Computational Relationships among Form, Function, and Phylogeny in the Catarrhine Ulnar Carpus, and the Evolutionary History of Ape and Human Locomotion

by

Craig L. Wuthrich

A dissertation submitted in partial fulfillment
of the requirements for the degree of
Doctor of Philosophy
(Anthropology)
in The University of Michigan
2017

Doctoral Committee:

Professor Laura M. MacLatchy, Chair
Associate Professor Jacinta C. Beehner
Associate Professor John D. Kingston
Assistant Professor Caley M. Orr, University of Colorado Denver
Research Scientist William J. Sanders

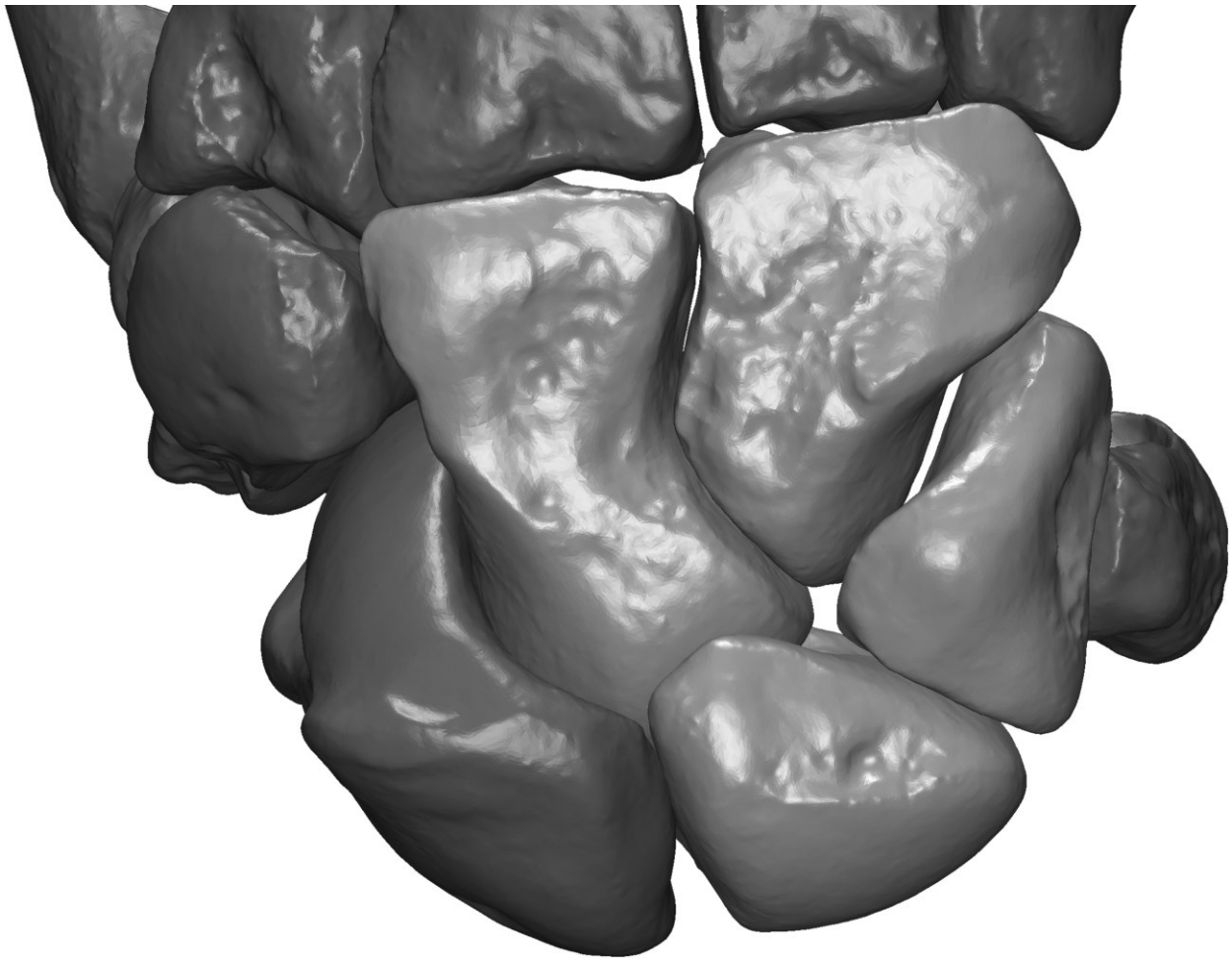

Craig L. Wuthrich

craigwut@umich.edu

ORCID iD: 0000-0002-3134-1719

Acknowledgements

My circuitous path to biological anthropology included two classes at the University of Colorado as a non-degree student near the end of several years in the private sector; for confirming my interest and facilitating my entrance into the field, I express appreciation to Matt Sponheimer and Michelle Sauther.

For access to extant specimens in their care, I thank Mark Omura and Judy Chupasko at the Museum of Comparative Zoology at Harvard University, Eileen Westwig at the American Museum of Natural History, Lyman Jelema at the Cleveland Museum of Natural History, Darrin Lunde at the Smithsonian National Museum of Natural History, Owen Lovejoy at Kent State University, and Stephen Hinshaw and Cody Thompson at the University of Michigan Museum of Zoology.

For access to scans or casts of fossil specimens, I thank Emma Mbua, Fredrick Manthi, and Blasto Onyango at the National Museums of Kenya, as well as Lee Berger, Matt Tocheri, William Kimbel, Michele Morgan, Caley Orr, and Mike Rose. Special thanks to the Rising Star team led by Lee Berger and to Doug Boyer at MorphoSource, Duke University, from which *H. naledi* scans were downloaded, for their contributions to open science.

For access, assistance, and training in the use of μCT and laser scanning equipment and 3D software, I thank Kathy Sweet and Karl Jepson in the department of orthopedic surgery at the University of Michigan, as well as Dana Begun, John Kingston, and the University of Michigan 3D Lab.

For assistance in figuring out the various analytical methods employed in this dissertation, I thank the authors of the many R packages used herein, and the overlapping communities of R, phylogenetics, and statistics researchers, developers, and enthusiasts at Stack Overflow, Cross Validated, r-sig-phylo, and various other personal sites and GitHub repositories. I also thank Charles Nunn and the other organizers and presenters of the 2010 AnthroTree Workshop (supported by NSF BCS-0923791) for providing my introduction to phylogenetic comparative methods,

For helpful conversations and comments, I thank Milford Wolpoff, Isaiah Nengo, Biren Patel, Craig Byron, and the members of my dissertation committee, with particular thanks to my advisor and committee chair, Laura MacLatchy, for her assistance and support over the years.

Finally, I thank Helen Dixon, my inspiration and witness.

Table of Contents

List of Tables

List of Figures

Abstract

Catarrhine wrist elements are commonly preserved in the fossil record, and the morphology of these specimens plays a prominent role in shaping our understanding of hominoid evolution. This joint complex may have special utility both in understanding how morphology tends to change in association with positional behavior, and in reconstructing the prevalence of these behaviors in extinct primates. However, we continue to lack a detailed understanding of the relationships among function, phylogeny and wrist morphology, including the degree to which quantifiably similar morphological variation should be expected in behaviorally convergent lineages. Quantitatively-confirmed morpho-functional links within the anthropoid wrist therefore remain exceedingly rare, hindering our ability to characterize the locomotor evolution of early catarrhine groups, including that of our own lineage.

This dissertation addresses this gap through analysis of 3D morphometrics derived from μCT and laser scans of a broad sample of extant and fossil anthropoid carpals, while ameliorating the confounding influences of allometry and phylogeny through their explicit inclusion in statistical models. Several cases of morphological convergence are identified in association with each of several behavioral modes. Features determined to meet both statistical and biomechanical criteria are selected as plausible locomotor or postural adaptations, and multivariate predictive models are demonstrated to be highly accurate in predicting differing degrees of reliance on the major anthropoid positional behaviors.

These predictive models and other insights are applied along with additional analytical techniques to a sample of seven morphologically diverse, formerly-undescribed catarrhine capitates from sites in the early Miocene Tinderet sequence of Western Kenya. Each specimen is formally described, and its taxonomic identity determined or constrained through estimation of body mass and analyses of taxonomic, phylogenetic, and functional affinities. The functional diversity of this fossil sample is also quantified, and found to be comparable to that of broad extant groups, with two specimens demonstrating substantial suspensory affinities, and another being uniquely great ape-like among capitates known from the early Miocene. The latter specimen is assigned to *Rangwapithecus gordoni*, and a new criterion by which to distinguish specimens of this taxon from *Proconsul africanus* is suggested. The range of variation in functionally diagnostic traits within this sample indicates a greater diversity of positional behavior among early Miocene catarrhines than what is generally recognized, and results add further support for the presence of a mid-sized, behaviorally-derived catarrhine at Songhor.

This study also contributes to the ongoing debate over human locomotor ancestry by modeling the adaptive landscape during hominoid locomotor evolution. It reconstructs various adaptive transitions across the clade, and estimates the prevalence of different positional behaviors in the populations ancestral to each of the various nested clades within Anthropoidea. While there is inconsistency in the patterns of morphological covariation among the different carpal elements, results are consistent in providing further support for the frequency of parallelism in the locomotor evolution of hominoids, particularly as it applies to suspension, with the last common ancestors of

both hominoids and great apes predicted to have been more generalized than any of the clade's extant representatives. The last common ancestor of humans and chimpanzees is also estimated to have lacked adaptations in association with knuckle-walking, providing further support for a relatively generalized ancestral morphotype at the root of the hominin clade – one that is not well modeled by any of the surviving hominoid lineages.

These results advance our understanding of the complex relationships among form, function, and phylogeny, and of the locomotor evolution of extant and fossil anthropoids, with important caveats, and provide guidance for future analyses of extant and fossil anthropoid functional morphology.

Chapter 1

Introduction

This dissertation represents an attempt to untangle the influence of positional behavior from the complex and overlapping influences of phylogeny and allometry on the morphology of the wrist in anthropoid primates, and to apply resulting insights toward increasing our understanding of human and ape[1] evolution, particularly as it relates to positional behavior (i.e., modes of locomotion and posture; Prost, 1965). From the first application of the paleobiological approach to primate evolution (Napier and Davis, 1959), morphology of the wrist, comprising either 8 or 9 carpals (due to fusion of the scaphoid and os centrale among hominines), the proximal metacarpal epiphyses, and the distal radius and ulna, has played a vital role in our understanding of positional behavior in fossil catarrhines, including that of our own putative ancestors. However, the reliability of functional inferences derived from carpal morphology is dependent on the fidelity of our understanding regarding how it is influenced by function. While there has been substantial progress on this front, the degree to which wrist morphology reliably reflects locomotor behavior across anthropoid lineages remains unclear, and specific

[1] In discussing groups within Hominoidea, the superfamily to which humans belong, "hominid" is used to refer to the clade we share with great apes, "hominine" to the clade we share with chimpanzees, bonobos, and gorillas, and "hominin" to all members of the human clade since our divergence from *Pan*. While the relatively recent understanding of our close relationship with other hominoids sometimes results in attempts to redefine long-established colloquial terms, their utility in referring to the paraphyletic subset of a clade's non-hominin representatives is retained here. To wit, "apes" refers to non-hominin hominoids, "great apes" to non-hominin hominids, and "African apes" to non-hominin hominines. "Asian apes" likewise refers to the paraphyletic group comprising pongines and hylobatids.

morphological traits quantitatively demonstrated to be diagnostic of a given locomotor mode remain rare.

Much of the lack of consensus in interpreting morpho-functional relationships within the wrist of hominoids and other anthropoids is due to confounding factors affecting the broader fields of functional morphology and biology in general. As with all biological traits, the skeletal elements comprising the wrists of anthropoids have evolved in each lineage to facilitate multiple functions while simultaneously reflecting a legion of non-adaptive influences. Even a brief summary of the confounds associated with inferring function from morphology is beyond the scope of this work (see also Abrams, 2001; Smith, 2016 and references therein). Several of these confounds feature prominently in subsequent chapters, chief among them the phylogenetic autocorrelation of biological data.

Morphological change associated with non-adaptive mechanisms tends to accumulate within lineages over time, which, along with that resulting from recent or ancestral selection, results in a strong tendency toward greater similarity in more closely related species. The essence of this phenomenon has long been understood, as demonstrated by its having served as the primary basis for the seminal work of both Linnæus (1735) and Darwin (1859). In accord with this tendency, adaptation associated with different positional behaviors in closely-related species tends to result in smaller-scale modification of a shared pattern (Lovejoy *et al.*, 1999, Hamrick, 1999). Biological samples derived from multiple species are therefore statistically nonindependent, violating the assumptions of standard quantitative methods. A statistical toolkit allowing the phylogenetic autocorrelation of biological data to be accounted for in quantitative

models has begun to take shape over the last three or so decades (Felsenstein, 1985). This work employs a variety of these tools in an attempt to account for some of the non-adaptive influences complicating our understanding of morpho-functional relationships in the anthropoid carpus.

This dissertation comprises three semi-autonomous studies neatly sandwiched between brief introductory and concluding chapters in fulfillment of the sacred rite by which the academy is instilled with a solidarity born of having formatted a roughly book-length document in *Microsoft Word*. Each chapter is intended to contain the information necessary to contextualize its goals, results, and conclusions; a thorough introduction to the issues addressed is therefore not attempted here.

Chapter 2 serves as the foundation of this work. In addition to summarizing my thought process in embarking on this project and introducing many of the methods employed, results from this chapter are the basis of several analyses in subsequent chapters. I test several dozen morpho-functional hypotheses in the wrists of anthropoids, and identify cases of morphological convergence in association with positional behavior while accounting for the influence of both phylogeny and allometry. The biomechanical underpinnings of each statistical relationship are then evaluated to gauge its plausibility as having emerged due to adaptation. I also build multivariate models to test the degree of correspondence between carpal morphology and positional behavior in extant anthropoids, thereby evaluating the generalizability and potential efficacy of these models in predicting the behavior of extinct members of the clade, and also explore the relative influences of different positional behaviors in shaping anthropoid wrist morphology.

In Chapter 3, I analyze a rare, morphologically diverse sample of catarrhine specimens of a single postcranial element, all recovered from the same geographically- and temporally-constrained setting of the early Miocene. I provide morphological descriptions for each of seven previously-undescribed capitates from Tinderet sites in Western Kenya, and constrain their taxonomic identities through body mass estimation, taxonomic and phylogenetic analyses, as well as reconstructions of positional behavior, in comparison with *Ekembo heseloni* and a large extant sample. The range of behavioral diversity implied by the Tinderet sample is also compared to those of different extant anthropoid groups. Results are contextualized in terms of their implications for early hominoid locomotor evolution and diversity, and a new criterion by which to distinguish specimens of *Proconsul africanus* and *Rangwapithecus gordoni* is suggested.

In Chapter 4, I analyze a broad range of hominin and non-hominin fossil specimens with the primary goal of contributing to the debate regarding the ancestral locomotor repertoire from which hominin bipedalism emerged. This study assesses both the overall morphology and the functional affinities of the human ulnar carpus, and those of the sampled fossil taxa, relative to those of a large non-hominin anthropoid sample. I reconstruct the locomotor evolution of the anthropoid clade as reflected in each of the analyzed carpal elements, and in the four combined, to assess the prevalence of homoplasy during hominoid locomotor evolution and to test competing hypotheses related to the ancestral positional repertoire of Hominoidea and those of its major nested clades. Additional analyses are conducted to test for functional distinctions among hominin taxa, with an emphasis on *Australopithecus sediba*.

The final chapter provides a brief summary of my conclusions, and describes some related caveats along with some future plans that may ameliorate some of them. Other research planned to build on and elaborate the results presented here are also outlined.

Chapter 1 references

Abrams, P., 2001. Adaptationism, optimality models, and tests of adaptive scenarios, in: Orzack, S.H., Sober, E. (Eds.), Adaptationism and Optimality. Cambridge University Press, pp. 273-302.

Darwin, C., 1859. On the Origin of Species. J. Murray, London.

Felsenstein, J., 1985. Phylogenies and the comparative method. The American Naturalist 125, 1-15.

Hamrick, M.W., 1999. A chondral modeling theory revisited. Journal of Theoretical Biology 201, 201-208.

Linnæus, C., 1735. Systema Naturæ. T. Haak, Lugduni Batavorum.

Lovejoy, C.O., Cohn, M.J., White, T.D., 1999. Morphological analysis of the mammalian postcranium: A developmental perspective. Proceedings of the National Academy of Sciences 96, 13247-13252.

Napier, J.R., Davis, P.R., 1959. The forelimb skeleton and associated remains of *Proconsul africanus*. Fossil Mammals of Africa 16, 1-69.

Prost, J.H., 1965. A definitional system for the classification of primate locomotion. American Anthropologist 67, 1198-1214.

Smith, R.J., 2016. Explanations for adaptations, just-so stories, and limitations on evidence in evolutionary biology. Evolutionary Anthropology 25, 276-287.

Chapter 2

Computational relationships between carpal joint surface morphology and positional behavior in extant anthropoids

Abstract

Despite the wrist theoretically having special utility in diagnosing the positional behavior of extinct primates, traits of the carpus quantitatively identified to consistently covary with positional behavior across the anthropoid clade remain exceedingly rare. This study seeks to remedy this by testing for covariance between positional behavior and aspects of carpal morphology in a broad sample of extant anthropoids. Shape traits hypothesized to be functionally significant were quantified using μCT and laser scan data, and analyzed along with quantitative and categorical characterizations of positional behavior while accounting for the confounding influences of allometry and phylogeny. The biomechanical underpinnings of univariate morpho-functional links are evaluated to determine which of the identified statistical relationships most plausibly result from adaptation. Multivariate relationships between shape and behavior are also explored – the differential influences wielded by locomotor and postural behaviors in shaping anthropoid wrist morphology are characterized, and the efficacy of carpal morphology in predicting anthropoid behavioral repertoires is evaluated.

Results indicate that morphology strongly covaries with positional behavior across the anthropoid clade. Instances of morphological convergence are identified in

association with each of several behavioral modes, and multivariate models predict the behavior of extant anthropoids with high accuracy. These results advance our understanding of the complex relationships among form, function, and phylogeny, and of the locomotor evolution of extant catarrhine groups, while guiding future behavioral reconstructions of fossil carpal specimens.

Introduction

The hands of anthropoid primates (catarrhines and platyrrhines) are used for a variety of tasks, including object manipulation (e.g., tool use, foraging, and social grooming), gathering sensory information, communication, and providing affection or comfort to other individuals (Fragaszy and Crast, 2016 and references therein). Much of the diversity in positional behavior among this clade's members can also be broadly construed according to differential use of the forelimbs (Schmitt *et al.*, 2016 and references therein). Suspension, vertical climbing, leaping, and the various types of quadrupedalism performed by anthropoids each generate distinct loading regimes (e.g., Fleagle, 1981; Rose, 1988; Swartz *et al.*, 1989; Carlson and Patel, 2006; Patel and Carlson, 2007, 2008; Tsegai *et al.*, 2013; Hunt, 2016), and to be best facilitated by different degrees of mobility (e.g., Sarmiento, 1988; Orr, 2010; Daver *et al.*, 2012). As a result, the anthropoid forelimb is thought to be especially adaptable (Rose, 1997).

Adaptability seems to be further enhanced in the carpus relative to more proximal skeletal elements. Variation in hand and wrist mobility among anthropoids results largely from corresponding variation in carpal morphology (Kivell, 2016), and this morphology is also important in maintaining stability and transmitting the forces generated during locomotion. Developmental constraints have been observed to

decrease in the forelimb on a gradient from proximal to distal (Hinchliffe, 1994, 2002; Shubin *et al.*, 1997; Hamrick, 2001, 2003, 2007), and analyses of primate forelimbs confirm that morphological variability increases distally, largely in accord with behavior (Etter, 1973; Hamrick, 1998, 1999, 2007; Cullinane, 2000). Aspects of carpal morphology may therefore have special utility in understanding morpho-functional relationships in extant anthropoids, and in reconstructing the behavior of extinct members of the clade.

The ulnar side of the wrist may have particular relevance in understanding how locomotor behavior is reflected in morphology. Suspension and vertical climbing are associated with greater mobility in ulnar deviation and supination (e.g. Lewis, 1969; Sarmiento, 1988; Rose, 1988) and greater strength in flexion (e.g., Susman and Stern, 1979), while differential loading of the ulnar side of the wrist has been hypothesized to distinguish these and other functional and taxonomic groups. For example, gorillas are hypothesized to transmit a greater proportion of ground reaction forces ulnarly relative to chimpanzees (Sarmiento, 1988; Inouye, 1994a, b; Dainton and Macho, 1999a; Matarazzo, 2013a, b). In addition, while the functional significance of variation among hominoids in features of the radial wrist has received ample attention (e.g., Tuttle, 1967; Rose, 1997; Richmond and Strait, 2000; Richmond *et al.*, 2001; Tocheri *et al.*, 2003, 2005; Begun, 2004; Marzke, 2010; Tallman, 2012; Orr, 2017), there has arguably been less attention paid to the condition of similarly important features in more ulnar wrist elements.

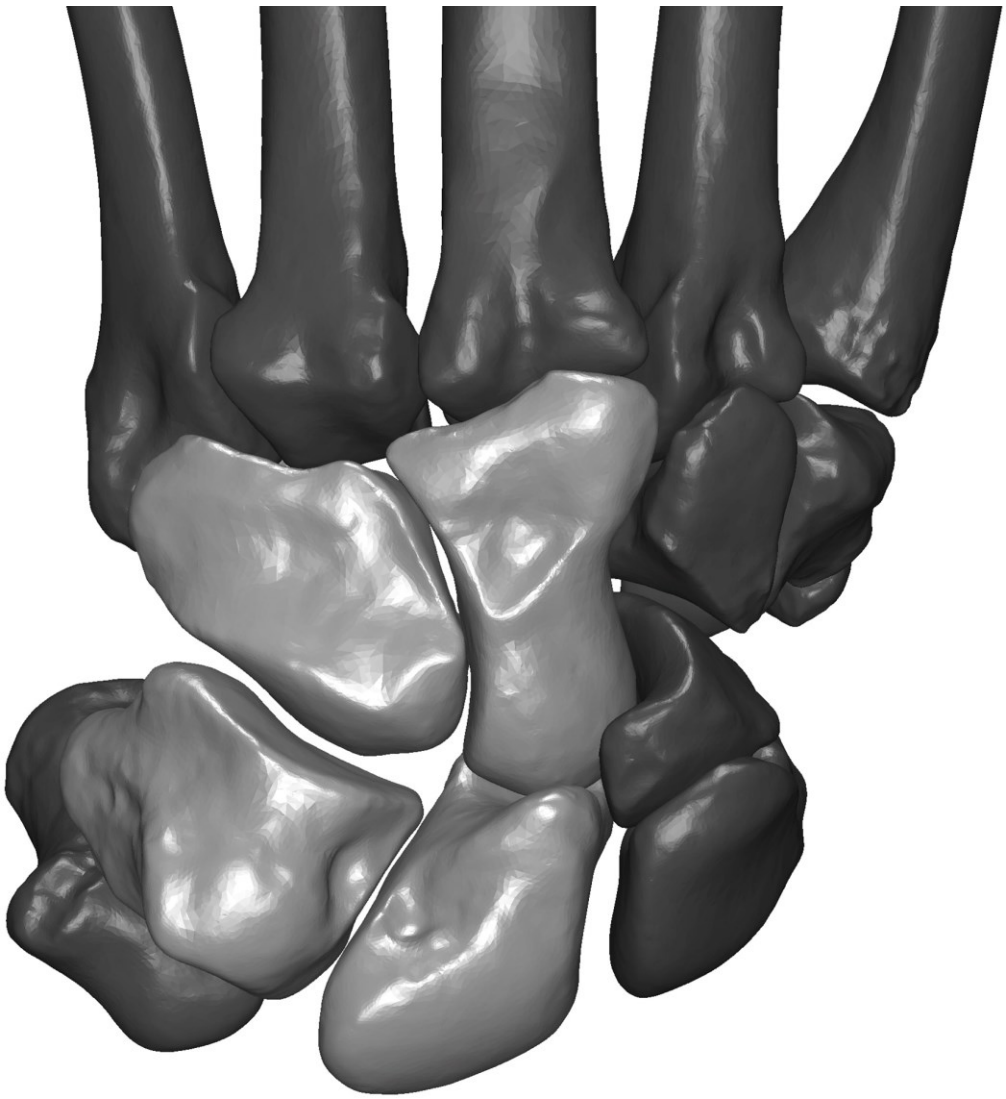

Fig. 2.1. Left wrist of *Cercopithecus mitis* (AMNH 82411) in dorsal view, with elements analyzed in this study highlighted.

Elements of the forelimb are commonly preserved in the catarrhine fossil record, and analysis of this material has been prominent in developing our understanding of ape and human evolution (reviewed in Nakatsukasa *et al.*, 2016 and Richmond *et al.*, 2016, respectively). However, the identification of reliable behavioral indicators in the anthropoid wrist is an ongoing concern, as cases of morphological convergence in behaviorally similar anthropoids have been more difficult to identify in the wrist relative

to the more proximal joint complexes of the forelimb (e.g., Rose, 1996; Larson, 1998; Young, 2003; Patel, 2010a). Aspects of carpal morphology are often assigned functional significance, but quantitative testing of these hypothesized morpho-functional links, including assessment of their generalizability across anthropoid lineages, has been substantially less common. As a result, specific wrist traits known to consistently covary with a given locomotor mode, or that are demonstrated to statistically distinguish among anthropoid behavioral repertoires, remain exceedingly rare.

An expectation of anatomical convergence in functionally convergent lineages is confounded by a host of factors (see Smith, 2016 and references therein), but there are additional complications to which the wrist is especially susceptible. The more proximal joint complexes of the appendicular skeleton are relatively simple, and may therefore have fewer adaptive pathways in facilitating similar behaviors, potentially increasing adaptive uniformity in behaviorally convergent lineages (Rose, 1997; Schmitt *et al.*, 2016; Byron *et al.*, in press). In contrast, the complex, interrelated joints of the carpus (as well as the tarsus; see Throckmorton, 2013) may provide a similar degree of mobility and stability in a variety of configurations (e.g., Lemelin and Schmitt, 1998; Jouffroy and Medina, 2002), with adaptive architectures and the relative contributions of constituent bones varying among lineages of similar function. The complexity of the small, oddly-shaped, and intricately-arranged elements of the carpus presents an additional, methodological barrier to understanding. While a great deal of information is contained in this morphology, much of it cannot be properly extracted using linear measurements, until recently the primary means of morphological quantification. These elements may be particularly productive targets of the modern 3D imaging and analysis

techniques utilized by a growing number of researchers (see Orr, 2016 and references therein).

If the degree to which positional behavior is reflected in skeletal morphology increases as a function of proximity with the substrate, distinct adaptive complexes may be induced in the wrist by variation within a broad behavioral class, such as grasping versus non-grasping palmigrady, contralateral versus ipsilateral grasping in different lineages of brachiators (Jenkins, 1981; Schmitt *et al.*, 2016, Byron *et al.*, *in press*), or even idiosyncratically in accord with more subtle variations in substrate use or hand posture. The need to maintain the grasping capability required for feeding, grooming, and other manipulative behaviors practiced among anthropoids may also limit the degree to which their hands and wrists can become specialized for locomotion (Vilensky and Larson, 1989). These factors have the potential to severely attenuate detectable covariance between wrist morphology and broadly-construed positional classes.

From within the noise of these myriad factors influencing anthropoid carpal morphology, this study attempts to isolate a functional signal associated with each of several positional behaviors. To this end, associated carpal elements from a broad set of anthropoid taxa are analyzed, with the confounding influences wielded by allometry and phylogeny ameliorated through their explicit inclusion in statistical models. The goals of this study are fourfold. The first is to investigate the consistency with which wrist morphology covaries with different locomotor and postural behaviors between lineages within the anthropoid clade, and to identify specific cases of morphological convergence in association with each. The second goal is to determine which of the traits found to covary with a function are most likely to be adaptive to that function. This

necessarily involves a degree of subjective interpretation, but is an essential step in separating statistical aberration from biological adaptation, with the latter becoming more likely as the plausibility of the underlying biomechanical relationship increases. The two remaining goals involve exploration of multivariate relationships between shape and behavior: this study evaluates the differential influences wielded by locomotor and postural behaviors in shaping anthropoid wrist morphology, as well as the efficacy with which anthropoid behavioral repertoires can be predicted based on functionally diagnostic aspects of carpal morphology.

Materials and methods

Sampling procedure

An associated set of four carpal elements – the capitate, hamate, lunate, and triquetrum – was sampled from each of 336 individuals representing 28 extant anthropoid taxa (Table 2.1). Most specimens (n = 1136) were scanned with a GE Healthcare model Pxs5-928EA μCT scanner, operating at an accelerated potential of 55 kV with a beam current of 450 μA, producing scan data with a resolution of 92 microns. An isosurface was derived from each of these scans and exported as a triangular mesh. The remaining specimens (n = 208) were scanned with a NextEngine 3D Scanner HD (Macro setting, two families of 6 scans with autorotation, 160k ppi for smaller specimens, 40k ppi for larger ones), creating a triangular mesh comparable to those produced by the μCT workflow. The efficacy of pooling scan data of different types has been demonstrated (Slizewski *et al.*, 2010, Tocheri, *et al.*, 2011; Polo and Felicismino, 2012). All meshes were processed to correct imperfections stemming from the scanning

process, osteochondral defects, or other minor issues of pathology or preservation to ensure comparability across the sample. Completed 3D models were then digitally segmented along articular margins with reference to the original specimen or high-resolution photographs thereof (see Fig. 2.2).

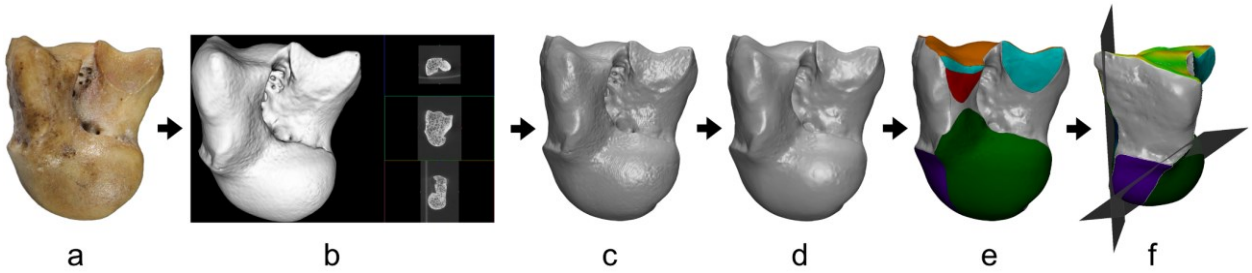

Fig. 2.2**.** A schematic representing the sampling workflow of this study. Each specimen, here represented by a left capitate of *Pan troglodytes troglodytes* (UMMZ 39507) in lateral view (a), was scanned (b), exported as a triangular mesh isosurface (c), processed and smoothed (d), and digitally segmented (e), followed by variable extraction (f).

Table 2.1. Comparative sample

Taxon	n	♂	♀	Total proportions[f]					Arboreal-only proportions					
				Quad[a]	*Susp*[b]	*Climb*[c]	*Leap*[d]	*Arb*[e]	*QuadA*	*SuspA*	*ClimbA*	*LeapA*	Class[g]	References
Pan troglodytes schweinfurthii	10	7	3	0.93	0.01	0.06	0	0.10	0.31	0.08	0.59	0.02	*KW*	Doran and Hunt, 1994; Carlson, 2005
Pan troglodytes troglodytes	12	6	6										*KW*	
Pan troglodytes verus	13	7	6	0.86	0.01	0.11	0	0.16	0.21	0.06	0.68	0.01	*KW*	Doran, 1993a; Carlson, 2005
Pan troglodytes ellioti	5	2	3										*KW*	
Pan paniscus	4	2	2	0.87	0.01	0.09	0	0.17	0.35	0.09	0.51	0.04	*KW*	Doran and Hunt, 1994[h]
Gorilla gorilla	26	15	11	0.92	0.01	0.06	0	0.10	0.19	0.13	0.62	0.02	*KW*	Remis, 1994[i]
Gorilla beringei	11	8	3	0.96	0.01	0.04	0	0.09	0.53	0.06	0.40	0.01	*KW*	Doran, 1996, 1997
Pongo pygmaeus	19	9	10	0.12	0.43	0.37	0.01	0.95	0.12	0.43	0.37	0.01	*S*	Cant, 1987[j]
Pongo abelii	14	4	10	0.18	0.38	0.35	0.01	0.95	0.18	0.38	0.35	0.01	*S*	Thorpe and Crompton, 2006
Hoolock hoolock	7	3	4	0	0.55	0.20	0.22	0.99	0	0.55	0.20	0.22	*S*	Sati and Alfred, 2002
Hylobates muelleri	4	2	2										*S*	
Hylobates lar	15	9	6	0	0.59	0.19	0.16	0.99	0	0.59	0.19	0.16	*S*	Nowak and Reichard, 2016
Symphalangus syndactylus	3	1	2	0	0.59	0.32	0.02	0.99	0	0.59	0.32	0.02	*S*	Hunt, 2004
Papio anubis	14	8	6	0.99	0	0.01	0.01	0.05	0.68	0	0.21	0.10	*DG*	Hunt, 1991
Lophocebus albigena	6	5	1	0.42	0	0.36	0.21	0.95	0.42	0	0.36	0.21	*PG*	Gebo and Chapman, 1995; Aronsen, 2004[k]
Mandrillus sphinx	8	6	2										*DG*	
Cercocebus agilis	2	2	0										*PG*	
Macaca fascicularis	18	11	7	0.68	0	0.26	0.06	0.97	0.68	0	0.26	0.06	*PG*	Cant, 1988[l]
Erythrocebus patas	7	5	2	0.94	0	0.05	0.01	0.08	0.60	0	0.30	0.10	*DG*	Isbell *et al.*, 1998[m]
Cercopithecus mitis	10	6	4	0.54	0	0.35	0.11	0.95	0.54	0	0.35	0.11	*PG*	Gebo and Chapman, 1995
Colobus guereza	9	6	3	0.41	0.01	0.20	0.38	0.96	0.41	0.01	0.20	0.38	*PG*	Gebo and Chapman, 1995
Procolobus rufomitratus	12	6	6	0.35	0.01	0.29	0.35	0.95	0.35	0.01	0.29	0.35	*PG*	Gebo and Chapman, 1995; Aronsen, 2004[k]
Nasalis larvatus	17	9	8										*PG*	
Trachypithecus sp.	17	7	10	0.60	0	0.13	0.28	0.99	0.60	0	0.13	0.28	*PG*	Fleagle, 1980
Presbytis melalophos	2	1	1	0.28	0.02	0.19	0.50	0.99	0.28	0.02	0.19	0.50	*PG*	Fleagle, 1980
Alouatta sp.	32	13	19	0.61	0.02	0.33	0.05	0.95	0.61	0.02	0.33	0.05	*PG*	Youlatos and Guillot, 2015[n]
Ateles geoffroyi	11	2	9	0.42	0.25	0.25	0.07	0.99	0.42	0.25	0.25	0.07	*S*	Mittermeier, 1978; Cant, 1986; Fontaine, 1990[k]
Cebus apella	28	20	8	0.37	0	0.40	0.21	0.95	0.37	0	0.40	0.21	*PG*	Wright, 2007; Youlatos, 1998[k]
Total n	336	182	154											

[a] Includes both quadrupedal and tripedal walking.
[b] Includes brachiation, forelimb swinging, orthograde clambering and transfering, and inverted walking or running (after Thorpe and Crompton, 2006).
[c] Includes vertical climbing and descent, scrambling, sliding, swaying, and bridging (after Doran, 1996).
[d] Includes both leap and drop.
[e] Refers to the proportion of all locomotion occuring on an arboreal substrate. When combined locomotion is not quantified but travel and feeding locomotion are, an average was taken, weighted by number of observations when available. Male and female data were also averaged if combined proportion was not provided. When no terrestrial locomotion was reported, *Arb* was estimated at .99.
[f] Highly arboreal species (*Arb* ≥ .95) are generally studied in terms of arboreal-only locomotor proportions; the total proportions of these taxa were not adjusted to reflect minor differences in *Arb*.
[g] Characterizes the dominant positional behavior in each taxon's locomotor repertoire; *KW*, knuckle-walking; *S*, orthograde clambering, climbing, suspension, and/or brachiation; *PG*, arboreal palmigrade quadrupedalism; *DG*, terrestrial digitigrade quadrupedalism.
[h] *Arb* estimated based on Doran, 1993b, total proportions extrapolated.
[i] *Arb* estimated and total proportions extrapolated.
[j] *Arb* calculated from Galdikas, 1978; *Leap* estimated based on *P. abelii* and subtracted from horizontal clambering, classified here under suspension.
[k] Average of reported values.
[l] *Arb* from Wheatley, 1982.
[m] *Arb* estimated, arboreal proportions extrapolated.
[n] Compiled values for sampled species averaged.

Shape variables

33 morphometric variables (Table 2.2) were extracted from the set of segmented models belonging to each individual. The relative size of an articulation was characterized by indexing its surface area against that of its parent bone. The average orientation of selected surfaces was characterized by a fitted least-squares plane. Most angular metrics are dihedral angles calculated between these planes; in one case (LuCpRaA), the first inertial axis (i.e., the normal vector) of the lunate's capitate facet was used to limit the metric's variation to within a parasagittal plane, and in another case (Tq1LuA) the first inertial axis of the triquetrum was used to characterize the orientation of its long axis relative to its lunate facet. In these cases, the angle is calculated between the inertial axis and its orthogonal projection onto the least-squares plane of interest. An additional four compound metrics were derived from these angular metrics by summing adjacent angles, or in one case (MCJAR) by indexing two such compound angles against each other.

Four additional shape variables were calculated for each individual. The concavity of the capitate's hamate facet (CpHmC) and the lunate's capitate facet (LuCpC) were characterized by the difference between the maximum and minimum deviance of the facet relative to its fitted plane, divided by the maximum length of the facet parallel to the axis of concavity. The topological complexity of the capitate's Mc3 surface (Cp3SD) was characterized by the standard deviation of its vertices relative to its fitted plane (weighted to account for triangle size), divided by the cube root of capitate volume. Capitate head position (CpHP) was measured linearly from its most proximal point to a plane extending from the dorsal nonarticular region of the bone

orthogonal to the plane of the Mc3 facet, divided by the square root of Mc3 surface area to account for isometry. Each shape variable characterizes a morphological trait hypothesized either here or elsewhere in the literature to be associated with one or more anthropoid functions (Table 2.2). In many cases, these hypotheses were left implicit by previous researchers, or limited in context; this study seeks to quantitatively test for the existence of these links, and to assess their generalizability to other anthropoids.

Table 2.2. Description of shape variables and associated functional hypotheses in non-hominin anthropoids. Listed hypotheses were not necessarily endorsed or explicitly stated in the provided references, and were often applied in a more limited taxonomic setting. See text for measurement details.

Metric	Description	Hypothesized Functional Implications	References
CpPx	Capitate proximoradial surface area	Greater area may reflect medial and/or lateral expansion of the capitate head or expansion of the concave distal portion of the scaphoid/centrale surface, perhaps associated with greater midcarpal mobility in supination, extension, and/or radial deviation in suspensors, or with a stable midcarpal joint during limited extension during terrestrial behavior, particularly in knuckle-walkers.	Jenkins, 1981; Rose, 1984; Ward, 1998
CpDn	Capitate dorsal nonarticular surface area	Greater area may correspond with a smaller articular arc on the dorsum of the capitate associated with limited extension of the midcarpus, possibly associated with terrestriality, especially knuckle-walking.	Richmond *et al.*, 2001; Begun, 2004; Orr, 2017
Cp2	Capitate Mc2 surface area	Restricted to the palmar portion of the capitate as part of the stable CJC of great apes; greater surface area may reflect a more proximal Mc2 origin as part of the distal wrist mortise in terrestrial cercopithecoids.	Lovejoy *et al.*, 2009; Selby *et al.*, 2016
Cp4	Capitate Mc4 surface area	A lack of articulation may reflect offset Mc3&4 bases and increased CMC stability in knuckle-walking taxa, while extensive articulation may aid axial load transmission in digitigrade taxa	Marzke *et al.*, 1994
Cp23A	Interior angle between the Mc2 and Mc3 facets of the capitate	Sagittal alignment of the Mc2 facet said to be unique to great apes and key to their CJC stability, although the more proximal origin of the Mc2 in digitigrade cercopithecoids may also be reflected in a more acute angle	Selby *et al.*, 2016
CpPxA	Interior angle between the proximoradial surface and the hamate facet of the capitate	Larger values reflect a stouter capitate and a lower degree of midcarpal joint curvature associated with terrestriality, whereas smaller values reflect a narrower capitate and greater midcarpal joint curvature associated with greater mobility in climbing or suspensory primates	Tuttle, 1967; Jenkins and Fleagle, 1975; Sarmiento, 1988; Hamrick, 1996b
CpScA	Interior angle between the scaphoid/centrale facet and the dorsal nonarticular surface of the capitate	Lower values reflect a more radial (as opposed to dorsal) orientation of the scaphoid/centrale facet, thought to be associated with habitual supination of the midcarpal joint in suspensory taxa	Jenkins and Fleagle, 1975; Jenkins, 1981; Rose, 1984
Cp3SD	Capitate Mc3 facet complexity	Larger values reflect topographical complexity or keeling related to increased CMC stability, usually thought to be associated with knuckle-walking, less commonly with suspension	McHenry, 1983; Marzke, 1983; Marzke and Marzke, 1987; Richmond *et al.*, 2001; Begun, 2004; Selby *et al.*, 2016
CpHmC	Capitate hamate surface concavity	Greater concavity may reduce shear during knuckle-walking or perhaps vertical-manus quadrupedalism more generally.	Sarmiento, 1985; Richmond *et al.*, 2001; Begun and Kivell, 2011

CpHP	Dorsopalmar position of the capitate head	Larger values reflect a more palmarly positioned capitate head, suggested to be associated with greater extension of the midcarpal joint as found in palmigrade primates	Lovejoy *et al.*, 2009; Selby *et al.*, 2016
HmPx	Hamate proximomedial surface area	Larger values may be associated with habitual loading of the wrist in ulnar deviation, and perhaps also increased mobility; smaller values may reflect limited ulnar deviation in knuckle-walkers	Spoor *et al.*, 1991; Preuschoft *et al.*, 1993; Richmond *et al.*, 2001; Begun and Kivell, 2011
Hm5	Hamate Mc5 surface area	Greater values may be associated with CMC mobility and/or ulnar loading in digitigrade primates, whereas lower values may reflect relatively low ulnar loading, especially of the fifth ray, during knuckle-walking	Marzke, 1983; Marzke *et al.*, 1992
Hm45A	Interior angle between the Mc5 and Mc4 facets of the hamate	Smaller values may reflect a more ulnar orientation of the Mc5 facet, perhaps related to the distal wrist mortise in cercopithecoids, particularly in accomodating the styloid-like proximomedially projecting Mc5 base in digitigrade taxa.	Selby *et al.*, 2016
HmPxA	Interior angle between the proximomedial surface and capitate facet of the hamate	Lower values indicate a narrow hamate and greater curvature of the midcarpal joint, which facilitates mobility in rotation and ulnar deviation at the midcarpal joint	Tuttle, 1967; Jenkins and Fleagle, 1975; Jenkins, 1981; Sarmiento, 1988; Orr and Atkinson, 2016
CpHmPxA[a]	Interior angle between the proximal surfaces of the capitate and hamate (CpPxA + HmPxA)	Lower values indicate higher curvature of the midcarpal joint facilitating midcarpal mobility; higher values indicate a midcarpal joint oriented orthogonal to axial compressive loads experienced among African apes and terrestrial cercopithecids	Tuttle, 1967; Jenkins and Fleagle, 1975; Jenkins, 1981; Sarmiento, 1988; Hamrick 1996b; Richmond, 2006
CMC34A	Exterior angle between the capitate Mc3 facet and the hamate Mc4 facet	Said to be parallel in most cercopithecoids but forming a V-shaped angle in baboons, may play a role in converting shear to compression during digitigrade quadrupedalism	Selby *et al.*, 2016
LuDs	Lunate distal surface area	Greater values may be associated with the transmission of axial loads during knuckle-walking	Jenkins and Fleagle, 1975
LuTq	Lunate triquetrum surface area	Larger values may be associated with increased compressive loading and stability; smaller values may reflect a reduced role in weight-bearing in suspensory taxa	Kivell *et al.*, 2013
LuSc	Lunate scaphoid/centrale surface area	Smaller values may be associated with greater loading of the radiolunate joint in wrist adduction during climbing	Kivell *et al.*, 2013
LuRa	Lunate radius surface area	Larger values may reflect enhanced ulnar loading in Asian apes relative to African apes, but have also been associated with climbing in hominoids; large and small values have both also been linked to pronograde weight support or terrestriality	Jenkins and Fleagle, 1975; Heinrich *et al.*, 1993; Zylstra, 1999; Richmond *et al.*, 2001; Lovejoy *et al.*, 2009; Ward *et al.*, 2012; Kivell *et al.*, 2013

LuDsTqA	Interior angle between the distal surface and triquetral facet of the lunate	A more obtuse angle orients the triquetrum distally, and may correspond with increased ulnar loading and/or distal migration of the triquetrum, associated with greater supination and ulnar deviation in suspensors	Corruccini, 1978; Sarmiento, 1985, 1988; Begun, 2004
LuDsScA	Interior angle between the distal surface and scaphoid/centrale facet of the lunate	Larger values serve to orient the distal facet normal to compressive axial forces produced during pronograde weight bearing; smaller values may be associated with a more curved midcarpal joint and greater midcarpal mobility	Sarmiento, 1988
LuScRaA	Interior angle of scaphoid/centrale and radius facets of the lunate	A more obtuse angle may be associated with the radial facets of the lunate and scaphoid being relatively coplanar to transmit axial compressive loads; a more acute angle may reflect a more radioulnarly curved and mobile proximal wrist joint.	Tuttle, 1967, 1969; Beard *et al.*, 1986; Begun, 2004; Richmond, 2006
LuCpRaA	Orientation of the radius facet of lunate relative to the first inertial axis of the capitate facet	May reflect the neutral or most stable position of the wrist in flexion-extension, characterizing the orientation of the radiocarpal and midcarpal joints relative to each other; greater values may be found in habitually palmigrade or palmigrade-capable species	Robertson, 1984; Rose, 1988
LuCpC	Lunate capitate surface dorsopalmar concavity	Greater concavity may enhance midcarpal stability throughout a larger range of motion during suspension	Dainton and Macho, 1999
TqHm	Triquetrum hamate facet area	Larger area may reflect greater midcarpal mobility in supination and ulnar deviation; and may be associated with more a distal origin of the pisiform, increasing leverage of the flexor carpi ulnaris during flexion	Kivell, 2011, Sarmiento, 1988
TqLu	Triquetrum lunate facet area	Larger values may be associated with greater compressive loading and stability; smaller values may reflect a reduced role in weight-bearing. Both large and small values have been associated with greater midcarpal mobility	Kivell, 2011; Kivell *et al.*, 2013
TqPi	Triquetrum pisiform facet area	Larger area may reflect increased intrinsic or extrinsic loading of triquetrum and pisiform, perhaps associated with terrestriality, while smaller values may reflect both lesser loading and the facet being limited to the more distal part of the bone	Sarmiento 1985, 1988
TqSt	Triquetrum ulnar styloid facet area	When present, a larger articulation may reflect greater distomedial displacement of the ulnar styloid, allowing greater ulnar deviation and supination at the proximal carpal joint	Beard *et al.*, 1986; Godinot and Beard, 1993
TqHmPiA	Orientation of pisiform facet of triquetrum relative to hamate facet	Larger values reflect a more distal or palmar (as opposed to proximal or medial) orientation of the pisiform facet, which may be reflected in the orientation of the pisiform, thought to increase flexor carpi ulnaris leverage during flexion in suspensory taxa	Sarmiento, 1988; Lewis, 1989; Hamrick, 1997
Tq1LuA	Orientation of the long axis (first inertial axis) of the triquetrum relative to lunate facet	Larger values may reflect a more distal orientation of the long axis of the triquetrum, associated with greater mobility in ulnar deviation and supination	Sarmiento, 1988

LuTqDsA[a]	Exterior angle between the distal surface of the lunate and the hamate facet of the triquetrum (360 - (LuDsTqA + TqHmLuA); the latter angle is not analyzed here)	Smaller values correspond with a narrower and more curved proximal surface of the midcarpal joint, which facilitates midcarpal mobility and the transmission of a greater variety of load vectors, but lesser ability in transmitting axial/unidirectional loading	Tuttle, 1967; Jenkins and Fleagle, 1975; Sarmiento, 1988; Hamrick, 1996a, b, c
MCJAR[a]	Ratio between the angles of the opposing midcarpal joint surfaces (LuTqDsA/CpHmPxA)	Greater congruence of opposing midcarpal joint surface curvature (values closer to 1) enhances load transmission, whereas larger values indicate relatively greater curvature of the distal surface, thought to enhance mobility	Bullough *et al.*, 1968; Sarmiento, 1988

[a] Denotes a compound metric

Behavioral data

Quantitative characterizations of locomotor behavior were compiled from published observations available for 22 of 28 sampled taxa (Table 2.1). The resulting locomotor variables represent the proportion of locomotor time spent in four different modes of locomotion: *Quad* = quadrupedalism/tripedalism; *Susp* = orthograde suspension, including brachiation, forelimb swinging, orthograde clambering and transferring, and inverted walking or running (after Thorpe and Crompton, 2006); *Climb* = vertical climbing, quadrupedal climbing and scrambling, vertical descent, bridging, sliding, and swaying (after Doran, 1996); *Leap* = leaping and dropping (see Hunt *et al.*, 1996 for definitions and discussion of behavioral terms). When locomotion during travel and feeding were quantified separately, these values were averaged, weighted by number of observations when available. Male and female proportions were similarly averaged if combined data were not provided.

Non-locomotor postures such as arm-hanging while feeding have been proposed to play important adaptive roles in hominoid evolution (e.g. Hunt, 1991), and there is a growing recognition that locomotion changes during ontogeny, and that behaviors preferred by sub-adults may disproportionately influence adult morphology (e.g., Sarringhaus *et al.*, 2016). However, the current lack of comparable ontogenetic and postural data for most of the sampled taxa made locomotor proportions a more feasible quantitative behavioral proxy.

Each locomotor mode is represented by an additional variable ending in the letter *A*, which measure arboreal-only locomotor proportions (e.g., *SuspA*). A final locomotor variable, *Arb*, characterizes the proportion of locomotion occurring on arboreal

substrates as opposed to on the ground. In highly arboreal species for which no or very limited terrestrial locomotion was observed, *Arb* was estimated at .99. Quantitative observations of the types and frequency of terrestrial locomotion in highly arboreal primates are uncommon; the total proportions of these species are therefore identical to their arboreal-only proportions, and do not reflect minor differences in *Arb* values. Proportions of bipedalism were also compiled, but are not analyzed here due to an expected lack of morphological association, as well as its strong collinearity with suspension in the sampled taxa. Some taxa therefore have total and arboreal-only proportions that do not sum to 1.

Sampled taxa were also assigned to one of four broad classes characterizing the hand/wrist postures most frequently employed during locomotion: *KW* = knuckle-walking; *S* = orthograde climbing, clambering, suspension and/or brachiation; *PG* = arboreal palmigrade quadrupedalism; *DG* = terrestrial digitigrade quadrupedalism. Some analyses were repeated using different combinations of these positional classes; *KW* and *DG* taxa combine to form a vertical manus group (*VM*), *S* and *PG* taxa form a palmigrade-capable group (after Orr, 2010), and *PG* and *DG* taxa form a pronograde monkey group. While categorical schemes are frequently used in analyzing behavioral variation in primates (e.g., Orr, 2010; Patel and Wunderlich, 2010; Polk *et al.*, 2010; Begun and Kivell, 2011; Fernandez *et al.*, 2015; Lewton, 2015; Selby *et al.*, 2016; Selby and Lovejoy, 2017), it is recognized that these are crude characterizations of the many behaviors performed by these animals (e.g., Hunt *et al.*, 1996; Walker, 1998). Members of the *KW* class, for example, are also all capable suspensors, but employ this behavior

relatively infrequently in adulthood, whereas members of the *S* class are more committed suspensors.

Included among the sampled taxa are several “phylogenetically-targeted” (Arnold and Nunn, 2010) dyads of closely-related but behaviorally dissimilar taxa, in an attempt to maximize the number of sampled lineages having undergone evolutionary changes in positional repertoire, which provide the best opportunities for testing functional hypotheses (Coddington, 1994). For example, each of the digitigrade taxa contribute to one of these dyads, with *Papio*, *Mandrillus*, and *Erythrocebus* having evolved digitigrady independently of each other (e.g., Gilbert *et al.* 2010; Gosselin-Ildari, 2013), in contrast to their closest relatives in the sample, respectively *Lophocebus*, *Cercocebus*, and *Cercopithecus*. *Macaca* serves as an outgroup to the papionin dyads, and *Cebus* the outgroup to an *Ateles-Alouatta* dyad. The colobine sample lacks positional class diversity, but captures substantial variation in locomotor proportions.

Preparatory analysis

The distributions of several locomotor proportions and two-thirds of the shape variables depart significantly from normality, as measured by Shapiro-Wilk (1965) tests. This is to be expected, however, given the statistical non-independence of biological data. Phylogenetic residuals of linear models were found to depart from normality only very rarely, and with no greater occurrence in the analysis of non-normally distributed variables. Shape and locomotor variables were therefore analyzed without transformation. For non-phylogenetic analyses, methods less sensitive to heteroscedasticity were preferred. Shape variables were scaled to units of standard

deviation for ease of regression coefficient comparison and to prevent bias in multivariate models due to unit heterogeneity.

The inclusion of redundant or irrelevant variables can cause important problems in multivariate models (e.g., Miller, 2002; Ritter, 2015). Shape variables were therefore subjected to a series of feature selection criteria. Pairwise collinearity was measured via Spearman correlation of combined sex-specific phylogenetic independent contrasts (PICs; Felsenstein, 1985). A certain amount of collinearity is expected in association with functional adaptation, phylogenetic or developmental constraints, and other influences, but variables with pairwise rho values exceeding 0.5 were prevented from inclusion in the same model. Multicollinearity was assessed in each subset selected for multivariate analysis via calculation of condition numbers.

A size surrogate was included as a covariate during hypothesis testing and feature selection, but not as a predictor in multivariate analyses. While potentially attenuating significance and predictive power, these steps increase the generalizability of the resulting models to taxa for which similar relationships among size, shape, and positional behavior cannot necessarily be assumed. The log-transformed volume of each carpal and combinations thereof were tested for size surrogate suitability via ordinary least squares (OLS) regression against log-transformed sex-specific body mass means and phylogenetic generalized least squares (PGLS; Grafen, 1989) of taxon means. Body mass data of sampled individuals were gathered from museum records when available, supplemented by data from Smith and Jungers (1997) and Delson and colleagues (2000). Analysis of covariance (ANCOVA) was used to detect heterogeneity of OLS regression slopes between sexes and superfamilies. Cases of

significant heterogeneity were further explored with *post hoc* Tukey (1949) tests with false discovery rate adjustment (Benjamini and Hochberg, 1995) to detect between-group differences. Spearman correlations between the PICs of each variable and the size surrogate were calculated to test for allometric scaling of shape and locomotor variables. Relationships between body size and positional classes were assessed using PGLS. Multivariate phylogenetic allometry of shape and locomotor variables was tested with a distance-based PGLS method (D-PGLS; Adams, 2014a).

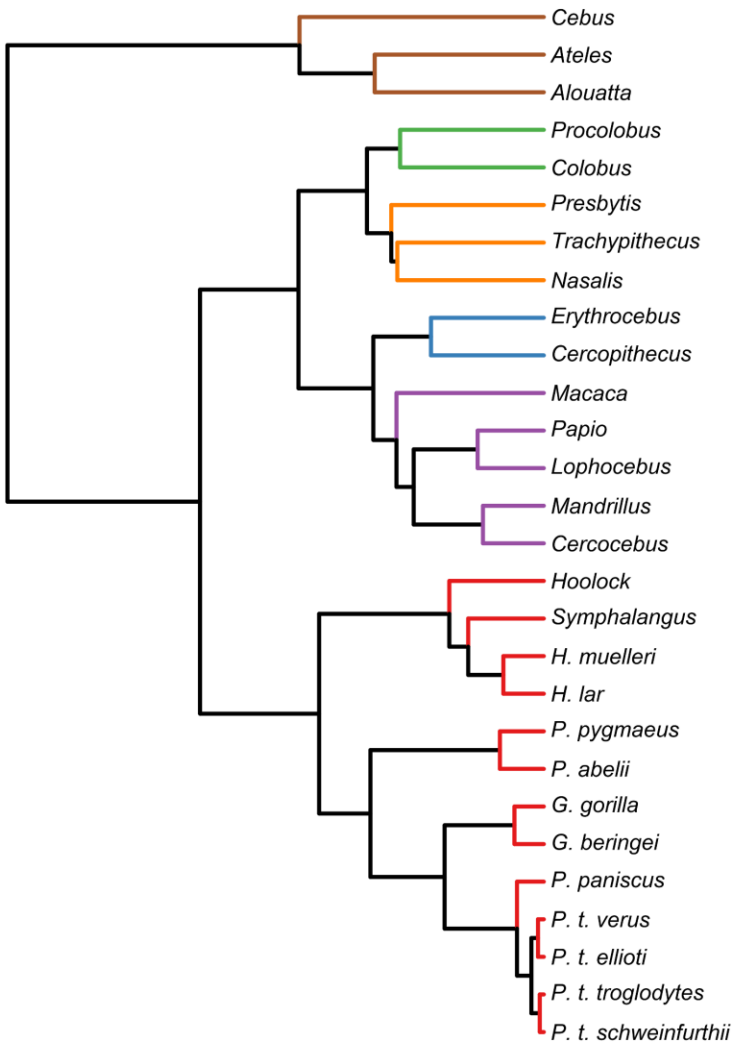

Fig. 2.3. Molecular relationships of the extant sample used in phylogenetic analyses.

The phylogenetic signal of individual shape and locomotor variables was estimated using both Pagel's lambda (Pagel, 1999) and Blomberg's K (Blomberg *et al.*, 2003); multivariate phylogenetic signal was estimated by K_{mult}, a generalization of the latter metric (Adams, 2014b). A consensus molecular tree based on Genbank data from version 3 of the 10ktrees project (Arnold *et al.*, 2010; Fig. 2.3) was used in analyses incorporating phylogenetic information.

Univariate hypothesis testing and feature selection

Shape and locomotor variable values were often extreme in sampled hylobatids, giving these data points high leverage in many of the functional analyses, and therefore the potential to yield significant correlations across the sample that in fact have no discernable functional pattern in the non-hylobatid sample (discussed further below). To take this into account, each of the analyses described in this section were repeated with hylobatids excluded.

Univariate relationships between the shape variables and the positional classes were assessed with PGLS regression, with λ estimated during model fitting. PGLS cannot be used with a categorical response variable, and therefore has limited utility in analyzing shape variation between positional classes while accounting for size. This limitation was overcome using phylogenetic generalized linear mixed modeling (PGLMM), of which PGLS can be considered a special case (de Villemereuil and Nakagawa, 2014). Unlike PGLS, the Bayesian Markov chain Monte Carlo (MCMC) PGLMM approach used here can also analyze multiple observations per taxon, allowing consideration of intra-taxon variation. Like other forms of multinomial logistic regression,

this method assigns a log odds ratio to each pairwise combination of the predictor variables and the non-reference classes of the dependent variable. With a palmigrade reference group, the coefficients therefore characterize the expected change in probability of belonging to *DG*, *KW*, and *S* relative to *PG* given a one standard deviation increase in the shape variable while holding the size variable constant. The use of PGLMM is described in detail elsewhere (Hadfield, 2010; Hadfield and Nakagawa, 2010; Carter and Worthington, 2016). This study takes the parameter expanded priors of the Bernoulli procedure followed by Carter and Worthington (2016; see Worthington, 2016 for R code), adjusted to accommodate a multiclass response variable (see Gelman, 2006 for background on this procedure). pMCMC values were also calculated for convenience in feature selection and hypothesis testing.

Investigation of the individual morpho-functional hypotheses (Table 2.2) was further supplemented through analysis of different positional schemes. *KW* and *S* were analyzed relative to pronograde monkeys, *DG* and *KW* relative to palmigrade-capable, *VM* relative to palmigrade-capable, and *VM* and *S* relative to *PG*. Inter- and intra-taxon variation were considered in separate analyses of each positional scheme, the former through analysis of taxon means, and the latter through analysis of all observations without taxonomic differentiation beyond that imposed by the phylogenetic structure.

Due to the time- and hardware-intensive nature of fitting a separate MCMC model for each shape variable in each of several different analyses, the number of iterations used to fit each model was limited. 5e6 iterations (5e5 burn-in period, 1e3 thinning interval) generally resulted in effective sample sizes (samples adjusted for Markov chain autocorrelation) exceeding 1000 for each coefficient, the minimum

recommended by de Villemereuil (2012). Analyses of observations especially prone to autocorrelation were repeated with 1e7 iterations to meet this threshold.

Results of phylogenetic regressions aided in selecting the subset of shape variables used to build multivariate classification models (Barr and Scott, 2014). Initially, shape variables were selected if found to significantly distinguish the taxon means of at least one of the three of three non-reference classes from those of the palmigrade class with hylobatids excluded. This subset was further winnowed to eliminate collinear variables, as discussed above. Finally, any variables excessively hindering the prediction of classes for which they were not chosen as significant were eliminated. This was done by averaging the p-values of each shape variable for the three non-reference classes and eliminating any with a mean greater than 0.4.

Univariate relationships between the shape variables and locomotor proportions were analyzed via PGLS. Allometry was accounted for by including the size surrogate as a covariate of shape with the locomotor proportion as the dependent variable. In addition to their use in testing the individual functional hypotheses (Table 2.2), results of these analyses aided in building a predictive model for each of the locomotor proportions. Shape variables found to correlate with a given locomotor proportion while accounting for allometry with hylobatids excluded were subjected to further model selection criteria as outlined below.

Multivariate analysis

Positional classes

Shape variables selected for inclusion in the positional classification model were first included in a final PGLMM analysis to estimate the subset's phylogenetic signal relative to the positional classes. The model's posterior mean λ did not differ significantly from zero. Because a phylogenetic model lacking phylogenetic signal yields results equivalent to those of non-phylogenetic methods, non-phylogenetic methods were chosen to construct and evaluate the classification model. Discriminant function analysis (DFA) was chosen for ease of visualization and interpretation. DFA assumes that all variables are normally distributed and that all classes have equal covariance matrices, is prone to over-fitting, and cannot detect non-linear relationships (Kovarovic *et al.*, 2011; Mitteroecker and Bookstein, 2011). A supplementary classifier was therefore built with a regularized multinomial logistic regression machine learning algorithm (*glmnet;* Friedman *et al.*, 2010), chosen for its less strict assumptions and ability to detect nonlinear relationships while further protecting against over-fitting and bias due to collinearity. This method incorporates elastic net regularization, in which predictor coefficients are shrunk in accord with collinearity as in ridge regression, while allowing uninformative or redundant variables to be ignored entirely as in LASSO regression (Tibshirani, 1996).

The classification accuracy of both models was calculated after 100 repetitions of k-fold cross-validation with random, non-stratified sampling. This technique reduces overfitting and variance while increasing model applicability to out-of-sample data (e.g., Kovarovic *et al.*, 2011). 10-fold CV was chosen for its favorable combination of variance

reduction and low bias relative to other CV techniques (Kuhn and Johnson, 2013). Models were trained and evaluated with priors proportional to class size (Sanchez, 1974). *glmnet* output was optimized by tuning alpha and lambda parameters (the regularization term and its weight, respectively; the latter not to be confused with Pagel's) on repeated runs.

Locomotor proportions

The subset of shape variables found to correlate with each locomotor proportion were subjected to a model selection algorithm detecting the PGLS models associated with the lowest second-order Akaike Information Criterion (AICc) values (Burnham and Anderson, 2002). A subset of three or four models was chosen for each locomotor proportion based on delta-AICc. From these, the final model for each locomotor proportion was chosen based on their relative accuracy in predicting extant locomotor proportions. λ was again estimated at 0 during the fitting of each candidate model; prediction and model evaluation was therefore carried out using non-phylogenetic quasibinomial logistic regression.

The six taxa for which quantitative locomotor observations were unavailable were used to aid model evaluation. Although not useful for quantifying prediction error, locomotor proportions estimated for these taxa were compared to published qualitative observations and to quantitative observations of taxa thought to be behaviorally similar. This approach was deemed superior to withholding taxa from the training set, as reducing the number of training taxa risks impoverishing the model-building process. Quantification of prediction error was carried out by calculating the percent standard

error of estimate (%SEE) of individual predictions generated during 100 repetitions of 10-fold cross validation.

The degree to which carpal morphology covaries with locomotion was further explored via calculation of RV coefficients (Escoufier, 1973; Klingenberg, 2009) between matrices (or blocks) of shape and locomotor variables and PICs thereof. Correspondence of the shape data with locomotion was assessed in turn relative to various combinations of locomotor proportions, including arboreal-only proportions and total proportions, with and without *Arb*. Relationships between shape and locomotor proportions were further assessed using two-block partial least squares (PLS) regression (Rohlf and Corti, 2000), which maximizes the covariance between blocks along each axis, as well as a phylogenetic equivalent (rPLS; Adams and Felice, 2014; Adams and Collyer, 2016). Taxa for which locomotor observations were not available were projected into PLS shape-space by scaling their shape data to match the training sample and multiplying the resulting matrix by one containing the singular vectors of the shape block.

A standardized Euclidean distance was calculated between each taxon's position in PLS shape-space and behavior-space, defined by the first two axes of each block's PLS scores scaled to match their proportions of covariance. This metric allows the average distance between shape and locomotor behavior to be compared between models with different inputs, and the degree to which form follows function to be compared between taxa.

Computational details

Computations were done in R (R Core Team, 2016) within RStudio (RStudio Team, 2016). PGLS was done with *caper* (Orme *et al.*, 2013); PGLMMs were fitted with *MCMCglmm* (Hadfield, 2010); RV tests were done with *FactoMineR* (Le *et al.*, 2008); two-block PLS was done with *Morpho* (Schlager, 2016) and *geomorph* (Adams and Otarola-Castillo, 2013); DFA was done with *MASS* (Venables and Ripley, 2002). Cross-validation of DFA and GLM models incorporated code taken from *ipred* (Peters and Hothorn, 2015); AICc model selection was done with *MuMIn* (Barton, 2016); *glmnet* (Friedman *et al.*, 2010) was used via wrapper functions in *caret* (Kuhn, 2016); %SEE was calculated with *MASSTIMATE* (Campione, 2016); Spearman correlations were done with *Hmisc* (Harrell *et al.*, 2016); Tukey tests were done with *multcomp* (Hothorn *et al.*, 2008). *ape* (Paradis *et al.*, 2004) was used to calculate PICs and to modify and visualize phylogenetic trees, the latter with the help of *phyclust* (Chen, 2011). Fig. 2.4, Fig. 2.6, Fig. 2.7, and Fig. 2.8 were produced with the aid of *ggplot2* (Wickham, 2009); 3D visualizations were produced in *3-Matic*.

Note: Hundreds of p-values were generated in the course of this study. They are considered for convenience in the aid of variable selection and interpreting relationship strengths, but are not individually relied upon as evidence for the validity of any conclusions presented. Multivariate models are instead evaluated through cross-validated prediction accuracy, while individual morpho-functional relationships are evaluated with consideration of prior functional hypotheses, results from multiple analyses with varying inputs, and the plausibility of their biomechanical underpinnings. p-values are therefore not adjusted for multiple comparison except where noted.

Despite the arbitrary nature of the $p \leq 0.05$ threshold, it is held here to indicate "statistical significance" for convenience in discussion.

Results

Univariate analysis

Log-transformed volumes of the capitate, lunate, and the four carpals combined were each determined to be effective surrogates for body size (Table 2.3). These variables each had OLS $R^2 \geq 0.97$, with slopes remaining homogenous between different sexes and superfamilies. Log-transformed sum carpal volume was chosen for use as the size surrogate in this study due to its higher R^2 and lower residual standard error values in both OLS and PGLS regression, and its lower λ estimate. Log-transformed hamate and triquetrum volumes were found to be less effective size surrogates. Log triquetrum volume slopes are very similar in hominoids and other anthropoids, but the intercept of hominoids is significantly different, as expected owing to their lack of stylotriquetrum articulation (Lewis, 1965 and references therein; note: ulnocarpal contact is often maintained in hylobatids via a novel accessory bone (Lewis, 1971; Jenkins, 1981; Sarmiento, 1988) that is not analyzed here). Meanwhile, the log hamate volume slope is significantly different in hominoids. Hylobatid carpals are large relative to body mass among the sampled taxa (save the triquetrum, which is large only relative to other hominoids), but their hamates are particularly disproportionate, which, combined with their small body size, is responsible for much of this heterogeneity.

Table 2.3**.** Results regression and analysis of covariance between sex-specific means (OLS) and taxon means (PGLS) of log-transformed body mass and log-transformed carpal volumes

	OLS					ANCOVA		PGLS					
	R^2	Inter-cept	b	p	RSE	p (sex)	p (superfamily)	R^2	λ	Inter-cept	b	p	RSE
Capitate	0.974	-2.404	0.806	**0.000**	0.166	0.317	0.420	0.973	0.411	-2.475	0.823	**0.000**	0.022
Hamate	0.956	-2.752	0.854	**0.000**	0.215	0.397	**0.005**[a]	0.945	0.824	-2.968	0.895	**0.000**	0.034
Lunate	0.971	-2.448	0.833	**0.000**	0.176	0.439	0.378	0.965	0.419	-2.441	0.838	**0.000**	0.025
Triquetrum	0.924	-3.633	1.069	**0.000**	0.283	0.463	**0.044**	0.919	0.878	-2.985	0.943	**0.000**	0.042
Sum	0.979	-4.033	0.883	**0.000**	0.151	0.292	0.068	0.985	0.000	-3.983	0.876	**0.000**	0.018

[a] Denotes significant between-group differences between anthropoid superfamilies in FDR-adjusted post hoc Tukey tests

Results of PGLS and PGLMM analyses for covariance between individual shape variables and positional classes are summarized in Table 2.4, with results of secondary positional scheme analyses available in Table 2.8. 16 of the 33 shape variables significantly distinguish suspensory and palmigrade taxon means, increasing to 21 with the size surrogate as a covariate. Seven of these shape traits remain significant when accounting for intra-taxon variation. With hylobatids excluded, 16 shape variables distinguish suspensory taxon means, 11 when accounting for size, and 5 when analyzing individual observations. Ten shape variables separate knuckle-walking and palmigrade taxon means. Only a single shape variable significantly distinguishes knuckle-walking taxon means when accounting for size, although this number increases to 6 in analysis of individual observations. Knuckle-walking is better distinguished with hylobatids excluded. Seven and 13 shape means distinguish knuckle-walking from palmigrady with and without accounting for allometry, as do 8 shape variables' individual observations. Digitigrady is the least distinguishable of the non-reference classes, with only 4 and 5 variables distinguishing taxon means with and without hylobatids, respectively. This drops to 2 and 3, respectively, when accounting for allometry, and 4 and 1 when analyzing individual observations, although several others fall just short of this threshold.

Table 2.4**.** Covariance of shape variables with positional classes relative to the palmigrade (*PG*) reference class. Reported results are from univariate phylogenetic generalized least squares (PGLS) regression of taxon means except where noted.

			DG						*KW*						*S*					
	R^2	λ	b	p	OR[a]	p[a]	OR[b]	p[b]	b	p	OR[a]	p[a]	OR[b]	p[b]	b	p	OR[a]	p[a]	OR[b]	p[b]
CpPx	0.18	0.82	0.19	0.64	1.62	0.21	1.21	0.20	0.69	0.35	-0.15	0.88	-0.22	0.81	-0.61	0.29	-2.48	**0.04**	-1.20	0.21
CpDn	0.02	0.99	0.26	0.58	1.61	0.14	0.97	0.22	-0.45	0.70	0.10	0.93	0.08	0.92	-0.39	0.65	-0.28	0.80	-0.51	0.52
Cp2	0.27	0.99	0.49	0.10	2.16	0.09	2.23	**0.04**	-1.56	**0.03**	-1.94	0.16	-1.34	0.19	-0.98	0.07	-3.03	**0.03**	-1.39	0.17
Cp4	0.16	1.00	-0.15	0.60	-0.03	1.00	0.18	0.88	-1.47	0.06	-2.54	0.09	-2.86	**0.02**	-0.42	0.44	1.23	0.30	0.90	0.41
Cp23A	0.23	0.89	-0.77	0.08	-1.74	0.12	-1.02	0.28	-0.54	0.52	-1.00	0.41	-1.22	0.19	0.64	0.32	1.41	0.19	0.72	0.41
CpPxA	0.69	0.79	-0.24	0.33	-0.71	0.57	0.20	0.86	0.26	0.53	1.37	0.34	1.06	0.32	-1.73	**0.00**	-4.41	**0.00**	-3.15	**0.00**
CpScA	0.25	1.00	-0.37	0.14	-1.17	0.26	-0.61	0.53	0.12	0.85	0.48	0.71	1.28	0.22	-0.84	0.08	-2.58	**0.01**	-1.43	0.14
Cp3SD	0.06	0.77	-0.19	0.73	0.66	0.55	0.53	0.58	0.84	0.37	0.37	0.78	-0.20	0.83	-0.07	0.92	-0.77	0.45	-0.53	0.58
CpHmC	0.38	1.00	0.23	0.38	1.97	0.17	2.18	0.06	0.23	0.72	0.75	0.61	-0.30	0.78	-1.31	**0.01**	-3.52	**0.01**	-2.53	**0.03**
CpHP	0.50	0.00	0.74	0.14	1.40	0.22	1.03	0.24	-1.42	**0.00**	-2.29	0.09	-1.45	0.12	-0.01	0.97	0.12	0.92	-0.13	0.87
HmPx	0.18	0.98	-0.47	0.24	-2.18	0.09	-1.62	0.11	-0.89	0.35	-0.86	0.53	0.28	0.80	0.55	0.43	1.64	0.14	0.85	0.38
Hm5	0.44	0.94	0.33	0.16	1.73	0.19	1.63	0.09	-1.23	**0.03**	-2.43	0.05	-2.17	**0.04**	-1.57	**0.00**	-3.15	**0.01**	-1.77	0.08
Hm45A	0.28	0.00	-0.78	0.20	-1.93	0.12	-0.89	0.32	0.26	0.55	-0.71	0.54	-0.54	0.55	0.97	**0.04**	1.44	0.19	0.61	0.51
HmPxA	0.13	0.93	0.35	0.39	1.24	0.34	0.96	0.33	0.61	0.49	-0.36	0.75	-0.10	0.93	-0.51	0.44	-2.01	0.07	-0.70	0.47
CpHmPxA	0.50	0.98	0.02	0.92	0.37	0.82	1.19	0.29	0.48	0.36	1.05	0.50	1.46	0.20	-1.25	**0.00**	-4.30	**0.00**	-3.95	**0.00**
CMC34A	0.52	0.00	-1.05	**0.04**	-2.82	**0.02**	-1.87	0.07	1.34	**0.00**	1.17	0.38	0.82	0.43	0.32	0.38	0.13	0.91	0.28	0.78
LuDs	0.76	0.00	-0.90	**0.01**	-3.00	**0.03**	-1.98	**0.03**	1.80	**0.00**	2.58	0.05	2.54	**0.01**	0.41	0.12	-0.10	0.95	-0.26	0.79
LuTq	0.67	0.00	0.69	0.09	1.72	0.16	0.98	0.25	0.46	0.13	1.26	0.32	0.71	0.39	-1.53	**0.00**	-3.78	**0.01**	-1.22	0.15
LuSc	0.19	0.98	0.02	0.95	0.96	0.48	0.81	0.39	-1.40	**0.03**	-2.19	0.11	-1.45	0.15	-0.35	0.46	-0.04	0.98	-0.16	0.85
LuRa	0.14	0.98	-0.01	0.97	0.80	0.51	0.62	0.48	0.64	0.47	1.79	0.20	0.54	0.55	-0.70	0.29	-2.27	0.05	-0.80	0.38
LuDsTqA	0.51	0.95	-0.30	0.26	-0.86	0.53	-1.14	0.30	-1.20	0.05	-2.10	0.14	-4.13	**0.00**	1.03	**0.03**	3.64	**0.00**	4.33	**0.00**
LuDsScA	0.27	0.80	0.46	0.23	1.76	0.13	0.84	0.30	0.36	0.60	0.80	0.53	0.43	0.62	-0.92	0.09	-3.11	**0.01**	-1.16	0.17
LuScRaA	0.19	0.80	-0.11	0.78	-0.56	0.58	0.47	0.58	-0.19	0.79	-0.47	0.68	0.22	0.79	-1.14	**0.05**	-3.13	**0.01**	-1.02	0.25
LuCpRaA	0.64	0.95	-1.27	**0.00**	-1.26	0.28	-0.09	0.93	-2.08	**0.00**	-3.69	**0.00**	-3.99	**0.00**	-1.16	**0.01**	-2.46	**0.04**	-0.24	0.81
LuCpC	0.68	0.00	-0.60	0.14	-2.21	0.11	-1.88	**0.04**	0.66	**0.03**	0.38	0.77	0.45	0.63	1.80	**0.00**	3.68	**0.00**	1.76	0.06
TqHm	0.14	0.87	-0.28	0.36	-1.79	0.19	-1.71	0.09	0.40	0.50	1.14	0.35	0.43	0.66	0.75	0.11	2.64	**0.03**	1.38	0.17
TqLu	0.08	0.97	0.05	0.86	-0.64	0.62	-0.53	0.61	0.78	0.25	1.66	0.22	0.49	0.64	0.01	0.98	0.48	0.69	0.46	0.66
TqPi	0.45	0.70	-0.23	0.53	-0.81	0.56	-0.12	0.92	0.88	0.12	2.27	0.12	1.33	0.20	-1.05	**0.03**	-3.77	**0.00**	-1.47	0.14

TqSt	0.36	1.00	0.19	0.17	1.30	0.34	2.43	**0.05**	-1.00	**0.01**	-2.08	0.11	-2.39	0.06	-0.75	**0.01**	-2.60	**0.04**	-1.25	0.30
TqHmPiA	0.46	0.59	0.35	0.34	0.14	0.90	-0.83	0.43	0.99	0.06	0.72	0.58	-0.75	0.47	1.83	**0.00**	4.44	**0.00**	2.45	**0.02**
Tq1LuA	0.83	0.00	-0.94	**0.00**	-2.17	0.09	-1.70	0.11	-1.40	**0.00**	-2.39	0.08	-3.12	**0.00**	1.01	**0.00**	3.07	**0.02**	2.84	**0.01**
LuTqDsA	0.44	0.80	0.40	0.23	2.08	0.14	1.89	0.07	0.56	0.33	0.48	0.71	0.25	0.82	-1.15	**0.01**	-3.73	**0.00**	-2.62	**0.01**
MCJAR	0.33	0.80	0.19	0.59	0.87	0.53	0.06	0.93	-0.17	0.78	-1.37	0.39	-1.03	0.34	1.25	**0.02**	3.90	**0.00**	1.67	0.11

Without hylobatids

			DG						*KW*						*S*					
	R^2	λ	b	p	OR^a	p^a	OR^b	p^b	b	p	OR^a	p^a	OR^b	p^b	b	p	OR^a	p^a	OR^b	p^b
CpPx	0.07	0.47	0.50	0.41	1.63	0.14	0.99	0.27	0.44	0.55	0.14	0.90	-0.01	0.99	-0.21	0.77	-1.03	0.35	-0.76	0.39
CpDn	0.09	0.97	0.31	0.47	2.34	**0.05**	1.24	0.15	-0.27	0.79	0.15	0.90	-0.55	0.51	-0.86	0.28	-2.22	0.08	-1.40	0.10
Cp2	0.28	0.99	0.47	0.13	2.21	0.08	1.94	0.05	-1.49	0.05	-2.11	0.14	-1.43	0.16	-0.94	0.11	-2.27	0.10	-1.34	0.19
Cp4	0.30	1.00	-0.15	0.46	0.20	0.86	0.67	0.52	-1.40	**0.01**	-3.05	**0.05**	-3.04	**0.01**	-0.89	**0.04**	-0.02	1.00	0.33	0.77
Cp23A	0.19	0.92	-0.94	0.07	-1.73	0.09	-0.62	0.50	-0.56	0.60	-1.15	0.28	-1.20	0.18	0.34	0.69	0.19	0.86	0.38	0.66
CpPxA	0.75	0.00	-0.63	0.09	-0.94	0.38	-0.02	0.98	0.29	0.28	1.23	0.32	0.78	0.43	-2.42	**0.00**	-3.36	**0.00**	-2.34	**0.02**
CpScA	0.18	1.00	-0.49	0.11	-1.80	0.11	-1.21	0.21	-0.03	0.97	0.53	0.63	1.47	0.13	-0.67	0.27	-1.01	0.38	-0.56	0.57
Cp3SD	0.07	0.96	-0.40	0.41	0.66	0.50	0.47	0.64	0.87	0.44	0.47	0.71	-0.23	0.81	0.40	0.64	-0.49	0.66	-0.49	0.61
CpHmC	0.35	0.93	0.41	0.25	2.32	0.05	1.74	0.09	0.12	0.88	1.10	0.39	-0.08	0.96	-1.50	**0.02**	-2.29	**0.05**	-1.73	0.09
CpHP	0.61	0.00	0.76	0.10	1.59	0.14	1.21	0.18	-1.46	**0.00**	-2.82	**0.02**	-2.06	**0.03**	-0.71	0.12	-1.15	0.32	-0.79	0.39
HmPx	0.18	0.94	-0.59	0.14	-2.20	0.06	-1.62	0.10	-0.89	0.30	-1.12	0.37	0.41	0.66	0.22	0.75	0.86	0.44	0.96	0.32
Hm5	0.84	0.00	0.40	0.16	1.92	0.14	1.29	0.16	-1.83	**0.00**	-2.90	**0.03**	-1.89	**0.05**	-1.43	**0.00**	-2.14	0.08	-1.39	0.15
Hm45A	0.52	0.00	-0.76	0.13	-2.22	0.07	-1.19	0.21	0.26	0.49	-0.53	0.65	-0.18	0.86	1.91	**0.00**	2.46	**0.04**	1.29	0.18
HmPxA	0.15	0.00	0.52	0.43	1.30	0.23	0.66	0.46	-0.60	0.22	0.02	0.99	0.15	0.87	-0.59	0.37	-0.38	0.69	-0.16	0.87
CpHmPxA	0.51	0.92	0.01	0.99	0.08	0.96	0.74	0.43	0.63	0.39	0.60	0.66	0.94	0.33	-1.94	**0.00**	-3.31	**0.01**	-2.82	**0.01**
CMC34A	0.62	0.00	-1.03	**0.03**	-2.71	**0.03**	-2.41	**0.02**	1.31	**0.00**	1.58	0.24	1.48	0.14	0.84	0.06	0.94	0.44	0.95	0.34
LuDs	0.89	0.00	-0.87	**0.00**	-2.89	**0.03**	-1.79	0.06	1.75	**0.00**	2.99	**0.02**	2.66	**0.01**	-0.23	0.33	-1.17	0.34	-0.60	0.52
LuTq	0.45	0.00	0.96	0.08	1.87	0.10	0.79	0.32	0.64	0.11	1.53	0.17	0.58	0.49	-1.32	**0.02**	-2.69	**0.02**	-1.16	0.17
LuSc	0.27	0.94	0.02	0.91	1.31	0.38	1.73	0.08	-1.30	**0.02**	-3.02	**0.03**	-2.32	**0.03**	-0.82	0.05	-1.94	0.16	-1.36	0.17
LuRa	0.06	0.96	0.01	0.98	0.75	0.49	0.38	0.65	0.60	0.53	2.10	0.10	0.54	0.54	-0.33	0.66	-1.02	0.38	-0.59	0.50
LuDsTqA	0.58	0.92	-0.41	0.17	-0.90	0.45	-1.02	0.32	-1.58	**0.02**	-2.50	0.06	-3.76	**0.00**	1.15	**0.03**	2.40	**0.04**	3.59	**0.00**
LuDsScA	0.31	0.00	1.27	**0.04**	1.73	0.06	0.66	0.39	0.34	0.44	1.01	0.34	0.45	0.58	-0.81	0.18	-1.73	0.16	-0.78	0.33
LuScRaA	0.32	0.00	-0.75	0.21	-0.74	0.44	0.15	0.87	-1.04	**0.02**	-0.49	0.65	0.19	0.82	-1.41	**0.02**	-1.87	0.09	-0.67	0.40

LuCpRaA	0.77	0.91	-1.26	**0.00**	-2.04	0.13	-0.76	0.47	-2.18	**0.00**	-4.05	**0.00**	-4.12	**0.00**	-0.88	**0.01**	-0.06	0.97	0.79	0.46
LuCpC	0.62	0.00	-0.78	0.08	-2.34	**0.05**	-1.48	0.10	0.86	**0.01**	0.35	0.77	0.45	0.62	1.90	**0.00**	2.81	**0.03**	1.57	0.08
TqHm	0.14	0.78	-0.33	0.35	-2.05	0.12	-1.46	0.15	0.74	0.23	1.19	0.34	0.40	0.70	0.62	0.24	1.59	0.19	1.19	0.23
TqLu	0.06	0.97	0.04	0.87	-0.28	0.82	-0.07	0.94	0.65	0.28	1.83	0.17	0.53	0.62	0.23	0.63	0.40	0.75	0.38	0.72
TqPi	0.64	0.00	-0.42	0.33	-1.33	0.34	-0.37	0.67	1.45	**0.00**	2.25	0.07	1.10	0.21	-0.68	0.12	-2.27	0.10	-0.80	0.37
TqSt	0.37	1.00	0.19	0.19	1.42	0.31	2.41	0.05	-1.08	**0.01**	-2.52	0.08	-2.36	0.07	-0.61	**0.04**	-1.14	0.39	-1.05	0.38
TqHmPiA	0.56	0.63	0.34	0.30	0.22	0.87	-0.77	0.46	0.96	0.05	0.65	0.62	-0.40	0.70	2.11	**0.00**	3.80	**0.00**	2.71	**0.01**
Tq1LuA	0.84	0.00	-0.96	**0.00**	-2.19	0.08	-1.47	0.15	-1.45	**0.00**	-2.55	**0.04**	-2.84	**0.01**	1.32	**0.00**	2.36	**0.04**	2.83	**0.02**
LuTqDsA	0.40	0.31	0.81	0.11	2.41	**0.04**	1.67	0.10	0.35	0.50	0.59	0.61	0.34	0.73	-1.38	**0.02**	-2.46	**0.03**	-1.94	0.06
MCJAR	0.43	0.68	0.69	0.14	1.53	0.15	0.45	0.62	-0.02	0.98	-0.64	0.56	-0.61	0.49	1.89	**0.01**	2.76	**0.01**	0.78	0.36

[a] Based on Bayesian phylogenetic generalized linear mixed model (PGLMM) regression of taxon means with size (log-transformed sum carpal volume) as a covariate. OR, odds ratio (log scale)

[b] Based on PGLMM analysis of all observations rather than taxon means

Covariance between shape and locomotor variables is reported in Table 2.5 and Table 2.9. *SuspA* and *Susp* are each correlated with 16 shape variables; without hylobatids, they maintain correlations with 10 and 7 traits, respectively. *Quad* and *ClimbA* share correlations with 8 and 6 shape metrics, respectively, regardless of whether hylobatids are included. *Climb* correlates with only 3 variables with hylobatids, but 12 without, the highest of the nine locomotor proportions. *Arb* is correlated with 9 and 10 shape variables with and without hylobatids. *QuadA* is correlated with the largest number of shape variables, with 17 significant relationships while accounting for allometry. However, the high-leverage data of hylobatids is especially apparent here – with this group excluded, significant covariance with *QuadA* is found in only four shape traits. *Leap* and *LeapA* covary with the fewest number of shape traits; only a single shape trait is correlated with either of the two leaping proportions across the sample, with one additional correlation revealed when excluding hylobatids.

Only four shape variables share an association with both *ClimbA* and *Climb*, and in three of these cases they covary in opposite directions. Only LuSc covaries in the same direction with both climbing proportions, and this is due to controlling for allometry – without size as a covariate it also covaries in opposite directions with the two climbing proportions. The implications of climbing's dichotomous shape correlations are investigated below.

Table 2.5**.** Relationships between shape variables and selected locomotor proportions based on PGLS regression

a	*Quad*						**b**	*SuspA*					
	R^2	λ	b	p	b^a	p^a		R^2	λ	b	p	b^a	p^a
CpPx	0.54	0.00	0.73	**0.00**	0.68	**0.00**		0.15	0.00	-0.28	0.07	-0.91	**0.00**
CpDn	0.06	1.00	0.20	0.26	0.23	0.14		0.00	1.00	-0.01	0.93	-0.01	0.92
Cp2	0.00	1.00	0.02	0.95	0.22	0.36		0.02	1.00	-0.11	0.56	-0.14	0.49
Cp4	0.05	1.00	-0.28	0.32	0.11	0.72		0.04	1.00	0.19	0.35	0.22	0.37
Cp23A	0.17	1.00	-0.44	0.06	-0.12	0.54		0.19	1.00	0.30	**0.04**	0.30	**0.05**
CpPxA	0.42	0.76	0.70	**0.00**	0.57	**0.01**		0.84	0.00	-0.86	**0.00**	-0.96	**0.00**
CpScA	0.02	1.00	0.21	0.54	0.28	0.34		0.32	1.00	-0.59	**0.01**	-0.60	**0.01**
Cp3SD	0.18	1.00	0.40	**0.05**	0.28	0.14		0.08	1.00	-0.19	0.20	-0.19	0.23
CpHmC	0.42	1.00	0.71	**0.00**	0.36	0.12		0.42	0.97	-0.54	**0.00**	-0.63	**0.00**
CpHP	0.00	1.00	0.04	0.80	0.04	0.79		0.01	1.00	0.06	0.64	0.06	0.65
HmPx	0.15	1.00	-0.35	0.08	-0.23	0.21		0.13	1.00	0.23	0.10	0.24	0.11
Hm5	0.21	1.00	0.59	**0.03**	0.46	0.06		0.21	1.00	-0.42	**0.03**	-0.42	**0.04**
Hm45A	0.01	1.00	-0.07	0.66	-0.12	0.35		0.01	1.00	0.05	0.62	0.06	0.59
HmPxA	0.10	1.00	0.30	0.15	0.21	0.26		0.16	1.00	-0.27	0.06	-0.27	0.07
CpHmPxA	0.39	0.97	0.74	**0.00**	0.50	**0.05**		0.73	0.00	-0.81	**0.00**	-0.95	**0.00**
CMC34A	0.06	1.00	0.20	0.27	0.10	0.58		0.01	1.00	-0.04	0.74	-0.04	0.80
LuDs	0.01	1.00	0.08	0.75	0.03	0.90		0.02	1.00	-0.11	0.53	-0.10	0.55
LuTq	0.56	0.99	0.75	**0.00**	0.24	0.12		0.20	1.00	-0.25	**0.04**	-0.25	**0.04**
LuSc	0.01	1.00	-0.14	0.63	0.09	0.75		0.09	1.00	0.28	0.17	0.29	0.19
LuRa	0.26	1.00	0.57	**0.01**	0.38	0.09		0.27	1.00	-0.41	**0.01**	-0.45	**0.01**
LuDsTqA	0.63	0.00	-0.79	**0.00**	-0.74	**0.00**		0.38	1.00	0.47	**0.00**	0.49	**0.00**
LuDsScA	0.24	0.99	0.51	**0.02**	0.24	0.20		0.29	1.00	-0.36	**0.01**	-0.36	**0.01**
LuScRaA	0.07	1.00	0.25	0.22	0.11	0.57		0.05	1.00	-0.14	0.32	-0.14	0.36
LuCpRaA	0.26	1.00	-0.59	**0.02**	-0.35	0.19		0.02	1.00	-0.11	0.54	-0.22	0.34
LuCpC	0.07	1.00	-0.21	0.22	-0.21	0.17		0.05	1.00	0.13	0.30	0.13	0.31
TqHm	0.13	1.00	-0.43	0.10	-0.42	0.06		0.31	1.00	0.48	**0.01**	0.48	**0.01**
TqLu	0.04	1.00	0.30	0.38	0.06	0.84		0.01	1.00	-0.13	0.59	-0.12	0.65
TqPi	0.49	1.00	0.70	**0.00**	0.16	0.36		0.10	1.00	-0.20	0.15	-0.20	0.16
TqSt	0.04	1.00	0.46	0.36	0.88	**0.05**		0.19	1.00	-0.71	**0.04**	-0.81	**0.03**
TqHmPiA	0.05	0.00	-0.20	0.31	-0.88	**0.00**		0.08	0.98	0.18	0.19	0.32	0.06
Tq1LuA	0.68	0.72	-0.79	**0.00**	-0.69	**0.00**		0.24	1.00	0.29	**0.02**	0.32	**0.02**
LuTqDsA	0.55	0.00	0.74	**0.00**	0.68	**0.00**		0.26	0.00	-0.33	**0.02**	-0.92	**0.00**
MCJAR	0.12	1.00	-0.42	0.12	-0.30	0.20		0.48	0.98	0.60	**0.00**	0.62	**0.00**

Without hylobatids

	R^2	λ	b	p	b^a	p^a	R^2	λ	b	p	b^a	p^a
CpPx	0.25	0.00	0.50	**0.03**	0.42	0.08	0.00	1.00	-0.01	0.93	-0.03	0.87
CpDn	0.28	1.00	0.50	**0.02**	0.50	**0.01**	0.14	1.00	-0.28	0.11	-0.30	0.09
Cp2	0.00	1.00	0.00	0.99	0.27	0.42	0.03	1.00	-0.18	0.50	-0.08	0.77
Cp4	0.00	1.00	-0.07	0.89	0.45	0.39	0.07	1.00	-0.42	0.29	-0.28	0.53
Cp23A	0.00	1.00	-0.03	0.88	-0.01	0.98	0.04	1.00	0.14	0.39	0.15	0.34

CpPxA	0.17	0.61	0.41	0.08	0.51	**0.02**	0.63	0.63	-0.71	**0.00**	-0.75	**0.00**
CpScA	0.02	1.00	-0.22	0.56	0.06	0.88	0.10	1.00	-0.39	0.20	-0.30	0.35
Cp3SD	0.10	1.00	0.34	0.18	0.27	0.27	0.00	1.00	-0.04	0.85	-0.08	0.69
CpHmC	0.22	0.65	0.57	**0.04**	0.28	0.30	0.15	1.00	-0.36	0.11	-0.48	**0.04**
CpHP	0.05	1.00	0.19	0.37	0.17	0.37	0.02	1.00	-0.10	0.56	-0.11	0.52
HmPx	0.10	1.00	-0.35	0.18	-0.23	0.36	0.01	1.00	0.08	0.71	0.15	0.49
Hm5	0.10	1.00	0.41	0.18	0.38	0.18	0.03	1.00	-0.18	0.48	-0.19	0.44
Hm45A	0.02	1.00	-0.13	0.52	-0.16	0.39	0.06	1.00	0.16	0.32	0.60	**0.00**
HmPxA	0.02	1.00	0.09	0.57	0.10	0.51	0.00	1.00	-0.03	0.80	-0.03	0.82
CpHmPxA	0.19	0.74	0.46	0.06	0.41	0.09	0.45	0.93	-0.60	**0.00**	-0.71	**0.00**
CMC34A	0.06	1.00	-0.24	0.33	-0.14	0.54	0.00	1.00	-0.02	0.93	0.03	0.87
LuDs	0.18	0.53	0.51	0.07	0.15	0.62	0.13	1.00	-0.39	0.13	-0.41	0.11
LuTq	0.32	0.00	0.57	**0.01**	0.50	**0.03**	0.10	1.00	-0.18	0.19	-0.60	**0.00**
LuSc	0.02	1.00	0.26	0.53	0.36	0.36	0.01	1.00	-0.15	0.64	-0.11	0.73
LuRa	0.17	0.99	0.54	0.08	0.36	0.24	0.06	1.00	-0.26	0.30	-0.40	0.13
LuDsTqA	0.46	0.00	-0.68	**0.00**	-0.63	**0.00**	0.37	0.99	0.56	**0.01**	0.72	**0.00**
LuDsScA	0.01	1.00	0.06	0.76	0.10	0.55	0.09	1.00	-0.18	0.21	-0.16	0.27
LuScRaA	0.02	1.00	0.13	0.54	0.06	0.74	0.00	1.00	0.03	0.83	0.00	0.98
LuCpRaA	0.54	1.00	-0.99	**0.00**	-1.22	**0.00**	0.00	1.00	0.02	0.95	0.52	0.17
LuCpC	0.05	1.00	-0.19	0.34	-0.26	0.16	0.53	0.00	0.73	**0.00**	0.62	**0.00**
TqHm	0.07	1.00	-0.32	0.28	-0.37	0.16	0.21	1.00	0.44	**0.05**	0.42	0.06
TqLu	0.01	1.00	0.17	0.74	-0.15	0.76	0.03	1.00	0.29	0.48	0.17	0.70
TqPi	0.19	0.00	0.43	0.06	0.05	0.75	0.00	1.00	0.01	0.91	0.05	0.70
TqSt	0.01	1.00	0.18	0.77	0.98	0.13	0.09	1.00	-0.60	0.22	-0.44	0.43
TqHmPiA	0.05	1.00	-0.21	0.38	-1.02	**0.00**	0.61	0.56	0.85	**0.00**	1.01	**0.00**
Tq1LuA	0.51	0.74	-0.70	**0.00**	-0.66	**0.00**	0.09	1.00	0.22	0.21	0.35	0.05
LuTqDsA	0.28	0.00	0.53	**0.02**	0.48	**0.03**	0.09	1.00	-0.18	0.21	-0.63	**0.00**
MCJAR	0.02	1.00	-0.12	0.60	-0.19	0.37	0.32	0.93	0.45	**0.01**	0.42	**0.02**

c	*ClimbA*						**d**	*Arb*					
	R^2	λ	b	p	b^a	p^a		R^2	λ	b	p	b^a	p^a
CpPx	0.12	0.51	0.35	0.11	0.23	0.31		0.21	0.00	-0.49	**0.03**	-0.30	0.09
CpDn	0.01	0.00	-0.09	0.64	-0.01	0.97		0.04	1.00	-0.19	0.36	-0.22	0.14
Cp2	0.02	0.00	-0.16	0.54	-0.11	0.66		0.01	1.00	-0.11	0.71	-0.42	0.08
Cp4	0.18	0.65	-0.48	**0.05**	-0.39	0.23		0.29	1.00	0.54	**0.01**	-0.43	0.12
Cp23A	0.20	0.00	-0.46	**0.04**	-0.33	0.05		0.19	0.00	0.49	**0.04**	0.37	**0.02**
CpPxA	0.25	0.69	0.54	**0.02**	0.45	**0.04**		0.12	0.00	-0.39	0.12	-0.31	0.05
CpScA	0.01	0.00	0.15	0.61	0.14	0.46		0.00	1.00	0.07	0.85	-0.03	0.92
Cp3SD	0.00	0.00	0.02	0.91	-0.02	0.91		0.18	1.00	-0.44	**0.05**	-0.08	0.69
CpHmC	0.16	0.51	0.41	0.07	0.30	0.18		0.28	0.00	-0.58	**0.01**	-0.37	**0.03**
CpHP	0.06	0.00	-0.23	0.25	-0.30	0.11		0.01	1.00	-0.07	0.70	-0.07	0.63
HmPx	0.06	0.00	-0.22	0.28	-0.12	0.61		0.46	1.00	0.68	**0.00**	0.20	0.27
Hm5	0.00	0.00	0.03	0.92	-0.01	0.94		0.09	1.00	-0.43	0.18	-0.24	0.35
Hm45A	0.06	0.63	0.19	0.29	0.09	0.62		0.03	1.00	0.12	0.48	0.20	0.11
HmPxA	0.01	0.00	0.11	0.63	0.04	0.84		0.03	1.00	-0.19	0.42	-0.05	0.78

CpHmPxA	0.15	0.61	0.43	0.08	0.31	0.17	0.13	1.00	-0.43	0.10	-0.05	0.86
CMC34A	0.06	0.00	0.24	0.28	0.24	0.25	0.01	1.00	-0.08	0.72	0.10	0.56
LuDs	0.20	0.00	0.46	**0.04**	0.40	0.05	0.01	1.00	0.09	0.75	0.16	0.44
LuTq	0.04	0.00	0.18	0.39	0.14	0.45	0.31	0.00	-0.57	**0.01**	-0.42	**0.01**
LuSc	0.71	0.00	-0.84	**0.00**	-0.86	**0.00**	0.33	1.00	0.58	**0.00**	-0.17	0.52
LuRa	0.36	0.00	0.58	**0.00**	0.45	**0.04**	0.53	1.00	-0.73	**0.00**	-0.34	0.13
LuDsTqA	0.33	0.62	-0.57	**0.01**	-0.49	**0.01**	0.29	0.00	0.55	**0.01**	0.42	**0.01**
LuDsScA	0.12	0.41	0.34	0.12	0.27	0.17	0.22	1.00	-0.50	**0.03**	-0.18	0.31
LuScRaA	0.03	0.46	0.18	0.43	0.03	0.90	0.04	1.00	-0.20	0.40	0.02	0.90
LuCpRaA	0.01	0.45	-0.12	0.65	0.04	0.89	0.46	1.00	0.89	**0.00**	0.58	**0.02**
LuCpC	0.01	0.46	-0.08	0.71	-0.08	0.69	0.04	0.00	0.17	0.39	0.35	**0.03**
TqHm	0.05	0.66	0.30	0.30	0.19	0.47	0.04	1.00	0.26	0.39	0.25	0.28
TqLu	0.33	0.32	0.66	**0.00**	0.52	0.10	0.33	1.00	-0.57	**0.01**	0.01	0.96
TqPi	0.31	0.43	0.53	**0.01**	0.45	**0.02**	0.16	1.00	-0.40	0.07	-0.05	0.75
TqSt	0.09	0.58	-0.51	0.18	-0.27	0.46	0.00	1.00	-0.01	0.99	-0.55	0.23
TqHmPiA	0.00	0.00	-0.07	0.77	-0.35	0.11	0.01	0.00	0.10	0.67	0.56	**0.00**
Tq1LuA	0.25	0.00	-0.45	**0.02**	-0.41	**0.02**	0.65	0.00	0.79	**0.00**	0.65	**0.00**
LuTqDsA	0.09	0.49	0.31	0.16	0.20	0.35	0.23	0.00	-0.51	**0.02**	-0.34	**0.04**
MCJAR	0.13	0.57	-0.40	0.09	-0.30	0.17	0.02	1.00	0.17	0.59	-0.01	0.96

Without hylobatids

	R^2	λ	b	p	b^a	p^a	R^2	λ	b	p	b^a	p^a
CpPx	0.01	0.75	0.08	0.70	0.05	0.83	0.17	0.35	-0.42	0.08	-0.28	0.15
CpDn	0.00	0.77	-0.02	0.91	0.04	0.84	0.13	1.00	-0.33	0.14	-0.42	**0.02**
Cp2	0.06	0.69	-0.26	0.31	-0.21	0.50	0.01	1.00	-0.11	0.75	-0.51	0.05
Cp4	0.04	0.71	-0.26	0.42	-0.14	0.73	0.25	0.00	0.50	**0.03**	-0.64	0.14
Cp23A	0.15	0.81	-0.32	0.11	-0.31	0.12	0.13	0.74	0.34	0.13	0.42	**0.02**
CpPxA	0.16	0.83	0.33	0.09	0.34	0.09	0.00	1.00	0.01	0.95	-0.33	0.06
CpScA	0.02	0.73	-0.15	0.60	-0.07	0.81	0.05	1.00	0.34	0.37	-0.07	0.84
Cp3SD	0.05	0.84	-0.21	0.37	-0.20	0.40	0.11	0.48	-0.35	0.17	-0.09	0.65
CpHmC	0.06	0.71	0.24	0.32	0.22	0.38	0.28	0.44	-0.59	**0.02**	-0.39	**0.04**
CpHP	0.09	0.72	-0.26	0.23	-0.34	0.10	0.03	1.00	-0.15	0.47	-0.13	0.44
HmPx	0.02	0.70	-0.13	0.58	-0.08	0.77	0.48	0.00	0.69	**0.00**	0.25	0.24
Hm5	0.10	0.62	-0.33	0.18	-0.40	0.13	0.05	1.00	-0.29	0.34	-0.25	0.29
Hm45A	0.01	0.78	0.08	0.68	0.03	0.88	0.11	0.72	0.31	0.17	0.41	**0.02**
HmPxA	0.06	0.77	-0.18	0.30	-0.19	0.28	0.01	1.00	-0.06	0.72	-0.07	0.59
CpHmPxA	0.03	0.78	0.15	0.49	0.14	0.50	0.06	0.72	-0.24	0.33	-0.33	0.07
CMC34A	0.03	0.71	-0.19	0.45	-0.27	0.25	0.00	1.00	0.06	0.80	-0.09	0.64
LuDs	0.34	0.50	0.58	**0.01**	0.57	**0.01**	0.26	0.00	-0.51	**0.03**	0.13	0.62
LuTq	0.00	0.77	-0.03	0.89	0.05	0.81	0.24	0.35	-0.48	**0.03**	-0.41	**0.02**
LuSc	0.69	0.00	-0.83	**0.00**	-0.89	**0.00**	0.28	0.00	0.53	**0.02**	-0.14	0.67
LuRa	0.40	0.28	0.63	**0.00**	0.56	**0.03**	0.55	0.00	-0.74	**0.00**	-0.43	0.09
LuDsTqA	0.20	0.75	-0.40	0.06	-0.38	0.06	0.27	0.41	0.50	**0.02**	0.46	**0.01**
LuDsScA	0.01	0.73	0.08	0.71	0.15	0.46	0.15	0.56	-0.38	0.10	-0.24	0.13
LuScRaA	0.02	0.70	-0.13	0.54	-0.27	0.22	0.02	1.00	-0.11	0.60	-0.02	0.92

LuCpRaA	0.44	0.00	-0.66	**0.00**	-0.49	0.25	0.69	1.00	1.11	**0.00**	1.02	**0.00**
LuCpC	0.03	0.77	0.17	0.46	0.13	0.60	0.03	1.00	0.15	0.47	0.24	0.11
TqHm	0.24	0.63	0.55	**0.03**	0.52	0.07	0.02	1.00	0.16	0.58	0.24	0.28
TqLu	0.35	0.39	0.69	**0.01**	0.74	**0.04**	0.33	0.00	-0.58	**0.01**	0.13	0.76
TqPi	0.27	0.59	0.42	**0.02**	0.50	**0.01**	0.21	0.00	-0.46	**0.05**	-0.07	0.60
TqSt	0.58	0.00	-0.76	**0.00**	-1.19	**0.01**	0.31	0.00	0.56	**0.01**	-0.82	0.12
TqHmPiA	0.00	0.76	0.01	0.98	-0.39	0.22	0.01	1.00	0.08	0.75	0.85	**0.00**
Tq1LuA	0.05	0.73	-0.18	0.37	-0.25	0.20	0.39	0.75	0.59	**0.00**	0.50	**0.00**
LuTqDsA	0.00	0.76	0.01	0.97	0.00	0.98	0.17	0.55	-0.41	0.08	-0.36	**0.05**
MCJAR	0.09	0.83	-0.26	0.20	-0.27	0.19	0.00	1.00	-0.05	0.83	0.05	0.80

[a] Based on PGLS model with size as a covariate

Evaluation of individual morpho-functional hypotheses

Discussion is based on analyses accounting for allometry and phylogeny except where noted. See Table 2.2 for metric descriptions, functional hypotheses, and references.

CpPx The proximoradial surface of the capitate was hypothesized to be enlarged to facilitate either suspension or terrestrialism. The size of the capitate's proximal surface tends to be somewhat reduced in suspensors relative to palmigrade anthropoids (Table 2.4), and is negatively correlated with *SuspA* (Table 2.5b) and *Susp* (Table 2.9b). However, the association of this trait with suspension is driven largely by the especially small size of this region in hylobatids (owing to a greatly increased contribution of the hamate to the midcarpal joint); with them excluded, all coefficients remain negative but none is significant.

Evidence for a positive association with terrestrialism is similarly weak. This trait does not distinguish knuckle-walkers (Table 2.4, Table 2.8a, b), and although values tend to be slightly greater in digitigrade taxa relative to palmigrade monkeys, the

relationship falls well short of significance (Table 2.4). It does covary significantly with *Quad* unless hylobatids are excluded (Table 2.5a), and inversely with *Arb* to a nearly-significant degree, but no functional relationships can be supported in the current sample.

CpDn The capitate's dorsal nonarticular region was hypothesized to be enlarged in association with limited midcarpal extension in terrestrial taxa, particular knuckle-walkers. This hypothesis is not supported as it relates to knuckle-walkers, which do not differ from most other anthropoids in this metric (see Fig. 2.6a, Table 2.4, Table 2.8a, b). However, the association of this trait with terrestriality among monkeys is very tentatively supported. The relative size of this region significantly separates the taxon means of the digitigrade sample from those of palmigrade anthropoids when hylobatids are excluded from the analysis (due to the effect their inclusion has on the estimated phylogenetic signal of the model; discussed further below). Intra-taxon variation of this trait is high, however, so this distinction drops below significance when all observations are analyzed. This trait also positively covaries with *Quad* and *QuadA* with hylobatids excluded, and negatively with *Arb*, reflecting both the weak association of this trait with digitigrady as well as the slightly elevated mean values of the African apes relative to *Pongo* but not hylobatids.

This shape variable is alone in sharing a significant relationship with leaping. It is negatively correlated with both *Leap* and *LeapA*, the latter falling just short of significance (Table 2.9d, e). This association is driven by the region tending to be smaller in colobines than cercopithecines, with the lowest values found *Presbytis* and

Colobus, the most prolific leapers of the sample. While this relationship may be coincidental, it may also be that leaping colobines are especially aided by mobility in extension, in association with either forceful flexion of the wrist at take-off or deceleration at landing, for which the forelimbs are largely responsible (Hunt, 2016).

Cp2 The size of the capitate's articulation with the Mc2 is thought to be low in the great apes, and was hypothesized here to be highest in digitigrade cercopithecines. Digitigrade individuals are indeed distinguished from palmigrade ones, although distinction of the classes' taxon means falls short of significance (Table 2.4). This trait also tends to be somewhat smaller in suspensory taxa, but knuckle-walking individuals are not distinct, and their taxon means are only distinguishable if allometry is not considered (Table 2.4, Table 2.8a).

Cp4 The size of the Mc4 articulation of the capitate was hypothesized to be lower in knuckle-walkers and higher in digitigrade primates. Knuckle-walkers are significantly distinguished from both palmigrade and palmigrade-capable anthropoids (Table 2.4, Table 2.8b), but the condition of this trait is similar in *Pongo* and *Gorilla*, and it also tends to covary with both *ClimbA* and *Climb* (Table 2.5c, Table 2.9c) Its association with knuckle-walking is therefore unclear (discussed further below). The hypothesized association of this trait with digitigrady is not supported, as this trait does not differ in the two positional classes of pronograde monkeys.

Cp23A The Mc2 facet of the capitate was hypothesized to share a more acute angle with the distal facet in great apes, and perhaps also in digitigrade primates. This angle is acute in great apes only relative to hylobatids; great apes are intermediate relative to sampled non-hominoids. Although neither knuckle-walking nor digitigrady is significantly distinguished from palmigrady by this metric (Table 2.4), vertical manus taxon means are significantly distinguished from those of both palmigrade and palmigrade-capable anthropoids (Table 2.8c, d). This trait is also positively correlated with *Arb* with or without including hylobatids (Table 2.5), reinforcing its inverse relationship with terrestriality.

CpPxA The proximal angle of the capitate was expected to be more acute in suspensors and more obtuse in terrestrial primates. An association with suspension is strongly supported. This angle is markedly acute in each of the hylobatid species as well as *Ateles* and *P. abelii*. Values are also usually low in *P. pygmaeus*, but variation is high, and a few individuals overlap with African apes (see Fig. 2.4a). This is nevertheless among the most effective sampled traits in distinguishing suspensory primates from other positional classes (Table 2.4, Table 2.8a, c), and shares a strong negative correlation with *Susp* and *SuspA* (Table 2.5, Table 2.9).

A relationship between this trait and terrestriality is unclear. It is positively correlated with *QuadA*, *Quad*, and *ClimbA* across the sample, and, with hylobatids excluded, maintains a positive correlation with *Quad*, and a negative one with *Climb* (the often-contradictory relationships of *ClimbA* and *Climb* are discussed below). While the positive correlations between this trait and the quadrupedal proportions would seem

consistent with its hypothesized terrestrial association, these correlations are highly driven by the low values of suspensors. This trait does not distinguish digitigrade, knuckle-walking, or vertical manus anthropoids from palmigrade or palmigrade-capable ones (Table 2.4, Table 2.8).

CpScA The orientation of the scaphoid/centrale facet relative to the dorsum of the capitate was expected to be more acute in suspensors. While Asian apes depart from the remainder of the sample, *Ateles* is not distinguished from other ceboids by this metric, in which this angle is especially obtuse. However, this may result from a failure of the metric to capture the desired variation; sampled *Ateles* specimens frequently possess significant palmar expansion of the centrale facet, corresponding with enhanced midcarpal supination, but reduced articulation of the capitate head with the lunate leaves more of its dorsal surface to articulate with the centrale, resulting in the average orientation of the centrale facet shifting dorsally. Variability of this trait is also high in the *Pongo* species, particularly in *P. pygmaeus*. As a result, this trait does not distinguish suspensory individuals, and significant covariance of taxon means with suspension is lost with hylobatids removed (Table 2.4, Table 2.5b, and Table 2.9b).

This trait is notable as the only one in the sample with a significant relationship to *LeapA*, and one of only two associated with *Leap* with hylobatids excluded (Table 2.9d, e). This is driven by an especially dorsal orientation of the centrale facet in *Colobus* and *Presbytis* and, to a lesser extent, in *Procolobus* (see Fig. 2.6b). The biomechanical underpinnings of this relationship, if any, are opaque, however.

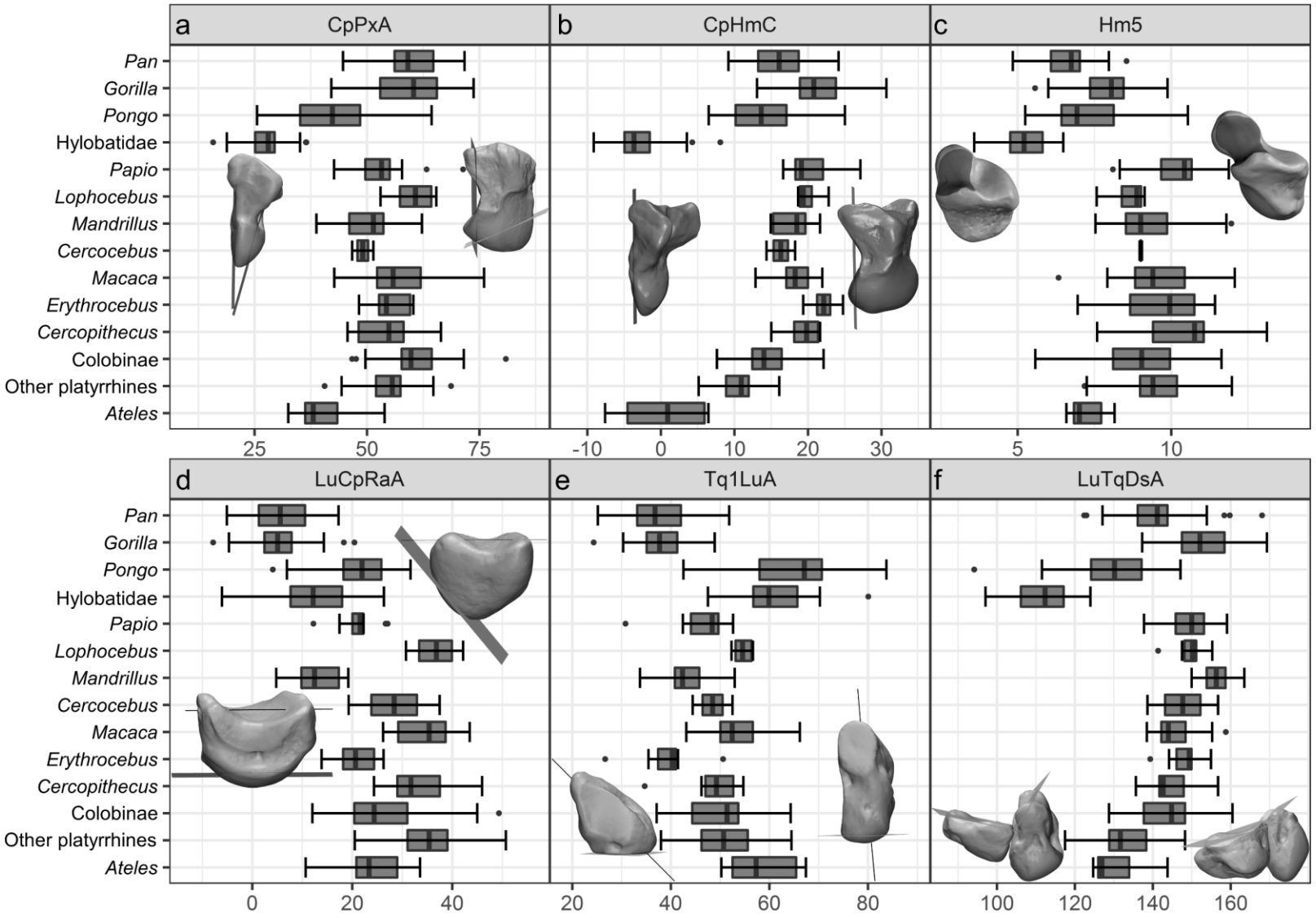

Fig. 2.4**.** Comparisons of selected shape variables. Boxes represent 25th and 75th percentiles, centerlines the medians, and whiskers the non-outlier ranges. Visualized models demonstrate the extremes of variation captured by the metric. Note that plotted values are not adjusted to account for phylogeny or allometry.

Cp3SD Capitate Mc3 facet topography is generally thought to be more complex in knuckle-walkers, and less often in suspensors as well. Neither hypothesis is supported here. Prior to isometric correction, the metric's characterization of articular complexity matches a qualitative assessment of the sample, with the *Gorilla* species having the highest values followed by *Pongo* and *Pan*, hylobatids having low values, and *Ateles* having higher values than the other ceboids. These results also correspond with observations of CMC mobility except in *Pongo*, for which this joint remains quite mobile despite their complex articular geometry (Orr, 2010). However, this trait is highly related to size across the sample – accounting for isometry eliminates any clear patterns of covariation (see Fig. 2.6c), and accounting for allometry causes most p-values to approach one (Table 2.4, Table 2.8). The raw metric also captures dorsopalmar concavity of the Mc3 surface, leading to slightly elevated values in digitigrade taxa relative to palmigrade ones. Accounting for isometry again eliminates this pattern, however.

Relatively high raw values in *Ateles* and *Pongo* indicate the possible benefit of this condition to suspension or climbing, particularly as body size increases. Low values in hylobatids and in the monkeys most reliant on climbing would likely require this narrative to be limited to the great apes, however, and this condition also seems to have been exapted in African apes to facilitate knuckle-walking.

CpHmC Concavity of the capitate's hamate facet was hypothesized here to be greater in terrestrial taxa, perhaps especially in knuckle-walkers. Concavity does tend to be greater in digitigrade anthropoids than in palmigrade or palmigrade-capable ones,

although the distinctions usually only approach significance (Table 2.4, Table 2.8b), and three *Mandrillus* specimens with low concavity depress this taxon's mean value. Mean concavity in *P. paniscus* and the *Gorilla* species rivals that of *Papio* and *Erythrocebus* for the highest of the sample, but *P. troglodytes* subspecies overlap extensively with the cercopithecoid sample (see Fig. 2.4b), and knuckle-walkers are indistinguishable from palmigrade anthropoids as a result.

The condition of this trait is most noteworthy in the brachiators, *Ateles* and the hylobatids, in which concavity is very low, with most specimens having negative concavity values as defined here. As a result, this trait distinguishes suspensory taxon means from those of palmigrade anthropoids and pronograde monkeys (Table 2.4, Table 2.8a, c), and shares significant negative correlations with *SuspA* and *Susp* (Table 2.5b, Table 2.9b). However, concavity in *Pongo* is not distinct from that of *Pan*, suggesting a functional relationship with brachiation rather than suspension more generally. This conclusion is further supported by other aspects of capitohamate joint morphology, discussed below.

CpHP The head of the capitate was hypothesized to be more palmarly positioned in palmigrade anthropoids relative to the other positional classes in association with their greater mobility in extension at the midcarpal joint. This hypothesis is tentatively supported only as it relates to the stiff midcarpal joints of knuckle-walkers, in which the capitate head is positioned dorsally relative to the palmigrade sample. However, this distinction reaches significance only with hylobatids excluded (Table 2.4), and *P. pygmaeus* values do not differ from those of *Gorilla*. Neither suspension nor digitigrady

is distinguished from palmigrady by this metric, and the capitate head tends to be positioned more palmarly in the digitigrade sample despite their lesser midcarpal mobility.

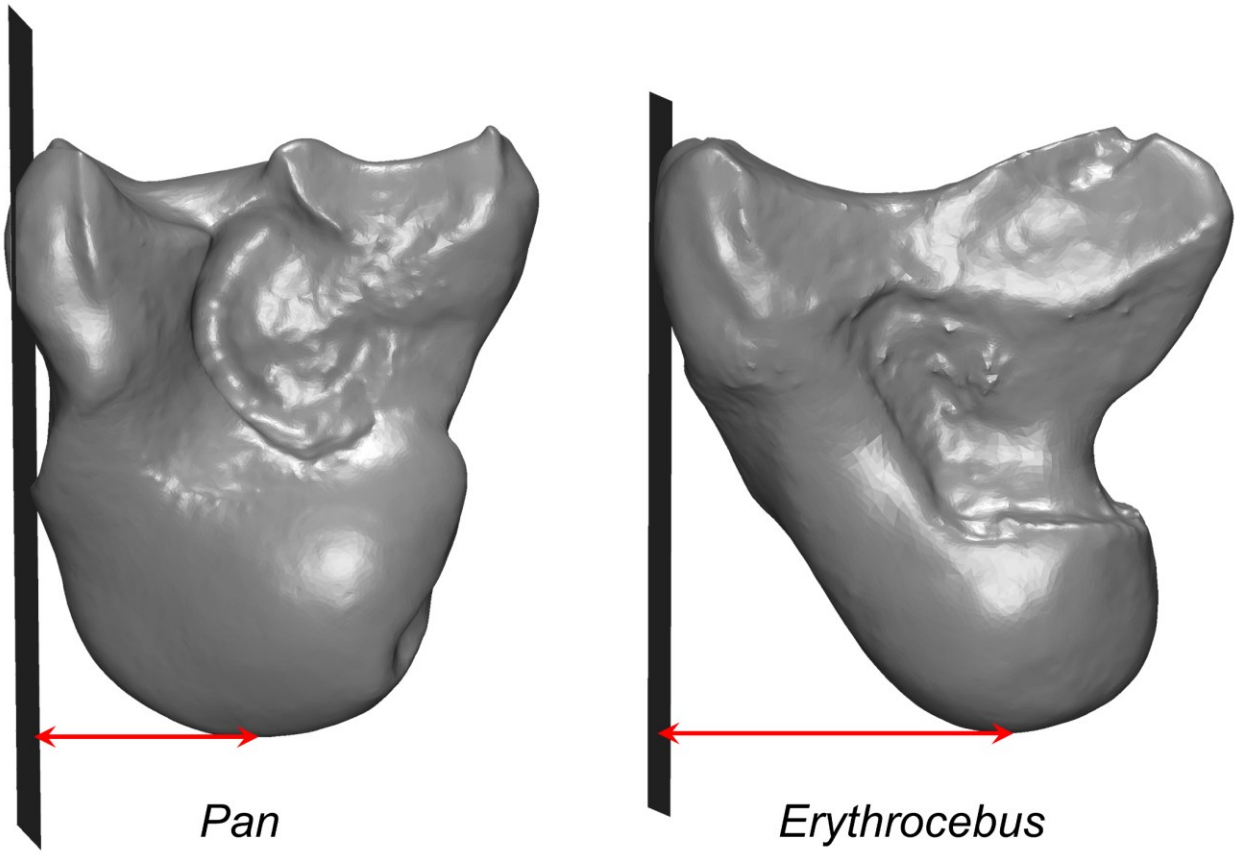

Fig. 2.5. Visualization of CpHP demonstrating variation in the dorsopalmar position of the capitate head. It tends to be more dorsally positioned in knuckle-walkers than in other positional classes, but does not otherwise covary with function.

HmPx The size of the hamate's proximal articulation was hypothesized to be reduced in knuckle-walkers, and expanded in association with either a more mobile midcarpus or with habitual loading during midcarpal ulnar deviation, perhaps as required during vertical climbing. The hypothesized reduction of this trait in knuckle-walkers is not supported, as it was not found to differ in knuckle-walkers compared to other anthropoids (Table 2.4, Table 2.8a, b).

This facet is relatively smaller in the digitigrade sample than the palmigrade sample, but to a degree only approaching significance (Table 2.4). An association of this trait with climbing is also not supported – it does share a weak positive correlation with *Climb* if allometry is not considered (Table 2.9c), but with size as a covariate the relationship is eliminated.

Hm5 The Mc5 facet of the hamate was hypothesized to be larger in digitigrade primates and smaller in knuckle-walkers. It is somewhat larger in the digitigrade sample, but again to a degree only approaching significance. An association with knuckle-walking has better statistical support, as this trait distinguishes the taxon means and individuals of the knuckle-walking and palmigrade samples with and without hylobatids included (Table 2.4). However, *Gorilla* is not distinguished from *Pongo* in this trait, and values are depressed across the hominoid sample (see Fig. 2.4c), which is at least partially attributable to hamulus expansion increasing the surface area against which facet area is indexed to account for isometry. This effect is largely accounted for by the phylogenetic component in the models, and the similarly reduced values of *Ateles* and even lower values of hylobatids point to suspensory behavior as the common factor. Nevertheless, the suspensors are less well distinguished from the palmigrade sample by this metric than are knuckle-walkers, and significant covariance with *SuspA* and *Susp* is lost with hylobatids excluded.

Hm45A The angle between the metacarpal facets of the hamate was hypothesized to be more acute in digitigrade taxa. This hypothesis is only tentatively supported here.

Mean values are reduced relative to the closest palmigrade relative of each digitigrade lineage, but the distinction again only approaches significance (Table 2.4). Significance is reached in distinguishing digitigrade taxon means from those of palmigrade-capable anthropoids (Table 2.8b), owing to these facets being closer to parallel in *Pongo* and *Ateles* (see Table 2.4, Table 2.5b, and Table 2.9b). This trait is also positively correlated with *Climb* (Table 2.9c), and to *Arb* without hylobatids (Table 2.5d), consistent with a negative association between this trait and terrestrialism in monkeys.

HmPxA The proximal angle of the hamate was expected to be more acute in suspensors and more obtuse in terrestrial primates. These hypotheses are mostly unsupported here. This angle is very acute in hylobatids, sufficient to produce a significant negative correlation with *Susp* (Table 2.9b), but values tend to be higher in *Ateles* than other ceboids, and are not notably reduced in *P. abelii*. *P. pygmaeus* is again extremely variable in this trait, with a mean value lower than that of *Gorilla* and *P. paniscus,* but not *P. troglodytes*. With hylobatids removed, *SuspA* and *Susp* coefficients are near zero.

The highest values in the sample belong to *Gorilla* and *Mandrillus*, but there is otherwise no terrestrial signal in the sample either. Values are lower in *P. troglodytes* than most sampled monkeys, and *Papio* and *Erythrocebus* are not dissimilar from the palmigrade sample.

CpHmPxA As the sum of the adjacent proximal angles of the capitate and hamate (CpPxA and HmPxA, discussed above), this trait estimates the degree of curvature of

the distal surface of the midcarpal joint. This angle was expected to be high in terrestrial taxa and low in suspensory ones. Because variance in HmPxA lacks a functional pattern, the functional signal of CpHmPxA resembles that of CpPxA. Suspensory taxon means and individuals are significantly distinguished from those of other positional classes with or without consideration of hylobatids (Table 2.4, Table 2.8a, c). The trait covaries negatively with *SuspA* and *Susp*, and positively with *Quad* and *QuadA* across the sample (Table 2.5a, b, Table 2.9a, b), maintaining the inverse relationship with the suspensory proportions and adding one with *Climb* with hylobatids excluded. By this metric, the midcarpal joints of knuckle-walkers and digitigrade cercopithecines are not found to be significantly broader than those of the palmigrade sample.

CMC34A The Mc3 facet of the capitate and the Mc4 facet of the hamate were hypothesized to be angled toward each other in digitigrade monkeys, relative to a more parallel arrangement in other anthropoids (Fig. 2.6d). This hypothesis is tentatively supported here, as this angle significantly distinguishes digitigrade cercopithecines from both palmigrade and palmigrade-capable anthropoids (Table 2.4,Table 2.8b). However, this result is largely due to the condition of this trait in *Mandrillus* and *Erythrocebus*, as *Papio* is not distinguished from *Lophocebus*, in which this trait is highly variable.

LuDs The distal surface of the lunate is hypothesized to be expanded in knuckle-walkers. This hypothesis is supported, with mean individual knuckle-walking values significantly distinguished from palmigrade and palmigrade-capable ones (Table 2.4, Table 2.8b). This trait is also positively correlated with *ClimbA* (Table 2.5c), driven by its

high values in African apes, raising ambiguity regarding the trait's more important functional association in this group (discussed below).

This trait is also noteworthy in being among those best distinguishing digitigrady and palmigrady, as values are significantly reduced in association with the former (Table 2.4; Table 2.8e). This is unexpected under an assumed regime of relatively anisotropic, axially-oriented forces like that of knuckle-walkers. The implications of this finding are discussed below.

LuTq The triquetrum facet of the lunate was hypothesized to be expanded in terrestrial taxa and reduced in suspensors. A negative association with suspension is supported – suspensory taxon means are all below those of their nearest relatives, and are significantly distinguished from those of the palmigrade sample (Table 2.4). This trait also covaries negatively with *SuspA* and *Susp*, maintaining significance with the former with hylobatids excluded (Table 2.5b, Table 2.9b). However, intra-taxon variability was high across the sample, resulting in analyses considering this variation falling short of significance.

A positive association between this trait and terrestrialism is only very tentatively supported. This facet tends to be somewhat larger in both digitigrade and knuckle-walking taxa, but not to a significant degree (Table 2.4, Table 2.8b). When considered in combination, the means of vertical manus taxa are significantly distinguishable from palmigrade-capable ones, but only approach significance in separating them from the palmigrade sample (Table 2.8c, d). This trait does positively correlate with *Quad*, and

negatively with *Arb* (Table 2.5a, d), providing additional support for some relationship with terrestriality.

LuSc The size of the scaphoid/centrale articulation of the lunate was hypothesized to be negatively correlated with climbing behavior. This hypothesis is supported, as its association with *ClimbA* is the strongest of the shape variables (Table 2.5c), driven by low values among the great apes as well as slightly reduced values in the monkeys most reliant on climbing. However, it is also found to significantly distinguish knuckle-walkers from palmigrade-capable anthropoids (Table 2.8b), and, with hylobatids removed, from palmigrade monkeys (Table 2.4). The functional association of this trait is therefore ambiguous; this is discussed further below.

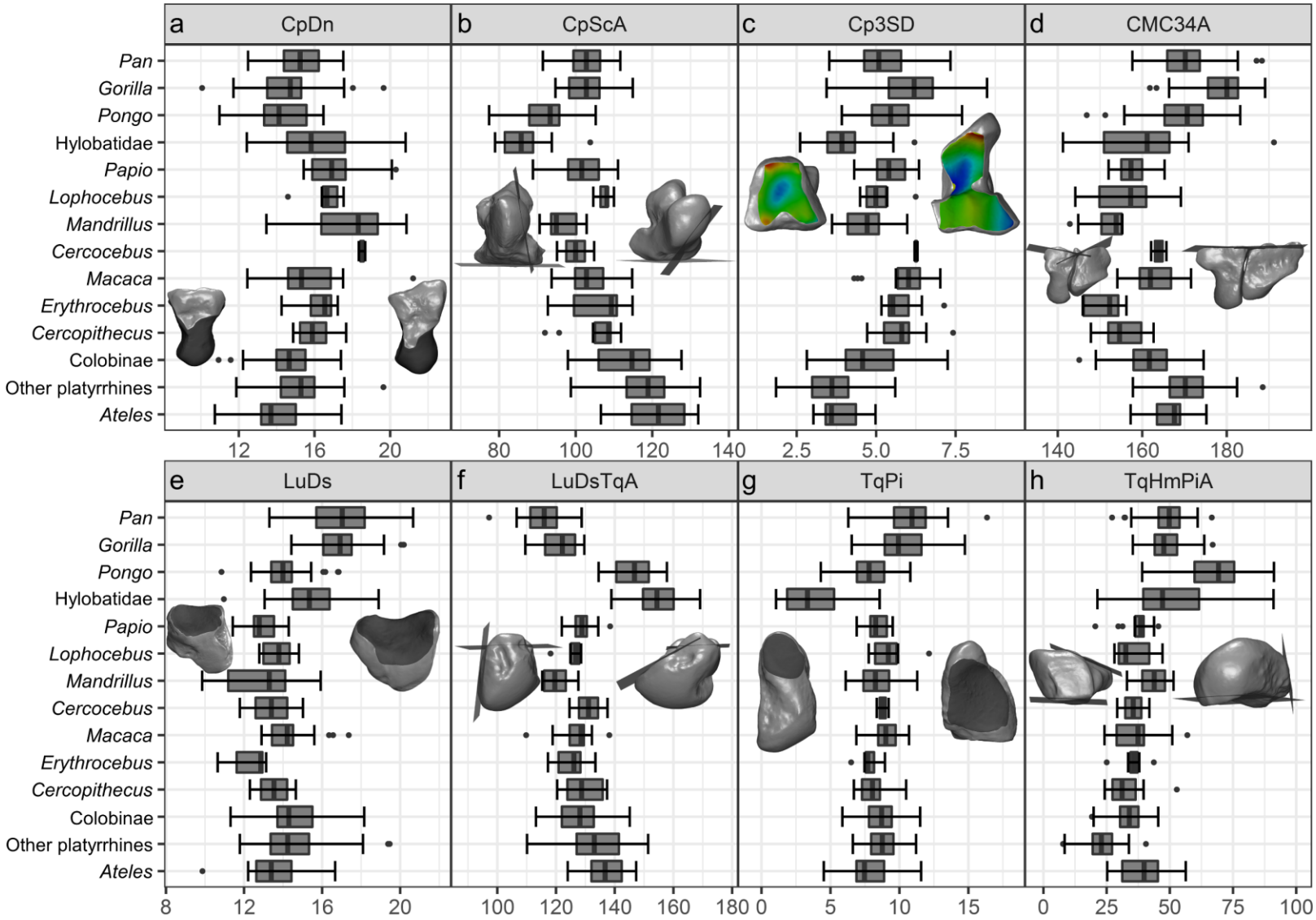

Fig. 2.6. Comparisons of additional shape variables. Boxes represent 25th and 75th percentiles, centerlines the medians, and whiskers the non-outlier ranges. Visualized models demonstrate the extremes of variation captured by the metric. Note that plotted values are not adjusted to account for phylogeny or allometry.

LuRa The size of the radial facet of the lunate has been hypothesized to vary positively in association with both suspension and climbing, and both positively and negatively in association with pronograde weight support. Some of the confusion regarding this trait seems related to how it is measured. Functional hypotheses are often premised on this facet being larger in Asian apes than in African apes, but when indexed against total lunate surface area, its average size is actually 7 and 3% smaller in *Pongo* than in *Pan* and *Gorilla*, respectively. Lunate surface area as a proportion of the sum of the four carpals is 19 and 27% greater in *Pongo*, however, and when this is used as the index, the radius facet is indeed 17 and 19% larger in *Pongo*. It is not clear whether this alternative procedure yields a metric more likely to reflect function, however.

Mean values of this trait (indexed against lunate surface area) are lowest in the hylobatids and *Ateles*, and are negatively correlated across the sample with *SuspA* and *Susp* (Table 2.5b, Table 2.9b), in contrast to the hypothesized positive association. The climbing hypothesis fares better, as this trait is positively correlated with *ClimbA* (Table 2.5c), driven by uniformly high values in great ape taxa. Hypotheses related to pronograde weight support are not supported – this trait does not distinguish digitigrade, knuckle-walking, or vertical manus taxa from palmigrade or palmigrade-capable ones (Table 2.4, Table 2.8a-d), and does not covary with *Quad* or *Arb*.

LuDsTqA The angle between the distal and triquetrum surfaces of the lunate was hypothesized to be more obtuse in suspensors. This hypothesis is supported. There is no overlap between Asian and African apes, and *Ateles* values are also high relative to the monkey sample, although its mean value falls below that of *Cebus* (see Fig. 2.6f).

Suspensors are significantly distinguished from other anthropoids by this trait (Table 2.4, Table 2.8a, c), which also strongly correlates with *SuspA* and *Susp* with and without hylobatids (Table 2.5b, Table 2.9b).

This angle is also found to be particularly acute in knuckle-walkers. Although the extreme values of Asian apes bias a phylogenetically-aware analysis in favor of this conclusion, the mean values of *Pan* taxa are the lowest of the sample, and those of the *Gorilla* species are lower than in any of the remaining taxa save *Mandrillus*. As a result, knuckle-walkers are significantly distinguished from both palmigrade and palmigrade-capable anthropoids (Table 2.4, Table 2.8a, b). This angle also covaries negatively with *Quad* and *QuadA*, but this angle is found to be only insignificantly more acute in the digitigrade sample despite its low value in *Mandrillus*.

LuDsScA The angle between the distal and scaphoid/centrale surfaces of the lunate was hypothesized to be more acute in suspensory taxa and more obtuse in terrestrial taxa. This trait does distinguish suspensory and palmigrade taxon means (Table 2.4) while sharing negative correlations with *SuspA* and *Susp* (Table 2.5b, Table 2.9b). These relationships owe to the very acute angle found in hylobatids, however. *Pongo* and *Ateles* do not differ from their nearest relatives, and no association with suspension remains with hylobatid observations excluded.

Knuckle-walking and digitigrade taxon means are somewhat elevated, but only the latter approaches significance (Table 2.4). African ape means are only slightly higher than those of the *Pongo* species, and while *Erythrocebus* and *Mandrillus* have the highest mean values of the sample, *Papio*'s is lower than the other cercopithecine

taxa. Vertical manus taxon means are nevertheless significantly higher than those of palmigrade-capable taxa (Table 2.8d). Intra-taxon variation of this metric is high, however, leading analyses in which it is considered to yield insignificant results.

LuScRaA The angle between the scaphoid/centrale and radial surfaces of the lunate was hypothesized to be more acute in suspensory taxa and more obtuse in terrestrial taxa. Neither hypothesis is strongly supported; although mean values in suspensory taxa are indeed significantly more acute than those of palmigrade taxa, this is largely due to the trait's condition among hylobatids (Table 2.4, Table 2.8c), as *Ateles* does not differ from other ceboids and this angle is only mildly more acute in *Pongo* species than in African apes. In this case, separation from palmigrade taxon means still approaches significance with hylobatids excluded, but this angle is again highly variable within taxa, yielding insignificant results when considering individual observations.

This trait also lacks the tentative terrestrial association of the previous one – values are elevated only in *Papio* of the digitigrade taxa, and the African apes do not differ from sampled monkeys. Furthermore, this trait does not correlate with any locomotor proportions, with or without hylobatids (Table 2.5, Table 2.9).

LuCpRaA In distinguishing *Pongo* from the African apes, the wrist of the former was said to have an "extension set" in association with its habitual slight extension during below-branch grasping (Robertson, 1984; see also Rose, 1988). As characterized by the angle between capitate and radial surfaces of the lunate (see Fig. 2.4d), this condition was hypothesized here to be further elaborated in the wrists of palmigrade

anthropoids, with these facets being closer to parallel in vertical manus taxa. This hypothesis is supported, and perhaps strongly so; interpretation is encumbered by the allometric signal of this trait far exceeding that of any other analyzed shape variable (Table 2.15a). Knuckle-walkers are significantly distinguished from palmigrade and palmigrade-capable anthropoids (Table 2.4, Table 2.8b), and the digitigrade taxa are all highly distinct from their nearest palmigrade relatives. However, accounting for allometry renders the latter covariance insignificant (Table 2.4). When combined, vertical manus anthropoids are significantly distinguished from palmigrade ones, and, to a lesser extent, from palmigrade-capable ones (Table 2.9c, d).

This trait also shares a strong positive correlation with *Climb* and *Arb*, and, with hylobatids removed, an additional negative correlation with *Quad* (Table 2.5a, d, Table 2.9c), in further support of its hypothesized function. The increased significance of this trait's relationships with terrestriality and postures thereof when allometric scaling is not considered likely reflects the reality of these relationships more accurately; problems introduced by accounting for allometry in analysis of morphological covariance with terrestriality are discussed below.

LuCpC The concavity of the capitate facet of the lunate was hypothesized to be enhanced in suspensory taxa and reduced in terrestrial taxa. The association with suspension is supported, as suspensors have significantly higher concavity than palmigrade quadrupeds in the sample (Table 2.4). This trait also shares a significant correlation with *SuspA,* although this is revealed only when hylobatids are excluded, despite their having the highest values of both concavity and suspension of the sample

(this is again related to their inclusion drastically reducing the estimated phylogenetic signal of the model; see Table 2.5b). An association between this trait and terrestriality is equivocal, as knuckle-walkers do not differ from palmigrade anthropoids in this trait. Digitigrady is, however, distinguished from palmigrady (Table 2.4), and digitigrade taxon means are distinct from palmigrade-capable ones (Table 2.8b). This trait is also positively correlated with *Arb* (Table 2.5d), offering some additional support for an inverse relationship with terrestriality.

TqHm The hamate facet of the triquetrum was hypothesized to be expanded in suspensory taxa. Support for this hypothesis is equivocal. Values are elevated in each of the hominoids relative to the monkeys, but this is at least largely due to the smaller triquetra of the former group (mean triquetrum volume of sampled monkeys is roughly double that of sampled apes as a proportion of the summed volume of the four carpals under analysis; see also Sarmiento, 1985). Values are particularly high among the Asian apes, however, and suspensory taxon means are therefore distinct from those of the palmigrade sample (Table 2.4) and share a positive correlation with *SuspA* (Table 2.5b). *Ateles* values are significantly lower than those of the other ceboids, however, so with hylobatids removed suspension and palmigrady are no longer distinct and the *SuspA* correlation falls just short of significance.

This trait also tends to be lower in digitigrade anthropoids, albeit not quite significantly so (Table 2.4). It also shares a strong inverse correlation with *QuadA*, and adds a positive correlation with *Climb* without hylobatids (Table 2.9a, c), potentially supporting a positive association between the size of this facet and midcarpal mobility

thought to facilitate more acrobatic arboreal behaviors. The sampled variation of this trait does comport reasonably well with available data on mobility in rotation and ulnar deviation (O'Connor and Rarey, 1979; Sarmiento, 2002; Orr, 2010; Orr and Atkinson, 2016), but these data are not analyzed here.

TqLu The lunate facet of the triquetrum was hypothesized to be expanded in terrestrial taxa and reduced in suspensory taxa. An association with terrestriality is not supported here. Knuckle-walking taxon means are elevated only insignificantly relative to those of the palmigrade sample, values do not differ between the digitigrade and palmigrade samples (Table 2.4), and its *Quad* and *Arb* coefficients are flat (Table 2.5a, d). A relationship with suspension is also not supported for this trait. *Pongo* values are not distinguishable from those of African apes, and suspensory coefficients are also near zero (Table 2.4, Table 2.8a, c). Reduction of this facet in the brachiators relative to their closest relatives leaves open the possibility of a relationship exclusive to this type of suspension, however.

TqPi The pisiform facet of the triquetrum was hypothesized to be expanded in terrestrial taxa and reduced in suspensory taxa. Results in both cases are equivocal. Six of seven sampled African ape taxa have mean values greater than the remainder of the sample, and values are markedly low in hylobatids (see Fig. 2.6g). However, the *Ateles* mean is only slightly reduced, and variation with the genus nearly encompasses that of all other sampled monkeys. *G. beringei* and the *Pongo* species are likewise indistinguishable from the monkey sample. This trait does distinguish suspensory and palmigrade means

(Table 2.4), and is negatively correlated with *Susp* (Table 2.9b), but these associations fall well short of significance with hylobatids excluded. Meanwhile, this trait does not differ between digitigrade and palmigrade primates, falls just short of significance in distinguishing knuckle-walking and palmigrady, and does not covary with *Quad* or *Arb*. Knuckle-walking taxon means are, however, distinguished from palmigrade-capable ones, and this trait covaries positively with *ClimbA* (Table 2.5c), owing to its large size in the African apes and in *Cebus* and *Lophocebus* to a lesser extent.

TqSt When present, the styloid facet of the triquetrum was hypothesized to be positively associated with mobility in supination and ulnar deviation at the antebrachiocarpal joint, perhaps in association with suspension. Results are equivocal. With only one monkey in the sample heavily reliant on suspension, the hypothesis cannot be properly assessed as it applies to this behavior. *Ateles* does have the highest mean value of the sample, and the occasional suspensors, most notably *Presbytis* and *Alouatta*, also have somewhat expanded styloid facets, consistent with the hypothesis.

The stronger relationship of this trait in the sample is with pronograde weight support. A larger styloid facet was found to distinguish digitigrade from palmigrade individuals (Table 2.4), and the size of this facet correlates positively with both *Quad* and *QuadA* across the sample despite its absence in apes (Table 2.5a, Table 2.9a).

TqHmPiA The angle between the hamate and pisiform facets of the triquetrum was hypothesized to be more obtuse in suspensory taxa. This hypothesis is strongly supported. Suspensors are significantly distinguished from palmigrade and pronograde

monkeys (Table 2.4, Table 2.8a, c), and the trait is positively correlated with both *SuspA* and *Susp* (Table 2.5b, Table 2.9b). In many cases, these associations are further strengthened by removing hylobatids, in which this trait is especially variable (see Fig. 2.6h). Although values are high in *Hoolock* and somewhat elevated in *Symphalangus*, the *Hylobates* species are not distinct from the African apes except in their greater variability. With or without the hylobatids, this trait is also correlated positively with *Arb* and negatively with *Quad* (Table 2.5a, d).

Tq1LuA The long axis of the triquetrum was hypothesized to be orthogonal relative to its lunate facet in suspensory taxa. This hypothesis is supported. The *Pongo* species and *H. lar* have the highest values in the sample, while the other hylobatid species are somewhat lower but still near the top of the monkey range, represented by *Ateles* (Fig. 2.4e). Suspensors are significantly distinguished from both palmigrade and pronograde monkeys (Table 2.4, Table 2.8a), and the trait is positively correlated with *SuspA* and *Susp* (Table 2.5b, Table 2.9b).

Lower values of this trait are associated with terrestriality. This angle is significantly more acute in each of the digitigrade taxa than in their closest palmigrade relatives (see Fig. 2.4e), although much of this variation is attributed to allometry, resulting in this distinction falling short of significance (Table 2.4). However, both knuckle-walking and vertical manus individuals have significantly less orthogonal triquetra than palmigrade ones (Table 2.4, Table 2.8c), and mean values of digitigrade, knuckle-walking, and vertical manus taxa are distinguished from those of palmigrade-

capable taxa (Table 2.8b, d). This angle also covaries negatively with *Quad* and *ClimbA*, and positively with *Climb* and *Arb*.

LuTqDsA The angle between the distal surfaces of the lunate and triquetrum was expected to be more acute in suspensors and more obtuse in terrestrial taxa. This compound metric incorporates LuDsTqA, discussed above, and results for the two traits are similar. The hypothesized association with suspension is supported. Each of the suspensory taxa tend to have lower values than their closest relatives of other positional classes, although the *Ateles* range of variation overlaps entirely with other ceboids (see Fig. 2.4f). Suspensory means and individual observations are significantly distinguished from those of palmigrade anthropoids with and without hylobatids (Table 2.4), and this angle covaries inversely with both *SuspA* and *Susp* (Table 2.5b, Table 2.9b).

An association with terrestrialism is also supported, albeit tentatively. This angle is slightly more obtuse on average in *Mandrillus* and *Erythrocebus* than their closest palmigrade relatives, but *Papio* is again not distinct from *Lophocebus*, so the distinction between digitigrade and palmigrade monkeys only approaches significance (Table 2.4). Knuckle-walkers are indistinguishable from other anthropoids in this metric, but when combined, vertical manus taxon means are significantly distinguished from palmigrade-capable ones (Table 2.8d). In further support of a terrestrial association, this trait is positively correlated with *Quad* and negatively correlated with *Arb* (Table 2.5a, d).

MCJAR The ratio between the angles of the opposing proximal and distal surfaces of the midcarpal joint was hypothesized to be greater in suspensors, and closer to 1 in

terrestrial taxa. The hypothesized association with suspension is supported. While this ratio is far higher in hylobatids than any other taxa, this trait distinguishes suspensory taxon means from those of palmigrade taxa even with this high-leverage data excluded (Table 2.4, Table 2.8c), and correlates with *SuspA* and *Susp* (Table 2.5b, Table 2.9b).

Knuckle-walkers do not differ from other anthropoids in this metric, and it tends to be slightly higher rather than lower in digitigrade taxa than palmigrade ones, albeit not significantly so. This trait also shares no relationship with either *Quad* or *Arb* (Table 2.5a, d). The congruence of midcarpal curvature may yet be functionally related to terrestriality, as the contribution of the scaphoid/centrale to the midcarpal joint is not considered here, but as characterized by this metric, an association with terrestriality is not supported.

Multivariate Analyses

Positional classification

The shape metrics of this study demonstrate remarkable effectiveness in distinguishing among anthropoid positional repertoires. This is particularly true for knuckle-walkers and suspensors, but despite individual traits separating digitigrade and palmigrade anthropoids only narrowly and inconsistently, the multivariate classifiers built in this study are also very effective in distinguishing these groups. Twenty shape variables significantly distinguish at least one of the non-reference positional classes from palmigrady with hylobatids excluded. The number of shape variables used to build the positional classifier number was winnowed to 16, with two variables eliminated due

to collinearity, and two others for adding excessive noise to the model, as described above.

Discriminant scores are visualized in Fig. 2.7. Variance along the first discriminant axis, which explains 58.3% of the variation, distinguishes knuckle-walkers from the other positional classes, with Tq1LuA, LuCpRaA, and LuDsTqA wielding the largest influence (Discriminant functions are shown in Table 2.6a; compare with *glmnet* coefficients, Table 2.6b). Suspensors are well separated from pronograde monkeys by the second discriminant function, which accounts for 35.4% of the sampled variation. Palmigrade and digitigrade anthropoids are distinguished almost entirely in the third dimension (Fig. 2.7b), comprising only 6.4% of the sampled variance, with inter-group differences in LuCpRaA, CpPxA, LuDs, and CMC34A having the greatest influence. Unlike the first two axes, the third axis does not cleanly distinguish between groups; two specimens of *Cercopithecus* are positioned on the digitigrade side of the decision boundary, and one of *Papio* on the palmigrade side.

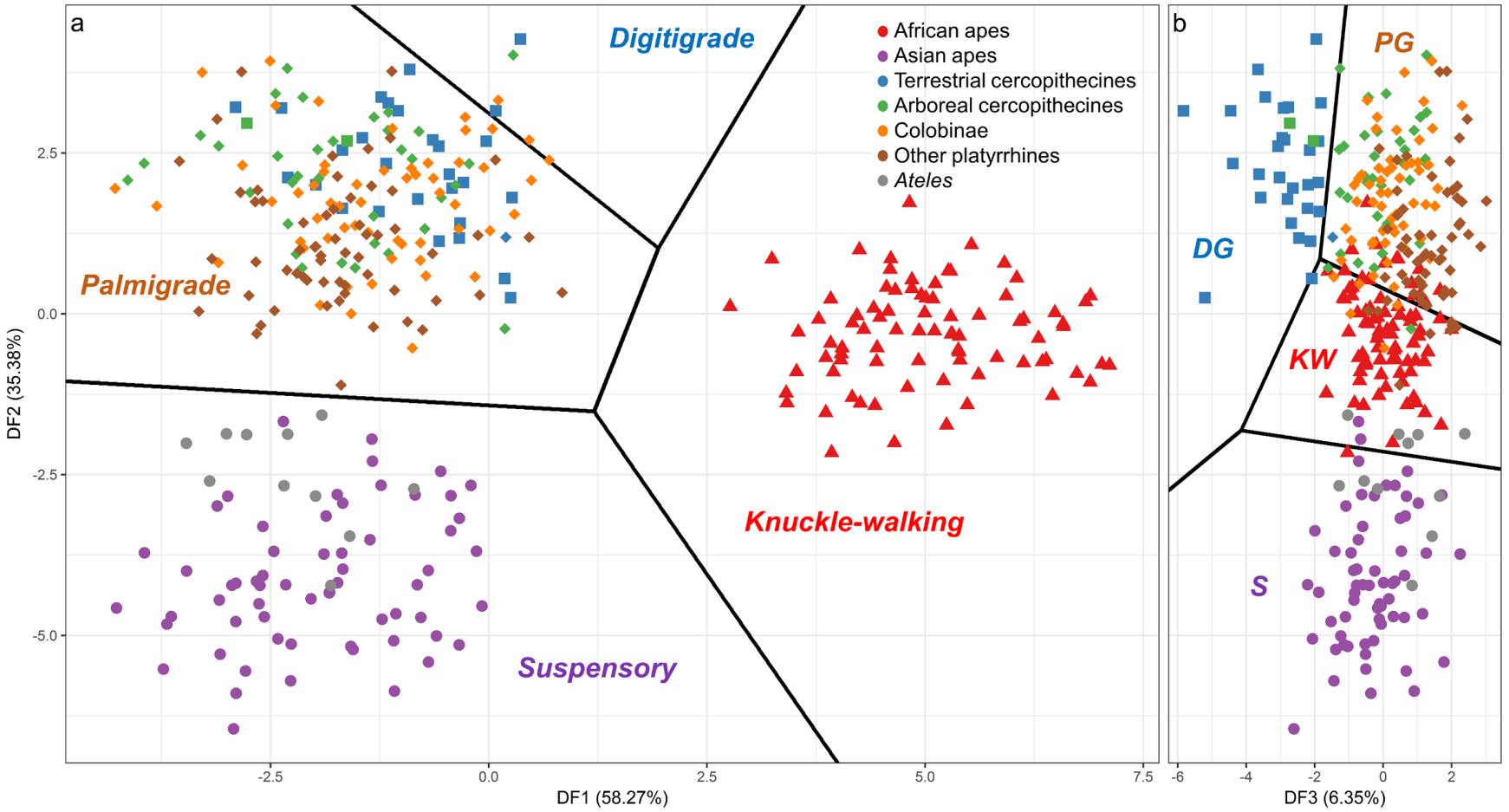

Fig. 2.7**.** Discriminant function analysis of 16 shape variables found to best distinguish positional classes. (a) visualizes the first two discriminant functions, and (b) the second and third. Observations are colored by taxonomic group (see legend) and shaped according to predicted positional classes (diamond = palmigrade; triangle = knuckle-walking; circle = suspensory; square = digitigrade). Black lines represent decision boundaries.

DFA results are consistent before and after cross-validation. One additional specimen of *Papio* was misclassified as palmigrade post-CV, with an initial *DG* posterior probability of 0.63 compared to a cross-validated mean of 0.45 (See Table 2.17). One *Cercopithecus* specimen, the individual most confidently misclassified by the DFA model, was also misclassified by the *glmnet* model. The only other inaccuracy of the final *glmnet* classifier is an *Ateles* specimen assigned a suspensory probability of 0.49, compared to the 0.60 assigned by the DFA classifier. The raw and balanced accuracy of both classifiers, calculated based on 33600 cross-validation trials, exceeded 98% (Table 2.6c). Both models identified suspensory and knuckle-walking anthropoids with extreme accuracy, with only rare misclassification during CV runs (Table 2.10a).

Table 2.6. Positional classification results

a	Discriminant functions			**b**	*glmnet* variable importance[a]			
	DF1	DF2	DF3		*DG*	*KW*	*PG*	*S*
CpDn	0.02	0.27	-0.16		0.96	0.00	0.00	0.78
Cp2	-0.49	0.43	-0.12		0.28	0.48	0.61	0.41
CpPxA	0.38	0.50	0.79		0.00	0.07	0.69	1.05
CpHmC	0.43	0.15	-0.43		0.61	0.17	0.25	0.53
CpHP	-0.44	0.09	-0.14		0.31	0.56	0.36	0.11
Hm5	-0.40	0.55	-0.46		0.85	0.44	0.27	0.68
Hm45A	-0.34	-0.15	0.02		0.09	0.07	0.00	0.39
CMC34A	0.46	-0.07	0.54		1.29	0.41	0.19	0.00
LuDs	0.33	0.25	0.60		0.80	0.45	0.58	0.23
LuTq	0.13	0.21	0.00		0.52	0.01	0.05	0.48
LuSc	-0.45	0.50	0.09		0.03	0.67	0.69	0.05
LuDsTqA	-0.56	-0.50	0.17		0.00	0.51	0.00	1.08
LuCpRaA	-0.65	0.69	1.04		0.55	0.71	2.37	0.00
LuCpC	0.05	-0.14	0.06		0.85	0.00	0.00	0.19
Tq1LuA	-0.89	-0.64	0.17		0.73	0.88	0.24	1.38
MCJAR	0.36	-0.20	-0.07		0.53	0.00	0.78	0.00

c	Classification accuracy[b]					
Model	Total	*DG*	*KW*	*PG*	*S*	Bal[c]
DFA	0.986	0.941	1.000	0.982	0.995	0.984
glmnet	0.993	0.978	1.000	0.992	0.994	0.993

[a] Absolute value of tuned model coefficients

[b] *glmnet* parameters were tuned with 20 repetitions of 10-fold CV; both DFA and *glmnet* model accuracy was calculated after 100 repetitions of 10-fold CV.

[c] Balanced accuracy is an average of a model's sensitivity and specificity (true positive rate and true negative rate)

Despite hylobatids being excluded from model building criteria, hylobatids were never misclassified during cross-validation, and mean posterior probabilities of both models exceeded 0.99 in every case (Table 2.17). The most notable difference between the classifiers was their ability to distinguish between digitigrade and palmigrade anthropoids. The DFA model misclassified palmigrade specimens as digitigrade 248% more often (265 vs. 107 trials; see Table 2.10a), and digitigrade specimens as palmigrade 271% more often than the *glmnet* model (171 vs. 63 trials). The DFA classifier was nevertheless highly accurate in classifying digitigrade specimens (sensitivity = 0.91, specificity = 0.99; see Table 2.10b).

Locomotor proportion estimation

Multivariate carpal shape strongly corresponds with each of the locomotor proportions apart from *Leap* and *LeapA*, which lacked sufficient morphological correspondence to allow predictive modeling. Models for the non-leaping proportions each consist of between 3 and 6 shape variables. In each case, PGLS R^2 exceeds 0.8 and λ is estimated at zero (Table 2.7a and Table 2.11a).

Table 2.7. Prediction results for selected locomotor proportions

a	Predictive models								
	PGLS			GLM					
	R^2	λ	p	Terms	Coef	SE	T	p	SEE%[a]
Quad	0.878	0.000	0.000	(Intercept)	0.22	0.05	4.2	0.000	16.0
				CpDn	0.05	0.05	1.0	0.321	
				LuTq	0.18	0.06	2.8	0.006	
				LuTqDsA	0.69	0.07	9.3	0.000	
				Tq1LuA	-0.94	0.06	-14.8	0.000	
SuspA	0.987	0.000	0.000	(Intercept)	-2.58	0.07	-38.1	0.000	7.9
				CpHmC	-0.40	0.07	-5.9	0.000	
				CpPxA	-0.36	0.08	-4.6	0.000	
				Tq1LuA	0.19	0.05	3.7	0.000	
				TqHm	0.52	0.06	8.9	0.000	
				TqHmPiA	0.55	0.06	9.7	0.000	
ClimbA	0.806	0.000	0.000	(Intercept)	-0.63	0.03	-24.3	0.000	9.6
				LuDs	0.16	0.03	5.8	0.000	
				LuDsTqA	-0.15	0.03	-5.4	0.000	
				LuSc	-0.37	0.03	-13.1	0.000	
Arb	0.906	0.000	0.000	(Intercept)	1.74	0.11	15.8	0.000	16.9
				Cp23A	0.70	0.12	5.8	0.000	
				CpDn	-0.38	0.09	-4.4	0.000	
				CpHmC	-1.40	0.13	-10.4	0.000	
				LuCpRaA	1.92	0.12	15.8	0.000	
				LuTq	-0.43	0.10	-4.3	0.000	

b	Predicted locomotor proportions of training taxa[b]											
	Quad			*SuspA*			*ClimbA*			*Arb*		
	Obs	Pred	Δ	Obs	Pred	Δ	Obs	Pred	Δ	Obs	Pred	Δ
P. t. schweinfurthii	0.93	0.82	0.11	0.08	0.06	0.02	0.59	0.54	0.05	0.10	0.27	0.17
P. t. verus	0.86	0.83	0.03	0.06	0.08	0.02	0.68	0.57	0.11	0.16	0.22	0.06
P. paniscus	0.87	0.80	0.07	0.09	0.09	0.00	0.51	0.58	0.07	0.17	0.19	0.02
G. gorilla	0.92	0.86	0.06	0.13	0.07	0.06	0.62	0.48	0.14	0.10	0.17	0.07

G. beringei	0.96	0.88	0.08	0.06	0.05	0.01	0.40	0.49	0.09	0.09	0.09	0.00
P. pygmaeus	0.12	0.17	0.05	0.43	0.40	0.03	0.37	0.38	0.01	0.95	0.82	0.13
P. abelii	0.18	0.25	0.07	0.38	0.34	0.04	0.35	0.38	0.03	0.95	0.87	0.08
Hoolock	0.00	0.13	0.13	0.55	0.57	0.02	0.20	0.21	0.01	0.99	0.89	0.10
H. lar	0.00	0.09	0.09	0.59	0.55	0.04	0.19	0.22	0.03	0.99	0.99	0.00
Symphalangus	0.00	0.21	0.21	0.59	0.64	0.05	0.32	0.29	0.03	0.99	0.96	0.03
Papio	0.99	0.79	0.20	0.00	0.03	0.03	0.21	0.29	0.08	0.05	0.39	0.34
Lophocebus	0.42	0.66	0.24	0.00	0.03	0.03	0.36	0.33	0.03	0.95	0.82	0.13
Macaca	0.68	0.60	0.08	0.00	0.04	0.04	0.26	0.31	0.05	0.97	0.90	0.07
Erythrocebus	0.94	0.85	0.09	0.00	0.02	0.02	0.30	0.29	0.01	0.08	0.26	0.18
Cercopithecus	0.54	0.69	0.15	0.00	0.03	0.03	0.35	0.32	0.03	0.95	0.77	0.18
Colobus	0.41	0.58	0.17	0.01	0.03	0.02	0.20	0.30	0.10	0.96	0.92	0.04
Procolobus	0.35	0.53	0.18	0.01	0.04	0.03	0.29	0.31	0.02	0.95	0.88	0.07
Trachypithecus	0.60	0.60	0.00	0.00	0.03	0.03	0.13	0.25	0.12	0.99	0.90	0.09
Presbytis	0.28	0.63	0.35	0.02	0.04	0.02	0.19	0.29	0.10	0.99	0.94	0.05
Alouatta	0.61	0.50	0.11	0.02	0.04	0.02	0.33	0.36	0.03	0.95	0.96	0.01
Ateles	0.42	0.27	0.15	0.25	0.13	0.12	0.25	0.31	0.06	0.99	0.98	0.01
Cebus	0.37	0.45	0.08	0.00	0.03	0.03	0.40	0.30	0.10	0.95	0.96	0.01

c Predicted locomotor proportions for other taxa

	Quad	*SuspA*	*ClimbA*	*Arb*
P. t. troglodytes	0.78	0.09	0.58	0.31
P. t. ellioti	0.79	0.08	0.58	0.28
H. muelleri	0.12	0.48	0.26	0.99
Mandrillus	0.87	0.04	0.31	0.22
Cercocebus	0.69	0.04	0.28	0.82
Nasalis	0.74	0.03	0.33	0.85

[a] Percent standard error of the estimate based on repeated individual predictions generated during cross validation

[b] Predictions calculated after 100 repetitions of 10-fold cross validation of quasibinomial logistic regression. Obs, observed proportions. Pred, predicted proportions. Δ, residual.

The *SuspA* model is the most accurate as characterized by %SEE. The only prediction delta of this model exceeding 0.06 is *Ateles*, which, while correctly predicted to be the most suspensory of the sample outside the Asian apes, is nevertheless underestimated by half (Table 2.7b). The other notable source of error in *SuspA* prediction was a general baseline proportion of 0.02-0.04 assigned to the nonsuspensory taxa. The *Susp* model was similarly accurate overall. Its *Ateles* prediction is slightly more accurate, and the baseline assigned to non-suspensors is closer to zero, but *Symphalangus* is underestimated by 0.15 (Table 2.11b). The *ClimbA* and *Climb* models are only slightly less accurate than the suspensory ones. The largest sources of error in the former are the greater *a priori* variance among African apes than predicted and overestimation of three of the four taxa most reliant on leaping.

The *Quad* and *Arb* models have the highest %SEE of the predictive models. Much of this is attributable to the high variance of these proportions, which range between 0 and 0.99 and between 0.05 and 0.99, respectively. Both of these models produce accurate predictions for most of the extant sample (Table 2.7b). The least accurate prediction of the *Quad* model is that for *Presbytis*, the taxon most reliant on leaping. The *Quad* model was conservative in predicting extreme values, resulting in inaccuracy due to the often-extreme values in the sample. It was nevertheless effective in distinguishing among highly terrestrial quadrupeds, arboreal quadrupeds, and the rarely-quadrupedal Asian apes, although the highest value among those assigned to the arboreal quadrupeds of the training sample falls only 0.10 short of the value predicted for *Papio*. Of the non-training taxa, *Nasalis* is predicted within only .05 of *Papio.* Although the former has been

suspected to have a significant terrestrial habit (Kawabe and Mano, 1972; Boonratana, 2000), this is likely a significant overestimate.

The *Arb* model was more accurate in most cases, but consistently over-estimated the arboreality of the most terrestrial taxa. The prediction for *Mandrillus* is lower than for the terrestrial cercopithecines of the training sample (Table 2.7c), but is still likely to be high, as this taxon is suspected to be nearly as terrestrial as the others (Sabater Pi, 1972; Hoshino, 1985). The *Arb* model is nevertheless effective in distinguishing between the terrestrial and arboreal taxa, with the nearest predictions between the two groups separated by a gulf of 0.38.

Predictions for the six taxa not used to train the prediction models (Table 2.7c, Table 2.11c) generally hold to expectations, save the *Quad* prediction for *Nasalis* discussed above. Predictions for the chimpanzee subspecies are consistent with those of the training subspecies, *Mandrillus* mirrors *Papio* and *Erythrocebus*, *H. muelleri* resembles the other hylobatids, and *Cercocebus* and *Nasalis* are similar to other arboreal quadrupeds in the sample.

Combined locomotor proportions

When shape is analyzed with locomotor proportions in concert, carpal morphology has a greater correlation with arboreal-only locomotor proportions than with total locomotor proportions (RV = 0.76 and 0.67, respectively; all p-values < 0.0001; Table 2.12a), despite the former providing a less complete characterization of a taxon's behavioral repertoire. This was hypothesized to be attributable to retention of suspensory and climbing adaptations in the African apes that belie their highly terrestrial

lifestyles post-adolescence, and tested by repeating the analyses with African apes removed. A greater association with arboreal proportions persisted (RV = 0.74 versus 0.71; Table 2.12a).

The shape-behavior correlation improves slightly when *Arb* is added to the arboreal proportions (RV = 0.77), whereas its addition to the total proportions further weakens the relationship (RV = 0.62). This is consistent with expectation given that the proportion of arboreality adds only redundant information to total locomotor proportions, whereas this information is not inherent in arboreal proportions. That the improvement is only incremental is notable, however. Due to the lack of morphological association with leaping, the shape-behavior relationship is maximized if *LeapA* is removed (RV = 0.80). When phylogeny is considered, shape-behavior correlation decreases substantially, corresponding with the high phylogenetic signal of most of the morphological variables under study, although it remains significant (total proportions RV = 0.40; arboreal proportions 0.41; with *Arb* added = 0.43; a best-fit set of *Quad*, *SuspA*, and *ClimbA* = 0.49; see Table 2.12b).

The structure of these relationships is highly influenced by the hylobatids; if they are excluded, shape is maximally correlated with a locomotor block consisting of *Arb* and the arboreal proportions whether or not phylogeny is considered (RV = 0.38 and 0.75, respectively; Table 2.12a, b). This set of proportions was used in the PLS analysis. Fig. 2.8a plots the first two resulting shape axes, which visualizes the correspondence between functional carpal traits and locomotion in each taxon, as well as the relative influences of locomotion and phylogeny in the evolution of carpal morphology. Old and New World monkeys form a tight group in shape-space, with only

Ateles a slight outlier. Phylogenetic structure is also evident within the large group of monkeys, with, for example, *Cebus* and *Lophocebus* having similar locomotor repertoires but morphology most like that of their closer, less behaviorally similar relatives. The terrestrial quadrupeds also loosely grouped in shape-space, but are not obviously distinguished from their close non-terrestrial relatives.

Fig. 2.8b depicts PLS behavior-space, a visualization of the sample's behavioral repertoires as characterized by the first two locomotion PLS axes. *Pongo* and *Ateles* are better separated from their closest relatives than in shape-space, as are the terrestrial monkeys. Despite the lack of correspondence between carpal morphology and leaping, the four taxa most reliant on leaping (*Presbytis*, *Colobus*, *Procolobus*, and *Trachypithecus*) are distinguished from the others in accord with their lower proportions of other behavioral modes. As shown in Table 2.13a, PLS1 positions more suspensory taxa toward the left and more quadrupedal taxa toward the right, while PLS2 places those more reliant on climbing during arboreal locomotion toward the bottom, and those more reliant on arboreal locomotion in general toward the top, particularly those doing the most leaping.

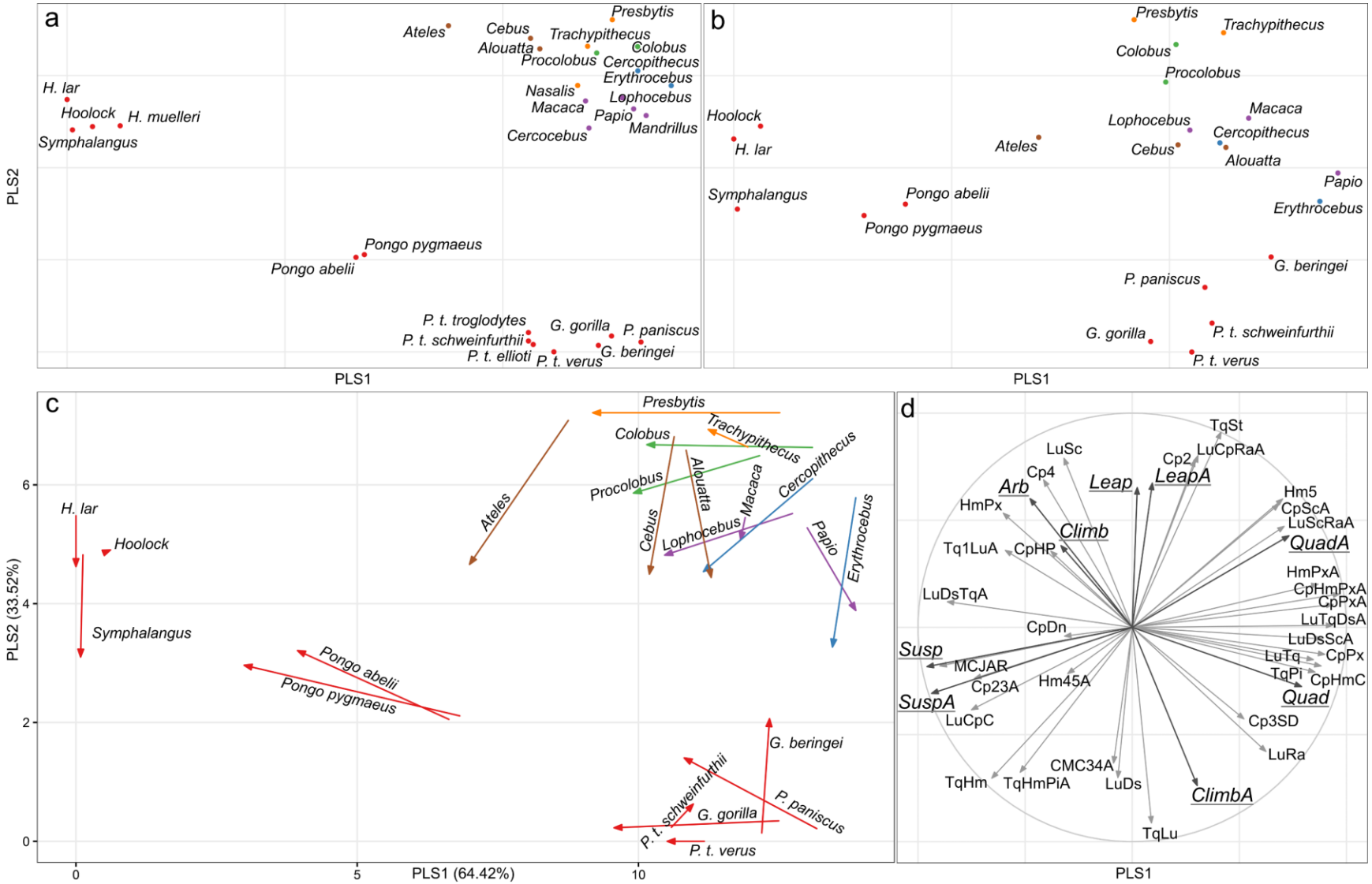

Fig. 2.8**.** Two-block partial least squares (PLS) analysis of shape and selected locomotor proportions (*QuadA*, *SuspA*, *ClimbA*, *LeapA*, *Arb*). (a) Shape-space, including projections of taxa lacking quantitative locomotor observations. (b) Behavior-space; (c) Overlay of a and b; arrows lead from each taxon's position in shape-space to its position in behavior-space, with length equal to standardized Euclidean distances. (d) Correlation circle depicting relationships between all shape and locomotor variables. See Table 2.13 for PLS vectors and Euclidean distances.

A comparison of Fig. 2.8a and Fig. 2.8b shows that locomotion varies more within broad taxonomic groups than does shape. This trend is visualized in Fig. 2.8c, an overlay of PLS shape-space and behavior-space including only the taxa used to train the model. Arrows lead from the position of each taxon in shape-space to its position in behavior-space, with length equal to the standardized Euclidean distance (listed in Table 2.13c). The monkeys and great apes are generally pulled away from their respective corners, with the more terrestrial monkeys and mountain gorillas pulled toward each other in behavior-space, the colobines moving laterally, and the ceboids and cercopithecines sharing a general downward trajectory. The latter trend corresponds to a shared preference in these groups for climbing over leaping during arboreal locomotion, as climbing is generally not reflected in the wrists of these animals in the same way as in the great apes (discussed below). Because of its very low correspondence with carpal morphology, taxa more reliant on leaping, led by *Presbytis* and *Colobus*, traverse greater distances between shape- and behavior-space than most other monkeys. The exception is *Ateles*, which is pulled downward in accord with its climbing habit and leftward toward the other suspensors, further separating this species from close relatives. The *Pongo* species also have relatively large Euclidean distances, reflecting the greater phylogenetic structure of morphological variance in the sample relative to locomotor variance.

Fig. 2.8d plots Pearson correlations between the shape variables and the first two PLS shape axes, with the light gray vectors representing r values between 0 (the origin) and 1 (represented by the circle). Correlations between the locomotor variables and shape axes are plotted in the same way, shown in dark gray. For example, the size

of the styloid facet on the triquetrum (TqSt) is correlated with the first axis at r = 0.36 and with the second axis at r = 0.93. The resulting vector is of length 1 and points toward the position in shape-space (Fig. 2.8a) of the non-hominoids, i.e., the sampled taxa with non-zero values for this trait. This assists interpretation of the other PLS plots by displaying how each shape and locomotor variable contributes to the structure of the analysis. All 9 locomotor variables are included in this plot, but the vectors of the variables contributing to Fig. 2.8a-c are not substantially changed. The correlation between any two variables is represented in Fig. 2.8d by the angle between their associated vectors, where angles approaching 90° represent no correlation and angles approaching 0° or 180° represent strongly positive or negative correlations, respectively. Hylobatids, the taxa with the highest *SuspA* and *Arb* and lowest *QuadA* values, are positioned far to the left in behavior-space (Fig. 2.8b,c), while their commensurately high values of, for example, MCJAR and LuDsTqA and low values of CpPxA and CpHmC (Fig. 2.8d) leave them positioned far to the left in shape-space as well (Fig. 2.8a,c). The African apes have high values of *ClimbA* and low values of *LeapA* and *Arb*, and are therefore positioned toward the bottom right corner, commensurate with their low values of, e.g., LuSc and Cp4, and high values of LuRa and TqLu.

Discussion

Adaptive convergence in the anthropoid carpus

This study successfully identifies aspects of wrist morphology that have evolved in association with various positional modes practiced among anthropoids. As noted at the outset, supporting these links as having evolved directly in adaptation to a given behavior is more difficult, but patterns of variation in several traits are consistent with their having convergently adapted to similar locomotor behavior in separate lineages, and are therefore worthy of further research. However, this study also demonstrates the complex, subtle, and variable nature of functional morphology, with many shape variables, particularly the surface area ratios, found to be highly variable within taxa and within positional classes. While this is consistent with our understanding of adaptation as a non-optimizing process (Abrams, 2001 and references therein), it potentially attenuates the utility of some morpho-functional units when inferring fossil behavior based on small sample sizes.

3D variables of the type analyzed here are thought to be especially well-suited to the complex articular geometry of the carpus (e.g., Orr, 2016), and they were generally found to be effective in quantifying important variation in anthropoid joint surface morphology. However, few articular features of the hamate were hypothesized to be related to function, and these were found to have little functional correspondence relative to the other carpal elements analyzed. Overall hamate morphology was still found to be significantly correlated with locomotor proportions ($RV = 0.53$, $p < 0.0001$), but a previous analysis found a greater correspondence of 0.73 between similar locomotor data and hamate morphology based on landmark data (Almecija *et al.*, 2015).

This may, however, reflect the functional signal of the hamulus, which is not analyzed here, particularly given the proportionally greater representation from hominoid taxa in their sample.

Results of this study also demonstrate some of the important drawbacks of accounting for the statistical non-independence associated with allometry and phylogeny inherent in biological research. Allometry seemed to wield only mild influence on the analyzed shape data. Multivariate phylogenetic allometry was low ($R^2 = 0.04$, $p = 0.03$), and only one variable was found to correlate with size at rho ≥ |0.5| and p ≤ 0.05) when accounting for phylogeny (Table 2.15). However, size was found to have a significant relationship with positional behavior. *Climb* and *Arb* were both significantly allometric, with *Leap*, *LeapA*, and *Quad* falling just short, while knuckle-walking and digitigrady were found to be significantly correlated with body size. Hence, accounting for allometric correlations between shape and positional variables stands to remove much of the very information being sought, particularly when analyzing traits associated with terrestriality or postures thereof. This was done to avoid making assumptions about size-function relationships being similar outside of the present sample, but constraints related to body size on substrate and positional mode preference have likely been present throughout the evolution of anthropoids (Remis, 1998 and references therein), with highly terrestrial species tending toward larger body sizes due to its greater energetic efficiency as well as a lesser need for arboreal agility (Hunt, 2016).

Similar problems are inherent in accounting for phylogeny. Despite attempts to bias the sample toward greater behavioral diversity within clades and limiting shape metrics to only those thought to have functional significance, the phylogenetic signal of

all shape and locomotor variables remains significant (Table 2.14a, b), and the multivariate phylogenetic signal of each set is similarly high (K_{mult} = 0.74 and 0.78, respectively). As with size, much of the morphological variance associated with a given function is therefore often instead attributed to phylogeny, despite shared functional adaptation likely playing a large role in the morphological differentiation between phylogenetic groups (Polly *et al.*, 2013).

This problem is exacerbated by the hylobatids, in which suspensory behavior and its associated morphology likely evolved largely in parallel with *Pongo* (Straus, 1949; Begun, 1993; Rose, 1997; Larson, 1998; Ward, 2015; Lovejoy *et al.*, 2009). Commonality of behavior and morphology between these groups is nevertheless treated as the result of homologous inheritance from a common ancestor by phylogenetic models. The already high-leverage data of hylobatids is given further influence by their basal position within the hominoid clade, often heavily influencing the phylogenetic signal estimated during the fitting of each model. As noted above, the statistical strength of a correlation between a shape variable and positional variable in which values of each are most extreme in hylobatids are often unintuitively hindered rather than helped by their presence, and other analyses in which their presence should not be relevant, such as traits separating digitigrady from palmigrady, can be significantly altered, due to their inclusion greatly altering the estimated phylogenetic signal of the model. For example, the hylobatid species have the highest *SuspA* values of sample, and among the highest LuCpC values as well (*Hylobates* species have the highest taxon means, *Hoolock* and *Symphalangus* are somewhat lower but still exceed those of nearly all other sampled taxa). Nevertheless, a strong positive correlation between these two

variables disappears at the inclusion of hylobatids – their presence in the model changes its estimated phylogenetic signal from 0 to 1 (Table 2.5b), reattributing almost all of the variation from suspensory frequency to phylogeny.

Despite these confounds, this study identifies morphologically convergent traits and complexes thereof in association with several anthropoid behaviors. The remainder of this subsection discusses the traits associated with some of these behaviors in turn, and evaluates the adaptive plausibility of each morpho-functional unit.

Suspension

Results presented here are consistent with the hypothesis that much of the forelimb morphology distinguishing suspensors from other anthropoids is related to facilitating greater mobility (e.g., Cartmill and Milton, 1977; Lewis, 1985a, b). Previous observations have found suspensors to have greater mediolateral curvature of the midcarpal joint (Tuttle, 1967; Sarmiento, 1988; Hamrick 1996b). A highly curved distal midcarpal surface in suspensors is confirmed, although as characterized here this condition results almost entirely from variation of the capitate, which is derived in each of the sampled suspensors (CpPxA; Fig. 2.4a). As observed previously by Kivell and colleagues (2013) and confirmed here, the proximal angle of the hamate (HmPxA) does not covary with suspension outside of hylobatids. Variation in curvature of the proximal midcarpal surface (LuTqDsA; Fig. 2.4f) also distinguishes suspensors, but this was again found to be attributable to only one of the two bones, as the lunate's contribution (LuDsTqA; Fig. 2.6f) distinguishes suspensory individuals better than the compound variable (LuTqDsA; see also Table 2.4, Table 2.8a, c). The ratio between proximal and

distal midcarpal curvature (MCJAR) was also highest in suspensors, in accord with the enhanced joint mobility such a lack of congruence is thought to provide (Bullough *et al.*, 1968; Sarmiento, 1988). Dorsopalmar curvature of the midcarpal joint, which is thought to covary with stability through a wider range of flexion/extension (Dainton and Macho, 1999), was also highest in sampled suspensors, as characterized by concavity of the lunate's capitate facet (LuCpC).

Other traits found to covary with suspension do not seem related to wrist mobility. Most of these seem instead to contribute to a functional complex of the ulnar carpus enhancing flexor carpi ulnaris leverage and transmitting forces generated thereby (see Fig. 2.9). The long axes of suspensory triquetra are more orthogonal to the lunate facet at their bases than in other anthropoids (Tq1LuA; Fig. 2.4e), which, in concert with a more distally oriented triquetrum facet of the lunate (LuDsTqA; Fig. 2.6f), gives the triquetra of suspensors a markedly distal orientation. This serves to reposition the distal-most portion of the triquetrum distally, an effect most pronounced in *Pongo*, in which the lunate's triquetrum facet, along with being distally reoriented has also been distally repositioned, resulting in the triquetrum having essentially joined the distal carpal row. The pisiform of suspensors is further displaced by its articulation being limited in most cases to the distal portion of the triquetrum; this change is reflected in the relative size of this facet being reduced in suspensors (TqPi; Fig. 2.6g). The distal position of the pisiform within the carpus in turn repositions the palmar-most extent of the flexor carpi ulnaris, resulting in its palmar relief from the wrist also being maximized more distally. This would seem to impart this muscle with especially high leverage as it crosses the midcarpal and ulnar carpometacarpal joints.

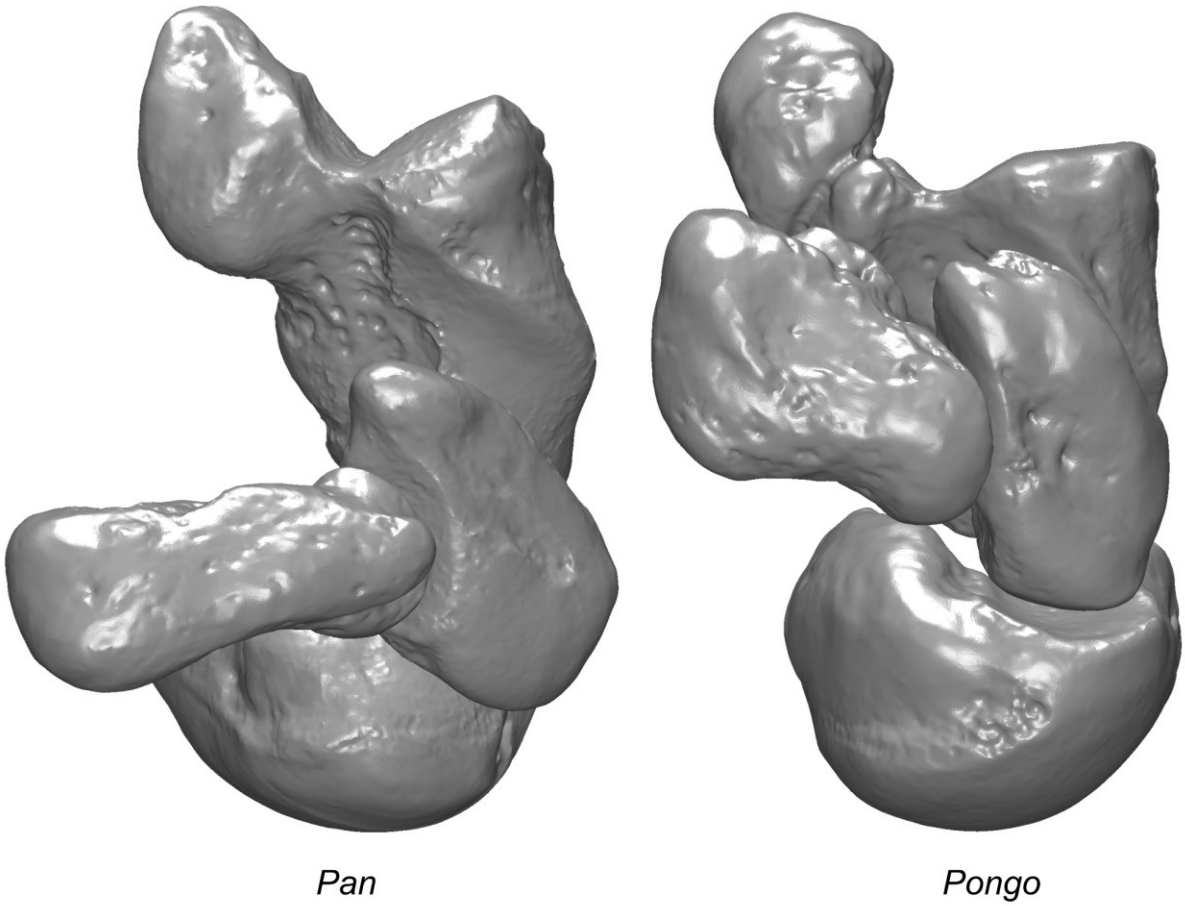

Fig. 2.9**.** Comparison of ulnar carpus reorganization in association with knuckle-walking and suspension. These positional classes are oppositely distinguished from palmigrade anthropoids in the size and orientation of the lunate's triquetrum facet (LuTq, LuDsTqA), the orientation of the long axis of the triquetrum (Tq1LuA), and the size and orientation of the triquetrum's pisiform facet (TqPi, TqHmPiA). In addition to differential loading regime mitigation, these features contribute to distal migration and reorientation of the pisiform in suspensors.

The distal orientation of the pisiform in suspensors arranges its long axis perpendicular to that of the forearm during mild wrist flexion, maximizing flexor carpi ulnaris leverage in this posture rather than during extension (Sarmiento, 1988; Lewis, 1989; Hamrick, 1997). Results of this study suggest the root of this reorientation may be found in the triquetrum rather than the pisiform itself: the facet on the triquetrum with which the pisiform articulates faces more palmarly and slightly distally in suspensors rather than proximoulnarly (TqHmPiA; Fig. 2.6h), which, in concert with their more

distally rather than palmarly oriented triquetra, is sufficient to significantly reorient the pisiform without any change in pisiform morphology. Whether the proximal morphology of suspensory pisiforms has been modified in furtherance of this effect is not analyzed here.

Two additional traits distinguishing suspensors may also participate in this ulnar functional complex. The size of the lunate's triquetrum facet (LuTq) is reduced, and, in Asian apes but not Ateles, the triquetrum's hamate facet (TqHm) tends to be slightly enlarged (Table 2.4, Table 2.5b, Table 2.8a, c, Table 2.9b). The former may simply reflect the triquetrum's reduced role in weight-bearing in these taxa (Kivell *et al.*, 2013), although the reorientation of this facet would suggest that the suspensory morphology reflects adaptation to a distinct loading regime rather than a similar regime of lesser magnitude. The distal repositioning of the triquetrum in suspensors would also likely result in a substantial portion of forces directed across the carpus, such as those originating in the pisiform, being more readily transmitted from the triquetrum into the hamate rather than the lunate, perhaps facilitated by its inconsistently enlarged articulation with the former.

The final trait distinguishing suspensors from other anthropoids is functionally distinct from the others. The hamate facet of the capitate in hylobatids and *Ateles* lacks the proximodistal concavity of all other taxa in the sample, often being assigned negative concavity values due to the facet's most medial extent often occurring near its center (CpHmC; Fig. 2.4b). This trait is also reduced in both *Pongo* species relative to *Gorilla*, and in *P. abelii* relative to *Pan*, although the high variability of *P. pygmaeus* encompasses the range of all five *Pan* taxa.

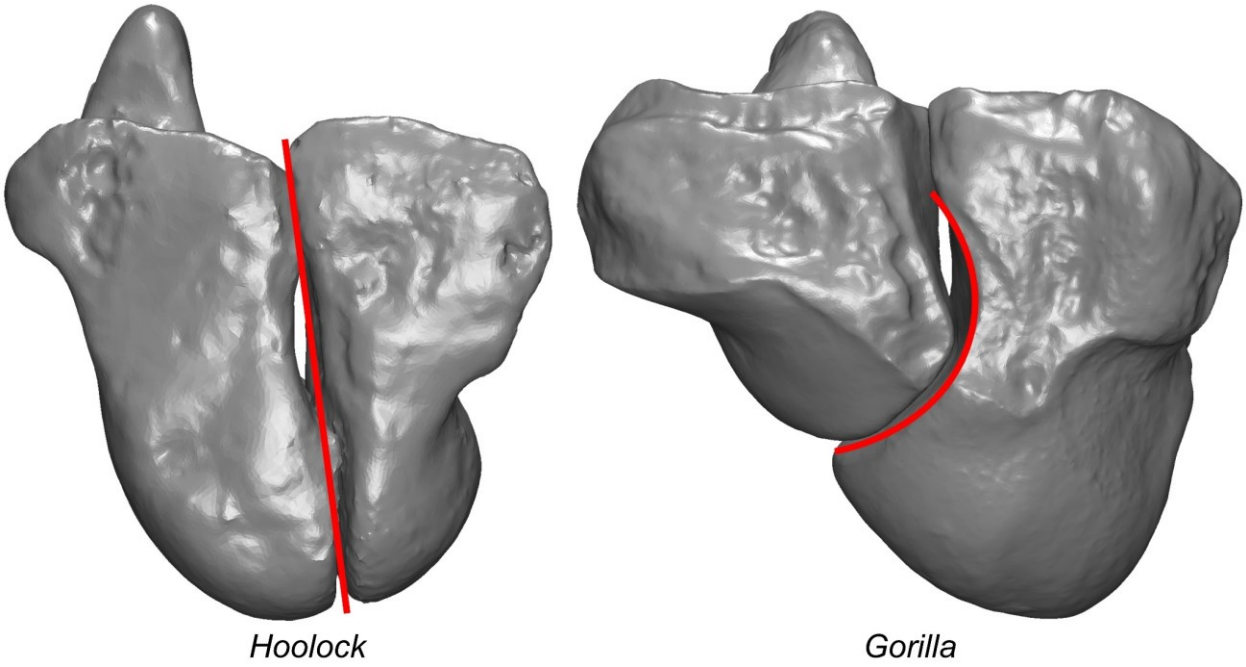

Fig. 2.10. Comparison of capitohamate joints in dorsal view. Most anthropoids display substantial proximodistal curvature, but this joint tends to be more planar in committed suspensors, especially in brachiators.

This trait seemingly contributes to a functional complex stabilizing the capitohamate joint against extrinsic forces. The distinct condition of this trait in the hylobatids and *Ateles,* along with several other aspects of capitohamate joint anatomy, point to a morphological reorganization of this joint in adaptation to brachiation. The opposing articular surfaces of the capitate-hamate joint span the dorsopalmar width of each bone both proximally and distally in each of the sampled brachiators, and the proximal and distal articulations are often separated from each other by large pits for the attachment of powerful capitohamate interosseous ligaments (Fig. 2.11). Distinct proximal and distal facets for articulation with the hamate are present in 12 of 13 *Ateles* capitate specimens and 26 of 29 sampled hylobatids, and similar discontinuity is found on the opposing surface of the hamate in 6 of 14 *Ateles* specimens and 27 of 29

hylobatids (Table 2.16b, c). This condition was rare in the remainder of the sample, with discontinuity present only in a minority of *Pongo* (8 of 34 capitates, 5 of 35 hamates) and *Nasalis* (4 of 17 capitates, 3 of 17 hamates), and in a single, possibly pathological *Procolobus* hamate.

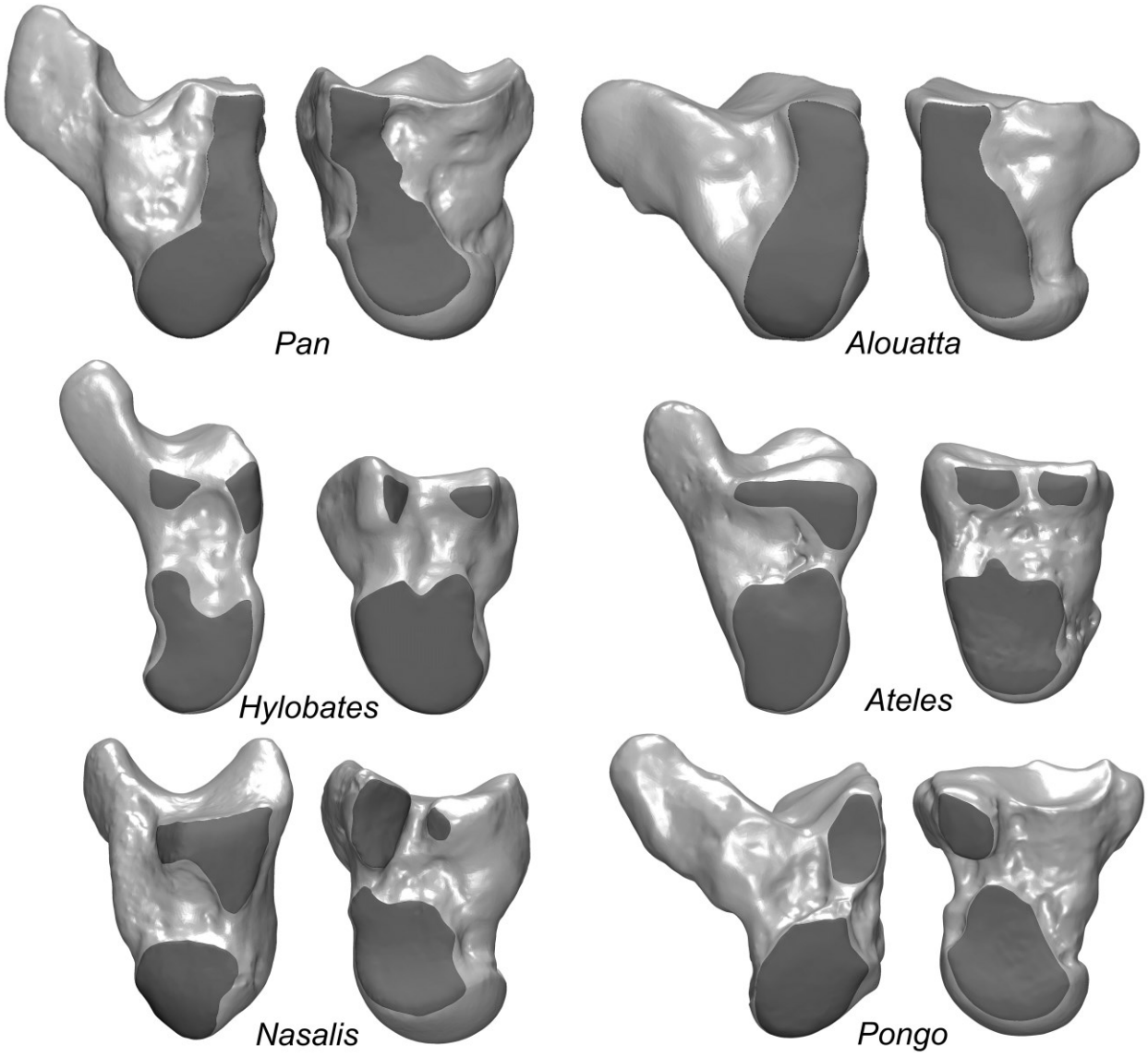

Fig. 2.11**.** Comparison of opposing capitohamate articulations. In each pairing, the hamate is shown on the left in lateral view, and the capitate on the right in medial view. Proximal is down, distal is up. All elements from the right side. *Pan* and *Alouatta* demonstrate the typical condition of most anthropoids; the others display a discontinuous articulation and deep ligament pits associated with reinforcement of the capitohamate joint, most commonly present in sampled brachiators.

The form of the discontinuity in *Pongo*, when present, is distinct from those found in the brachiating taxa. The distal articulations of the opposing surfaces are limited to the dorsal portion of each bone, as seen in most other anthropoids, and the ligament pit is palmarly positioned in most instances, rather than directly between the separate facets. The discontinuity seems less related to hypertrophy of the interosseous ligament, and may instead be related to medial displacement of the distal portion of the articulation. This condition is common in sampled *Pongo* specimens, but is often especially pronounced in specimens with the proximodistal articular discontinuity.

The condition of this joint in *Nasalis* also seems to be that of a brachiator. Proximodistal curvature is more similar to *Pongo* in being only slightly reduced relative to most of the sample, but in other ways its articulation with the hamate resembles those of the brachiating taxa. In addition to the occasional separation of the proximal and distal capitohamate articulations discussed above, the interosseous ligament pits of *Nasalis* specimens tend to be especially excavated. In 14 of 17 capitates there is also an accessory facet positioned palmarly to, and oriented opposite of, the palmarly-oriented distal portion of the hamate facet (or the dorsodistal facet when distinct; see Table 2.16b). This is akin to the condition of hylobatids, in which the distal hamate facet of the capitate is curved such that its palmar and dorsal portions face each other, although they are less often split into distinct facets (13 of 29 specimens). This morphology forms a mortise that articulates both palmarly and dorsally with the reciprocally beveled distal portion of the hamate, enhancing the ability of the capitohamate joint to resist dislocation due to dorsopalmar shear, such as might be generated by differential loading of the third and fourth rays during brachiation.

Meanwhile, more of the responsibility for resisting shear caused by force vectors concentrated near the proximodistal axis, for which the proximodistal curvature of the capitohamate joint seen in most of the sampled taxa is presumably useful, seems to have been shifted onto soft tissue structures in the brachiating taxa, including hypertrophied inter-carpal ligaments.

It is unclear whether the enhanced capitohamate joint stability that *Nasalis* seems to share with sampled brachiators actually relates to brachiation, to some other behavior with a matching loading regime, or to non-adaptive factors. Although *Nasalis* is closely related to known Old World brachiators *Rhinopithecus* (Le, 2014) and *Pygathrix* (Wright *et al.*, 2008), and has been suspected of brachiation based on its limb proportions (Byron and Covert, 2004; Byron *et al.*, 2015), its locomotor repertoire remains largely unknown.

Suspension seems to have a complex relationship with size. It is most commonly practiced by hominoids, most of whom are large, but large body size does not by itself correlate with suspensory behavior. Furthermore, its detected covariance with morphology actually increases when accounting for size, contrary to the other studied behaviors. Morphological adaptation to suspension may therefore be modulated as a function of body size, perhaps due to compromises necessary at larger body sizes to allow for transferring greater loads or in association with terrestrialism. Its lack of correlation with body size in the sample likely enhances the ability of this study's methodology to identify associated wrist traits, perhaps partially accounting for the number and strength of the suspensory correlations detected.

Knuckle-walking

Identification of knuckle-walking adaptations is confounded by its practice among anthropoids being isolated to a single lineage of large-bodied apes also reliant on suspension and vertical climbing. Morphology adapted for knuckle-walking is necessarily compromised to facilitate these other behaviors, and as discussed above, much of their uniqueness is obscured when accounting for allometric scaling. Several traits are nevertheless identified here as functionally distinct in African apes. The distal surface of the lunate is larger (LuDs; Fig. 2.6e), shares a more acute angle with the triquetrum facet (LuDsTqA; Fig. 2.6f), and is oriented nearly parallel with the radius facet (LuCpRaA; Fig. 2.4d). African apes also have relatively smaller capitate Mc4 and hamate Mc5 facets (Cp4 and Hm5; Fig. 2.4c), and the long axis of the triquetrum is highly angled relative to its articulation with the lunate (Tq1LuA; Fig. 2.4e). African apes also less reliably tend to have a more dorsally positioned capitate head (CpHP) and a smaller scaphoid facet on the lunate (LuSc).

Half of these eight potentially knuckle-walking-related traits – LuDs, LuSc, LuDsTqA, and Tq1LuA – also covary significantly with *ClimbA* (Table 2.5c). However, with one exception these correlations seem to be dictated by the African apes rather than reflecting generalizable morpho-functional relationships – only LuSc maintains a significant relationship with climbing behavior if African apes are excluded (this trait is discussed further below).

African apes are consistently distinguished by their low Hm5 values, in accord with hypotheses related to reduced loading of the fifth ray during knuckle-walking (Marzke, 1983; Marzke *et al.*, 1992). However, the pattern of variation in the sample

makes interpretation of this trait difficult. As discussed above, the lowest mean value of this trait outside of hominoids is found in *Ateles*, and the four hylobatid species have the lowest values of all (see Fig. 2.4c), indicating this condition may have a better relationship with brachiation than knuckle-walking. Furthermore, the size of this facet is not notably reduced in the *Gorilla* species – *G. beringei* is indistinguishable from *Pongo*, while *G. gorilla* has the highest values of the hominoid sample. It may be that the condition of this trait in *Pan* is related to their preferential loading of rays 2-4, whereas differences in hand posture result in a more even distribution of loading across the medial digits in *Gorilla* (Sarmiento 1988; Inouye 1994a, b; Dainton and Macho 1999; Matarazzo 2013a, b). Morphology associated with reduced loading of the fifth ray therefore cannot be considered adaptive to knuckle-walking more broadly.

Two more of the remaining traits have a dubious relationship to knuckle-walking despite statistically significant covariance. A lack of Mc4-capitate articulation has been noted in association with the bases of the third and fourth metacarpals being offset, hypothesized to increase the stability of the carpometacarpal joints in knuckle-walking taxa (Marzke *et al.*, 1994). A facet for the Mc4 was indeed absent in all sampled *Pan* capitates, and in 58% of the *Gorilla* sample (Table 2.16a). However, it was also absent in 41% of *Pongo* specimens. Loss or reduction of this articulation may therefore be better attributed to phylogeny, with its variable presence having emerged due to either nonadaptive factors or in association with vertical climbing or some other ancestral function benefited from increased CMC stability above a certain body size.

Capitate head position (CpHP) was hypothesized to covary with mobility in midcarpal extension among hominoids (Lovejoy *et al.*, 2009), the rigid-wristed African

apes presumably having the most dorsally-positioned capitate heads and therefore lowest values of this trait (see Fig. 2.5). African apes are only distinct with hylobatids removed, however, and the *Gorilla* and *Pongo* ranges overlap extensively. *Ateles* is also found to have a significantly more dorsal capitate head than other ceboids, and it tends to be somewhat more palmarly positioned in the relatively rigid-wristed digitigrade sample relative to their palmigrade relatives. The lack of covariance between this trait and mobility in midcarpal extension across the sample renders its hypothesized adaptive significance in African apes somewhat dubious.

The remaining traits, LuDs, LuCpRaA, LuDsTqA, and Tq1LuA, are the best candidates for being adapted to knuckle-walking. In each case, African apes are clearly and consistently distinguished from other anthropoids, and the African ape variant of each trait has a plausible biomechanical link to knuckle-walking. Axial compressive loading is high during knuckle-walking (e.g., Tuttle, 1967; Jenkins and Fleagle, 1975). Because stress across the distal facet of the lunate (LuDs) resulting from these forces decreases as a function of its surface area, its large size in knuckle-walkers (Fig. 2.6e) is of clear benefit. The adaptive benefit of a near-parallel orientation of the lunate's proximal and distal facets (LuCpRaA) is likewise straight-forward. The angle between these surfaces, which is most extreme in the palmigrade sample (Fig. 2.4d), seems to indicate the degree of extension associated with maximum stability, and likely corresponds to wrist posture during habitual locomotion. In accord with their especially limited mobility in extension at the antebrachiocarpal joint (Orr, 2010), the proximal and distal surfaces of African ape lunates are both oriented orthogonally relative to axial compressive loading, enhancing the bone's ability to transmit these forces into the

radius during maximum extension. The lack of distinction in this metric between the African ape genera seems to contrast with observed kinematic differences between the African ape genera (Kivell and Schmitt, 2009). Gorillas are thought to load their wrists in a neutral posture rather than at full extension as is generally the case in terrestrial mammals, including *Pan*. The near-parallel orientation of the distal and radius surfaces of the lunate in both genera would best comport with a more neutral posture for both, however. This morphology may therefore be compromised by the need to maintain stability during wrist flexion during suspension and vertical climbing.

The angle between the distal and triquetrum surfaces of the lunate (LuDsTqA) has been repeatedly noted as relatively obtuse in Asian apes (Corruccini, 1978; Sarmiento, 1985, 1988; Begun, 2004). Results of this study confirm this observation, as discussed above, but also find this angle to be especially acute in African apes (Fig. 2.6f). During knuckle-walking, loading is generally considered to be biased toward the radial side of the wrist (Heinrich *et al.*, 1993; Begun, 2004; Ward *et al.*, 2012), although this has not been experimentally confirmed (e.g., Kivell, 2016). In apparent association with this loading bias, the scaphoid of African apes is medially expanded, which results in the lunate being displaced medially (Begun, 2004). This displacement seems to result in the proximodistal alignment of the capitate and lunate with the axis of the forearm being increased somewhat during ulnar deviation. This in turn results in the distal lunate surface facing somewhat laterally in anatomical position. This being the case, the angle between this surface and the triquetrum facet will naturally be more acute given the same absolute orientation of the latter.

Perhaps more importantly, the midcarpal joint of *Pan* possesses a “screw-clamp” mechanism, originally identified in humans (MacConaill, 1941) and later confirmed experimentally in *Pan* (Orr, 2010), in which the lunate is pinned between the scaphoid and triquetrum during extension as the latter twists within its spiral facet on the hamate into a close-packed position. Although the morphology of *Gorilla* is consistent with this mechanism, its existence has not been experimentally confirmed. The more acute angle of African apes may reflect a reorientation of the lunate-triquetrum articulation to increase its orthogonality relative to transverse loading of the proximal carpal row as a result of the screw-clamp. A more acute angle also tends to reflect a wider (i.e., less curved) proximal surface of the midcarpal joint, as characterized by LuTqDsA, although this was found to be the case only in *Gorilla* and *P. paniscus* of the sample, with estimated curvature in the four *P. troglodytes* subspecies exceeding that of most sampled cercopithecoids (Fig. 2.4f).

The acute angle observed here between the lunate facet and long axis of the triquetrum (Tq1LuA; Fig. 2.4e) in African apes also has a straight-forward biomechanical link with knuckle-walking. The palmarly-leaning triquetrum of African apes yields a more proximally- (i.e., less distally-) directed pisiform, without requiring morphological change in the pisiform itself. This deepens the carpal tunnel and enhances the leverage of the flexor carpi ulnaris during wrist extension to the degree an equivalent change in pisiform morphology would; the advantage of the triquetrum being the source of this reorientation rather than the pisiform itself seems to be that in maintaining the spacial relationship between the triquetrum and pisiform while displacing the articulation between them palmarly, forces entering the carpus via the

pisiform are transmitted by the triquetrum largely as compression into the lunate and hamate, rather than as shear, allowing them to be safely transmitted across the carpus and into the forearm via the radius. This is facilitated not only by the triquetrum's now more oblique rather than orthogonal relationship with the lunate, but also due to a large portion of the hamate now being positioned dorsal to the triquetrum, opposite the pisiform. This mechanism is distinct from that of digitigrade monkeys, in which Tq1LuA is nearly as acute, as they can transmit pisiform-originating forces directly from the pisiform and triquetrum into the antebrachium via their articulation with the ulnar styloid process, eliminating much of the potential peril to the soft tissue of the ulnar carpus. The potential utility of this condition for digitigrady is discussed below.

Climbing

Climbing is unlike the other locomotor modes analyzed here in that arboreal and total proportions are uncorrelated in the sample (rho = 0.01), and there is almost no consistency between them in morphological correspondence. The lack of collinearity between *ClimbA* and *Climb* is due to larger primates tending to be less arboreal but more prone to climbing when they do take to the trees. Furthermore, since all climbing is arboreal by definition, the difference between a taxon's total and arboreal-only proportions is a function of its arboreality (see Fig. 2.8d). The African apes are the most reliant of the sample on climbing during arboreal locomotion, so their high degree of terrestriality results in these differences being drastic. Their distinct anatomy further exacerbates this problem, giving African apes sufficient influence to dictate the morphology associated with high values of C*limbA*, and to an only slightly lesser extent,

with low values of *Climb*. This makes congruence between traits associated with *ClimbA* and *Climb* virtually impossible.

The lack of consistent morphological covariance with climbing may be further explained by observational methodology. Climbing has often been a broad or amorphous designation in the literature, and although steps have been taken to remedy this (Hunt *et al.*, 1996 and succeeding studies), continuing methodological discrepancies in field observations and a necessary reliance on older studies due to a lack of recent ones for many taxa necessitate grouping several behaviors of dubious kinematic and kinetic similarity into a single class. Even vertical climbing in the most limited sense seems to be comparable across anthropoids only in purpose, with the hand-over-hand climbing of African apes bearing very little resemblance to the series of vertical leaps ("pulse-climbing"; Hunt, 1992) used by baboons to the same end. This may further explain the lack of overlap between traits associated with *ClimbA* and *Climb* – those related to the former are more likely to correspond to stereotypical vertical climbing as performed by great apes, while those related to the latter more likely reflect a suite of behaviors practiced by highly arboreal monkeys.

Only a single trait – the size of the scaphoid facet of the lunate (LuSc) – overcomes these confounds to demonstrate a consistent relationship with *Climb* and *ClimbA*. This trait covaries negatively with *ClimbA*, and the significance of this relationship is maintained with the exclusion of hylobatids, African apes, or both. Coefficients relative to *Climb* are also negative, approaching significance despite the low *Climb* values of African apes, and becoming highly significant upon the exclusion of this group. Reduction in the size of this facet and expansion of the radius facet were

noted by Kivell and colleagues (2013) as distinguishing *Pan* and *Pongo* from other anthropoids, which they hypothesized to reflect high loading of the radiolunate joint in adduction during climbing. As measured here, the lunate's scaphoid facet is only marginally larger in the *Gorilla* species than in *Pan* and *Pongo*, with all three genera having significantly lower values than other taxa of the sample. However, it is not obvious how this condition assists in mitigating loads borne during ulnar deviation. Because the radius, lunate, and capitate are somewhat aligned with the axis of the forearm during wrist adduction, an increase in the proportion of loading along this axis being transmitted directly into the antebrachium without passing between the scaphoid and lunate may be worthy of experimental testing. Utility not requiring ulnar deviation may be more likely given this trait's covariance with climbing in sampled monkeys as well, unless this covariance is coincidental in the sample.

The size of the capitate's Mc4 facet (Cp4) may also have some relationship with climbing at larger body sizes. It is inversely correlated with both *ClimbA* and *Climb* when accounting for size (Table 2.5c, Table 2.9c), due to its substantial reduction or absense in great apes, but has no relationship to either with African apes removed. The size of the lunate's radius facet (LuRa), the other trait noted by Kivell and colleagues (2013) as potentially related to climbing, is again distinct in each of the great ape genera as measured here, and positively correlated with *ClimbA* with and without hylobatids. Coefficients relative to *Climb* are negative, however, indicating its relationship with climbing is limited to the great apes, consistent with its hypothesized utility in transmitting loads during ulnar deviation of the antebrachiocarpal joint, which is limited in non-hominoid anthropoids.

Hm45A is the only other trait with a tenuous relationship to climbing; the hamate's metacarpal facets tend to become nearer to parallel as values of *Climb* increase, a relationship remaining significant with either hylobatids or African apes removed. This trait also covaries with *ClimbA* in the same direction, although to a degree that only approaches significance with African apes excluded from the analysis. While this angle was predicted to be more acute in digitigrade cercopithecines, in which *Climb* values are indeed low, the benefit of larger values of this trait to climbing is not apparent.

Digitigrady

Given the sometimes-subtle differences in wrist postures between digitigrade and palmigrade monkeys (e.g., Patel, 2009, 2010b), and the difficulty of previous researchers in finding corresponding anatomy (e.g., Patel, 2010a), the number of shape variables found to distinguish these groups is surprisingly high. As with the sampled suspensors, digitigrady is thought to have emerged independently in each of the sampled terrestrial monkey lineages (Gilbert *et al.* 2010; Gosselin-Ildari, 2013), so these traits may be examples of adaptive convergence. However, these features are spread throughout the carpus, effect sizes are often low, and statistically significant correlations sometimes belie a lack of consistency among the digitigrade genera. For example, there are several variables in which *Mandrillus* and *Erythrocebus* are distinct from their closest palmigrade relatives in accord with the associated morpho-functional hypothesis, while *Papio* does not differ from *Lophocebus* or other palmigrade cercopithecines. This is unexpected given the more vertical manus of *Papio* relative to

Erythrocebus (Richmond, 2006; Patel, 2009) and the more distant relationship of *Erythrocebus* relative to the digitigrade papionins. This may correspond with adaptive variation between lineages, or it may be a function of a single adaptive complex being spread throughout the carpus, rendering poor predictors of most individual metrics but allowing a combination thereof to be highly diagnostic.

Traits distinguishing digitigrady seem to contribute to a small number of discrete functional complexes, most prominently the distal wrist mortise. Much like the proximal mortise formed by the radial and ulnar styloid processes articulating the proximal carpal row medially and laterally, the distal wrist mortise of digitigrade taxa is formed by the more proximal origin of the second and fifth metacarpals, which therefore have a more mediolateral relationship with the distal-most portions of the capitate and hamate than is found in other primates. To wit, the Mc2 facet of the capitate (Cp2) tends to be larger and more radially oriented (Cp23A), and the Mc5 facet of the hamate tends to be oriented (Hm45A) ulnarly to articulate with the cylindrical and proximoulnarly projecting metacarpal base. As part of this complex, the Mc3 facet of the capitate and adjacent Mc4 facet of the hamate tend to be angled slightly toward each other in digitigrade taxa (CMC34A), as opposed to the more planar relationship found in palmigrade taxa. During CMC extension, Mc2 and Mc3 supinate slightly, and MC4 and MC5 pronate slightly, so that at full extension the arch formed by the metacarpals is reduced, aligning them transversely with each other and locking them together (Marzke, 1983). The angulation of the third and fourth metacarpal facets may aid in redirecting resulting mediolateral force vectors proximally through the capitate and hamate (Selby *et al.*, 2016).

The central column of the wrist seems to have narrowed in digitigrade taxa, judging by the reduced size of the lunate and capitate's distal surfaces (LuDs, Cp3; see Chapter 3), both of which are apparently due to mediolateral narrowing, and a variable tendency toward a narrower proximal angle of the capitate (CpPxA). Force vectors transmitted through this portion of the wrist have been hypothesized to be similar during knuckle-walking and digitigrady (see Schmitt *et al.*, 2016 and references therein), but these groups are distinguished from palmigrade primates in opposite directions by this metric. The narrowing of the central column in digitigrade taxa may accord with their habitual reliance on a locomotor mode prioritizing parasagittal movement at body sizes low enough to not require articular expansion.

Additional traits may reflect reduced mobility and greater stability in association with digitigrady. Mean concavity values of the capitate's hamate facet (CpHmC; Fig. 2.4b) are slightly increased in digitigrade lineages, while the lunate's capitate facet is less concave (LuCpC) and significantly closer to parallel with the radius facet in each of the digitigrade taxa relative to their closest palmigrade relatives (LuCpRaA; see Fig. 2.4d, Fig. 2.12). However, despite the latter trait being among the most distinctive digitigrade traits, it falls short of significance in the statistical models – the larger body size of the digitigrade member of each dyad conspire with similarly low values among African apes to cause most of this trait's variance to be attributed to allometry. The extent of the hamate-triquetrum articulation, as characterized by HmPx and TqHm, is also somewhat reduced in accord with limited midcarpal mobility, although the relationship with both variables is significant only at $p < 0.1$.

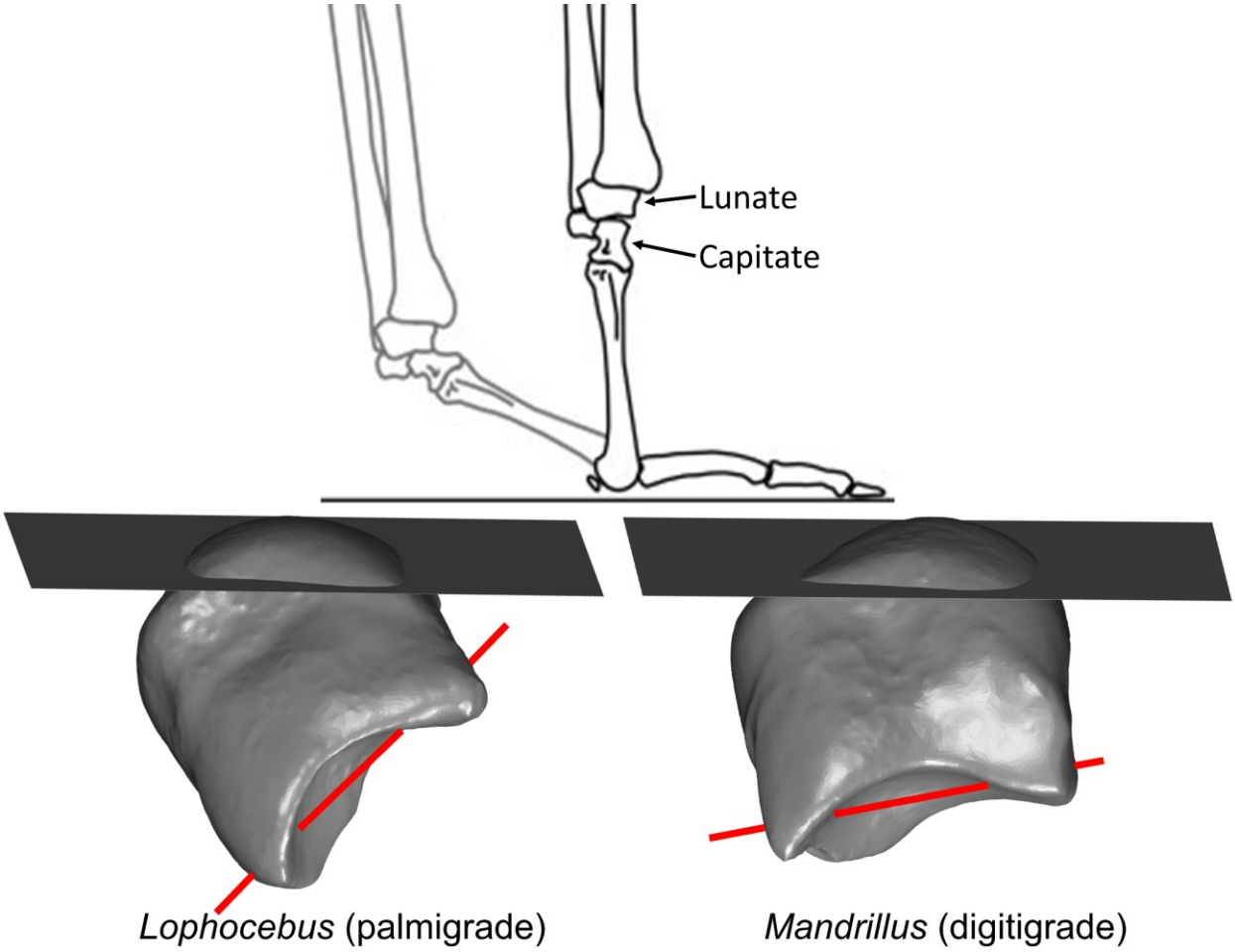

Fig. 2.12. Comparison of the angle between the radius and capitate facets of the lunate (LuCpRaA) demonstrating its covariance with wrist posture during habitual loading among cercopithecoids. Postural diagram modified from Patel, 2009.

Other than LuCpRaA, Tq1LuA is the trait best distinguishing the digitigrade and palmigrade samples when allometry is not accounted for, as the long axis of the triquetrum is significantly less orthogonal relative to its lunate surface in each of the digitigrade taxa relative to other cercopithecines. Ape triquetra, even those of knuckle-walkers, are oriented distally relative to those of non-hominoids, which are more transversely aligned with the lunate and scaphoid. Because of this, the lower Tq1LuA values of knuckle-walkers reflect the triquetrum leaning palmarly, whereas similarly low values in digitigrade anthropoids correspond to the distal portion of the triquetrum being

displaced medially as well as palmarly. This reorients both the pisiform and styloid articulations somewhat proximally, with the latter facet also facing slightly more ulnarly.

This reorientation of the pisiform facet could have analogous utility as discussed above for knuckle-walkers, but implications for the styloid articulation are less clear. The styloid facet is bounded dorsally by a process extending away from the body of the triquetrum, and it is this projection that interrupts the motion of the styloid at maximum supination. A process directed more dorsally (i.e., a more proximally-facing styloid facet) rather than proximally (i.e., a more palmarly-facing styloid facet) would seem to be less effective in limiting supination or maintaining stability at its extent. However, this condition may reorient the styloid facet more orthogonally relative to the ulnar axis during terrestrial quadrupedalism, in which the wrist is maximally pronated and extended, and somewhat ulnarly deviated (Jenkins and Fleagle, 1975). In this posture, the styloid process is positioned more palmarly relative to the carpus, and the styloid facet of the triquetrum is rotated palmarly to match. This would potentially increase the stability of the ulnar column of the wrist, loading of which may be higher in digitigrade primates due to ground reaction forces at higher body sizes in addition to the thumb not participating in weight support (Whitehead, 1993).

Terrestriality

Several traits were found to distinguish between vertical manus and palmigrade-capable taxa. However, in some cases this owes to the signal being sufficiently strong in either the digitigrade or knuckle-walking class to overcome a lack of signal, or even an opposite one, in the other. As evident in Fig. 2.7, even the metrics in which

digitigrade taxa are most distinct share far greater resemblance with palmigrade monkeys than with knuckle-walking apes. *Arb* is the locomotor variable with the strongest relationship to body size (Table 2.15b), and allometry therefore plays an especially large role in searching for a terrestrial signal in morphology, since accounting for allometric effects removes much of the morphological correlation associated with a size-correlated behavior. Greater consideration was therefore given to analyses not accounting for allometry in evaluating terrestrial traits. Shape variables discussed in this section are those distinguishing vertical manus and palmigrade-capable taxa and in which the digitigrade and knuckle-walking classes vary in same direction relative to the palmigrade or palmigrade-capable samples, while also covarying with *Quad* and oppositely with *Arb*. Seven traits were found to meet these criteria. Of these, LuTqDsA is less significant than one of its constituents, LuDsTqA, and was eliminated, leaving six traits potentially corresponding with terrestriality *per se*, rather than with a specific postural class. These are discussed in order of increasing significance.

The orientation of the capitate's Mc2 surface (Cp23A) is positively correlated with *Arb*, but a negative covariance with *Quad* only approaches significance, reaching it when African apes are removed due to the resulting decrease in estimated λ value. This angle was hypothesized to be acute in all great apes (Selby *et al.*, 2016); it is here found to be slightly more acute in African apes than in *Pongo*, and slightly more acute in digitigrade vs palmigrade anthropoids, although the distinction of both groups from the palmigrade sample falls short of significance. When combined, it does distinguish vertical manus taxon means from those of palmigrade and palmigrade-capable taxa. The hypothesized function in both cases is in enhancing CMC stability from transverse

force vectors, but there is sufficient noise in the data for this morpho-functional link to be considered very tentative.

The triquetrum facet of the lunate (LuTq) is slightly expanded in African apes relative to Asian apes and in digitigrade versus palmigrade cercopithecines. Intra-taxon variability is high, however, leading to a great deal of overlap and significance only in distinguishing taxon means. Concavity of the capitate's hamate facet (CpHmC) also seems somewhat related to terrestriality, but its significance is again tentative. This trait distinguishes digitigrade taxa with borderline significance and average concavity is greatest in the *Gorilla* species and *P. paniscus*, but values in *Pan* are similar to those of various palmigrade monkeys. Even so, this trait's covariance with *Quad, Arb,* and vertical manus postures is significant to a degree similar to Cp23A.

LuDsTqA covaries negatively with *Quad* and positively with *Arb* with or without hylobatids, distinguishes vertical manus individuals from palmigrade ones, and vertical manus taxon means from palmigrade-capable ones. However, while this angle is markedly acute in *Mandrillus*, it is only slightly reduced in *Erythrocebus* and not at all in *Papio* (Fig. 2.6f), so the association with general terrestriality is again inconsistent. Furthermore, the biomechanics of how this trait would facilitate digitigrady is not clear. While it is plausibly related to the screw-clamp mechanism in knuckle-walkers, a similar mechanism does not exist in cercopithecoids, in which stability of the proximal row is instead maintained by short and strong inter-carpal ligaments (Orr, 2010), resulting in far less inter-carpal mobility throughout the wrist's range of flexion and extension and obviating the need for a mechanism enhancing midcarpal stability only at full extension. The association of this angle with terrestriality could be found in its contribution to a

wider, less curved wrist joint, but while greater curvature of both distal and proximal midcarpal surfaces were found to be associated with suspension, there is little functional pattern in these traits among non-suspensors.

As discussed above, LuCpRaA and Tq1LuA distinguish digitigrady and knuckle-walking from palmigrady, although their significance in distinguishing digitigrady is mostly lost to allometry. The mechanism of the latter trait in facilitating terrestriality also seems to be at least somewhat distinct between the two postures, as also discussed above. Both traits significantly distinguish the taxon means and individual observations of vertical manus anthropoids from those of palmigrade ones. The degree to which terrestriality *per se* is reflected in wrist anatomy remains unclear, but these two traits seem to have the strongest case of those analyzed here.

Adaptive influence of different positional behaviors

Of the variety of anthropoid behaviors, some have greater correspondence to wrist morphology than others. As noted above, leaping was found to have very little correlation with carpal morphology, whereas suspension, quadrupedalism, and arboreality are strongly reflected in carpal shape. The prominence of the former two locomotor modes is especially apparent in the PLS analyses (Fig. 2.8), in which much of the variation is shown to occur along an axis separating more suspensory taxa from more quadrupedal ones. Statistical results ostensibly indicate that climbing also wields a significant adaptive influence on the wrist, but fewer shape variables are found to covary with *ClimbA* or *Climb* (Fig. 2.8d, Table 2.5c, Table 2.9c), and even fewer of these statistical relationships are found to be consistent across the sample. Metrics

associated with *ClimbA* may be worthy of further study, but the distinct biomechanics of different climbing behaviors may obviate the utility of the phylogenetic method in seeking a consistent morphological signal, particularly in the analysis of available quantitative behavioral observations.

Results of this study can also address the degree to which specialization results in unique adaptations as opposed to elaboration of traits possessed by taxa performing similar behaviors with less frequency. There is a great deal of overlap in the shape variables associated with *Quad* and *QuadA* in univariate analyses, with the exceptions involving traits that distinguish digitigrady or knuckle-walking. When accounting for size, the number of traits associated with *Quad* decreases significantly, but the remaining variables are all correlated in the same direction, and usually to a somewhat smaller degree, with *QuadA*. This supports the intuitive notion that highly quadrupedal primates possess many of the same traits as moderate quadrupeds, and often in exaggerated form, reflecting a degree of similarity in loading regimes regardless of substrate. It is also apparent, however, that the different postures used during quadrupedalism also result in morphological divergence.

There is also a high degree of overlap between traits associated with *SuspA* and *Susp*, as expected given that the two variables differ only among the African apes, with all other suspensors being highly arboreal. Differences between total and arboreal suspensory proportions in African apes have very little effect on multivariate morphological correspondence, and most individual correlations remain largely unchanged. Notable exceptions include the size and orientation of the pisiform facet, which are correlated with *Susp* but not *SuspA* due to the more terrestrial morphology of

African apes, as discussed above. Another way to address this question is by assessing the presence of nascent suspensory traits in the occasional suspensors of the sample. The suspensory predictions for *Alouatta*, *Presbytis*, *Colobus*, and *Procolobus* (Table 2.7b) are no higher than the baseline values assigned to non-suspensors, and in individual shape metrics these taxa show no discernible pattern of variation in the direction of more suspensory primates, suggesting that the occasional suspensory behavior of these taxa has not resulted in significant carpal reorganization. This finding may imply that occasional suspension does not require substantial adaptation in the carpus, potentially rendering this morphology useful only in recognizing committed suspensors in the fossil record and not incipient or facultative ones.

PLS results and RV correlations indicate that total locomotor proportions have a weaker relationship with carpal morphology than do arboreal-only locomotor proportions. This is counterintuitive, as the total proportions attempt to characterize the entirety of each taxon's locomotor repertoire, whereas arboreal-only proportions provide no information about terrestriality, which represents a large majority of the repertoire in a quarter of the sampled taxa. Much of this effect is attributable to African apes, as the discrepancy is reduced by more than half with them excluded from the analysis. Climbing and suspensory behaviors in African apes become increasingly rare in the years approaching adulthood (Doran, 1997; Remis, 1998; Sarringhaus *et al.*, 2014), so these activities may have an outsized morphological impact relative to the adult locomotor proportions analyzed here. The discrepancy is also partially attributable to the terrestrial cercopithecines, however, the only other sampled taxa in which arboreal and total locomotor proportions differ.

The quantitative behavioral variables analyzed here do not account for time spent using different postures or substrates in non-locomotor activities. Many of the sampled highly terrestrial taxa are known to spend a far greater proportion of their time in the canopy than might be suggested by the *Arb* values assigned here (e.g., *E. patas*, Nakagawa, 1989; *P. anubis* and *P. t. schweinfurthii*, Hunt, 1989; *P. t. verus*, Doran, 1993), but a greater proportion of this time is spent eating or resting. It may seem counterintuitive to expect time spent sitting in trees to be relevant in analyzing locomotor morphology, but this proportion may serve as a better proxy for the adaptive benefit of being able to access the trees. Given the utility of trees in providing food, protection from predators, and other survival essentials, the retention of arboreal adaptations in highly terrestrial anthropoids may be somewhat reminiscent of fallback foods (Marshall and Wrangham, 2007) in making an outsized contribution to survival relative to proportional utilization. Knuckle-walking has been characterized as an adaptive compromise that facilitates a terrestrial lifestyle while allowing maintenance of arboreal abilities (e.g., Tuttle, 1969; Richmond *et al.*, 2001; Begun and Kivell, 2011); a similarly important compromise may be found in other terrestrial primates as well. The need to maintain the grasping capability required for feeding, grooming, and other manipulative behaviors may also contribute to explaining these results (Vilensky and Larson, 1989), perhaps in concert with the relative recency of the behavioral shifts within the sampled terrestrial lineages.

Conclusion

Results indicate that when accounting for allometry and phylogeny, carpal morphology strongly covaries with positional behavior across the anthropoid clade, allowing extant anthropoids to be classified according to positional behavior with high accuracy, and for the frequency of different locomotor modes to be accurately estimated. Both locomotor behavior and the morphological traits with which it covaries most strongly are found to maintain high phylogenetic signal, with locomotion tending to vary to a greater extent than morphology within phylogenetic groups, and locomotor and morphological diversity are found to be far greater among hominoids than in other anthropoids. Wrist morphology is found to have greater correspondence to arboreal-only locomotor proportions than to total locomotor proportions, suggesting an outsized importance of arboreal behaviors on survivorship relative to their frequency of use in terrestrial anthropoids.

This study also identifies several cases of morphological convergence in association with each of several positional modes. Potential suspensory adaptations function to increase midcarpal and antebrachiocarpal mobility, enhance flexor carpi ulnaris leverage and transmit forces generated thereby, and stabilize the capitohamate joint against non-stereotypical force vectors.

Features associated with digitigrady function to stabilize the midcarpal joint during loading at maximum extension, contribute to a distal mortise aiding the stability of the ulnar carpometacarpal joints, and facilitate load transmission across the ulnocarpal joint. Although various confounds complicate interpretation of potential knuckle-walking adaptations, several traits common to African apes are found to have statisitical and biomechanical relationships with this behavior, largely related to facilitating transmission

of compressive axial loading. Several features shared by knuckle-walkers and digitigrade cercopithecines are also identified as potentially diagnostic of terrestriality more generally. Climbing is found to be reflected differently in the wrists of apes and monkeys, consistent with the biomechanical dissimilarity of the behaviors between the groups, while leaping is found to have very little influence on wrist morphology.

Chapter 2 references

Abrams, P., 2001. Adaptationism, optimality models, and tests of adaptive scenarios, in: Orzack, S.H., Sober, E. (Eds.), Adaptationism and Optimality. Cambridge University Press, pp. 273-302.

Adams, D.C., 2014a. A method for assessing phylogenetic least squares models for shape and other high-dimensional multivariate data. Evolution 68, 2675-2688.

Adams, D.C., 2014b. A generalized K statistic for estimating phylogenetic signal from shape and other high-dimensional multivariate data. Systematic Biology 63, 685-697.

Adams, D.C., Otárola-Castillo, E., 2013. geomorph: an R package for the collection and analysis of geometric morphometric shape data. Methods in Ecology and Evolution 4, 393-399.

Adams, D.C., Felice, R.N., 2014. Assessing trait covariation and morphological integration on phylogenies using evolutionary covariance matrices. PloS One 9, e94335.

Adams, D.C., Collyer, M.L., 2016. On the comparison of the strength of morphological integration across morphometric datasets. Evolution 70, 2623-2631.

Almecija, S., Orr, C.M., Tocheri, M.W., Patel, B.A., Jungers, W.L., 2015. Exploring phylogenetic and functional signals in complex morphologies: the hamate of extant anthropoids as a test-case study. Anatomical Record 298, 212-229.

Andrews, P., Martin, L., 1987. Cladistic relationships of extant and fossil hominoids. Journal of Human Evolution 16, 101-118.

Arnold, C., Nunn, C.L., 2010. Phylogenetic targeting of research effort in evolutionary biology. American Naturalist 176, 601-612.

Arnold, C., Matthews, L.J., Nunn, C.L., 2010. The 10kTrees website: A new online resource for primate phylogeny. Evolutionary Anthropology 19, 114-118.

Aronsen, G.P., 2004. Positional behavior and support use in three arboreal monkeys of the Kibale forest, Uganda: the influences of forest structure, microhabitats, and energetics. Ph.D. Dissertation, Yale University.

Barr, W.A., Scott, R.S., 2014. Phylogenetic comparative methods complement discriminant function analysis in ecomorphology. American Journal of Physical Anthropology 153, 663-674.

Barton, K., 2016. MuMIn: multi-model inference. R package version 1.15.6.

Beard, K.C., Teaford, M.F., Walker, A., 1986. New wrist bones of *Proconsul africanus* and *P. nyanzae* from Rusinga Island, Kenya. Folia Primatologica 47, 97-118.

Begun, D.R., 1993. New catarrhine phalanges from Rudabanya (Northeastern Hungary) and the problem of parallelism and convergence in hominoid postcranial morphology. Journal of Human Evolution 24, 373-402.

Begun, D.R., 2004. Knuckle-walking and the origin of human bipedalism, in: Meldrum, D.J., Hilton, C.E. (Eds.), From Biped to Strider: The Emergence of Modern Human Walking, Running and Resource Transport. Kluwer Academic/Plenum Publishers, New York, pp. 9-33.

Begun, D.R., Kivell, T.L., 2011. Knuckle-walking in *Sivapithecus*? The combined effects of homology and homoplasy with possible implications for pongine dispersals. Journal of Human Evolution 60, 158-170.

Benjamini, Y., Hochberg, Y., 1995. Controlling the false discovery rate: A practical and powerful approach to multiple testing. Journal of the Royal Statistical Society B 57, 289-300.
Biewener, A.A., 1983. Allometry of quadrupedal locomotion: the scaling of duty factor, bone curvature and limb orientation to body size. Journal of Experimental Biology 105, 147-171.
Blomberg, S.P., Garland, T., Jr., Ives, A.R., 2003. Testing for phylogenetic signal in comparative data: behavioral traits are more labile. Evolution 57, 717-745.
Boonratana, R., 1993. The ecology and behaviour of the proboscis monkey (*Nasalis larvatus*) in the Lower Kinabatangan, Sabah. Asian Primates 4, 13-14.
Boonratana, R., 2000. Ranging behavior of proboscis monkeys (*Nasalis larvatus*) in the lower Kinabatangan, Northern Borneo. International Journal of Primatology 21, 497-518.
Brinckmann, P., Frobin, W., Hierholzer, E., 1981. Stress on the articular surface of the hip joint in healthy adults and persons with idiopathic osteoarthrosis of the hip joint. Journal of Biomechanics 14, 149-156.
Bullough, P., Goodfellow, J., Greenwald, A.S., O'Connor, J., 1968. Incongruent surfaces in the human hip joint. Nature 217, 1290.
Burnham, K.P., Anderson, D.R., 2002. Model Selection and Inference: A Practical Information-Theoretical Approach, 2nd Ed. Springer-Verlag, New York.
Byron, C.D., Covert, H.H., 2004. Unexpected locomotor behaviour: brachiation by an Old World monkey (*Pygathrix nemaeus*) from Vietnam. Journal of Zoology 263, 101-106.
Byron, C.D., Hensel, C., Morrison, J., Nguyen, H., 2015. The skeletal anatomy of the douc langurs (Genus *Pygathrix*). Vietnamese Journal of Primatology 2, 13-24.
Byron, C., Granatosky, M.C., Covert, H., In press. An anatomical and mechanical analysis of the douc monkey (genus *Pygathrix*), and its role in understanding the evolution of brachiation. American Journal of Physical Anthropology.
Campione, N.E., 2016. MASSTIMATE: body mass estimation equations for vertebrates. R package version 1.3.
Cant, J.G.H., 1986. Locomotion and feeding postures of spider and howling monkeys: field study and evolutionary interpretation. Folia Primatologica 46, 1-14.
Cant, J.G.H., 1987. Positional behavior of female Bornean orangutans (*Pongo pygmaeus*). American Journal of Primatology 12, 71-90.
Cant, J.G.H., 1988. Positional behavior of long-tailed macaques (*Macaca fascicularis*) in northern Sumatra. American Journal of Physical Anthropology 76, 29-37.
Carlson, K.J., 2005. Investigating the form-function interface in African apes: Relationships between principal moments of area and positional behaviors in femoral and humeral diaphyses. American Journal of Physical Anthropology 127, 312-334.
Carlson, K.J., Patel, B.A., 2006. Habitual use of the primate forelimb is reflected in the material properties of subchondral bone in the distal radius. Journal of Anatomy 208, 659-670.
Carlson, K.J., Doran-Sheehy, D.M., Hunt, K.D., Nishida, T., Yamanaka, A., Boesch, C., 2006. Locomotor behavior and long bone morphology in individual free-ranging chimpanzees. Journal of Human Evolution 50, 394-404.

Carter, K.E., Worthington, S., 2016. The evolution of anthropoid molar proportions. BMC Evolutionary Biology 16, 110.
Cartmill, M., Milton, K., 1977. The lorisiform wrist joint and the evolution of "brachiating" adaptations in the Hominoidea. American Journal of Physical Anthropology 47, 249-272.
Chen, W.-C., 2011. Overlapping Codon model, Phylogenetic Clustering, and Alternative Partial Expectation Conditional Maximization Algorithm. Ph.D. Dissertation, Iowa State University.
Coddington, J.A., 1994. The roles of homology and convergence in studies of adaptation, in: Eggleton, P., Vane-Wright, R.I. (Eds.), Phylogenetics and ecology. Academic Press for the Linnean Society, London, pp. 53-78.
Collard, M., Wood, B., 2000. How reliable are human phylogenetic hypotheses? Proceedings of the National Academy of Sciences 97, 5003-5006.
Collard, M., Wood, B., 2001. How reliable are current estimates of fossil catarrhine phylogeny? An assessment using extant great apes and Old World monkeys, in: Bonis, L.d., Koufos, G.D. (Eds.), Phylogeny of Eurasian Neogene Hominoid Primates. Cambridge University Press, Cambridge, pp. 118-150.
Corruccini, R.S., 1978. Comparative osteometrics of the hominoid wrist joint, with special reference to knuckle-walking. Journal of Human Evolution 7, 307-321.
Cullinane, D.M., 2000. Axial versus appendicular: constraint versus selection. American Zoologist 40, 136-145.
Dainton, M., Macho, G.A., 1999a. Did knuckle walking evolve twice? Journal of Human Evolution 36, 171-194.
Dainton, M., Macho, G.A., 1999b. Heterochrony: somatic, skeletal and dental development in *Gorilla*, *Homo*, and *Pan*, in: Hoppa, R.D., Fitzgerald, C.M. (Eds.), Human Growth in the past: studies from bones and teeth. Cambridge University Press, Cambridge, pp. 32-64.
Daver, G., Berillon, G., Grimaud-Herve, D., 2012. Carpal kinematics in quadrupedal monkeys: towards a better understanding of wrist morphology and function. Journal of Anatomy 220, 42-56.
de Villemereuil, P., 2012. Estimation of a biological trait heritability using the animal model: How to use the MCMCglmm R package. (White paper)
de Villemereuil, P., Nakagawa, S., 2014. General quantitative genetic methods for comparative biology, in: Garamszegi, L.Z. (Ed.), Modern Phylogenetic Comparative Methods and Their Application in Evolutionary Biology. Springer-Verlag, Berlin Heidelberg, pp. 287-303.
Delson, E., Terranova, C.J., Jungers, W.L., Sargis, E.J., Jablonski, N.G., Dechow, P.C., 2000. Body mass in Cercopithecidae (Primates, Mammalia): Estimation and scaling in extinct and extant taxa. American Museum of Natural History, Anthropological Papers 83.
Doran, D.M., 1993a. Sex differences in adult chimpanzee positional behavior: The influence of body size on locomotion and posture. American Journal of Physical Anthropology 91, 99-115.
Doran, D.M., 1993b. Comparative locomotor behavior of chimpanzees and bonobos: the influence of morphology on locomotion. American Journal of Physical Anthropology 91, 83-98.

Doran, D.M., 1996. Comparative positional behavior of the African apes, in: McGrew, W., Marchant, L., Nishida, T. (Eds.), Great Ape Societies. Cambridge University Press, pp. 213-224.
Doran, D.M., 1997. Ontogeny of locomotion in mountain gorillas and chimpanzees. Journal of Human Evolution 32, 323-344.
Doran, D.M., Hunt, K.D., 1994. Comparative locomotor behavior of chimpanzees and bonobos, in: Wrangham, R., McGrew, W.C., De Waal, F.B.M., Heltne, P. (Eds.), Chimpanzee Cultures. Harvard University Press, pp. 93-108.
Escoufier, Y., 1973. Le traitement des variables vectorielles. Biometrics 29, 751-760.
Etter, H.F., 1973. Terrestrial adaptations in the hands of Cercopithecinae. Folia Primatologica 20, 331-350.
Felsenstein, J., 1985. Phylogenies and the comparative method. The American Naturalist 125, 1-15.
Fernandez, P.J., Almecija, S., Patel, B.A., Orr, C.M., Tocheri, M.W., Jungers, W.L., 2015. Functional aspects of metatarsal head shape in humans, apes, and Old World monkeys. Journal of Human Evolution 86, 136-146.
Fleagle, J.G., 1980. Locomotion and posture, in: Chivers, D.J. (Ed.), Malayan Forest Primates. Plenum Press, New York, pp. 191-207.
Fleagle, J.G., Lieberman, D.E., 2015. Major transformations in the evolution of primate locomotion, in: Dial, K.P., Shubin, N., Brainerd, E.L. (Eds.), Great Transformations in Vertebrate Evolution. University of Chicago Press, Chicago, IL, pp. 257-278.
Fleagle, J.G., Stern, J.T., Jungers, W.L., Susman, R.L., Vangor, A.K., Wells, J.P., 1981. Climbing: a biomechanical link with brachiation and with bipedalism. Symposia of the Zoological Society of London 48, 359-375.
Fontaine, R., 1990. Positional behavior in *Saimiri boliviensis* and *Ateles geoffroyi*. American Journal of Physical Anthropology 82, 485-508.
Fragaszy, D.M., Crast, J., 2016. Functions of the hand in primates, in: Kivell, T.L., Lemelin, P., Richmond, B.G., Schmitt, D. (Eds.), The Evolution of the Primate Hand. Springer, New York, pp. 313-344.
Friedman, J., Hastie, T., Tibshirani, R., 2010. Regularization paths for generalized linear models via coordinate descent. Journal of Statistical Software 33, 1-22.
Frost, H.M., 1997. Why do marathon runners have less bone than weight lifters? A vital-biomechanical view and explanation. Bone 20, 183-189.
Galdikas, B.M.F., 1978. Orangutan Adaptation at Tanjung Puting Reserve, Central Borneo. Ph.D. Dissertation, UCLA.
Gebo, D.L., Chapman, C.A., 1995. Positional behavior in five sympatric Old World monkeys. American Journal of Physical Anthropology 97, 49-76.
Gelman, A., 2006. Prior distributions for variance parameters in hierarchical models (comment on article by Browne and Draper). Bayesian Analysis 1, 515-534.
Gelman, A., Carlin, J.B., Stern, H.S., Dunson, D.B., Vehtari, A., Rubin, D.B., 2014. Bayesian Data Analysis, 3rd ed. CRC Press.
Gilbert, C.C., Rossie, J.B., 2007. Congruence of molecules and morphology using a narrow allometric approach. Proceedings of the National Academy of Sciences 104, 11910-11914.

Gilbert, C.C., Goble, E.D., Hill, A., 2010. Miocene Cercopithecoidea from the Tugen Hills, Kenya. Journal of Human Evolution 59, 465-483.
Godinot, M., Beard, K.C., 1993. A survey of fossil primate hands, in: Preuschoft, H., Chivers, D.J. (Eds.), Hands of Primates. Springer, pp. 335-378.
Gosselin-Ildari, A.D., 2013. The Evolution of Cercopithecoid Locomotion: a Morphometric, Phylogenetic, and Character Mapping Approach. Ph.D. dissertation, Stony Brook University.
Gould, S.J., Lewontin, R.C., 1979. The spandrels of San Marco and the Panglossian paradigm: a critique of the adaptationist programme. Proceedings of the Royal Society B 205, 581-598.
Grafen, A., 1989. The phylogenetic regression. Philosophical Transactions of the Royal Society of London B 326, 119-157.
Hadfield, J.D., 2010. MCMC methods for multi-response generalized linear mixed models: The MCMCglmm R package. Journal of Statistical Software 33, 1-22.
Hadfield, J.D., Nakagawa, S., 2010. General quantitative genetic methods for comparative biology: phylogenies, taxonomies and multi-trait models for continuous and categorical characters. Journal of Evolutionary Biology 23, 494-508.
Hamrick, M.W., 1996a. Functional morphology of the Lemuriform wrist joints and the relationship between wrist morphology and positional behavior in arboreal primates. American Journal of Physical Anthropology 99, 319-344.
Hamrick, M.W., 1996b. Locomotor adaptations reflected in the wrist joints of early tertiary primates (Adapiformes). American Journal of Physical Anthropology 100, 585-604.
Hamrick, M.W., 1996c. Articular size and curvature as determinants of carpal joint mobility and stability in strepsirhine primates. Journal of Morphology 230, 113-127.
Hamrick, M.W., 1997. Functional osteology of the primate carpus with special reference to Strepsirhini. American Journal of Physical Anthropology 104, 105-116.
Hamrick, M.W., 1998. Functional and adaptive significance of primate pads and claws: evidence from New World anthropoids. American Journal of Physical Anthropology 106, 113-127.
Hamrick, M.W., 1999. Pattern and process in the evolution of primate nails and claws. Journal of Human Evolution 37, 293-297.
Hamrick, M.W., 2001. Development and evolution of the mammalian limb: adaptive diversification of nails, hooves, and claws. Evolution & Development 3, 355-363.
Hamrick, M.W., 2003. Evolution and development of mammalian limb integumentary structures. Journal of Experimental Zoology 298B, 152-163.
Hamrick, M.W., 2007. Evolvability, limb morphology, and primate origins, in: Ravosa, M.J., Dagosto, M. (Eds.), Primate Origins. Springer, New York, pp. 381-401.
Harcourt-Smith, W.E.H., Aiello, L.C., 2004. Fossils, feet and the evolution of human bipedal locomotion. Journal of Anatomy 204, 403-416.
Harrell, F.E., Jr., Dupont, C., 2016. Hmisc: Harrell miscellaneous. R package version 4.0-0.

Heinrich, R.E., Rose, M.D., Leakey, R.E., Walker, A.C., 1993. Hominid radius from the middle Pliocene of Lake Turkana, Kenya. American Journal of Physical Anthropology 92, 139-148.
Hinchliffe, J.R., 1994. Evolutionary developmental biology of the tetrapod limb. Development, 163-168.
Hinchliffe, J.R., 2002. Developmental basis of limb evolution. International Journal of Developmental Biology 46, 835-845.
Hoshino, J., 1985. Feeding ecology of mandrills (*Mandrillus sphinx*) in Campo animal reserve, Cameroon. Primates 26, 248-273.
Hothorn, T., Bretz, F., Westfall, P., 2008. Simultaneous inference in general parametric models. Biometrical Journal 50, 346-363.
Hunt, K.D., 1989. Positional Behavior in *Pan troglodytes* at the Mahale Mountains and the Gombe Stream National Parks, Tanzania. Ph.D. Dissertation, University of Michigan.
Hunt, K.D., 1991. Positional behavior in the Hominoidea. International Journal of Primatology 12, 95-18.
Hunt, K.D., 1992. Positional behavior of *Pan troglodytes* in the Mahale mountains and Gombe stream national parks, Tanzania. American Journal of Physical Anthropology 87, 83-105.
Hunt, K.D., Cant, J.G.H., Gebo, D.L., Rose, M.D., Walker, S.E., Youlatos, D., 1996. Standardized descriptions of primate locomotion and postural modes. Primates 37, 363-387.
Hunt, K., D., 2004. The special demands of great ape locomotion and posture, in: Russon, A.E., Begun, D.R. (Eds.), The Evolution of Thought. Cambridge University Press, Cambridge, pp. 172-189.
Hunt, K.D., 2016. Why are there apes? Evidence for the co-evolution of ape and monkey ecomorphology. Journal of Anatomy 228, 630-685.
Hunt, K.D., Cant, J.G.H., Gebo, D.L., Rose, M.D., Walker, S.E., Youlatos, D., 1996. Standardized descriptions of primate locomotion and postural modes. Primates 37, 363-387.
Inouye, S.E., 1992. Ontogeny and allometry of African ape manual rays. Journal of Human Evolution 23, 107-138.
Inouye, S.E., 1994a. Ontogeny of knuckle-walking hand postures in African apes. Journal of Human Evolution 26, 459-485.
Inouye, S.E., 1994b. The Ontogeny of Knuckle-walking Behavior and Associated Morphology in the African Apes. Ph.D. Dissertation, Northwestern University.
Inouye, S.E., Shea, B.T., 2004. The implications of variation in knuckle-walking features for models of African hominoid locomotor evolution. Journal of Anthropological Sciences 82, 67-88.
Isbell, L.A., Pruetz, J.D., Lewis, M., Young, T.P., 1998. Locomotor activity differences between sympatric patas monkeys (*Erythrocebus patas*) and vervet monkeys (*Cercopithecus aethiops*): implications for the evolution of long hindlimb length in *Homo*. American Journal of Physical Anthropology 105, 199-207.
Jenkins Jr., F.A., Fleagle, J.G., 1975. Knuckle-walking and the functional anatomy of the wrists in living apes, in: Tuttle, R.H. (Ed.), Primate Functional Morphology and Evolution. Mouton, The Hague, pp. 213-231.

Jenkins Jr., F.A., 1981. Wrist rotation in primates: A critical adaptation for brachiators. Symposia of the Zoological Society of London 48, 429-451.
Jouffroy, F.K., Medina, M.F., 2002. Radio-ulnar deviation of the primate carpus: An X-ray study. Zeitschrift fuer Morphologie und Anthropologie 83, 275-289.
Kawabe, M., Mano, T., 1972. Ecology and behavior of the wild proboscis monkey, *Nasalis larvatus* (Wurmb), in Sabeh, Malaysia. Primates 13, 213-228.
Kivell, T.L., 2011. A comparative analysis of the hominin triquetrum (SKX 3498) from Swartkrans, South Africa. South African Journal of Science 107, #515, 10 pages.
Kivell, T.L., 2016. The primate wrist, in: Kivell, T.L., Lemelin, P., Richmond, B.G., Schmitt, D. (Eds.), The Evolution of the Primate Hand. Springer, New York, pp. 17-54.
Kivell, T.L., Schmitt, D., 2009. Independent evolution of knuckle-walking in African apes shows that humans did not evolve from a knuckle-walking ancestor. Proceedings of the National Academy of Sciences 106, 14241-14246.
Kivell, T.L., Barros, A.P., Smaers, J.B., 2013. Different evolutionary pathways underlie the morphology of wrist bones in hominoids. BMC Evolutionary Biology 13, 229.
Klingenberg, C.P., 2009. Morphometric integration and modularity in configurations of landmarks: tools for evaluating *a priori* hypotheses. Evolution & Development 11, 405-421.
Kovarovic, K., Aiello, L.C., Cardini, A., Lockwood, C.A., 2011. Discriminant function analyses in archaeology: Are classification rates too good to be true? Journal of Archaeological Science 38, 3006-3018.
Kuhn, M., 2016. caret: classification and regression training. R package version 6.0-73.
Kuhn, M., Johnson, K., 2013. Applied Predictive Modeling. Springer, New York.
Larson, S.G., 1998. Parallel evolution in the hominoid trunk and forelimb. Evolutionary Anthropology 6, 87-99.
Le, K.Q., 2014. Positional Behavior and Support Use of the Tonkin Snub-nosed Monkeys (*Rhinopithecus avunculus*) in Khau Ca forest, Ha Giang Province, Vietnam. Ph.D. Dissertation, University of Colorado.
Le, S., Josse, J., Husson, F., 2008. FactoMineR: An R package for multivariate analysis. Journal of Statistical Software 25, 1-18.
Lemelin, P., Schmitt, D., 1998. The relation between hand morphology and quadrupedalism in primates. American Journal of Physical Anthropology 105, 185-197.
Lewis, O.J., 1965. Evolutionary change in the primate wrist and inferior radio-ulnar joints. The Anatomical Record 151, 275-286.
Lewis, O.J., 1969. The hominoid wrist joint. American Journal of Physical Anthropology 30, 251-268.
Lewis, O.J., 1971. Brachiation and the early evolution of the Hominoidea. Nature 230, 577-579.
Lewis, O.J., 1985a. Derived morphology of the wrist articulations and theories of hominoid evolution. Part I. The lorisine joints. Journal of Anatomy 140, 447-460.
Lewis, O.J., 1985b. Derived morphology of the wrist articulations and theories of hominoid evolution. Part II. The midcarpal joints of higher primates. Journal of Anatomy 142, 151-172.

Lewis, O.J., 1989. Functional Morphology of the Evolving Hand and Foot. Clarendon Press, Oxford.
Lewton, K.L., 2015. Pelvic form and locomotor adaptation in strepsirrhine primates. Anatomical Record 298, 230-248.
Lovejoy, C.O., Cohn, M.J., White, T.D., 1999. Morphological analysis of the mammalian postcranium: A developmental perspective. Proceedings of the National Academy of Sciences 96, 13247-13252.
Lovejoy, C.O., Heiple, K.G., Meindl, R.S., 2001. Reply to Richmond and Strait (2000). Nature 410, 325-326.
Lovejoy, C.O., Simpson, S.W., White, T.D., Asfaw, B., Suwa, G., 2009. Careful climbing in the Miocene: The forelimbs of *Ardipithecus ramidus* and humans are primitive. Science 326, 70e1-8.
MacConaill, M.A., 1941. The mechanical anatomy of the carpus and its bearings on some surgical problems. Journal of Anatomy 75, 166-175.
Martin, R.B., Burr, D.B., Sharkey, N.A., 1998. Skeletal Tissue Mechanics. Springer.
Marshall, A.J., Wrangham, R.W., 2007. Evolutionary consequences of fallback foods. International Journal of Primatology 28, 1219-1235.
Marzke, M.W., 1983. Joint functions and grips of the *Australopithecus afarensis* hand, with special reference to the region of the capitate. Journal of Human Evolution 12, 197-211.
Marzke, M.W., Marzke, R.F., 1987. The third metacarpal styloid process in humans: origin and functions. American Journal of Physical Anthropology 73, 415-431.
Marzke, M.W., Wullstein, K.L., Viegas, S.F., 1992. Evolution of the power ("squeeze") grip and its morphological correlates in hominids. American Journal of Physical Anthropology 89, 283-298.
Marzke, M.W., Wullstein, K.L., Viegas, S.F., 1994. Variability at the carpometacarpal and midcarpal joints involving the fourth metacarpal, hamate, and lunate in Catarrhini. American Journal of Physical Anthropology 93, 229-240.
Marzke, M.W., Tocheri, M.W., Steinberg, B., Femiani, J.D., Reece, S.P., Linscheid, R.L., Orr, C.M., Marzke, R.F., 2010. Comparative 3D quantitative analyses of trapeziometacarpal joint surface curvatures among living catarrhines and fossil hominins. American Journal of Physical Anthropology 141, 38-51.
Matarazzo, S., 2013a. Manual pressure distribution patterns of knuckle-walking apes. American Journal of Physical Anthropology 152, 44-50.
Matarazzo, S.A., 2013b. Knuckle-walking Signal in the Manual Phalanges and Metacarpals of the Great Apes (*Pan* and *Gorilla*). Ph.D. Dissertation, University of Massachusetts - Amherst.
McHenry, H.M., 1983. The capitate of *Australopithecus afarensis* and *A. africanus*. American Journal of Physical Anthropology 62, 187-198.
Mendel, F.C., 1979. The wrist joint of two-toed sloths and its relevance to brachiating adaptations in the Hominoidea. Journal of Morphology 162, 413-424.
Miller, A.J., 2002. Subset Selection in Regression, 2nd ed. CRC Press, New York.
Mittermeier, R.A., 1978. Locomotion and posture in *Ateles geoffroyi* and *Ateles paniscus*. Folia Primatologica 30, 161-193.

Mitteroecker, P., Bookstein, F., 2011. Linear discrimination, ordination, and the visualization of selection gradients in modern morphometrics. Evolutionary Biology 38, 100-114.
Nakagawa, N., 1989. Activity budget and diet of patas monkeys in Kala Maloue national-park, Cameroon - a preliminary-report. Primates 30, 27-34.
Nakatsukasa, M., Almécija, S., Begun, D.R., 2016. The hands of Miocene hominoids, in: Kivell, T.L., Lemelin, P., Richmond, B.G., Schmitt, D. (Eds.), The Evolution of the Primate Hand. Springer, New York, pp. 485-514.
Nowak, M.G., Reichard, U.H., 2016. The torso-orthograde positional behavior of wild white-handed gibbons (*Hylobates lar*), in: Reichard, U.H., Hirai, H., Barelli, C. (Eds.), Evolution of Gibbons and Siamang. Springer, New York, pp. 203-225.
O'Connor, B.L., Rarey, K.E., 1979. Normal amplitudes of radioulnar pronation and supination in several genera of anthropoid primates. American Journal of Physical Anthropology 51, 39-44.
Orme, D., Freckleton, R., Thomas, G., Petzoldt, T., Fritz, S., Isaac, N., Pearse, W., 2013. caper: comparative analyses of phylogenetics and evolution in R. R package version 0.5.2.
Orr, C.M., 2010. Adaptations to knuckle-walking and digitigrady: a three-dimensional kinematic and morphometric analysis of the anthropoid wrist. Ph.D. Dissertation, Arizona State University.
Orr, C.M., 2016. Functional morphology of the primate hand: Recent approaches using biomedical imaging, computer modeling, and engineering methods, in: Kivell, T.L., Lemelin, P., Richmond, B.G., Schmitt, D. (Eds.), The Evolution of the Primate Hand. Springer, New York, pp. 227-257.
Orr, C.M., 2017. Locomotor hand postures, carpal kinematics during wrist extension, and associated morphology in anthropoid primates. Anatomical Record 300, 382-401.
Orr, C.M., Atkinson, R., 2016. Carpal kinematics and morphological correlates of ulnar deviation mobility in anthropoids. American Journal of Physical Anthropology 159, 245-245.
Pagel, M., 1999. Inferring the historical patterns of biological evolution. Nature 401, 877-884.
Paradis, E., Claude, J., Strimmer, K., 2004. APE: analyses of phylogenetics and evolution in R language. Bioinformatics 20, 289-290.
Patel, B.A., 2009. Not so fast: speed effects on forelimb kinematics in cercopithecine monkeys and implications for digitigrade postures in primates. American Journal of Physical Anthropology 140, 92-112.
Patel, B.A., 2010a. Functional morphology of cercopithecoid primate metacarpals. Journal of Human Evolution 58, 320-337.
Patel, B.A., 2010b. The interplay between speed, kinetics, and hand postures during primate terrestrial locomotion. American Journal of Physical Anthropology 141, 222-234.
Patel, B.A., Carlson, K.J., 2007. Bone density spatial patterns in the distal radius reflect habitual hand postures adopted by quadrupedal primates. Journal of Human Evolution 52, 130-141.

Patel, B.A., Carlson, K.J., 2008. Apparent density patterns in subchondral bone of the sloth and anteater forelimb. Biology Letters 4, 486-489.
Patel, B.A., Wunderlich, R.E., 2010. Dynamic pressure patterns in the hands of olive baboons (*Papio anubis*) during terrestrial locomotion: implications for cercopithecoid primate hand morphology. The Anatomical record 293, 710-718.
Peters, A., Hothorn, T., 2015. ipred: Improved Predictors. R package version 0.9-5.
Pilbeam, D., 1996. Genetic and morphological records of the Hominoidea and hominid origins: a synthesis. Molecular Phylogenetics and Evolution 5, 155-168.
Polk, J.D., Williams, S.A., Peterson, J.V., Roseman, C.C., Godfrey, L.R., 2010. Subchondral bone apparent density and locomotor behavior in extant primates and subfossil lemurs *Hadropithecus* and *Pachylemur*. International Journal of Primatology 31, 275-299.
Polly, P.D., Lawing, A.M., Fabre, A.-C., Goswami, A., 2013. Phylogenetic principal components analysis and geometric morphometrics. Hystrix 24, 33-41.
Polo, M.E., Felicisimo, A.M., 2012. Analysis of uncertainty and repeatability of a low-cost 3D laser scanner. Sensors 12, 9046-9054.
Preuschoft, H., Godinot, M., Beard, K.C., Nieschalk, U., Jouffroy, F.K., 1993. Biomechanical considerations to explain important morphological characters of primate hands, in: Preuschoft, H., Chivers, D.J. (Eds.), Hands of Primates. Springer, pp. 245-256.
R Core Team, 2016. R: A language and environment for statistical computing. R Foundation for Statistical Computing, Vienna, Austria.
Remis, M.J., 1994. Feeding Ecology and Positional Behavior of Western Lowland Gorillas (*Gorilla gorilla gorilla*) in the Central African Republic. Ph.D. Dissertation, Yale University.
Richmond, B.G., 2006. Functional morphology of the midcarpal joint in knuckle-walkers and terrestrial quadrupeds, in: Ishida, H., Tuttle, R., Pickford, M., Ogihara, N., Nakatsukasa, M. (Eds.), Human Origins and Environmental Backgrounds. Springer, New York, pp. 105-122.
Richmond, B.G., Strait, D.S., 2000. Evidence that humans evolved from a knuckle-walking ancestor. Nature 404, 382-385.
Richmond, B.G., Begun, D.R., Strait, D.S., 2001. Origin of human bipedalism: The knuckle-walking hypothesis revisited. American Journal of Physical Anthropology Suppl 33, 70-105.
Richmond, B.G., Roach, N.T., Ostrofsky, K.R., 2016. Evolution of the early hominin hand, in: Kivell, T.L., Lemelin, P., Richmond, B.G., Schmitt, D. (Eds.), The Evolution of the Primate Hand. Springer, New York, pp. 515-543.
Ritter, G., 2015. Robust Cluster Analysis and Variable Selection. CRC Press, New York.
Robertson, M.L., 1984. The Carpus of *Proconsul africanus*: Functional Analysis and Comparison with Selected Nonhuman Primates. Ph.D. Dissertation, University of Michigan.
Rohlf, F.J., Corti, M., 2000. Use of two-block partial least-squares to study covariation in shape. Systematic Biology 49, 740-753.
Rose, M.D., 1984. Hominoid postcranial specimens from the middle Miocene Chinji formation, Pakistan. Journal of Human Evolution 13, 503-516.

Rose, M.D., 1988. Another look at the anthropoid elbow. Journal of Human Evolution 17, 193-224.
Rose, M.D., 1993. Locomotor anatomy of Miocene hominoids, in: Gebo, D.L. (Ed.), Postcranial Adaptation in Nonhuman Primates. Northern Illinois University Press, DeKalb, pp. 252-272.
Rose, M.D., 1996. Functional morphological similarities in the locomotor skeleton of Miocene catarrhines and platyrrhine monkeys. Folia Primatologica 66, 7-14.
Rose, M.D., 1997. Functional and phylogenetic features of the forelimb in Miocene hominoids, in: Begun, D.R., Ward, C.V., Rose, M.D. (Eds.), Function, Phylogeny, and Fossils: Miocene Hominoid Evolution and Adaptations. Plenum Press, New York, pp. 79-100.
RStudio Team, 2016. RStudio: Integrated Development for R. RStudio, Inc., Boston, MA.
Sabater Pi, J., 1972. Contribution to the ecology of *Mandrillus sphinx* of Rio Muni (Republic of Equatorial Guinea). Folia Primatologica 17, 304-319.
Sanchez, P.M., 1974. The unequal group size problem in discriminant analysis. Journal of the Academy of Marketing Science 2, 629-633.
Sarmiento, E.E., 1985. Functional Differences in the Skeleton of Wild and Captive Orangutans and their Adaptive Significance. Ph.D. Dissertation, New York University.
Sarmiento, E.E., 1988. Anatomy of the hominoid wrist joint: its evolutionary and functional implications. International Journal of Primatology 9, 281-345.
Sarmiento, E.E., 1994. Terrestrial traits in the hands and feet of gorillas. American Museum Novitates 3091, 1-56.
Sarmiento, E.E., 2002. Forearm rotation and the "origin of the hominoid lifestyle": a reply to Stern and Larson (2001). American Journal of Physical Anthropology 119, 92-94.
Sarringhaus, L.A., MacLatchy, L.M., Mitani, J.C., 2014. Locomotor and postural development of wild chimpanzees. Journal of Human Evolution 66, 29-38.
Sati, J.P., Alfred, J.R.B., 2002. Locomotion and posture in hoolock gibbon. Annals of Forestry 10, 298-306.
Schmitt, D., Hanna, J.B., 2004. Substrate alters forelimb to hindlimb peak force ratios in primates. Journal of Human Evolution 46, 239-254.
Schmitt, D., Zeininger, A., Granatosky, M.C., 2016. Patterns, variability, and flexibility of hand posture during locomotion in primates, in: Kivell, T.L., Lemelin, P., Richmond, B.G., Schmitt, D. (Eds.), The Evolution of the Primate Hand. Springer, New York, pp. 345-369.
Selby, M.S., Simpson, S.W., Lovejoy, C.O., 2016. The functional anatomy of the carpometacarpal complex in anthropoids and its implications for the evolution of the hominoid hand. Anatomical Record 299, 583-600.
Selby, M.S., Lovejoy, C.O., 2017. Evolution of the hominoid scapula and its implications for earliest hominid locomotion. American Journal of Physical Anthropology 162, 682-700.
Shapiro, S.S., Wilk, M.B., 1965. An analysis of variance test for normality (complete samples). Biometrika 52, 591-611.

Shubin, N., Tabin, C., Carroll, S., 1997. Fossils, genes and the evolution of animal limbs. Nature 388, 639-648.
Slizewski, A., Friess, M., Semal, P., 2010. Surface scanning of anthropological specimens: nominal-actual comparison with low cost laser scanner and high end fringe light projection surface scanning systems. Quartar 57, 179-187.
Smith, R.J., Jungers, W.L., 1997. Body mass in comparative primatology. Journal of Human Evolution 32, 523-559.
Smith, R.J., 2016. Explanations for adaptations, just-so stories, and limitations on evidence in evolutionary biology. Evolutionary Anthropology 25, 276-287.
Spoor, C.F., Sondaar, P.Y., Hussain, S.T., 1991. A new hominoid hamate and first metacarpal from the late Miocene Nagri formation of Pakistan. Journal of Human Evolution 21, 413-424.
Straus, J., William L., 1949. The riddle of man's ancestry. The Quarterly Review of Biology 24, 200-223.
Susman, R.L., Stern, J.T., Jr., 1979. Telemetered electromyography of flexor digitorum profundus and flexor digitorum superficialis in *Pan troglodytes* and implications for interpretation of the OH 7 hand. American Journal of Physical Anthropology 50, 565-574.
Swartz, S.M., Bertram, J.E.A., Biewener, A.A., 1989. Telemetered in vivo strain analysis of locomotor mechanics of brachiating gibbons. Nature 342, 270-272.
Tallman, M., 2012. Morphology of the distal radius in extant hominoids and fossil hominins: implications for the evolution of bipedalism. The Anatomical Record 295, 454-464.
Thorpe, S.K., Crompton, R.H., 2006. Orangutan positional behavior and the nature of arboreal locomotion in Hominoidea. American Journal of Physical Anthropology 131, 384-401.
Throckmorton, Z.J., 2013. Variation and Non-adaptive Evolution of the Hominin Foot. Ph.D. Dissertation, University of Wisconsin.
Tibshirani, R., 1996. Regression shrinkage and selection via the lasso. Journal of the Royal Statistical Society B 58, 267-288.
Tocheri, M.W., Marzke, M.W., Liu, D., Bae, M., Jones, G.P., Williams, R.C., Razdan, A., 2003. Functional capabilities of modern and fossil hominid hands: three-dimensional analysis of trapezia. American Journal of Physical Anthropology 122, 101-112.
Tocheri, M.W., Razdan, A., Williams, R.C., Marzke, M.W., 2005. A 3D quantitative comparison of trapezium and trapezoid relative articular and nonarticular surface areas in modern humans and great apes. Journal of Human Evolution 49, 570-586.
Tocheri, M.W., Solhan, C.R., Orr, C.M., Femiani, J., Frohlich, B., Groves, C.P., Harcourt-Smith, W.E., Richmond, B.G., Shoelson, B., Jungers, W.L., 2011. Ecological divergence and medial cuneiform morphology in gorillas. Journal of Human Evolution 60, 171-184.
Tsegai, Z.J., Kivell, T.L., Gross, T., Nguyen, N.H., Pahr, D.H., Smaers, J.B., Skinner, M.M., 2013. Trabecular bone structure correlates with hand posture and use in hominoids. PLoS One 8, e78781.

Tukey, J.W., 1949. Comparing Individual Means in the Analysis of Variance. Biometrics 5, 99-114.
Tuttle, R.H., 1967. Knuckle-walking and the evolution of hominoid hands. American Journal of Physical Anthropology 26, 171-206.
Tuttle, R.H., 1969. Quantitative and functional studies on the hands of the Anthropoidea. I. The Hominoidea. Journal of Morphology 128, 309-364.
Venables, W.N., Ripley, B.D., 2002. Modern Applied Statistics with S. 4th edition. Springer, New York.
Venkataraman, V.V., Kraft, T.S., DeSilva, J.M., Dominy, N.J., 2013. Phenotypic plasticity of climbing-related traits in the ankle joint of great apes and rainforest hunter-gatherers. Human Biology 85, 309-328.
Vilensky, J.A., Larson, S.G., 1989. Primate locomotion: utilization and control of symmetrical gaits. Annual Review of Anthropology 18, 17-35.
Walker, S.E., 1998. Fine-grained differences within positional categories: a case study of *Pithecia* and *Chiropotes*, in: Strasser, E., Fleagle, J., Rosenberger, A., McHenry, H. (Eds.), Primate Locomotion: Recent Advances. Springer, pp. 31-43.
Ward, C.V., 1998. *Afropithecus*, *Proconsul*, and the primitive hominoid skeleton, in: Strasser, E., Fleagle, J., Rosenberger, A., McHenry, H. (Eds.), Primate Locomotion: Recent Advances. Springer, pp. 337-352.
Ward, C.V., 2015. Postcranial and locomotor adaptations of hominoids, in: Henke, W., Tattersall, I. (Eds.), Handbook of Paleoanthropology. Springer-Verlag, Berlin, pp. 1363-1386.
Ward, C.V., Kimbel, W.H., Harmon, E.H., Johanson, D.C., 2012. New postcranial fossils of *Australopithecus afarensis* from Hadar, Ethiopia (1990-2007). Journal of Human Evolution 63, 1-51.
Wheatley, B.P., 1982. Energetics of foraging in *Macaca fascicularis* and *Pongo pygrnaeus* and a selective advantage of large body size in the orang-utan. Primates 23, 348-363.
Wickham, H., 2009. Elegant Graphics for Data Analysis. Springer-Verlag, New York.
Whitehead, P.F., 1993. Aspects of the anthropoid wrist and hand, in: Gebo, D.L. (Ed.), Postcranial adaptation in nonhuman primates. Northern Illinois University Press, DeKalb, pp. 96-120.
Worthington, S., 2016. Anthropoid morphometric and phylogenetic data, with R replication code [Data set], BMC Evolutionary Biology. Zenodo.
Wright, K.A., 2007. The relationship between locomotor behavior and limb morphology in brown (*Cebus apella*) and weeper (*Cebus olivaceus*) capuchins. American Journal of Primatology. 69, 736-756.
Wright, K.A., Stevens, N.J., Covert, H.H., Nadler, T., 2008. Comparisons of suspensory behaviors among *Pygathrix cinerea*, *P. nemaeus*, and *Nomascus leucogenys* in Cuc Phuong National Park, Vietnam. International Journal of Primatology 29, 1467-1480.
Youlatos, D., 1998. Positional behavior of two sympatric Guianan capuchin monkeys, the brown capuchin (*Cebus apella*) and the wedge-capped capuchin *(Cebus olivaceus*). Mammalia 62, 351-365.

Youlatos, D., Guillot, D., 2015. Howler monkey positional behavior, in: Kowalewski, M.M., Garber, P.A., Cortés-Ortiz, L., Urbani, B., Youlatos, D. (Eds.), Howler Monkeys. Springer, New York, pp. 191-218.
Young, R.W., 2003. Evolution of the human hand: the role of throwing and clubbing. Journal of Anatomy 202, 165-174.
Zhao, C., Zhao, K.D., Babb, A., An, K.-N., 2013. Biomechanics of the wrist and hand, in: Winkelstein, B.A. (Ed.), Orthopaedic Biomechanics. CRC Press, Boca Raton, pp. 233-264.
Zylstra, M., 1999. Functional morphology of the hominoid forelimb: implications for knuckle-walking and the origin of hominid bipedalism. Ph.D., University of Toronto.

Supplementary material

Table 2.8. Covariance of shape variables with positional classes relative to the reference class. Results based on univariate phylogenetic generalized least squares (PGLS) of taxon means except where noted

a *KW* & *S* vs pronograde monkeys

			KW						*S*					
	R^2	λ	b	p	OR^a	p^a	OR^b	p^b	b	p	OR^a	p^a	OR^b	p^b
CpPx	0.17	0.83	0.68	0.36	0.41	0.81	0.23	0.84	-0.62	0.27	-1.77	0.23	-0.53	0.65
CpDn	0.01	0.99	-0.48	0.68	0.27	0.87	0.27	0.78	-0.41	0.63	-0.57	0.66	-0.39	0.69
Cp2	0.18	0.99	-1.61	**0.04**	-1.38	0.38	-0.74	0.53	-1.02	0.07	-2.32	0.15	-0.53	0.64
Cp4	0.15	1.00	-1.46	0.05	-2.21	0.18	-2.49	0.07	-0.41	0.45	0.82	0.59	0.77	0.53
Cp23A	0.11	0.92	-0.48	0.60	-0.86	0.56	-0.86	0.42	0.69	0.33	1.81	0.18	0.72	0.49
CpPxA	0.67	0.80	0.29	0.49	1.32	0.41	1.12	0.37	-1.70	**0.00**	-3.74	**0.01**	-2.52	**0.04**
CpScA	0.18	1.00	0.15	0.81	0.45	0.78	1.06	0.37	-0.81	0.09	-2.07	0.14	-1.43	0.23
Cp3SD	0.06	0.72	0.84	0.34	0.59	0.70	0.11	0.93	-0.07	0.91	-0.22	0.86	0.03	0.99
CpHmC	0.35	1.00	0.21	0.75	1.09	0.50	0.31	0.81	-1.33	**0.01**	-3.24	**0.03**	-1.65	0.20
CpHP	0.29	0.42	-1.61	**0.01**	-2.01	0.16	-1.30	0.29	-0.27	0.57	0.43	0.76	0.13	0.92
HmPx	0.13	0.98	-0.84	0.39	-0.89	0.58	-0.11	0.92	0.59	0.41	1.30	0.36	0.28	0.81
Hm5	0.41	0.93	-1.27	**0.02**	-2.13	0.14	-1.29	0.30	-1.60	**0.00**	-2.78	0.06	-0.73	0.55
Hm45A	0.22	0.00	0.43	0.32	-0.65	0.63	-0.41	0.71	1.13	**0.01**	1.57	0.24	0.61	0.58
HmPxA	0.10	0.93	0.57	0.51	-0.06	0.96	0.01	0.98	-0.54	0.41	-1.49	0.29	-0.55	0.63
CpHmPxA	0.50	0.98	0.48	0.35	1.36	0.43	2.36	0.08	-1.26	**0.00**	-3.70	**0.02**	-3.39	**0.01**
CMC34A	0.20	0.47	1.40	**0.02**	0.99	0.53	0.65	0.57	0.35	0.48	-0.04	0.99	-0.01	1.00
LuDs	0.33	0.75	1.65	**0.01**	2.11	0.16	2.10	0.09	0.06	0.89	-0.76	0.62	-0.89	0.44
LuTq	0.63	0.00	0.31	0.30	1.30	0.41	0.57	0.59	-1.68	**0.00**	-3.46	**0.04**	-0.90	0.39
LuSc	0.19	0.98	-1.40	**0.03**	-1.68	0.28	-1.18	0.33	-0.35	0.45	0.34	0.83	0.04	0.98
LuRa	0.14	0.98	0.64	0.46	1.57	0.31	0.42	0.71	-0.70	0.28	-1.95	0.18	-0.46	0.67
LuDsTqA	0.80	0.00	-0.79	**0.00**	-1.84	0.22	-3.50	**0.02**	1.63	**0.00**	3.03	**0.05**	3.38	**0.01**
LuDsScA	0.21	0.83	0.31	0.65	0.93	0.54	0.49	0.66	-0.94	0.09	-2.70	0.08	-0.72	0.53
LuScRaA	0.19	0.81	-0.17	0.81	0.44	0.80	0.44	0.69	-1.11	0.05	-2.63	0.09	-0.91	0.42
LuCpRaA	0.69	0.00	-1.93	**0.00**	-2.59	0.10	-3.12	**0.02**	-1.13	**0.00**	-0.68	0.64	0.80	0.53
LuCpC	0.65	0.00	0.79	**0.01**	-0.03	0.99	-0.30	0.77	1.93	**0.00**	3.20	**0.03**	0.87	0.41
TqHm	0.11	0.87	0.43	0.47	0.55	0.70	0.02	0.98	0.78	0.09	2.10	0.15	0.99	0.43
TqLu	0.08	0.97	0.77	0.24	1.08	0.48	0.26	0.86	0.00	0.99	0.18	0.91	0.36	0.77
TqPi	0.45	0.69	0.91	0.10	1.96	0.22	1.11	0.34	-1.02	**0.03**	-2.99	0.06	-1.17	0.31

TqSt	0.31	1.00	-1.01	**0.01**	-1.40	0.36	-1.15	0.44	-0.76	**0.01**	-1.96	0.19	-0.81	0.58
TqHmPiA	0.44	0.61	0.93	0.07	0.00	0.99	-0.95	0.48	1.78	**0.00**	3.48	**0.02**	2.14	0.10
Tq1LuA	0.75	0.00	-1.20	**0.00**	-1.89	0.22	-2.55	**0.05**	1.21	**0.00**	2.91	**0.04**	2.23	0.06
LuTqDsA	0.40	0.81	0.52	0.37	0.93	0.60	0.85	0.49	-1.18	**0.01**	-3.25	**0.04**	-1.74	0.16
MCJAR	0.32	0.81	-0.20	0.75	-1.33	0.44	-0.95	0.46	1.23	**0.02**	3.25	**0.04**	1.62	0.19

Without hylobatids

			KW						*S*					
	R^2	λ	b	p	OR^a	p^a	OR^b	p^b	b	p	OR^a	p^a	OR^b	p^b
CpPx	0.03	0.57	0.46	0.56	0.52	0.69	0.47	0.67	-0.19	0.79	-0.56	0.69	-0.13	0.91
CpDn	0.06	0.98	-0.30	0.76	0.79	0.60	0.22	0.83	-0.88	0.26	-2.10	0.14	-0.54	0.59
Cp2	0.18	0.99	-1.54	0.05	-1.60	0.32	-0.75	0.52	-0.97	0.11	-1.73	0.25	-0.46	0.69
Cp4	0.28	1.00	-1.38	**0.01**	-2.58	0.13	-2.56	**0.05**	-0.88	**0.04**	-0.02	0.98	0.56	0.65
Cp23A	0.03	0.95	-0.48	0.69	-0.94	0.50	-0.92	0.38	0.40	0.67	1.06	0.44	0.49	0.63
CpPxA	0.71	0.00	0.42	0.12	1.28	0.37	0.93	0.40	-2.29	**0.00**	-2.85	**0.03**	-1.85	0.10
CpScA	0.07	1.00	0.02	0.98	0.43	0.76	1.06	0.39	-0.63	0.31	-1.34	0.33	-1.17	0.33
Cp3SD	0.04	0.92	0.89	0.39	0.84	0.57	0.26	0.81	0.42	0.61	0.03	0.98	0.22	0.84
CpHmC	0.30	0.95	0.07	0.93	1.21	0.43	0.38	0.74	-1.54	**0.02**	-2.32	0.09	-1.07	0.35
CpHP	0.30	0.51	-1.62	**0.01**	-2.52	0.08	-1.40	0.22	-0.78	0.15	-0.56	0.68	-0.02	0.99
HmPx	0.08	0.96	-0.83	0.37	-0.99	0.51	-0.27	0.81	0.27	0.70	0.69	0.63	0.09	0.95
Hm5	0.83	0.00	-1.91	**0.00**	-2.65	**0.05**	-1.07	0.36	-1.51	**0.00**	-1.84	0.19	-0.46	0.69
Hm45A	0.46	0.00	0.42	0.25	-0.77	0.60	-0.46	0.68	2.07	**0.00**	2.28	0.10	0.78	0.48
HmPxA	0.13	0.00	-0.71	0.13	0.03	0.99	0.18	0.86	-0.70	0.27	-0.27	0.83	-0.17	0.88
CpHmPxA	0.51	0.92	0.63	0.38	0.83	0.57	1.65	0.17	-1.94	**0.00**	-2.86	**0.04**	-2.35	**0.04**
CMC34A	0.24	0.44	1.36	**0.02**	1.27	0.40	0.66	0.57	0.68	0.21	0.48	0.73	-0.01	1.00
LuDs	0.81	0.00	1.94	**0.00**	2.79	0.07	2.18	0.07	-0.04	0.89	-1.56	0.31	-1.22	0.29
LuTq	0.36	0.00	0.43	0.28	1.39	0.35	0.67	0.53	-1.53	**0.01**	-2.57	0.07	-0.69	0.51
LuSc	0.27	0.94	-1.30	**0.01**	-2.34	0.13	-1.29	0.29	-0.82	**0.05**	-1.05	0.49	-0.23	0.84
LuRa	0.06	0.96	0.60	0.52	1.98	0.20	0.56	0.61	-0.33	0.65	-1.09	0.45	-0.22	0.84
LuDsTqA	0.54	0.90	-1.53	**0.02**	-2.04	0.18	-3.46	**0.01**	1.20	**0.03**	2.17	0.11	2.77	**0.03**
LuDsScA	0.08	0.46	0.15	0.83	0.92	0.48	0.55	0.61	-0.74	0.30	-1.61	0.26	-0.41	0.70
LuScRaA	0.10	0.63	-0.52	0.51	0.31	0.86	0.46	0.67	-1.05	0.15	-1.89	0.19	-0.65	0.53
LuCpRaA	0.75	0.00	-1.93	**0.00**	-3.32	**0.03**	-3.64	**0.01**	-0.53	0.12	0.75	0.63	1.19	0.35
LuCpC	0.56	0.00	1.03	**0.00**	0.09	0.89	-0.34	0.76	2.07	**0.00**	2.55	0.08	0.68	0.51
TqHm	0.10	0.78	0.78	0.20	0.76	0.59	-0.01	0.99	0.65	0.21	1.21	0.41	0.80	0.52
TqLu	0.06	0.97	0.64	0.27	1.32	0.38	0.37	0.78	0.22	0.62	0.32	0.83	0.50	0.70

TqPi	0.62	0.00	1.54	**0.00**	2.17	0.14	1.11	0.30	-0.59	0.17	-1.97	0.22	-0.64	0.56
TqSt	0.32	1.00	-1.10	**0.01**	-2.02	0.21	-1.46	0.33	-0.62	**0.04**	-0.81	0.58	-0.44	0.76
TqHmPiA	0.53	0.64	0.90	0.07	0.04	0.96	-0.82	0.54	2.07	**0.00**	3.09	**0.03**	2.18	0.08
Tq1LuA	0.74	0.00	-1.24	**0.00**	-1.97	0.19	-2.58	**0.05**	1.53	**0.00**	2.42	0.10	2.28	0.07
LuTqDsA	0.29	0.49	0.34	0.58	0.73	0.63	0.88	0.44	-1.37	**0.03**	-2.20	0.12	-1.20	0.30
MCJAR	0.35	0.76	-0.14	0.85	-0.74	0.60	-0.58	0.57	1.80	**0.01**	2.54	0.07	0.90	0.37

b *DG* & *KW* vs palmigrade-capable

			DG						*KW*					
	R^2	λ	b	p	OR^a	p^a	OR^b	p^b	b	p	OR^a	p^a	OR^b	p^b
CpPx	0.14	0.86	0.20	0.62	1.91	0.15	0.84	0.41	1.18	0.06	0.44	0.70	0.00	0.99
CpDn	0.01	0.99	0.27	0.56	1.94	0.10	0.92	0.30	-0.14	0.88	-0.52	0.75	-1.24	0.20
Cp2	0.16	0.99	0.51	0.10	2.49	0.06	1.67	0.18	-0.76	0.21	-1.50	0.31	-1.85	0.16
Cp4	0.14	1.00	-0.14	0.62	0.17	0.91	1.06	0.41	-1.13	0.07	-2.56	0.10	-3.16	**0.03**
Cp23A	0.18	0.93	-0.77	0.07	-2.03	0.08	-0.69	0.54	-1.05	0.15	-0.85	0.51	-0.59	0.61
CpPxA	0.25	0.96	-0.16	0.60	0.39	0.73	0.00	0.99	1.58	**0.01**	2.07	0.15	0.55	0.65
CpScA	0.15	1.00	-0.35	0.18	-0.67	0.62	-0.45	0.71	0.80	0.14	0.78	0.59	0.47	0.71
Cp3SD	0.06	0.78	-0.19	0.73	0.49	0.67	0.19	0.86	0.89	0.23	0.52	0.71	0.05	0.96
CpHmC	0.18	1.00	0.26	0.38	2.34	0.09	1.86	0.15	1.30	**0.04**	1.07	0.45	-0.12	0.94
CpHP	0.50	0.00	0.74	0.12	1.28	0.27	0.79	0.44	-1.41	**0.00**	-2.32	0.08	-1.90	0.09
HmPx	0.16	0.98	-0.48	0.23	-2.17	0.10	-1.26	0.27	-1.34	0.09	-1.14	0.40	0.13	0.90
Hm5	0.07	0.99	0.39	0.19	2.22	0.11	1.39	0.21	0.03	0.96	-1.22	0.38	-2.01	0.10
Hm45A	0.11	0.61	-0.80	0.17	-2.30	0.05	-0.97	0.32	-0.71	0.28	-0.90	0.37	0.49	0.63
HmPxA	0.10	0.96	0.36	0.36	1.71	0.18	1.30	0.27	1.04	0.16	0.22	0.86	-0.38	0.75
CpHmPxA	0.26	0.99	0.05	0.83	1.15	0.42	1.00	0.41	1.50	**0.01**	1.53	0.34	-0.15	0.90
CMC34A	0.31	0.46	-0.93	**0.04**	-2.55	**0.05**	-2.16	0.07	1.11	**0.02**	1.26	0.37	2.30	0.07
LuDs	0.52	0.56	-0.79	**0.02**	-2.20	0.08	-1.44	0.19	1.56	**0.00**	2.59	**0.04**	2.35	**0.05**
LuTq	0.26	0.72	0.70	0.12	2.13	0.08	0.50	0.61	1.40	**0.02**	1.76	0.15	0.66	0.50
LuSc	0.17	0.98	0.03	0.92	1.12	0.47	1.15	0.36	-1.12	**0.03**	-2.55	0.07	-2.82	**0.04**
LuRa	0.10	0.99	0.00	1.00	0.79	0.49	0.00	0.99	1.20	0.11	1.87	0.20	1.20	0.27
LuDsTqA	0.38	0.98	-0.33	0.25	-1.61	0.15	0.05	0.98	-2.02	**0.00**	-2.91	**0.02**	-2.62	**0.05**
LuDsScA	0.15	0.87	0.46	0.24	2.02	0.10	0.50	0.59	1.06	0.09	1.08	0.39	0.50	0.60
LuScRaA	0.04	0.90	-0.01	0.98	0.42	0.74	0.31	0.76	0.71	0.30	-0.14	0.94	-0.50	0.63
LuCpRaA	0.51	0.98	-1.25	**0.00**	-1.14	0.37	-0.21	0.87	-1.14	**0.04**	-2.92	**0.03**	-2.95	**0.02**
LuCpC	0.11	0.78	-0.56	0.21	-2.70	**0.05**	-1.38	0.20	-0.75	0.22	-0.38	0.74	1.15	0.31

TqHm	0.04	0.93	-0.29	0.34	-2.34	0.11	-2.13	0.09	-0.21	0.69	0.78	0.61	2.19	0.08
TqLu	0.08	0.97	0.05	0.86	-0.77	0.61	-1.43	0.24	0.77	0.15	2.31	0.12	2.39	0.06
TqPi	0.27	0.85	-0.19	0.61	-0.05	0.98	-0.39	0.71	1.64	**0.01**	2.68	0.07	1.41	0.20
TqSt	0.12	1.00	0.20	0.19	1.74	0.25	2.79	0.07	-0.39	0.22	-2.00	0.18	-3.43	**0.03**
TqHmPiA	0.05	0.91	0.26	0.54	-0.80	0.53	-0.71	0.55	-0.63	0.36	-0.36	0.73	1.07	0.37
Tq1LuA	0.62	0.62	-1.03	**0.01**	-2.58	**0.01**	-0.84	0.47	-2.22	**0.00**	-3.03	**0.00**	-1.66	0.17
LuTqDsA	0.26	0.90	0.42	0.23	2.49	0.07	1.63	0.16	1.49	**0.01**	1.09	0.39	0.02	0.99
MCJAR	0.12	0.92	0.14	0.71	-0.11	0.93	-0.09	0.95	-1.13	0.09	-1.63	0.33	-0.39	0.77

Without hylobatids

			DG						*KW*					
	R^2	λ	b	p	OR^a	p^a	OR^b	p^b	b	p	OR^a	p^a	OR^b	p^b
CpPx	0.06	0.51	0.48	0.41	1.65	0.18	0.61	0.56	0.56	0.39	0.37	0.72	-0.08	0.94
CpDn	0.03	0.98	0.32	0.46	2.19	0.08	1.02	0.28	0.31	0.72	-0.24	0.91	-1.09	0.27
Cp2	0.17	0.99	0.48	0.13	2.49	0.09	1.69	0.18	-0.85	0.20	-1.66	0.27	-1.85	0.16
Cp4	0.12	1.00	-0.14	0.54	0.52	0.71	1.36	0.31	-0.79	0.12	-2.66	0.09	-3.07	**0.04**
Cp23A	0.18	0.93	-0.94	0.06	-1.91	0.09	-0.59	0.61	-0.79	0.38	-0.84	0.48	-0.55	0.65
CpPxA	0.21	0.86	-0.33	0.50	-0.10	0.97	-0.15	0.87	1.75	**0.04**	1.96	0.12	0.37	0.72
CpScA	0.13	1.00	-0.48	0.12	-1.56	0.27	-0.73	0.51	0.43	0.52	0.51	0.70	0.20	0.87
Cp3SD	0.06	0.96	-0.41	0.38	0.21	0.83	0.13	0.90	0.60	0.52	0.45	0.77	0.00	0.99
CpHmC	0.13	0.98	0.42	0.29	2.47	**0.03**	1.45	0.23	1.15	0.16	1.31	0.30	-0.03	0.96
CpHP	0.56	0.00	0.91	0.05	1.63	0.19	0.90	0.39	-1.31	**0.00**	-2.20	0.10	-1.76	0.12
HmPx	0.18	0.93	-0.59	0.13	-2.11	0.12	-1.05	0.35	-1.04	0.16	-1.22	0.38	0.15	0.89
Hm5	0.14	0.96	0.46	0.17	2.10	0.13	1.17	0.26	-0.72	0.27	-1.95	0.17	-1.97	0.10
Hm45A	0.17	0.76	-0.78	0.15	-2.52	**0.04**	-1.01	0.32	-1.10	0.15	-1.02	0.35	0.42	0.70
HmPxA	0.12	0.00	0.64	0.31	1.44	0.22	0.89	0.41	-0.47	0.31	0.15	0.89	-0.36	0.73
CpHmPxA	0.22	0.97	0.06	0.88	0.88	0.44	0.50	0.63	1.98	**0.02**	1.55	0.20	-0.18	0.87
CMC34A	0.28	0.69	-0.87	**0.04**	-2.69	**0.04**	-2.23	0.08	0.89	0.10	1.27	0.36	2.18	0.08
LuDs	0.89	0.00	-0.82	**0.00**	-2.26	0.09	-1.47	0.19	1.80	**0.00**	2.94	**0.04**	2.28	0.06
LuTq	0.25	0.20	1.08	0.06	2.16	0.05	0.36	0.70	1.01	0.05	1.90	0.09	0.58	0.54
LuSc	0.10	0.97	0.05	0.85	1.48	0.34	1.30	0.29	-0.74	0.14	-2.39	0.10	-2.53	0.05
LuRa	0.05	0.96	0.02	0.96	0.51	0.66	-0.20	0.83	0.83	0.31	1.89	0.19	1.02	0.33
LuDsTqA	0.44	0.96	-0.44	0.17	-1.54	0.15	0.06	0.97	-2.36	**0.00**	-3.02	**0.01**	-2.36	0.07
LuDsScA	0.18	0.33	1.10	0.06	1.85	0.07	0.29	0.74	0.57	0.31	1.21	0.24	0.37	0.71
LuScRaA	0.01	0.77	-0.15	0.78	-0.05	0.96	0.19	0.84	0.16	0.84	-0.38	0.76	-0.49	0.60
LuCpRaA	0.69	0.95	-1.25	**0.00**	-1.88	0.15	-0.20	0.88	-1.59	**0.00**	-3.63	**0.01**	-2.95	**0.03**

LuCpC	0.11	0.66	-0.73	0.15	-2.70	**0.04**	-1.20	0.25	-0.36	0.58	-0.32	0.76	1.04	0.34
TqHm	0.06	0.87	-0.34	0.33	-2.34	0.13	-1.75	0.16	0.28	0.62	1.19	0.40	2.10	0.10
TqLu	0.05	0.97	0.04	0.88	-0.99	0.52	-1.58	0.20	0.50	0.33	2.18	0.18	2.16	0.08
TqPi	0.59	0.00	-0.27	0.53	-1.02	0.50	-0.55	0.58	1.59	**0.00**	2.61	**0.05**	0.99	0.31
TqSt	0.22	1.00	0.20	0.20	1.76	0.27	2.81	0.07	-0.67	0.05	-2.32	0.14	-3.63	**0.02**
TqHmPiA	0.05	0.90	0.27	0.52	-0.52	0.69	-0.67	0.58	-0.54	0.46	-0.11	0.90	0.99	0.42
Tq1LuA	0.60	0.68	-1.04	**0.01**	-2.55	**0.02**	-0.76	0.51	-2.29	**0.00**	-3.06	**0.01**	-1.65	0.17
LuTqDsA	0.22	0.69	0.74	0.15	2.71	**0.03**	1.21	0.26	1.30	0.06	1.29	0.23	0.03	0.99
MCJAR	0.15	0.88	0.53	0.29	1.00	0.41	0.15	0.85	-1.28	0.14	-1.22	0.28	-0.19	0.88

c *S* & vertical manus vs *PG*

			S						*VM*					
	R^2	λ	b	p	OR^a	p^a	OR^b	p^b	b	p	OR^a	p^a	OR^b	p^b
CpPx	0.18	0.81	-0.80	0.11	-2.32	0.06	-0.72	0.47	0.30	0.41	0.81	0.51	0.65	0.51
CpDn	0.01	0.99	-0.12	0.87	-0.13	0.91	-0.29	0.73	0.17	0.70	1.27	0.24	0.59	0.49
Cp2	0.04	0.99	-0.22	0.67	-2.32	0.07	-0.53	0.62	0.23	0.46	0.54	0.67	0.47	0.66
Cp4	0.06	1.00	0.08	0.87	0.94	0.47	0.24	0.84	-0.31	0.27	-1.15	0.39	-0.98	0.40
Cp23A	0.22	0.90	0.56	0.31	1.15	0.29	0.34	0.72	-0.72	0.06	-2.21	0.07	-1.47	0.14
CpPxA	0.66	0.82	-1.89	**0.00**	-4.16	**0.00**	-2.99	**0.01**	-0.12	0.56	0.57	0.68	0.62	0.58
CpScA	0.24	1.00	-1.02	**0.01**	-2.42	**0.02**	-1.25	0.26	-0.31	0.18	-0.42	0.70	0.10	0.93
Cp3SD	0.03	0.71	-0.41	0.51	-0.67	0.52	-0.35	0.74	0.13	0.79	0.73	0.53	0.26	0.80
CpHmC	0.38	1.00	-1.31	**0.00**	-3.43	**0.01**	-1.72	0.16	0.23	0.34	2.27	0.11	1.03	0.39
CpHP	0.02	0.86	0.19	0.76	0.06	0.93	-0.06	0.96	-0.22	0.62	-0.15	0.92	-0.12	0.91
HmPx	0.17	0.98	0.71	0.22	1.45	0.25	0.35	0.74	-0.52	0.16	-2.02	0.13	-0.93	0.37
Hm5	0.24	0.98	-0.97	**0.02**	-2.76	**0.01**	-0.89	0.35	0.13	0.59	-0.36	0.72	0.13	0.89
Hm45A	0.16	0.50	0.74	0.19	1.15	0.30	0.41	0.69	-0.44	0.36	-1.77	0.14	-0.88	0.39
HmPxA	0.13	0.93	-0.61	0.27	-1.87	0.08	-0.47	0.67	0.39	0.29	0.63	0.61	0.65	0.54
CpHmPxA	0.48	0.98	-1.42	**0.00**	-4.22	**0.00**	-3.48	**0.01**	0.08	0.68	1.30	0.40	1.73	0.15
CMC34A	0.07	0.90	-0.64	0.29	-0.06	0.96	-0.13	0.91	-0.48	0.26	-1.45	0.20	-0.61	0.56
LuDs	0.13	0.94	-0.96	0.06	-0.43	0.71	-0.52	0.59	-0.31	0.36	-0.38	0.74	-0.07	0.96
LuTq	0.67	0.00	-1.53	**0.00**	-3.73	**0.01**	-0.72	0.41	0.53	0.05	2.02	0.14	1.09	0.23
LuSc	0.03	0.98	0.18	0.67	-0.10	0.94	-0.17	0.87	-0.17	0.52	-0.63	0.65	-0.12	0.93
LuRa	0.13	0.98	-0.94	0.09	-1.99	0.09	-0.42	0.68	0.07	0.83	1.53	0.20	0.73	0.46
LuDsTqA	0.46	0.97	1.35	**0.00**	3.44	**0.02**	3.53	**0.01**	-0.43	0.09	-2.12	0.13	-3.04	**0.02**
LuDsScA	0.27	0.80	-0.88	0.06	-2.97	**0.03**	-0.80	0.36	0.44	0.20	1.98	0.10	0.79	0.36

LuScRaA	0.19	0.80	-1.11	**0.03**	-3.09	**0.01**	-0.87	0.36	-0.13	0.71	-0.61	0.54	0.50	0.60
LuCpRaA	0.60	0.96	-0.86	**0.02**	-2.41	**0.03**	-0.87	0.46	-1.39	**0.00**	-2.86	**0.02**	-2.46	**0.04**
LuCpC	0.37	0.46	1.26	**0.00**	3.31	**0.01**	0.92	0.35	-0.15	0.66	-1.34	0.27	-1.00	0.31
TqHm	0.09	0.91	0.46	0.26	2.29	0.06	0.87	0.43	-0.17	0.55	-0.66	0.58	-0.77	0.48
TqLu	0.04	0.97	-0.26	0.53	0.51	0.67	0.52	0.66	0.15	0.57	0.28	0.80	0.02	0.99
TqPi	0.35	0.77	-1.38	**0.00**	-3.45	**0.01**	-1.34	0.20	0.04	0.89	1.03	0.49	0.49	0.64
TqSt	0.07	1.00	-0.30	0.23	-2.40	**0.05**	-1.40	0.31	0.04	0.78	-0.08	0.92	0.56	0.68
TqHmPiA	0.41	0.69	1.62	**0.00**	4.24	**0.00**	2.12	0.07	0.50	0.12	0.08	0.93	-1.02	0.39
Tq1LuA	0.81	0.00	1.01	**0.00**	2.79	0.05	2.17	0.07	-1.26	**0.00**	-3.18	**0.02**	-2.99	**0.01**
LuTqDsA	0.45	0.79	-1.21	**0.00**	-3.54	**0.01**	-1.87	0.11	0.43	0.14	1.79	0.20	1.38	0.23
MCJAR	0.32	0.80	1.38	**0.00**	3.67	**0.00**	1.57	0.19	0.11	0.73	-0.66	0.68	-0.44	0.72

Without hylobatids

			S						*VM*					
	R^2	λ	b	p	OR^a	p^a	OR^b	p^b	b	p	OR^a	p^a	OR^b	p^b
CpPx	0.07	0.49	-0.19	0.77	-0.74	0.49	-0.69	0.47	0.47	0.33	0.92	0.38	0.69	0.48
CpDn	0.08	0.97	-0.66	0.33	-1.70	0.15	-0.30	0.71	0.22	0.56	1.61	0.12	0.60	0.47
Cp2	0.04	0.99	-0.25	0.66	-1.64	0.19	-0.46	0.67	0.22	0.48	0.46	0.71	0.55	0.62
Cp4	0.12	1.00	-0.46	0.25	-0.09	0.95	0.20	0.87	-0.30	0.16	-1.04	0.45	-1.03	0.37
Cp23A	0.18	0.93	0.21	0.78	-0.08	0.91	0.36	0.71	-0.87	0.06	-2.23	**0.02**	-1.46	0.15
CpPxA	0.67	0.32	-2.54	**0.00**	-3.19	**0.00**	-2.95	**0.01**	-0.17	0.58	0.08	0.97	0.62	0.59
CpScA	0.17	1.00	-0.83	0.11	-1.12	0.33	-1.23	0.26	-0.44	0.12	-0.59	0.60	0.11	0.93
Cp3SD	0.01	0.96	-0.04	0.96	-0.37	0.72	-0.35	0.73	-0.23	0.62	0.75	0.46	0.25	0.82
CpHmC	0.34	0.94	-1.40	**0.01**	-2.14	**0.05**	-1.67	0.18	0.36	0.26	2.43	0.06	1.07	0.39
CpHP	0.01	0.88	-0.24	0.71	-0.52	0.59	-0.12	0.91	-0.19	0.63	-0.25	0.76	-0.19	0.86
HmPx	0.18	0.94	0.32	0.59	0.61	0.59	0.31	0.77	-0.64	0.08	-2.05	0.08	-0.95	0.37
Hm5	0.12	0.97	-0.81	0.14	-1.58	0.15	-0.84	0.39	0.12	0.71	-0.41	0.70	0.19	0.86
Hm45A	0.43	0.00	1.91	**0.00**	2.07	0.08	0.40	0.70	-0.05	0.89	-1.67	0.13	-0.89	0.39
HmPxA	0.03	0.56	-0.08	0.92	-0.09	0.93	-0.46	0.67	0.37	0.49	0.78	0.44	0.66	0.55
CpHmPxA	0.50	0.92	-2.16	**0.00**	-3.10	**0.01**	-3.49	**0.01**	0.11	0.73	0.61	0.63	1.74	0.17
CMC34A	0.07	0.90	-0.42	0.50	0.44	0.69	-0.22	0.84	-0.48	0.22	-1.02	0.33	-0.69	0.51
LuDs	0.24	0.93	-1.20	**0.02**	-1.41	0.19	-0.43	0.66	-0.27	0.36	-0.11	0.93	0.01	0.98
LuTq	0.44	0.00	-1.32	**0.02**	-2.49	**0.04**	-0.71	0.43	0.74	**0.04**	2.06	0.08	1.09	0.23
LuSc	0.04	0.97	-0.34	0.41	-1.52	0.25	-0.19	0.87	-0.15	0.52	-1.04	0.39	-0.14	0.90
LuRa	0.04	0.96	-0.54	0.41	-0.83	0.46	-0.47	0.63	0.09	0.82	1.47	0.16	0.69	0.48
LuDsTqA	0.49	0.94	1.55	**0.00**	2.17	0.07	2.91	**0.02**	-0.60	**0.05**	-2.15	0.10	-2.68	**0.02**

LuDsScA	0.18	0.39	-0.47	0.45	-1.56	0.19	-0.81	0.36	0.70	0.14	1.79	0.06	0.77	0.38
LuScRaA	0.31	0.00	-1.41	**0.02**	-1.90	0.09	-0.86	0.36	-0.95	**0.02**	-0.72	0.45	0.50	0.60
LuCpRaA	0.72	0.95	-0.57	0.09	-0.29	0.83	-0.90	0.43	-1.41	**0.00**	-3.95	**0.00**	-2.48	**0.04**
LuCpC	0.26	0.57	1.20	**0.04**	2.35	0.06	0.89	0.34	-0.25	0.52	-1.13	0.29	-1.03	0.28
TqHm	0.02	0.88	0.18	0.73	1.09	0.39	0.89	0.43	-0.15	0.63	-0.69	0.57	-0.74	0.51
TqLu	0.01	0.97	0.01	0.98	0.33	0.79	0.49	0.67	0.12	0.60	0.46	0.72	-0.01	0.99
TqPi	0.23	0.36	-1.08	0.08	-2.28	0.10	-1.33	0.23	0.37	0.39	0.80	0.48	0.50	0.64
TqSt	0.02	1.00	-0.16	0.59	-1.08	0.43	-1.41	0.30	0.03	0.84	-0.25	0.85	0.54	0.69
TqHmPiA	0.51	0.70	1.90	**0.00**	3.58	**0.01**	2.11	0.06	0.49	0.10	0.14	0.94	-1.06	0.36
Tq1LuA	0.82	0.00	1.32	**0.00**	2.14	0.10	2.12	0.08	-1.30	**0.00**	-3.17	**0.01**	-3.01	**0.01**
LuTqDsA	0.37	0.47	-1.21	**0.03**	-2.13	0.07	-1.75	0.13	0.63	0.12	1.54	0.19	1.48	0.20
MCJAR	0.40	0.73	2.10	**0.00**	2.79	**0.01**	1.61	0.17	0.48	0.23	0.35	0.74	-0.40	0.74

d Vertical manus vs palmigrade-capable

			VM					
	R^2	λ	b	p	OR^a	p^a	OR^b	p^b
CpPx	0.07	0.86	0.49	0.16	1.54	0.22	0.62	0.57
CpDn	0.01	0.99	0.19	0.65	1.13	0.26	0.21	0.81
Cp2	0.03	0.99	0.27	0.36	1.03	0.39	0.31	0.80
Cp4	0.06	1.00	-0.33	0.23	-1.15	0.45	-0.85	0.56
Cp23A	0.18	0.93	-0.84	**0.02**	-2.32	**0.04**	-1.05	0.40
CpPxA	0.02	0.98	0.19	0.53	1.70	0.20	0.34	0.78
CpScA	0.01	1.00	-0.13	0.58	0.19	0.86	-0.22	0.88
Cp3SD	0.01	0.71	0.26	0.56	0.70	0.53	0.09	0.94
CpHmC	0.10	1.00	0.45	0.11	2.55	0.07	1.33	0.37
CpHP	0.02	0.88	-0.26	0.52	-0.33	0.80	-0.29	0.80
HmPx	0.12	0.98	-0.65	0.07	-2.29	0.10	-0.93	0.47
Hm5	0.06	0.99	0.32	0.23	0.72	0.60	0.16	0.89
Hm45A	0.11	0.62	-0.77	0.09	-2.00	**0.04**	-0.44	0.66
HmPxA	0.08	0.96	0.51	0.15	1.36	0.28	0.78	0.56
CpHmPxA	0.06	1.00	0.33	0.20	2.06	0.14	0.75	0.58
CMC34A	0.03	0.90	-0.33	0.41	-1.08	0.33	-0.32	0.78
LuDs	0.00	0.95	-0.11	0.73	0.24	0.84	0.07	0.95
LuTq	0.23	0.71	0.97	**0.01**	2.58	**0.04**	0.76	0.43
LuSc	0.03	0.98	-0.20	0.42	-0.83	0.60	-0.57	0.67
LuRa	0.02	0.99	0.23	0.49	1.59	0.19	0.70	0.52

LuDsTqA	0.17	0.99	-0.66	**0.03**	-3.05	**0.01**	-1.57	0.27
LuDsScA	0.13	0.87	0.64	0.06	2.30	**0.05**	0.56	0.56
LuScRaA	0.01	0.91	0.18	0.61	0.14	0.91	0.24	0.81
LuCpRaA	0.51	0.98	-1.23	**0.00**	-2.44	0.07	-1.95	0.15
LuCpC	0.11	0.77	-0.63	0.09	-2.12	0.07	-0.53	0.63
TqHm	0.04	0.93	-0.27	0.30	-1.24	0.33	-0.29	0.82
TqLu	0.02	0.97	0.20	0.43	0.68	0.65	0.54	0.66
TqPi	0.03	0.90	0.28	0.42	1.65	0.23	0.38	0.75
TqSt	0.02	1.00	0.09	0.52	0.29	0.81	-0.05	0.98
TqHmPiA	0.00	0.90	0.02	0.95	-1.30	0.28	0.00	0.98
Tq1LuA	0.65	0.00	-1.65	**0.00**	-3.60	**0.00**	-1.93	0.14
LuTqDsA	0.17	0.90	0.71	**0.03**	2.49	0.07	1.27	0.33
MCJAR	0.01	0.95	-0.14	0.67	-1.22	0.39	-0.31	0.84

Without hylobatids

			VM					
	R^2	λ	b	p	OR^a	p^a	OR^b	p^b
CpPx	0.06	0.50	0.52	0.24	1.14	0.31	0.37	0.73
CpDn	0.03	0.98	0.31	0.40	1.45	0.19	0.29	0.75
Cp2	0.03	0.99	0.25	0.40	0.89	0.50	0.32	0.82
Cp4	0.06	1.00	-0.24	0.25	-0.92	0.55	-0.60	0.68
Cp23A	0.18	0.93	-0.91	**0.04**	-2.15	**0.04**	-0.93	0.47
CpPxA	0.00	0.92	0.15	0.75	1.26	0.23	0.08	0.94
CpScA	0.06	1.00	-0.33	0.24	-0.48	0.76	-0.47	0.70
Cp3SD	0.01	0.96	-0.22	0.60	0.43	0.70	0.01	1.00
CpHmC	0.10	0.97	0.56	0.12	2.69	**0.04**	0.99	0.45
CpHP	0.01	0.88	-0.15	0.69	-0.13	0.93	-0.10	0.94
HmPx	0.17	0.93	-0.69	**0.05**	-2.26	0.10	-0.74	0.55
Hm5	0.03	0.98	0.25	0.42	0.29	0.82	0.00	0.99
Hm45A	0.16	0.73	-0.88	**0.05**	-2.18	**0.04**	-0.48	0.63
HmPxA	0.03	0.59	0.41	0.40	0.94	0.41	0.42	0.72
CpHmPxA	0.05	0.98	0.42	0.30	1.74	0.08	0.33	0.79
CMC34A	0.05	0.89	-0.40	0.28	-1.14	0.34	-0.42	0.72
LuDs	0.00	0.95	-0.09	0.77	0.40	0.76	0.02	0.98
LuTq	0.25	0.21	1.04	**0.01**	2.52	**0.04**	0.62	0.52
LuSc	0.01	0.97	-0.10	0.66	-0.59	0.72	-0.31	0.83

LuRa	0.01	0.96	0.17	0.64	1.37	0.26	0.47	0.67
LuDsTqA	0.22	0.97	-0.80	**0.02**	-2.85	**0.01**	-1.27	0.33
LuDsScA	0.15	0.46	0.81	0.06	2.00	0.07	0.31	0.73
LuScRaA	0.00	0.77	-0.06	0.90	-0.26	0.83	0.06	0.93
LuCpRaA	0.68	0.96	-1.32	**0.00**	-3.49	**0.02**	-2.28	0.11
LuCpC	0.10	0.70	-0.61	0.14	-1.87	0.09	-0.40	0.71
TqHm	0.02	0.89	-0.19	0.53	-0.97	0.45	-0.20	0.87
TqLu	0.01	0.97	0.12	0.58	0.54	0.73	0.36	0.78
TqPi	0.27	0.00	1.03	**0.01**	1.33	0.27	0.12	0.92
TqSt	0.01	1.00	0.05	0.73	-0.11	0.95	-0.24	0.91
TqHmPiA	0.00	0.89	0.07	0.84	-1.09	0.38	0.08	0.95
Tq1LuA	0.64	0.00	-1.58	**0.00**	-3.58	**0.00**	-1.69	0.18
LuTqDsA	0.21	0.63	0.94	**0.03**	2.34	**0.05**	0.95	0.42
MCJAR	0.00	0.91	0.10	0.83	-0.53	0.61	-0.07	0.99

[a] Based on Bayesian phylogenetic generalized linear mixed model (PGLMM) regression of taxon means with size (log-transformed sum carpal volume) as a covariate. OR, odds ratio (log scale)

[b] Based on PGLMM analysis of individual observations

Table 2.9. Relationships between shape variables and additional locomotor proportions based on PGLS regression

a	*QuadA*						**b**	*Susp*					
	R^2	λ	b	p	b^a	p^a		R^2	λ	b	p	b^a	p^a
CpPx	0.27	0.00	0.50	**0.01**	0.79	**0.00**		0.24	1.00	-0.35	**0.02**	-0.36	**0.03**
CpDn	0.09	0.88	0.26	0.18	0.27	0.16		0.00	1.00	0.02	0.90	0.01	0.92
Cp2	0.02	0.79	0.15	0.55	0.24	0.40		0.01	1.00	-0.07	0.72	-0.11	0.59
Cp4	0.02	0.80	-0.16	0.52	-0.15	0.66		0.06	1.00	0.22	0.27	0.24	0.34
Cp23A	0.17	0.45	-0.40	0.06	-0.44	**0.04**		0.18	1.00	0.29	**0.05**	0.29	0.06
CpPxA	0.33	0.00	0.56	**0.00**	0.70	**0.00**		0.91	0.00	-0.95	**0.00**	-0.96	**0.00**
CpScA	0.19	0.60	0.49	**0.04**	0.49	0.06		0.37	1.00	-0.65	**0.00**	-0.67	**0.00**
Cp3SD	0.34	0.85	0.57	**0.00**	0.61	**0.01**		0.05	1.00	-0.16	0.30	-0.15	0.37
CpHmC	0.29	0.00	0.55	**0.01**	0.77	**0.00**		0.45	1.00	-0.57	**0.00**	-0.59	**0.00**
CpHP	0.00	0.83	0.05	0.78	0.07	0.74		0.03	1.00	0.09	0.47	0.09	0.48
HmPx	0.13	0.75	-0.33	0.11	-0.38	0.11		0.17	1.00	0.27	0.05	0.27	0.07
Hm5	0.67	0.00	0.82	**0.00**	0.83	**0.00**		0.26	1.00	-0.47	**0.02**	-0.47	**0.02**
Hm45A	0.01	0.82	-0.08	0.64	-0.10	0.59		0.02	1.00	0.07	0.51	0.08	0.47
HmPxA	0.31	0.00	0.53	**0.01**	0.72	**0.00**		0.23	1.00	-0.32	**0.02**	-0.32	**0.03**
CpHmPxA	0.41	0.00	0.64	**0.00**	0.76	**0.00**		0.74	0.96	-0.84	**0.00**	-0.88	**0.00**
CMC34A	0.03	0.82	0.16	0.47	0.14	0.57		0.02	1.00	-0.08	0.56	-0.07	0.65
LuDs	0.00	0.82	0.00	0.99	-0.01	0.95		0.03	1.00	-0.14	0.41	-0.13	0.44
LuTq	0.26	0.61	0.47	**0.02**	0.52	**0.01**		0.19	1.00	-0.25	**0.04**	-0.24	0.05
LuSc	0.00	0.82	-0.08	0.76	-0.02	0.95		0.09	1.00	0.28	0.18	0.27	0.23
LuRa	0.12	0.75	0.35	0.12	0.40	0.12		0.27	1.00	-0.41	**0.01**	-0.44	**0.02**
LuDsTqA	0.18	0.54	-0.40	**0.05**	-0.46	**0.03**		0.43	1.00	0.51	**0.00**	0.51	**0.00**
LuDsScA	0.24	0.55	0.48	**0.02**	0.53	**0.01**		0.22	1.00	-0.31	**0.03**	-0.31	**0.04**
LuScRaA	0.10	0.62	0.31	0.15	0.31	0.17		0.14	1.00	-0.25	0.09	-0.25	0.12
LuCpRaA	0.01	0.76	0.10	0.69	0.24	0.43		0.01	1.00	-0.07	0.70	-0.19	0.41
LuCpC	0.30	0.44	-0.55	**0.01**	-0.54	**0.01**		0.12	1.00	0.19	0.12	0.19	0.13
TqHm	0.70	0.00	-0.83	**0.00**	-0.93	**0.00**		0.16	1.00	0.35	0.06	0.35	0.07
TqLu	0.00	0.82	0.05	0.87	-0.03	0.94		0.03	1.00	-0.20	0.43	-0.17	0.51
TqPi	0.09	0.64	0.29	0.16	0.31	0.17		0.25	1.00	-0.32	**0.02**	-0.31	**0.02**
TqSt	0.27	0.00	0.78	**0.01**	1.12	**0.00**		0.15	1.00	-0.64	0.08	-0.75	**0.04**
TqHmPiA	0.14	0.64	-0.40	0.08	-0.52	**0.04**		0.17	1.00	0.26	0.06	0.32	**0.03**
Tq1LuA	0.16	0.74	-0.35	0.06	-0.37	0.07		0.27	1.00	0.31	**0.01**	0.32	**0.02**
LuTqDsA	0.34	0.00	0.56	**0.00**	0.77	**0.00**		0.30	0.00	-0.36	**0.01**	-0.92	**0.00**
MCJAR	0.33	0.00	-0.56	**0.01**	-0.70	**0.00**		0.49	1.00	0.61	**0.00**	0.61	**0.00**

Without hylobatids												
	R^2	λ	b	p	b^a	p^a	R^2	λ	b	p	b^a	p^a
CpPx	0.02	0.53	0.16	0.53	0.36	0.11	0.03	1.00	-0.12	0.46	-0.13	0.43
CpDn	0.43	0.60	0.65	**0.00**	0.60	**0.00**	0.10	1.00	-0.23	0.20	-0.23	0.20
Cp2	0.24	0.00	0.49	**0.03**	0.22	0.51	0.01	1.00	-0.11	0.69	-0.03	0.93
Cp4	0.23	0.00	0.47	**0.04**	0.13	0.73	0.04	1.00	-0.32	0.43	-0.21	0.65
Cp23A	0.01	0.51	-0.07	0.77	-0.08	0.73	0.03	1.00	0.12	0.45	0.13	0.42
CpPxA	0.06	0.47	0.23	0.32	0.22	0.30	0.73	0.00	-0.86	**0.00**	-0.83	**0.00**
CpScA	0.01	0.48	0.14	0.62	-0.09	0.78	0.15	1.00	-0.48	0.11	-0.45	0.17
Cp3SD	0.19	0.77	0.49	0.06	0.48	**0.04**	0.00	1.00	0.03	0.88	0.00	1.00
CpHmC	0.07	0.59	0.30	0.27	0.38	0.09	0.18	1.00	-0.40	0.07	-0.43	0.06
CpHP	0.30	0.00	0.55	**0.02**	0.41	0.07	0.00	1.00	-0.04	0.82	-0.05	0.79
HmPx	0.01	0.62	-0.13	0.65	-0.43	0.16	0.04	1.00	0.16	0.44	0.23	0.30
Hm5	0.44	0.00	0.66	**0.00**	0.57	**0.04**	0.06	1.00	-0.26	0.30	-0.27	0.28
Hm45A	0.05	0.50	-0.21	0.37	-0.22	0.32	0.49	0.00	0.70	**0.00**	0.66	**0.00**
HmPxA	0.07	0.53	0.22	0.29	0.25	0.24	0.03	1.00	-0.10	0.47	-0.09	0.49
CpHmPxA	0.12	0.46	0.33	0.15	0.31	0.15	0.51	0.98	-0.65	**0.00**	-0.65	**0.00**
CMC34A	0.00	0.57	-0.01	0.98	0.05	0.85	0.00	1.00	0.05	0.79	0.09	0.65
LuDs	0.00	0.56	0.00	1.00	0.02	0.95	0.19	1.00	-0.47	0.06	-0.49	0.05
LuTq	0.09	0.61	0.29	0.21	0.34	0.11	0.08	1.00	-0.16	0.23	-0.16	0.25
LuSc	0.35	0.00	0.59	**0.01**	0.49	0.15	0.02	1.00	-0.18	0.58	-0.15	0.65
LuRa	0.00	0.55	-0.02	0.93	0.18	0.56	0.06	1.00	-0.25	0.33	-0.36	0.17
LuDsTqA	0.03	0.53	-0.16	0.50	-0.23	0.29	0.46	0.99	0.63	**0.00**	0.83	**0.00**
LuDsScA	0.03	0.58	0.17	0.47	0.20	0.36	0.03	1.00	-0.10	0.48	-0.09	0.55
LuScRaA	0.00	0.54	0.03	0.89	0.04	0.86	0.03	1.00	-0.12	0.48	-0.14	0.39
LuCpRaA	0.01	0.47	0.10	0.72	-0.34	0.47	0.01	1.00	0.11	0.68	0.61	0.11
LuCpC	0.24	0.19	-0.51	**0.03**	-0.40	0.08	0.08	1.00	0.19	0.23	0.17	0.29
TqHm	0.53	0.00	-0.73	**0.00**	-0.83	**0.01**	0.05	1.00	0.22	0.36	0.20	0.40
TqLu	0.25	0.00	-0.50	**0.03**	-0.20	0.63	0.01	1.00	0.15	0.71	0.04	0.92
TqPi	0.03	0.57	-0.17	0.45	-0.14	0.55	0.07	1.00	-0.14	0.27	-0.12	0.36
TqSt	0.39	0.00	0.62	**0.00**	0.93	0.08	0.05	1.00	-0.44	0.37	-0.31	0.59
TqHmPiA	0.32	0.00	-0.57	**0.01**	-0.43	0.22	0.51	0.86	0.78	**0.00**	1.17	**0.00**
Tq1LuA	0.09	0.56	-0.28	0.21	-0.29	0.17	0.13	1.00	0.26	0.14	0.34	0.06
LuTqDsA	0.09	0.50	0.30	0.20	0.38	0.06	0.13	1.00	-0.22	0.13	-0.68	**0.00**
MCJAR	0.05	0.47	-0.22	0.34	-0.13	0.59	0.25	1.00	0.37	**0.03**	0.35	**0.04**

	c	*Climb*						d	*LeapA*					
	R^2	λ	b	p	b^a	p^a		R^2	λ	b	p	b^a	p^a
CpPx	0.12	0.00	-0.34	0.12	-0.19	0.38		0.01	1.00	-0.09	0.65	0.01	0.96
CpDn	0.00	0.00	-0.06	0.80	-0.14	0.48		0.12	1.00	-0.25	0.11	-0.27	0.06
Cp2	0.03	0.00	0.17	0.44	-0.30	0.27		0.02	1.00	0.15	0.54	0.02	0.93
Cp4	0.17	0.98	0.41	0.06	-0.74	0.06		0.13	1.00	0.40	0.10	0.22	0.43
Cp23A	0.03	0.00	0.20	0.42	0.11	0.58		0.00	1.00	0.00	0.99	-0.07	0.71
CpPxA	0.07	0.00	-0.28	0.23	-0.22	0.26		0.00	1.00	0.00	1.00	0.07	0.74
CpScA	0.01	0.00	-0.14	0.61	-0.16	0.45		0.18	1.00	0.56	**0.05**	0.52	0.05
Cp3SD	0.16	0.00	-0.39	0.07	-0.19	0.41		0.14	1.00	-0.31	0.09	-0.23	0.21
CpHmC	0.12	0.00	-0.34	0.12	-0.19	0.38		0.00	1.00	-0.02	0.93	0.12	0.61
CpHP	0.05	0.00	0.22	0.34	0.03	0.88		0.06	1.00	-0.16	0.28	-0.16	0.25
HmPx	0.19	0.00	0.44	**0.04**	0.20	0.44		0.01	1.00	-0.08	0.67	-0.19	0.29
Hm5	0.01	0.00	0.08	0.73	-0.11	0.62		0.00	1.00	-0.08	0.76	0.02	0.94
Hm45A	0.18	0.00	0.43	**0.05**	0.55	**0.00**		0.17	1.00	-0.24	0.05	-0.21	0.08
HmPxA	0.05	0.00	-0.24	0.31	-0.15	0.47		0.00	1.00	0.00	0.99	0.07	0.71
CpHmPxA	0.07	0.00	-0.29	0.23	-0.21	0.30		0.00	1.00	0.00	1.00	0.13	0.62
CMC34A	0.01	0.00	-0.11	0.62	0.25	0.30		0.08	1.00	-0.20	0.22	-0.13	0.41
LuDs	0.10	0.00	-0.32	0.15	-0.07	0.77		0.09	1.00	-0.28	0.17	-0.25	0.20
LuTq	0.22	0.00	-0.47	**0.03**	-0.35	0.09		0.01	1.00	0.06	0.72	0.09	0.55
LuSc	0.04	0.00	0.19	0.40	-0.49	0.12		0.06	1.00	0.28	0.27	0.15	0.57
LuRa	0.15	0.00	-0.39	0.07	-0.12	0.65		0.01	1.00	-0.09	0.68	0.07	0.76
LuDsTqA	0.18	0.00	0.43	**0.05**	0.32	0.12		0.04	1.00	0.20	0.36	0.11	0.61
LuDsScA	0.08	0.00	-0.29	0.20	-0.19	0.37		0.00	1.00	-0.04	0.84	-0.01	0.97
LuScRaA	0.04	0.00	-0.22	0.40	-0.18	0.37		0.00	1.00	0.05	0.77	0.18	0.33
LuCpRaA	0.42	0.74	0.93	**0.00**	0.84	**0.01**		0.10	1.00	0.32	0.16	0.12	0.66
LuCpC	0.07	0.00	0.29	0.24	0.34	0.08		0.00	1.00	-0.04	0.80	-0.04	0.77
TqHm	0.09	0.00	0.45	0.17	0.36	0.11		0.01	1.00	-0.12	0.61	-0.13	0.57
TqLu	0.11	0.00	-0.33	0.14	0.30	0.42		0.03	1.00	-0.22	0.47	-0.06	0.85
TqPi	0.07	0.00	-0.26	0.24	-0.11	0.62		0.00	1.00	0.03	0.88	0.04	0.82
TqSt	0.05	0.00	0.23	0.30	-0.27	0.36		0.04	1.00	0.41	0.36	0.19	0.67
TqHmPiA	0.01	0.00	0.10	0.71	0.40	0.11		0.04	1.00	-0.16	0.36	-0.06	0.72
Tq1LuA	0.49	0.00	0.70	**0.00**	0.60	**0.00**		0.05	1.00	0.17	0.30	0.08	0.65
LuTqDsA	0.12	0.00	-0.35	0.11	-0.24	0.23		0.00	1.00	-0.06	0.76	0.02	0.93
MCJAR	0.03	0.00	0.18	0.46	0.11	0.57		0.00	1.00	-0.07	0.78	-0.16	0.48

Without hylobatids

	R^2	λ	b	p	b^a	p^a	R^2	λ	b	p	b^a	p^a
CpPx	0.24	0.00	-0.49	**0.03**	-0.35	0.13	0.00	1.00	0.00	0.99	0.01	0.92
CpDn	0.04	0.37	-0.21	0.41	-0.35	0.11	0.18	1.00	-0.27	0.07	-0.27	0.06
Cp2	0.03	0.00	0.19	0.44	-0.47	0.15	0.07	1.00	0.24	0.28	0.13	0.58
Cp4	0.23	0.00	0.48	**0.04**	-0.40	0.46	0.02	1.00	0.18	0.60	-0.08	0.83
Cp23A	0.02	0.43	0.14	0.57	0.18	0.44	0.00	1.00	0.02	0.87	0.01	0.95
CpPxA	0.13	0.00	-0.36	0.14	-0.44	**0.03**	0.01	1.00	0.06	0.68	0.05	0.76
CpScA	0.02	0.00	0.15	0.54	-0.49	0.12	0.37	1.00	0.65	**0.01**	0.58	**0.02**
Cp3SD	0.17	0.00	-0.41	0.08	-0.21	0.42	0.15	1.00	-0.28	0.10	-0.24	0.15
CpHmC	0.19	0.00	-0.44	0.06	-0.29	0.20	0.00	1.00	-0.04	0.83	-0.01	0.96
CpHP	0.02	0.00	0.15	0.55	-0.17	0.42	0.01	1.00	-0.06	0.70	-0.05	0.74
HmPx	0.21	0.00	0.46	**0.05**	0.18	0.52	0.01	1.00	0.07	0.68	0.00	1.00
Hm5	0.05	0.00	0.21	0.38	-0.29	0.33	0.01	1.00	-0.07	0.75	-0.05	0.79
Hm45A	0.17	0.21	0.41	0.08	0.53	**0.01**	0.11	1.00	-0.18	0.17	-0.17	0.19
HmPxA	0.08	0.34	-0.27	0.24	-0.32	0.13	0.01	1.00	0.04	0.72	0.04	0.74
CpHmPxA	0.16	0.16	-0.41	0.09	-0.51	**0.01**	0.03	1.00	0.12	0.49	0.10	0.57
CMC34A	0.01	0.25	0.13	0.64	-0.25	0.35	0.07	1.00	0.19	0.26	0.14	0.41
LuDs	0.18	0.00	-0.42	0.07	-0.17	0.54	0.02	1.00	-0.12	0.60	-0.09	0.68
LuTq	0.30	0.00	-0.54	**0.02**	-0.45	**0.04**	0.01	1.00	0.04	0.73	0.04	0.74
LuSc	0.03	0.00	0.19	0.45	-0.57	0.16	0.03	1.00	0.20	0.48	0.15	0.58
LuRa	0.16	0.00	-0.40	0.09	-0.16	0.63	0.10	1.00	-0.28	0.20	-0.19	0.40
LuDsTqA	0.38	0.00	0.62	**0.00**	0.54	**0.01**	0.02	1.00	-0.10	0.60	-0.10	0.59
LuDsScA	0.14	0.00	-0.37	0.12	-0.31	0.14	0.00	1.00	0.01	0.93	-0.01	0.91
LuScRaA	0.06	0.52	-0.25	0.33	-0.38	0.10	0.06	1.00	0.14	0.31	0.18	0.17
LuCpRaA	0.74	0.99	1.36	**0.00**	1.54	**0.00**	0.10	1.00	0.28	0.20	0.06	0.85
LuCpC	0.12	0.38	0.39	0.14	0.60	**0.00**	0.06	1.00	-0.14	0.30	-0.11	0.41
TqHm	0.07	0.69	0.39	0.26	0.89	**0.00**	0.00	1.00	-0.02	0.93	0.01	0.95
TqLu	0.09	0.00	-0.31	0.20	0.67	0.18	0.15	1.00	-0.57	0.10	-0.44	0.21
TqPi	0.13	0.00	-0.36	0.13	-0.21	0.36	0.04	1.00	0.09	0.42	0.05	0.64
TqSt	0.09	0.00	0.31	0.20	-1.50	**0.01**	0.09	1.00	0.52	0.21	0.27	0.57
TqHmPiA	0.00	0.39	0.08	0.79	0.82	**0.01**	0.12	1.00	-0.23	0.15	-0.15	0.40
Tq1LuA	0.51	0.52	0.72	**0.00**	0.65	**0.00**	0.04	1.00	0.12	0.44	0.05	0.77
LuTqDsA	0.26	0.00	-0.51	**0.02**	-0.45	**0.03**	0.02	1.00	0.06	0.62	0.06	0.59
MCJAR	0.04	0.31	0.20	0.42	0.44	0.05	0.01	1.00	-0.06	0.71	-0.02	0.89

e	*Leap*					
	R^2	λ	b	p	b^a	p^a
CpPx	0.03	1.00	-0.15	0.48	-0.02	0.92
CpDn	0.15	1.00	-0.29	0.08	-0.32	**0.03**
Cp2	0.00	1.00	0.01	0.97	-0.17	0.47
Cp4	0.10	1.00	0.38	0.15	0.08	0.78
Cp23A	0.00	1.00	0.02	0.94	-0.08	0.68
CpPxA	0.00	1.00	0.08	0.75	0.17	0.42
CpScA	0.17	1.00	0.57	0.06	0.51	0.06
Cp3SD	0.13	1.00	-0.33	0.09	-0.22	0.24
CpHmC	0.01	1.00	-0.11	0.65	0.06	0.81
CpHP	0.06	1.00	-0.17	0.28	-0.17	0.23
HmPx	0.00	1.00	0.04	0.84	-0.09	0.60
Hm5	0.02	1.00	-0.18	0.50	-0.06	0.82
Hm45A	0.08	1.00	-0.17	0.21	-0.13	0.30
HmPxA	0.01	1.00	-0.07	0.71	0.01	0.94
CpHmPxA	0.00	1.00	0.00	0.99	0.17	0.51
CMC34A	0.04	1.00	-0.15	0.40	0.05	0.77
LuDs	0.02	1.00	-0.16	0.49	-0.13	0.52
LuTq	0.00	1.00	-0.03	0.84	0.01	0.96
LuSc	0.05	1.00	0.28	0.31	0.09	0.72
LuRa	0.04	1.00	-0.21	0.36	-0.02	0.94
LuDsTqA	0.04	1.00	0.20	0.39	0.08	0.72
LuDsScA	0.01	1.00	-0.10	0.62	-0.06	0.74
LuScRaA	0.00	1.00	0.01	0.97	0.16	0.38
LuCpRaA	0.19	1.00	0.48	**0.04**	0.24	0.36
LuCpC	0.00	1.00	0.05	0.78	0.08	0.55
TqHm	0.01	1.00	-0.12	0.63	-0.13	0.56
TqLu	0.04	1.00	-0.27	0.40	-0.06	0.84
TqPi	0.00	1.00	-0.02	0.90	-0.01	0.95
TqSt	0.02	1.00	0.32	0.51	0.01	0.98
TqHmPiA	0.01	1.00	-0.08	0.66	0.06	0.74
Tq1LuA	0.08	1.00	0.23	0.19	0.08	0.66
LuTqDsA	0.02	1.00	-0.12	0.54	-0.02	0.89
MCJAR	0.01	1.00	-0.11	0.67	-0.23	0.32

Without hylobatids

	R^2	λ	b	p	b^a	p^a
CpPx	0.01	1.00	-0.05	0.75	-0.03	0.85
CpDn	0.23	1.00	-0.34	**0.04**	-0.34	**0.02**
Cp2	0.01	1.00	0.10	0.70	-0.10	0.69
Cp4	0.01	1.00	0.14	0.71	-0.26	0.50
Cp23A	0.00	1.00	0.03	0.87	0.01	0.97
CpPxA	0.04	1.00	0.14	0.40	0.11	0.45
CpScA	0.34	1.00	0.69	**0.01**	0.55	**0.04**
Cp3SD	0.14	1.00	-0.30	0.12	-0.23	0.18
CpHmC	0.03	1.00	-0.14	0.52	-0.10	0.63
CpHP	0.01	1.00	-0.08	0.62	-0.06	0.66
HmPx	0.07	1.00	0.21	0.28	0.12	0.53
Hm5	0.03	1.00	-0.16	0.48	-0.14	0.50
Hm45A	0.03	1.00	-0.10	0.49	-0.08	0.56
HmPxA	0.00	1.00	-0.01	0.93	-0.02	0.88
CpHmPxA	0.03	1.00	0.14	0.47	0.11	0.55
CMC34A	0.03	1.00	0.13	0.49	0.05	0.79
LuDs	0.00	1.00	0.03	0.92	0.07	0.77
LuTq	0.00	1.00	-0.03	0.84	-0.03	0.78
LuSc	0.02	1.00	0.19	0.55	0.12	0.67
LuRa	0.18	1.00	-0.42	0.07	-0.30	0.19
LuDsTqA	0.01	1.00	-0.09	0.66	-0.09	0.63
LuDsScA	0.00	1.00	-0.03	0.81	-0.07	0.57
LuScRaA	0.03	1.00	0.10	0.52	0.16	0.26
LuCpRaA	0.22	1.00	0.48	**0.04**	0.26	0.44
LuCpC	0.00	1.00	-0.04	0.78	0.01	0.97
TqHm	0.00	1.00	-0.03	0.88	0.01	0.96
TqLu	0.15	1.00	-0.63	0.10	-0.42	0.26
TqPi	0.01	1.00	0.05	0.67	0.00	0.98
TqSt	0.05	1.00	0.43	0.35	-0.03	0.96
TqHmPiA	0.04	1.00	-0.15	0.42	0.01	0.94
Tq1LuA	0.06	1.00	0.17	0.31	0.07	0.68
LuTqDsA	0.00	1.00	0.01	0.94	0.01	0.92
MCJAR	0.04	1.00	-0.14	0.39	-0.09	0.54

[a] based on PGLS model with size as a covariate

Table 2.10. Additional positional classification results

a	Cross-validation trials								
	DFA				*glmnet*				
	DG	*KW*	*PG*	*S*	*DG*	*KW*	*PG*	*S*	Total
DG	2729	0	171	0	2837	0	63	0	2900
KW	0	8100	0	0	3	8097	0	0	8100
PG	265	0	15032	3	107	0	15182	11	15300
S	0	0	37	7263	0	0	46	7254	7300
b	Additional per-class accuracy metrics								
Bal[a]	0.953	1.000	0.986	0.999	0.980	1.000	0.993	0.998	
Sen[b]	0.911	1.000	0.986	1.000	0.963	1.000	0.993	0.998	
Spec[c]	0.994	1.000	0.985	0.999	0.998	1.000	0.994	0.998	
PPV[d]	0.941	1.000	0.982	0.995	0.978	1.000	0.992	0.994	
NPV[e]	0.991	1.000	0.989	1.000	0.996	1.000	0.994	1.000	
c	Mean prediction posterior probabilities				Mean probabilities by *a priori* class				
DFA	0.916	1.000	0.972	0.984	0.880	1.000	0.965	0.984	
glmnet	0.838	0.982	0.953	0.961	0.832	0.982	0.951	0.959	
d	*glmnet* tuned parameters								
alpha	0.4813559								
lambda	0.0032373								

[a] Balanced accuracy – average of sensitivity and specificity
[b] Sensitivity – correct predictions relative to the number of *a priori* cases of that class in the sample. Also known as recall or true positive rate.
[c] Specificity – rate at which observations not assigned to a class actually do not belong to that class, also known as the true negative rate.
[d] Positive prediction value – probability that an observation predicted to belong to a class actually belongs to that class.
[e] Negative prediction value – probability than an observation not predicted to belong to a class actually does not belong to that class

Table 2.11. Prediction results for additional locomotor proportions

a	Predictive models								
	PGLS			GLM					
	R^2	λ	p	Terms	Coef	SE	T	p	SEE%[a]
QuadA	0.831	0.000	0.000	(Intercept)	-0.58	0.04	-14.9	0.000	13.1
				Cp3SD	0.08	0.04	2.0	0.047	
				CpDn	0.04	0.04	1.0	0.301	
				Hm5	0.38	0.04	8.8	0.000	
				TqHm	-0.60	0.05	-12.4	0.000	
Susp	0.989	0.000	0.000	(Intercept)	-3.30	0.10	-34.7	0.000	8.5
				CpPxA	-0.68	0.11	-6.4	0.000	
				Hm45A	0.16	0.05	3.1	0.002	
				LuTqDsA	-0.53	0.08	-6.9	0.000	

				MCJAR	0.05	0.06	0.8	0.437	
				Tq1LuA	0.74	0.06	11.6	0.000	
				TqHmPiA	0.42	0.05	7.8	0.000	
Climb	0.872	0.000	0.000	(Intercept)	-1.34	0.03	-39.5	0.000	8.8
				Hm45A	0.19	0.03	5.8	0.000	
				LuCpRaA	0.60	0.04	15.6	0.000	
				LuTq	-0.19	0.03	-5.5	0.000	
				TqHm	0.19	0.04	5.1	0.000	

b Predicted locomotor proportions of training taxa[b]

	QuadA			*Susp*			*Climb*		
	Obs	Pred	Δ	Obs	Pred	Δ	Obs	Pred	Δ
P. t. schweinfurthii	0.31	0.23	0.08	0.01	0.01	0.00	0.06	0.12	0.06
P. t. verus	0.21	0.22	0.01	0.01	0.01	0.00	0.11	0.11	0.00
P. paniscus	0.35	0.18	0.17	0.01	0.02	0.01	0.09	0.10	0.01
G. gorilla	0.19	0.26	0.07	0.01	0.01	0.00	0.06	0.12	0.06
G. beringei	0.53	0.35	0.18	0.01	0.01	0.00	0.04	0.09	0.05
P. pygmaeus	0.12	0.18	0.06	0.43	0.39	0.04	0.37	0.30	0.07
P. abelii	0.18	0.23	0.05	0.38	0.37	0.01	0.35	0.28	0.07
Hoolock	0.00	0.13	0.13	0.55	0.59	0.04	0.20	0.17	0.03
H. lar	0.00	0.13	0.13	0.59	0.54	0.05	0.19	0.21	0.02
Symphalangus	0.00	0.09	0.09	0.59	0.44	0.15	0.32	0.20	0.12
Papio	0.68	0.59	0.09	0.00	0.02	0.02	0.01	0.14	0.13
Lophocebus	0.42	0.49	0.07	0.00	0.02	0.02	0.36	0.26	0.10
Macaca	0.68	0.54	0.14	0.00	0.03	0.03	0.26	0.26	0.00
Erythrocebus	0.60	0.61	0.01	0.00	0.01	0.01	0.05	0.14	0.09
Cercopithecus	0.54	0.60	0.06	0.00	0.02	0.02	0.35	0.26	0.09
Colobus	0.41	0.54	0.13	0.01	0.02	0.01	0.20	0.18	0.02
Procolobus	0.35	0.40	0.05	0.01	0.02	0.01	0.29	0.28	0.01
Trachypithecus	0.60	0.55	0.05	0.00	0.02	0.02	0.13	0.21	0.08
Presbytis	0.28	0.47	0.19	0.02	0.02	0.00	0.19	0.17	0.02
Alouatta	0.61	0.44	0.17	0.02	0.03	0.01	0.33	0.33	0.00
Ateles	0.42	0.44	0.02	0.25	0.16	0.09	0.25	0.24	0.01
Cebus	0.37	0.48	0.11	0.00	0.03	0.03	0.40	0.33	0.07

c Proportions predicted for other taxa

	QuadA	*Susp*	*Climb*
P. t. troglodytes	0.21	0.01	0.13
P. t. ellioti	0.21	0.02	0.11
H. muelleri	0.12	0.44	0.23
Mandrillus	0.54	0.01	0.10
Cercocebus	0.52	0.03	0.23
Nasalis	0.51	0.01	0.14

[a] Percent standard error of the estimate based on repeated individual predictions generated during cross validation

[b] Predictions calculated after 100 repetitions of 10-fold cross validation of quasibinomial logistic regression. Obs, observed proportion. Pred, predicted proportion. Δ, residual.

Table 2.12. RV correlations between shape and locomotor proportion matrices

a	RV	p	RV[a]	p[a]	RV[b]	p[b]	RV[c]	p[c]
Total proportions	0.67	**0.00**	0.71	**0.00**	0.56	**0.00**	0.68	**0.00**
with *Arb*	0.62	**0.00**	0.63	**0.00**	0.56	**0.00**	0.64	**0.00**
Arboreal proportions	0.76	**0.00**	0.74	**0.00**	0.69	**0.00**	0.70	**0.00**
with *Arb*	0.77	**0.00**	0.73	**0.00**	0.75	**0.00**	0.73	**0.00**
without *LeapA*	0.80	**0.00**	0.76	**0.00**	0.73	**0.00**	0.70	**0.00**
Quad, SuspA, ClimbA	0.79	**0.00**	0.77	**0.00**	0.70	**0.00**	0.70	**0.00**
b With phylogenetic independent contrasts of tip data								
Total proportions	0.40	**0.01**	0.46	**0.03**	0.29	0.21	0.53	**0.01**
with *Arb*	0.36	**0.03**	0.41	0.06	0.28	0.21	0.52	**0.02**
Arboreal proportions	0.41	**0.01**	0.52	**0.01**	0.35	0.12	0.52	**0.02**
with *Arb*	0.43	**0.01**	0.52	**0.02**	0.38	0.11	0.58	**0.01**
without *LeapA*	0.43	**0.01**	0.53	**0.01**	0.36	0.11	0.55	**0.02**
Quad, SuspA, ClimbA	0.49	**0.00**	0.54	**0.01**	0.36	0.11	0.54	**0.01**

[a] African apes excluded
[b] Hylobatids excluded
[c] African apes and hylobatids excluded

Table 2.13. PLS results

a	Locomotor PLS vectors				
	PLS 1	PLS 2	PLS 3	PLS 4	PLS 5
QuadA	0.58	0.23	-0.52	-0.09	0.58
SuspA	-0.72	-0.10	-0.21	0.21	0.61
ClimbA	0.17	-0.63	0.44	-0.47	0.41
LeapA	0.12	0.51	0.70	0.33	0.36
Arb	-0.31	0.53	0.03	-0.79	0.01
b	Shape PLS vectors				
CpPx	0.22	-0.09	-0.12	0.01	-0.18
CpDn	-0.03	-0.04	-0.50	0.15	0.40
Cp2	0.10	0.25	0.01	0.10	-0.04
Cp4	-0.06	0.22	-0.09	-0.04	0.15
Cp23A	-0.21	0.04	0.07	0.15	-0.13
CpPxA	0.25	-0.01	0.15	-0.08	0.02
CpScA	0.19	0.15	0.15	-0.15	0.16
Cp3SD	0.13	-0.16	-0.43	0.08	-0.12
CpHmC	0.22	-0.10	-0.05	0.07	-0.12
CpHP	-0.07	0.13	-0.36	0.17	-0.08
HmPx	-0.14	0.20	0.09	-0.17	0.17
Hm5	0.21	0.16	-0.23	-0.08	-0.19
Hm45A	-0.09	-0.09	-0.33	-0.56	0.00
HmPxA	0.22	0.03	-0.09	-0.03	0.07
CpHmPxA	0.25	0.01	0.06	-0.06	0.04
CMC34A	-0.03	-0.23	-0.13	-0.28	0.29
LuDs	-0.03	-0.25	0.18	-0.11	0.33

LuTq	0.22	-0.09	-0.01	0.18	-0.07
LuSc	-0.05	0.32	0.01	0.25	0.03
LuRa	0.15	-0.26	-0.07	0.01	-0.17
LuDsTqA	-0.23	0.12	-0.11	0.01	-0.14
LuDsScA	0.22	-0.07	-0.04	0.03	-0.07
LuScRaA	0.19	0.14	0.17	-0.01	-0.12
LuCpRaA	0.09	0.27	-0.07	-0.39	-0.19
LuCpC	-0.21	-0.11	-0.03	-0.19	-0.16
TqHm	-0.21	-0.21	0.18	-0.05	-0.12
TqLu	-0.01	-0.31	-0.01	0.00	-0.22
TqPi	0.20	-0.13	0.15	-0.18	-0.09
TqSt	0.14	0.28	-0.12	-0.09	0.08
TqHmPiA	-0.18	-0.16	-0.06	0.06	-0.21
Tq1LuA	-0.19	0.22	-0.01	-0.23	-0.39
LuTqDsA	0.24	-0.04	-0.04	0.08	-0.12
MCJAR	-0.24	-0.02	-0.06	0.18	-0.11

c Euclidean distances[a]	
P. t. schweinfurthii	0.55
P. t. verus	0.66
P. paniscus	2.64
G. gorilla	2.93
G. beringei	1.93
P. pygmaeus	3.93
P. abelii	2.93
Hoolock	0.03
H. lar	0.85
Symphalangus	1.72
Papio	1.64
Lophocebus	2.38
Macaca	0.38
Erythrocebus	2.55
Cercopithecus	2.49
Colobus	2.94
Procolobus	2.35
Trachypithecus	0.76
Presbytis	3.32
Alouatta	2.19
Ateles	2.99
Cebus	2.35
Sample mean	2.02
Sample median	2.35

[a] Standardized taxon means between PLS shape- and behavior-space

Table 2.14. Estimated phylogenetic signal of analyzed variables

a	λ	p	K	p
CpPx	0.89	0.00	0.42	0.00
CpDn	0.99	0.00	0.58	0.00
Cp2	0.99	0.00	1.13	0.00
Cp4	1.01	0.00	1.93	0.00
Cp23A	0.97	0.00	0.66	0.00
CpPxA	0.98	0.00	0.91	0.00
CpScA	1.00	0.00	2.08	0.00
Cp3SD	0.81	0.02	0.52	0.00
CpHmC	1.01	0.00	1.32	0.00
CpHP	0.89	0.00	0.50	0.00
HmPx	0.99	0.00	0.77	0.00
Hm5	0.99	0.00	1.41	0.00
Hm45A	0.54	0.16	0.31	0.02
HmPxA	1.00	0.00	0.70	0.00
CpHmPxA	1.00	0.00	1.44	0.00
CMC34A	0.86	0.00	0.44	0.00
LuDs	0.94	0.00	0.72	0.00
LuTq	0.82	0.00	0.45	0.00
LuSc	0.99	0.00	1.43	0.00
LuRa	0.99	0.00	0.89	0.00
LuDsTqA	0.99	0.00	1.00	0.00
LuDsScA	0.90	0.00	0.46	0.01
LuScRaA	0.91	0.00	0.58	0.00
LuCpRaA	0.99	0.00	0.98	0.00
LuCpC	0.81	0.00	0.34	0.01
TqHm	0.93	0.00	1.10	0.00
TqLu	0.98	0.00	1.69	0.00
TqPi	0.93	0.00	0.68	0.00
TqSt	1.01	0.00	5.96	0.00
TqHmPiA	0.90	0.00	0.72	0.00
Tq1LuA	0.91	0.00	0.34	0.01
LuTqDsA	0.93	0.00	0.52	0.00
MCJAR	0.96	0.00	0.78	0.00
b Locomotor variables				
QuadA	0.81	0.00	0.56	0.00
SuspA	1.00	0.00	1.55	0.00
ClimbA	0.80	0.00	0.51	0.02
LeapA	1.00	0.00	1.00	0.00
Quad	1.00	0.00	0.81	0.00
Susp	1.00	0.00	1.50	0.00
Climb	0.29	0.70	0.48	0.01
Leap	1.00	0.00	0.88	0.00
Arb	1.00	0.01	0.69	0.01

Table 2.15. PIC Spearman correlation tests for allometric scaling

a	Males		Females		Means	
	rho	p	rho	p	rho	p
CpPx	0.07	0.74	0.14	0.49	0.13	0.51
CpDn	0.05	0.79	0.07	0.73	0.22	0.28
Cp2	-0.10	0.61	-0.11	0.57	-0.10	0.62
Cp4	-0.26	0.19	-0.27	0.18	-0.29	0.14
Cp23A	0.00	0.99	-0.01	0.94	-0.04	0.84
CpPxA	0.20	0.31	-0.07	0.72	0.10	0.61
CpScA	-0.21	0.30	-0.15	0.44	-0.26	0.19
Cp3SD	0.01	0.97	0.17	0.39	0.11	0.58
CpHmC	0.20	0.31	-0.07	0.73	0.12	0.57
CpHP	0.20	0.31	-0.17	0.39	0.00	1.00
HmPx	-0.39	**0.04**	-0.30	0.12	-0.34	0.08
Hm5	0.28	0.16	0.13	0.51	0.11	0.59
Hm45A	-0.18	0.37	0.19	0.33	-0.09	0.64
HmPxA	0.27	0.18	0.10	0.61	0.16	0.43
CpHmPxA	0.24	0.23	0.02	0.93	0.10	0.63
CMC34A	0.11	0.60	0.25	0.20	0.22	0.27
LuDs	0.01	0.95	-0.02	0.93	0.17	0.41
LuTq	0.06	0.76	0.13	0.51	0.18	0.37
LuSc	-0.11	0.60	-0.03	0.88	-0.06	0.76
LuRa	0.04	0.86	0.01	0.98	0.00	1.00
LuDsTqA	-0.21	0.29	-0.29	0.14	-0.26	0.19
LuDsScA	-0.01	0.98	-0.07	0.75	-0.01	0.95
LuScRaA	0.00	0.99	0.39	**0.04**	0.23	0.24
LuCpRaA	-0.49	**0.01**	-0.74	**0.00**	-0.62	**0.00**
LuCpC	-0.19	0.35	-0.02	0.93	-0.19	0.35
TqHm	-0.10	0.63	-0.16	0.43	-0.09	0.64
TqLu	0.10	0.63	0.11	0.57	0.06	0.77
TqPi	0.05	0.81	-0.27	0.18	-0.33	0.09
TqSt	-0.15	0.45	-0.15	0.46	-0.05	0.81
TqHmPiA	0.14	0.50	0.34	0.09	0.49	**0.01**
Tq1LuA	-0.22	0.27	-0.26	0.18	-0.26	0.20
LuTqDsA	0.43	**0.03**	0.19	0.33	0.33	0.09
MCJAR	-0.09	0.66	0.10	0.63	0.11	0.57
b Locomotor variables						
QuadA	0.04	0.87	-0.08	0.72	0.06	0.78
SuspA	0.13	0.57	0.07	0.77	0.11	0.65
ClimbA	0.26	0.25	0.20	0.38	0.14	0.56
LeapA	-0.56	**0.01**	-0.40	0.07	-0.47	**0.03**
Quad	0.41	0.07	0.29	0.21	0.39	0.08
Susp	0.12	0.60	0.10	0.65	0.16	0.47
Climb	-0.38	0.09	-0.54	**0.01**	-0.57	**0.01**
Leap	-0.55	**0.01**	-0.36	0.11	-0.46	**0.03**
Arb	-0.70	**0.00**	-0.58	**0.01**	-0.70	**0.00**

Table 2.16. Condition of selected articulations in sampled specimens. Tot, total. Cont, continuous. D, dorsal only. P, palmar only. D&P, separate dorsal and palmar facets. Na, absent. Plm acc, palmar accessory facet.

	a	Capitate - Mc4					**b**	Capitate - hamate				**c**	Hamate - capitate			
	Tot	Cont	D	P	D&P	Na		Cont	D&P	Dist D&P	Plm acc		Tot	Cont	D&P	Dist D&P	Plm acc
Pan	44	0	0	0	0	44		44	0	0	2		44	44	0	0	0
Gorilla	38	0	16	0	0	22		38	0	0	0		37	38	0	0	0
Pongo	34	0	19	0	1	14		26	8	0	0		35	30	5	0	0
Hylobatids	29	12	0	2	15	0		3	26	12	1		29	2	27	12	1
Papio	14	5	1	1	7	0		14	0	0	0		14	14	0	0	0
Lophocebus	6	1	0	1	4	0		6	0	0	0		6	6	0	0	0
Mandrillus	9	0	0	4	5	0		9	0	0	0		8	8	0	0	0
Cercocebus	2	0	0	0	2	0		2	0	0	0		2	2	0	0	0
Macaca	18	1	0	0	17	0		18	0	0	1		18	18	0	0	0
Erythrocebus	7	7	0	0	0	0		7	0	0	0		7	7	0	0	0
Cercopithecus	11	1	0	1	9	0		11	0	0	0		11	11	0	0	0
Colobus	9	0	0	1	8	0		9	0	0	0		9	9	0	0	0
Procolobus	13	0	2	1	10	0		13	0	0	0		13	12	1	0	0
Nasalis	17	1	0	0	16	0		13	4	3	11		17	14	3	1	3
Trachypithecus	17	1	0	0	16	0		17	0	0	0		17	17	0	0	1
Presbytis	2	0	0	0	2	0		2	0	0	0		2	2	0	0	0
Alouatta	32	23	0	0	9	0		32	0	0	0		32	32	0	0	0
Ateles	13	13	0	0	0	0		1	12	1	0		14	8	6	0	0
Cebus	28	28	0	0	0	0		28	0	0	0		28	28	0	0	0

Table 2.17. Individual positional classifications and average posterior probabilities after 100 repetitions of 10-fold cross-validation

			DFA					*glmnet*				
Specimen	Taxon	Class	*DG*	*KW*	*PG*	*S*	Pred	*DG*	*KW*	*PG*	*S*	Pred
AMNH 51202	*P. t. schweinfurthii*	*KW*	0.00	1.00	0.00	0.00	*KW*	0.00	1.00	0.00	0.00	*KW*
AMNH 51205	*P. t. schweinfurthii*	*KW*	0.00	1.00	0.00	0.00	*KW*	0.02	0.97	0.01	0.00	*KW*
AMNH 51278	*P. t. schweinfurthii*	*KW*	0.00	1.00	0.00	0.00	*KW*	0.00	1.00	0.00	0.00	*KW*
AMNH 51376	*P. t. schweinfurthii*	*KW*	0.00	1.00	0.00	0.00	*KW*	0.00	1.00	0.00	0.00	*KW*
AMNH 51377	*P. t. schweinfurthii*	*KW*	0.00	1.00	0.00	0.00	*KW*	0.00	1.00	0.00	0.00	*KW*
AMNH 51379	*P. t. schweinfurthii*	*KW*	0.00	1.00	0.00	0.00	*KW*	0.00	1.00	0.00	0.00	*KW*
AMNH 51381	*P. t. schweinfurthii*	*KW*	0.00	1.00	0.00	0.00	*KW*	0.00	0.99	0.01	0.00	*KW*
AMNH 51393	*P. t. schweinfurthii*	*KW*	0.00	1.00	0.00	0.00	*KW*	0.01	0.99	0.00	0.00	*KW*
AMNH 201588	*P. t. schweinfurthii*	*KW*	0.00	1.00	0.00	0.00	*KW*	0.00	1.00	0.00	0.00	*KW*
NMNH 236971	*P. t. schweinfurthii*	*KW*	0.00	1.00	0.00	0.00	*KW*	0.00	1.00	0.00	0.00	*KW*
AMNH 54330	*P. t. troglodytes*	*KW*	0.00	1.00	0.00	0.00	*KW*	0.02	0.97	0.01	0.00	*KW*
AMNH 90189	*P. t. troglodytes*	*KW*	0.00	1.00	0.00	0.00	*KW*	0.00	1.00	0.00	0.00	*KW*
AMNH 90190	*P. t. troglodytes*	*KW*	0.00	1.00	0.00	0.00	*KW*	0.01	0.86	0.14	0.00	*KW*
AMNH 90191	*P. t. troglodytes*	*KW*	0.00	1.00	0.00	0.00	*KW*	0.00	1.00	0.00	0.00	*KW*
AMNH 90292	*P. t. troglodytes*	*KW*	0.00	1.00	0.00	0.00	*KW*	0.00	0.99	0.01	0.00	*KW*
AMNH 167342	*P. t. troglodytes*	*KW*	0.00	1.00	0.00	0.00	*KW*	0.00	1.00	0.00	0.00	*KW*
AMNH 167343	*P. t. troglodytes*	*KW*	0.00	1.00	0.00	0.00	*KW*	0.00	1.00	0.00	0.00	*KW*
AMNH 167344	*P. t. troglodytes*	*KW*	0.00	1.00	0.00	0.00	*KW*	0.00	1.00	0.00	0.00	*KW*
AMNH 167346	*P. t. troglodytes*	*KW*	0.00	1.00	0.00	0.00	*KW*	0.00	1.00	0.00	0.00	*KW*
AMNH 201469	*P. t. troglodytes*	*KW*	0.00	1.00	0.00	0.00	*KW*	0.00	0.99	0.00	0.00	*KW*
UMMZ 39507	*P. t. troglodytes*	*KW*	0.00	1.00	0.00	0.00	*KW*	0.00	1.00	0.00	0.00	*KW*
MCZ 15312	*P. t. troglodytes*	*KW*	0.00	1.00	0.00	0.00	*KW*	0.00	0.98	0.01	0.01	*KW*
AMNH 89351	*P. t. verus*	*KW*	0.00	1.00	0.00	0.00	*KW*	0.00	1.00	0.00	0.00	*KW*
AMNH 89353	*P. t. verus*	*KW*	0.00	1.00	0.00	0.00	*KW*	0.00	1.00	0.00	0.00	*KW*
AMNH 89354	*P. t. verus*	*KW*	0.00	1.00	0.00	0.00	*KW*	0.00	1.00	0.00	0.00	*KW*
AMNH 89355	*P. t. verus*	*KW*	0.00	1.00	0.00	0.00	*KW*	0.00	1.00	0.00	0.00	*KW*
AMNH 89406	*P. t. verus*	*KW*	0.00	1.00	0.00	0.00	*KW*	0.00	1.00	0.00	0.00	*KW*
AMNH 174860	*P. t. verus*	*KW*	0.00	1.00	0.00	0.00	*KW*	0.00	1.00	0.00	0.00	*KW*
AMNH 174861	*P. t. verus*	*KW*	0.00	1.00	0.00	0.00	*KW*	0.00	1.00	0.00	0.00	*KW*

			DFA					*glmnet*				
Specimen	Taxon	Class	*DG*	*KW*	*PG*	*S*	Pred	*DG*	*KW*	*PG*	*S*	Pred
NMNH 256973	*P. t. verus*	*KW*	0.00	1.00	0.00	0.00	*KW*	0.00	0.73	0.26	0.01	*KW*
NMNH 477333	*P. t. verus*	*KW*	0.00	1.00	0.00	0.00	*KW*	0.00	1.00	0.00	0.00	*KW*
NMNH 481803	*P. t. verus*	*KW*	0.00	1.00	0.00	0.00	*KW*	0.00	0.98	0.02	0.00	*KW*
NMNH 481804	*P. t. verus*	*KW*	0.00	1.00	0.00	0.00	*KW*	0.00	1.00	0.00	0.00	*KW*
UMMZ 76276	*P. t. verus*	*KW*	0.00	1.00	0.00	0.00	*KW*	0.00	1.00	0.00	0.00	*KW*
UMMZ 76277	*P. t. verus*	*KW*	0.00	1.00	0.00	0.00	*KW*	0.00	1.00	0.00	0.00	*KW*
MCZ 20041	*P. t. ellioti*	*KW*	0.00	1.00	0.00	0.00	*KW*	0.00	1.00	0.00	0.00	*KW*
MCZ 23163	*P. t. ellioti*	*KW*	0.00	1.00	0.00	0.00	*KW*	0.00	0.98	0.02	0.00	*KW*
MCZ 23167	*P. t. ellioti*	*KW*	0.00	1.00	0.00	0.00	*KW*	0.00	1.00	0.00	0.00	*KW*
MCZ 26849	*P. t. ellioti*	*KW*	0.00	1.00	0.00	0.00	*KW*	0.00	1.00	0.00	0.00	*KW*
UMMZ 167199	*P. t. ellioti*	*KW*	0.00	1.00	0.00	0.00	*KW*	0.00	1.00	0.00	0.00	*KW*
AMNH 86857	*P. paniscus*	*KW*	0.00	1.00	0.00	0.00	*KW*	0.00	0.98	0.00	0.02	*KW*
MCZ 38018	*P. paniscus*	*KW*	0.00	1.00	0.00	0.00	*KW*	0.06	0.94	0.00	0.00	*KW*
MCZ 38019	*P. paniscus*	*KW*	0.00	1.00	0.00	0.00	*KW*	0.00	0.99	0.01	0.00	*KW*
MCZ 38020	*P. paniscus*	*KW*	0.00	1.00	0.00	0.00	*KW*	0.28	0.72	0.00	0.00	*KW*
AMNH 54355	*G. gorilla*	*KW*	0.00	1.00	0.00	0.00	*KW*	0.00	0.97	0.03	0.00	*KW*
AMNH 54356	*G. gorilla*	*KW*	0.00	1.00	0.00	0.00	*KW*	0.00	0.99	0.00	0.01	*KW*
AMNH 69398	*G. gorilla*	*KW*	0.00	1.00	0.00	0.00	*KW*	0.02	0.96	0.01	0.00	*KW*
AMNH 81651	*G. gorilla*	*KW*	0.00	1.00	0.00	0.00	*KW*	0.00	1.00	0.00	0.00	*KW*
AMNH 81652	*G. gorilla*	*KW*	0.00	1.00	0.00	0.00	*KW*	0.00	1.00	0.00	0.00	*KW*
AMNH 90289	*G. gorilla*	*KW*	0.00	1.00	0.00	0.00	*KW*	0.00	1.00	0.00	0.00	*KW*
AMNH 167335	*G. gorilla*	*KW*	0.00	1.00	0.00	0.00	*KW*	0.00	1.00	0.00	0.00	*KW*
AMNH 167337	*G. gorilla*	*KW*	0.00	1.00	0.00	0.00	*KW*	0.00	0.97	0.01	0.02	*KW*
AMNH 167338	*G. gorilla*	*KW*	0.00	1.00	0.00	0.00	*KW*	0.00	0.99	0.01	0.00	*KW*
AMNH 167339	*G. gorilla*	*KW*	0.00	1.00	0.00	0.00	*KW*	0.00	0.99	0.01	0.00	*KW*
AMNH 167340	*G. gorilla*	*KW*	0.00	1.00	0.00	0.00	*KW*	0.00	0.98	0.01	0.01	*KW*
AMNH 201471	*G. gorilla*	*KW*	0.00	1.00	0.00	0.00	*KW*	0.00	0.97	0.01	0.02	*KW*
AMNH 214103	*G. gorilla*	*KW*	0.00	1.00	0.00	0.00	*KW*	0.00	1.00	0.00	0.00	*KW*
MCZ 17684	*G. gorilla*	*KW*	0.00	1.00	0.00	0.00	*KW*	0.00	1.00	0.00	0.00	*KW*
MCZ 20038	*G. gorilla*	*KW*	0.00	1.00	0.00	0.00	*KW*	0.00	0.97	0.03	0.00	*KW*

			DFA					*glmnet*				
Specimen	Taxon	Class	*DG*	*KW*	*PG*	*S*	Pred	*DG*	*KW*	*PG*	*S*	Pred
MCZ 20039	*G. gorilla*	*KW*	0.00	1.00	0.00	0.00	*KW*	0.00	0.99	0.00	0.00	*KW*
MCZ 20043	*G. gorilla*	*KW*	0.00	1.00	0.00	0.00	*KW*	0.00	1.00	0.00	0.00	*KW*
MCZ 23160	*G. gorilla*	*KW*	0.00	1.00	0.00	0.00	*KW*	0.00	1.00	0.00	0.00	*KW*
MCZ 23162	*G. gorilla*	*KW*	0.00	1.00	0.00	0.00	*KW*	0.00	0.97	0.02	0.01	*KW*
MCZ 26850	*G. gorilla*	*KW*	0.00	1.00	0.00	0.00	*KW*	0.01	0.96	0.01	0.02	*KW*
MCZ 29047	*G. gorilla*	*KW*	0.00	1.00	0.00	0.00	*KW*	0.00	0.98	0.01	0.00	*KW*
MCZ 29049	*G. gorilla*	*KW*	0.00	1.00	0.00	0.00	*KW*	0.00	0.99	0.01	0.00	*KW*
MCZ 37264	*G. gorilla*	*KW*	0.00	1.00	0.00	0.00	*KW*	0.00	1.00	0.00	0.00	*KW*
MCZ 38326	*G. gorilla*	*KW*	0.00	1.00	0.00	0.00	*KW*	0.00	1.00	0.00	0.00	*KW*
MCZ 57482	*G. gorilla*	*KW*	0.00	1.00	0.00	0.00	*KW*	0.00	0.95	0.05	0.01	*KW*
UMMZ 17886	*G. gorilla*	*KW*	0.00	1.00	0.00	0.00	*KW*	0.01	0.99	0.00	0.00	*KW*
AMNH 54089	*G. beringei*	*KW*	0.00	1.00	0.00	0.00	*KW*	0.00	1.00	0.00	0.00	*KW*
AMNH 54090	*G. beringei*	*KW*	0.00	1.00	0.00	0.00	*KW*	0.00	1.00	0.00	0.00	*KW*
AMNH 54091	*G. beringei*	*KW*	0.00	1.00	0.00	0.00	*KW*	0.00	0.99	0.01	0.00	*KW*
AMNH 115609	*G. beringei*	*KW*	0.00	1.00	0.00	0.00	*KW*	0.00	1.00	0.00	0.00	*KW*
NMNH 395636	*G. beringei*	*KW*	0.00	1.00	0.00	0.00	*KW*	0.00	1.00	0.00	0.00	*KW*
NMNH 396934	*G. beringei*	*KW*	0.00	1.00	0.00	0.00	*KW*	0.00	0.99	0.01	0.00	*KW*
NMNH 396935	*G. beringei*	*KW*	0.00	1.00	0.00	0.00	*KW*	0.00	0.98	0.01	0.00	*KW*
NMNH 396937	*G. beringei*	*KW*	0.00	1.00	0.00	0.00	*KW*	0.00	1.00	0.00	0.00	*KW*
NMNH 397351	*G. beringei*	*KW*	0.00	1.00	0.00	0.00	*KW*	0.00	0.99	0.00	0.00	*KW*
MCZ 23182	*G. beringei*	*KW*	0.00	1.00	0.00	0.00	*KW*	0.01	0.98	0.01	0.00	*KW*
MCZ 38017	*G. beringei*	*KW*	0.00	1.00	0.00	0.00	*KW*	0.00	0.98	0.01	0.00	*KW*
AMNH 28252	*P. pygmaeus*	*S*	0.00	0.00	0.09	0.91	*S*	0.06	0.01	0.25	0.68	*S*
AMNH 28253	*P. pygmaeus*	*S*	0.00	0.00	0.00	1.00	*S*	0.00	0.01	0.03	0.96	*S*
NMNH 145301	*P. pygmaeus*	*S*	0.00	0.00	0.00	1.00	*S*	0.00	0.00	0.02	0.98	*S*
NMNH 145302	*P. pygmaeus*	*S*	0.00	0.00	0.00	1.00	*S*	0.00	0.03	0.02	0.94	*S*
NMNH 145304	*P. pygmaeus*	*S*	0.00	0.00	0.01	0.99	*S*	0.00	0.04	0.09	0.87	*S*
NMNH 145305	*P. pygmaeus*	*S*	0.00	0.00	0.00	1.00	*S*	0.00	0.00	0.09	0.91	*S*
NMNH 145308	*P. pygmaeus*	*S*	0.00	0.00	0.00	1.00	*S*	0.00	0.02	0.16	0.82	*S*
NMNH 145309	*P. pygmaeus*	*S*	0.00	0.00	0.00	1.00	*S*	0.00	0.00	0.00	1.00	*S*

			DFA					*glmnet*				
Specimen	Taxon	Class	*DG*	*KW*	*PG*	*S*	Pred	*DG*	*KW*	*PG*	*S*	Pred
NMNH 145310	*P. pygmaeus*	*S*	0.00	0.00	0.00	1.00	*S*	0.00	0.01	0.00	0.99	*S*
MCZ 37362	*P. pygmaeus*	*S*	0.00	0.00	0.00	1.00	*S*	0.00	0.00	0.03	0.96	*S*
MCZ 37363	*P. pygmaeus*	*S*	0.00	0.00	0.01	0.99	*S*	0.00	0.01	0.04	0.95	*S*
MCZ 37364	*P. pygmaeus*	*S*	0.00	0.00	0.00	1.00	*S*	0.00	0.00	0.00	1.00	*S*
MCZ 37365	*P. pygmaeus*	*S*	0.00	0.00	0.15	0.85	*S*	0.00	0.00	0.30	0.70	*S*
NMNH 142170	*P. pygmaeus*	*S*	0.00	0.00	0.00	1.00	*S*	0.00	0.00	0.00	1.00	*S*
NMNH 153805	*P. pygmaeus*	*S*	0.00	0.00	0.00	1.00	*S*	0.00	0.01	0.01	0.98	*S*
NMNH 153823	*P. pygmaeus*	*S*	0.00	0.00	0.00	1.00	*S*	0.00	0.00	0.00	1.00	*S*
AMNH 61586	*P. pygmaeus*	*S*	0.00	0.00	0.00	1.00	*S*	0.00	0.00	0.01	0.99	*S*
AMNH 202511	*P. pygmaeus*	*S*	0.00	0.00	0.00	1.00	*S*	0.00	0.00	0.03	0.97	*S*
AMNH 239847	*P. pygmaeus*	*S*	0.00	0.00	0.00	1.00	*S*	0.00	0.00	0.06	0.94	*S*
CMNH HTB1030	*P. abelii*	*S*	0.00	0.00	0.00	1.00	*S*	0.00	0.00	0.02	0.97	*S*
CMNH HTB1055	*P. abelii*	*S*	0.00	0.00	0.00	1.00	*S*	0.00	0.00	0.00	1.00	*S*
CMNH HTB1168	*P. abelii*	*S*	0.00	0.00	0.00	1.00	*S*	0.00	0.05	0.00	0.95	*S*
CMNH HTB1444	*P. abelii*	*S*	0.00	0.00	0.00	1.00	*S*	0.00	0.00	0.00	1.00	*S*
NMNH 143590	*P. abelii*	*S*	0.00	0.00	0.00	1.00	*S*	0.00	0.00	0.00	1.00	*S*
NMNH 143593	*P. abelii*	*S*	0.00	0.00	0.00	1.00	*S*	0.00	0.00	0.07	0.93	*S*
NMNH 143594	*P. abelii*	*S*	0.00	0.00	0.00	1.00	*S*	0.00	0.01	0.00	0.99	*S*
NMNH 143596	*P. abelii*	*S*	0.00	0.00	0.00	1.00	*S*	0.00	0.00	0.00	1.00	*S*
NMNH 143597	*P. abelii*	*S*	0.00	0.00	0.00	1.00	*S*	0.00	0.00	0.00	1.00	*S*
NMNH 143598	*P. abelii*	*S*	0.00	0.00	0.00	1.00	*S*	0.00	0.00	0.00	1.00	*S*
NMNH 143600	*P. abelii*	*S*	0.00	0.00	0.00	1.00	*S*	0.00	0.00	0.00	1.00	*S*
NMNH 143601	*P. abelii*	*S*	0.00	0.00	0.00	1.00	*S*	0.00	0.00	0.00	1.00	*S*
NMNH 143602	*P. abelii*	*S*	0.00	0.00	0.00	1.00	*S*	0.00	0.00	0.00	1.00	*S*
NMNH 270807	*P. abelii*	*S*	0.00	0.00	0.00	1.00	*S*	0.00	0.00	0.00	1.00	*S*
AMNH 80068	*Hoolock*	*S*	0.00	0.00	0.00	1.00	*S*	0.00	0.00	0.00	1.00	*S*
AMNH 83418	*Hoolock*	*S*	0.00	0.00	0.00	1.00	*S*	0.00	0.00	0.00	1.00	*S*
AMNH 83420	*Hoolock*	*S*	0.00	0.00	0.00	1.00	*S*	0.00	0.00	0.00	0.99	*S*
AMNH 83423	*Hoolock*	*S*	0.00	0.00	0.00	1.00	*S*	0.00	0.00	0.00	1.00	*S*
AMNH 83425	*Hoolock*	*S*	0.00	0.00	0.00	1.00	*S*	0.00	0.00	0.00	1.00	*S*

			DFA					*glmnet*				
Specimen	Taxon	Class	*DG*	*KW*	*PG*	*S*	Pred	*DG*	*KW*	*PG*	*S*	Pred
AMNH 112676	*Hoolock*	*S*	0.00	0.00	0.00	1.00	*S*	0.00	0.00	0.00	1.00	*S*
AMNH 112720	*Hoolock*	*S*	0.00	0.00	0.00	1.00	*S*	0.00	0.00	0.00	1.00	*S*
MCZ 37378	*H. muelleri*	*S*	0.00	0.00	0.00	1.00	*S*	0.00	0.00	0.00	1.00	*S*
MCZ 37380	*H. muelleri*	*S*	0.00	0.00	0.00	1.00	*S*	0.00	0.00	0.00	1.00	*S*
MCZ 37381	*H. muelleri*	*S*	0.00	0.00	0.00	1.00	*S*	0.00	0.00	0.00	1.00	*S*
MCZ 37383	*H. muelleri*	*S*	0.00	0.00	0.00	1.00	*S*	0.00	0.00	0.00	1.00	*S*
MCZ 41417	*H. lar*	*S*	0.00	0.00	0.00	1.00	*S*	0.00	0.00	0.00	1.00	*S*
MCZ 41524	*H. lar*	*S*	0.00	0.00	0.00	1.00	*S*	0.00	0.00	0.00	1.00	*S*
MCZ 41525	*H. lar*	*S*	0.00	0.00	0.00	1.00	*S*	0.00	0.00	0.00	1.00	*S*
MCZ 41526	*H. lar*	*S*	0.00	0.00	0.00	1.00	*S*	0.00	0.00	0.00	1.00	*S*
MCZ 41527	*H. lar*	*S*	0.00	0.00	0.00	1.00	*S*	0.00	0.00	0.00	1.00	*S*
MCZ 41529	*H. lar*	*S*	0.00	0.00	0.00	1.00	*S*	0.00	0.00	0.00	1.00	*S*
MCZ 41530	*H. lar*	*S*	0.00	0.00	0.00	1.00	*S*	0.00	0.00	0.00	1.00	*S*
MCZ 41531	*H. lar*	*S*	0.00	0.00	0.00	1.00	*S*	0.00	0.00	0.00	1.00	*S*
MCZ 41532	*H. lar*	*S*	0.00	0.00	0.00	1.00	*S*	0.00	0.00	0.00	1.00	*S*
MCZ 41534	*H. lar*	*S*	0.00	0.00	0.00	1.00	*S*	0.00	0.00	0.00	1.00	*S*
MCZ 41536	*H. lar*	*S*	0.00	0.00	0.00	1.00	*S*	0.00	0.00	0.00	1.00	*S*
AMNH 43063	*H. lar*	*S*	0.00	0.00	0.00	1.00	*S*	0.00	0.00	0.00	1.00	*S*
MCZ 41565	*H. lar*	*S*	0.00	0.00	0.00	1.00	*S*	0.00	0.00	0.00	1.00	*S*
UMMZ 160908	*H. lar*	*S*	0.00	0.00	0.00	1.00	*S*	0.00	0.00	0.00	1.00	*S*
UMMZ 160909	*H. lar*	*S*	0.00	0.00	0.00	1.00	*S*	0.00	0.00	0.00	1.00	*S*
AMNH 106581	*Symphalangus*	*S*	0.00	0.00	0.00	1.00	*S*	0.00	0.00	0.00	1.00	*S*
AMNH 106583	*Symphalangus*	*S*	0.00	0.00	0.00	1.00	*S*	0.00	0.00	0.00	1.00	*S*
MCZ 27867	*Symphalangus*	*S*	0.00	0.00	0.00	1.00	*S*	0.00	0.00	0.00	1.00	*S*
AMNH 51380	*Papio*	*DG*	1.00	0.00	0.00	0.00	*DG*	1.00	0.00	0.00	0.00	*DG*
AMNH 52668	*Papio*	*DG*	0.74	0.00	0.26	0.00	*DG*	0.89	0.03	0.07	0.00	*DG*
AMNH 52676	*Papio*	*DG*	0.99	0.00	0.01	0.00	*DG*	0.95	0.00	0.05	0.00	*DG*
AMNH 82097	*Papio*	*DG*	0.36	0.00	0.64	0.00	***PG***	0.71	0.02	0.27	0.00	*DG*
AMNH 187369	*Papio*	*DG*	0.69	0.00	0.31	0.00	*DG*	0.53	0.00	0.47	0.00	*DG*
MCZ 15378	*Papio*	*DG*	0.98	0.00	0.02	0.00	*DG*	0.88	0.00	0.12	0.00	*DG*

			DFA					*glmnet*				
Specimen	Taxon	Class	*DG*	*KW*	*PG*	*S*	Pred	*DG*	*KW*	*PG*	*S*	Pred
NMNH 236976	*Papio*	*DG*	0.95	0.00	0.05	0.00	*DG*	0.92	0.00	0.08	0.00	*DG*
NMNH 239743	*Papio*	*DG*	0.76	0.00	0.24	0.00	*DG*	0.81	0.01	0.18	0.00	*DG*
NMNH 384223	*Papio*	*DG*	0.98	0.00	0.02	0.00	*DG*	0.93	0.00	0.07	0.00	*DG*
NMNH 384227	*Papio*	*DG*	0.71	0.00	0.29	0.00	*DG*	0.79	0.00	0.21	0.00	*DG*
NMNH 384228	*Papio*	*DG*	0.93	0.00	0.07	0.00	*DG*	0.63	0.03	0.33	0.01	*DG*
NMNH 384229	*Papio*	*DG*	0.77	0.00	0.23	0.00	*DG*	0.67	0.00	0.33	0.00	*DG*
NMNH 384234	*Papio*	*DG*	0.81	0.00	0.19	0.00	*DG*	0.75	0.00	0.25	0.00	*DG*
NMNH 384235	*Papio*	*DG*	0.45	0.00	0.55	0.00	***PG***	0.58	0.01	0.41	0.00	*DG*
AMNH 52596	*Lophocebus*	*PG*	0.00	0.00	1.00	0.00	*PG*	0.01	0.00	0.99	0.00	*PG*
AMNH 52609	*Lophocebus*	*PG*	0.01	0.00	0.99	0.00	*PG*	0.02	0.00	0.98	0.00	*PG*
AMNH 52627	*Lophocebus*	*PG*	0.02	0.00	0.98	0.00	*PG*	0.07	0.00	0.93	0.00	*PG*
MCZ 37928	*Lophocebus*	*PG*	0.01	0.00	0.99	0.00	*PG*	0.07	0.00	0.93	0.00	*PG*
AMNH 167678	*Lophocebus*	*PG*	0.00	0.00	1.00	0.00	*PG*	0.00	0.00	1.00	0.00	*PG*
NMNH 578579	*Lophocebus*	*PG*	0.01	0.00	0.99	0.00	*PG*	0.05	0.00	0.95	0.00	*PG*
AMNH 89361	*Mandrillus*	*DG*	0.96	0.00	0.04	0.00	*DG*	0.72	0.01	0.27	0.00	*DG*
AMNH 89362	*Mandrillus*	*DG*	0.75	0.00	0.25	0.00	*DG*	0.81	0.01	0.18	0.00	*DG*
AMNH 89364	*Mandrillus*	*DG*	1.00	0.00	0.00	0.00	*DG*	1.00	0.00	0.00	0.00	*DG*
AMNH 89367	*Mandrillus*	*DG*	1.00	0.00	0.00	0.00	*DG*	1.00	0.00	0.00	0.00	*DG*
AMNH 170364	*Mandrillus*	*DG*	0.83	0.00	0.17	0.00	*DG*	0.54	0.01	0.45	0.00	*DG*
AMNH 170366	*Mandrillus*	*DG*	1.00	0.00	0.00	0.00	*DG*	1.00	0.00	0.00	0.00	*DG*
MCZ 34137	*Mandrillus*	*DG*	1.00	0.00	0.00	0.00	*DG*	0.97	0.00	0.03	0.00	*DG*
MCZ 34177	*Mandrillus*	*DG*	1.00	0.00	0.00	0.00	*DG*	0.99	0.00	0.00	0.00	*DG*
AMNH 52634	*Cercocebus*	*PG*	0.29	0.00	0.71	0.00	*PG*	0.14	0.00	0.86	0.00	*PG*
AMNH 81250	*Cercocebus*	*PG*	0.08	0.00	0.92	0.00	*PG*	0.27	0.00	0.72	0.01	*PG*
AMNH 103654	*Macaca*	*PG*	0.00	0.00	1.00	0.00	*PG*	0.01	0.00	0.98	0.00	*PG*
AMNH 103659	*Macaca*	*PG*	0.02	0.00	0.98	0.00	*PG*	0.01	0.00	0.97	0.01	*PG*
AMNH 175460	*Macaca*	*PG*	0.00	0.00	1.00	0.00	*PG*	0.00	0.00	1.00	0.00	*PG*
MCZ 35626	*Macaca*	*PG*	0.00	0.00	1.00	0.00	*PG*	0.01	0.00	0.98	0.00	*PG*
MCZ 35629	*Macaca*	*PG*	0.00	0.00	1.00	0.00	*PG*	0.00	0.00	1.00	0.00	*PG*
MCZ 35652	*Macaca*	*PG*	0.00	0.00	1.00	0.00	*PG*	0.00	0.00	0.94	0.06	*PG*

			DFA					*glmnet*				
Specimen	Taxon	Class	*DG*	*KW*	*PG*	*S*	Pred	*DG*	*KW*	*PG*	*S*	Pred
MCZ 35658	*Macaca*	*PG*	0.18	0.00	0.82	0.00	*PG*	0.30	0.01	0.69	0.00	*PG*
MCZ 35677	*Macaca*	*PG*	0.00	0.00	1.00	0.00	*PG*	0.00	0.00	1.00	0.00	*PG*
MCZ 35681	*Macaca*	*PG*	0.00	0.00	1.00	0.00	*PG*	0.00	0.00	1.00	0.00	*PG*
MCZ 35693	*Macaca*	*PG*	0.01	0.00	0.99	0.00	*PG*	0.01	0.00	0.99	0.00	*PG*
MCZ 35694	*Macaca*	*PG*	0.00	0.00	1.00	0.00	*PG*	0.00	0.00	1.00	0.00	*PG*
MCZ 35700	*Macaca*	*PG*	0.02	0.00	0.98	0.00	*PG*	0.02	0.00	0.98	0.00	*PG*
MCZ 35701	*Macaca*	*PG*	0.00	0.00	1.00	0.00	*PG*	0.00	0.00	1.00	0.00	*PG*
MCZ 35729	*Macaca*	*PG*	0.01	0.00	0.99	0.00	*PG*	0.02	0.00	0.97	0.00	*PG*
MCZ 35736	*Macaca*	*PG*	0.00	0.00	1.00	0.00	*PG*	0.00	0.00	1.00	0.00	*PG*
UMMZ 130418	*Macaca*	*PG*	0.00	0.00	1.00	0.00	*PG*	0.00	0.00	1.00	0.00	*PG*
UMMZ 161308	*Macaca*	*PG*	0.00	0.00	1.00	0.00	*PG*	0.00	0.00	1.00	0.00	*PG*
UMMZ 56349	*Macaca*	*PG*	0.00	0.00	1.00	0.00	*PG*	0.00	0.08	0.77	0.15	*PG*
AMNH 34709	*Erythrocebus*	*DG*	0.98	0.00	0.02	0.00	*DG*	0.81	0.00	0.19	0.00	*DG*
AMNH 34712	*Erythrocebus*	*DG*	0.99	0.00	0.01	0.00	*DG*	0.91	0.00	0.09	0.00	*DG*
AMNH 34713	*Erythrocebus*	*DG*	1.00	0.00	0.00	0.00	*DG*	0.98	0.00	0.02	0.00	*DG*
AMNH 34714	*Erythrocebus*	*DG*	0.96	0.00	0.04	0.00	*DG*	0.59	0.00	0.41	0.00	*DG*
NMNH 257013	*Erythrocebus*	*DG*	1.00	0.00	0.00	0.00	*DG*	0.93	0.00	0.07	0.00	*DG*
NMNH 399317	*Erythrocebus*	*DG*	0.95	0.00	0.05	0.00	*DG*	0.88	0.01	0.12	0.00	*DG*
NMNH 538311	*Erythrocebus*	*DG*	1.00	0.00	0.00	0.00	*DG*	0.99	0.00	0.01	0.00	*DG*
AMNH 52368	*Cercopithecus*	*PG*	0.87	0.00	0.13	0.00	***DG***	0.43	0.00	0.57	0.00	*PG*
AMNH 52398	*Cercopithecus*	*PG*	0.01	0.00	0.99	0.00	*PG*	0.00	0.00	1.00	0.00	*PG*
AMNH 52401	*Cercopithecus*	*PG*	0.00	0.00	1.00	0.00	*PG*	0.00	0.00	1.00	0.00	*PG*
AMNH 52410	*Cercopithecus*	*PG*	0.09	0.00	0.91	0.00	*PG*	0.28	0.00	0.72	0.00	*PG*
AMNH 82411	*Cercopithecus*	*PG*	0.00	0.00	1.00	0.00	*PG*	0.02	0.00	0.98	0.00	*PG*
AMNH 82412	*Cercopithecus*	*PG*	0.02	0.00	0.98	0.00	*PG*	0.01	0.00	0.99	0.00	*PG*
AMNH 82415	*Cercopithecus*	*PG*	0.30	0.00	0.70	0.00	*PG*	0.37	0.01	0.61	0.01	*PG*
MCZ 37930	*Cercopithecus*	*PG*	0.10	0.00	0.90	0.00	*PG*	0.18	0.00	0.82	0.00	*PG*
MCZ 37934	*Cercopithecus*	*PG*	0.47	0.00	0.53	0.00	*PG*	0.03	0.00	0.97	0.00	*PG*
UMMZ 39508	*Cercopithecus*	*PG*	0.99	0.00	0.01	0.00	***DG***	0.79	0.00	0.21	0.00	***DG***
AMNH 27711	*Colobus*	*PG*	0.00	0.00	1.00	0.00	*PG*	0.00	0.00	1.00	0.00	*PG*

			DFA					*glmnet*				
Specimen	Taxon	Class	*DG*	*KW*	*PG*	*S*	Pred	*DG*	*KW*	*PG*	*S*	Pred
AMNH 99468	*Colobus*	*PG*	0.00	0.00	1.00	0.00	*PG*	0.01	0.00	0.98	0.01	*PG*
NMNH 452621	*Colobus*	*PG*	0.00	0.00	1.00	0.00	*PG*	0.00	0.00	1.00	0.00	*PG*
AMNH 52223	*Colobus*	*PG*	0.01	0.00	0.99	0.00	*PG*	0.16	0.02	0.78	0.04	*PG*
AMNH 52229	*Colobus*	*PG*	0.00	0.00	1.00	0.00	*PG*	0.00	0.00	1.00	0.00	*PG*
AMNH 52240	*Colobus*	*PG*	0.00	0.00	1.00	0.00	*PG*	0.00	0.01	0.98	0.01	*PG*
AMNH 52241	*Colobus*	*PG*	0.00	0.00	1.00	0.00	*PG*	0.00	0.00	1.00	0.00	*PG*
AMNH 52248	*Colobus*	*PG*	0.00	0.00	1.00	0.00	*PG*	0.01	0.00	0.99	0.00	*PG*
AMNH 187392	*Colobus*	*PG*	0.00	0.00	1.00	0.00	*PG*	0.00	0.00	1.00	0.00	*PG*
AMNH 52278	*Procolobus*	*PG*	0.00	0.00	1.00	0.00	*PG*	0.00	0.00	1.00	0.00	*PG*
AMNH 52287	*Procolobus*	*PG*	0.00	0.00	1.00	0.00	*PG*	0.00	0.00	0.96	0.04	*PG*
AMNH 52298	*Procolobus*	*PG*	0.00	0.00	1.00	0.00	*PG*	0.00	0.00	1.00	0.00	*PG*
AMNH 52303	*Procolobus*	*PG*	0.00	0.00	1.00	0.00	*PG*	0.00	0.00	1.00	0.00	*PG*
AMNH 52334	*Procolobus*	*PG*	0.08	0.00	0.92	0.00	*PG*	0.01	0.01	0.96	0.02	*PG*
AMNH 54279	*Procolobus*	*PG*	0.01	0.00	0.99	0.00	*PG*	0.02	0.04	0.93	0.01	*PG*
AMNH 86709	*Procolobus*	*PG*	0.00	0.00	1.00	0.00	*PG*	0.00	0.00	0.99	0.00	*PG*
MCZ 37931	*Procolobus*	*PG*	0.00	0.00	1.00	0.00	*PG*	0.00	0.01	0.90	0.10	*PG*
MCZ 37932	*Procolobus*	*PG*	0.00	0.00	1.00	0.00	*PG*	0.00	0.00	0.99	0.00	*PG*
MCZ 37933	*Procolobus*	*PG*	0.00	0.00	1.00	0.00	*PG*	0.00	0.00	0.99	0.00	*PG*
MCZ 37935	*Procolobus*	*PG*	0.00	0.00	1.00	0.00	*PG*	0.00	0.00	1.00	0.00	*PG*
MCZ 37936	*Procolobus*	*PG*	0.00	0.00	1.00	0.00	*PG*	0.00	0.00	0.99	0.00	*PG*
AMNH 28255	*Nasalis*	*PG*	0.00	0.00	1.00	0.00	*PG*	0.00	0.00	0.98	0.01	*PG*
AMNH 103668	*Nasalis*	*PG*	0.01	0.00	0.99	0.00	*PG*	0.01	0.01	0.98	0.00	*PG*
AMNH 103669	*Nasalis*	*PG*	0.01	0.00	0.99	0.00	*PG*	0.09	0.01	0.87	0.03	*PG*
AMNH 103670	*Nasalis*	*PG*	0.20	0.00	0.80	0.00	*PG*	0.09	0.06	0.85	0.01	*PG*
AMNH 103671	*Nasalis*	*PG*	0.03	0.00	0.97	0.00	*PG*	0.01	0.00	0.98	0.00	*PG*
AMNH 106272	*Nasalis*	*PG*	0.07	0.00	0.93	0.00	*PG*	0.05	0.01	0.94	0.00	*PG*
AMNH 106273	*Nasalis*	*PG*	0.20	0.00	0.80	0.00	*PG*	0.26	0.04	0.70	0.01	*PG*
AMNH 106274	*Nasalis*	*PG*	0.02	0.00	0.97	0.00	*PG*	0.03	0.02	0.82	0.13	*PG*
AMNH 106275	*Nasalis*	*PG*	0.42	0.00	0.58	0.00	*PG*	0.19	0.04	0.72	0.05	*PG*
MCZ 7099	*Nasalis*	*PG*	0.00	0.00	1.00	0.00	*PG*	0.00	0.00	1.00	0.00	*PG*

			DFA					*glmnet*				
Specimen	Taxon	Class	*DG*	*KW*	*PG*	*S*	Pred	*DG*	*KW*	*PG*	*S*	Pred
MCZ 37325	*Nasalis*	*PG*	0.01	0.00	0.99	0.00	*PG*	0.01	0.00	0.98	0.00	*PG*
MCZ 37329	*Nasalis*	*PG*	0.13	0.00	0.87	0.00	*PG*	0.02	0.00	0.98	0.00	*PG*
MCZ 37342	*Nasalis*	*PG*	0.05	0.00	0.95	0.00	*PG*	0.00	0.01	0.98	0.00	*PG*
MCZ 41554	*Nasalis*	*PG*	0.05	0.00	0.95	0.00	*PG*	0.03	0.01	0.96	0.00	*PG*
MCZ 41555	*Nasalis*	*PG*	0.02	0.00	0.98	0.00	*PG*	0.04	0.03	0.92	0.00	*PG*
MCZ 41556	*Nasalis*	*PG*	0.01	0.00	0.99	0.00	*PG*	0.00	0.01	0.98	0.00	*PG*
MCZ 41560	*Nasalis*	*PG*	0.01	0.00	0.99	0.00	*PG*	0.02	0.01	0.97	0.00	*PG*
AMNH 101504	*Trachypithecus*	*PG*	0.00	0.00	1.00	0.00	*PG*	0.00	0.00	0.99	0.00	*PG*
AMNH 102461	*Trachypithecus*	*PG*	0.00	0.00	0.98	0.02	*PG*	0.01	0.07	0.69	0.23	*PG*
AMNH 106598	*Trachypithecus*	*PG*	0.00	0.00	1.00	0.00	*PG*	0.00	0.00	0.98	0.02	*PG*
MCZ 35636	*Trachypithecus*	*PG*	0.00	0.00	1.00	0.00	*PG*	0.00	0.00	1.00	0.00	*PG*
MCZ 35640	*Trachypithecus*	*PG*	0.00	0.00	1.00	0.00	*PG*	0.00	0.00	0.98	0.02	*PG*
MCZ 35675	*Trachypithecus*	*PG*	0.00	0.00	1.00	0.00	*PG*	0.00	0.00	1.00	0.00	*PG*
MCZ 35682	*Trachypithecus*	*PG*	0.00	0.00	1.00	0.00	*PG*	0.00	0.00	1.00	0.00	*PG*
MCZ 35685	*Trachypithecus*	*PG*	0.00	0.00	1.00	0.00	*PG*	0.00	0.00	0.99	0.00	*PG*
MCZ 37387	*Trachypithecus*	*PG*	0.01	0.00	0.99	0.00	*PG*	0.03	0.00	0.96	0.00	*PG*
MCZ 37391	*Trachypithecus*	*PG*	0.00	0.00	1.00	0.00	*PG*	0.00	0.00	1.00	0.00	*PG*
MCZ 37394	*Trachypithecus*	*PG*	0.02	0.00	0.98	0.00	*PG*	0.04	0.00	0.95	0.00	*PG*
MCZ 37396	*Trachypithecus*	*PG*	0.00	0.00	1.00	0.00	*PG*	0.02	0.03	0.95	0.00	*PG*
MCZ 37399	*Trachypithecus*	*PG*	0.00	0.00	1.00	0.00	*PG*	0.01	0.00	0.99	0.00	*PG*
MCZ 37665	*Trachypithecus*	*PG*	0.00	0.00	1.00	0.00	*PG*	0.00	0.00	1.00	0.00	*PG*
MCZ 37671	*Trachypithecus*	*PG*	0.00	0.00	1.00	0.00	*PG*	0.00	0.00	1.00	0.00	*PG*
AMNH 112976	*Trachypithecus*	*PG*	0.00	0.00	1.00	0.00	*PG*	0.01	0.00	0.99	0.00	*PG*
AMNH 112977	*Trachypithecus*	*PG*	0.01	0.00	0.99	0.00	*PG*	0.01	0.00	0.99	0.00	*PG*
AMNH 106599	*Presbytis*	*PG*	0.01	0.00	0.99	0.00	*PG*	0.01	0.01	0.97	0.01	*PG*
AMNH 106606	*Presbytis*	*PG*	0.05	0.00	0.95	0.00	*PG*	0.03	0.00	0.97	0.00	*PG*
AMNH 211527	*Alouatta*	*PG*	0.00	0.00	1.00	0.00	*PG*	0.00	0.00	1.00	0.00	*PG*
AMNH 211528	*Alouatta*	*PG*	0.00	0.00	1.00	0.00	*PG*	0.00	0.00	1.00	0.00	*PG*
AMNH 211531	*Alouatta*	*PG*	0.00	0.00	1.00	0.00	*PG*	0.00	0.00	1.00	0.00	*PG*
AMNH 211532	*Alouatta*	*PG*	0.00	0.00	1.00	0.00	*PG*	0.00	0.01	0.98	0.00	*PG*

			DFA					*glmnet*				
Specimen	Taxon	Class	*DG*	*KW*	*PG*	*S*	Pred	*DG*	*KW*	*PG*	*S*	Pred
AMNH 211535	*Alouatta*	*PG*	0.00	0.00	1.00	0.00	*PG*	0.00	0.00	1.00	0.00	*PG*
AMNH 211542	*Alouatta*	*PG*	0.00	0.00	1.00	0.00	*PG*	0.00	0.00	1.00	0.00	*PG*
AMNH 211543	*Alouatta*	*PG*	0.00	0.00	1.00	0.00	*PG*	0.00	0.00	1.00	0.00	*PG*
AMNH 211544	*Alouatta*	*PG*	0.00	0.00	1.00	0.00	*PG*	0.00	0.00	1.00	0.00	*PG*
AMNH 23333	*Alouatta*	*PG*	0.00	0.00	1.00	0.00	*PG*	0.00	0.00	1.00	0.00	*PG*
AMNH 23342	*Alouatta*	*PG*	0.00	0.00	1.00	0.00	*PG*	0.00	0.00	1.00	0.00	*PG*
AMNH 187999	*Alouatta*	*PG*	0.00	0.00	1.00	0.00	*PG*	0.00	0.00	1.00	0.00	*PG*
AMNH 188006	*Alouatta*	*PG*	0.00	0.00	1.00	0.00	*PG*	0.00	0.00	0.96	0.04	*PG*
AMNH 30193	*Alouatta*	*PG*	0.00	0.00	1.00	0.00	*PG*	0.00	0.00	1.00	0.00	*PG*
AMNH 42313	*Alouatta*	*PG*	0.00	0.00	1.00	0.00	*PG*	0.00	0.01	0.99	0.00	*PG*
AMNH 42316	*Alouatta*	*PG*	0.00	0.01	0.99	0.00	*PG*	0.00	0.07	0.91	0.02	*PG*
AMNH 132790	*Alouatta*	*PG*	0.00	0.00	1.00	0.00	*PG*	0.00	0.01	0.93	0.06	*PG*
MCZ 30436	*Alouatta*	*PG*	0.00	0.00	1.00	0.00	*PG*	0.00	0.00	0.99	0.01	*PG*
MCZ 30437	*Alouatta*	*PG*	0.00	0.00	1.00	0.00	*PG*	0.00	0.00	0.95	0.05	*PG*
MCZ 31694	*Alouatta*	*PG*	0.00	0.00	1.00	0.00	*PG*	0.00	0.00	1.00	0.00	*PG*
MCZ 31695	*Alouatta*	*PG*	0.00	0.00	1.00	0.00	*PG*	0.00	0.00	0.99	0.00	*PG*
MCZ 32160	*Alouatta*	*PG*	0.00	0.00	1.00	0.00	*PG*	0.00	0.00	1.00	0.00	*PG*
MCZ 28735	*Alouatta*	*PG*	0.00	0.00	1.00	0.00	*PG*	0.00	0.01	0.98	0.01	*PG*
UMMZ 116300	*Alouatta*	*PG*	0.00	0.00	1.00	0.00	*PG*	0.00	0.00	1.00	0.00	*PG*
UMMZ 116301	*Alouatta*	*PG*	0.00	0.00	1.00	0.00	*PG*	0.00	0.00	0.99	0.00	*PG*
UMMZ 77301	*Alouatta*	*PG*	0.00	0.00	1.00	0.00	*PG*	0.01	0.04	0.93	0.03	*PG*
UMMZ 124689	*Alouatta*	*PG*	0.00	0.00	1.00	0.00	*PG*	0.00	0.00	1.00	0.00	*PG*
UMMZ 124690	*Alouatta*	*PG*	0.00	0.00	1.00	0.00	*PG*	0.00	0.00	1.00	0.00	*PG*
UMMZ 146506	*Alouatta*	*PG*	0.00	0.00	1.00	0.00	*PG*	0.00	0.00	0.99	0.00	*PG*
UMMZ 63503	*Alouatta*	*PG*	0.00	0.00	0.99	0.01	*PG*	0.00	0.00	0.97	0.02	*PG*
UMMZ 63504	*Alouatta*	*PG*	0.01	0.00	0.99	0.00	*PG*	0.10	0.00	0.89	0.00	*PG*
UMMZ 63511	*Alouatta*	*PG*	0.00	0.00	1.00	0.00	*PG*	0.00	0.01	0.98	0.00	*PG*
UMMZ 63512	*Alouatta*	*PG*	0.00	0.00	1.00	0.00	*PG*	0.00	0.00	0.99	0.01	*PG*
AMNH 28418	*Ateles*	*S*	0.00	0.00	0.35	0.65	*S*	0.00	0.00	0.51	0.49	***PG***
AMNH 28420	*Ateles*	*S*	0.00	0.00	0.04	0.96	*S*	0.00	0.00	0.21	0.79	*S*

			DFA					*glmnet*				
Specimen	Taxon	Class	*DG*	*KW*	*PG*	*S*	Pred	*DG*	*KW*	*PG*	*S*	Pred
MCZ 47269	*Ateles*	*S*	0.00	0.00	0.00	1.00	*S*	0.00	0.00	0.06	0.94	*S*
UMMZ 116302	*Ateles*	*S*	0.00	0.00	0.00	1.00	*S*	0.00	0.00	0.00	0.99	*S*
NMNH 276631	*Ateles*	*S*	0.00	0.00	0.26	0.74	*S*	0.00	0.03	0.12	0.86	*S*
NMNH 276657	*Ateles*	*S*	0.00	0.00	0.00	1.00	*S*	0.00	0.03	0.01	0.96	*S*
UMMZ 63165	*Ateles*	*S*	0.00	0.00	0.00	1.00	*S*	0.00	0.00	0.07	0.92	*S*
UMMZ 63166	*Ateles*	*S*	0.00	0.00	0.12	0.88	*S*	0.00	0.00	0.19	0.81	*S*
UMMZ 63171	*Ateles*	*S*	0.00	0.00	0.10	0.90	*S*	0.00	0.00	0.21	0.79	*S*
NMNH 244863	*Ateles*	*S*	0.00	0.00	0.00	1.00	*S*	0.00	0.00	0.01	0.99	*S*
NMNH 396348	*Ateles*	*S*	0.00	0.00	0.00	1.00	*S*	0.00	0.00	0.00	1.00	*S*
UMMZ 126129	*Cebus*	*PG*	0.00	0.00	0.65	0.35	*PG*	0.00	0.01	0.54	0.45	*PG*
UMMZ 126130	*Cebus*	*PG*	0.00	0.00	1.00	0.00	*PG*	0.00	0.00	0.99	0.00	*PG*
AMNH 133606	*Cebus*	*PG*	0.00	0.00	1.00	0.00	*PG*	0.00	0.00	0.99	0.01	*PG*
AMNH 133607	*Cebus*	*PG*	0.00	0.00	1.00	0.00	*PG*	0.00	0.00	0.98	0.02	*PG*
AMNH 133608	*Cebus*	*PG*	0.00	0.00	1.00	0.00	*PG*	0.00	0.00	0.98	0.02	*PG*
AMNH 133622	*Cebus*	*PG*	0.00	0.00	1.00	0.00	*PG*	0.01	0.00	0.95	0.03	*PG*
AMNH 133624	*Cebus*	*PG*	0.00	0.00	1.00	0.00	*PG*	0.00	0.00	1.00	0.00	*PG*
AMNH 133626	*Cebus*	*PG*	0.00	0.00	1.00	0.00	*PG*	0.00	0.00	1.00	0.00	*PG*
AMNH 133628	*Cebus*	*PG*	0.00	0.00	1.00	0.00	*PG*	0.00	0.00	0.92	0.08	*PG*
AMNH 133629	*Cebus*	*PG*	0.00	0.00	1.00	0.00	*PG*	0.00	0.00	0.99	0.01	*PG*
AMNH 133631	*Cebus*	*PG*	0.00	0.00	1.00	0.00	*PG*	0.00	0.00	0.95	0.05	*PG*
AMNH 133633	*Cebus*	*PG*	0.00	0.00	1.00	0.00	*PG*	0.00	0.00	0.95	0.04	*PG*
AMNH 133635	*Cebus*	*PG*	0.00	0.00	1.00	0.00	*PG*	0.00	0.00	0.99	0.01	*PG*
AMNH 133637	*Cebus*	*PG*	0.00	0.00	1.00	0.00	*PG*	0.00	0.00	0.99	0.01	*PG*
AMNH 133638	*Cebus*	*PG*	0.00	0.00	1.00	0.00	*PG*	0.00	0.00	0.99	0.01	*PG*
AMNH 133640	*Cebus*	*PG*	0.00	0.00	1.00	0.00	*PG*	0.00	0.02	0.96	0.02	*PG*
AMNH 133654	*Cebus*	*PG*	0.00	0.00	1.00	0.00	*PG*	0.00	0.00	1.00	0.00	*PG*
AMNH 133656	*Cebus*	*PG*	0.00	0.00	1.00	0.00	*PG*	0.00	0.00	1.00	0.00	*PG*
AMNH 133660	*Cebus*	*PG*	0.00	0.00	1.00	0.00	*PG*	0.00	0.00	0.99	0.01	*PG*
AMNH 133662	*Cebus*	*PG*	0.00	0.00	1.00	0.00	*PG*	0.00	0.00	1.00	0.00	*PG*
AMNH 133666	*Cebus*	*PG*	0.00	0.00	1.00	0.00	*PG*	0.00	0.00	1.00	0.00	*PG*

			DFA					*glmnet*				
Specimen	Taxon	Class	*DG*	*KW*	*PG*	*S*	Pred	*DG*	*KW*	*PG*	*S*	Pred
AMNH 133667	*Cebus*	*PG*	0.00	0.00	1.00	0.00	*PG*	0.00	0.00	0.99	0.00	*PG*
AMNH 133668	*Cebus*	*PG*	0.00	0.00	1.00	0.00	*PG*	0.01	0.00	0.99	0.00	*PG*
AMNH 133674	*Cebus*	*PG*	0.00	0.00	1.00	0.00	*PG*	0.00	0.00	0.97	0.03	*PG*
AMNH 133677	*Cebus*	*PG*	0.00	0.00	1.00	0.00	*PG*	0.00	0.00	0.98	0.02	*PG*
AMNH 133815	*Cebus*	*PG*	0.00	0.00	1.00	0.00	*PG*	0.00	0.00	0.99	0.01	*PG*
AMNH 133851	*Cebus*	*PG*	0.00	0.00	1.00	0.00	*PG*	0.01	0.00	0.99	0.00	*PG*
AMNH 133862	*Cebus*	*PG*	0.00	0.00	1.00	0.00	*PG*	0.00	0.00	1.00	0.00	*PG*

Chapter 3

Tinderet capitate morphology, and locomotor diversity among early Miocene catarrhines

Abstract

A great deal of taxonomic diversity has been recognized among early Miocene catarrhines, but characterization of locomotor diversity within this group has lagged behind. With rare exception, catarrhines of the early Miocene are thought to deviate little from the positional repertoire best represented by *Ekembo heseloni*, consisting largely of above-branch quadrupedalism. Our understanding of early Miocene catarrhine behavior is hindered by the rarity of instances in which multiple species are represented by the same postcranial element, particularly from the same geographical and temporal setting. This chapter provides morphological descriptions and computational analysis of seven capitates belonging to non-cercopithecoid catarrhines from three sites within the Tinderet Miocene sequence of Western Kenya. 3D morphometrics from a broad sample of extant anthropoids are used to construct models to predict the positional behavior of each specimen, and the functional diversity of the sampled catarrhines present in this early Miocene setting is quantified and compared to that of extant groups. These results, along with body mass estimates, are used to constrain the taxonomic identity of each specimen.

The functional diversity of the Tinderet sample is found to be comparable to that of broad extant groups. Four specimens are classified as arboreal quadrupeds, two of which have estimated locomotor proportions distinct from those of *E. heseloni*. Two other specimens demonstrate significant reliance on below-branch behaviors, and suggest the presence of a currently unrecognized small-bodied suspensor at Songhor. The final specimen, KNM-SO 1002, is uniquely great ape-like among capitates known from the early Miocene, and possesses features often associated with knuckle-walking. Along with previous observations of isolated postcrania, this specimen suggests the presence of a behaviorally-derived mid-sized ape at Songhor, the identity of which may be *Rangwapithecus gordoni*. This study documents the presence of a wide range of behavioral repertoires in an early Miocene setting, and points to a broader trend of functional diversity among early Miocene catarrhines beyond what is generally recognized.

Introduction

The early Miocene (ca. 23-16 Ma) of Africa is home to a great variety of catarrhine species. However, postcranial evidence has seemed to suggest that the functional diversity of this group lagged far behind its taxonomic diversity, with the majority of specimens interpreted to facilitate a similarly limited range of behaviors (Ward, 2015). This functional repertoire, best characterized in *Ekembo heseloni* due to its extensive postcranial hypodigm (Napier and Davis, 1959; Walker and Pickford, 1983; Walker *et al.*, 1993; Walker, 1997), is thought to have been dominated by above-branch palmigrade quadrupedalism, likely supplemented by occasional slow climbing or careful clambering (e.g., McHenry and Corruccini, 1983; Cartmill and Milton, 1977; Rose, 1983,

1993, 1996; Beard *et al.*, 1986, 1993; Kelley, 1997; Ward, 1998; Daver and Nakatsukasa, 2015), and possibly some leaping (Ruff, 2002; Ryan *et al.*, 2012). This positional habit has become the null hypothesis in the study of early and middle Miocene catarrhine functional morphology, with postcranial specimens only rarely thought to deviate sufficiently from those of *E. heseloni* to indicate significant behavioral divergence.

A handful of taxa depart from this pattern. Specimens of *Dendropithecus macinnesi* from Rusinga are thought to have supplemented the paradigmatic behavioral repertoire with increased reliance on climbing (Rose *et al.*, 1992; Rose, 1994) and perhaps some below-branch suspension (Napier and Davis, 1959; Preuschoft, 1973; Simons and Fleagle, 1973; Fleagle, 1983; Rose, 1983, 1993). *Simiolus enjiessi* specimens from Kalodirr have been reconstructed similarly (Rose *et al.*, 1992). Among putative apes, every species of the early Miocene has been reconstructed as behaviorally similar to *E. heseloni* aside from *Morotopithecus bishopi*, a very early and potentially isolated instance of adaptation for orthograde climbing (Sanders and Bodenbender, 1994; Gebo *et al.*, 1997; MacLatchy *et al.*, 2000; MacLatchy, 2004).

Behavioral variation finally emerges in the middle Miocene, with specimens of *Equatorius africanus* hinting at the appearance of incipient terrestriality (McCrossin *et al.*, 1998; Ward *et al.*, 1999; *Sherwood et al., 2002*) and *Nacholapithecus kerioi* evincing enhanced climbing abilities (Rose *et al.*, 1996; Ishida *et al.*, 2004). However, behavioral patterns clearly distinct from those of *E. heseloni* are either not generally recognized or not yet well-characterized in the hominoid lineage until the late-middle Miocene of Eurasia (e.g., Rose, 1984; Moya-Sola *et al.*, 2004).

Among the factors inhibiting our understanding of early catarrhine positional behavior is the relative dearth of instances in which the same postcranial element has been recovered from multiple early Miocene species. In addition to encumbering the functional analysis of individual taxa, this hinders characterization of functional diversity among these animals. Seven capitates belonging to non-cercopithecoid catarrhines were recovered between 1931 and 1996 from Songhor, Chamtwara, and Mteitei Valley, potentially penecontemporaneous sites within the Tinderet Miocene sequence of Western Kenya (see Fig. 3.1). Several of these specimens are mentioned in the work of previous researchers (e.g., Harrison, 1982; Rose, 1984), but none has been formally described. Here I present morphological descriptions and computational analysis of this rare collection of overlapping postcranial specimens.

Table 3.1. Fossil catarrhines known from Songhor, Chamtwara, and Mteitei Valley, with published body mass estimates

Taxon	Localities	Body mass[a]	References
Proconsul africanus	SO, CA, MV	Similar to *E. heseloni*[b]	Harrison, 2010
Proconsul major	SO, CA, MV	63.4 - 86.7kg[c]	Rafferty *et al.*, 1995
Rangwapithecus gordoni	SO	Similar to *E. heseloni*	Andrews, 1978; Langdon, 1984
Dendropithecus macinnesi	SO, CA	6 - 8kg	Bilsborough and Rae, 2015; Harrison, 2013
Kalepithecus songhorensis	SO, CA, MV	5 - 6kg	Harrison, 2013
Limnopithecus evansi	SO, MV	5kg	Harrison, 2010
Limnopithecus legetet	CA	5kg	Harrison, 2010
Micropithecus clarki	CA	3 - 4.5kg	Fleagle and Simons, 1978; Harrison, 2013

[a] Body mass estimates of all species at Tinderet other than *P. major* are based on qualitative comparisons.
[b] E. heseloni estimates are based on postcranial articular sizes or shaft dimensions, with adult size extrapolated based on the size of different extant anthropoids at similar developmental stages. They range between approximately 8 and 19kg (Rafferty *et al.*, 1995, Ruff 2003).
[c] Estimated for 3 specimens from Songhor and Napak based on linear regression with tibial and humeral shaft dimensions, and talar and tibial articular size

Fig. 3.1. Fossil sites preserving the specimens analyzed in this study.

The fossil assemblages of these three sites reflect the taxonomic diversity of early catarrhines, with eight species currently recognized as having been present in this temporally and geographically constrained setting (Table 3.1). Taxonomic attribution of these specimens is confounded by the lack of capitates recovered in association with craniodental material attributed to any of the catarrhine species known from these sites; I therefore constrain the possible identity of each specimen through body mass estimation, qualitative and quantitative affinity to extant anthropoid taxa, and, when

possible, by comparing the functional affinities of each specimen to results of previous functional analyses of postcrania attributed to species known from these sites.

I reconstruct the likely behavioral repertoires of each fossil specimen through analysis of morphometric traits found to be associated with positional behaviors and frequencies thereof in a broad sample of extant anthropoids. The functional diversity of this sample is also quantitatively characterized and compared to that of extant anthropoid groups. I discuss how the diversity present in this limited setting might aid our understanding of catarrhine evolution.

Discovery and context

Five of the seven Tinderet capitates were recovered at Songhor (35° 13' E, 00° 02' S), a site discovered in 1932 by L.S.B Leakey and Donald MacInnes (MacInnes, 1943). This locality's fossiliferous sediments, accumulated by sub-aerial deposition, consist of a sequence of tuffs divided into 4 main units, from oldest to youngest – the Calcified Tuff Member, the Red Bed Member, the Grey Tuff Member, and the Tuff and Agglomerate Member (Pickford and Andrews, 1981). A sample from a biotite collected at the base of the calcified Tuff Member, the oldest of the four, yielded a K/Ar age estimate of between 19.2 and 20.5 Ma (Bishop *et al.*, 1969); adjustment for new radiometric constants produce a marginally earlier range of 19.7-21 Ma (Cote *et al.*, 2016). Efforts to re-date this and many other East African Miocene sites are currently underway (McNulty *et al.*, 2014). KNM-SO 1000, KNM-SO 1001, and KNM-SO 1002 were recovered during the Leakey and MacInnes survey beginning in 1966. KNM-SO 31245 and KNM-SO 31246 were recovered in 1996 after renewed excavation and

sieving of Red Bed Member sediments by Nengo and colleagues (Nengo and Rae, 1992) in collecting area 5 (Pickford and Andrews, 1981).

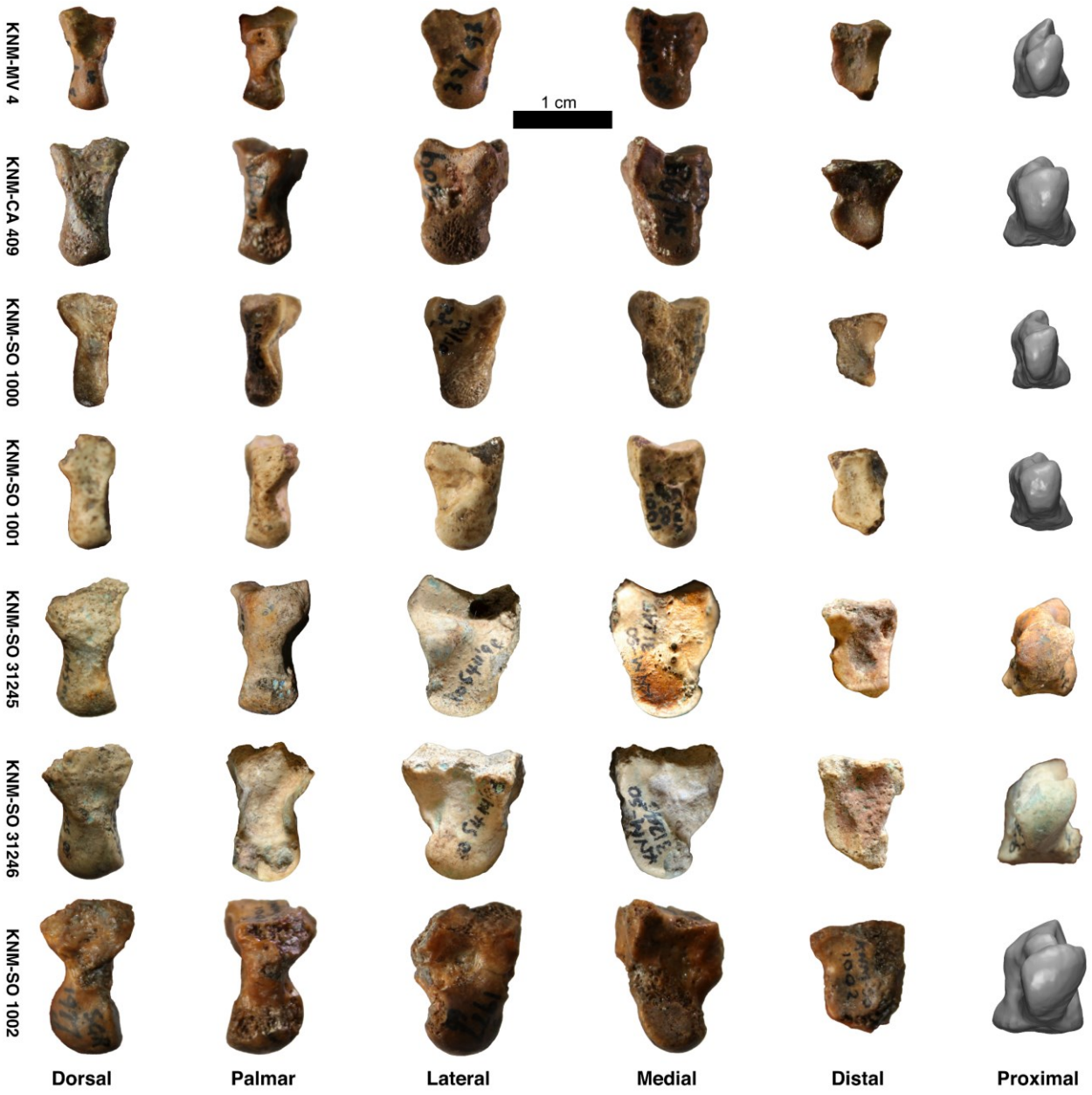

Fig. 3.2. Tinderet fossil sample in standard anatomical views. All specimens roughly to scale. KNM-SO 1000, a left capitate, was mirrored for ease of comparison. Missing photographic views are represented by 3D models.

The remaining two capitates were discovered at nearby Chamtwara (35° 15' 57.6" E, 0° 07' 32.6" S) and Mteitei Valley (35° 18' 30.75" E, 0° 00' 40.6" N), apparently by Leakey and MacInnes' 1930s expedition based on their field numbers. These three Tinderet sites have distinct fossil assemblages (see Table 3.1): *Proconsul africanus*, *Proconsul major*, and *Kalepithecus songhorensis* are common to all, but *Dendropithecus macinnesi* has been identified only at Songhor and Chamtwara of the Tinderet sites (Harrison, 2010 and references therein). *Limnopithecus legetet* and *Micropithecus clarki* are common at Chamtwara but not known at Songhor or Mteitei Valley, which instead yield *Limnopithecus evansi* (Harrison, 1981, 1988). *Rangwapithecus gordoni* may have been a temporally and geographically restricted taxon (Cote *et al.*, 2014), perhaps associated with a specialization for folivory (Kay and Ungar, 1997; but see Shearer *et al.*, 2015). It is known almost exclusively from Songhor, save for a mandible (Cote *et al.*, 2014) and partial cranium (McNulty *et al.*, 2015a) from Lower Kapurtay, an adjacent site discovered in 1996 by Nengo and Malit (Gebo *et al.*, 2009), although a lower third molar from Moroto II, Uganda has also been provisionally attributed to this genus (Jansma and MacLatchy, 2015).

Table 3.2. Sampled extant (a) and fossil (b) capitates. See Chapter 2 for details on positional behavior variables and references

a Extant taxon				Total proportions					Arboreal-only proportions				
	n	♂	♀	*Quad*	*Susp*	*Climb*	*Leap*	*Arb*	*QuadA*	*SuspA*	*ClimbA*	*LeapA*	Class
Pan troglodytes schweinfurthii	10	7	3	0.93	0.01	0.06	0	0.10	0.31	0.08	0.59	0.02	*KW*
Pan troglodytes troglodytes	12	6	6										*KW*
Pan troglodytes verus	13	7	6	0.86	0.01	0.11	0	0.16	0.21	0.06	0.68	0.01	*KW*
Pan troglodytes ellioti	5	2	3										*KW*
Pan paniscus	4	2	2	0.87	0.01	0.09	0	0.17	0.35	0.09	0.51	0.04	*KW*
Gorilla gorilla	26	15	11	0.92	0.01	0.06	0	0.10	0.19	0.13	0.62	0.02	*KW*
Gorilla beringei	12	9	3	0.96	0.01	0.04	0	0.09	0.53	0.06	0.40	0.01	*KW*
Pongo pygmaeus	19	9	10	0.12	0.43	0.37	0.01	0.95	0.12	0.43	0.37	0.01	*S*
Pongo abelii	15	5	10	0.18	0.38	0.35	0.01	0.95	0.18	0.38	0.35	0.01	*S*
Hoolock hoolock	7	3	4	0	0.55	0.20	0.22	0.99	0	0.55	0.20	0.22	*S*
Hylobates muelleri	4	2	2										*S*
Hylobates lar	15	9	6	0	0.59	0.19	0.16	0.99	0	0.59	0.19	0.16	*S*
Symphalangus syndactylus	3	1	2	0	0.59	0.32	0.02	0.99	0	0.59	0.32	0.02	*S*
Papio anubis	14	8	6	0.99	0	0.01	0.01	0.05	0.68	0	0.21	0.10	*DG*
Lophocebus albigena	6	5	1	0.42	0	0.36	0.21	0.95	0.42	0	0.36	0.21	*PG*
Mandrillus sphinx	9	7	2										*DG*
Cercocebus agilis	2	2	0										*PG*
Macaca fascicularis	18	11	7	0.68	0	0.26	0.06	0.97	0.68	0	0.26	0.06	*PG*
Erythrocebus patas	7	5	2	0.94	0	0.05	0.01	0.08	0.60	0	0.30	0.10	*DG*
Cercopithecus mitis	11	7	4	0.54	0	0.35	0.11	0.95	0.54	0	0.35	0.11	*PG*
Colobus guereza	9	6	3	0.41	0.01	0.20	0.38	0.96	0.41	0.01	0.20	0.38	*PG*
Procolobus rufomitratus	13	7	6	0.35	0.01	0.29	0.35	0.95	0.35	0.01	0.29	0.35	*PG*
Nasalis larvatus	17	9	8										*PG*
Trachypithecus sp.	17	7	10	0.60	0	0.13	0.28	0.99	0.60	0	0.13	0.28	*PG*
Presbytis melalophos	2	1	1	0.28	0.02	0.19	0.50	0.99	0.28	0.02	0.19	0.50	*PG*
Alouatta sp.	32	13	19	0.61	0.02	0.33	0.05	0.95	0.61	0.02	0.33	0.05	*PG*
Ateles geoffroyi	13	2	11	0.42	0.25	0.25	0.07	0.99	0.42	0.25	0.25	0.07	*S*
Cebus apella	28	20	8	0.37	0	0.40	0.21	0.95	0.37	0	0.40	0.21	*PG*
Total n	343	187	156										

b Fossil specimens	
Undescribed	KNM-MV 4
	KNM-CA 409
	KNM-SO 1000
	KNM-SO 1001
	KNM-SO 31245
	KNM-SO 31246
	KNM-SO 1002
Ekembo heseloni	KNM KPS III C26
	KNM KPS III C28
	KNM KPS VIII C27
	KNM-RU 2036M

Materials and methods

Sample and Data Collection

Extant comparanda comprise 343 specimens from 28 taxa, selected to sample the locomotor diversity within a range of anthropoid clades (Table 3.2a, Fig. 3.9c). Extant taxa were assigned locomotor proportions and categories of positional behavior based on published observations (see Chapter 2 references and details). The Tinderet sample is compared to four *E. heseloni* capitates from Rusinga (Table 3.2b).

The sampling procedure is detailed in Chapter 2. Specimens were µCT or laser scanned to produce 3D models from which surface areas, angles, and other shape metrics were extracted (Table 3.3). Metrics subject to isometry were indexed to render them scale-free (Jungers *et al.*, 1995). CpPx, which characterizes the size of the capitate's proximoradial surface, is the sum of two other shape variables, CpSc and CpLu, and was excluded from multivariate analyses of "all" shape metrics.

Table 3.3. Description of capitate shape variables

Metric	Description
CpPx[a]	Capitate proximoradial surface area
CpSc	Surface area of scaphoid/centrale facet of capitate relative to capitate surface area
CpLu	Surface area of lunate facet of capitate relative to capitate surface area
CpDn	Capitate dorsal nonarticular surface area
Cp3	Surface area of Mc3 facet of capitate relative to capitate surface area
CpHm	Surface area of hamate facet(s) of capitate relative to total surface area
Cp2	Capitate Mc2 surface area
Cp4	Capitate Mc4 surface area
Cp23A	Orientation of Mc2 facet of capitate relative to Mc3 facet
Cp3HmA	Angle between Mc3 and hamate facets of capitate
CpPxA	Orientation of proximoradial surface of the capitate relative to hamate facet
CpScA	Orientation of scaphoid/centrale facet of capitate relative to dorsal nonarticular surface
Cp3SD	Capitate Mc3 facet complexity
CpHmC	Capitate hamate surface concavity
CpHP	Dorsopalmar position of the capitate head

[a] Sum of CpSc and CpLu. CpPx and its constituents were not included together in multivariate analyses

Taphonomic damage to fossil specimens was virtually repaired, guided by preserved anatomy and with reference to that of contemporaneous specimens (Fig. 3.3). Morphometric values dependent on missing anatomy (7 total values from 4 specimens) were imputed via a bootstrap-aggregated decision tree algorithm trained with the combined set of extant and fossil shape data, which fits a model for each variable as a function of all the others. Qualitative observations were made on the original fossils at the National Museums of Kenya, Nairobi.

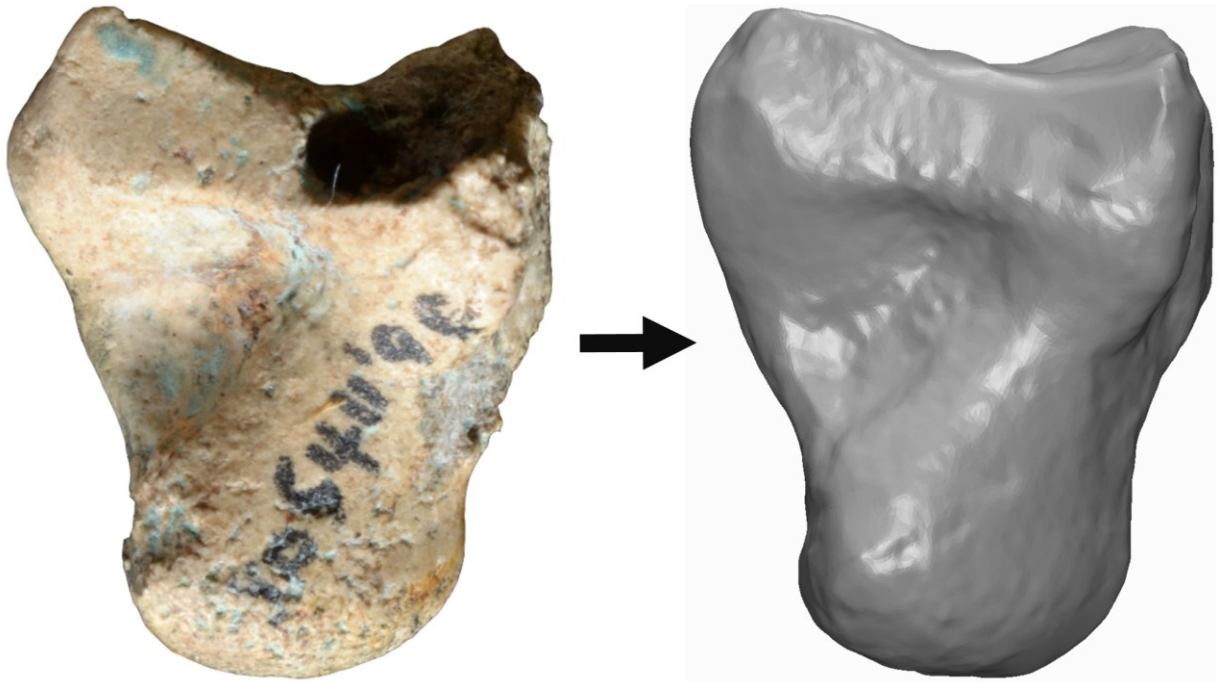

Fig. 3.3. Representative example (KNM-SO 31245) of virtual reconstruction of missing fossil morphology.

Body mass estimation and preparatory analyses

Fossil body mass estimates were calculated based on the known relationship between capitate volume and body mass (see Chapter 2). To encompass the possible phylogenetic, locomotor, and size ranges of the fossil specimens, all sex-specific body mass data were included in building the model except male *Gorilla*, which was excluded as an outlier due to its extreme size relative to the fossil specimens and its very low relative capitate volume. Smith (1984, 1985) has recommended limiting the range of training set body masses to those similar to the experimental set; the other extant apes were nevertheless included to account for possible scaling variation between anthropoid groups.

"Classical calibration" was used to produce maximum likelihood estimates based on regression of morphometric data against body mass (Konigsberg *et al.*, 1998; Uhl *et al.*, 2013). All data were log-transformed to correct for heteroscedasticity and improve model fit, as is common in scaling analyses (e.g., Rafferty *et al.*, 1995). It has been suggested that log-log allometric regressions can be misleading (e.g., Packard, 2013, 2015), but I follow others (e.g., Lemaitre *et al.*, 2015) in judging the superior interpretability and transferability of this approach to outweigh any slight increase in accuracy that may be afforded by suggested alternatives. Systematic underestimation resulting from detransformation of logged predictions into standard linear space was ameliorated by applying the quasi-maximum likelihood estimator correction factor (Sprugel, 1983). Different correction factors tend to converge when representing less than about 10% of the detransformed values (Smith, 1993); that used here equaled roughly 1%, so variation associated with different correction factors would necessarily be trivial. Because sex-specific means were used to predict individual body masses, confidence intervals are not meaningful (Smith, 1985). Prediction error was therefore characterized with percent mean prediction error (%MPE) and percent standard error of the estimate (%SEE) after 100 repetitions of 10-fold cross validation (CV).

Functional analyses

Covariance between shape variables and locomotor proportions in the extant sample was tested using phylogenetic generalized least squares (PGLS) regression. An additional PGLS model was fitted for each shape variable with size as a covariate to account for the influence of allometry. PGLS was also used to test the covariance of

each shape variable between positional classes. Because PGLS does not allow dependent factors, these relationships were assessed while accounting for the influence of allometry using Bayesian phylogenetic generalized linear mixed models (PGLMM; Hadfield, 2010; Hadfield and Nakagawa, 2010; Carter and Worthington, 2016, Gelman, 2006; see also Chapter 2). Separate PGLMM regressions were fitted to both taxon means and individual observations of each shape variable, with size as a covariate. All PGLS and PGLMM analyses were repeated with hylobatids excluded to allow the influence of this group's high-leverage data to be considered when evaluating functional relationships.

Two positional classifiers were built. Discriminant function analysis (DFA) was chosen for interpretability and ease of visualization. This was supplemented by *glmnet*, a regularized multinomial logistic regression machine learning algorithm (Friedman *et al.*, 2010), chosen for its complementary properties. Relative to DFA, *glmnet* is less prone to overfitting and bias due to collinearity, less stringent in its assumptions regarding heteroscedasticity, and can detect non-linear relationships (Kovarovic *et al.*, 2011; Mitteroecker and Bookstein, 2011). Shape variables were selected for inclusion in these models with consideration of all four PGLMM analyses (taxon means and individual observations, with and without hylobatids). Selected predictors each distinguish the individual observations of either suspensory, knuckle-walking, or digitigrade anthropoids from those of the palmigrade reference class at $p \leq 0.1$ with hylobatids excluded, while covarying with similar or greater significance in at least one of the other three analyses. The classification accuracy of both models was calculated after 100 repetitions of 10-fold CV.

Models to estimate the locomotor proportions of the fossil specimens were built in a multi-step process. First, shape variables found not to significantly covary with the locomotor variable under consideration in either PGLS regression (i.e., with or without hylobatids) were eliminated from consideration. Subsets of the remaining variables were then ranked by ascending second-order Akaike Information Criterion (AICc; Burnham and Anderson, 2002). The three or four top-ranked subsets resulting from this process, which generally had similar AICc values, were used to predict the locomotor proportions of the extant sample, with accuracy calculated after 100 10-fold CV repetitions of quasibinomial logistic regression. The most accurate of these models, as judged by %SEE, was chosen to estimate the frequency of that locomotor behavior in the fossil specimens.

For several of the locomotor proportions, individual shape variables did not sufficiently covary with behavior for this process to produce effective predictive models. In these cases, models were built with all shape variables as predictors. Although these models were effective in predicting extant locomotor proportions, they do not account for phylogeny or allometry, and base predictions on functionally uninformative morphological features. Their predictions therefore reflect the overall resemblance of each specimen relative to the extant sample, and a larger proportion of their accuracy in predicting extant proportions is likely attributable to overfitting. Predictions assigned by these models are nevertheless provided to aid in evaluating the possible locomotor repertoires of the Tinderet sample, but are given less consideration.

Functional affinities of the Tinderet specimens were further explored using two-block partial least squares (PLS) regression (Rohlf and Corti, 2000). The first block

consists of the extant shape variables, while the second block comprises the arboreal-only locomotor proportions and proportion of arboreality (*Arb*; see Table 3.2), chosen as the combination with the strongest relationship to wrist morphology (see Chapter 2). The fossil specimens, along with extant taxa for which locomotor observations are unavailable, were projected into PLS shape-space by multiplying their scaled shape variable matrix by one containing the singular vectors of the PLS shape block. The functional diversity of the Tinderet sample was characterized by calculating the Euclidean area of the convex hull enveloping the constituent data points of the Tinderet sample in PLS shape-space, relative to those calculated for extant groups.

Taxonomic and phylogenetic analyses

The fossil specimens were also assigned to one of the three anthropoid superfamilies using classifiers built with DFA and *glmnet* as described above. Shape variable covariance between these groups was assessed using multinomial logistic regression with size as a covariate. Variables were validated for inclusion in the taxonomic classifiers if found to significantly distinguish both hominoid and ceboid observations from those of cercopithecoids.

The phylogenetic affinities of the fossil specimens were further explored via hierarchical clustering analysis. Significantly allometric variables have been found to adversely affect phylogenetic reconstruction (Worthington, 2012), so efforts were made to avoid their inclusion. Allometric scaling was assessed in a phylogenetic context. Sex-specific means of each shape variable and the size surrogate were first transformed into phylogenetic independent contrasts (PICs; Felsenstein, 1985). Spearman correlations

were then calculated between the PICs of size and each shape variable. The phylogenetic signal of each shape variable was also estimated using both Pagel's lambda (Pagel, 1999) and Blomberg's K (Blomberg *et al.*, 2003).

Relative dissimilarity among the extant taxa and fossil specimens was estimated by calculating a matrix of Euclidean distances based on the shape variables found to have significant phylogenetic signal and insignificant allometric scaling. Hierarchical clustering was then carried out using BioNJ. This and other neighbor-joining algorithms (Saitou and Nei, 1987; Studier and Kappler, 1988) improve on standard agglomerative methods by seeking to join the pair of tips that minimizes the branch lengths of the entire tree at each stage of clustering. BioNJ adds an additional approximation of distance variance and covariance, accounting somewhat for non-independence due to shared evolutionary history (Gascuel, 1997). Trees were outgroup-rooted using *Cebus*, providing a basis for approximating trait polarity and yielding trees that depict estimated phylogenetic, rather than only phenetic, relationships. Separate clustering analyses were carried out for each fossil specimen; relationships between fossil and extant specimens are represented by multiple dendrograms to best represent the phylogenetic placement of the fossils in individual analyses.

All variables were scaled to prevent bias due to unit heterogeneity and for convenience in comparing coefficients. Fossil shape variables were scaled according to the mean and standard deviation of the extant sample to ensure comparability. Phylogenetic information was taken from Arnold and colleagues (2010; Fig. 3.9c). All analyses were done in R (R Core Team, 2016). See Chapter 2 for computational details.

Results

Morphological descriptions

KNM-MV 4 This right capitate is the smallest of the fossil sample (See Fig. 3.2), similar in size to the average of sampled blue monkeys. It is well preserved and complete save for abrasion of the lateral approximately two-thirds of the dorsodistal margin. The capitate head is narrow both dorsopalmarly and mediolaterally, condyloid, and pronated substantially relative to the body, the latter resulting in the proximal region of the hamate facet facing somewhat dorsally. Distally, ligament notches are absent laterally and medially, allowing the Mc2 and Mc4 facets to run uninterrupted along the dorsopalmar entirety of these margins, a condition unique among the fossil sample with the possible exception of KNM-SO 31246 (see below). The palmar portion of the Mc4 facet widens and tilts medially, increasing in degree as it approaches its palmar extent. The Mc2 and Mc4 facets are separated by a wide and topographically mild articulation for the Mc3. In these features this specimen is most reminiscent of *Cebus* of the extant sample.

In other features, KNM-MV 4 more closely resembles its sampled Miocene contemporaries. It lacks the lateral expansion of the distal portion of the body that characterizes the platyrrhines in the sample, and the distal portion of the hamate facet is oriented palmarly relative to the proximal portion. The topography of the Mc3 articular surface follows the basic pattern of the other fossils of the sample: the distal-most extent of the dorsal Mc3 margin occurs a short distance from its lateral extent, and the dorsal portion of the surface lateral to this point withdraws proximally before abutting the Mc2 facet. The remainder of the Mc3 surface is gently concave dorsopalmarly, and the

proximal half slopes distally toward the raised margin it shares with the palmar portion of the Mc2 facet, just distal to a rugose, palmarly projecting ridge for attachment of palmar intercarpal ligaments. However, this topography is generally less pronounced, resulting in a surface deviating only slightly from planar.

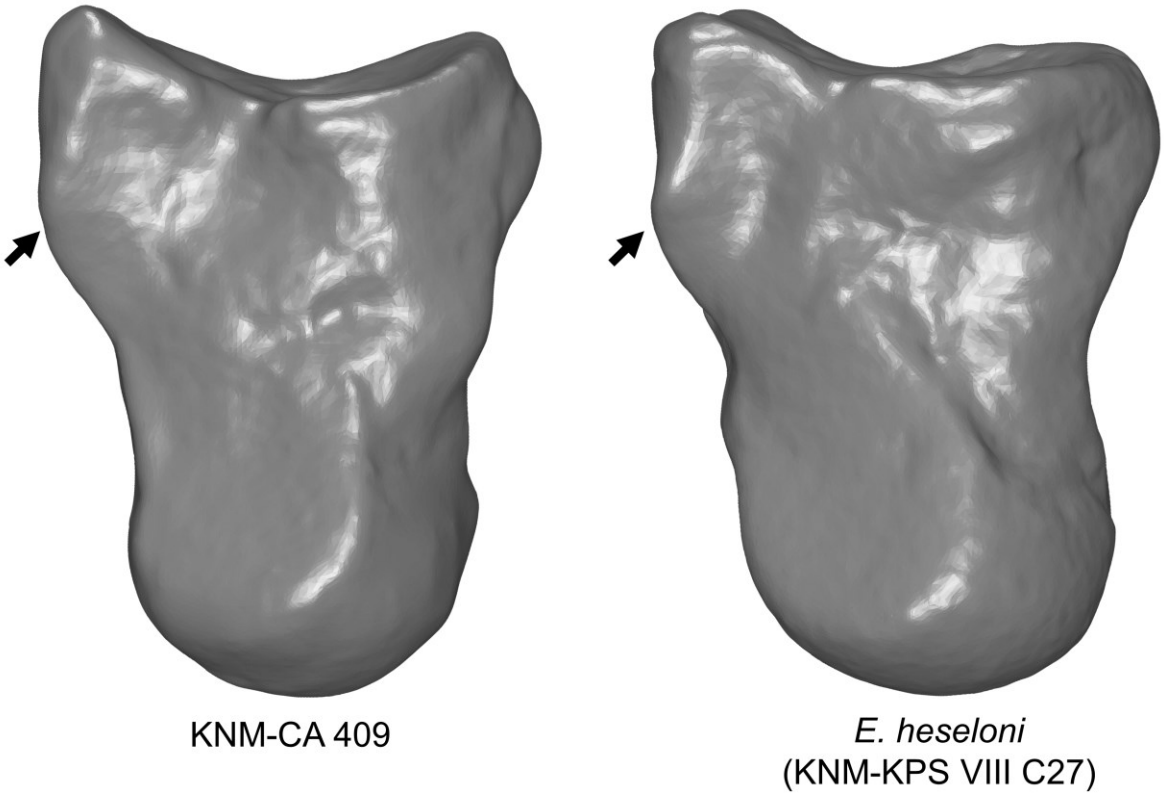

Fig. 3.4. Comparison of dorsodistal lip morphology in fossil specimens.

KNM-CA 409 The Chamtwara specimen is a nearly complete, right capitate, most similar in size to sampled patas monkeys and colobins. The centrale facet suffers from minor weathering, and small portions are abraded along the bone's dorsodistal margin and along the distal extent of its proximal surface both palmarly and dorsally.

This specimen resembles those from Rusinga in much of its morphology. The midline of the Mc2 facet is constricted proximally, likely due to encroachment by the capitotrapezoid interosseous ligament. The dorsal extent of this articular surface is expanded distally where it abuts the dorsodistal margin of the bone, and its wide palmar portion projects distally where it meets the reciprocally angled Mc3 facet to form a raised ridge along their shared palmar border. The palmar portion of the Mc3 facet is mildly concave both proximodistally and mediolaterally, while the dorsolateral portion is moderately withdrawn proximally. A lateral projection along the dorsal margin of the distal hamate facet is also evident in KNM-CA 409, which serves to orient the distal portion of the hamate facet somewhat palmarly. This palmar orientation is common in extant apes, but the angulation that clearly delineates this portion from the medially-oriented remainder of the hamate facet has previously been identified exclusively in *E. heseloni*, in which this portion rides along the dorsum of the hamate (Beard *et al.*, 1986). This angulation is not quite as pronounced in KNM-CA 409 (Fig. 3.4), but it is nevertheless clearly distinguished from the remainder of the hamate facet.

More proximally, the morphology of this specimen departs somewhat from that of the Rusinga specimens. While its most proximal point occurs palmarly relative to the other Tinderet specimens, it is positioned dorsally relative to each of the Rusinga specimens. This point is also lateral to the midline, and the most proximal surface is moderately angular in palmar or dorsal view rather than smoothly curved, resulting in a clear delineation between the lunate and centrale facets. The capitate head is not visibly pronated relative to the body, and resembles a quarter sphere in proximal view, as the lunate facet faces dorsally rather than dorsolaterally as in most others of the fossil

sample (Fig. 3.2, proximal view). The palmar extent of the centrale facet roughly matches that of the contralateral hamate facet, whereas in each of the Rusinga specimens the centrale articulation extends palmarly to a significant degree, even accounting for the head's pronated position. The lunate facet terminates more proximally on the dorsum of the bone relative to all others of the fossil sample. These features indicate significant differences in midcarpal mobility, with KNM-CA 409 perhaps having facilitated a relatively limited range of extension and supination.

KNM- SO 1000 This left capitate is slightly larger than KNM-MV 4, of a size with sampled lutungs or smaller spider monkeys. It is extremely gracile, with an apparent fineness ratio (i.e., proximodistal length relative to mediolateral or dorsopalmar width) exceeding that of most hylobatids. The hamate surface is weathered, very long, and dorsopalmarly narrow, with only mild concavity. The head is narrow both dorsopalmarly and especially mediolaterally, and is not pronated relative to the body of the capitate, orienting its hamate facet directly medially. The proximal facet remains parallel with the dorsal nonarticular region for some distance near its medial margin with the hamate facet before angling sharply toward its palmar margin, rather than curving toward it immediately. The centrale facet is therefore more radially oriented, and is also palmarly expanded relative to the hamate facet, which, given cooperative soft tissue, would allow the centrale to translate farther palmarly, enhancing the range of mid-carpal supination (Jenkins, 1981). The centrale facet remains convex at its distal extent, terminating in the neck region proximal to where the body angles laterally in the region of the trapezoid

articulation. This condition occurs often in *Pongo* and *Gorilla*, but only rarely in hylobatids and *Pan* (see Fig. 3.10b).

Distally, the Mc3 surface is mediolaterally narrow, and winnows progressively before coming to a palmolateral point. The entire facet is uniformly concave along its medial border; laterally, it shares the withdrawn dorsal portion and distally projecting palmar portion with its contemporaries, although the latter feature may be most pronounced in this specimen. The latter condition displaces the palmar Mc2 articulation more distally, resembling an inchoate form of the hook-like process common in *Pongo* specimens (Rose, 1984). A distal notch is present laterally, resulting in a discontinuous Mc2 facet and adding to the great ape resemblance of the anterior Mc2 morphology. A distal notch is not in evidence medially, but the slight projection of the distal portion of the hamate facet may have allowed a carpometacarpal ligament to pass, a possibility supported by the specimen's discontinuous Mc4 facet. The body flares laterally to a small degree in the region of the dorsal Mc2 and trapezoid facets, perhaps increasing its embrasure with the trapezoid to some degree. The hamate facet is also discontinuous, with the most distal portion separated from the remainder by a small area of increased rugosity. This allies it somewhat with the brachiators of the extant sample (see Fig. 3.5), although the small size of the intervening region is more comparable with that variably present in *Pongo* and *Nasalis*, and particularly the former, as it lacks the latter's especially deep excavation of the medial surface and distomedial margin for attachment and passage of capitohamate and carpometacarpal ligaments.

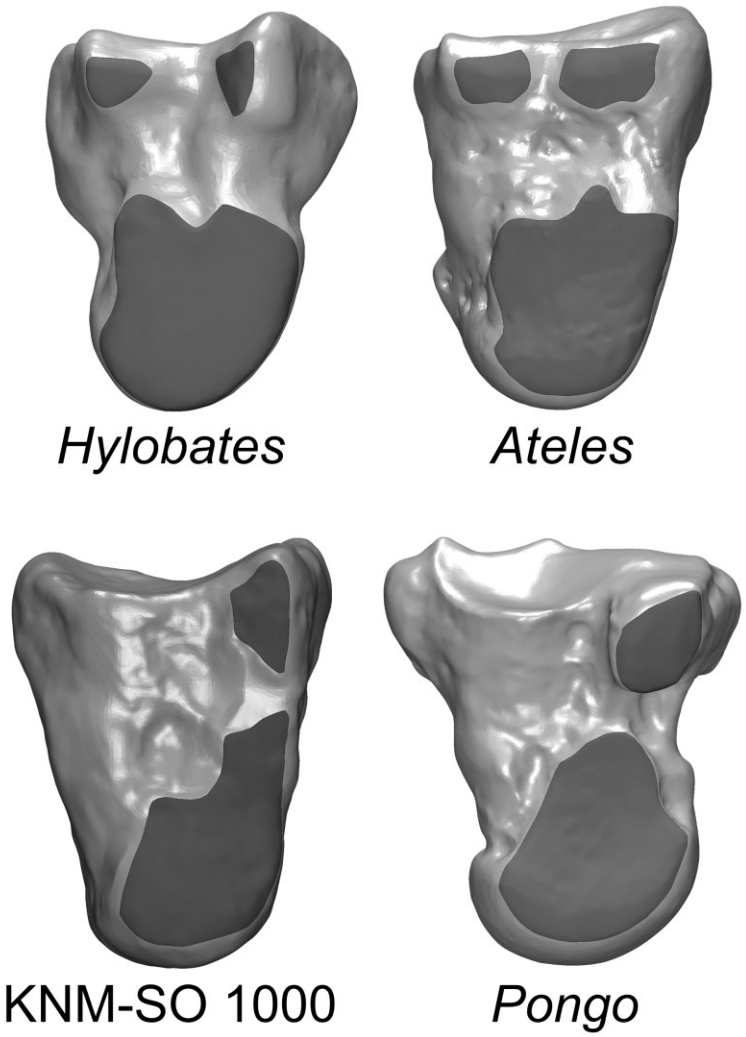

Fig. 3.5. Visualization of the hamate articulation (CpHm) in specimens displaying discontinuity. See Table 3.17b for variation among sampled taxa.

KNM-SO 1001 This right capitate is similar in size to KNM-SO 1000 as measured by volume and surface area, but is shorter and stouter, more similar in its dimensions to the Rusinga specimens and KNM-CA 409. It is well preserved except for small deletions along the distal margins palmarly and dorsomedially, and a larger one dorsolaterally. Despite its small size, this specimen resembles those from Rusinga in many ways. A distal notch is present medially and absent laterally, and it has large, continuous facets for both the Mc2 and hamate, both in accord with most of the fossil sample but unlike

KNM-SO 1000. The Mc3 surface is also more similar to others of the fossil sample than to KNM-SO 1000. Its mediolateral width remains relatively uniform from dorsal to palmar, and its medial and palmar borders are angled less acutely to each other than in the other Songhor specimen of similar size. Mc3 topography is less pronounced, with relatively continuous dorsopalmar concavity akin to that of the Rusinga specimens, lacking any hook-like projection palmarly. The facet's distal extent occurs along the Mc2 margin, but does not result in notable distal displacement of the palmar Mc2 articulation.

Like KNM-SO 1000 and KNM-CA 409, the capitate head of KNM-SO 1001 lacks pronation, and its distinct lunate facet maintains a directly dorsal orientation across its mediolateral width before forming an angular border with the centrale facet. Unlike others of the fossil sample, the lunate and centrale facets are nearly orthogonal to each other, with the latter having a markedly lateral orientation. The hamate facet of this specimen is also the least concave of the fossil sample, falling just outside the upper range of *Ateles*.

KNM-SO 31245 This right capitate is larger than those described above, just larger than the KPS III individual of *E. heseloni* and most similar in size to female proboscis monkeys of the sample. It suffers from abrasion along the lunate-centrale and lunate-hamate facet margins palmarly, and along the dorsodistal margin of the hamate facet. More severe damage is present distally, where the dorsal margin of the Mc3 facet has been eroded, progressing in severity toward the lateral extent where the deletion includes the dorsal portion of the Mc2 surface. Despite this damage, the dorsopalmar continuity of the Mc2 surface is evident, with the facet maintaining uniform width at the

midline, as opposed to the proximal impingement adjacent to the lateral ligament concavity seen in the other fossil specimens.

This specimen is relatively stout, with the head, neck, and body all mediolaterally expanded slightly. The distal facet is relatively uniform in width, neither narrowing palmarly nor coming to a point palmolaterally, although the prominent ligament attachment site just proximal to the Mc3 facet projects palmarly beyond the MC3 articular surface, as commonly occurs in apes and in each of the fossil specimens save two of the Rusinga specimens. The distal portion of the hamate facet may have a slight palmar orientation, but the abrasion of the margin renders the morphology unclear. The head is pronated, and the centrale facet seems to be somewhat palmarly expanded, though the erosion in this area hinders comparison.

KNM-SO 31246 Also from the right side, KNM-SO 31246 resembles KNM-SO 31245 in many ways while being more pronounced in many of their distinctive shared features. It is also larger, most similar in size to a large proboscis monkey or a small mandrill. While weathering is minor, the specimen suffers from severe erosion along the palmar margin of the lunate facet, growing in severity medially in the region formerly abutting the hamate facet. Damage is most extensive distally, where the Mc3 facet is properly represented in only a small palmomedial region. The unaffected area demonstrates the absence of a distal notch medially, contrary to the condition of KNM-SO 31245. The Mc2 facet has also been almost entirely deleted, although an attachment site for a lateral ligament is preserved. The distal position of this excavation suggests that

encroachment on the Mc2 articulation would have been significant, but the presence of a distolateral notch cannot be determined.

Overall mediolateral expansion is more pronounced than in KNM-SO 31245, and the hamate facet's proximodistal concavity is high relative to most of the fossil sample. It also has a weakly expressed dorsal ridge, akin to those sometimes present in great apes. A dorsal portion of the centrale facet is distally expanded, its distal extent positioned palmar to this slightly raised and angular portion of the body (Fig. 3.10). The distal portion of the hamate facet of KNM-SO 31246 also has a distinct palmar orientation, comparable to the condition of extant apes and lacking the unique morphology of *E. heseloni*. Head pronation is also exaggerated relative to KNM-SO 31245, approaching the degree found in KNM-MV 4 (see Fig. 3.2, proximal view). Its centrale facet appears to have been palmarly expanded in life, but the palmar-most extent of this articulation is now absent. In overall morphology, this specimen bears some resemblance to the less morphologically elaborated *Gorilla* specimens of the sample.

KNM-SO 1002 This right capitate is the largest of the fossil sample, similar in size to the smallest of the *Papio* sample. It suffers from erosion like that of KNM-SO 31246, albeit not as severe, with most of the Mc3 facet and a central portion of the Mc2 facet having been preserved. Palmar portions of the lunate and centrale facets also suffer from erosion, which extends distally and medially to transect the hamate facet, terminating near the dorsodistal border of the lunate surface.

The head of this specimen, large, globular, and greatly expanded laterally, while being somewhat pronated. The body is expanded both medially and laterally, and the neck is highly waisted. A dorsal portion of the centrale facet is distally expanded, positioning its distal extent palmar to the laterally-expanded body (Fig. 3.10). The erosion of the dorsal margin separating the body and head prevents examination of morphology in this region, but the surface just proximal to this area is well preserved and markedly concave, with the lunate surface angling dorsally where it may have contributed to a raised ridge. While a raised ridge in this area is fairly common, the preserved anatomy suggests it may have been quite robust in this specimen, perhaps resembling that of *Nacholapithecus* (Ogihara *et al.*, 2016). The distal portion of the hamate facet maintains a palmar orientation, and is the most concave of the fossil sample, largely owing to the medial expansion of the body. Just palmar to this facet lies a deep excavation for the capitohamate ligament, the most pronounced of the fossil sample. KNM-SO 1002 also shares with many extant apes a distinct indentation for displacement of the palmar horn of the lunate, perhaps related functionally to load bearing in flexion.

The preserved portion of the Mc2 surface is sufficient to demonstrate its dorsopalmar continuity, as well as a mildly distal orientation, a feature most pronounced in Asian apes among non-hominin anthropoids. Its continuous Mc2 facet aligns KNM-SO 1002 with its contemporaries other than KNM-SO 1000, but distinguishes it from the typical condition of extant apes (Table 3.17a). A distal notch is absent medially, although like KNM-SO 1000, the medial projection of the distal hamate surface leaves a possible passage for a carpometacarpal ligament. The preserved portion of the distal

facet displays topography like that of contemporaneous catarrhines, lacking the complex Mc3 articulation most pronounced in African apes, *Pongo*, and *Ateles* of the extant sample. The morphology of the head is intermediate between *Pan* and cercopithecines; it appears to lack the palmar extension of the lunate and centrale facets generally seen in *Pan*, but its proximal outline is roughly a quarter sphere, as is commonly true of *Pan*.

Body size estimation

Body mass estimates for each of the fossil capitates are shown in Table 3.4a, with regression coefficients and associated uncertainty values in Table 3.4b. *E. heseloni* body size is estimated at 11.5kg (weighted mean to account for C26 and C28 both belonging to the KPS III individual), comparable to the 10.9kg estimate of Rafferty and colleagues (1995; Table 3.1).

Most of the Tinderet specimens can be differentiated into two size groups. KNM MV 4, KNM-SO 1000, and KNM-SO 1001 belong to the smaller group, with body mass estimates between 5 and 6 kg. These estimates are incongruent with the *Proconsul* species and *Rangwapithecus*, but are potentially compatible with all other catarrhine species known from these sites. Estimates for KNM-SO 31245, KNM-SO 31246, and KNM-SO 1002 fall between 12 and 16 kg, compatible with *P. africanus* and *R. gordoni*. KNM- CA 409 falls between the two groups at 9.2 kg; this is within the range estimated for *E. heseloni*, and therefore is also compatible with the two mid-sized Tinderet species. However, because the estimated ranges of the relevant fossil taxa are based

on qualitative comparisons of limited material, the size of this specimen could potentially comport with *D. macinnesi* as well.

Table 3.4. Fossil body mass estimates. qmle CF, quasi-maximum likelihood estimator correction factor; RSE, residual standard error; %SEE, percent standard error of estimate; %MPE, percent mean prediction error. See text for details.

a	Specimen	BM (kg)
Undescribed	KNM-MV 4	5.3
	KNM-CA 409	9.2
	KNM-SO 1000	6.0
	KNM-SO 1001	5.9
	KNM-SO 31245	12.4
	KNM-SO 31246	15.4
	KNM-SO 1002	15.9
E. heseloni	KPS III(L) C26	12.1
	KPS III(R) C28	12.1
	KPS VIII C27	11.6
	KNM-RU 2036M	10.7
	Mean	11.5

b	Regression coefficients and uncertainty values						
R^2	Inter-cept	Slope	p	qmle CF	RSE	% SEE	% MPE
0.977	-2.30	0.786	0.000	1.01	0.147	16.15	12.36

Functional analyses

Positional classification

Nine shape variables were found to distinguish between extant positional classes by the criteria described above (see Table 3.5; Table 3.9), and were included in the positional classifiers. The first two discriminant functions are visualized in Fig. 3.6. Most suspensors are distinguished from pronograde monkeys along the first axis, while the African apes overlap with both groups. Knuckle-walkers are largely distinguished from

members of the other positional classes along the second discriminant axis. Digitigrade anthropoids are poorly distinguished by the first two axes.

The third axis, accounting for 6.3% of the variation, separates digitigrade individuals from non-cercopithecines monkeys, but does little to distinguish between the cercopithecine postural modes. Difficulty in separating digitigrade and palmigrade cercopithecines is the most prominent source of misclassification error for both models. Overall, however, the cross-validated accuracy of each exceeds 90% when accounting for differential class prevalence in the sample (Table 3.5a; see Table 3.10 for additional positional classifier details and Table 3.18 for predictions and posterior probabilities for extant individuals).

The positional classifications of the fossil sample are entirely congruent between the two models (Table 3.5c). KNM-SO 1000 and KNM-SO 1001 are classified as suspensory, KNM-SO 1002 is classified as a knuckle-walker, and the remainder as palmigrade. The posterior probabilities assigned to these predictions by both models are generally high. The lowest-confidence predictions of the *glmnet* model were those for KNM-SO 31245 and KNM SO 1002, which were assigned a probability of 0.83. All others were 0.92 or higher. Posterior probabilities of DFA classification were 0.8 or greater for the Tinderet specimens, with most again exceeding 0.9. Nevertheless, the discriminant scores of the fossil specimens classified as suspensory or knuckle-walking position them near the decision boundaries separating these classes from the palmigrade sample (Fig. 3.6). This reflects the subtle, perhaps incipient nature of the positional adaptations of these specimens.

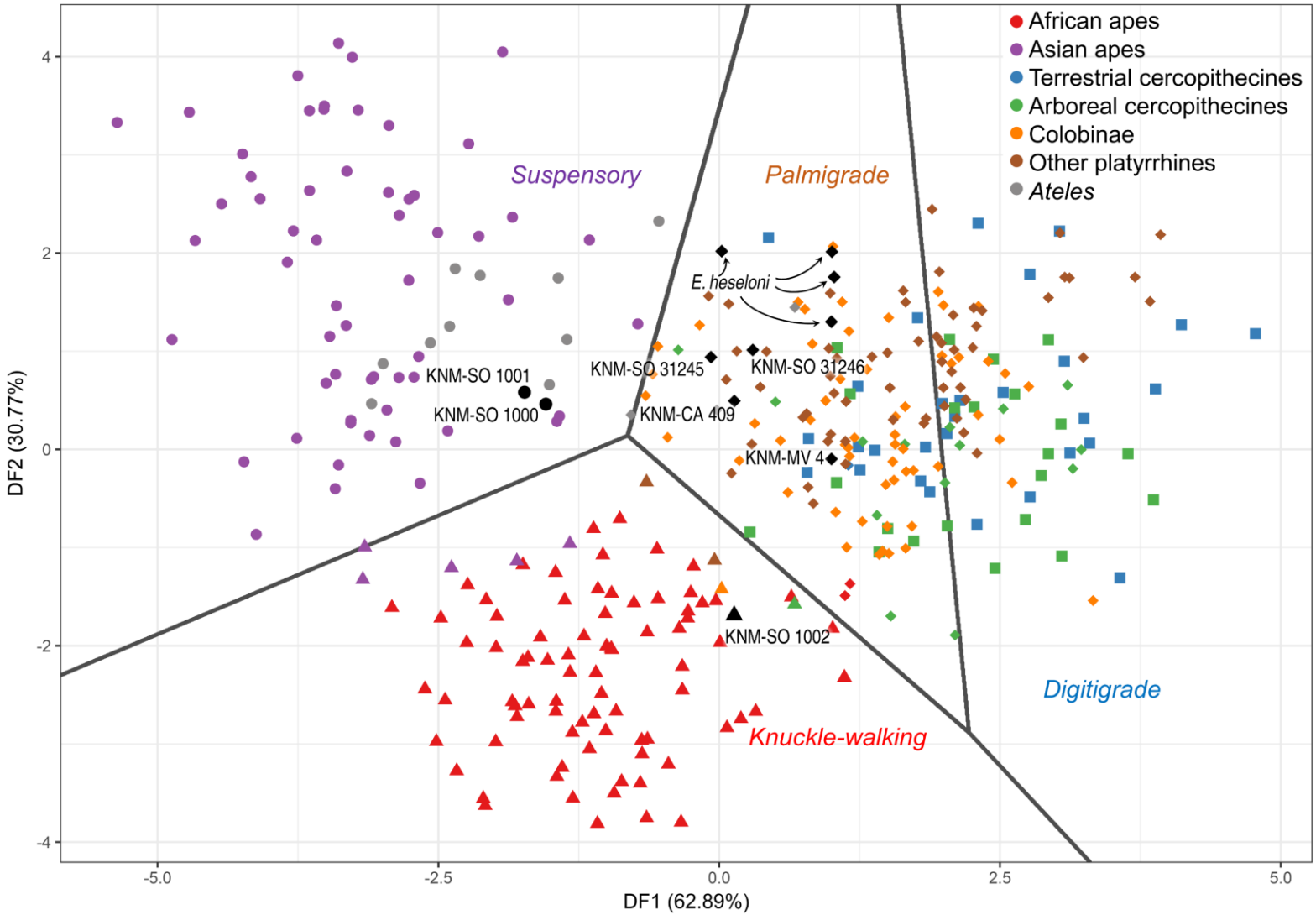

Fig. 3.6. Plot of scores for first two discriminant functions based on 9 shape variables best separating extant positional classes. Data points are colored according to *a priori* class and shaped according to predicted class (diamond = palmigrade; triangle = knuckle-walking; circle = suspensory; square = digitigrade). Gray lines represent decision boundaries. See Table 3.5 for discriminant functions, classification accuracy, and posterior probabilities.

Table 3.5. Positional classification results

a Extant classification accuracy[a]

Model	Total	*DG*	*KW*	*PG*	*S*	Bal[b]
DFA	0.881	0.633	0.957	0.895	0.870	0.901
glmnet	0.906	0.621	0.976	0.914	0.927	0.919

b	Discriminant functions			*glmnet* variable importance[c]			
	DF1	DF2	DF3	*DG*	*KW*	*PG*	*S*
CpSc	0.40	-0.40	-0.35	0.43	1.87	0.21	2.09
CpDn	0.41	-0.19	-0.44	1.44	0.00	0.53	2.01
Cp3	-0.02	-0.31	0.20	1.35	1.78	0.00	0.00
Cp2	0.72	0.58	-0.13	2.50	2.38	0.87	0.99
Cp4	0.76	0.46	0.33	1.67	7.47	2.44	0.00
CpPxA	0.69	-0.93	0.52	0.00	3.24	0.66	4.51
CpScA	0.49	0.36	0.37	0.60	0.40	1.21	1.41
CpHmC	0.76	-0.15	-0.53	2.39	0.58	0.00	3.88
CpHP	0.29	0.49	-0.07	1.77	1.67	1.44	1.54

c Fossil classification results

DFA	*DG*	*KW*	*PG*	*S*	Max	Class
KNM-MV 4	0.04	0.01	0.94	0.00	0.94	*PG*
KNM-CA 409	0.14	0.04	0.80	0.03	0.80	*PG*
KNM-SO 1000	0.00	0.08	0.03	0.89	0.89	*S*
KNM-SO 1001	0.00	0.04	0.01	0.95	0.95	*S*
KNM-SO 31245	0.01	0.01	0.93	0.06	0.93	*PG*
KNM-SO 31246	0.02	0.00	0.96	0.02	0.96	*PG*
KNM-SO 1002	0.00	0.89	0.11	0.00	0.89	*KW*
KPS III(L) C26	0.35	0.00	0.65	0.00	0.65	*PG*
KPS III(R) C28	0.24	0.00	0.76	0.00	0.76	*PG*
KPS VIII C27	0.06	0.00	0.94	0.00	0.94	*PG*
KNM-RU 2036M	0.15	0.00	0.67	0.19	0.67	*PG*
glmnet	*DG*	*KW*	*PG*	*S*	Max	Class
KNM-MV 4	0.00	0.00	1.00	0.00	1.00	*PG*
KNM-CA 409	0.01	0.00	0.99	0.00	0.99	*PG*
KNM-SO 1000	0.00	0.00	0.01	0.99	0.99	*S*
KNM-SO 1001	0.00	0.00	0.00	1.00	1.00	*S*
KNM-SO 31245	0.00	0.00	0.83	0.17	0.83	*PG*
KNM-SO 31246	0.00	0.00	0.96	0.04	0.96	*PG*
KNM-SO 1002	0.00	0.83	0.17	0.00	0.83	*KW*
KPS III(L) C26	0.06	0.00	0.94	0.00	0.94	*PG*
KPS III(R) C28	0.03	0.00	0.97	0.00	0.97	*PG*
KPS VIII C27	0.01	0.00	0.99	0.00	0.99	*PG*
KNM-RU 2036M	0.05	0.00	0.92	0.03	0.92	*PG*

[a] glmnet parameters were tuned with 20 repetitions of 10-fold CV; both DFA and glmnet model accuracy was calculated after 100 repetitions of 10-fold CV.
[b] Balanced accuracy is an average of a model's sensitivity and specificity (true positive rate and true negative rate).
[c] Absolute value of tuned model coefficients.

Locomotor proportion estimation

The described procedure produced effective predictive models for only *Susp*, *SuspA*, *QuadA*, and, to a lesser extent, *Quad*. The other locomotor proportions had lesser correspondence to capitate morphology – in lieu of inaccurate models built using the ame procedure, models to predict *ClimbA*, *Climb*, and *Arb* reported here were built using all shape variables as predictors (see Table 3.12). Due to the essential lack of correspondence between capitate morphology and leaping behavior, neither process was successful in producing effective models to predict *LeapA* or *Leap*.

Fossil estimates of non-leaping locomotor proportions are presented in Table 3.6. They are largely consistent with the classification results, but the different locomotor estimates for each specimen do not necessarily tell a consistent story. KNM-SO 1000 and KNM-SO 1001 are assigned the highest values of *SuspA*, with the latter estimated to be the fossil individual most reliant on suspension during arboreal locomotion, with a frequency exceeding that of extant *Ateles*. This is surprising, given the greater qualitative resemblance of KNM-SO 1000 to extant suspensors. This is reflected in the *Susp* estimates, of which the latter specimen is assigned the highest value. KNM-SO 1001 is also estimated as more suspensory than most of its Miocene contemporaries, but its prediction matches that of KNM-RU 2036, and is only slightly greater than several of the specimens reconstructed as palmigrade. This is inconsistent with the high *SuspA* estimate of this specimen, barring a major terrestrial component, which would also be inconsistent with the high degree of arboreality estimated for this specimen. *QuadA* is estimated to be very low in KNM SO 1001, but only slightly reduced in KNM-SO 1000 relative to most others of the Miocene sample. This trend is reversed in *Quad*,

with KNM-SO 1000 assigned the lowest value of the fossil sample and KNM-SO 1001 representing the sample median.

Table 3.6. Estimated locomotor proportions, based on GLM models from variable subsets selected using PGLS. See Table 3.12 for model details

Specimen	*QuadA*	*Quad*	*SuspA*	*Susp*	*ClimbA*[a]	*Climb*[a]	*Arb*[a]
KNM-MV 4	0.35	0.57	0.07	0.03	0.42	0.28	0.77
KNM-CA 409	0.61	0.54	0.06	0.08	0.34	0.19	0.47
KNM-SO 1000	0.37	0.24	0.19	0.19	0.42	0.32	0.86
KNM-SO 1001	0.16	0.50	0.32	0.10	0.36	0.19	0.89
KNM-SO 31245	0.40	0.31	0.12	0.07	0.31	0.26	0.93
KNM-SO 31246	0.41	0.32	0.09	0.06	0.29	0.29	0.95
KNM-SO 1002	0.42	0.76	0.04	0.01	0.37	0.16	0.74
KPS III(L) C26	0.51	0.51	0.10	0.08	0.25	0.27	0.88
KPS III(R) C28	0.46	0.51	0.09	0.09	0.29	0.27	0.81
KPS VIII C27	0.48	0.52	0.08	0.05	0.32	0.29	0.83
KNM-RU 2036M	0.52	0.27	0.11	0.10	0.28	0.27	0.79
E. heseloni mean	0.49	0.45	0.09	0.08	0.29	0.27	0.83

[a] Models based on selected functionally significant traits performed poorly in estimating these proportions; estimates in these cases were calculated using all shape variables, and therefore reflect overall extant affinities and may be less reliable.

KNM-SO 1002 is predicted as the least suspensory of the fossil sample, with estimates corresponding to the baseline values assigned to non-suspensors of the extant sample (Table 3.12). Its *Quad* estimate is the highest of the fossil sample, and exceeds the estimated (but not observed) values of most extant taxa as well, including most of the African apes. Its *QuadA* estimate, meanwhile, is similar to those assigned to many other extant and fossil specimens, which would be consistent with a substantial terrestrial component. This is not supported by the only slightly reduced *Arb* estimate assigned to this specimen, although as described above, output of the *Arb* model is likely to be less reliable.

Locomotor estimates for the fossil specimens classifed as palmigrade are fairly consistent with each other. The Rusinga specimens are all predicted very similarly save for a low *Quad* estimate for KNM-RU 2036, while KNM SO 31245 and KNM-SO 31246 are very similar to each other and, to a somewhat lesser degree, to the Rusinga specimens. KNM-SO 409 has a slightly elevated *QuadA* estimate and a substantially lower *Arb* estimate, while KNM-MV 4 has slightly lower estimates for *QuadA* and *Susp*. These specimens are otherwise estimated to have locomotion similar to that of the Rusinga specimens.

Analysis of locomotor diversity

The PLS shape scores of all extant centroids and fossil specimens are visualized in Fig. 3.7a. The *E. heseloni* specimens group together in the center of the monkey group, flanked by the ceboids and colobins. KNM-SO 31245 and KNM-SO 31246 are nearby, positioned near *Procolobus* between the Rusinga specimens and papionins. KNM-SO 1000 and KNM-SO 1002 plot among the great apes. KNM-CA 409, KNM-MV 4, and KNM-SO 1001 are positioned between the great ape and monkey groups, with the latter separated somewhat from the other specimens in the general direction of the hylobatids. The Euclidean area of the Tinderet sample's convex hull approaches that of the combined monkey centroids, although the great ape sample occludes the greatest portion of shape-space (Table 3.13c).

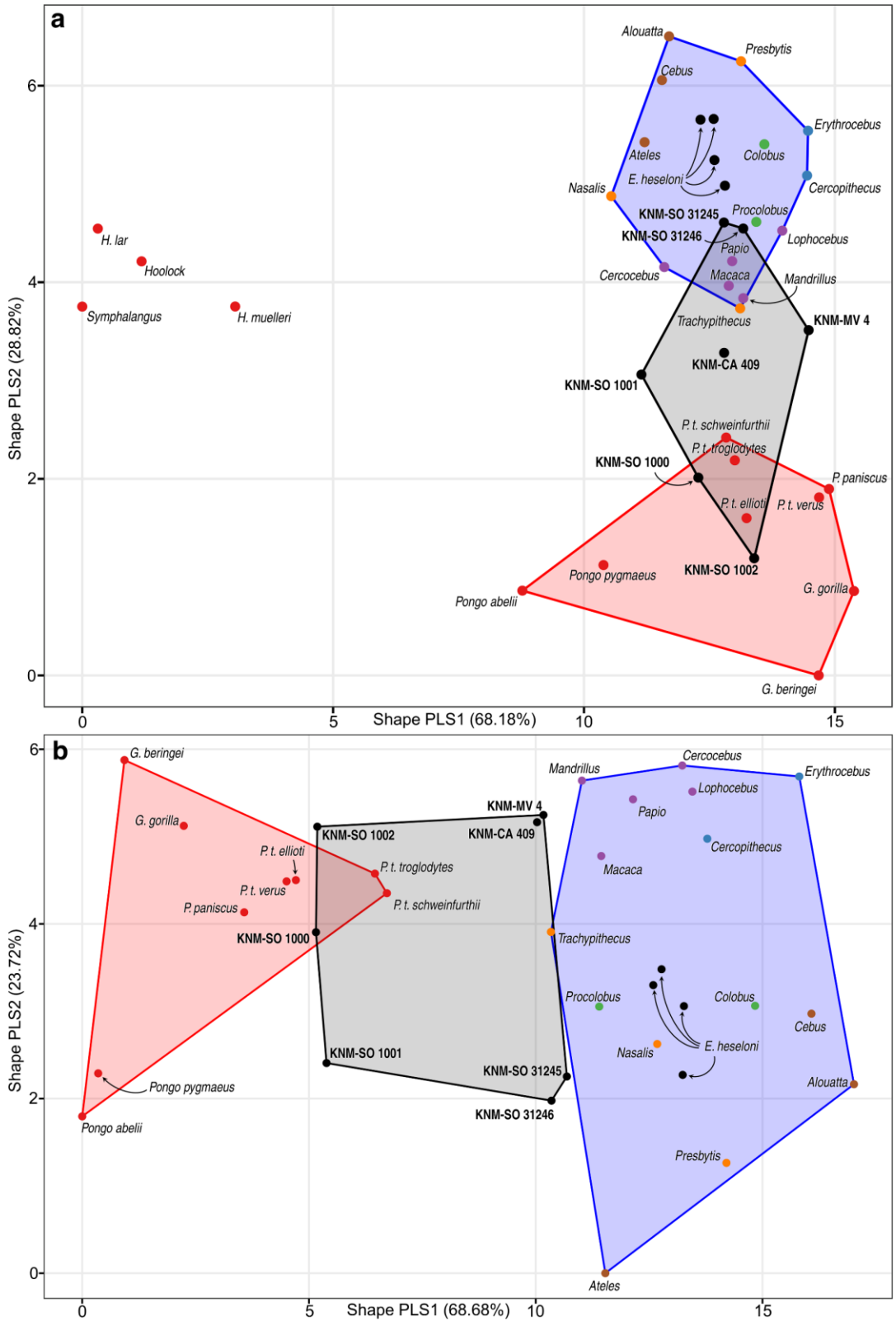

Fig. 3.7. PLS shape-space with convex hulls characterizing the functional diversity of the Tinderet sample relative to extant great apes and monkeys, with (a) and without (b) inclusion of hylobatids. The Euclidean area of the Tinderet sample approaches or exceeds that of broad extant groups.

Much of the separation between groups occurs along the second PLS axis, but the structure of the shape space is dominated by the extreme shape and locomotor variables of the hylobatids. Most morphological covariation occurs along the first axis, with high suspension and low quadrupedalism on the left, high quadrupedalism and low suspension on the right, and relatively little morphological covariation with climbing or leaping.

With hylobatids excluded, morphological covariation with suspension still wields the strongest influence, excluding hylobatids, but parity with other behaviors is greatly increased (Table 3.13a). This results in recognition of far greater functional diversity among the monkeys; the Euclidean area of the convex hull formed by the Old and New World monkey centroids in the new PLS shape-space (Fig. 3.7b) approaches that of the Tinderet and great ape samples combined (Table 3.13c). Diversity among the Tinderet sample in this analysis exceeds that of the great ape centroids, with their convex hulls comprising 15.6% and 13.0% of the shape-space, respectively. The groups are largely distinguished by the first axis, with increasing values reflecting morphology associated with more quadrupedalism and less climbing and suspension. Within the broad groupings, most of the variation occurs along the second axis, which is most strongly influenced by morphological covariates of suspension and arboreality. Morphology associated with greater proportions of *SuspA* and *Arb* is positioned lower on this axis, while more terrestrial taxa and those more reliant on quadrupedalism and climbing during arboreal locomotion are positioned toward the top.

As in the first PLS analysis, *E. heseloni* specimens form a cluster in the center of the monkey group, and KNM-SO 31245 and KNM-SO 31246 are again positioned

nearest to the Rusinga specimens of the Tinderet sample. KNM-SO 1000 is positioned among the great apes as before, while KNM-SO 1002 plots nearest the *Pan* centroids just outside the great ape hull. KNM-CA 409 and KNM-MV 4 plot nearest the cercopithecines this time, while KNM -SO 1001 is again separated from the other fossils in accord with its morphological resemblance to extant suspensors.

Taxonomic and phylogenetic analyses

Superfamily classification

Nine shape variables met the criteria for inclusion in the taxonomic classifiers. In the taxonomic DFA (Fig. 3.8), hominoids are distinguished from ceboids and, to a lesser extent, from cercopithecoids by the first discriminant function. This axis is dominated by the orientation of the scaphoid/central facet (CpScA) and the relative size of the Mc4 facet (Cp4; Table 3.7b), which tend to be low among hominoids and high among ceboids (Table 3.14a). The second discriminant function separates most cercopithecoids and ceboids, while also contributing to the hominoid-cercopithecoid distinction. Values along this axis increase most strongly in association with a larger and more distally oriented Mc2 surface (Cp2, Cp23A), and a larger and more proximally oriented proximodradial surface (CpPx, CpPxA).

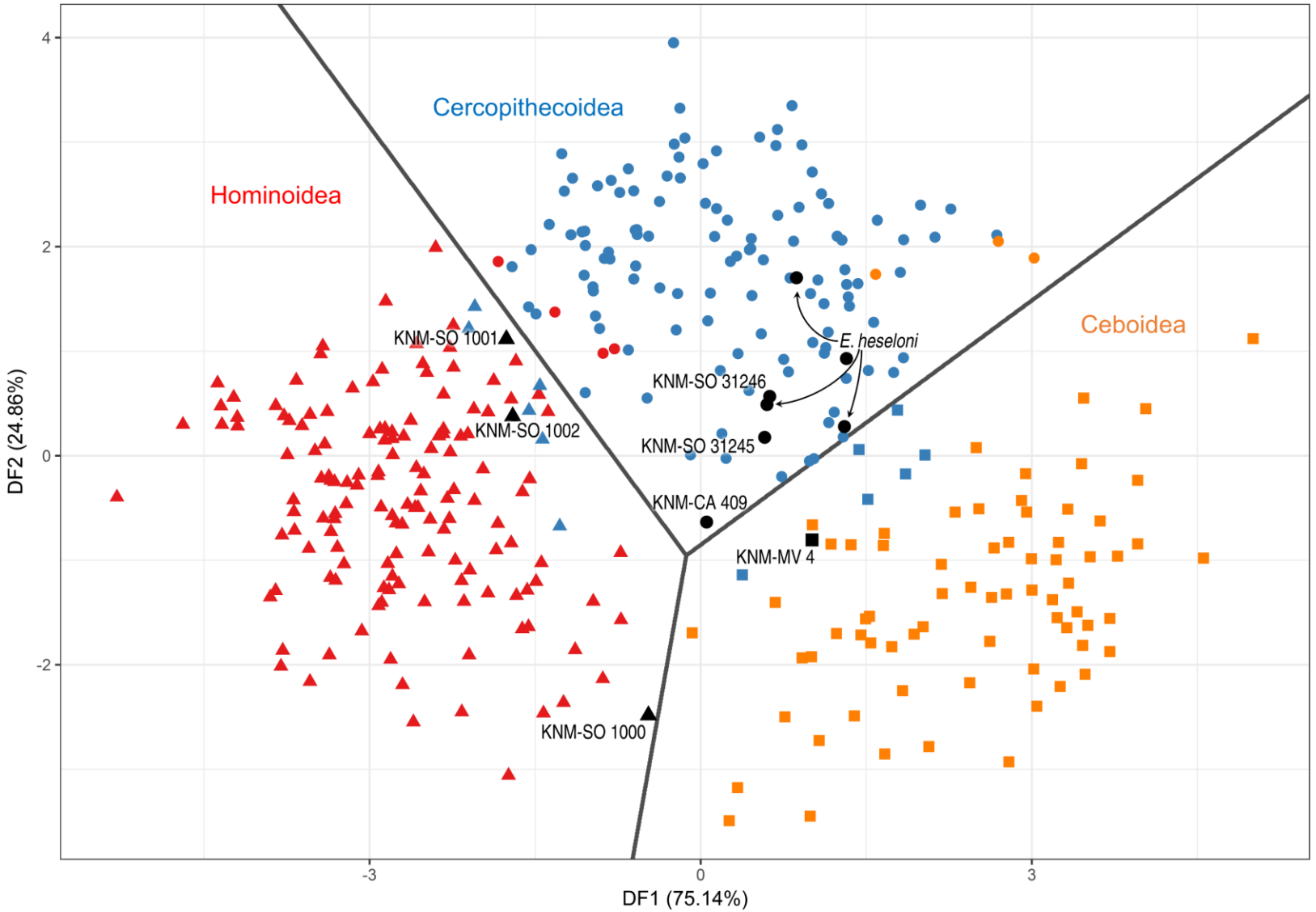

Fig. 3.8. Plot of scores for first two discriminant functions based on 9 shape variables best separating broad taxonomic groups. Data points are colored according to *a priori* class and shaped according to predicted class (triangle = Hominoidea; circle = Cercopithecoidea; square = Ceboidea). Gray lines represent decision boundaries. See Table 3.7 and Table 3.15 for classification accuracy, discriminant functions, posterior probabilities, and other model details.

In the *glmnet* model, platyrrhines are most strongly distinguished from other anthropoids by their large Mc4 facets and dorsally-oriented centrale facets, and cercopithecoids by their large proximoradial facets and hamate facet concavity. Hominoids are meanwhile best distinguished by small Mc2 and Mc4 facets and radially-oriented scaphoid/centrale facets (Table 3.7b).

Both models were effective in classifying the extant specimens, with the balanced accuracy of both exceeding 95% (Table 3.7a; see Table 3.15 for additional details). Fossil predictions are congruent between classifiers with the exception of KNM-MV 4, which the DFA classifies as a ceboid and *glmnet* classifies as a cercopithecoid with similar confidence (Table 3.7c). KNM-SO 1000, KNM-SO 1001, and KNM-SO 1002 are classified as hominoids, with the Rusinga sample and the remaining Tinderet specimens classified among the cercopithecoids. Posterior probabilities of the *glmnet* predictions are again high, while the DFA model lacks confidence about KNM-SO 1000, KNM-SO 1001, and KNM-CA 409, as well as one of the Rusinga specimens. This uncertainty is reflected in the DFA plot (Fig. 3.8), in which the fossil specimens again tend to plot very near the decision boundaries.

Table 3.7. Taxonomic classification results. Hom, Hominoidea; Cerc, Cercopithecoidea; Plat, Platyrrhini. See Table 3.5 and text for details

a Extant classification accuracy

Model	Total	Cerc	Hom	Plat	Bal
DFA	0.943	0.907	0.971	0.947	0.955
glmnet	0.947	0.930	0.961	0.945	0.960

b	Discriminant functions		*glmnet* variable importance		
	DF1	DF2	Cerc	Hom	Plat
CpPx	0.08	0.62	1.05	0.00	1.34
Cp2	0.55	0.96	0.00	3.24	0.04
Cp4	0.99	-0.01	0.00	3.17	3.31
Cp23A	-0.41	0.49	0.00	0.16	1.45
CpPxA	-0.09	0.43	0.26	0.00	1.63
CpScA	1.22	-0.37	0.00	3.00	5.10
Cp3SD	-0.19	0.32	0.00	0.02	1.56
CpHmC	0.08	0.14	0.81	0.39	0.00
CpHP	0.31	0.37	0.03	1.69	0.00

c Fossil classification results

DFA	Cerc	Hom	Plat	Max	Class
KNM-MV 4	0.11	0.00	0.89	0.89	Plat
KNM-CA 409	0.52	0.17	0.32	0.52	Cerc
KNM-SO 1000	0.01	0.60	0.39	0.60	Hom
KNM-SO 1001	0.37	0.63	0.00	0.63	Hom
KNM-SO 31245	0.83	0.01	0.16	0.83	Cerc
KNM-SO 31246	0.93	0.01	0.07	0.93	Cerc
KNM-SO 1002	0.14	0.86	0.00	0.86	Hom
KPS III(L) C26	0.99	0.00	0.01	0.99	Cerc
KPS III(R) C28	0.89	0.00	0.11	0.89	Cerc
KPS VIII C27	0.58	0.00	0.42	0.58	Cerc
KNM-RU 2036M	0.92	0.01	0.08	0.92	Cerc
glmnet	Cerc	Hom	Plat	Max	Class
KNM-MV 4	0.90	0.02	0.08	0.90	Cerc
KNM-CA 409	0.80	0.19	0.00	0.80	Cerc
KNM-SO 1000	0.04	0.96	0.01	0.96	Hom
KNM-SO 1001	0.16	0.84	0.00	0.84	Hom
KNM-SO 31245	0.94	0.01	0.05	0.94	Cerc
KNM-SO 31246	0.98	0.00	0.01	0.98	Cerc
KNM-SO 1002	0.14	0.86	0.00	0.86	Hom
KPS III(L) C26	1.00	0.00	0.00	1.00	Cerc
KPS III(R) C28	0.99	0.00	0.01	0.99	Cerc
KPS VIII C27	0.97	0.00	0.03	0.97	Cerc
KNM-RU 2036M	0.99	0.00	0.01	0.99	Cerc

Hierarchical clustering

All shape variables were found to have significant phylogenetic signal as quantified by both Pagel's lambda and Blomberg's K (Table 3.14b), and no significant allometric correlations were found in PICs of the tip data from either sex (Table 3.16). All variables were therefore included in the hierarchical clustering analysis. The BioNJ algorithm effectively represents the underlying distance matrix, with an extant cophenetic correlation coefficient of 0.953. Relationships between the extant taxa and fossil specimens are represented in two separate dendrograms, Fig. 3.9a and b.

The capitate metrics again effectively distinguish among the major anthropoid superfamilies, but relationships within these groups often vary from those based on molecular data (Fig. 3.9c). *E. heseloni*, KNM-CA 409, and KNM-MV 4 are positioned as basal catarrhines, while KNM-SO 31245 and KNM-SO 31246 plot together as sister to a group comprising the hominoids, cercopithecines, and two of the three presbytins. KNM-SO 1000 and KNM-SO 1001 are grouped within an Asian ape clade, with the former more similar to hylobatids and the latter more similar to the *Pongo* species. KNM-SO 1002 is positioned as a basal member of the African ape clade.

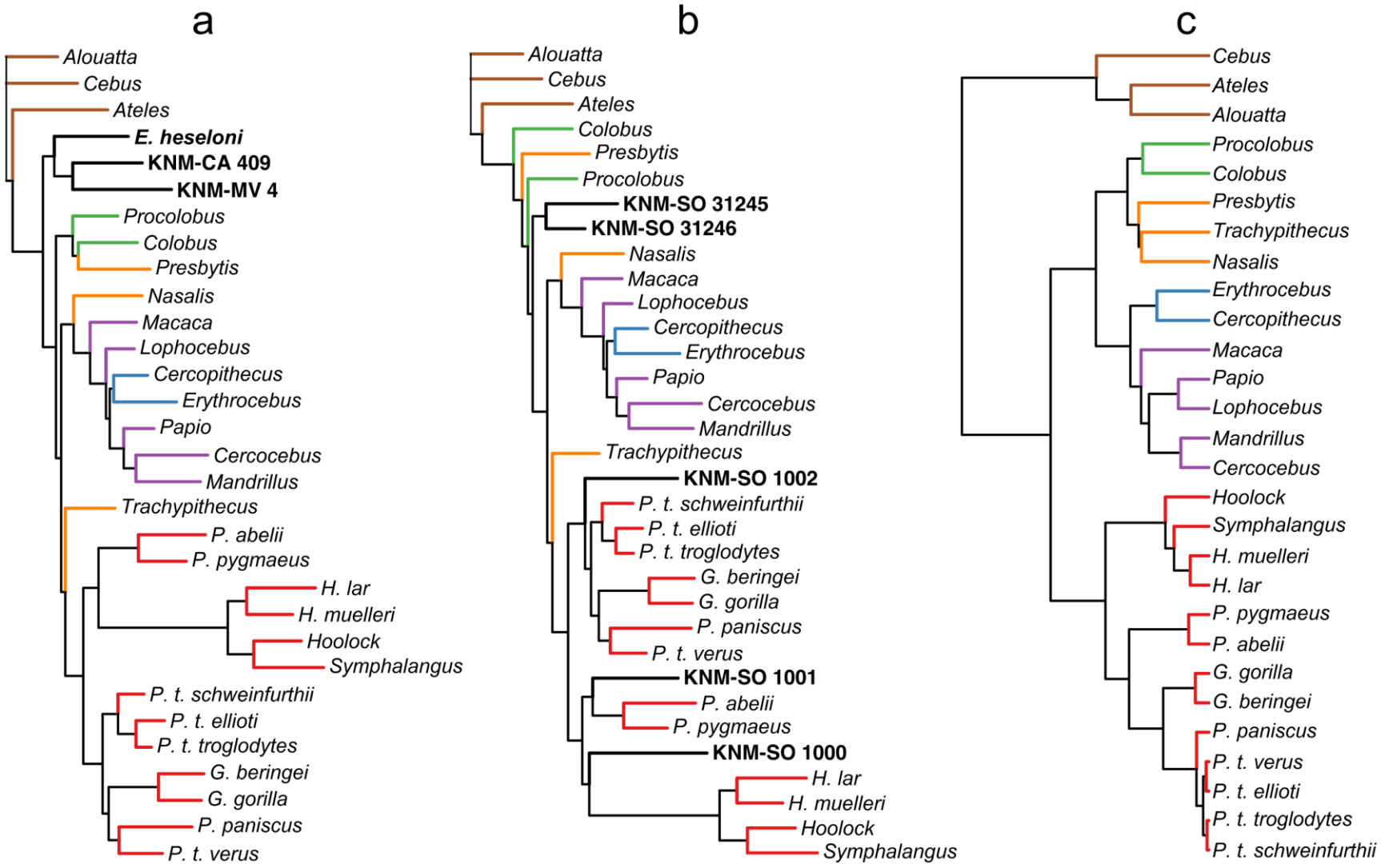

Fig. 3.9. Phenetic and phylogenetic relationships among extant and fossil specimens. (a and b) BioNJ dendrograms, (c) molecular phylogeny utilized in phylogenetic comparative analyses. Branch tips colored according to major anthropoid taxonomic divisions.

Discussion

Positional reconstructions

While both KNM-SO 31245 and KNM-SO 31246 have some qualitative resemblance to extant terrestrial taxa, the quantitative results are not consistent with terrestrialism as more than a minor behavioral component. They are estimated to have the highest proportion of arboreality of the fossil sample, are classified as palmigrade by both positional classifiers, group nearest to highly arboreal monkeys in PLS shape-space, and were found in all analyses to have great affinity with the sampled specimens of *E. heseloni*, for which significant terrestrial locomotion has not been suggested. The metrics of this study are limited in their ability to identify a terrestrial signal, however. While this may reflect the conservative nature of capitate morphology (Corruccini *et al.*, 1975; Blue, 2002), some potentially relevant features, such as capitate neck waisting or the presence of a raised ridge along the dorsal margin of the proximal surface, were not quantitatively characterized here. The lack of quantitative likeness to extant terrestrial primates nevertheless suggests behavioral habits comparable to those of *E. heseloni*.

KNM-MV 4 is also reconstructed as an arboreal palmigrade quadruped, but with perhaps slightly less reliance on quadrupedalism than *E. heseloni*, and perhaps some greater frequency of climbing as well. *Cebus* is perhaps this specimen's best functional analog of the extant sample (compare Table 3.6 and Table 3.12b). The shape metrics of KNM-MV 4 all fall within the range of variation of the *Cebus* sample, with three exceptions: The Mc4 articulation is especially large in *Cebus*, and although KNM-MV 4 has the largest Mc4 articulation of the fossil sample, it exceeds only one outlier specimen of *Cebus* in size. *Cebus* has the most acute Cp23A of the extant sample, but

it is even more acute in KNM-MV 4, falling just outside the range of all sampled specimens. The final exception is found in the size of the hamate facet, among the least functionally-informative of the analyzed metrics, which is relatively small in the Mteitei Valley specimen.

KNM-CA 409 is estimated to be the most reliant of the fossil sample on quadrupedalism during arboreal locomotion, and is most similar in most estimates to observations of *Alouatta*. KNM-CA 409 is also estimated as the least arboreal of the fossil sample, and the only specimen for which the arboreality estimate departs significantly from *E. heseloni*, but estimates of arboreality may be less reliable due to its relative lack of correspondence in individual shape variables, as detailed above. KNM-CA 409 is also the only specimen of the Tinderet sample assigned more than a trivial probability of digitigrady by either of the positional classifiers, and does have several features aligning it with terrestrial monkeys to some extent, including its large dorsal nonarticular region, lack of head pronation or palmar centrale facet expansion, acute Mc2-Mc3 facet angle, and relatively small Mc3 surface with somewhat elevated topography. It is nevertheless designated with high confidence as an arboreal quadruped by both positional classifiers.

The behavioral regimes of KNM-SO 1000 and KNM-SO 1001 seem likely to have included a significant degree of below-branch suspension. Both are classified with high confidence as suspensory by the positional classifiers. Locomotor proportion estimates for KNM-SO 1000 are most similar to those observed in *Ateles*, but with somewhat less predicted suspension and more climbing. Estimates of *QuadA*, *SuspA*, and *ClimbA* assigned to KNM-SO 1001 align it more closely with *Pongo*, although this is

contradicted by a relatively low *Susp* prediction. Both specimens are relatively narrow (CpPxA), with low hamate facet concavity (CpHmC), and small, radially-oriented centrale facets (CpSc, CpScA), each of which is associated with suspensory behavior in extant anthropoids (Table 3.9 and Table 3.11; see also Chapter 2 and Kivell, 2016 and references therein). KNM-SO 1000 also has a relatively small and discontinuous Mc2 articulation. This discontinuity, unique among the fossil sample, has been linked to hypertrophy of the lateral carpometacarpal ligament, leading to a hypothesized association with suspension (Lovejoy *et al.*, 2009). This trait was variably present within each of the sampled anthropoid subfamilies, however, with no apparent functional correspondence (Table 3.17a). Qualitative observations have been use to argue that the size of the canal transmitting this ligament is the more diagnostic feature (Selby *et al.*, 2016), a conclusion not examined here.

The discontinuous hamate facet of KNM-SO 1000 (Fig. 3.5) is less common in extant anthropoids. It is typical only in the brachiators of the extant sample (*Ateles* and the hylobatids), otherwise occurring only in a minority of sampled *Pongo* and *Nasalis* specimens (Table 3.17b). This feature may be associated with hypertrophy of the capitohamate interosseous ligament, which would assist in stabilizing this joint against sudden load transmission gradients experienced during brachiation or other acrobatic arboreal behaviors.

The locomotor behavior of KNM-SO 1002 is likely distinct from the others of the fossil sample, but characterization of its repertoire is difficult. It is classified with high confidence as a knuckle-walker by both positional classifiers, and is assigned the lowest values of *SuspA* and *Susp* among the fossil sample, as well as the highest estimate of

Quad. It is also assigned a low *Climb* estimate and a relatively high *ClimbA* value, which are also reminiscent of the African ape pattern. However, these two predictions, along with its moderate *Arb* estimate, are based on suboptimal models required by the relative lack of functional signal in individual shape variables and may therefore be unreliable. The large, globular head, highly-waisted neck, medially and laterally expanded body, moderately-expressed dorsal ridge, and concave hamate facet of KNM-SO 1002 contribute to a profile in dorsal or palmar view that is uniquely great ape-like among early or middle Miocene capitates. This is especially surprising given the early date.

Many of these features have been interpreted as contributing to enhanced midcarpal stability to better transmit loads generated during knuckle-walking (e.g., Corruccini, 1978; Richmond *et al.*, 2001; Begun, 2004). This interpretation of these features has come into question, however, due to the relative rarity of these and other reputed knuckle-walking traits in *Gorilla*, their inconsistent presence in *Pan*, and their variable presence in non-knuckle-walking taxa (e.g., Shea and Inouye, 1993; McCrossin and Benefit, 1997; Richmond, 2006; Kivell and Schmitt, 2009; Orr, 2010). An understanding of how knuckle-walking is reflected in the wrist remains elusive, as its extant practitioners comprise a single group of closely-related species whose morphology is also adapted to facilitate vertical climbing and suspension.

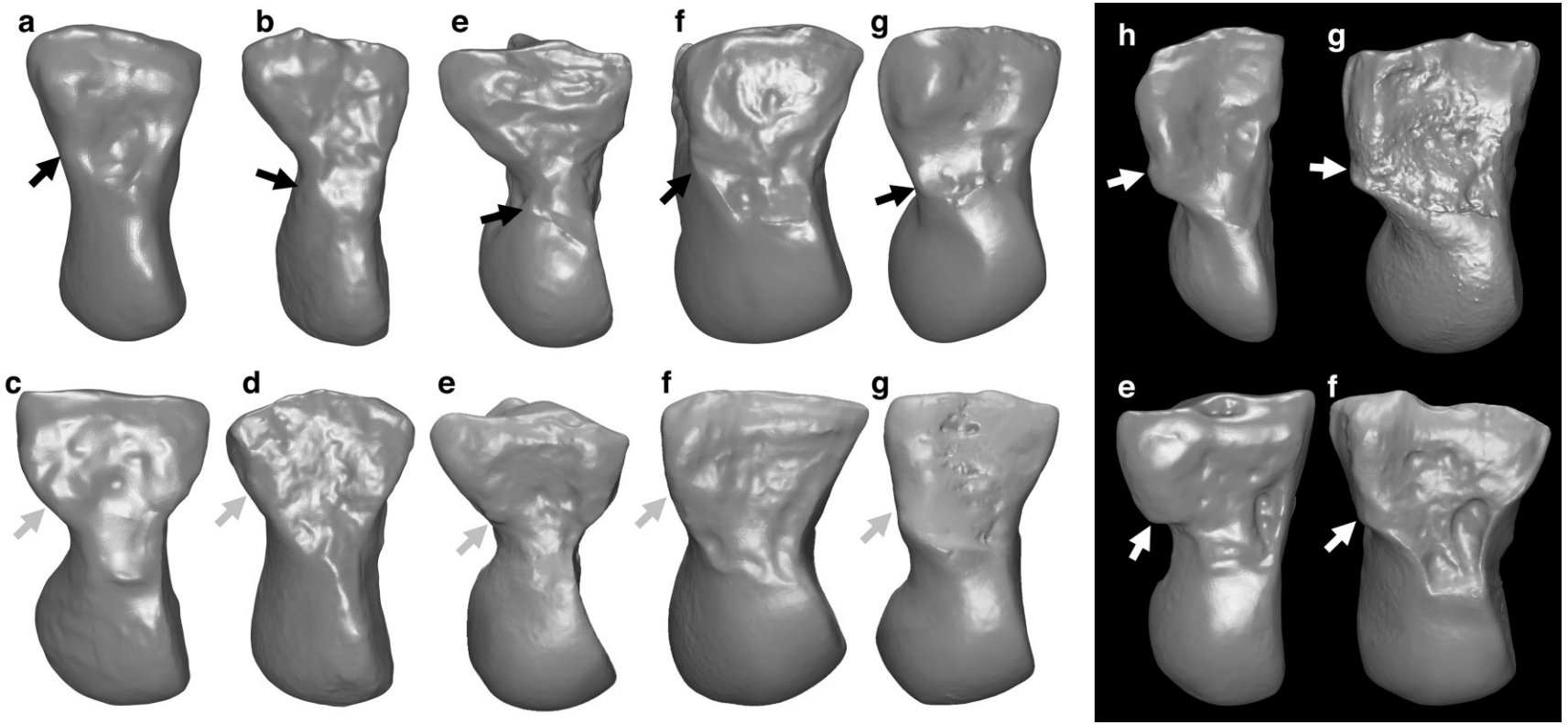

Fig. 3.10. Variation in scaphoid/centrale facet dorsal margin morphology. Right capitates in dorsal view, with arrows pointing to the facet's dorsodistal extent (black arrows = distal extent visible in dorsal view; light arrows = distal extent occurs palmar to a laterally-projecting portion of the body). Inset: elaborated condition described in the text. (a) KNM-MV 4, (b) KNM-SO 1000, (c) KNM-SO 1002, (d) KNM-SO 31246, (e) *Pongo*, (f) *Gorilla*, (g) *Pan*, (h) *Hoolock*.

The condition of KNM-SO 1002 and KNM-SO 31246, wherein the distal extent of the centrale facet is positioned palmarly to a laterally-projecting portion of the body's dorsal margin (Fig. 3.10c, d), would seems to aid stability during wrist extension, justifying its putative knuckle-walking utility. However, this condition appears in *Pongo* and *Gorilla* with similar frequency. In most specimens of *Pan* but only occasionally in *Gorilla* and rarely in *Pongo,* an elaborated condition appears in which the entire dorsum of the body projects laterally, reorienting a large portion of the scaphoid facet palmarly (see Fig. 3.10 inset). This projection's proximal extent tends to be sharply-angled, and is often confluent with a raised ridge separating the head and body. The greater frequency in *Pan* of these features may be explained, as other reputed knuckle-walking traits have been, by a more extended wrist posture during stance phase (Inouye, 1992, 1994; Inouye and Shea, 2004; Kivell and Schmitt, 2009; but see Finestone *et al*., 2015, 2016).

However, hylobatids also frequently possess morphology matching the most elaborated African ape examples of this trait (Fig. 3.10h), which, despite their behavioral disparities, this may indicate some unrecognized kinematic affinity with *Pan*, perhaps relating not to habitual loading in extension but rather a shared need to limit over-pronation of the midcarpal joint (or over-supination of the forearm below a fixed grasp), with this need being either reduced or otherwise accommodated in others of the extant and fossil sample. Given the above (see also Kivell, 2016 and references therein), these features do not seem to be related exclusively to knuckle-walking. Deciphering the functional signal in KNM-SO 1002's morphology will therefore likely require a detailed understanding of differential carpal kinematics among the great apes. Vertical climbing may explain many of these features, but this conclusion would require an explanation of

the lesser prevalence of these features in *Gorilla* despite the utility thereof presumably increasing with body size (Kivell and Schmitt, 2009).

If the reputed knuckle-walking features of this specimen are interpreted to evince its performance of this behavior, homoplasy is a far more parsimonious explanation than is a knuckle-walking ancestry for all apes. The former scenario could still contribute to the debate over the locomotor evolution of hominines by providing evidence for the homoplastic evolvability of the behavior (see Begun and Kivell, 2011). However, a non-knuckle-walking explanation for the qualitative and quantitative African ape affinities of this specimen is favored here.

Taxonomic allocation

Results of this study constrain the possible taxonomic identities of the Tinderet specimens; because no capitates have been found in association with craniodental remains for any of the species known from Tinderet, however, definitive identification of the taxon to which each belongs is not possible.

KNM-MV 4 is in some ways the most primitive specimen of the sample. It has a qualitative resemblance to some platyrrhine specimens, and is classified among them in the taxonomic DFA. The hierarchical clustering analysis also suggests a basal position relative to most others of the Tinderet sample. If possible taxonomic identities are limited to those previously identified at the same locality, *L. legetet* is ruled out. Size is less useful in this case; this specimen is probably too large for *M. clarki* and too small for *D. macinnesi*, but the likelihood of an uncharacterized degree of body size dimorphism in these taxa prevents ruling them out on this basis. The lack of morphology

indicating increased reliance on climbing or suspension does reduce the plausibility of the latter, but postcrania are unknown for *M. clarki*. *L. evansi* and *K. songhorensis* are the best size matches based on current evidence; unfortunately, the phylogenetic relationships of these two species remain unresolved and their functional affinities remain unknown, preventing the identity of KNM-MV 4 from being further constrained.

The identities of KNM-SO 1000 and KNM-SO 1001 are limited by size and locality to the same four species, although known *M. clarki* specimens indicate a body size range unlikely to encompass specimens of this size. None of the available allocations comports well with the hominoid classification of these specimens, although the DFA model was nearly split in both cases, assigning KNM-SO 1000 a 0.39 platyrrhine probability and KNM-SO 1001 a 0.37 cercopithecoid probability (Table 3.7c). Results of the functional analyses are consistent with interpretations of postcrania assigned to *D. macinnesi*, perhaps increasing the likelihood of this allocation, but the positional behavior of the other options is entirely unknown. Furthermore, although a strong suspensory signal is identified in both specimens, they are quantitatively and qualitatively dissimilar from each other. The morphology of KNM-SO 1000 is clearly distinct from the rest of the fossil sample, but KNM-SO 1001 has much in common with the Rusinga specimens and KNM-CA 409. Setting aside its small size, KNM-SO 1001 is distinguished from the latter specimens largely by its low hamate facet concavity (CpHmC) and the radial orientation of its centrale facet (CpScA). While either KNM-SO 1000 or 1001 may belong to *D. macinnesi*, there is little basis for deciding which of the two has the better case for inclusion in this taxon, and their disparate morphology makes a conspecific relationship between them seem unlikely. However, there is not

another species of appropriate size known at Songhor interpreted to have a derived behavioral pattern, so a taxonomic distinction between these specimens would imply a suspensory habit for *L. evansi, K. songhorensis*, or some other undiscovered small-bodied catarrhine at Songhor. Whether this is more parsimonious than a conspecific relationship between KNM-SO 1000 and KNM-SO 1001 cannot be determined with current evidence. In the interim, both are referred to *cf. D. macinnesi*.

KNM-SO 31245 and KNM-SO 31246 have the most quantitative affinity to *E. heseloni* of the Tinderet sample – they plot near or among the Rusinga specimens in positional and taxonomic DFA and PLS shape-space, and are estimated to have equivalent behavioral habits. However, they are qualitatively distinct from KNM-CA 409 and the Rusinga specimens, often in ways reminiscent of African apes or other terrestrial catarrhines. Meanwhile, KNM-CA 409 has greater qualitative resemblance to *E. heseloni,* including the presence of the dorsodistal lip formerly exclusive to this taxon, and group more closely with the Rusinga specimens in the hierarchical clustering analysis. KNM-CA 409 is slightly smaller than the Rusinga specimens, but this mirrors the relationship between the dental size of the two species (Harrison, 2010). A special similitude between *E. heseloni* and KNM-CA 409 is not evinced by the predictive models, however; their placement in DFA and PLS shape-space is not particularly close, and, as discussed above, their predicted locomotor repertoires have significant differences.

The implications of resemblance to the Rusinga specimens are not entirely clear. Until recently this could reasonably have been interpreted to support the allocation of these specimens to *Proconsul africanus*, but this may no longer be the case since the

reallocation of their long-time Kisingiri congeners to *Ekembo* (McNulty *et al.*, 2015b), leaving the Tinderet species with a very limited postcranial hypodigm. Available postcrania attributed to *P. africanus*, as well those attributed to *P. major*, are anatomically and functionally similar to overlapping specimens of *E. heseloni* (e.g., Rose *et al.*, 1992), but as discussed above, this is true of most early Miocene catarrhines. There is only one other taxon of appropriate size available – *R. gordoni*, the more prevalent of the mid-sized catarrhines at Songhor based on allocation of dental remains (Cote *et al.*, 2014). Mid-sized unassociated postcrania at Songhor and the nearby lower Kapurtay have previously been tentatively referred to this taxon on the basis of size. This material includes a proximal femur interpreted to be adapted for increased climbing or suspension (Harrison, 1982), two medial cuneiforms also thought to be derived relative to *P. africanus* (Nengo and Rae, 1992), and four specimens of the elbow joint, described as equivalent in function to *E. heseloni* (Gebo *et al.*, 2009).

KNM-SO 1002 is larger than the Rusinga capitates, meeting the historical criterion for inclusion in this taxon, but *R. gordoni* does not seem to significantly depart from *P. africanus* or *E. heseloni* in craniodental size, obviating the utility of this criterion. I nevertheless provisionally allocate this specimen to *R. gordoni* here, and propose that the presence of derived, ape-like features relative to *P. africanus*, as seen in KNM-SO 1002 as well as the unassociated femur and tarsals discussed above, may be a better criterion for distinguishing between these taxa than is body size.

The attribution of KNM-SO 1002 to a behaviorally derived *R. gordoni* raises another dilemma, however. Unless a third mid-sized catarrhine was present at Songhor, KNM-SO 31245, KNM-SO 31246, and KNM-CA 409 are all necessarily attributed to *P.*

africanus. The similarity of the two Songhor specimens supports their conspecificity, but inclusion of the latter specimen yields a species with a high degree of morphological diversity, compared to the consistency noted for the overlapping hand and wrist elements of *E. heseloni* (Beard *et al.*, 1993), confirmed here for the capitate specimens. The allocation of these three specimens to *P. africanus* is therefore tentative.

Locomotor diversity in the early Miocene and implications for hominoid evolution

This sample of seven overlapping elements provides a rare opportunity to evaluate the functional diversity among catarrhines of a geographically and temporally constrained setting that pre-dates the increased functional diversity of the hominoid radiation in Eurasia (Casanovas-Vilar *et al.*, 2011). The specimens analyzed here evince the well-known taxonomic diversity of the Tinderet Miocene sequence, but it is out-paced in this sample by functional diversity, with multiple broadly construed positional behaviors present, and two additional cases of functionally distinct specimens being provisionally allocated to the same species. And, as characterized in the PLS analysis, the functionally-associated morphological diversity present in seven Tinderet capitates approaches or exceeds that of different broad extant groups represented by a larger number of extant centroids.

The morphology of KNM-SO 1002 lends further support to the presence of a mid-sized catarrhine at Songhor with a behavioral repertoire more similar in some ways to extant apes than to *E. heseloni.* Although unlikely due to the seemingly less derived anatomy of later African Miocene catarrhines, I cannot rule out homology in explaining the great ape features of KNM-SO 1002. The cladistic event separating hylobatids from

great apes is estimated to have coincided with the time period represented at these Tinderet localities (mean: 20.19 Ma, median: 19.43 Ma; see Hedges *et al.*, 2015), and although the mosaicism of later hominoid evolution has changed the calculus regarding the parsimony of extant ape homology (e.g., Begun, 1993; Almecija *et al.*, 2009; Casanovas-Vilar *et al.*, 2011; Morgan *et al.*, 2015; Ward, 2015), functional morphology shared among extant members of these lineages is very unlikely to have evolved entirely in parallel (e.g., Schmitt, 2003; Nowak and Reichard, 2016). The nyanzapithecines, of which *R. gordoni* is perhaps the basal member (Rossie and MacLatchy, 2006; Hill *et al.*, 2013), are sometimes thought to have a close relationship with crown hominoids relative to their Miocene contemporaries (e.g., Stevens *et al.*, 2013), but there is not consensus on this point (Begun, 2015 and references therein). Whether ape-like traits preserved at Songhor (and Moroto) offer a glimpse of the ancestral crown hominoid morphotype, or only of early examples of the evolutionary experimentation characterizing later hominoid evolution, is difficult to address with current evidence. While the depositional and diagenetic environment of Miocene Tinderet sediments seems to have been unconducive to the preservation of associated catarrhine crania and postcrania, continued work at these and other early Miocene sites leading to additional sets of overlapping postcranial elements like that presented here will be important in further characterizing functional diversity among early catarrhines.

The specimens analyzed here represent a geographically- and temporally-limited setting within the early Miocene. The morphological diversity of this sample (summarized in Table 3.8) therefore offers a snapshot of differing lifestyles among a community of penecontemporaneous catarrhines. These results indicate the likelihood

of a broader phenomenon of behavioral diversity among the early members of this clade. Although confident conclusions cannot be made based on a single skeletal element, this collection of overlapping postcranial specimens raises the possibility of early hominoids and their contemporaries having diversified to fill multiple ecological niches quite early in their evolutionary career, well before the previously-inferred locomotor diversification of the later Miocene of Eurasia.

Table 3.8. Summary of findings

Specimen	BM (kg)	Taxonomic classification				Positional classification				Estimated locomotor proportions							Plausible identity[a]
		DFA	prob	*glmnet*	prob	DFA	prob	*glmnet*	prob	*QuadA*	*Quad*	*SuspA*	*Susp*	*ClimbA*	*Climb*	*Arb*	
KNM-MV 4	5.3	Plat	0.89	Cerc	0.90	*PG*	0.94	*PG*	1.00	0.35	0.57	0.07	0.03	0.42	0.28	0.77	*L. evansi, K. songhorensis*
KNM-CA 409	9.2	Cerc	0.52	Cerc	0.80	*PG*	0.80	*PG*	0.99	0.61	0.54	0.06	0.08	0.34	0.19	0.47	***cf. P. africanus***
KNM-SO 1000	6.0	Hom	0.60	Hom	0.96	*S*	0.89	*S*	0.99	0.37	0.24	0.19	0.19	0.42	0.32	0.86	***cf. D. macinnesi***, *L. evansi, K. songhorensis*
KNM-SO 1001	5.9	Hom	0.63	Hom	0.84	*S*	0.95	*S*	1.00	0.16	0.50	0.32	0.10	0.36	0.19	0.89	***cf. D. macinnesi***, *L. evansi, K. songhorensis*
KNM-SO 31245	12.4	Cerc	0.83	Cerc	0.94	*PG*	0.93	*PG*	0.83	0.40	0.31	0.12	0.07	0.31	0.26	0.93	***cf. P. africanus***, *R. gordoni*
KNM-SO 31246	15.4	Cerc	0.93	Cerc	0.98	*PG*	0.96	*PG*	0.96	0.41	0.32	0.09	0.06	0.29	0.29	0.95	***cf. P. africanus***, *R. gordoni*
KNM-SO 1002	15.9	Hom	0.86	Hom	0.86	*KW*	0.89	*KW*	0.83	0.42	0.76	0.04	0.01	0.37	0.16	0.74	***R. gordoni***, *P. africanus*
E. heseloni means	11.5	Cerc	0.85	Cerc	0.99	*PG*	0.75	*PG*	0.95	0.49	0.45	0.09	0.08	0.29	0.27	0.83	

[a] Preferred allocations are in bold.

Conclusions

Results of this study document a degree of functional diversity beyond what is generally recognized among early Miocene catarrhines. This sample of seven overlapping postcranial specimens from a geographically- and temporally-limited setting is found to vary in functionally-related morphology to a degree approaching or exceeding that of broad extant anthropoid groups characterized by a larger number of taxon centroids. The taxonomic diversity of this time period is also reflected in the Tinderet sample, with as many as six species represented. The identity of each specimen cannot be determined with confidence, however; when accounting for body size, known species to which these specimens can be attributed are insufficient in number.

KNM-SO 31245, KNM-SO 31246, KNM-CA 409, and KNM-MV 4 are classified as arboreal quadrupeds, with the latter two predicted to have locomotor proportions distinct from those of *E. heseloni*. KNM-SO 1000 and KNM-SO 1001 are inferred to have been significantly reliant on below-branch behaviors, but morphological distinctions between these two specimens suggest they are not conspecific. KNM-SO 1002 is uniquely great ape-like among capitates known from the early Miocene. It possesses several features often associated with knuckle-walking, interpreted here as reinforcing our lack of understanding of how knuckle-walking is reflected in wrist morphology, rather than as evidence for the evolution of knuckle-walking in the early Miocene. This specimen adds to a growing body of evidence indicating the presence of a functionally-derived, mid-sized catarrhine at Songhor, and documents another example of great ape-like locomotor adaptation occurring very early in hominoid evolution.

Chapter 3 references

Almecija, S., Alba, D.M., Moya-Sola, S., 2009. *Pierolapithecus* and the functional morphology of Miocene ape hand phalanges: paleobiological and evolutionary implications. Journal of Human Evolution 57, 284-297.

Andrews, P.J., 1978. A revision of the Miocene Hominoidea of East Africa. Bulletin of the British Museum of Natural History 30, 85-224.

Arnold, C., Matthews, L.J., Nunn, C.L., 2010. The 10kTrees website: A new online resource for primate phylogeny. Evolutionary Anthropology 19, 114-118.

Beard, K.C., Teaford, M.F., Walker, A., 1986. New wrist bones of *Proconsul africanus* and *P. nyanzae* from Rusinga Island, Kenya. Folia Primatologica 47, 97-118.

Beard, K.C., Teaford, M.F., Walker, A., 1993. New hand bones of the early Miocene hominoid *Proconsul* and their implications for the evolution of the hominoid wrist, in: Holger, P., Chivers, D.J. (Eds.), Hands of Primates. Springer, pp. 387-403.

Begun, D.R., 1993. New catarrhine phalanges from Rudabanya (Northeastern Hungary) and the problem of parallelism and convergence in hominoid postcranial morphology. Journal of Human Evolution 24, 373-402.

Begun, D.R., 2004. Knuckle-walking and the origin of human bipedalism, in: Meldrum, D.J., Hilton, C.E. (Eds.), From Biped to Strider: The Emergence of Modern Human Walking, Running and Resource Transport. Kluwer Academic/Plenum Publishers, New York, pp. 9-33.

Begun, D.R., 2015. Fossil record of Miocene hominoids, in: Henke, W., Tattersall, I. (Eds.), Handbook of Paleoanthropology. Springer-Verlag, Berlin, pp. 1261-1332.

Begun, D.R., Kivell, T.L., 2011. Knuckle-walking in *Sivapithecus*? The combined effects of homology and homoplasy with possible implications for pongine dispersals. Journal of Human Evolution 60, 158-170.

Bilsborough, A., Rae, T.C., 2007. Hominoid cranial diversity and adaptation, in: Henke, W. (Ed.), Handbook of Paleoanthropology. Springer, Heidelberg, pp. 1031-1105.

Bishop, W.W., Miller, J.A., Fitch, F.J., 1969. New potassium-argon age determinations relevant to the Miocene fossil mammal sequence in East Africa. American Journal of Science 267, 669-699.

Blomberg, S.P., Garland, T., Jr., Ives, A.R., 2003. Testing for phylogenetic signal in comparative data: behavioral traits are more labile. Evolution 57, 717-745.

Blue, K.T., 2002. Functional morphology of the forelimb in *Victoriapithecus* and its implications for phylogeny within the Catarrhini. Ph.D. Dissertation, University of Chicago.

Burnham, K.P., Anderson, D.R., 2002. Model Selection and Inference: A Practical Information-Theoretical Approach, 2nd ed. Springer-Verlag, New York.

Byron, C.D., Covert, H.H., 2004. Unexpected locomotor behaviour: brachiation by an Old World monkey (*Pygathrix nemaeus*) from Vietnam. Journal of Zoology 263, 101-106.

Cartmill, M., Milton, K., 1977. The lorisiform wrist joint and the evolution of "brachiating" adaptations in the Hominoidea. American Journal of Physical Anthropology 47, 249-272.

Casanovas-Vilar, I., Alba, D.M., Garces, M., Robles, J.M., Moya-Sola, S., 2011. Updated chronology for the Miocene hominoid radiation in Western Eurasia. Proceedings of the National Academy of Sciences 108, 5554-5559.

Corruccini, R.S., Ciochon, R.L., McHenry, H.M., 1975. Osteometric shape relationships in the wrist joint of some anthropoids. Folia Primatologica 24, 250-274.
Corruccini, R.S., 1978. Comparative osteometrics of the hominoid wrist joint, with special reference to knuckle-walking. Journal of Human Evolution 7, 307-321.
Cote, S., Malit, N., Nengo, I., 2014. Additional mandibles of *Rangwapithecus gordoni*, an early Miocene catarrhine from the Tinderet localities of Western Kenya. American Journal of Physical Anthropology 153, 341-352.
Cote, S., McNulty, K.P., Stevens, N.J., Nengo, I.O., 2016. A detailed assessment of the maxillary morphology of *Limnopithecus evansi* with implications for the taxonomy of the genus. Journal of Human Evolution 94, 83-91.
Daver, G., Nakatsukasa, M., 2015. *Proconsul heseloni* distal radial and ulnar epiphyses from the Kaswanga Primate Site, Rusinga Island, Kenya. Journal of Human Evolution 80, 17-33.
Delson, E., Terranova, C.J., Jungers, W.L., Sargis, E.J., Jablonski, N.G., Dechow, P.C., 2000. Body mass in Cercopithecidae (Primates, Mammalia): Estimation and scaling in extinct and extant taxa. American Museum of Natural History, Anthropological Papers 83.
Felsenstein, J., 1985. Phylogenies and the comparative method. The American Naturalist 125, 1-15.
Finestone, E.M., Brown, M., Ross, S.R., Pontzer, H., 2015. The kinematics of knuckle-walking: To what extent is gait and posture conserved in the African great apes? Paleoanthropology meetings, San Francisco.
Finestone, E.M., Brown, M.H., Ross, S.R., Pontzer, H., 2016. Videographic analysis of kinematics in great apes: To what extent are gait and posture conserved? American Journal of Physical Anthropology 159, 143-143.
Fleagle, J.G., 1983. Locomotor adaptations of Oligocene and Miocene hominoids and their phyletic implications, in: Ciochon, R.L., Corruccini, R.S. (Eds.), New Interpretations of Ape and Human Ancestry. Plenum Press, New York, pp. 301-324.
Fleagle, J.G., Simons, E.L., 1978. *Micropithecus clarki*, a small ape from the Miocene of Uganda. American Journal of Physical Anthropology 49, 427-440.
Friedman, J., Hastie, T., Tibshirani, R., 2010. Regularization paths for generalized linear models via coordinate descent. Journal of Statistical Software 33, 1-22.
Gascuel, O., 1997. BIONJ: An improved version of the NJ algorithm based on a simple model of sequence data. Molecular Biology and Evolution 14, 685-695.
Gebo, D.L., MacLatchy, L., Kityo, R., Deino, A., Kingston, J., Pilbeam, D., 1997. A hominoid genus from the early Miocene of Uganda. Science 276, 401-404.
Gebo, D.L., Malit, N.R., Nengo, I.O., 2009. New proconsuloid postcranials from the early Miocene of Kenya. Primates 50, 311-319.
Gilbert, C.C., Rossie, J.B., 2007. Congruence of molecules and morphology using a narrow allometric approach. Proceedings of the National Academy of Sciences 104, 11910-11914.
Harrison, T., 1981. New finds of small fossil apes from the Miocene locality at Koru in Kenya. Journal of Human Evolution 10, 129-137.
Harrison, T., 1982. Small-bodied apes from the Miocene of East Africa. Ph.D. Dissertation, University College London.

Harrison, T., 1988. A taxonomic revision of the small catarrhine primates from the Early Miocene of East Africa. Folia Primatologica 50, 59-108.
Harrison, T., 2010. Dendropithecoidea, Proconsuloidea, and Hominoidea, in: Werdelin, L., Sanders, W.J. (Eds.), Cenozoic Mammals of Africa. University of California Press, Berkeley, pp. 429-469.
Harrison, T., 2013. Catarrhine origins, in: Begun, D.R. (Ed.), A Companion to Paleoanthropology. Blackwell Publishing Ltd., pp. 376-396.
Hedges, S.B., Marin, J., Suleski, M., Paymer, M., Kumar, S., 2015. Tree of life reveals clock-like speciation and diversification. Molecular Biology and Evolution 32, 835-845.
Hill, A., Nengo, I.O., Rossie, J.B., 2013. A *Rangwapithecus gordoni* mandible from the early Miocene site of Songhor, Kenya. Journal of Human Evolution 65, 490-500.
Inouye, S.E., 1992. Ontogeny and allometry of African ape manual rays. Journal of Human Evolution 23, 107-138.
Inouye, S.E., 1994. Ontogeny of knuckle-walking hand postures in African apes. Journal of Human Evolution 26, 459-485.
Inouye, S.E., Shea, B.T., 2004. The implications of variation in knuckle-walking features for models of African hominoid locomotor evolution. Journal of Anthropological Sciences 82, 67-88.
Ishida, H., Kunimatsu, Y., Takano, T., Nakano, Y., Nakatsukasa, M., 2004. *Nacholapithecus* skeleton from the Middle Miocene of Kenya. Journal of Human Evolution 46, 69-103.
Jansma, R.J.W., MacLatchy, L.M., 2015. First evidence of Nyanzapithecinae at Moroto II, Uganda. American Journal of Physical Anthropology 156, 177-177.
Jenkins Jr., F.A., 1981. Wrist rotation in primates: A critical adaptation for brachiators. Symposia of the Zoological Society of London 48, 429-451.
Jungers, W.L., Falsetti, A.B., Wall, C.E., 1995. Shape, relative size, and size-adjustments in morphometrics. Yearbook of Physical Anthropology 38, 137-161.
Kay, R.F., Ungar, P.S., 1997. Dental evidence for diet in some Miocene catarrhines with comments on the effects of phylogeny on the interpretation of adaptation, in: Begun, D.R., Ward, C.V., Rose, M.D. (Eds.), Function, Phylogeny, and Fossils. Plenum Press, New York, pp. 131-151.
Kelley, J., 1997. Paleobiological and phylogenetic significance of life history in Miocene hominoids, in: Begun, D.R., Ward, C.V., Rose, M.D. (Eds.), Function, Phylogeny, and Fossils. Plenum Press, New York, pp. 173-208.
Kivell, T.L., 2016. The primate wrist, in: Kivell, T.L., Lemelin, P., Richmond, B.G., Schmitt, D. (Eds.), The Evolution of the Primate Hand. Springer, New York, pp. 17-54.
Kivell, T.L., Schmitt, D., 2009. Independent evolution of knuckle-walking in African apes shows that humans did not evolve from a knuckle-walking ancestor. Proceedings of the National Academy of Sciences 106, 14241-14246.
Konigsberg, L.W., Hens, S.M., Jantz, L.M., Jungers, W.L., 1998. Stature estimation and calibration: Bayesian and maximum likelihood perspectives in physical anthropology. Yearbook of Physical Anthropology 41, 65-92.

Lefort, V., Desper, R., Gascuel, O., 2015. Fastme 2.0: A comprehensive, accurate, and fast distance-based phylogeny inference program. Molecular Biology and Evolution 32, 2798-2800.
Lemaitre, J.F., Vanpe, C., Plard, F., Pelabon, C., Gaillard, J.M., 2015. Response to Packard: make sure we do not throw out the biological baby with the statistical bath water when performing allometric analyses. Biology Letters 11, 20150144.
Lovejoy, C.O., Simpson, S.W., White, T.D., Asfaw, B., Suwa, G., 2009. Careful climbing in the Miocene: The forelimbs of *Ardipithecus ramidus* and humans are primitive. Science 326, 70e1-8.
MacInnes, D.G., 1943. Notes on the East African Miocene primates. The Journal of the East Africa and Uganda Natural History Society 17, 141-181.
Maclatchy, L., 2004. The oldest ape. Evolutionary Anthropology 13, 90-103.
MacLatchy, L., Gebo, D., Kityo, R., Pilbeam, D., 2000. Postcranial functional morphology of *Morotopithecus bishopi*, with implications for the evolution of modern ape locomotion. Journal of Human Evolution 39, 159-183.
McCrossin, M.L., Benefit, B.R., 1997. On the relationships and adaptations of *Kenyapithecus*, a large-bodied hominoid from the Middle Miocene of Eastern Africa, in: Begun, D.R., Ward, C.V., Rose, M.D. (Eds.), Function, Phylogeny, and Fossils: Miocene Hominoid Evolution and Adaptations. Plenum Press, New York, pp. 241-267.
McCrossin, M.L., Benefit, B.R., Gitau, S.N., Palmer, A.K., Blue, K.T., 1998. Fossil evidence for the origins of terrestriality among Old World higher primates, in: Strasser, E., Fleagle, J., Rosenberger, A., McHenry, H. (Eds.), Primate Locomotion: Recent Advances. Plenum Press, New York, pp. 353-396.
McHenry, H.M., Corruccini, R.S., 1983. The wrist of *Proconsul africanus* and the origins of hominoid postcranial adaptations, in: Ciochon, R.L., Corruccini, R.S. (Eds.), New Interpretation of Ape and Human Ancestry. Plenum Press, New York, pp. 353-367.
McNulty, K.P., MacLatchy, L., Rossie, J.B., Peppe, D.J., Deino, A.L., Mbua, E.N., Manthi, F.K., Nengo, I.O., Miller, E.R., Stevens, N.J., Cote, S., Lehmann, T., Gutierrez, M., 2014. Research on East African catarrhine and hominoid evolution: Results from the first year. American Journal of Physical Anthropology 153, 182-182.
McNulty, K.P., Nengo, I.O., Fox, D.L., Stevens, N.J., Manthi, F.K., Mbua, E.N., Peppe, D.J., 2015a. New partial cranium from an early Miocene locality at Lower Kapurtay. American Journal of Physical Anthropology 156, 222-222.
McNulty, K.P., Begun, D.R., Kelley, J., Manthi, F.K., Mbua, E.N., 2015b. A systematic revision of *Proconsul* with the description of a new genus of early Miocene hominoid. Journal of Human Evolution 84, 42-61.
Miller, A.J., 2002. Subset Selection in Regression, 2nd ed. CRC Press, New York.
Mitteroecker, P., Bookstein, F., 2011. Linear discrimination, ordination, and the visualization of selection gradients in modern morphometrics. Evolutionary Biology 38, 100-114.
Morgan, M.E., Lewton, K.L., Kelley, J., Otárola-Castillo, E., Barry, J.C., Flynn, L.J., Pilbeam, D., 2015. A partial hominoid innominate from the Miocene of Pakistan:

Description and preliminary analyses. Proceedings of the National Academy of Sciences 112, 82-87.
Moya-Sola, S., Kohler, M., Alba, D.M., Casanovas-Vilar, I., Galindo, J., 2004. *Pierolapithecus catalaunicus*, a new Middle Miocene great ape from Spain. Science 306, 1339-1344.
Napier, J.R., Davis, P.R., 1959. The forelimb skeleton and associated remains of *Proconsul africanus*. Fossil Mammals of Africa 16, 1-69.
Nengo, I.O., Rae, T.C., 1992. New hominoid fossils from the early Miocene site of Songhor, Kenya. Journal of Human Evolution 23, 423-429.
Nowak, M.G., Reichard, U.H., 2016. Locomotion and posture in ancestral hominoids prior to the split of hylobatids, in: Reichard, U.H., Hirai, H., Barelli, C. (Eds.), Evolution of Gibbons and Siamang. Siamang, New York, pp. 55-89.
Ogihara, N., Almecija, S., Nakatsukasa, M., Nakano, Y., Kikuchi, Y., Kunimatsu, Y., Makishima, H., Shimizu, D., Takano, T., Tsujikawa, H., Kagaya, M., Ishida, H., 2016. Carpal bones of *Nacholapithecus kerioi,* a middle Miocene hominoid from northern Kenya. American Journal of Physical Anthropology 160, 469-482.
Orr, C.M., 2010. Adaptations to Knuckle-walking and Digitigrady: a Three-dimensional Kinematic and Morphometric Analysis of the Anthropoid Wrist. Ph.D. Dissertation, Arizona State University.
Packard, G.C., 2013. Fitting statistical models in bivariate allometry: scaling metabolic rate to body mass in mustelid carnivores. Comparative Biochemistry and Physiology Part A: Molecular & Integrative Physiology 166, 70-73.
Packard, G.C., 2015. Allometric variation in the antlers of cervids: a comment on Lemaitre *et al.* Biology Letters 11, 20140923.
Pagel, M., 1999. Inferring the historical patterns of biological evolution. Nature 401, 877-884.
Pickford, M., Andrews, P., 1981. The Tinderet Miocene sequence in Kenya. Journal of Human Evolution 10, 11-33.
Preuschoft, H., 1973. Body posture and locomotion in some East African Miocene Dryopithecinae. Journal of Human Evolution 11, 13-46.
R Core Team, 2016. R: A language and environment for statistical computing. R Foundation for Statistical Computing, Vienna, Austria.
Rafferty, K.L., Walker, A., Ruff, C.B., Rose, M.D., Andrews, P.J., 1995. Postcranial estimates of body weight in *Proconsul*, with a note on a distal tibia of *P. major* from Napak, Uganda. American Journal of Physical Anthropology 97, 391-402.
Richmond, B.G., Begun, D.R., Strait, D.S., 2001. Origin of human bipedalism: The knuckle-walking hypothesis revisited. American Journal of Physical Anthropology Suppl 33, 70-105.
Richmond, B.G., 2006. Functional morphology of the midcarpal joint in knuckle-walkers and terrestrial quadrupeds, in: Ishida, H., Tuttle, R., Pickford, M., Ogihara, N., Nakatsukasa, M. (Eds.), Human Origins and Environmental Backgrounds. Springer, New York, pp. 105-122.
Rohlf, F.J., Corti, M., 2000. Use of two-block partial least-squares to study covariation in shape. Systematic Biology 49, 740-753.

Rose, M.D., 1983. Miocene hominoid postcranial morphology: monkey-like, ape-like, neither, or both?, in: Ciochon, R.L., Corruccini, R.S. (Eds.), New Interpretations of Ape and Human Ancestry. Plenum Press, New York, pp. 405-417.
Rose, M.D., 1984. Hominoid postcranial specimens from the middle Miocene Chinji formation, Pakistan. Journal of Human Evolution 13, 503-516.
Rose, M.D., 1993. Locomotor anatomy of Miocene hominoids, in: Gebo, D.L. (Ed.), Postcranial Adaptation in Nonhuman Primates. Northern Illinois University Press, DeKalb, pp. 252-272.
Rose, M.D., 1994. Quadrupedalism in some Miocene catarrhines. Journal of Human Evolution 26, 387-411.
Rose, M.D., 1996. Functional morphological similarities in the locomotor skeleton of Miocene catarrhines and platyrrhine monkeys. Folia Primatologica 66, 7-14.
Rose, M.D., Leakey, M.G., Leakey, R.E.F., Walker, A.C., 1992. Postcranial specimens of *Simiolus enjiessi* and other primitive catarrhines from the early Miocene of Lake Turkana, Kenya. Journal of Human Evolution 22, 171-237.
Rose, M.D., Nakano, Y., Ishida, H., 1996. *Kenyapithecus* postcranial specimens from Nachola, Kenya. African Study Monographs Supplement 24, 3-56.
Rossie, J.B., MacLatchy, L., 2006. A new pliopithecoid genus from the early Miocene of Uganda. Journal of Human Evolution 50, 568-586.
Rossie, J.B., Seiffert, E.R., 2006. Continental paleobiogeography as phylogenetic evidence, in: Lehman, S.M., Fleagle, J.G. (Eds.), Primate Biogeography. Springer, New York, pp. 469-522.
Ruff, C.B., 2002. Long bone articular and diaphyseal structure in old world monkeys and apes. I: locomotor effects. American Journal of Physical Anthropology 119, 305-342.
Ruff, C.B., 2003. Long bone articular and diaphyseal structure in Old World monkeys and apes. II: Estimation of body mass. American Journal of Physical Anthropology 120, 16-37.
Ryan, T.M., Silcox, M.T., Walker, A., 2012. Evolution of locomotion in Anthropoidea: the semicircular canal evidence. Proceedings of the Royal Society B 279, 3467-3475.
Saitou, N., Nei, M., 1987. The neighbor-joining method: a new method for reconstructing phylogenetic trees. Molecular Biology and Evolution 4, 406-425.
Sanchez, P.M., 1974. The unequal group size problem in discriminant analysis. Journal of the Academy of Marketing Science 2, 629-633.
Sanders, W.J., Bodenbender, B.E., 1994. Morphometric analysis of lumbar vertebra UMP 67-28: implications for spinal function and phylogeny of the Miocene Moroto hominoid. Journal of Human Evolution 26, 203-237.
Schmitt, D., 2003. Substrate size and primate forelimb mechanics: implications for understanding the evolution of primate locomotion. International Journal of Primatology 24, 1023-1036.
Selby, M.S., Simpson, S.W., Lovejoy, C.O., 2016. The functional anatomy of the carpometacarpal complex in anthropoids and its implications for the evolution of the hominoid hand. Anatomical Record 299, 583-600.
Shea, B.T., Inouye, S.E., 1993. Knuckle-walking ancestors. Science 259, 293-294.

Shearer, B.M., Ungar, P.S., McNulty, K.P., Harcourt-Smith, W.E.H., Dunsworth, H.M., Teaford, M.F., 2015. Dental microwear profilometry of African non-cercopithecoid catarrhines of the Early Miocene. Journal of Human Evolution 78, 33-43.
Simm, J., Magrans de Abril, I., Sugiyama, M., 2014. Tree-based ensemble multi-task learning method for classification and regression. IEICE Transactions on Information and Systems E97-D, 1677-1681.
Simons, E. L., Fleagle, J. G., 1973. The history of extinct gibbon-like primates. Gibbon and Siamang 2, 121-148.
Singleton, M., 2000. The phylogenetic affinities of *Otavipithecus namibiensis*. Journal of Human Evolution 38, 537-573.
Slizewski, A., Friess, M., Semal, P., 2010. Surface scanning of anthropological specimens: nominal-actual comparison with low cost laser scanner and high end fringe light projection surface scanning systems. Quartar 57, 179-187.
Smith, R.J., 1984. Allometric scaling in comparative biology: problems of concept and method. American Journal of Physiology 246, R152-R160.
Smith, R.J., 1985. The present as a key to the past: body weight of Miocene hominoids as a test of allometric methods for paleontological inference, in: Jungers, W.L. (Ed.), Size and Scaling in Primate Biology. Plenum Press, New York, pp. 437-448.
Smith, R.J., 1993. Logarithmic transformation bias in allometry. American Journal of Physical Anthropology 90, 215-228.
Smith, R.J., Jungers, W.L., 1997. Body mass in comparative primatology. Journal of Human Evolution 32, 523-559.
Sprugel, D.G., 1983. Correcting for bias in log-transformed allometric equations. Ecology 64, 209-210.
Stern, J.T., Susman, R.L., 1983. The locomotor anatomy of *Australopithecus afarensis*. American Journal of Physical Anthropology 60, 279-317.
Stevens, N.J., Seiffert, E.R., O'Connor, P.M., Roberts, E.M., Schmitz, M.D., Krause, C., Gorscak, E., Ngasala, S., Hieronymus, T.L., Temu, J., 2013. Palaeontological evidence for an Oligocene divergence between Old World monkeys and apes. Nature 497, 611-614.
Studier, J.A., Keppler, K.J., 1988. A note on the neighbor-joining algorithm of Saitou and Nei. Molecular Biology and Evolution 5, 729-731.
Teaford, M.F., Ungar, P.S., 2000. Diet and the evolution of the earliest human ancestors. Proceedings of the National Academy of Sciences 97, 13506-13511.
Tocheri, M.W., Solhan, C.R., Orr, C.M., Femiani, J., Frohlich, B., Groves, C.P., Harcourt-Smith, W.E., Richmond, B.G., Shoelson, B., Jungers, W.L., 2011. Ecological divergence and medial cuneiform morphology in gorillas. Journal of Human Evolution 60, 171-184.
Uhl, N.M., Rainwater, C.W., Konigsberg, L.W., 2013. Testing for size and allometric differences in fossil hominin body mass estimation. American Journal of Physical Anthropology 151, 215-229.
Walker, A., 1997. *Proconsul* function and phylogeny, in: Begun, D.R., Ward, C.V., Rose, M.D. (Eds.), Function, Phylogeny, and Fossils: Miocene Hominoid Evolution and Adaptations. Plenum Press, New York, pp. 209-224.

Walker, A.C., Pickford, M., 1983. New postcranial fossils of *Proconsul africanus* and *Proconsul nyanzae*, in: Ciochon, R.L., Corruccini, R.S. (Eds.), New Interpretations of Ape and Human Ancestry. Plenum Press, New York, pp. 325-351.
Walker, A., Teaford, M.F., Martin, L., Andrews, P., 1993. A new species of *Proconsul* from the early Miocene of Rusinga/Mfangano Islands, Kenya. Journal of Human Evolution 25, 43-56.
Ward, C.V., 1998. *Afropithecus*, *Proconsul*, and the primitive hominoid skeleton, in: Strasser, E., Fleagle, J., Rosenberger, A., McHenry, H. (Eds.), Primate Locomotion: Recent Advances. Springer, pp. 337-352.
Ward, C.V., 2015. Postcranial and locomotor adaptations of hominoids, in: Henke, W., Tattersall, I. (Eds.), Handbook of Paleoanthropology. Springer-Verlag, Berlin, pp. 1363-1386.
Ward, S., Brown, B., Hill, A., Kelley, J., Downs, W., 1999. *Equatorius*: a new hominoid genus from the Middle Miocene of Kenya. Science 285, 1382-1386

Supplementary material

Table 3.9. Covariance of shape variables with positional classes relative to the palmigrade (PG) reference class. Reported results are from univariate phylogenetic generalized least squares (PGLS) regression of taxon means except where noted.

			DG						*KW*						*S*					
	R^2	λ	b	p	OR[a]	p[a]	OR[b]	p[b]	b	p	OR[a]	p[a]	OR[b]	p[b]	b	p	OR[a]	p[a]	OR[b]	p[b]
CpPx	0.18	0.82	0.12	0.77	1.44	0.25	1.17	0.21	0.63	0.39	-0.25	0.82	-0.24	0.80	-0.64	0.27	-2.45	**0.04**	-1.15	0.22
CpSc	0.20	0.71	0.06	0.88	1.82	0.17	0.90	0.27	-0.38	0.57	-0.24	0.83	0.87	0.31	-1.16	**0.04**	-3.43	**0.01**	-1.56	0.06
CpLu	0.06	0.96	0.16	0.72	0.61	0.65	0.45	0.63	1.10	0.28	-0.42	0.70	-0.73	0.44	0.20	0.79	-0.52	0.62	0.27	0.77
CpDn	0.03	0.99	0.32	0.50	1.62	0.14	0.89	0.25	-0.42	0.72	0.13	0.90	0.08	0.91	-0.37	0.67	-0.23	0.86	-0.56	0.47
Cp3	0.22	0.77	-0.53	0.26	-1.31	0.24	-1.13	0.24	1.21	0.13	0.86	0.47	1.26	0.21	-0.24	0.70	-0.89	0.37	-0.33	0.73
CpHm	0.05	0.62	-0.15	0.78	-0.36	0.76	-0.19	0.83	-0.70	0.36	-0.40	0.75	0.17	0.83	-0.04	0.95	0.09	0.93	0.08	0.89
Cp2	0.30	0.98	0.46	0.11	2.13	0.10	2.24	**0.02**	-1.66	**0.02**	-1.94	0.16	-1.25	0.21	-1.13	**0.03**	-3.16	**0.02**	-1.48	0.13
Cp4	0.16	1.00	-0.17	0.55	-0.23	0.88	-0.01	0.99	-1.43	0.06	-2.48	0.10	-2.55	**0.03**	-0.38	0.49	1.31	0.28	0.87	0.40
Cp23A	0.26	0.88	-0.83	0.06	-1.83	0.13	-1.07	0.23	-0.50	0.54	-1.09	0.39	-1.31	0.17	0.71	0.26	1.48	0.19	0.72	0.41
Cp3HmA	0.08	0.71	0.64	0.25	1.34	0.21	1.13	0.24	0.57	0.51	0.23	0.86	-0.11	0.90	-0.04	0.95	-0.71	0.51	0.11	0.89
CpPxA	0.67	0.81	-0.23	0.33	-0.74	0.55	0.22	0.83	0.28	0.51	1.39	0.34	1.15	0.27	-1.69	**0.00**	-4.39	**0.00**	-3.01	**0.00**
CpScA	0.25	1.00	-0.37	0.13	-1.25	0.24	-0.72	0.46	0.14	0.82	0.49	0.71	1.49	0.15	-0.82	0.08	-2.60	**0.02**	-1.39	0.16
Cp3SD	0.06	0.78	-0.14	0.79	0.76	0.49	0.56	0.56	0.89	0.34	0.40	0.76	-0.18	0.82	0.02	0.98	-0.65	0.53	-0.50	0.59
CpHmC	0.39	1.00	0.23	0.37	2.03	0.15	2.32	0.06	0.18	0.78	0.75	0.65	-0.39	0.73	-1.36	**0.01**	-3.50	**0.00**	-2.61	**0.02**
CpHP	0.50	0.00	0.73	0.15	1.38	0.22	0.96	0.29	-1.42	**0.00**	-2.27	0.08	-1.43	0.12	0.01	0.99	0.18	0.85	-0.20	0.82
Without hylobatids																				
CpPx	0.05	0.47	0.40	0.51	1.55	0.16	0.90	0.32	0.38	0.61	0.11	0.96	-0.12	0.90	-0.23	0.75	-1.01	0.35	-0.82	0.36
CpSc	0.17	0.73	0.05	0.91	1.85	0.16	0.63	0.44	-0.34	0.64	-0.23	0.85	0.82	0.32	-1.22	0.07	-2.96	**0.01**	-1.57	0.05
CpLu	0.16	0.77	0.15	0.75	0.07	0.94	0.13	0.89	1.01	0.21	0.16	0.91	-0.36	0.69	1.29	0.07	2.02	0.12	0.84	0.36
CpDn	0.10	0.97	0.37	0.38	2.33	**0.05**	1.27	0.11	-0.24	0.81	0.12	0.91	-0.51	0.53	-0.83	0.29	-2.25	0.08	-1.37	0.09
Cp3	0.20	0.60	-0.68	0.19	-1.82	0.11	-2.25	**0.03**	1.13	0.12	1.45	0.18	2.27	**0.03**	0.23	0.72	0.65	0.54	0.89	0.38
CpHm	0.03	0.68	-0.13	0.80	-0.52	0.64	-0.46	0.60	-0.60	0.45	-0.46	0.71	0.27	0.77	-0.13	0.86	0.52	0.63	0.31	0.75
Cp2	0.30	0.99	0.44	0.14	2.21	0.08	1.96	0.06	-1.57	**0.04**	-1.95	0.15	-1.29	0.23	-1.10	0.06	-2.50	0.06	-1.45	0.16
Cp4	0.29	1.00	-0.17	0.40	0.08	0.93	0.41	0.70	-1.35	**0.02**	-2.89	0.06	-2.71	**0.02**	-0.84	**0.05**	0.00	1.00	0.39	0.71
Cp23A	0.21	0.90	-1.02	0.05	-1.83	0.07	-0.70	0.43	-0.51	0.62	-1.28	0.24	-1.26	0.16	0.44	0.60	0.28	0.80	0.41	0.63
Cp3HmA	0.16	0.00	1.05	0.12	1.35	0.14	0.76	0.39	0.36	0.46	0.62	0.53	0.16	0.86	0.86	0.20	1.02	0.27	0.63	0.47

CpPxA	0.74	0.00	-0.65	0.08	-1.01	0.33	-0.05	0.95	0.30	0.27	1.15	0.37	0.79	0.41	-2.39	**0.00**	-3.32	**0.00**	-2.38	**0.02**
CpScA	0.19	1.00	-0.50	0.10	-1.86	0.09	-1.44	0.13	0.00	1.00	0.56	0.62	1.69	0.10	-0.64	0.28	-1.01	0.36	-0.51	0.59
Cp3SD	0.07	0.97	-0.38	0.43	0.78	0.44	0.51	0.60	0.95	0.41	0.48	0.70	-0.15	0.87	0.55	0.54	-0.31	0.79	-0.36	0.72
CpHmC	0.36	0.94	0.40	0.25	2.30	0.07	1.82	0.09	0.04	0.96	1.06	0.42	-0.18	0.87	-1.57	**0.02**	-2.36	**0.03**	-1.90	0.08
CpHP	0.60	0.00	0.75	0.10	1.65	0.14	1.17	0.19	-1.46	**0.00**	-2.79	**0.03**	-2.00	**0.03**	-0.68	0.14	-1.08	0.33	-0.83	0.35

[a] Based on Bayesian phylogenetic generalized linear mixed model (PGLMM) regression of taxon means with size (log-transformed sum carpal volume) as a covariate. OR, odds ratio (log scale)

[b] Based on PGLMM analysis of all observations rather than taxon means

Table 3.10. Additional extant positional classification results

a	Cross-validation trials								
	DFA				*glmnet*				
	DG	*KW*	*PG*	*S*	*DG*	*KW*	*PG*	*S*	Total
DG	1900	0	1100	0	1868	0	1132	0	3000
KW	0	7846	354	0	0	7989	46	165	8200
PG	1205	417	13868	10	825	203	14150	322	15500
S	0	500	487	6613	0	189	352	7059	7600

b	Additional per-class accuracy metrics							
	DFA				*glmnet*			
Bal[a]	0.788	0.941	0.894	0.981	0.829	0.973	0.915	0.958
Sen[b]	0.612	0.895	0.877	0.998	0.694	0.953	0.902	0.935
Spec[c]	0.965	0.986	0.912	0.964	0.964	0.992	0.927	0.980
PPV[d]	0.633	0.957	0.895	0.870	0.623	0.974	0.913	0.929
NPV[e]	0.962	0.965	0.897	1.000	0.974	0.985	0.919	0.982

c	Mean prediction posterior probabilities				Mean probabilities by *a priori* class			
DFA	0.756	0.946	0.908	0.969	0.610	0.939	0.865	0.861
glmnet	0.801	0.959	0.931	0.958	0.589	0.949	0.884	0.915

d	*glmnet* tuned parameters
alpha	0.9632653
lambda	0.0005459

[a] Balanced accuracy – average of sensitivity and specificity
[b] Sensitivity – correct predictions relative to the number of *a priori* cases of that class in the sample. Also known as recall or true positive rate.
[c] Specificity – rate at which observations not assigned to a class actually do not belong to that class, also known as the true negative rate.
[d] Positive prediction value – probability that an observation predicted to belong to a class actually belongs to that class.
[e] Negative prediction value – probability than an observation not predicted to belong to a class actually does not belong to that class

Table 3.11. Relationships between shape variables and selected locomotor proportions based on PGLS regression

a	*QuadA*						**b**	*Quad*						**c**	*SuspA*					
	R^2	λ	b	p	b^a	p^a		R^2	λ	b	p	b^a	p^a		R^2	λ	b	p	b^a	p^a
CpPx	0.26	0.56	0.49	**0.02**	0.78	**0.00**		0.53	0.00	0.72	**0.00**	0.67	**0.00**		0.14	1.00	-0.26	0.08	-0.27	0.10
CpSc	0.11	0.58	0.33	0.14	0.32	0.17		0.04	1.00	0.19	0.39	0.71	**0.00**		0.07	1.00	-0.19	0.24	-0.20	0.23
CpLu	0.10	0.79	0.30	0.16	0.46	0.10		0.02	1.00	0.14	0.48	-0.06	0.74		0.05	1.00	-0.14	0.34	-0.14	0.38
CpDn	0.10	0.88	0.27	0.15	0.28	0.14		0.06	1.00	0.20	0.26	0.21	0.16		0.00	1.00	-0.02	0.89	-0.02	0.88
Cp3	0.05	0.72	0.20	0.34	0.19	0.38		0.03	1.00	0.13	0.48	0.05	0.76		0.06	1.00	-0.14	0.29	-0.13	0.32
CpHm	0.11	0.86	-0.30	0.13	-0.30	0.16		0.01	1.00	-0.08	0.64	-0.02	0.91		0.08	1.00	0.14	0.21	0.14	0.23
Cp2	0.02	0.79	0.17	0.52	0.25	0.39		0.00	1.00	0.03	0.90	0.23	0.35		0.02	1.00	-0.13	0.51	-0.16	0.44
Cp4	0.02	0.80	-0.17	0.51	-0.19	0.59		0.05	1.00	-0.29	0.30	0.13	0.68		0.05	1.00	0.20	0.32	0.24	0.35
Cp23A	0.17	0.53	-0.40	0.05	-0.46	**0.03**		0.19	0.87	-0.46	**0.04**	-0.20	0.32		0.21	1.00	0.31	**0.03**	0.31	**0.04**
Cp3HmA	0.03	0.77	0.14	0.44	0.13	0.51		0.00	1.00	-0.01	0.96	-0.05	0.69		0.04	1.00	-0.09	0.40	-0.08	0.43
CpPxA	0.34	0.48	0.56	**0.00**	0.71	**0.00**		0.42	0.59	0.70	**0.00**	0.55	**0.01**		0.84	0.58	-0.86	**0.00**	-0.96	**0.00**
CpScA	0.19	0.57	0.49	**0.04**	0.49	0.05		0.02	1.00	0.21	0.53	0.29	0.32		0.33	1.00	-0.60	**0.01**	-0.62	**0.01**
Cp3SD	0.31	0.85	0.55	**0.01**	0.59	**0.01**		0.19	1.00	0.43	**0.04**	0.31	0.11		0.06	1.00	-0.18	0.25	-0.17	0.29
CpHmC	0.29	0.65	0.54	**0.01**	0.77	**0.00**		0.39	0.72	0.69	**0.00**	0.36	0.13		0.43	1.00	-0.54	**0.00**	-0.63	**0.00**
CpHP	0.00	0.82	0.06	0.76	0.08	0.71		0.00	1.00	0.04	0.80	0.05	0.72		0.01	1.00	0.06	0.64	0.06	0.65
Without hylobatids																				
CpPx	0.02	0.53	0.16	0.53	0.35	0.12		0.23	0.00	0.48	**0.04**	0.02	0.93		0.00	1.00	0.00	0.98	-0.02	0.90
CpSc	0.43	0.60	0.65	**0.00**	0.33	0.18		0.02	1.00	0.16	0.54	0.63	**0.01**		0.52	0.00	-0.72	**0.00**	-0.63	**0.01**
CpLu	0.06	0.72	-0.28	0.30	0.12	0.76		0.00	1.00	-0.06	0.80	-0.20	0.37		0.03	1.00	0.13	0.49	0.08	0.69
CpDn	0.23	0.00	0.47	**0.04**	0.60	**0.00**		0.27	1.00	0.48	**0.02**	0.48	**0.01**		0.15	1.00	-0.28	0.10	-0.29	0.09
Cp3	0.01	0.51	-0.07	0.77	-0.10	0.64		0.00	1.00	0.01	0.96	-0.03	0.88		0.00	1.00	0.00	0.99	-0.02	0.90
CpHm	0.05	0.52	-0.18	0.37	-0.28	0.31		0.00	1.00	-0.06	0.78	-0.02	0.90		0.08	1.00	0.19	0.24	0.21	0.19
Cp2	0.06	0.47	0.23	0.32	0.22	0.50		0.00	1.00	0.03	0.93	0.28	0.40		0.04	1.00	-0.21	0.43	-0.13	0.66
Cp4	0.01	0.48	0.14	0.62	0.07	0.86		0.00	1.00	-0.11	0.84	0.50	0.37		0.06	1.00	-0.39	0.33	-0.23	0.62
Cp23A	0.16	0.00	-0.40	0.09	-0.07	0.75		0.00	1.00	-0.05	0.82	-0.03	0.89		0.06	1.00	0.16	0.33	0.16	0.30
Cp3HmA	0.19	0.77	0.49	0.06	-0.14	0.51		0.03	1.00	-0.10	0.45	-0.09	0.46		0.01	1.00	0.03	0.74	0.04	0.71
CpPxA	0.07	0.59	0.30	0.27	0.23	0.28		0.17	0.62	0.41	0.08	0.42	0.06		0.62	0.65	-0.70	**0.00**	-0.75	**0.00**
CpScA	0.30	0.00	0.55	**0.02**	-0.10	0.73		0.02	1.00	-0.22	0.57	0.06	0.87		0.10	1.00	-0.40	0.18	-0.33	0.32
Cp3SD	0.01	0.62	-0.13	0.65	0.48	**0.04**		0.11	1.00	0.36	0.16	0.29	0.23		0.00	1.00	0.01	0.98	-0.03	0.88

CpHmC	0.16	0.38	-0.37	0.09	0.38	0.08		0.20	0.71	0.55	0.05	0.28	0.31		0.15	1.00	-0.37	0.10	-0.48	**0.04**
CpHP	0.44	0.00	0.66	**0.00**	0.40	0.07		0.05	1.00	0.19	0.36	0.19	0.33		0.02	1.00	-0.09	0.57	-0.10	0.57
d	*Susp*						**e**	*ClimbA*						**f**	*Climb*					
	R^2	λ	b	p	b^a	p^a		R^2	λ	b	p	b^a	p^a		R^2	λ	b	p	b^a	p^a
CpPx	0.23	1.00	-0.34	**0.02**	-0.34	**0.03**		0.13	0.71	0.36	0.10	0.23	0.31		0.11	0.00	-0.33	0.14	-0.18	0.40
CpSc	0.17	1.00	-0.30	0.06	-0.32	**0.05**		0.05	0.80	0.24	0.30	0.30	0.14		0.04	0.34	-0.23	0.36	-0.40	0.06
CpLu	0.05	1.00	-0.14	0.32	-0.13	0.42		0.05	0.73	0.21	0.33	-0.04	0.88		0.07	0.00	-0.26	0.24	0.21	0.49
CpDn	0.00	1.00	0.01	0.91	0.01	0.93		0.01	0.81	-0.10	0.61	-0.02	0.92		0.00	0.30	-0.06	0.78	-0.14	0.49
Cp3	0.08	1.00	-0.16	0.21	-0.15	0.26		0.16	0.79	0.37	0.07	0.29	0.09		0.04	0.32	-0.20	0.40	-0.05	0.81
CpHm	0.02	1.00	0.08	0.49	0.07	0.55		0.00	0.79	-0.05	0.81	0.16	0.48		0.07	0.00	0.26	0.23	-0.07	0.78
Cp2	0.01	1.00	-0.09	0.66	-0.13	0.53		0.02	0.78	-0.15	0.56	-0.08	0.74		0.02	0.00	0.16	0.48	-0.32	0.24
Cp4	0.07	1.00	0.23	0.25	0.25	0.33		0.18	0.70	-0.48	**0.05**	-0.35	0.30		0.17	0.00	0.41	0.06	-0.79	0.05
Cp23A	0.19	1.00	0.30	**0.04**	0.29	0.06		0.19	0.78	-0.45	**0.04**	-0.34	**0.04**		0.04	0.42	0.21	0.39	0.13	0.53
Cp3HmA	0.03	1.00	-0.09	0.41	-0.08	0.46		0.04	0.75	0.16	0.39	0.10	0.59		0.01	0.00	-0.10	0.65	0.04	0.84
CpPxA	0.91	0.00	-0.95	**0.00**	-0.96	**0.00**		0.24	0.81	0.54	**0.02**	0.43	**0.04**		0.07	0.18	-0.28	0.23	-0.23	0.25
CpScA	0.37	1.00	-0.65	**0.00**	-0.67	**0.00**		0.01	0.80	0.14	0.63	0.16	0.40		0.01	0.42	-0.15	0.61	-0.17	0.42
Cp3SD	0.05	1.00	-0.15	0.32	-0.14	0.40		0.00	0.79	0.03	0.89	-0.02	0.92		0.16	0.00	-0.40	0.06	-0.21	0.37
CpHmC	0.46	1.00	-0.57	**0.00**	-0.59	**0.00**		0.16	0.69	0.41	0.07	0.29	0.19		0.11	0.00	-0.34	0.12	-0.19	0.38
CpHP	0.03	1.00	0.09	0.46	0.09	0.47		0.07	0.72	-0.24	0.23	-0.29	0.12		0.05	0.00	0.21	0.34	0.03	0.91
Without hylobatids																				
CpPx	0.03	1.00	-0.11	0.47	-0.12	0.43		0.01	0.75	0.10	0.64	0.06	0.80		0.21	0.00	-0.46	**0.05**	-0.32	0.16
CpSc	0.17	1.00	-0.36	0.07	-0.34	0.11		0.04	0.79	0.19	0.40	0.26	0.26		0.03	0.34	-0.18	0.49	-0.52	**0.03**
CpLu	0.03	1.00	0.13	0.48	0.10	0.63		0.01	0.79	-0.11	0.66	-0.52	0.12		0.09	0.00	-0.30	0.22	0.39	0.33
CpDn	0.09	1.00	-0.22	0.21	-0.22	0.21		0.00	0.78	-0.04	0.84	0.06	0.78		0.04	0.37	-0.21	0.39	-0.34	0.11
Cp3	0.00	1.00	-0.04	0.81	-0.05	0.75		0.10	0.81	0.26	0.18	0.23	0.27		0.02	0.33	-0.16	0.53	-0.05	0.84
CpHm	0.01	1.00	0.07	0.65	0.09	0.60		0.00	0.77	0.04	0.86	0.08	0.75		0.08	0.00	0.29	0.23	-0.10	0.65
Cp2	0.02	1.00	-0.14	0.60	-0.08	0.79		0.05	0.70	-0.25	0.34	-0.29	0.32		0.03	0.00	0.17	0.48	-0.47	0.15
Cp4	0.03	1.00	-0.30	0.46	-0.18	0.71		0.04	0.71	-0.26	0.42	-0.05	0.90		0.23	0.00	0.48	**0.04**	-0.45	0.43
Cp23A	0.04	1.00	0.13	0.41	0.14	0.39		0.14	0.80	-0.31	0.12	-0.38	**0.05**		0.03	0.44	0.16	0.51	0.19	0.40
Cp3HmA	0.01	1.00	0.04	0.69	0.04	0.67		0.00	0.77	-0.05	0.78	-0.05	0.79		0.01	0.00	-0.08	0.73	0.06	0.63
CpPxA	0.73	0.00	-0.85	**0.00**	-0.83	**0.00**		0.16	0.83	0.33	0.09	0.33	0.09		0.13	0.00	-0.36	0.13	-0.43	**0.04**
CpScA	0.15	1.00	-0.48	0.11	-0.46	0.17		0.02	0.72	-0.16	0.57	-0.06	0.83		0.02	0.00	0.15	0.54	-0.48	0.13

Cp3SD	0.00	1.00	0.06	0.78	0.03	0.88	0.04	0.83	-0.20	0.39	-0.19	0.43	0.18	0.00	-0.42	0.07	-0.23	0.35
CpHmC	0.19	1.00	-0.41	0.07	-0.44	0.05	0.06	0.71	0.25	0.31	0.21	0.38	0.18	0.00	-0.42	0.07	-0.28	0.22
CpHP	0.00	1.00	-0.03	0.85	-0.03	0.85	0.09	0.72	-0.27	0.20	-0.33	0.11	0.02	0.00	0.14	0.56	-0.20	0.34
g	*LeapA*						**h**	*Leap*						**i**	*Arb*			
	R^2	λ	b	p	b^a	p^a	R^2	λ	b	p	b^a	p^a	R^2	λ	b	p	b^a	p^a
CpPx	0.01	1.00	-0.09	0.65	0.01	0.95	0.02	1.00	-0.14	0.49	-0.01	0.95	0.20	0.52	-0.48	**0.04**	-0.30	0.09
CpSc	0.06	1.00	0.22	0.27	0.17	0.38	0.03	1.00	0.16	0.46	0.09	0.64	0.01	1.00	-0.12	0.65	-0.48	**0.00**
CpLu	0.08	1.00	-0.23	0.19	-0.12	0.53	0.08	1.00	-0.24	0.19	-0.08	0.66	0.01	1.00	-0.09	0.68	0.22	0.24
CpDn	0.12	1.00	-0.24	0.11	-0.25	0.08	0.14	1.00	-0.28	0.08	-0.30	**0.04**	0.04	1.00	-0.18	0.35	-0.21	0.17
Cp3	0.01	1.00	-0.06	0.72	0.00	0.98	0.00	1.00	0.02	0.90	0.10	0.53	0.00	1.00	-0.03	0.88	0.09	0.58
CpHm	0.09	1.00	0.19	0.18	0.15	0.26	0.05	1.00	0.15	0.32	0.10	0.46	0.00	1.00	-0.01	0.97	-0.10	0.50
Cp2	0.02	1.00	0.15	0.53	0.03	0.89	0.00	1.00	0.01	0.96	-0.16	0.49	0.01	1.00	-0.13	0.68	-0.42	0.08
Cp4	0.13	1.00	0.40	0.10	0.22	0.46	0.10	1.00	0.38	0.15	0.06	0.83	0.29	0.00	0.54	**0.01**	-0.48	0.10
Cp23A	0.00	1.00	0.00	0.99	-0.07	0.71	0.00	1.00	0.02	0.92	-0.07	0.70	0.21	0.74	0.50	**0.03**	0.39	**0.01**
Cp3HmA	0.00	1.00	0.00	0.99	0.03	0.80	0.00	1.00	-0.03	0.84	0.01	0.93	0.00	1.00	0.01	0.96	0.07	0.57
CpPxA	0.00	1.00	0.00	0.99	0.07	0.75	0.00	1.00	0.07	0.76	0.17	0.43	0.12	0.69	-0.39	0.12	-0.32	0.05
CpScA	0.18	1.00	0.56	**0.05**	0.51	0.06	0.17	1.00	0.57	0.06	0.51	0.06	0.00	1.00	0.07	0.85	-0.04	0.90
Cp3SD	0.15	1.00	-0.33	0.08	-0.25	0.17	0.15	1.00	-0.36	0.07	-0.25	0.18	0.17	0.57	-0.43	0.05	-0.12	0.56
CpHmC	0.00	1.00	-0.02	0.94	0.12	0.59	0.01	1.00	-0.11	0.66	0.07	0.77	0.28	0.56	-0.58	**0.01**	-0.37	**0.03**
CpHP	0.06	1.00	-0.16	0.27	-0.17	0.22	0.06	1.00	-0.17	0.28	-0.18	0.20	0.01	1.00	-0.07	0.70	-0.09	0.55
Without hylobatids																		
CpPx	0.00	1.00	0.00	0.99	0.02	0.89	0.01	1.00	-0.04	0.76	-0.02	0.90	0.15	0.37	-0.39	0.11	-0.27	0.18
CpSc	0.05	1.00	0.17	0.35	0.11	0.53	0.02	1.00	0.12	0.56	0.03	0.88	0.01	1.00	-0.08	0.75	-0.50	**0.01**
CpLu	0.04	1.00	-0.13	0.42	-0.06	0.70	0.04	1.00	-0.14	0.41	-0.05	0.79	0.00	1.00	0.01	0.96	0.21	0.26
CpDn	0.17	1.00	-0.26	0.08	-0.26	0.06	0.22	1.00	-0.32	**0.04**	-0.32	**0.02**	0.12	1.00	-0.32	0.14	-0.42	**0.01**
Cp3	0.00	1.00	-0.03	0.80	-0.01	0.92	0.01	1.00	0.05	0.73	0.08	0.54	0.00	1.00	0.04	0.85	0.09	0.55
CpHm	0.08	1.00	0.17	0.24	0.15	0.28	0.04	1.00	0.13	0.41	0.10	0.49	0.00	1.00	-0.03	0.89	-0.08	0.62
Cp2	0.07	1.00	0.24	0.28	0.14	0.56	0.01	1.00	0.10	0.70	-0.09	0.71	0.01	1.00	-0.13	0.71	-0.51	0.05
Cp4	0.02	1.00	0.18	0.61	-0.13	0.74	0.01	1.00	0.15	0.71	-0.33	0.41	0.25	0.00	0.50	**0.03**	-0.72	0.11
Cp23A	0.00	1.00	0.02	0.87	0.01	0.93	0.00	1.00	0.03	0.85	0.01	0.93	0.15	0.74	0.36	0.11	0.44	**0.01**
Cp3HmA	0.01	1.00	0.03	0.71	0.03	0.75	0.00	1.00	0.01	0.91	0.00	0.97	0.01	1.00	0.05	0.70	0.04	0.72
CpPxA	0.01	1.00	0.06	0.68	0.04	0.76	0.04	1.00	0.14	0.40	0.11	0.45	0.00	1.00	0.01	0.97	-0.32	0.07

CpScA	0.36	1.00	0.65	**0.01**	0.59	**0.02**	0.34	1.00	0.69	**0.01**	0.55	**0.04**	0.05	1.00	0.35	0.37	-0.07	0.84
Cp3SD	0.16	1.00	-0.30	0.09	-0.26	0.13	0.16	1.00	-0.32	0.09	-0.27	0.13	0.11	0.51	-0.35	0.16	-0.13	0.54
CpHmC	0.00	1.00	-0.04	0.84	-0.01	0.97	0.02	1.00	-0.14	0.53	-0.09	0.65	0.26	0.45	-0.57	**0.02**	-0.38	**0.05**
CpHP	0.01	1.00	-0.06	0.69	-0.06	0.68	0.02	1.00	-0.08	0.62	-0.08	0.58	0.03	1.00	-0.15	0.47	-0.15	0.36

[a] Based on PGLS model with size as a covariate

Table 3.12. Prediction results for selected locomotor proportions

a Predictive models

	PGLS			GLM					
	R^2	λ	p	Terms	Coef	SE	T	p	SEE%[a]
QuadA	0.901	0.000	**0.000**	(Intercept)	-0.55	0.04	-12.8	0.000	15.4
				Cp23A	-0.09	0.05	-1.9	0.061	
				Cp3SD	0.27	0.05	6.0	0.000	
				CpDn	0.26	0.05	5.6	0.000	
				CpHP	0.22	0.05	4.9	0.000	
				CpScA	0.70	0.05	13.0	0.000	
Quad	0.638	0.421	**0.000**	(Intercept)	0.15	0.06	2.3	0.020	20.5
				CpDn	0.36	0.07	5.3	0.000	
				CpPx	0.70	0.07	9.7	0.000	
				CpPxA	0.79	0.08	10.3	0.000	
SuspA	0.969	0.000	**0.000**	(Intercept)	-2.55	0.07	-34.6	0.000	8.5
				CpDn	-0.36	0.06	-6.3	0.000	
				CpHmC	-0.23	0.07	-3.24	0.001	
				CpPxA	-0.62	0.09	-6.8	0.000	
				CpSc	-0.48	0.06	-7.6	0.000	
				CpScA	-0.54	0.08	-6.8	0.000	
Susp	0.945	0.000	**0.000**	(Intercept)	-3.10	0.12	-26.2	0.000	9.6
				CpPxA	-1.34	0.08	-17.8	0.000	
				CpSc	-0.79	0.09	-9.0	0.000	
ClimbA	0.951	1.000	**0.009**	(all)					10.0
Climb	0.895	0.000	0.069	(all)					11.0
Arb	0.892	0.000	0.075	(all)					25.2

b Predicted locomotor proportions of training taxa[b]

	QuadA			*Quad*			*SuspA*			*Susp*		
	Obs	Pred	Δ	Obs	Pred	Δ	Obs	Pred	Δ	Obs	Pred	Δ
P. t. schweinfurthii	0.31	0.30	0.01	0.93	0.61	0.32	0.08	0.06	0.02	0.01	0.03	0.02
P. t. verus	0.21	0.26	0.05	0.86	0.69	0.17	0.06	0.06	0.00	0.01	0.02	0.01
P. paniscus	0.35	0.28	0.07	0.87	0.70	0.17	0.09	0.06	0.03	0.01	0.03	0.02
G. gorilla	0.19	0.33	0.14	0.92	0.76	0.16	0.13	0.06	0.07	0.01	0.03	0.02
G. beringei	0.53	0.41	0.12	0.96	0.73	0.23	0.06	0.07	0.01	0.01	0.05	0.04
P. pygmaeus	0.12	0.20	0.08	0.12	0.33	0.21	0.43	0.34	0.09	0.43	0.25	0.18
P. abelii	0.18	0.23	0.05	0.18	0.33	0.15	0.38	0.37	0.01	0.38	0.36	0.02
Hoolock	0.00	0.17	0.17	0.00	0.10	0.10	0.55	0.44	0.11	0.55	0.51	0.04
H. lar	0.00	0.15	0.15	0.00	0.07	0.07	0.59	0.61	0.02	0.59	0.58	0.01
Symphalangus	0.00	0.19	0.19	0.00	0.12	0.12	0.59	0.56	0.03	0.59	0.59	0.00
Papio	0.68	0.45	0.23	0.99	0.77	0.22	0.00	0.03	0.03	0.00	0.02	0.02
Lophocebus	0.42	0.51	0.09	0.42	0.79	0.37	0.00	0.02	0.02	0.00	0.01	0.01
Macaca	0.68	0.41	0.27	0.68	0.74	0.06	0.00	0.04	0.04	0.00	0.02	0.02
Erythrocebus	0.60	0.57	0.03	0.94	0.68	0.26	0.00	0.04	0.04	0.00	0.04	0.04
Cercopithecus	0.54	0.49	0.05	0.54	0.73	0.19	0.00	0.04	0.04	0.00	0.02	0.02

Colobus	0.41	0.48	0.07	0.41	0.71	0.30	0.01	0.02	0.01	0.01	0.01	0.00
Procolobus	0.35	0.37	0.02	0.35	0.62	0.27	0.01	0.05	0.04	0.01	0.03	0.02
Trachypithecus	0.60	0.51	0.09	0.60	0.65	0.05	0.00	0.06	0.06	0.00	0.03	0.03
Presbytis	0.28	0.39	0.11	0.28	0.49	0.21	0.02	0.05	0.03	0.02	0.03	0.01
Alouatta	0.61	0.52	0.09	0.61	0.49	0.12	0.02	0.04	0.02	0.02	0.03	0.01
Ateles	0.42	0.46	0.04	0.42	0.28	0.14	0.25	0.13	0.12	0.25	0.17	0.08
Cebus	0.37	0.45	0.08	0.37	0.44	0.07	0.00	0.06	0.06	0.00	0.05	0.05

c Predictions of locomotor proportions less reflected in capitate morphology

	ClimbA			*Climb*			*Arb*		
	Obs	Pred	Δ	Obs	Pred	Δ	Obs	Pred	Δ
P. t. schweinfurthii	0.59	0.47	0.12	0.06	0.13	0.07	0.10	0.41	0.31
P. t. verus	0.68	0.52	0.16	0.11	0.15	0.04	0.16	0.35	0.19
P. paniscus	0.51	0.45	0.06	0.09	0.18	0.09	0.17	0.36	0.19
G. gorilla	0.62	0.54	0.08	0.06	0.13	0.07	0.10	0.19	0.09
G. beringei	0.40	0.48	0.08	0.04	0.14	0.10	0.09	0.21	0.12
P. pygmaeus	0.37	0.40	0.03	0.37	0.21	0.16	0.95	0.75	0.20
P. abelii	0.35	0.32	0.03	0.35	0.24	0.11	0.95	0.87	0.08
Hoolock	0.20	0.27	0.07	0.20	0.29	0.09	0.99	0.99	0.00
H. lar	0.19	0.21	0.02	0.19	0.29	0.10	0.99	1.00	0.01
Symphalangus	0.32	0.18	0.14	0.32	0.23	0.09	0.99	1.00	0.01
Papio	0.21	0.30	0.09	0.01	0.18	0.17	0.05	0.54	0.49
Lophocebus	0.36	0.33	0.03	0.36	0.18	0.18	0.95	0.48	0.47
Macaca	0.26	0.31	0.05	0.26	0.17	0.09	0.97	0.65	0.32
Erythrocebus	0.30	0.27	0.03	0.05	0.27	0.22	0.08	0.64	0.56
Cercopithecus	0.35	0.30	0.05	0.35	0.21	0.14	0.95	0.62	0.33
Colobus	0.20	0.35	0.15	0.20	0.21	0.01	0.96	0.84	0.12
Procolobus	0.29	0.33	0.04	0.29	0.27	0.02	0.95	0.87	0.08
Trachypithecus	0.13	0.29	0.16	0.13	0.20	0.07	0.99	0.87	0.12
Presbytis	0.19	0.29	0.10	0.19	0.28	0.09	0.99	0.95	0.04
Alouatta	0.33	0.30	0.03	0.33	0.31	0.02	0.95	0.96	0.01
Ateles	0.25	0.31	0.06	0.25	0.34	0.09	0.99	0.99	0.00
Cebus	0.40	0.34	0.06	0.40	0.30	0.10	0.95	0.95	0.00

d Predicted locomotor proportions for other taxa

	QuadA	*Quad*	*SuspA*	*Susp*	*ClimbA*	*Climb*	*Arb*
P. t. troglodytes	0.30	0.62	0.06	0.02	0.47	0.14	0.42
P. t. ellioti	0.29	0.63	0.07	0.03	0.49	0.14	0.43
H. muelleri	0.19	0.08	0.55	0.44	0.25	0.24	1.00
Mandrillus	0.39	0.75	0.04	0.03	0.33	0.20	0.44
Cercocebus	0.58	0.77	0.03	0.02	0.22	0.16	0.70
Nasalis	0.41	0.65	0.05	0.02	0.21	0.22	0.95

[a] Percent standard error of the estimate based on repeated individual predictions generated during cross validation

[b] Predictions calculated after 100 repetitions of 10-fold cross validation of quasibinomial logistic regression. Obs, observed proportions. Pred, predicted proportions. Δ, residual.

Table 3.13. PLS results

a Locomotor PLS vectors						Without hylobatids				
	PLS1	PLS2	PLS3	PLS4	PLS5	PLS1	PLS2	PLS3	PLS4	PLS5
QuadA	0.54	0.28	-0.50	0.26	0.56	0.47	0.38	-0.55	0.15	-0.56
SuspA	-0.71	-0.22	-0.24	-0.09	0.62	-0.54	-0.51	-0.39	-0.23	-0.49
ClimbA	0.29	-0.56	0.60	0.28	0.40	-0.43	0.31	0.46	0.53	-0.47
LeapA	0.03	0.58	0.51	-0.51	0.37	0.45	-0.28	0.58	-0.39	-0.48
Arb	-0.36	0.47	0.26	0.76	-0.02	0.31	-0.64	-0.04	0.70	0.04
b Shape PLS vectors										
CpSc	0.31	0.27	-0.08	-0.29	0.31	0.34	0.27	0.13	-0.05	-0.05
CpLu	0.21	-0.32	-0.11	0.15	-0.53	-0.37	0.05	-0.07	-0.25	-0.01
CpDn	-0.04	-0.11	-0.60	0.09	0.57	0.10	0.51	-0.48	0.26	-0.20
Cp3	0.26	-0.10	0.14	0.61	0.21	-0.12	0.07	0.17	0.48	-0.48
CpHm	-0.04	0.31	0.05	0.19	0.12	0.22	-0.17	0.00	0.07	-0.32
Cp2	0.14	0.52	-0.16	-0.23	-0.27	0.44	-0.07	-0.03	-0.38	-0.05
Cp4	-0.15	0.40	-0.18	0.39	-0.13	0.36	-0.13	-0.24	0.34	0.35
Cp23A	-0.37	0.00	0.07	-0.27	-0.06	-0.06	-0.30	-0.07	-0.25	-0.03
Cp3HmA	0.27	-0.05	0.04	0.13	-0.21	-0.14	-0.09	0.09	-0.32	-0.36
CpPxA	0.44	0.09	0.13	-0.12	0.06	0.24	0.40	0.52	-0.04	0.12
CpScA	0.30	0.38	0.09	0.21	-0.01	0.39	-0.14	0.18	-0.07	-0.47
Cp3SD	0.25	-0.27	-0.49	0.03	-0.11	-0.18	0.32	-0.31	-0.18	-0.32
CpHmC	0.41	-0.10	-0.09	-0.35	0.00	-0.04	0.47	0.17	-0.30	0.18
CpHP	-0.14	0.21	-0.52	0.06	-0.30	0.29	0.02	-0.47	-0.29	-0.02
c Convex hull Euclidean area[a]										
	Monkeys		Great apes		Tinderet	Monkeys		Great apes		Tinderet
	6.89		8.93		6.11	27.23		12.96		15.58

[a] As proportion of scaled PLS shape-space

Table 3.14. (a) Covariance of shape variables with Hominoidea and Platyrrhini relative to Cercopithecoidea. Reported results are from univariate ordinary least squares (OLS) regression of individual observations except where noted. (b) Phylogenetic signal estimated with Pagel's lambda and Blomberg's K.

a		Hominoidea				Platyrrhini				**b**	Phylogenetic signal			
	R^2	b	p	OR[a]	p[a]	b	p	OR[a]	p[a]		λ	p	K	p
CpPx	0.19	-0.70	**0.00**	-3.47	**0.00**	-1.00	**0.00**	-1.53	**0.00**		0.88	**0.00**	0.42	**0.01**
CpSc	0.23	-1.26	**0.00**	-1.76	**0.00**	-0.59	**0.00**	-0.51	**0.01**		0.86	**0.00**	0.36	**0.00**
CpLu	0.11	0.36	**0.00**	-1.65	**0.00**	-0.59	**0.00**	-1.09	**0.00**		0.97	**0.00**	0.65	**0.00**
CpDn	0.05	-0.43	**0.00**	-0.27	0.10	-0.59	**0.00**	-0.66	**0.00**		0.99	**0.00**	0.57	**0.00**
Cp3	0.24	0.44	**0.00**	0.01	0.96	1.24	**0.00**	1.69	**0.00**		0.91	**0.00**	0.52	**0.00**
CpHm	0.21	-0.29	**0.01**	0.34	0.12	1.09	**0.00**	1.51	**0.00**		0.71	**0.00**	0.48	**0.00**
Cp2	0.47	-1.57	**0.00**	-3.13	**0.00**	-0.69	**0.00**	-0.88	**0.00**		0.99	**0.00**	1.12	**0.00**
Cp4	0.35	-0.43	**0.00**	1.79	**0.00**	1.13	**0.00**	1.81	**0.00**		1.01	**0.00**	1.96	**0.00**
Cp23A	0.15	0.41	**0.00**	1.26	**0.00**	-0.80	**0.00**	-1.06	**0.00**		0.97	**0.00**	0.65	**0.00**

Cp3HmA	0.09	-0.67	**0.00**	-2.40	**0.00**	-0.47	**0.00**	-0.05	0.81	0.76	**0.02**	0.34	**0.02**
CpPxA	0.14	-0.79	**0.00**	-3.31	**0.00**	-0.51	**0.00**	-0.55	**0.01**	0.98	**0.00**	0.91	**0.00**
CpScA	0.39	-1.00	**0.00**	-2.98	**0.00**	0.94	**0.00**	2.47	**0.00**	1.00	**0.00**	2.09	**0.00**
Cp3SD	0.18	0.06	0.60	-0.96	**0.00**	-1.08	**0.00**	-2.00	**0.00**	0.82	**0.02**	0.52	**0.00**
CpHmC	0.30	-0.67	**0.00**	-6.53	**0.00**	-1.37	**0.00**	-3.23	**0.00**	1.01	**0.00**	1.32	**0.00**
CpHP	0.17	-0.89	**0.00**	-0.45	**0.02**	-0.88	**0.00**	-0.72	**0.00**	0.88	**0.00**	0.50	**0.00**

[a] Based on multinomial logistic regression with size (log-transformed sum carpal volume) as a covariate. OR, odds ratio (log scale)

Table 3.15. Additional extant taxonomic classification results. See Table 3.5 and Table 3.7 for abbreviations and definitions.

a	Cross-validation trials						
	DFA			*glmnet*			
	Cerc	Hom	Plat	Cerc	Hom	Plat	Total
Cerc	11336	632	532	11630	656	214	12500
Hom	417	14083	0	444	13940	116	14500
Plat	300	85	6915	309	92	6899	7300
b	Additional per-class accuracy metrics						
Bal	0.944	0.965	0.957	0.950	0.960	0.971	
Sen	0.941	0.952	0.929	0.940	0.949	0.957	
Spec	0.948	0.979	0.986	0.961	0.972	0.985	
PPV	0.907	0.971	0.947	0.931	0.962	0.945	
NPV	0.967	0.964	0.980	0.966	0.962	0.988	
c	Mean prediction posterior probabilities			Mean probabilities by *a priori* class			
DFA	0.932	0.966	0.968	0.869	0.953	0.935	
glmnet	0.906	0.938	0.925	0.949	0.960	0.954	
d	*glmnet* tuned parameters						
alpha	0.9921053						
lambda	0.0010833						

Table 3.16. Spearman correlations between phylogenetic independent contrasts of shape variables and size surrogate

	Males		Females		Pooled	
	rho	p	rho	p	rho	p
CpPx	0.10	0.83	0.11	0.88	0.10	0.70
CpSc	-0.27	0.57	-0.08	0.88	-0.18	0.48
CpLu	0.45	0.24	0.16	0.88	0.33	0.13
CpDn	0.20	0.57	0.08	0.88	0.13	0.70
Cp3	-0.32	0.57	-0.04	0.90	-0.19	0.48
CpHm	-0.22	0.57	-0.44	0.28	-0.32	0.13
Cp2	-0.07	0.85	-0.12	0.88	-0.08	0.77

Cp4	-0.31	0.57	-0.24	0.88	-0.30	0.14
Cp23A	0.11	0.83	-0.07	0.88	0.00	0.98
Cp3HmA	0.04	0.85	0.18	0.88	0.12	0.70
CpPxA	0.19	0.57	-0.07	0.88	0.06	0.84
CpScA	-0.24	0.57	-0.25	0.88	-0.24	0.29
Cp3SD	-0.05	0.85	-0.02	0.90	-0.05	0.84
CpHmC	0.18	0.57	-0.04	0.90	0.10	0.70
CpHP	0.20	0.57	-0.15	0.88	0.02	0.93

Table 3.17. Condition of selected articulations in extant sample

	a	Mc2			**b** Hamate		
	Tot	Cont	P only	D&P	Prox & dist	Dist D&P	Plm acc
Pan	44	1	3	40	0	0	2
Gorilla	38	0	25	13	0	0	0
Pongo	34	0	1	33	8	0	0
Hylobatids	29	0	0	29	26	12	1
Papio	14	10	0	4	0	0	0
Lophocebus	6	6	0	0	0	0	0
Mandrillus	9	7	0	2	0	0	0
Cercocebus	2	1	0	1	0	0	0
Macaca	18	18	0	0	0	0	1
Erythrocebus	7	7	0	0	0	0	0
Cercopithecus	11	8	0	3	0	0	0
Colobus	9	1	0	8	0	0	0
Procolobus	13	10	0	3	0	0	0
Nasalis	17	13	0	4	4	3	11
Trachypithecus	17	14	0	3	0	0	0
Presbytis	2	2	0	0	0	0	0
Alouatta	32	28	0	4	0	0	0
Ateles	13	12	0	1	12	1	0
Cebus	28	17	0	11	0	0	0

Table 3.18. List of specimens with average posterior probabilities calculated after 100 cross-validation repeats. Misclassified individuals are highlighted.

		a	Positional classification										**b**	Taxonomic classification								
			DFA					*glmnet*						DFA				*glmnet*				
Specimen	Taxon	Class	*DG*	*KW*	*PG*	*S*	Pred	*DG*	*KW*	*PG*	*S*	Pred	Class	Cerc	Hom	Plat	Pred	Cerc	Hom	Plat	Pred
AMNH 51202	*P. t. schwein.*	*KW*	0.00	1.00	0.00	0.00	*KW*	0.00	1.00	0.00	0.00	*KW*	Hom	0.00	1.00	0.00	Hom	0.00	1.00	0.00	Hom
AMNH 51205	*P. t. schwein.*	*KW*	0.03	0.19	0.78	0.00	***PG***	0.01	0.69	0.30	0.00	*KW*	Hom	0.10	0.90	0.00	Hom	0.29	0.71	0.00	Hom
AMNH 51278	*P. t. schwein.*	*KW*	0.00	0.99	0.00	0.01	*KW*	0.00	0.97	0.00	0.02	*KW*	Hom	0.00	1.00	0.00	Hom	0.00	1.00	0.00	Hom
AMNH 51376	*P. t. schwein.*	*KW*	0.00	0.99	0.01	0.01	*KW*	0.00	1.00	0.00	0.00	*KW*	Hom	0.10	0.90	0.00	Hom	0.05	0.95	0.00	Hom
AMNH 51377	*P. t. schwein.*	*KW*	0.00	0.99	0.01	0.00	*KW*	0.00	1.00	0.00	0.00	*KW*	Hom	0.00	1.00	0.00	Hom	0.01	0.99	0.00	Hom
AMNH 51379	*P. t. schwein.*	*KW*	0.00	0.97	0.03	0.00	*KW*	0.00	1.00	0.00	0.00	*KW*	Hom	0.03	0.97	0.00	Hom	0.02	0.98	0.00	Hom
AMNH 51381	*P. t. schwein.*	*KW*	0.00	0.98	0.00	0.02	*KW*	0.00	0.79	0.00	0.21	*KW*	Hom	0.00	1.00	0.00	Hom	0.00	1.00	0.00	Hom
AMNH 51393	*P. t. schwein.*	*KW*	0.00	1.00	0.00	0.00	*KW*	0.00	1.00	0.00	0.00	*KW*	Hom	0.00	1.00	0.00	Hom	0.00	1.00	0.00	Hom
AMNH 201588	*P. t. schwein.*	*KW*	0.00	1.00	0.00	0.00	*KW*	0.00	1.00	0.00	0.00	*KW*	Hom	0.00	1.00	0.00	Hom	0.00	1.00	0.00	Hom
NMNH 236971	*P. t. schwein.*	*KW*	0.00	1.00	0.00	0.00	*KW*	0.00	1.00	0.00	0.00	*KW*	Hom	0.00	1.00	0.00	Hom	0.00	1.00	0.00	Hom
AMNH 54330	*P. t. trog.*	*KW*	0.00	1.00	0.00	0.00	*KW*	0.00	1.00	0.00	0.00	*KW*	Hom	0.00	1.00	0.00	Hom	0.00	1.00	0.00	Hom
AMNH 90189	*P. t. trog.*	*KW*	0.00	0.98	0.02	0.00	*KW*	0.00	0.74	0.25	0.01	*KW*	Hom	0.00	1.00	0.00	Hom	0.00	1.00	0.00	Hom
AMNH 90190	*P. t. trog.*	*KW*	0.04	0.47	0.49	0.00	***PG***	0.00	0.96	0.03	0.00	*KW*	Hom	0.17	0.83	0.00	Hom	0.16	0.84	0.00	Hom
AMNH 90191	*P. t. trog.*	*KW*	0.00	1.00	0.00	0.00	*KW*	0.00	1.00	0.00	0.00	*KW*	Hom	0.00	1.00	0.00	Hom	0.00	1.00	0.00	Hom
AMNH 90292	*P. t. trog.*	*KW*	0.00	0.95	0.04	0.00	*KW*	0.00	0.98	0.02	0.00	*KW*	Hom	0.01	0.99	0.00	Hom	0.01	0.99	0.00	Hom
AMNH 167342	*P. t. trog.*	*KW*	0.00	0.97	0.03	0.00	*KW*	0.00	1.00	0.00	0.00	*KW*	Hom	0.04	0.96	0.00	Hom	0.03	0.97	0.00	Hom
AMNH 167343	*P. t. trog.*	*KW*	0.00	1.00	0.00	0.00	*KW*	0.00	1.00	0.00	0.00	*KW*	Hom	0.00	1.00	0.00	Hom	0.00	1.00	0.00	Hom
AMNH 167344	*P. t. trog.*	*KW*	0.06	0.14	0.80	0.00	***PG***	0.05	0.57	0.38	0.00	*KW*	Hom	0.69	0.31	0.00	**Cerc**	0.86	0.14	0.00	**Cerc**
AMNH 167346	*P. t. trog.*	*KW*	0.00	0.99	0.00	0.01	*KW*	0.00	1.00	0.00	0.00	*KW*	Hom	0.00	1.00	0.00	Hom	0.00	1.00	0.00	Hom
AMNH 201469	*P. t. trog.*	*KW*	0.00	0.83	0.16	0.01	*KW*	0.00	0.90	0.07	0.03	*KW*	Hom	0.18	0.82	0.00	Hom	0.11	0.89	0.00	Hom
UMMZ 39507	*P. t. trog.*	*KW*	0.00	1.00	0.00	0.00	*KW*	0.00	1.00	0.00	0.00	*KW*	Hom	0.00	1.00	0.00	Hom	0.00	1.00	0.00	Hom
MCZ 15312	*P. t. trog.*	*KW*	0.00	0.98	0.02	0.00	*KW*	0.00	1.00	0.00	0.00	*KW*	Hom	0.01	0.99	0.00	Hom	0.01	0.99	0.00	Hom
AMNH 89351	*P. t. verus*	*KW*	0.00	1.00	0.00	0.00	*KW*	0.00	1.00	0.00	0.00	*KW*	Hom	0.00	1.00	0.00	Hom	0.00	1.00	0.00	Hom
AMNH 89353	*P. t. verus*	*KW*	0.00	1.00	0.00	0.00	*KW*	0.00	1.00	0.00	0.00	*KW*	Hom	0.00	1.00	0.00	Hom	0.00	1.00	0.00	Hom
AMNH 89354	*P. t. verus*	*KW*	0.00	1.00	0.00	0.00	*KW*	0.00	1.00	0.00	0.00	*KW*	Hom	0.00	1.00	0.00	Hom	0.00	1.00	0.00	Hom
AMNH 89355	*P. t. verus*	*KW*	0.00	1.00	0.00	0.00	*KW*	0.00	1.00	0.00	0.00	*KW*	Hom	0.00	1.00	0.00	Hom	0.00	1.00	0.00	Hom
AMNH 89406	*P. t. verus*	*KW*	0.00	1.00	0.00	0.00	*KW*	0.00	1.00	0.00	0.00	*KW*	Hom	0.00	1.00	0.00	Hom	0.00	1.00	0.00	Hom
AMNH 174860	*P. t. verus*	*KW*	0.00	1.00	0.00	0.00	*KW*	0.00	1.00	0.00	0.00	*KW*	Hom	0.02	0.98	0.00	Hom	0.01	0.99	0.00	Hom
AMNH 174861	*P. t. verus*	*KW*	0.01	0.37	0.62	0.00	***PG***	0.00	1.00	0.00	0.00	*KW*	Hom	0.86	0.14	0.00	**Cerc**	0.88	0.12	0.00	**Cerc**
NMNH 256973	*P. t. verus*	*KW*	0.00	0.90	0.10	0.00	*KW*	0.00	0.99	0.01	0.00	*KW*	Hom	0.39	0.61	0.00	Hom	0.18	0.82	0.00	Hom
NMNH 477333	*P. t. verus*	*KW*	0.00	1.00	0.00	0.00	*KW*	0.00	1.00	0.00	0.00	*KW*	Hom	0.00	1.00	0.00	Hom	0.00	1.00	0.00	Hom
NMNH 481803	*P. t. verus*	*KW*	0.00	0.95	0.05	0.00	*KW*	0.00	0.99	0.01	0.00	*KW*	Hom	0.01	0.99	0.00	Hom	0.02	0.98	0.00	Hom
NMNH 481804	*P. t. verus*	*KW*	0.00	0.99	0.01	0.00	*KW*	0.00	1.00	0.00	0.00	*KW*	Hom	0.02	0.98	0.00	Hom	0.02	0.98	0.00	Hom

		a	Positional classification										**b**	Taxonomic classification								
			DFA					*glmnet*						DFA				*glmnet*				
Specimen	Taxon	Class	*DG*	*KW*	*PG*	*S*	Pred	*DG*	*KW*	*PG*	*S*	Pred	Class	Cerc	Hom	Plat	Pred	Cerc	Hom	Plat	Pred
UMMZ 76276	*P. t. verus*	*KW*	0.00	1.00	0.00	0.00	*KW*	0.00	1.00	0.00	0.00	*KW*	Hom	0.00	1.00	0.00	Hom	0.00	1.00	0.00	Hom
UMMZ 76277	*P. t. verus*	*KW*	0.00	0.93	0.00	0.07	*KW*	0.00	0.56	0.00	0.44	*KW*	Hom	0.00	1.00	0.00	Hom	0.00	1.00	0.00	Hom
MCZ 20041	*P. t. ellioti*	*KW*	0.00	0.91	0.08	0.00	*KW*	0.00	1.00	0.00	0.00	*KW*	Hom	0.07	0.93	0.00	Hom	0.14	0.86	0.00	Hom
MCZ 23163	*P. t. ellioti*	*KW*	0.00	1.00	0.00	0.00	*KW*	0.00	1.00	0.00	0.00	*KW*	Hom	0.00	1.00	0.00	Hom	0.00	1.00	0.00	Hom
MCZ 23167	*P. t. ellioti*	*KW*	0.00	1.00	0.00	0.00	*KW*	0.00	0.97	0.00	0.03	*KW*	Hom	0.00	1.00	0.00	Hom	0.00	1.00	0.00	Hom
MCZ 26849	*P. t. ellioti*	*KW*	0.00	0.88	0.06	0.05	*KW*	0.00	0.48	0.25	0.27	*KW*	Hom	0.01	0.99	0.00	Hom	0.01	0.99	0.00	Hom
UMMZ 167199	*P. t. ellioti*	*KW*	0.00	1.00	0.00	0.00	*KW*	0.00	1.00	0.00	0.00	*KW*	Hom	0.00	1.00	0.00	Hom	0.00	1.00	0.00	Hom
AMNH 86857	*P. paniscus*	*KW*	0.01	0.84	0.09	0.06	*KW*	0.00	0.93	0.00	0.06	*KW*	Hom	0.40	0.60	0.00	Hom	0.39	0.61	0.00	Hom
MCZ 38018	*P. paniscus*	*KW*	0.00	0.94	0.06	0.00	*KW*	0.00	1.00	0.00	0.00	*KW*	Hom	0.05	0.95	0.00	Hom	0.03	0.97	0.00	Hom
MCZ 38019	*P. paniscus*	*KW*	0.00	0.98	0.02	0.00	*KW*	0.00	1.00	0.00	0.00	*KW*	Hom	0.02	0.98	0.00	Hom	0.02	0.98	0.00	Hom
MCZ 38020	*P. paniscus*	*KW*	0.00	0.99	0.01	0.00	*KW*	0.00	1.00	0.00	0.00	*KW*	Hom	0.00	1.00	0.00	Hom	0.00	1.00	0.00	Hom
AMNH 54355	*G. gorilla*	*KW*	0.00	1.00	0.00	0.00	*KW*	0.00	1.00	0.00	0.00	*KW*	Hom	0.02	0.98	0.00	Hom	0.02	0.98	0.00	Hom
AMNH 54356	*G. gorilla*	*KW*	0.00	0.94	0.01	0.05	*KW*	0.00	0.22	0.05	0.73	***S***	Hom	0.04	0.95	0.01	Hom	0.08	0.92	0.00	Hom
AMNH 69398	*G. gorilla*	*KW*	0.01	0.62	0.37	0.00	*KW*	0.00	0.99	0.01	0.00	*KW*	Hom	0.80	0.20	0.00	**Cerc**	0.96	0.04	0.00	**Cerc**
AMNH 81651	*G. gorilla*	*KW*	0.00	1.00	0.00	0.00	*KW*	0.00	1.00	0.00	0.00	*KW*	Hom	0.00	1.00	0.00	Hom	0.00	1.00	0.00	Hom
AMNH 81652	*G. gorilla*	*KW*	0.00	1.00	0.00	0.00	*KW*	0.00	1.00	0.00	0.00	*KW*	Hom	0.00	1.00	0.00	Hom	0.00	1.00	0.00	Hom
AMNH 90289	*G. gorilla*	*KW*	0.00	1.00	0.00	0.00	*KW*	0.00	1.00	0.00	0.00	*KW*	Hom	0.00	1.00	0.00	Hom	0.00	1.00	0.00	Hom
AMNH 167335	*G. gorilla*	*KW*	0.00	1.00	0.00	0.00	*KW*	0.00	1.00	0.00	0.00	*KW*	Hom	0.00	1.00	0.00	Hom	0.00	1.00	0.00	Hom
AMNH 167337	*G. gorilla*	*KW*	0.00	0.95	0.00	0.05	*KW*	0.00	0.68	0.02	0.30	*KW*	Hom	0.01	0.99	0.00	Hom	0.01	0.99	0.00	Hom
AMNH 167338	*G. gorilla*	*KW*	0.00	1.00	0.00	0.00	*KW*	0.00	1.00	0.00	0.00	*KW*	Hom	0.00	1.00	0.00	Hom	0.00	1.00	0.00	Hom
AMNH 167339	*G. gorilla*	*KW*	0.00	1.00	0.00	0.00	*KW*	0.00	1.00	0.00	0.00	*KW*	Hom	0.00	1.00	0.00	Hom	0.00	1.00	0.00	Hom
AMNH 167340	*G. gorilla*	*KW*	0.00	1.00	0.00	0.00	*KW*	0.00	1.00	0.00	0.00	*KW*	Hom	0.01	0.99	0.00	Hom	0.02	0.98	0.00	Hom
AMNH 201471	*G. gorilla*	*KW*	0.00	1.00	0.00	0.00	*KW*	0.00	1.00	0.00	0.00	*KW*	Hom	0.00	1.00	0.00	Hom	0.00	1.00	0.00	Hom
AMNH 214103	*G. gorilla*	*KW*	0.00	1.00	0.00	0.00	*KW*	0.00	1.00	0.00	0.00	*KW*	Hom	0.00	1.00	0.00	Hom	0.00	1.00	0.00	Hom
MCZ 17684	*G. gorilla*	*KW*	0.00	1.00	0.00	0.00	*KW*	0.00	1.00	0.00	0.00	*KW*	Hom	0.00	1.00	0.00	Hom	0.00	1.00	0.00	Hom
MCZ 20038	*G. gorilla*	*KW*	0.00	0.93	0.07	0.00	*KW*	0.00	1.00	0.00	0.00	*KW*	Hom	0.33	0.67	0.00	Hom	0.25	0.75	0.00	Hom
MCZ 20039	*G. gorilla*	*KW*	0.00	0.99	0.01	0.00	*KW*	0.00	0.96	0.04	0.00	*KW*	Hom	0.01	0.99	0.00	Hom	0.01	0.99	0.00	Hom
MCZ 20043	*G. gorilla*	*KW*	0.00	1.00	0.00	0.00	*KW*	0.00	1.00	0.00	0.00	*KW*	Hom	0.00	1.00	0.00	Hom	0.00	1.00	0.00	Hom
MCZ 23160	*G. gorilla*	*KW*	0.00	1.00	0.00	0.00	*KW*	0.00	1.00	0.00	0.00	*KW*	Hom	0.00	1.00	0.00	Hom	0.00	1.00	0.00	Hom
MCZ 23162	*G. gorilla*	*KW*	0.00	1.00	0.00	0.00	*KW*	0.00	1.00	0.00	0.00	*KW*	Hom	0.07	0.93	0.00	Hom	0.02	0.98	0.00	Hom
MCZ 26850	*G. gorilla*	*KW*	0.00	0.97	0.00	0.03	*KW*	0.00	0.95	0.01	0.03	*KW*	Hom	0.02	0.98	0.00	Hom	0.02	0.98	0.00	Hom
MCZ 29047	*G. gorilla*	*KW*	0.00	1.00	0.00	0.00	*KW*	0.00	1.00	0.00	0.00	*KW*	Hom	0.00	1.00	0.00	Hom	0.00	1.00	0.00	Hom
MCZ 29049	*G. gorilla*	*KW*	0.00	0.99	0.01	0.00	*KW*	0.00	1.00	0.00	0.00	*KW*	Hom	0.16	0.84	0.00	Hom	0.18	0.82	0.00	Hom
MCZ 37264	*G. gorilla*	*KW*	0.00	1.00	0.00	0.00	*KW*	0.00	1.00	0.00	0.00	*KW*	Hom	0.00	1.00	0.00	Hom	0.00	1.00	0.00	Hom

		a	Positional classification										b	Taxonomic classification								
			DFA					*glmnet*						DFA				*glmnet*				
Specimen	Taxon	Class	*DG*	*KW*	*PG*	*S*	Pred	*DG*	*KW*	*PG*	*S*	Pred	Class	Cerc	Hom	Plat	Pred	Cerc	Hom	Plat	Pred
MCZ 38326	*G. gorilla*	*KW*	0.00	1.00	0.00	0.00	*KW*	0.00	1.00	0.00	0.00	*KW*	Hom	0.00	1.00	0.00	Hom	0.00	1.00	0.00	Hom
MCZ 57482	*G. gorilla*	*KW*	0.00	1.00	0.00	0.00	*KW*	0.00	0.87	0.00	0.13	*KW*	Hom	0.00	1.00	0.00	Hom	0.00	1.00	0.00	Hom
UMMZ 17886	*G. gorilla*	*KW*	0.00	1.00	0.00	0.00	*KW*	0.00	1.00	0.00	0.00	*KW*	Hom	0.00	1.00	0.00	Hom	0.00	1.00	0.00	Hom
AMNH 54089	*G. beringei*	*KW*	0.00	1.00	0.00	0.00	*KW*	0.00	1.00	0.00	0.00	*KW*	Hom	0.00	1.00	0.00	Hom	0.00	1.00	0.00	Hom
AMNH 54090	*G. beringei*	*KW*	0.00	0.84	0.16	0.00	*KW*	0.00	0.91	0.09	0.00	*KW*	Hom	0.05	0.95	0.00	Hom	0.17	0.83	0.00	Hom
AMNH 54091	*G. beringei*	*KW*	0.02	0.83	0.15	0.00	*KW*	0.01	0.85	0.14	0.00	*KW*	Hom	0.09	0.91	0.00	Hom	0.19	0.81	0.00	Hom
AMNH 115609	*G. beringei*	*KW*	0.00	1.00	0.00	0.00	*KW*	0.00	1.00	0.00	0.00	*KW*	Hom	0.00	1.00	0.00	Hom	0.00	1.00	0.00	Hom
NMNH 395636	*G. beringei*	*KW*	0.00	1.00	0.00	0.00	*KW*	0.00	1.00	0.00	0.00	*KW*	Hom	0.00	1.00	0.00	Hom	0.01	0.99	0.00	Hom
NMNH 396934	*G. beringei*	*KW*	0.00	0.94	0.04	0.02	*KW*	0.00	0.98	0.02	0.00	*KW*	Hom	0.05	0.95	0.00	Hom	0.05	0.95	0.00	Hom
NMNH 396935	*G. beringei*	*KW*	0.00	0.97	0.01	0.03	*KW*	0.00	0.95	0.03	0.03	*KW*	Hom	0.00	1.00	0.00	Hom	0.01	0.99	0.00	Hom
NMNH 396937	*G. beringei*	*KW*	0.00	1.00	0.00	0.00	*KW*	0.00	1.00	0.00	0.00	*KW*	Hom	0.00	1.00	0.00	Hom	0.00	1.00	0.00	Hom
NMNH 397351	*G. beringei*	*KW*	0.00	1.00	0.00	0.00	*KW*	0.00	1.00	0.00	0.00	*KW*	Hom	0.00	1.00	0.00	Hom	0.00	1.00	0.00	Hom
NMNH 545041	*G. beringei*	*KW*	0.00	0.99	0.01	0.00	*KW*	0.00	1.00	0.00	0.00	*KW*	Hom	0.00	1.00	0.00	Hom	0.01	0.99	0.00	Hom
MCZ 23182	*G. beringei*	*KW*	0.00	1.00	0.00	0.00	*KW*	0.00	1.00	0.00	0.00	*KW*	Hom	0.00	1.00	0.00	Hom	0.00	1.00	0.00	Hom
MCZ 38017	*G. beringei*	*KW*	0.00	1.00	0.00	0.00	*KW*	0.00	1.00	0.00	0.00	*KW*	Hom	0.00	1.00	0.00	Hom	0.00	1.00	0.00	Hom
AMNH 28252	*P. pygmaeus*	*S*	0.00	0.96	0.03	0.01	***KW***	0.00	0.48	0.14	0.39	***KW***	Hom	0.00	1.00	0.00	Hom	0.01	0.99	0.00	Hom
AMNH 28253	*P. pygmaeus*	*S*	0.00	0.97	0.01	0.02	***KW***	0.00	0.38	0.01	0.61	*S*	Hom	0.00	1.00	0.00	Hom	0.01	0.99	0.00	Hom
NMNH 145301	*P. pygmaeus*	*S*	0.00	0.90	0.00	0.10	***KW***	0.00	0.26	0.00	0.74	*S*	Hom	0.00	1.00	0.00	Hom	0.00	1.00	0.00	Hom
NMNH 145302	*P. pygmaeus*	*S*	0.00	0.63	0.00	0.37	***KW***	0.00	0.00	0.00	1.00	*S*	Hom	0.00	1.00	0.00	Hom	0.00	1.00	0.00	Hom
NMNH 145304	*P. pygmaeus*	*S*	0.00	0.08	0.00	0.92	*S*	0.00	0.00	0.00	1.00	*S*	Hom	0.00	1.00	0.00	Hom	0.00	1.00	0.00	Hom
NMNH 145305	*P. pygmaeus*	*S*	0.00	0.00	0.00	1.00	*S*	0.00	0.00	0.00	1.00	*S*	Hom	0.00	1.00	0.00	Hom	0.00	1.00	0.00	Hom
NMNH 145308	*P. pygmaeus*	*S*	0.00	0.92	0.00	0.08	***KW***	0.00	0.95	0.00	0.05	***KW***	Hom	0.00	1.00	0.00	Hom	0.00	1.00	0.00	Hom
NMNH 145309	*P. pygmaeus*	*S*	0.00	0.15	0.00	0.85	*S*	0.00	0.00	0.00	1.00	*S*	Hom	0.00	1.00	0.00	Hom	0.00	1.00	0.00	Hom
NMNH 145310	*P. pygmaeus*	*S*	0.00	0.01	0.00	0.99	*S*	0.00	0.00	0.00	1.00	*S*	Hom	0.00	1.00	0.00	Hom	0.00	1.00	0.00	Hom
MCZ 37362	*P. pygmaeus*	*S*	0.00	0.22	0.20	0.58	*S*	0.00	0.00	0.27	0.73	*S*	Hom	0.01	0.99	0.00	Hom	0.02	0.98	0.00	Hom
MCZ 37363	*P. pygmaeus*	*S*	0.00	0.00	0.00	1.00	*S*	0.00	0.00	0.00	1.00	*S*	Hom	0.00	1.00	0.00	Hom	0.00	1.00	0.00	Hom
MCZ 37364	*P. pygmaeus*	*S*	0.00	0.00	0.00	1.00	*S*	0.00	0.00	0.00	1.00	*S*	Hom	0.00	1.00	0.00	Hom	0.00	1.00	0.00	Hom
MCZ 37365	*P. pygmaeus*	*S*	0.01	0.01	0.59	0.39	***PG***	0.01	0.00	0.27	0.71	*S*	Hom	0.91	0.09	0.00	**Cerc**	0.99	0.01	0.00	**Cerc**
NMNH 142170	*P. pygmaeus*	*S*	0.00	0.00	0.00	1.00	*S*	0.00	0.00	0.00	1.00	*S*	Hom	0.00	1.00	0.00	Hom	0.01	0.99	0.00	Hom
NMNH 153805	*P. pygmaeus*	*S*	0.00	0.23	0.00	0.77	*S*	0.00	0.04	0.01	0.94	*S*	Hom	0.00	1.00	0.00	Hom	0.00	1.00	0.00	Hom
NMNH 153823	*P. pygmaeus*	*S*	0.00	0.01	0.00	0.99	*S*	0.00	0.00	0.00	1.00	*S*	Hom	0.00	1.00	0.00	Hom	0.00	1.00	0.00	Hom
AMNH 61586	*P. pygmaeus*	*S*	0.00	0.06	0.00	0.94	*S*	0.00	0.00	0.00	1.00	*S*	Hom	0.00	1.00	0.00	Hom	0.00	1.00	0.00	Hom
AMNH 202511	*P. pygmaeus*	*S*	0.00	0.04	0.00	0.96	*S*	0.00	0.00	0.00	1.00	*S*	Hom	0.00	1.00	0.00	Hom	0.00	1.00	0.00	Hom
AMNH 239847	*P. pygmaeus*	*S*	0.00	0.01	0.00	0.99	*S*	0.00	0.00	0.00	1.00	*S*	Hom	0.00	1.00	0.00	Hom	0.00	1.00	0.00	Hom

		a	Positional classification										b	Taxonomic classification								
			DFA					*glmnet*						DFA				*glmnet*				
Specimen	Taxon	Class	*DG*	*KW*	*PG*	*S*	Pred	*DG*	*KW*	*PG*	*S*	Pred	Class	Cerc	Hom	Plat	Pred	Cerc	Hom	Plat	Pred
MCZ 50960	*P. abelii*	*S*	0.00	0.04	0.00	0.96	*S*	0.00	0.00	0.00	1.00	*S*	Hom	0.00	1.00	0.00	Hom	0.00	1.00	0.00	Hom
CMNH HTB1030	*P. abelii*	*S*	0.00	0.00	0.00	1.00	*S*	0.00	0.00	0.00	1.00	*S*	Hom	0.00	1.00	0.00	Hom	0.00	1.00	0.00	Hom
CMNH HTB1055	*P. abelii*	*S*	0.00	0.00	0.00	1.00	*S*	0.00	0.00	0.00	1.00	*S*	Hom	0.00	1.00	0.00	Hom	0.00	1.00	0.00	Hom
CMNH HTB1168	*P. abelii*	*S*	0.00	0.00	0.00	1.00	*S*	0.00	0.00	0.00	1.00	*S*	Hom	0.00	1.00	0.00	Hom	0.00	1.00	0.00	Hom
CMNH HTB1444	*P. abelii*	*S*	0.00	0.00	0.00	1.00	*S*	0.00	0.00	0.00	1.00	*S*	Hom	0.00	1.00	0.00	Hom	0.00	1.00	0.00	Hom
NMNH 143590	*P. abelii*	*S*	0.00	0.01	0.00	0.99	*S*	0.00	0.00	0.00	1.00	*S*	Hom	0.00	1.00	0.00	Hom	0.00	1.00	0.00	Hom
NMNH 143593	*P. abelii*	*S*	0.00	0.23	0.08	0.68	*S*	0.03	0.04	0.73	0.20	***PG***	Hom	0.01	0.99	0.00	Hom	0.01	0.99	0.00	Hom
NMNH 143594	*P. abelii*	*S*	0.00	0.00	0.00	1.00	*S*	0.00	0.00	0.00	1.00	*S*	Hom	0.00	1.00	0.00	Hom	0.00	1.00	0.00	Hom
NMNH 143596	*P. abelii*	*S*	0.00	0.01	0.00	0.99	*S*	0.00	0.00	0.00	1.00	*S*	Hom	0.00	1.00	0.00	Hom	0.00	1.00	0.00	Hom
NMNH 143597	*P. abelii*	*S*	0.00	0.02	0.00	0.98	*S*	0.00	0.00	0.00	1.00	*S*	Hom	0.00	1.00	0.00	Hom	0.00	1.00	0.00	Hom
NMNH 143598	*P. abelii*	*S*	0.00	0.00	0.00	1.00	*S*	0.00	0.00	0.00	1.00	*S*	Hom	0.00	1.00	0.00	Hom	0.00	1.00	0.00	Hom
NMNH 143600	*P. abelii*	*S*	0.00	0.00	0.00	1.00	*S*	0.00	0.00	0.00	1.00	*S*	Hom	0.00	1.00	0.00	Hom	0.00	1.00	0.00	Hom
NMNH 143601	*P. abelii*	*S*	0.00	0.00	0.00	1.00	*S*	0.00	0.00	0.00	1.00	*S*	Hom	0.30	0.70	0.00	Hom	0.44	0.56	0.00	Hom
NMNH 143602	*P. abelii*	*S*	0.00	0.00	0.00	1.00	*S*	0.00	0.00	0.00	1.00	*S*	Hom	0.00	1.00	0.00	Hom	0.00	1.00	0.00	Hom
NMNH 270807	*P. abelii*	*S*	0.00	0.00	0.00	1.00	*S*	0.00	0.00	0.00	1.00	*S*	Hom	0.04	0.96	0.00	Hom	0.09	0.91	0.00	Hom
AMNH 80068	*Hoolock*	*S*	0.01	0.00	0.03	0.96	*S*	0.03	0.00	0.48	0.49	*S*	Hom	0.00	1.00	0.00	Hom	0.02	0.97	0.00	Hom
AMNH 83418	*Hoolock*	*S*	0.00	0.00	0.00	1.00	*S*	0.00	0.00	0.00	1.00	*S*	Hom	0.00	1.00	0.00	Hom	0.01	0.99	0.00	Hom
AMNH 83420	*Hoolock*	*S*	0.00	0.00	0.00	1.00	*S*	0.00	0.00	0.00	1.00	*S*	Hom	0.00	1.00	0.00	Hom	0.00	1.00	0.00	Hom
AMNH 83423	*Hoolock*	*S*	0.00	0.00	0.00	1.00	*S*	0.00	0.00	0.00	1.00	*S*	Hom	0.00	1.00	0.00	Hom	0.00	1.00	0.00	Hom
AMNH 83425	*Hoolock*	*S*	0.00	0.00	0.00	1.00	*S*	0.00	0.00	0.00	1.00	*S*	Hom	0.01	0.99	0.00	Hom	0.09	0.90	0.02	Hom
AMNH 112676	*Hoolock*	*S*	0.00	0.00	0.00	1.00	*S*	0.00	0.00	0.00	1.00	*S*	Hom	0.00	1.00	0.00	Hom	0.00	1.00	0.00	Hom
AMNH 112720	*Hoolock*	*S*	0.00	0.00	0.00	1.00	*S*	0.00	0.00	0.00	1.00	*S*	Hom	0.00	1.00	0.00	Hom	0.00	1.00	0.00	Hom
MCZ 37378	*H. muelleri*	*S*	0.00	0.00	0.00	1.00	*S*	0.00	0.00	0.00	1.00	*S*	Hom	0.00	1.00	0.00	Hom	0.00	1.00	0.00	Hom
MCZ 37380	*H. muelleri*	*S*	0.00	0.00	0.00	1.00	*S*	0.00	0.00	0.00	1.00	*S*	Hom	0.00	1.00	0.00	Hom	0.00	1.00	0.00	Hom
MCZ 37381	*H. muelleri*	*S*	0.00	0.00	0.00	1.00	*S*	0.00	0.00	0.00	1.00	*S*	Hom	0.05	0.95	0.00	Hom	0.05	0.95	0.00	Hom
MCZ 37383	*H. muelleri*	*S*	0.00	0.00	0.00	1.00	*S*	0.00	0.00	0.00	1.00	*S*	Hom	0.00	1.00	0.00	Hom	0.00	1.00	0.00	Hom
MCZ 41417	*H. lar*	*S*	0.00	0.00	0.00	1.00	*S*	0.00	0.00	0.00	1.00	*S*	Hom	0.00	1.00	0.00	Hom	0.01	0.97	0.02	Hom
MCZ 41524	*H. lar*	*S*	0.00	0.00	0.00	1.00	*S*	0.00	0.00	0.00	1.00	*S*	Hom	0.00	1.00	0.00	Hom	0.00	1.00	0.00	Hom
MCZ 41525	*H. lar*	*S*	0.00	0.00	0.00	1.00	*S*	0.00	0.00	0.00	1.00	*S*	Hom	0.01	0.94	0.05	Hom	0.01	0.21	0.78	**Plat**
MCZ 41526	*H. lar*	*S*	0.00	0.00	0.00	1.00	*S*	0.00	0.00	0.00	1.00	*S*	Hom	0.00	1.00	0.00	Hom	0.00	1.00	0.00	Hom
MCZ 41527	*H. lar*	*S*	0.00	0.00	0.00	1.00	*S*	0.00	0.00	0.00	1.00	*S*	Hom	0.01	0.98	0.01	Hom	0.03	0.84	0.13	Hom
MCZ 41529	*H. lar*	*S*	0.00	0.00	0.00	1.00	*S*	0.00	0.00	0.00	1.00	*S*	Hom	0.00	1.00	0.00	Hom	0.00	1.00	0.00	Hom
MCZ 41530	*H. lar*	*S*	0.00	0.00	0.00	1.00	*S*	0.00	0.00	0.00	1.00	*S*	Hom	0.00	0.99	0.01	Hom	0.00	0.90	0.10	Hom
MCZ 41531	*H. lar*	*S*	0.00	0.00	0.00	1.00	*S*	0.00	0.00	0.00	1.00	*S*	Hom	0.01	0.99	0.00	Hom	0.01	0.99	0.00	Hom

		a	Positional classification										b	Taxonomic classification								
			DFA					*glmnet*						DFA				*glmnet*				
Specimen	Taxon	Class	*DG*	*KW*	*PG*	*S*	Pred	*DG*	*KW*	*PG*	*S*	Pred	Class	Cerc	Hom	Plat	Pred	Cerc	Hom	Plat	Pred
MCZ 41532	*H. lar*	*S*	0.00	0.00	0.00	1.00	*S*	0.00	0.00	0.00	1.00	*S*	Hom	0.00	1.00	0.00	Hom	0.00	0.99	0.00	Hom
MCZ 41534	*H. lar*	*S*	0.00	0.00	0.00	1.00	*S*	0.00	0.00	0.00	1.00	*S*	Hom	0.17	0.80	0.03	Hom	0.28	0.47	0.25	Hom
MCZ 41536	*H. lar*	*S*	0.00	0.00	0.00	1.00	*S*	0.00	0.00	0.00	1.00	*S*	Hom	0.01	0.99	0.00	Hom	0.01	0.99	0.00	Hom
AMNH 43063	*H. lar*	*S*	0.00	0.00	0.00	1.00	*S*	0.00	0.00	0.00	1.00	*S*	Hom	0.03	0.97	0.00	Hom	0.04	0.96	0.00	Hom
MCZ 41565	*H. lar*	*S*	0.00	0.00	0.00	1.00	*S*	0.00	0.00	0.00	1.00	*S*	Hom	0.05	0.89	0.06	Hom	0.09	0.78	0.13	Hom
UMMZ 160908	*H. lar*	*S*	0.00	0.00	0.00	1.00	*S*	0.00	0.00	0.00	1.00	*S*	Hom	0.01	0.99	0.00	Hom	0.01	0.99	0.00	Hom
UMMZ 160909	*H. lar*	*S*	0.00	0.00	0.00	1.00	*S*	0.00	0.00	0.00	1.00	*S*	Hom	0.01	0.99	0.00	Hom	0.01	0.99	0.00	Hom
AMNH 106581	*Symphalangus*	*S*	0.00	0.00	0.00	1.00	*S*	0.00	0.00	0.00	1.00	*S*	Hom	0.01	0.99	0.00	Hom	0.01	0.99	0.00	Hom
AMNH 106583	*Symphalangus*	*S*	0.00	0.00	0.00	1.00	*S*	0.00	0.00	0.00	1.00	*S*	Hom	0.00	1.00	0.00	Hom	0.00	1.00	0.00	Hom
MCZ 27867	*Symphalangus*	*S*	0.00	0.00	0.00	1.00	*S*	0.00	0.00	0.00	1.00	*S*	Hom	0.00	1.00	0.00	Hom	0.01	0.99	0.00	Hom
AMNH 51380	*Papio*	*DG*	0.98	0.00	0.02	0.00	*DG*	0.97	0.00	0.03	0.00	*DG*	Cerc	0.15	0.85	0.00	**Hom**	0.20	0.80	0.00	**Hom**
AMNH 52668	*Papio*	*DG*	0.56	0.00	0.44	0.00	*DG*	0.19	0.00	0.81	0.00	***PG***	Cerc	1.00	0.00	0.00	Cerc	1.00	0.00	0.00	Cerc
AMNH 52676	*Papio*	*DG*	0.93	0.00	0.07	0.00	*DG*	0.96	0.00	0.04	0.00	*DG*	Cerc	1.00	0.00	0.00	Cerc	1.00	0.00	0.00	Cerc
AMNH 82097	*Papio*	*DG*	0.33	0.00	0.67	0.00	***PG***	0.22	0.00	0.78	0.00	***PG***	Cerc	1.00	0.00	0.00	Cerc	1.00	0.00	0.00	Cerc
AMNH 187369	*Papio*	*DG*	0.50	0.00	0.50	0.00	***PG***	0.07	0.00	0.93	0.00	***PG***	Cerc	0.99	0.00	0.01	Cerc	1.00	0.00	0.00	Cerc
MCZ 15378	*Papio*	*DG*	0.33	0.00	0.67	0.00	***PG***	0.59	0.00	0.41	0.00	*DG*	Cerc	1.00	0.00	0.00	Cerc	1.00	0.00	0.00	Cerc
NMNH 236976	*Papio*	*DG*	0.53	0.00	0.47	0.00	*DG*	0.69	0.00	0.31	0.00	*DG*	Cerc	1.00	0.00	0.00	Cerc	1.00	0.00	0.00	Cerc
NMNH 239743	*Papio*	*DG*	0.25	0.00	0.75	0.00	***PG***	0.29	0.00	0.71	0.00	***PG***	Cerc	0.97	0.03	0.00	Cerc	0.98	0.02	0.00	Cerc
NMNH 384223	*Papio*	*DG*	0.95	0.00	0.05	0.00	*DG*	0.99	0.00	0.01	0.00	*DG*	Cerc	1.00	0.00	0.00	Cerc	1.00	0.00	0.00	Cerc
NMNH 384227	*Papio*	*DG*	0.82	0.00	0.18	0.00	*DG*	0.75	0.00	0.25	0.00	*DG*	Cerc	0.98	0.02	0.00	Cerc	0.99	0.01	0.00	Cerc
NMNH 384228	*Papio*	*DG*	0.61	0.00	0.39	0.00	*DG*	0.71	0.00	0.29	0.00	*DG*	Cerc	0.97	0.03	0.00	Cerc	0.98	0.02	0.00	Cerc
NMNH 384229	*Papio*	*DG*	0.71	0.00	0.29	0.00	*DG*	0.43	0.00	0.57	0.00	***PG***	Cerc	1.00	0.00	0.00	Cerc	1.00	0.00	0.00	Cerc
NMNH 384234	*Papio*	*DG*	0.11	0.01	0.88	0.00	***PG***	0.07	0.01	0.91	0.00	***PG***	Cerc	0.99	0.01	0.00	Cerc	0.99	0.01	0.00	Cerc
NMNH 384235	*Papio*	*DG*	0.25	0.00	0.75	0.00	***PG***	0.10	0.00	0.90	0.00	***PG***	Cerc	0.98	0.00	0.02	Cerc	1.00	0.00	0.00	Cerc
AMNH 52596	*Lophocebus*	*PG*	0.43	0.00	0.57	0.00	*PG*	0.20	0.00	0.80	0.00	*PG*	Cerc	1.00	0.00	0.00	Cerc	1.00	0.00	0.00	Cerc
AMNH 52609	*Lophocebus*	*PG*	0.24	0.02	0.74	0.00	*PG*	0.25	0.00	0.75	0.00	*PG*	Cerc	0.55	0.45	0.00	Cerc	0.72	0.28	0.00	Cerc
AMNH 52627	*Lophocebus*	*PG*	0.29	0.00	0.71	0.00	*PG*	0.11	0.00	0.89	0.00	*PG*	Cerc	0.79	0.00	0.21	Cerc	1.00	0.00	0.00	Cerc
MCZ 37928	*Lophocebus*	*PG*	0.75	0.00	0.25	0.00	***DG***	0.66	0.01	0.32	0.00	***DG***	Cerc	1.00	0.00	0.00	Cerc	1.00	0.00	0.00	Cerc
AMNH 167678	*Lophocebus*	*PG*	0.10	0.00	0.90	0.00	*PG*	0.06	0.00	0.94	0.00	*PG*	Cerc	1.00	0.00	0.00	Cerc	1.00	0.00	0.00	Cerc
NMNH 578579	*Lophocebus*	*PG*	0.19	0.00	0.81	0.00	*PG*	0.06	0.00	0.94	0.00	*PG*	Cerc	0.95	0.00	0.05	Cerc	1.00	0.00	0.00	Cerc
AMNH 89361	*Mandrillus*	*DG*	0.21	0.00	0.75	0.04	***PG***	0.24	0.00	0.73	0.03	***PG***	Cerc	1.00	0.00	0.00	Cerc	1.00	0.00	0.00	Cerc
AMNH 89362	*Mandrillus*	*DG*	0.87	0.00	0.13	0.00	*DG*	0.90	0.00	0.10	0.00	*DG*	Cerc	0.93	0.07	0.00	Cerc	0.92	0.08	0.00	Cerc
AMNH 89364	*Mandrillus*	*DG*	0.97	0.00	0.03	0.00	*DG*	0.96	0.00	0.04	0.00	*DG*	Cerc	1.00	0.00	0.00	Cerc	1.00	0.00	0.00	Cerc
AMNH 89367	*Mandrillus*	*DG*	0.98	0.00	0.02	0.00	*DG*	1.00	0.00	0.00	0.00	*DG*	Cerc	0.98	0.02	0.00	Cerc	0.99	0.01	0.00	Cerc

		a	Positional classification										b	Taxonomic classification								
			DFA					*glmnet*						DFA				*glmnet*				
Specimen	Taxon	Class	*DG*	*KW*	*PG*	*S*	Pred	*DG*	*KW*	*PG*	*S*	Pred	Class	Cerc	Hom	Plat	Pred	Cerc	Hom	Plat	Pred
AMNH 170364	*Mandrillus*	*DG*	0.71	0.00	0.29	0.00	*DG*	0.77	0.00	0.23	0.00	*DG*	Cerc	0.89	0.11	0.00	Cerc	0.93	0.07	0.00	Cerc
AMNH 170366	*Mandrillus*	*DG*	0.98	0.00	0.02	0.00	*DG*	0.99	0.00	0.01	0.00	*DG*	Cerc	0.66	0.34	0.00	Cerc	0.76	0.24	0.00	Cerc
MCZ 34090	*Mandrillus*	*DG*	0.86	0.00	0.14	0.00	*DG*	0.91	0.00	0.09	0.00	*DG*	Cerc	0.15	0.85	0.00	**Hom**	0.17	0.83	0.00	**Hom**
MCZ 34137	*Mandrillus*	*DG*	0.31	0.04	0.65	0.00	***PG***	0.16	0.01	0.84	0.00	***PG***	Cerc	0.94	0.06	0.00	Cerc	0.89	0.11	0.00	Cerc
MCZ 34177	*Mandrillus*	*DG*	0.79	0.00	0.21	0.00	*DG*	0.65	0.01	0.34	0.00	*DG*	Cerc	1.00	0.00	0.00	Cerc	1.00	0.00	0.00	Cerc
AMNH 52634	*Cercocebus*	*PG*	0.98	0.00	0.02	0.00	***DG***	0.98	0.00	0.02	0.00	***DG***	Cerc	0.99	0.01	0.00	Cerc	0.99	0.01	0.00	Cerc
AMNH 81250	*Cercocebus*	*PG*	0.65	0.00	0.35	0.00	***DG***	0.47	0.00	0.53	0.00	*PG*	Cerc	1.00	0.00	0.00	Cerc	1.00	0.00	0.00	Cerc
AMNH 103654	*Macaca*	*PG*	0.06	0.66	0.29	0.00	***KW***	0.01	0.26	0.73	0.00	*PG*	Cerc	0.31	0.69	0.00	**Hom**	0.22	0.78	0.00	**Hom**
AMNH 103659	*Macaca*	*PG*	0.13	0.00	0.86	0.00	*PG*	0.09	0.00	0.91	0.00	*PG*	Cerc	0.99	0.01	0.00	Cerc	0.99	0.01	0.00	Cerc
AMNH 175460	*Macaca*	*PG*	0.01	0.00	0.99	0.00	*PG*	0.01	0.00	0.99	0.00	*PG*	Cerc	1.00	0.00	0.00	Cerc	1.00	0.00	0.00	Cerc
MCZ 35626	*Macaca*	*PG*	0.08	0.02	0.90	0.00	*PG*	0.02	0.00	0.98	0.00	*PG*	Cerc	0.92	0.08	0.00	Cerc	0.96	0.04	0.00	Cerc
MCZ 35629	*Macaca*	*PG*	0.13	0.00	0.87	0.00	*PG*	0.05	0.00	0.95	0.00	*PG*	Cerc	1.00	0.00	0.00	Cerc	1.00	0.00	0.00	Cerc
MCZ 35652	*Macaca*	*PG*	0.36	0.42	0.22	0.00	***KW***	0.01	0.97	0.02	0.00	***KW***	Cerc	0.59	0.41	0.00	Cerc	0.53	0.47	0.00	Cerc
MCZ 35658	*Macaca*	*PG*	0.22	0.02	0.76	0.00	*PG*	0.06	0.00	0.94	0.00	*PG*	Cerc	0.97	0.03	0.00	Cerc	0.98	0.02	0.00	Cerc
MCZ 35677	*Macaca*	*PG*	0.54	0.01	0.45	0.00	***DG***	0.14	0.01	0.85	0.00	*PG*	Cerc	0.93	0.07	0.00	Cerc	0.94	0.06	0.00	Cerc
MCZ 35681	*Macaca*	*PG*	0.15	0.01	0.83	0.00	*PG*	0.12	0.00	0.86	0.02	*PG*	Cerc	0.96	0.04	0.00	Cerc	0.97	0.03	0.00	Cerc
MCZ 35693	*Macaca*	*PG*	0.17	0.00	0.83	0.00	*PG*	0.04	0.00	0.96	0.00	*PG*	Cerc	0.99	0.00	0.01	Cerc	1.00	0.00	0.00	Cerc
MCZ 35694	*Macaca*	*PG*	0.80	0.03	0.17	0.00	***DG***	0.60	0.00	0.39	0.00	***DG***	Cerc	0.14	0.86	0.00	**Hom**	0.18	0.82	0.00	**Hom**
MCZ 35700	*Macaca*	*PG*	0.50	0.00	0.50	0.00	*PG*	0.20	0.00	0.80	0.00	*PG*	Cerc	0.97	0.03	0.00	Cerc	0.99	0.01	0.00	Cerc
MCZ 35701	*Macaca*	*PG*	0.00	0.11	0.89	0.00	*PG*	0.00	0.00	1.00	0.00	*PG*	Cerc	0.85	0.15	0.00	Cerc	0.89	0.11	0.00	Cerc
MCZ 35729	*Macaca*	*PG*	0.13	0.00	0.87	0.00	*PG*	0.04	0.00	0.96	0.00	*PG*	Cerc	1.00	0.00	0.00	Cerc	1.00	0.00	0.00	Cerc
MCZ 35736	*Macaca*	*PG*	0.22	0.00	0.78	0.00	*PG*	0.12	0.00	0.88	0.00	*PG*	Cerc	1.00	0.00	0.00	Cerc	1.00	0.00	0.00	Cerc
UMMZ 130418	*Macaca*	*PG*	0.02	0.06	0.92	0.00	*PG*	0.00	0.00	1.00	0.00	*PG*	Cerc	0.79	0.21	0.00	Cerc	0.88	0.12	0.00	Cerc
UMMZ 161308	*Macaca*	*PG*	0.52	0.00	0.48	0.00	***DG***	0.24	0.00	0.76	0.00	*PG*	Cerc	0.98	0.02	0.00	Cerc	0.99	0.01	0.00	Cerc
UMMZ 56349	*Macaca*	*PG*	0.01	0.02	0.76	0.21	*PG*	0.01	0.00	0.20	0.79	***S***	Cerc	0.99	0.01	0.00	Cerc	0.99	0.01	0.00	Cerc
AMNH 34709	*Erythrocebus*	*DG*	0.47	0.00	0.53	0.00	***PG***	0.59	0.00	0.41	0.00	*DG*	Cerc	0.99	0.00	0.01	Cerc	1.00	0.00	0.00	Cerc
AMNH 34712	*Erythrocebus*	*DG*	0.28	0.00	0.72	0.00	***PG***	0.53	0.00	0.47	0.00	*DG*	Cerc	0.99	0.00	0.01	Cerc	1.00	0.00	0.00	Cerc
AMNH 34713	*Erythrocebus*	*DG*	0.80	0.00	0.20	0.00	*DG*	0.82	0.00	0.18	0.00	*DG*	Cerc	0.98	0.00	0.02	Cerc	1.00	0.00	0.00	Cerc
AMNH 34714	*Erythrocebus*	*DG*	0.63	0.00	0.37	0.00	*DG*	0.32	0.00	0.68	0.00	***PG***	Cerc	0.93	0.00	0.07	Cerc	0.99	0.00	0.01	Cerc
NMNH 257013	*Erythrocebus*	*DG*	0.68	0.00	0.32	0.00	*DG*	0.78	0.00	0.22	0.00	*DG*	Cerc	1.00	0.00	0.00	Cerc	1.00	0.00	0.00	Cerc
NMNH 399317	*Erythrocebus*	*DG*	0.40	0.00	0.60	0.00	***PG***	0.17	0.00	0.83	0.00	***PG***	Cerc	0.99	0.00	0.01	Cerc	1.00	0.00	0.00	Cerc
NMNH 538311	*Erythrocebus*	*DG*	0.52	0.00	0.48	0.00	*DG*	0.87	0.00	0.13	0.00	*DG*	Cerc	1.00	0.00	0.00	Cerc	1.00	0.00	0.00	Cerc
AMNH 52368	*Cercopithecus*	*PG*	0.87	0.00	0.13	0.00	***DG***	0.75	0.00	0.25	0.00	***DG***	Cerc	0.99	0.00	0.01	Cerc	1.00	0.00	0.00	Cerc
AMNH 52398	*Cercopithecus*	*PG*	0.78	0.00	0.22	0.00	***DG***	0.80	0.00	0.20	0.00	***DG***	Cerc	1.00	0.00	0.00	Cerc	1.00	0.00	0.00	Cerc

		a	Positional classification										b	Taxonomic classification								
			DFA					*glmnet*						DFA				*glmnet*				
Specimen	Taxon	Class	*DG*	*KW*	*PG*	*S*	Pred	*DG*	*KW*	*PG*	*S*	Pred	Class	Cerc	Hom	Plat	Pred	Cerc	Hom	Plat	Pred
AMNH 52401	*Cercopithecus*	*PG*	0.31	0.00	0.69	0.00	*PG*	0.20	0.00	0.80	0.00	*PG*	Cerc	0.99	0.00	0.01	Cerc	1.00	0.00	0.00	Cerc
AMNH 52410	*Cercopithecus*	*PG*	0.51	0.00	0.49	0.00	***DG***	0.29	0.00	0.71	0.00	*PG*	Cerc	1.00	0.00	0.00	Cerc	1.00	0.00	0.00	Cerc
AMNH 82411	*Cercopithecus*	*PG*	0.14	0.00	0.86	0.00	*PG*	0.07	0.00	0.93	0.00	*PG*	Cerc	0.98	0.00	0.02	Cerc	1.00	0.00	0.00	Cerc
AMNH 82412	*Cercopithecus*	*PG*	0.44	0.00	0.56	0.00	*PG*	0.29	0.00	0.71	0.00	*PG*	Cerc	1.00	0.00	0.00	Cerc	1.00	0.00	0.00	Cerc
AMNH 82415	*Cercopithecus*	*PG*	0.20	0.00	0.80	0.00	*PG*	0.66	0.00	0.34	0.00	***DG***	Cerc	0.99	0.01	0.00	Cerc	0.99	0.01	0.00	Cerc
MCZ 37930	*Cercopithecus*	*PG*	0.71	0.00	0.29	0.00	***DG***	0.39	0.00	0.61	0.00	*PG*	Cerc	1.00	0.00	0.00	Cerc	1.00	0.00	0.00	Cerc
MCZ 37934	*Cercopithecus*	*PG*	0.15	0.00	0.85	0.00	*PG*	0.12	0.00	0.88	0.00	*PG*	Cerc	1.00	0.00	0.00	Cerc	1.00	0.00	0.00	Cerc
MCZ 38079	*Cercopithecus*	*PG*	0.84	0.00	0.16	0.00	***DG***	0.91	0.00	0.09	0.00	***DG***	Cerc	1.00	0.00	0.00	Cerc	1.00	0.00	0.00	Cerc
UMMZ 39508	*Cercopithecus*	*PG*	0.65	0.00	0.35	0.00	***DG***	0.72	0.00	0.28	0.00	***DG***	Cerc	0.97	0.03	0.00	Cerc	0.98	0.02	0.00	Cerc
AMNH 27711	*Colobus*	*PG*	0.00	0.02	0.98	0.00	*PG*	0.00	0.02	0.98	0.00	*PG*	Cerc	0.97	0.00	0.03	Cerc	1.00	0.00	0.00	Cerc
AMNH 99468	*Colobus*	*PG*	0.01	0.26	0.59	0.14	*PG*	0.00	0.02	0.61	0.36	*PG*	Cerc	0.16	0.09	0.75	**Plat**	0.50	0.37	0.13	Cerc
NMNH 452621	*Colobus*	*PG*	0.01	0.00	0.99	0.00	*PG*	0.00	0.00	1.00	0.00	*PG*	Cerc	0.14	0.00	0.86	**Plat**	0.65	0.00	0.35	Cerc
AMNH 52223	*Colobus*	*PG*	0.00	0.00	1.00	0.00	*PG*	0.00	0.00	1.00	0.00	*PG*	Cerc	0.79	0.00	0.21	Cerc	0.61	0.00	0.39	Cerc
AMNH 52229	*Colobus*	*PG*	0.00	0.01	0.99	0.00	*PG*	0.00	0.00	1.00	0.00	*PG*	Cerc	0.61	0.00	0.39	Cerc	0.95	0.00	0.05	Cerc
AMNH 52240	*Colobus*	*PG*	0.01	0.00	0.99	0.00	*PG*	0.00	0.00	1.00	0.00	*PG*	Cerc	0.45	0.00	0.55	**Plat**	0.87	0.00	0.13	Cerc
AMNH 52241	*Colobus*	*PG*	0.00	0.01	0.99	0.00	*PG*	0.00	0.00	1.00	0.00	*PG*	Cerc	0.76	0.00	0.24	Cerc	0.97	0.00	0.03	Cerc
AMNH 52248	*Colobus*	*PG*	0.02	0.00	0.98	0.00	*PG*	0.00	0.00	1.00	0.00	*PG*	Cerc	0.13	0.00	0.87	**Plat**	0.47	0.00	0.53	**Plat**
AMNH 187392	*Colobus*	*PG*	0.00	0.02	0.98	0.00	*PG*	0.00	0.01	0.99	0.00	*PG*	Cerc	0.13	0.00	0.87	**Plat**	0.70	0.00	0.30	Cerc
AMNH 52278	*Procolobus*	*PG*	0.02	0.00	0.98	0.00	*PG*	0.01	0.00	0.99	0.00	*PG*	Cerc	0.97	0.00	0.03	Cerc	0.97	0.00	0.03	Cerc
AMNH 52287	*Procolobus*	*PG*	0.02	0.02	0.95	0.00	*PG*	0.04	0.00	0.96	0.01	*PG*	Cerc	0.80	0.16	0.04	Cerc	0.94	0.06	0.00	Cerc
AMNH 52298	*Procolobus*	*PG*	0.08	0.00	0.92	0.00	*PG*	0.16	0.00	0.84	0.00	*PG*	Cerc	0.77	0.00	0.23	Cerc	0.93	0.00	0.07	Cerc
AMNH 52303	*Procolobus*	*PG*	0.02	0.00	0.98	0.00	*PG*	0.03	0.00	0.97	0.00	*PG*	Cerc	0.99	0.00	0.01	Cerc	1.00	0.00	0.00	Cerc
AMNH 52334	*Procolobus*	*PG*	0.01	0.11	0.54	0.34	*PG*	0.01	0.00	0.76	0.23	*PG*	Cerc	0.24	0.76	0.00	**Hom**	0.32	0.68	0.00	**Hom**
MCZ 37943	*Procolobus*	*PG*	0.00	0.81	0.19	0.00	***KW***	0.00	0.35	0.65	0.00	*PG*	Cerc	0.03	0.96	0.00	**Hom**	0.02	0.98	0.00	**Hom**
AMNH 54279	*Procolobus*	*PG*	0.01	0.02	0.97	0.00	*PG*	0.00	0.00	1.00	0.00	*PG*	Cerc	0.82	0.07	0.11	Cerc	0.95	0.03	0.02	Cerc
AMNH 86709	*Procolobus*	*PG*	0.01	0.00	0.99	0.00	*PG*	0.01	0.10	0.89	0.00	*PG*	Cerc	0.99	0.00	0.01	Cerc	0.99	0.00	0.01	Cerc
MCZ 37931	*Procolobus*	*PG*	0.00	0.00	1.00	0.00	*PG*	0.00	0.00	1.00	0.00	*PG*	Cerc	0.53	0.00	0.47	Cerc	0.15	0.00	0.85	**Plat**
MCZ 37932	*Procolobus*	*PG*	0.13	0.00	0.86	0.00	*PG*	0.20	0.00	0.80	0.00	*PG*	Cerc	0.98	0.01	0.01	Cerc	0.99	0.01	0.00	Cerc
MCZ 37933	*Procolobus*	*PG*	0.00	0.00	1.00	0.00	*PG*	0.00	0.00	0.99	0.00	*PG*	Cerc	0.98	0.00	0.02	Cerc	0.99	0.00	0.01	Cerc
MCZ 37935	*Procolobus*	*PG*	0.01	0.00	0.99	0.00	*PG*	0.01	0.00	0.99	0.00	*PG*	Cerc	0.88	0.00	0.12	Cerc	0.93	0.00	0.07	Cerc
MCZ 37936	*Procolobus*	*PG*	0.05	0.00	0.95	0.00	*PG*	0.11	0.00	0.89	0.00	*PG*	Cerc	1.00	0.00	0.00	Cerc	1.00	0.00	0.00	Cerc
AMNH 28255	*Nasalis*	*PG*	0.01	0.00	0.99	0.00	*PG*	0.01	0.00	0.99	0.00	*PG*	Cerc	1.00	0.00	0.00	Cerc	1.00	0.00	0.00	Cerc
AMNH 103668	*Nasalis*	*PG*	0.04	0.00	0.96	0.00	*PG*	0.02	0.00	0.98	0.00	*PG*	Cerc	1.00	0.00	0.00	Cerc	1.00	0.00	0.00	Cerc
AMNH 103669	*Nasalis*	*PG*	0.16	0.00	0.84	0.00	*PG*	0.34	0.00	0.66	0.00	*PG*	Cerc	1.00	0.00	0.00	Cerc	1.00	0.00	0.00	Cerc

		a	Positional classification										b	Taxonomic classification								
			DFA					*glmnet*						DFA				*glmnet*				
Specimen	Taxon	Class	*DG*	*KW*	*PG*	*S*	Pred	*DG*	*KW*	*PG*	*S*	Pred	Class	Cerc	Hom	Plat	Pred	Cerc	Hom	Plat	Pred
AMNH 103670	*Nasalis*	*PG*	0.01	0.00	0.99	0.00	*PG*	0.01	0.00	0.99	0.00	*PG*	Cerc	1.00	0.00	0.00	Cerc	0.99	0.00	0.01	Cerc
AMNH 103671	*Nasalis*	*PG*	0.04	0.00	0.96	0.00	*PG*	0.02	0.00	0.98	0.00	*PG*	Cerc	1.00	0.00	0.00	Cerc	1.00	0.00	0.00	Cerc
AMNH 106272	*Nasalis*	*PG*	0.04	0.00	0.96	0.00	*PG*	0.15	0.00	0.85	0.00	*PG*	Cerc	0.99	0.01	0.00	Cerc	1.00	0.00	0.00	Cerc
AMNH 106273	*Nasalis*	*PG*	0.08	0.00	0.92	0.00	*PG*	0.14	0.00	0.86	0.00	*PG*	Cerc	0.99	0.01	0.00	Cerc	0.99	0.01	0.00	Cerc
AMNH 106274	*Nasalis*	*PG*	0.01	0.00	0.99	0.00	*PG*	0.06	0.00	0.94	0.00	*PG*	Cerc	1.00	0.00	0.00	Cerc	1.00	0.00	0.00	Cerc
AMNH 106275	*Nasalis*	*PG*	0.02	0.00	0.98	0.00	*PG*	0.02	0.00	0.98	0.00	*PG*	Cerc	0.98	0.02	0.00	Cerc	0.99	0.01	0.00	Cerc
MCZ 7099	*Nasalis*	*PG*	0.02	0.00	0.97	0.00	*PG*	0.01	0.00	0.99	0.00	*PG*	Cerc	0.99	0.01	0.00	Cerc	0.99	0.01	0.00	Cerc
MCZ 37325	*Nasalis*	*PG*	0.04	0.00	0.96	0.00	*PG*	0.12	0.00	0.88	0.00	*PG*	Cerc	1.00	0.00	0.00	Cerc	1.00	0.00	0.00	Cerc
MCZ 37329	*Nasalis*	*PG*	0.03	0.00	0.96	0.00	*PG*	0.04	0.00	0.96	0.00	*PG*	Cerc	0.99	0.01	0.00	Cerc	1.00	0.00	0.00	Cerc
MCZ 37342	*Nasalis*	*PG*	0.03	0.00	0.97	0.00	*PG*	0.04	0.00	0.96	0.00	*PG*	Cerc	1.00	0.00	0.00	Cerc	1.00	0.00	0.00	Cerc
MCZ 41554	*Nasalis*	*PG*	0.03	0.00	0.97	0.00	*PG*	0.09	0.00	0.91	0.00	*PG*	Cerc	1.00	0.00	0.00	Cerc	1.00	0.00	0.00	Cerc
MCZ 41555	*Nasalis*	*PG*	0.00	0.00	0.99	0.00	*PG*	0.00	0.00	1.00	0.00	*PG*	Cerc	1.00	0.00	0.00	Cerc	1.00	0.00	0.00	Cerc
MCZ 41556	*Nasalis*	*PG*	0.03	0.00	0.97	0.00	*PG*	0.06	0.00	0.94	0.00	*PG*	Cerc	1.00	0.00	0.00	Cerc	1.00	0.00	0.00	Cerc
MCZ 41560	*Nasalis*	*PG*	0.02	0.00	0.98	0.00	*PG*	0.04	0.00	0.96	0.00	*PG*	Cerc	1.00	0.00	0.00	Cerc	1.00	0.00	0.00	Cerc
AMNH 101504	*Trachypithecus*	*PG*	0.01	0.01	0.87	0.11	*PG*	0.01	0.00	0.97	0.02	*PG*	Cerc	0.57	0.43	0.00	Cerc	0.71	0.29	0.00	Cerc
AMNH 102461	*Trachypithecus*	*PG*	0.01	0.00	0.99	0.00	*PG*	0.00	0.00	1.00	0.00	*PG*	Cerc	0.61	0.01	0.38	Cerc	0.83	0.00	0.17	Cerc
AMNH 106598	*Trachypithecus*	*PG*	0.00	0.03	0.80	0.18	*PG*	0.00	0.00	0.34	0.66	***S***	Cerc	0.99	0.01	0.00	Cerc	0.99	0.01	0.00	Cerc
MCZ 35636	*Trachypithecus*	*PG*	0.01	0.00	0.98	0.00	*PG*	0.00	0.00	1.00	0.00	*PG*	Cerc	0.60	0.00	0.40	Cerc	0.50	0.00	0.50	**Plat**
MCZ 35640	*Trachypithecus*	*PG*	0.00	0.02	0.72	0.26	*PG*	0.00	0.00	0.43	0.57	***S***	Cerc	0.63	0.02	0.35	Cerc	0.91	0.02	0.07	Cerc
MCZ 35675	*Trachypithecus*	*PG*	0.00	0.00	1.00	0.00	*PG*	0.00	0.00	1.00	0.00	*PG*	Cerc	0.96	0.00	0.04	Cerc	0.98	0.00	0.02	Cerc
MCZ 35682	*Trachypithecus*	*PG*	0.06	0.00	0.94	0.00	*PG*	0.04	0.00	0.96	0.00	*PG*	Cerc	1.00	0.00	0.00	Cerc	1.00	0.00	0.00	Cerc
MCZ 35685	*Trachypithecus*	*PG*	0.00	0.00	1.00	0.00	*PG*	0.00	0.00	1.00	0.00	*PG*	Cerc	0.97	0.01	0.02	Cerc	0.98	0.01	0.01	Cerc
MCZ 37387	*Trachypithecus*	*PG*	0.01	0.07	0.92	0.00	*PG*	0.00	0.00	1.00	0.00	*PG*	Cerc	0.86	0.14	0.00	Cerc	0.88	0.12	0.00	Cerc
MCZ 37391	*Trachypithecus*	*PG*	0.01	0.06	0.93	0.00	*PG*	0.00	0.01	0.99	0.00	*PG*	Cerc	0.99	0.01	0.00	Cerc	0.98	0.02	0.00	Cerc
MCZ 37394	*Trachypithecus*	*PG*	0.01	0.00	0.99	0.00	*PG*	0.00	0.00	1.00	0.00	*PG*	Cerc	0.86	0.00	0.14	Cerc	0.98	0.00	0.02	Cerc
MCZ 37396	*Trachypithecus*	*PG*	0.00	0.03	0.96	0.00	*PG*	0.00	0.00	1.00	0.00	*PG*	Cerc	0.91	0.04	0.04	Cerc	0.95	0.03	0.02	Cerc
MCZ 37399	*Trachypithecus*	*PG*	0.00	0.02	0.98	0.00	*PG*	0.00	0.00	1.00	0.00	*PG*	Cerc	0.99	0.01	0.01	Cerc	0.99	0.01	0.00	Cerc
MCZ 37665	*Trachypithecus*	*PG*	0.01	0.00	0.99	0.00	*PG*	0.00	0.00	1.00	0.00	*PG*	Cerc	0.97	0.00	0.03	Cerc	0.98	0.00	0.02	Cerc
MCZ 37671	*Trachypithecus*	*PG*	0.02	0.02	0.96	0.00	*PG*	0.01	0.00	0.99	0.00	*PG*	Cerc	0.95	0.05	0.00	Cerc	0.95	0.05	0.00	Cerc
AMNH 112976	*Trachypithecus*	*PG*	0.01	0.04	0.95	0.00	*PG*	0.01	0.00	0.99	0.00	*PG*	Cerc	0.91	0.09	0.00	Cerc	0.93	0.07	0.00	Cerc
AMNH 112977	*Trachypithecus*	*PG*	0.00	0.02	0.97	0.00	*PG*	0.00	0.00	0.97	0.03	*PG*	Cerc	0.89	0.11	0.00	Cerc	0.93	0.07	0.00	Cerc
AMNH 106599	*Presbytis*	*PG*	0.00	0.00	0.99	0.00	*PG*	0.00	0.01	0.99	0.00	*PG*	Cerc	0.98	0.00	0.02	Cerc	1.00	0.00	0.00	Cerc
AMNH 106606	*Presbytis*	*PG*	0.03	0.00	0.97	0.00	*PG*	0.04	0.00	0.96	0.00	*PG*	Cerc	0.99	0.00	0.01	Cerc	0.97	0.00	0.03	Cerc
AMNH 211527	*Alouatta*	*PG*	0.02	0.00	0.98	0.00	*PG*	0.01	0.00	0.99	0.00	*PG*	Plat	0.97	0.00	0.03	**Cerc**	0.45	0.00	0.55	Plat

		a	Positional classification										b	Taxonomic classification								
			DFA					*glmnet*						DFA				*glmnet*				
Specimen	Taxon		Class	*DG*	*KW*	*PG*	*S*	Pred	*DG*	*KW*	*PG*	*S*	Pred	Class	Cerc	Hom	Plat	Pred	Cerc	Hom	Plat	Pred
AMNH 211528	*Alouatta*		*PG*	0.13	0.00	0.87	0.00	*PG*	0.04	0.00	0.96	0.00	*PG*	Plat	0.89	0.00	0.11	**Cerc**	0.39	0.00	0.61	Plat
AMNH 211531	*Alouatta*		*PG*	0.06	0.00	0.94	0.00	*PG*	0.11	0.00	0.89	0.00	*PG*	Plat	0.99	0.00	0.01	**Cerc**	0.92	0.00	0.08	**Cerc**
AMNH 211532	*Alouatta*		*PG*	0.00	0.00	1.00	0.00	*PG*	0.00	0.00	1.00	0.00	*PG*	Plat	0.00	0.00	1.00	Plat	0.00	0.00	1.00	Plat
AMNH 211535	*Alouatta*		*PG*	0.00	0.00	1.00	0.00	*PG*	0.00	0.00	1.00	0.00	*PG*	Plat	0.05	0.00	0.95	Plat	0.00	0.00	1.00	Plat
AMNH 211542	*Alouatta*		*PG*	0.00	0.00	1.00	0.00	*PG*	0.00	0.00	1.00	0.00	*PG*	Plat	0.01	0.00	0.99	Plat	0.00	0.00	1.00	Plat
AMNH 211543	*Alouatta*		*PG*	0.00	0.00	1.00	0.00	*PG*	0.00	0.00	1.00	0.00	*PG*	Plat	0.10	0.00	0.90	Plat	0.01	0.00	0.99	Plat
AMNH 211544	*Alouatta*		*PG*	0.00	0.00	1.00	0.00	*PG*	0.00	0.00	1.00	0.00	*PG*	Plat	0.00	0.00	1.00	Plat	0.00	0.00	1.00	Plat
AMNH 23333	*Alouatta*		*PG*	0.03	0.00	0.97	0.00	*PG*	0.00	0.00	1.00	0.00	*PG*	Plat	0.01	0.00	0.99	Plat	0.00	0.00	1.00	Plat
AMNH 23342	*Alouatta*		*PG*	0.01	0.00	0.99	0.00	*PG*	0.00	0.00	1.00	0.00	*PG*	Plat	0.00	0.00	1.00	Plat	0.00	0.00	1.00	Plat
AMNH 187999	*Alouatta*		*PG*	0.01	0.00	0.99	0.00	*PG*	0.00	0.00	1.00	0.00	*PG*	Plat	0.00	0.00	1.00	Plat	0.00	0.00	1.00	Plat
AMNH 188006	*Alouatta*		*PG*	0.01	0.00	0.99	0.00	*PG*	0.00	0.00	1.00	0.00	*PG*	Plat	0.00	0.00	1.00	Plat	0.00	0.00	1.00	Plat
AMNH 30193	*Alouatta*		*PG*	0.00	0.00	1.00	0.00	*PG*	0.00	0.00	1.00	0.00	*PG*	Plat	0.01	0.00	0.99	Plat	0.00	0.00	1.00	Plat
AMNH 42313	*Alouatta*		*PG*	0.00	0.00	1.00	0.00	*PG*	0.00	0.00	1.00	0.00	*PG*	Plat	0.00	0.00	1.00	Plat	0.00	0.00	1.00	Plat
AMNH 42316	*Alouatta*		*PG*	0.00	0.00	1.00	0.00	*PG*	0.00	0.00	1.00	0.00	*PG*	Plat	0.00	0.00	1.00	Plat	0.00	0.00	1.00	Plat
AMNH 132790	*Alouatta*		*PG*	0.00	0.00	1.00	0.00	*PG*	0.00	0.00	1.00	0.00	*PG*	Plat	0.00	0.00	1.00	Plat	0.00	0.00	1.00	Plat
MCZ 30436	*Alouatta*		*PG*	0.00	0.04	0.96	0.00	*PG*	0.00	0.00	1.00	0.00	*PG*	Plat	0.01	0.00	0.99	Plat	0.09	0.00	0.91	Plat
MCZ 30437	*Alouatta*		*PG*	0.00	0.00	1.00	0.00	*PG*	0.00	0.00	1.00	0.00	*PG*	Plat	0.00	0.00	1.00	Plat	0.00	0.00	1.00	Plat
MCZ 31694	*Alouatta*		*PG*	0.00	0.03	0.97	0.00	*PG*	0.00	0.00	1.00	0.00	*PG*	Plat	0.28	0.01	0.71	Plat	0.33	0.00	0.67	Plat
MCZ 31695	*Alouatta*		*PG*	0.00	0.48	0.47	0.06	***KW***	0.00	0.03	0.89	0.07	*PG*	Plat	0.00	0.00	1.00	Plat	0.00	0.00	0.99	Plat
MCZ 32160	*Alouatta*		*PG*	0.00	0.69	0.31	0.00	***KW***	0.00	0.62	0.38	0.00	***KW***	Plat	0.00	0.01	0.99	Plat	0.04	0.03	0.94	Plat
MCZ 28735	*Alouatta*		*PG*	0.00	0.00	0.99	0.01	*PG*	0.00	0.00	0.88	0.12	*PG*	Plat	0.00	0.00	1.00	Plat	0.00	0.00	1.00	Plat
UMMZ 116300	*Alouatta*		*PG*	0.00	0.00	1.00	0.00	*PG*	0.00	0.00	1.00	0.00	*PG*	Plat	0.01	0.00	0.99	Plat	0.00	0.00	1.00	Plat
UMMZ 116301	*Alouatta*		*PG*	0.00	0.01	0.99	0.00	*PG*	0.00	0.00	1.00	0.00	*PG*	Plat	0.09	0.00	0.91	Plat	0.08	0.00	0.92	Plat
UMMZ 77301	*Alouatta*		*PG*	0.02	0.00	0.98	0.00	*PG*	0.00	0.00	1.00	0.00	*PG*	Plat	0.00	0.00	1.00	Plat	0.01	0.00	0.99	Plat
UMMZ 124689	*Alouatta*		*PG*	0.00	0.00	1.00	0.00	*PG*	0.00	0.00	1.00	0.00	*PG*	Plat	0.00	0.00	1.00	Plat	0.00	0.00	1.00	Plat
UMMZ 124690	*Alouatta*		*PG*	0.00	0.00	1.00	0.00	*PG*	0.00	0.00	1.00	0.00	*PG*	Plat	0.00	0.00	1.00	Plat	0.00	0.00	1.00	Plat
UMMZ 146506	*Alouatta*		*PG*	0.01	0.00	0.99	0.00	*PG*	0.00	0.00	1.00	0.00	*PG*	Plat	0.00	0.00	1.00	Plat	0.00	0.00	1.00	Plat
UMMZ 63503	*Alouatta*		*PG*	0.04	0.00	0.96	0.00	*PG*	0.01	0.00	0.99	0.00	*PG*	Plat	0.01	0.00	0.99	Plat	0.00	0.00	1.00	Plat
UMMZ 63504	*Alouatta*		*PG*	0.02	0.00	0.97	0.00	*PG*	0.00	0.00	1.00	0.00	*PG*	Plat	0.00	0.00	1.00	Plat	0.01	0.00	0.99	Plat
UMMZ 63511	*Alouatta*		*PG*	0.00	0.00	0.99	0.00	*PG*	0.00	0.00	0.97	0.03	*PG*	Plat	0.04	0.00	0.96	Plat	0.07	0.00	0.93	Plat
UMMZ 63512	*Alouatta*		*PG*	0.00	0.00	1.00	0.00	*PG*	0.00	0.00	1.00	0.00	*PG*	Plat	0.01	0.00	0.99	Plat	0.00	0.00	1.00	Plat
AMNH 28418	*Ateles*		*S*	0.00	0.00	0.99	0.00	***PG***	0.00	0.00	1.00	0.00	***PG***	Plat	0.00	0.00	1.00	Plat	0.00	0.00	1.00	Plat
AMNH 28420	*Ateles*		*S*	0.00	0.00	0.72	0.28	***PG***	0.00	0.00	0.05	0.95	*S*	Plat	0.00	0.00	1.00	Plat	0.00	0.00	1.00	Plat
MCZ 34320	*Ateles*		*S*	0.00	0.00	0.00	1.00	*S*	0.00	0.00	0.00	1.00	*S*	Plat	0.00	0.00	1.00	Plat	0.00	0.00	1.00	Plat

		a	Positional classification										b	Taxonomic classification								
			DFA					*glmnet*						DFA				*glmnet*				
Specimen	Taxon	Class	*DG*	*KW*	*PG*	*S*	Pred	*DG*	*KW*	*PG*	*S*	Pred	Class	Cerc	Hom	Plat	Pred	Cerc	Hom	Plat	Pred
MCZ 34322	*Ateles*	*S*	0.00	0.01	0.23	0.76	*S*	0.00	0.00	0.04	0.96	*S*	Plat	0.01	0.00	0.99	Plat	0.01	0.00	0.99	Plat
MCZ 47269	*Ateles*	*S*	0.00	0.00	0.00	1.00	*S*	0.00	0.00	0.00	1.00	*S*	Plat	0.10	0.53	0.37	**Hom**	0.09	0.61	0.30	**Hom**
UMMZ 116302	*Ateles*	*S*	0.00	0.00	0.01	0.99	*S*	0.00	0.00	0.00	1.00	*S*	Plat	0.00	0.00	1.00	Plat	0.00	0.00	1.00	Plat
NMNH 276631	*Ateles*	*S*	0.01	0.00	0.99	0.00	***PG***	0.00	0.00	0.98	0.02	***PG***	Plat	0.02	0.00	0.98	Plat	0.01	0.00	0.99	Plat
NMNH 276657	*Ateles*	*S*	0.00	0.00	0.00	1.00	*S*	0.00	0.00	0.00	1.00	*S*	Plat	0.00	0.05	0.95	Plat	0.00	0.00	1.00	Plat
UMMZ 63165	*Ateles*	*S*	0.00	0.15	0.63	0.21	***PG***	0.00	0.00	0.20	0.80	*S*	Plat	0.08	0.02	0.89	Plat	0.48	0.08	0.44	**Cerc**
UMMZ 63166	*Ateles*	*S*	0.00	0.06	0.21	0.73	*S*	0.00	0.00	0.03	0.97	*S*	Plat	0.00	0.00	1.00	Plat	0.00	0.00	1.00	Plat
UMMZ 63171	*Ateles*	*S*	0.00	0.00	0.00	1.00	*S*	0.00	0.00	0.00	1.00	*S*	Plat	0.00	0.00	1.00	Plat	0.00	0.00	1.00	Plat
NMNH 244863	*Ateles*	*S*	0.00	0.00	0.06	0.94	*S*	0.00	0.00	0.00	1.00	*S*	Plat	0.01	0.00	0.99	Plat	0.07	0.00	0.93	Plat
NMNH 396348	*Ateles*	*S*	0.00	0.01	0.00	0.99	*S*	0.00	0.00	0.00	1.00	*S*	Plat	0.00	0.06	0.94	Plat	0.00	0.19	0.80	Plat
UMMZ 126129	*Cebus*	*PG*	0.00	0.00	0.96	0.04	*PG*	0.00	0.00	0.74	0.26	*PG*	Plat	0.00	0.00	1.00	Plat	0.00	0.00	1.00	Plat
UMMZ 126130	*Cebus*	*PG*	0.00	0.00	0.92	0.08	*PG*	0.00	0.00	0.63	0.37	*PG*	Plat	0.00	0.00	1.00	Plat	0.00	0.00	1.00	Plat
AMNH 133606	*Cebus*	*PG*	0.02	0.00	0.98	0.00	*PG*	0.00	0.00	1.00	0.00	*PG*	Plat	0.00	0.00	1.00	Plat	0.00	0.00	1.00	Plat
AMNH 133607	*Cebus*	*PG*	0.00	0.00	1.00	0.00	*PG*	0.00	0.00	1.00	0.00	*PG*	Plat	0.00	0.00	1.00	Plat	0.00	0.00	1.00	Plat
AMNH 133608	*Cebus*	*PG*	0.00	0.00	1.00	0.00	*PG*	0.00	0.00	1.00	0.00	*PG*	Plat	0.00	0.00	1.00	Plat	0.00	0.00	1.00	Plat
AMNH 133622	*Cebus*	*PG*	0.00	0.03	0.97	0.00	*PG*	0.00	0.00	1.00	0.00	*PG*	Plat	0.00	0.00	1.00	Plat	0.07	0.00	0.93	Plat
AMNH 133624	*Cebus*	*PG*	0.00	0.00	1.00	0.00	*PG*	0.00	0.00	1.00	0.00	*PG*	Plat	0.00	0.00	1.00	Plat	0.00	0.00	1.00	Plat
AMNH 133626	*Cebus*	*PG*	0.00	0.00	0.99	0.00	*PG*	0.00	0.00	1.00	0.00	*PG*	Plat	0.14	0.00	0.86	Plat	0.82	0.01	0.17	**Cerc**
AMNH 133628	*Cebus*	*PG*	0.02	0.00	0.98	0.00	*PG*	0.00	0.00	0.95	0.05	*PG*	Plat	0.00	0.00	1.00	Plat	0.00	0.00	1.00	Plat
AMNH 133629	*Cebus*	*PG*	0.00	0.00	1.00	0.00	*PG*	0.00	0.00	1.00	0.00	*PG*	Plat	0.02	0.00	0.98	Plat	0.03	0.00	0.97	Plat
AMNH 133631	*Cebus*	*PG*	0.00	0.00	1.00	0.00	*PG*	0.00	0.00	1.00	0.00	*PG*	Plat	0.00	0.00	1.00	Plat	0.00	0.00	1.00	Plat
AMNH 133633	*Cebus*	*PG*	0.00	0.00	1.00	0.00	*PG*	0.00	0.00	1.00	0.00	*PG*	Plat	0.00	0.00	1.00	Plat	0.00	0.00	1.00	Plat
AMNH 133635	*Cebus*	*PG*	0.00	0.00	1.00	0.00	*PG*	0.00	0.00	1.00	0.00	*PG*	Plat	0.00	0.00	1.00	Plat	0.00	0.00	1.00	Plat
AMNH 133637	*Cebus*	*PG*	0.00	0.00	1.00	0.00	*PG*	0.00	0.00	1.00	0.00	*PG*	Plat	0.00	0.00	1.00	Plat	0.00	0.00	1.00	Plat
AMNH 133638	*Cebus*	*PG*	0.00	0.00	1.00	0.00	*PG*	0.00	0.00	1.00	0.00	*PG*	Plat	0.01	0.00	0.99	Plat	0.01	0.00	0.99	Plat
AMNH 133640	*Cebus*	*PG*	0.00	0.00	1.00	0.00	*PG*	0.00	0.00	1.00	0.00	*PG*	Plat	0.00	0.00	1.00	Plat	0.00	0.00	1.00	Plat
AMNH 133654	*Cebus*	*PG*	0.00	0.00	1.00	0.00	*PG*	0.00	0.00	1.00	0.00	*PG*	Plat	0.00	0.00	1.00	Plat	0.00	0.00	1.00	Plat
AMNH 133656	*Cebus*	*PG*	0.00	0.01	0.99	0.00	*PG*	0.00	0.00	1.00	0.00	*PG*	Plat	0.00	0.00	1.00	Plat	0.01	0.00	0.99	Plat
AMNH 133660	*Cebus*	*PG*	0.00	0.08	0.92	0.00	*PG*	0.00	0.00	0.95	0.05	*PG*	Plat	0.01	0.00	0.98	Plat	0.16	0.02	0.82	Plat
AMNH 133662	*Cebus*	*PG*	0.00	0.00	1.00	0.00	*PG*	0.00	0.00	1.00	0.00	*PG*	Plat	0.00	0.00	1.00	Plat	0.00	0.00	1.00	Plat
AMNH 133666	*Cebus*	*PG*	0.01	0.00	0.99	0.00	*PG*	0.00	0.00	1.00	0.00	*PG*	Plat	0.02	0.00	0.98	Plat	0.01	0.00	0.99	Plat
AMNH 133667	*Cebus*	*PG*	0.01	0.00	0.99	0.00	*PG*	0.00	0.00	1.00	0.00	*PG*	Plat	0.06	0.00	0.94	Plat	0.16	0.00	0.84	Plat
AMNH 133668	*Cebus*	*PG*	0.01	0.00	0.99	0.00	*PG*	0.00	0.00	1.00	0.00	*PG*	Plat	0.00	0.00	1.00	Plat	0.00	0.00	1.00	Plat
AMNH 133674	*Cebus*	*PG*	0.00	0.00	1.00	0.00	*PG*	0.00	0.00	1.00	0.00	*PG*	Plat	0.00	0.00	1.00	Plat	0.00	0.00	1.00	Plat

		a	Positional classification									**b**	Taxonomic classification								
			DFA					*glmnet*					DFA					*glmnet*			
Specimen	Taxon	Class	*DG*	*KW*	*PG*	*S*	Pred	*DG*	*KW*	*PG*	*S*	Pred	Class	Cerc	Hom	Plat	Pred	Cerc	Hom	Plat	Pred
AMNH 133677	*Cebus*	*PG*	0.00	0.00	1.00	0.00	*PG*	0.00	0.00	1.00	0.00	*PG*	Plat	0.00	0.00	1.00	Plat	0.00	0.00	1.00	Plat
AMNH 133815	*Cebus*	*PG*	0.01	0.00	0.99	0.00	*PG*	0.00	0.00	1.00	0.00	*PG*	Plat	0.00	0.00	1.00	Plat	0.00	0.00	1.00	Plat
AMNH 133851	*Cebus*	*PG*	0.00	0.00	1.00	0.00	*PG*	0.00	0.00	1.00	0.00	*PG*	Plat	0.00	0.00	1.00	Plat	0.00	0.00	1.00	Plat
AMNH 133862	*Cebus*	*PG*	0.00	0.01	0.97	0.02	*PG*	0.00	0.00	0.98	0.02	*PG*	Plat	0.01	0.00	0.99	Plat	0.16	0.01	0.83	Plat

Chapter 4

Evolutionary history of the hominoid ulnar carpus and its implications for hominin locomotor ancestry

Abstract

The ancestral locomotor repertoire from which hominin bipedalism emerged remains a subject of frequent debate, with multiple competing hypotheses maintaining support among active researchers. This study contributes to this ongoing debate by reconstructing the morphological and locomotor evolution of hominoids based on patterns of morphometric variation in a broad sample of extant and fossil anthropoid carpals, including extant and extinct hominins. In addition to reconstructing adaptive transitions associated with locomotor behavior, I estimate the prevalence of different locomotor behaviors at the origin of nested clades within Hominoidea, including the one we share with *Pan*.

While there is inconsistency of morphological covariation with function and phylogeny among carpal elements, results are consistent in supporting frequent parallelism during hominoid locomotor evolution. This support is strongest as it applies to suspensory behaviors, with the last common ancestors of both apes and great apes predicted to have been far more generalized than any of the clades' extant representatives. The last common ancestor of humans and chimpanzees is also estimated to have lacked adaptations in association with knuckle-walking, providing

further support for the hominin clade having descended from a relatively generalized ancestral morphotype that is not well modeled by any of the surviving hominoid lineages.

Introduction

There has long been uncertainty regarding the ancestral behavioral repertoire from which hominin bipedalism originated, as direct fossil evidence continues to be elusive for the time period when human ancestors are hypothesized to have diverged phylogenetically from other hominoids (>7 Ma; Langergraber *et al.*, 2012; Steiper and Seiffert, 2012). The knuckle walking hypothesis of hominin locomotor ancestry first rose to prominence as evidence supporting a close relationship between humans and apes began to accumulate (Washburn, 1967). A knuckle-walking phase in the ancestry of humans won broader acceptance after molecular confirmation of a *Pan-Homo* clade (e.g., Ruvolo *et al.*, 1991; Ruvolo, 1997), owing to the perceived parsimony of humans having descended from an African ape-like ancestor.

Evidence from the wrist has featured prominently in arguments supporting the knuckle-walking hypothesis (e.g., Richmond and Strait, 2000; Richmond *et al.*, 2001; Begun, 1992, 2004, Orr, 2005; Richmond, 2006; Kivell and Begun, 2007; Williams, 2010). Likewise, many of the challenges to this hypothesis have focused on anatomical, developmental, or postural heterogeneity in the wrists of African ape genera, from which the parallel evolution of this behavior in African ape genera has been inferred (Tuttle, 1967; Inouye, 1992, 1994; Shea and Inouye, 1993; Dainton and Macho, 1999; Inouye and Shea, 2004; Kivell and Schmitt, 2009; Lovejoy *et al.*, 2009a; Patel *et al.*, 2009;

Matarazzo, 2008, 2013; but see Steiper and Young, 2006; Langergraber *et al.*, 2012; Scally *et al.*, 2012).

Alternative hypotheses related to the ancestral locomotor repertoire have varied. An orthograde climber and suspensor entirely lacking in terrestrial behavior but otherwise resembling one or both extant African ape genera has been suggested (e.g., Keith, 1902, 1923; Gregory, 1927; Napier, 1964; Tuttle, 1969, 1974, 1981; Hunt, 1996). Other researchers have envisioned a more generalized heritage including neither knuckle-walking nor suspension, but rather either arboreal bipedalism (e.g., Wolpoff, 1997; Thorpe and Crompton, 2006; Stanford, 2006; Thorpe *et al.*, 2015), perhaps in combination with "compressive orthogrady" (Crompton *et al.*, 2010) or other incipient orthograde behaviors (Harrison, 1991; Ward, 2015), or above-branch pronograde quadrupedalism with occasional bouts of careful climbing and bridging (Lovejoy *et al.*, 2009a). A slightly modified version of the knuckle-walking hypothesis has also been proposed, in which a portion of the adaptation associated with knuckle-walking, or even the transition from a more generalized terrestrial posture, may have occurred in parallel (e.g., Sarmiento, 1988; Gebo, 1992, 1996), the similar genetic and phenotypic variation among the basal members of each branch having led to similarly constrained adaptive responses under similar selective pressures (Roth, 1984; Begun, 2007).

The likelihood of frequent parallelism during hominoid locomotor evolution has been largely supported as the Miocene ape fossil record has grown. Most notably, there are no suspensory adaptations preserved in any of the various catarrhine taxa of sufficient antiquity to be considered ancestral to crown hominoids (e.g., Straus, 1949; Begun, 1993; Rose, 1997; Larson, 1998; Ward, 2015), supporting the homoplastic

acquisition of this behavior in hylobatids and pongines, as has occurred one or more times in each of the other anthropoid superfamilies, namely atelines (e.g., Youlatos, 1996; Jones, 2008) and douc langers (e.g., Byron *et al.*, 2004; Wright *et al.*, 2008; Granatosky, 2015). The presence of orthograde climbing or clambering behaviors in the basal hominoid repertoire remains possible, however, as associated adaptations of sufficient antiquity have been inferred for *Morotopithecus* (Gebo *et al.*, 1997; MacLatchy *et al.*, 2000), and may have been present in *Rangwapithecus* as well (see Chapter 3). The relative ubiquity of more generalized taxa in the early and middle Miocene may indicate a lack of homology between these early locomotor adaptations and those of crown hominoids, however, preserving the possibility of the hominoid LCA having locomoted in a manner more closely resembling palmigrade monkeys than extant hominoids (Lovejoy *et al.*, 2009a).

Suspensory adaptations have been identified in the middle-Miocene hominids *Hispanopithecus* (Almecija *et al.*, 2007; Alba *et al.*, 2010, 2012; Pina *et al.*, 2012; Susanna *et al.*, 2014) and *Rudapithecus* (Kivell and Begun, 2009; Begun, 2015), supplementing those generally accepted to be present in the late Miocene *Oreopithecus* (e.g., Jungers, 1987; Harrison and Rook, 1997; Wunderlich *et al.*, 1999; Russo and Shapiro, 2013; but see Kohler and Moya-Sola, 1997; Moya-Sola *et al.*, 1999, 2005; Rook *et al.*, 1999). Other middle Miocene hominids like *Sivapithecus* and *Pierolapithecus* are generally interpreted to lack suspensory adaptations, however (Rose, 1997; Moya-Sola *et al.*, 2004; Almecija *et al.*, 2009; Hammond *et al.*, 2013; Pina *et al.*, 2014; but see Deane and Begun, 2008, 2010), and the differing mosaics of primitive and derived features of the suspensory Miocene apes, along with their inferred

maintenance of substantial above-branch quadrupedalism (Alba *et al.*, 2012; Tallman *et al.*, 2013), again suggest that the relationship between their suspensory adaptations and those of extant great apes is not homologous in nature (e.g., Rose, 1986; Madar *et al.*, 2002; Moya-Sola *et al.*, 2004; Almecija *et al.*, 2009; Alba *et al.*, 2010). Miocene apes also lack adaptations for knuckle-walking (Harcourt-Smith, 2015), with the possible exception of *Sivapithecus* (Begun and Kivell, 2011), although postcrania from earlier representatives of the *Pan* and *Gorilla* lineages are unknown.

Examination of the presence of morphology associated with non-bipedal modes of locomotion in fossil hominins has also contributed to this debate, as phylogenetic lag is hypothesized to result in ancestral locomotor adaptations being retained in the hominin lineage, perhaps even to the present (Richmond and Strait, 2000; Richmond *et al.*, 2001). A knuckle-walking signal in the wrists of hominins would potentially be particularly informative. While an autapomorphically increased reliance on arboreal behaviors in a branch of the hominin clade is plausible, it would seem less likely for an already terrestrially competent biped to have secondarily acquired a knuckle-walking habit. The detection of knuckle-walking adaptations in hominins would therefore indicate the likely contribution of this behavior to the ancestral locomotor repertoire. Morphology associated with climbing or suspensory behaviors could yet inform the ancestral repertoire, but only if shown to be consistently or increasingly present in hominins of increasing antiquity.

However, there is little agreement on which features constitute adaptations for relevant behaviors, which has prevented consensus on the locomotor affinities of individual hominin species or the presence of temporal trends potentially informing the

ancestral repertoire. For example, the shoulder and forearm of *Australopithecus sediba* (but not the hand and wrist; see Kivell *et al.*, 2011) have been interpreted as adapted for suspension and climbing (Churchill *et al.*, 2013; Rein *et al.*, 2017), and similar inferences have been made for *A. africanus* (McHenry and Berger, 1998; Green *et al.*, 2007) and *H. habilis* (Johanson *et al.*, 1987). The predicted use of derived arboreal behaviors in these species exceeds those inferred for earlier species like *A. afarensis or Ar. ramidus* (Lovejoy *et al.*, 2009a, b), so while potentially evincing the evolvability of these behaviors, are not necessarily germane to reconstructions of positional behavior in the *Pan-Homo* LCA. In contrast, Young and colleagues (2015) argue that human scapulae evolved on a relatively direct path from an ancestral condition resembling *Pan* without notable variance among hominins in accord with locomotor function (but see Almecija, 2016). Meanwhile, Selby and Lovejoy (2017) judge all known hominin scapulae to be similarly nonsuspensory, and instead prefer a narrative in which humans retained the morphology of their generalized ancestors, with apes subsequently acquiring similarly derived morphology in parallel.

This study addresses these uncertainties through a series of morphometric and evolutionary analyses on continuous 3D shape variables derived from a broad sample of extant and fossil anthropoid carpals, including extant and extinct hominins. In addition to reconstructing the evolutionary history of each element's morphology, this study uses the subsets of shape traits identified in Chapter 2 as most diagnostic of suspension, knuckle-walking, and other positional behaviors to test alternative hypotheses related to the homology and homoplasy of hominoid locomotor behaviors. It also presents a reevaluation of functional affinities in the wrists of several hominin species, and

discusses their implications for our understanding of the positional repertoire from which hominin bipedalism emerged.

Table 4.1. Description of shape variables

Metric	Description
CpPx	Capitate proximoradial surface area
CpTd	Capitate trapezoid surface area
CpDn	Capitate dorsal nonarticular surface area
Cp3	Capitate Mc3 surface area
CpHm	Capitate hamate surface area
Cp2	Capitate Mc2 surface area
Cp4	Capitate Mc4 surface area
Cp23A	Interior angle between the Mc2 and Mc3 facets of the capitate
Cp3HmA	Interior angle between Mc3 and hamate facets of the capitate
CpPxA	Interior angle between the proximoradial surface and the hamate facet of the capitate
CpScA	Interior angle between the scaphoid/centrale facet and the dorsal nonarticular surface of the capitate
Cp3SD	Capitate Mc3 facet complexity
CpHmC	Capitate hamate surface concavity
CpHP	Dorsopalmar position of the capitate head
HmPx	Hamate proximomedial surface area
HmCp	Hamate capitate surface area
Hm4	Hamate Mc4 surface area
Hm5	Hamate Mc5 surface area
Hm45A	Interior angle between the Mc5 and Mc4 facets of the hamate
Hm5CpA	interior angle between Mc5 and capitate facets of hamate
Hm4CpA	interior angle between Mc4 and capitate facets of hamate
HmPxA	Interior angle between the proximomedial surface and capitate facet of the hamate
LuDs	Lunate distal surface area
LuTq	Lunate triquetrum surface area
LuSc	Lunate scaphoid/centrale surface area
LuRa	Lunate radius surface area
LuDsTqA	Interior angle between the distal surface and triquetral facet of the lunate
LuDsScA	Interior angle between the distal surface and scaphoid/centrale facet of the lunate
LuScRaA	Interior angle of scaphoid/centrale and radius facets of the lunate
LuTqRaA	Interior angle of triquetrum and radius facets of the lunate
LuCpRaA	Orientation of the radius facet of lunate relative to the first inertial axis of the capitate facet
LuCpC	Lunate capitate surface dorsopalmar concavity
TqHm	Triquetrum hamate facet area
TqLu	Triquetrum lunate facet area
TqPi	Triquetrum pisiform facet area
TqHmPiA	Orientation of pisiform facet of triquetrum relative to hamate facet
TqHmLuA	Interior angle of hamate and lunate facets of the triquetrum
TqLuPiA	Interior angle of lunate and pisiform facets of the triquetrum
Tq1LuA	Orientation of the long axis (first inertial axis) of the triquetrum relative to lunate facet

Materials and methods

Sampling procedure

Scale-free morphometrics (Table 4.1) were extracted from 3D models created from μCT or laser scans of carpal elements from 377 extant and 32 fossil individuals, including 15 hominins (Table 4.2, Table 4.3) using the procedure detailed in Chapter 2. Scans of original specimens were used for *H. naledi*, *A. sediba*, *A. africanus*, and the upper Pleistocene specimens, including *H. floresiensis*. Scan data of *A. afarensis* and the non-hominin fossil sample were derived from high-quality casts. Damage to fossil specimens was virtually reconstructed based on extrapolation from preserved anatomy and comparison to other specimens. In a few cases of severe damage, morphometrics were imputed using a bootstrap-aggregated decision tree algorithm trained on the complete extant and fossil data set of that element. The majority of the human sample is from the Libben collection at Kent State University (Lovejoy *et al.*, 1977; Meindl, *et al.*, 2008), with additional specimens from the Cleveland Museum of Natural History and the American Museum of Natural History. See Table 2.17 and Table 3.18 for the provenience of other extant specimens.

Table 4.2. Extant sample

Taxon	n	♂	♀
Homo sapiens	32	16	16
Pan troglodytes schweinfurthii	10	7	3
Pan troglodytes troglodytes	12	6	6
Pan troglodytes verus	13	7	6
Pan troglodytes ellioti	5	2	3
Pan paniscus	4	2	2
Gorilla gorilla	26	15	11
Gorilla beringei	12	9	3
Pongo pygmaeus	20	9	11
Pongo abelii	15	5	10
Hoolock hoolock	7	3	4
Hylobates muelleri	4	2	2
Hylobates lar	15	9	6
Symphalangus syndactylus	3	1	2
Papio anubis	14	8	6
Lophocebus albigena	6	5	1
Mandrillus sphinx	9	7	2
Cercocebus agilis	2	2	0
Macaca fascicularis	18	11	7
Erythrocebus patas	7	5	2
Cercopithecus mitis	11	7	4
Colobus guereza	9	6	3
Procolobus rufomitratus	13	7	6
Nasalis larvatus	17	9	8
Trachypithecus sp.	17	7	10
Presbytis melalophos	2	1	1
Alouatta sp.	32	13	19
Ateles geoffroyi	14	2	12
Cebus apella	28	20	8
Total n	377	203	174

Table 4.3. Hominin and non-hominin fossil samples

Taxon	Specimen	Elements
Early *Homo sapiens*	Tianyuan	H
	Qafzeh 9	C, H
Homo sapiens neanderthalensis	Kebara 2	C, H
	Shanidar 4	C, H
	Tabun 1	C
	Regourdou 1	H
Homo naledi	UW 101	C, H, L, T (R) L (L)
Homo floresiensis	LB1-45	C
	LB20, LB21+22[a]	C, H
Australopithecus sediba	MH2 UW 88	C, H, L, T (R) C, H (L)
Australopithecus africanus	TM1526	C
Australopithecus afarensis	AL 288-1w	C
	AL 333	C, H
	KNM-WT 22944	C, H, L
	AL 444-3	L
Oreopithecus bambolii	BH 36	H
Sivapithecus parvada	NG 940	H
Sivapithecus indicus	GSP 17119	C
Equatorius africanus	KNM-TH 28860N	H
Afropithecus turkanensis	KNM-WK 18365	C
Rangwapithecus gordoni	KNM-SO 1002[b]	C
Ekembo heseloni	KPS III	C, H, L, T
	KPS VIII C27	C
	KNM-RU 2036	C, H, L, T
Ekembo nyanzae	KNM-RU 15100	L, T
cf. Proconsul africanus	KNM-CA 409[b]	C
	KNM-SO 31245[b]	C
	KNM-SO 31246[b]	C
cf. Dendropithecus macinnesi	KNM-SO 1000[b]	C
	KNM-SO 1001[b]	C
Limnopithecus/Kalepithecus	KNM-MV 4[b]	C
Pliopithecus vindobonensis	YPM30452	C

[a] Digital composite of hamate antimeres; see Orr *et al.*, 2013
[b] Taxonomic allocations from Chapter 3

Shape analysis

Because the fossil sample of each carpal element varies, combined analysis of the four elements was supplemented with independent analysis of each. To aid in characterizing both the absolute variation of sampled morphology as well as that

relative to expectation given known or estimated relationships among sampled taxa, extant and fossil samples were subjected to both standard principal components analysis (PCA), phylogenetic PCA (pPCA; Revell, 2009, 2012). The degree of phylogenetic autocorrelation in each sample was estimated during model fitting; variance in accord with Brownian motion results in a λ (Pagel, 1999) estimate of 1, whereas a pPCA with an estimated λ of 0 is equivalent to a standard PCA.

Locomotor affinities in the human and fossil samples were further explored using discriminant function analysis (DFA), with input consisting of shape variables found to best distinguish among non-human anthropoid positional classes (see Chapter 2 for selection criteria and discussion of the extant sample's *a priori* positional classes). Models were trained using prior probabilities proportional to class size (Sanchez, 1974); humans and fossil specimens were projected into DFA morphospace without influencing its structure using flat priors. Classification accuracy was calculated after 100 repetitions of 10-fold cross validation, again with flat priors. Combined PCA, pPCA, and DFA analyses were performed using a subset of shape variables derived from all four analyzed elements. This subset comprises 14 morphometrics determined in Chapter 2 to be adapted in extant hominoids for either suspension, knuckle-walking, or both.

Analyses incorporating phylogenetic information utilize a molecular phylogeny from version 3 of the 10k Trees Project (Arnold *et al.*, 2010). Fossil taxa were added to the tree in accord with consensus phylogenetic placement and accepted date estimates (Bishop *et al.*, 1969; Bar-Yosef, 1998, Ward *et al.*, 1999; Shang *et al.*, 2007; Harrison, 2010; Peppe *et al.*, 2011; Casanovas-Vilar *et al.*, 2011; Ward *et al.*, 2012; Begun, 2015; Harrison and Rein, 2016; Sutikna *et al.*, 2016; Cote *et al.*, 2016). *Homo naledi* was

estimated at 1 Ma with a divergence date of 2 Ma based on recent inference (Thackeray, 2015; Dembo *et al.*, 2016; Schroeder *et al.*, 2017; [The 236-335 ka date for *H. naledi* (Dirks *et al.*, 2017), revealed during final revisions of this document, is not expected to substantially change any of the reported results]).

Modeling morphological and locomotor evolution

The adaptive landscape during anthropoid evolution was modeled using a multi-regime Ornstein-Uhlenbeck (OU) procedure (Hansen, 1997) implemented in the R package *ouch* (Butler and King, 2004; King and Butler, 2009), via wrapper functions in the R package *surface* (Ingram and Mahler, 2013). OU methods are descended from those using Brownian motion (Einstein, 1905), in which change (d) in a continuous trait (X) over time (t) is modeled as change according to random noise (B) of a given intensity (σ) over time, to wit:

$$dX(t) = \sigma dB(t)$$

OU methods retain these parameters while additionally estimating the contribution of stabilizing selection, thereby modeling change in a continuous trait over time as random change of a given intensity modulated by the estimated rate (α) at which selection has moved it toward, or maintained its position near, an estimated adaptive optimum (θ):

$$dX(t) = \sigma dB(t) + \alpha(\theta - X(t))dt$$

A multi-regime OU model has increased utility in testing evolutionary hypotheses by allowing multiple optima to be identified within a phylogeny, as would be expected in cases of different clades having faced different selective regimes. The *surface*

implementation of this method allows shifts in the rate and direction of adaptive evolution to be identified based on statistical goodness of fit (AICc; Akaike, 1974; Burham and Anderson, 2002), as opposed to choosing the best fit model from among those suggested by the researcher *a priori*. This is done in a two-step process. The "forward pass" sequentially identifies the shift of adaptive regime within the phylogeny that best improves the AICc score until no more can be found. The "backward pass" then iteratively determines the ΔAICc resulting from the pairwise collapse of regimes identified in the forward pass, collapsing the convergent regimes best improving model fit until no more can be found.

Multi-regime OU models were built with phylogenetic PCA scores to account for phylogenetic autocorrelation in assessing the similarity of adaptive regimes among clades. At least two pPCs were used as *surface* inputs in each case; scores from the third pPC were included when warranted by the log-likelihood ratio threshold recommended by Bookstein (2014).

Ancestral state estimation

The morphospace formed by the first two principal components was transformed into phylomorphospace by projecting the phylogeny into it (Rohlf, 2002). The position of each ancestral state (i.e., the internal nodes of the tree) was estimated using a maximum likelihood (ML) approach (Felsenstein, 1985, 1988; Schluter *et al.*, 1997). Standard PCA was used to visualize the absolute morphological diversity across the sample of each element; phylomorphospace plots based on pPCs are available as supplementary material at the end of the chapter.

To further explore the locomotor ancestry of the hominin clade, an additional, less inclusive DFA was performed using the shape variables of each element best distinguishing knuckle-walking from suspension. Phylogenetic trait maps were created from these results to estimate and visualize the process by which these behaviors evolved. This was done by mapping discriminant scores along the axis best separating knuckle-walking and suspension (the second axis for the hamate, the first in all other cases) onto the tips of the phylogeny, estimating ancestral states using the same ML procedure used for phylomorphospace plots, and then estimating the rate of evolution along each branch via interpolation (equation 3 of Felsenstein, 1985; Revell, 2013). In accord with the finding in Chapter 2 that positional behavior is poorly reflected in anthropoid hamate morphology, a less inclusive subset of hamate morphometrics diagnostic of knuckle-walking and suspension could not be identified. Its phylogenetic trait map therefore uses the second discriminant function of its original DFA described in the *Shape analysis* subsection.

Three additional phylogenetic trait maps were created using morphometric subsets derived from all four analyzed elements. The first uses the shape variables best distinguishing suspension from other positional classes, and the second using those best distinguishing knuckle-walking from other positional classes. Finally, to aid in testing the hypothesis that a more generalized form of terrestrial behavior may be homologous in African apes even if knuckle-walking is not, a third combined trait map was created using the shape variables best distinguishing terrestrial and arboreal anthropoids without regard to hand posture.

Results

Capitate

Early and modern human capitates stand apart from those of other extant anthropoids in overall morphology (Fig. 4.1; see also Table 4.4a). Recent hominin taxa fall between the hylobatids and a relatively undifferentiated group of other anthropoids along the first axis, while the second axis distinguishes humans and most fossil hominins from other anthropoids. *H. naledi* in particular is distinguished from all other taxa to a degree approaching that of the human sample. There is little separation between *Pan* and cercopithecoids, and the *Pan-Homo* LCA is reconstructed as being most similar to *Mandrillus*, and nearest *A. africanus* of the fossil sample. The great ape LCA meanwhile is not estimated to have substantially evolved since the hominoid LCA, with both positioned near *Pongo pygmaeus*, *Nasalis*, *Afropithecus*, and *S. indicus.* The anthropoid LCA (labeled “root” in phylomorphospace) is nearest *E. heseloni*, and the *Alouatta* centroid of the extant sample.

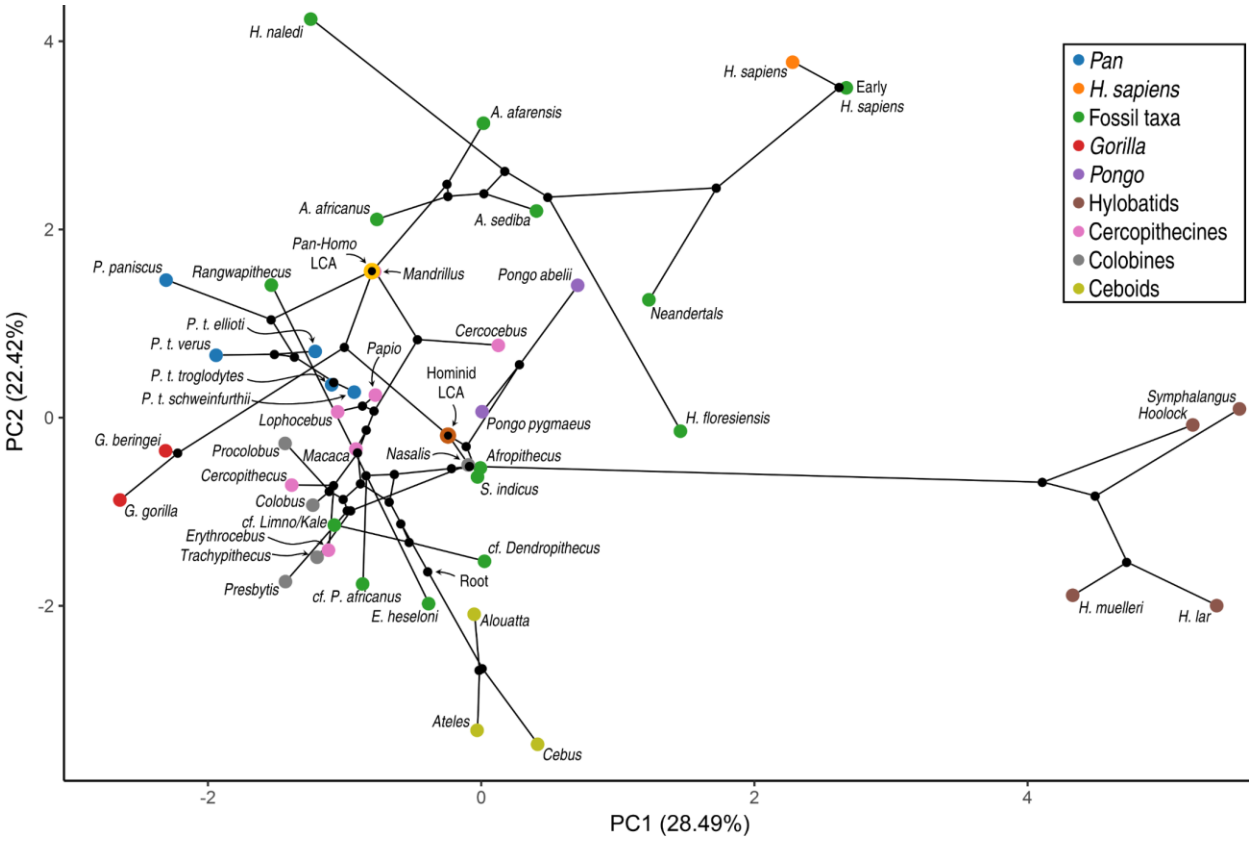

Fig. 4.1. Phylomorphospace representing the evolutionary history of anthropoid capitate morphology. The phylogeny is projected onto the first two principal components of all extant and fossil capitate shape variables, with ancestral states estimated via maximum likelihood. *Pan-Homo* and great ape LCAs are highlighted. See Table 4.4a for eigenvalues.

The multi-regime OU model (Fig. 4.2) estimates the hylobatid and hominid lineages to have adaptive diverged shortly after their phylogenetic split. Both clades are estimated to have transitioned away from the ancestral regime shared by the non-hominoids and stem hominoids of the sample other than *R. gordoni* (KNM-SO 1002; see Chapter 3), in which there was an adaptive transition after branching from the other early Miocene hominoids of the sample. *Pan* and *Pongo* are estimated to have maintained the ancestral hominid regime, while *Gorilla* shifted from the hominid regime after their divergence from the *Pan-Homo* lineage. The hominins are estimated to have followed suit in shifting away from the ancestral hominid regime after branching from

Pan, with another transition leading to *H. floresiensis* and Neandertals, and a third and final adaptive shift in the hominin clade occurring as recent *H. sapiens* converged toward (without approaching) the adaptive optimum of hylobatids (their similar recent trajectory is more apparent in pPCA phylomorphospace; see Fig. 4.28).

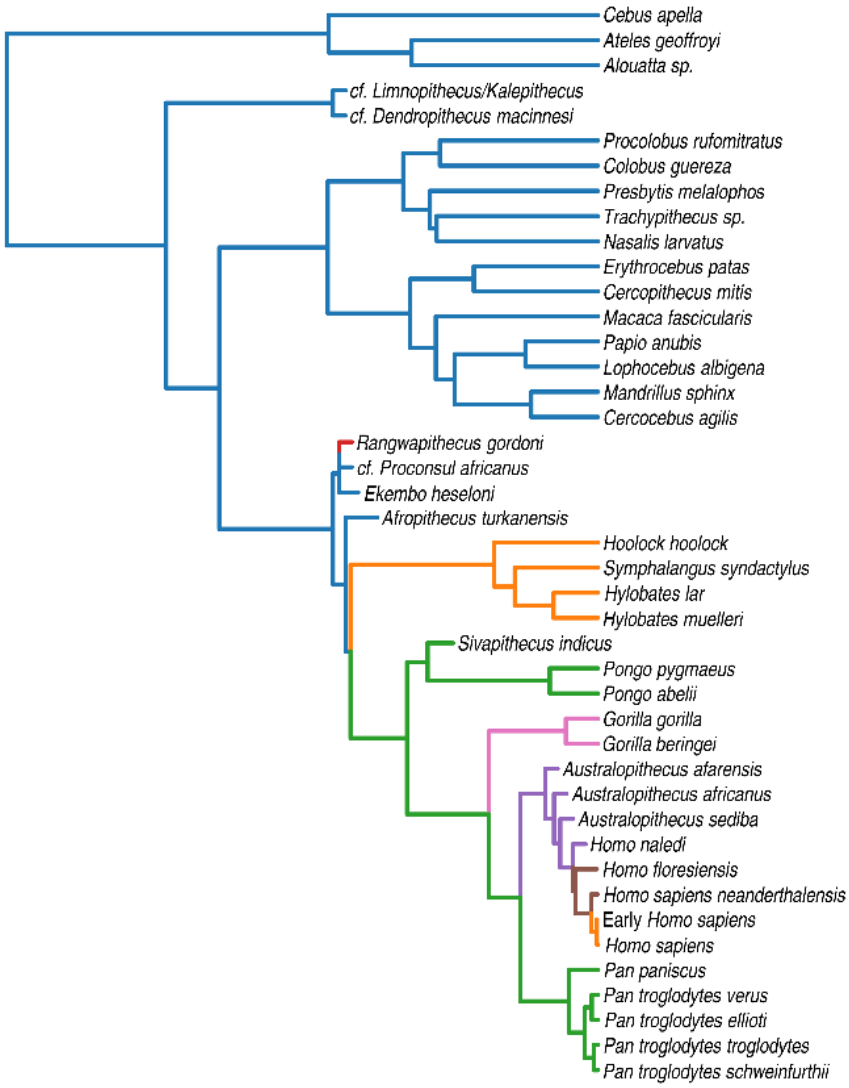

Fig. 4.2. Estimated adaptive regimes during anthropoid capitate evolution. Adaptive optima and evolutionary trajectories are based on the first three phylogenetic principal components of all capitate shape variables, accounting for 59.5% of the variation among sampled extant and fossil taxa (see Fig. 4.28 and Table 4.5a). Branches are colored according to adaptive regime; the shared regime of hylobatids and recent hominins reflects convergent similarity of adaptive optima.

Table 4.4. PCA eigenvalues of individual elements

a Capitate			**b** Hamate			**c** Lunate			**d** Triquetrum		
	PC1	PC2		PC1	PC2		PC1	PC2		PC1	PC2
CpPx	-0.35	0.19	HmPx	0.39	0.04	LuDs	-0.33	-0.28	TqHm	-0.39	-0.14
CpTd	0.16	0.39	HmCp	-0.35	-0.30	LuTq	-0.28	0.38	TqLu	-0.53	0.13
CpDn	0.16	0.40	Hm4	-0.32	0.12	LuSc	0.41	0.05	TqPi	-0.09	0.62
Cp3	-0.26	-0.26	Hm5	-0.24	0.50	LuRa	-0.43	0.12	TqHmPiA	-0.43	-0.37
CpHm	0.09	-0.38	Hm45A	0.12	-0.64	LuDsTqA	0.40	-0.26	TqHmLuA	-0.34	0.14
Cp2	-0.10	-0.04	Hm5CpA	0.46	0.03	LuDsScA	-0.38	0.25	TqLuPiA	0.50	0.00
Cp4	0.23	-0.39	Hm4CpA	0.40	0.44	LuScRaA	0.19	0.37	Tq1LuA	0.06	-0.65
Cp23A	0.27	0.34	HmPxA	-0.43	0.18	LuTqRaA	-0.23	-0.42			
Cp3HmA	-0.34	0.20				LuCpRaA	0.24	0.29			
CpPxA	-0.38	0.14				LuCpC	-0.01	-0.50			
CpScA	-0.31	-0.22									
Cp3SD	-0.20	-0.17									
CpHmC	-0.41	0.16									
CpHP	0.21	-0.05									

In DFA morphospace (Fig. 4.3), most humans and fossil specimens show the greatest functional resemblance to pronograde monkeys. The human sample is classified among them with high confidence, with similar mean posterior probabilities for palmigrady and digitigrady (see Table 4.12a). Non-hominin fossils assigned to other classes include *Rangwapithecus*, classified as a knuckle-walker, and the two specimens allocated to *cf. Dendropithecus* in the previous chapter, which are estimated along with *S. indicus* (*contra* Begun and Kivell, 2011) as suspensors.

It is notable that of the four taxa estimated to be most similar to the hominid LCA in overall morphology (Fig. 4.1), *S. indicus* and *Pongo pygmaeus* are suspensors, while *Afropithecus* and *Nasalis* are palmigrade quadrupeds. This potentially demonstrates the process by which functional adaptation is often thought to occur, as selected features are subtly modified in response to selection while maintaining a broadly similar morphological pattern born of shared ancestry (Lovejoy *et al.* 1999, Hamrick 1999).

Hominin capitates not grouping with extant pronograde monkeys include those of *H. floresiensis*, which plot in the area of overlap between the *Pan* and *Pongo* samples in line with previous analyses of this hominin's primitive carpal morphology (Tocheri *et al.*, 2007; Orr *et al.*, 2013). They are classified as knuckle-walkers along with two of the three Neandertals (Shanidar 4 and Tabun 1) as well as AL 288-1. The specimen attributed to *A. africanus* plots near the 80% CI of the *Pongo* sample somewhat further removed from the African apes, but although it is assigned the highest suspensory probability of the hominins it is also classified among the knuckle-walkers.

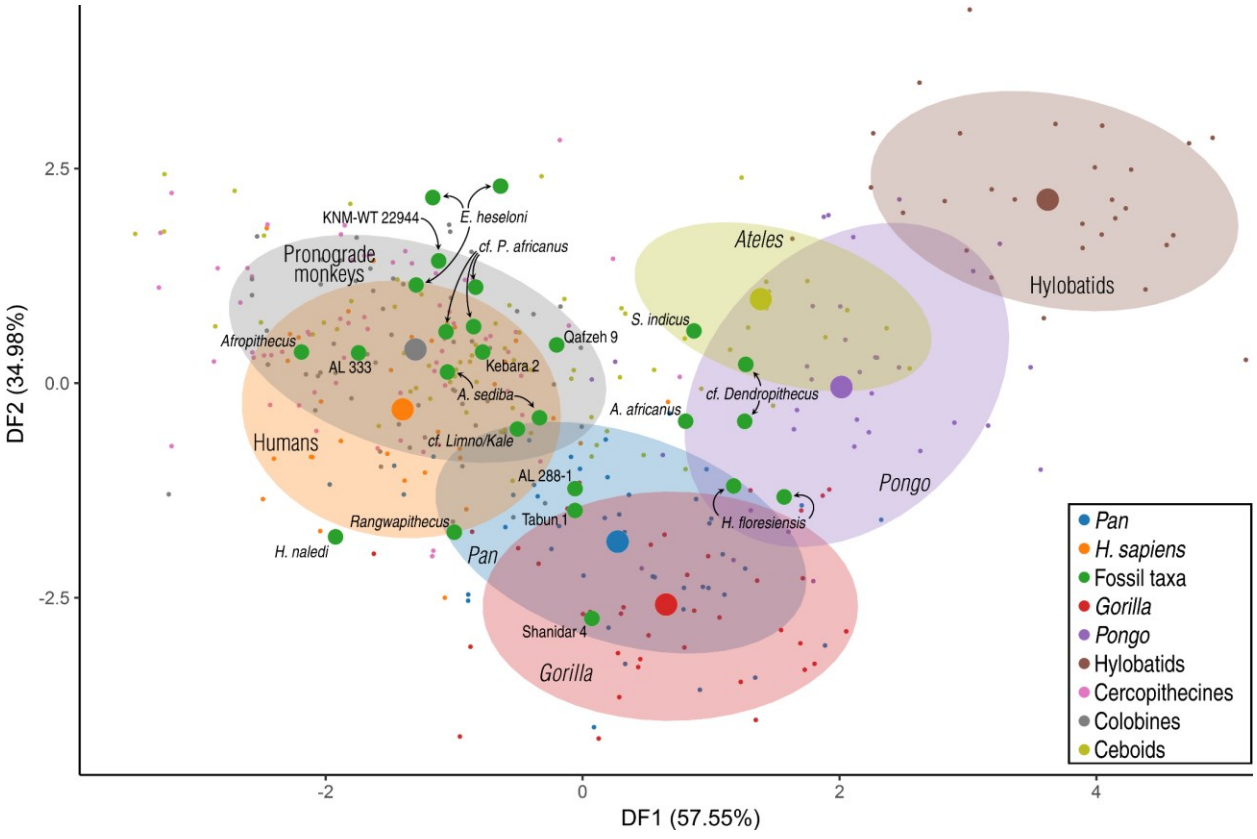

Fig. 4.3. Discriminant function analysis of seven functionally diagnostic shape variables of the capitate. See Chapter 2 for selection criteria, Table 4.6a for variables and scaling, Table 4.9 for accuracy metrics, and Table 4.12a for predictions and posterior probabilities of humans and fossil specimens. Small and medium points represent extant and fossil observations, respectively. Large points represent group means; shaded ellipses are 80% confidence intervals.

The capitate's phylogenetic trait map (Fig. 4.4, Table 4.7a) effectively distinguishes suspensors from other anthropoids, and estimates the LCAs of humans with *Pan*, *Gorilla*, and *Pongo* to have all lacked a degree of suspensory adaptation approaching those of extant suspensors. This model does not effectively distinguish knuckle-walkers from pronograde monkeys, however, and therefore lacks utility in estimating the evolution of terrestriality.

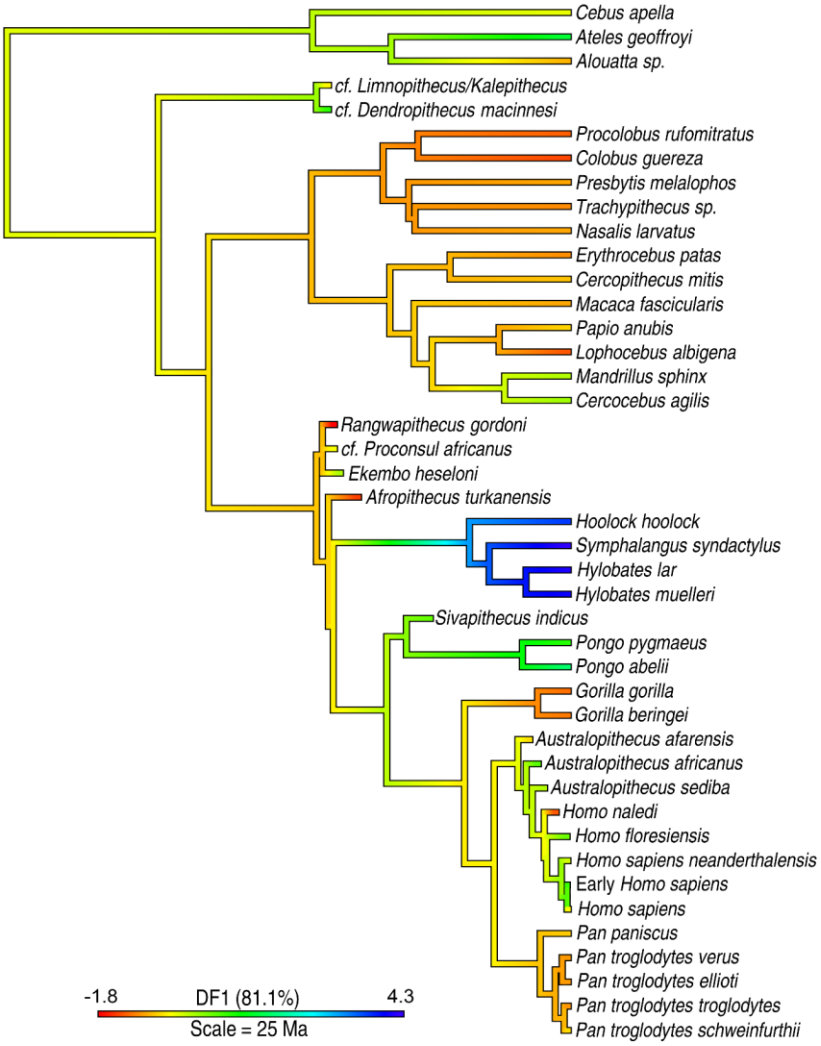

Fig. 4.4. Estimated anthropoid locomotor evolution based on three capitate shape variables identified in Chapter 2 as best distinguishing knuckle-walking and suspension. Bluer hues represent increasing suspensory specialization. Ancestral states estimated via maximum likelihood. See Table 4.7a for variables and scaling.

Table 4.5. Phylogenetic PCA eigenvalues of individual elements

a Capitate			**b** Hamate			**c** Lunate			**d** Triquetrum		
	PC1	PC2		PC1	PC2		PC1	PC2		PC1	PC2
CpPx	-0.09	0.31	HmPx	0.44	0.13	LuDs	-0.18	-0.28	TqHm	-0.33	-0.07
CpTd	0.38	0.18	HmCp	-0.28	0.41	LuTq	0.22	0.56	TqLu	-0.03	-0.14
CpDn	0.33	0.24	Hm4	-0.33	0.28	LuSc	-0.02	-0.23	TqPi	-0.57	-0.23
Cp3	-0.44	-0.18	Hm5	-0.19	0.06	LuRa	-0.33	0.43	TqHmPiA	0.34	0.00
CpHm	0.07	-0.55	Hm45A	0.36	0.76	LuDsTqA	0.22	-0.18	TqHmLuA	0.41	-0.58
Cp2	0.11	0.17	Hm5CpA	0.46	0.05	LuDsScA	-0.52	0.35	TqLuPiA	-0.46	0.22
Cp4	0.12	-0.25	Hm4CpA	0.29	-0.40	LuScRaA	0.59	0.04	Tq1LuA	0.25	0.74
Cp23A	0.36	0.01	HmPxA	-0.40	0.06	LuTqRaA	-0.34	-0.33			
Cp3HmA	-0.19	0.39				LuCpRaA	-0.16	-0.09			
CpPxA	-0.21	0.31				LuCpC	-0.10	-0.32			
CpScA	-0.17	0.09									
Cp3SD	-0.39	-0.24									
CpHmC	-0.20	0.20									
CpHP	0.28	-0.20									

Hamate

In contrast to the 8-regime model fit to the capitate data, the best-fit OU model for the hamate (Fig. 4.6) finds only three. The ancestral regime is estimated to have been maintained across nearly the entire anthropoid clade, with most variation occurring within clades rather than between them (Fig. 4.5, Fig. 4.29). The exceptions to this are found among the hylobatids, as well as *Oreopithecus*, which is estimated to have converged with them toward a highly distinct optimum.

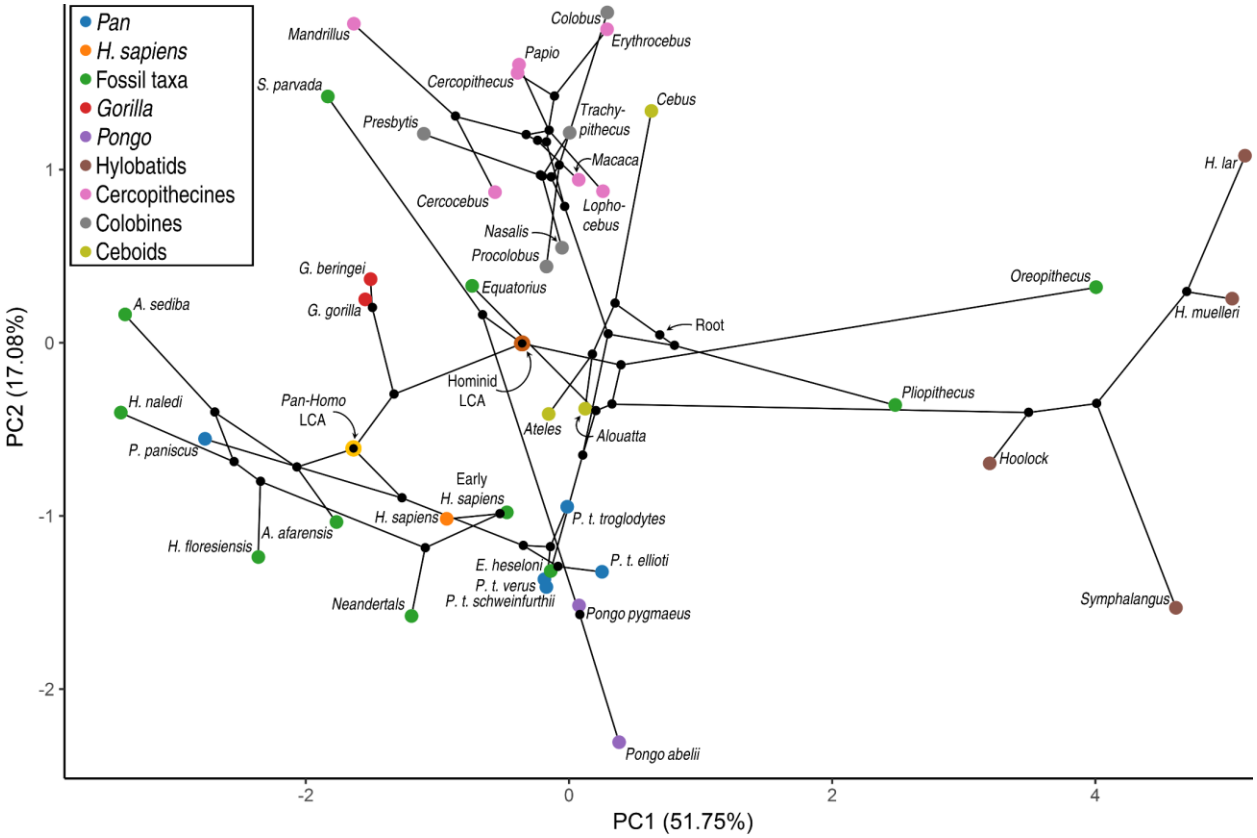

Fig. 4.5. Phylomorphospace representing the evolutionary history of anthropoid hamate morphology. The phylogeny is projected onto the first two principal components of all extant and fossil hamate shape variables, with ancestral states estimated via maximum likelihood. *Pan-Homo* and great ape LCAs are highlighted. See Table 4.4b for eigenvalues

Pliopithecus also seems to have converged with hylobatids, albeit to a somewhat lesser degree and from a more proximate ancestral node than *Oreopithecus*. Bonobos, meanwhile, diverge sharply from the relatively homogenous chimpanzee subspecies. Positioned in the intervening space are humans, most of the hominins, and the reconstructed *Pan-Homo* LCA. The only adaptive shift identified by the OU model in the sampled hamate variation outside the specialized suspensors s a recent shift among upper Pleistocene hominins, which, as is evident in phylomorphospace, are estimated to have come to secondarily resemble extant chimpanzees and orangutans, the latter also estimated to have converged with chimpanzees after branching from an ancestor

more like *Equatorius* and extant pronograde monkeys. This ancestral estimate is influenced by *S. parvada*, which, contrary to the capitate of *S. indicus*, is found to be substantially derived relative to the hominid LCA, with a trajectory opposite that of its presumed pongine relatives.

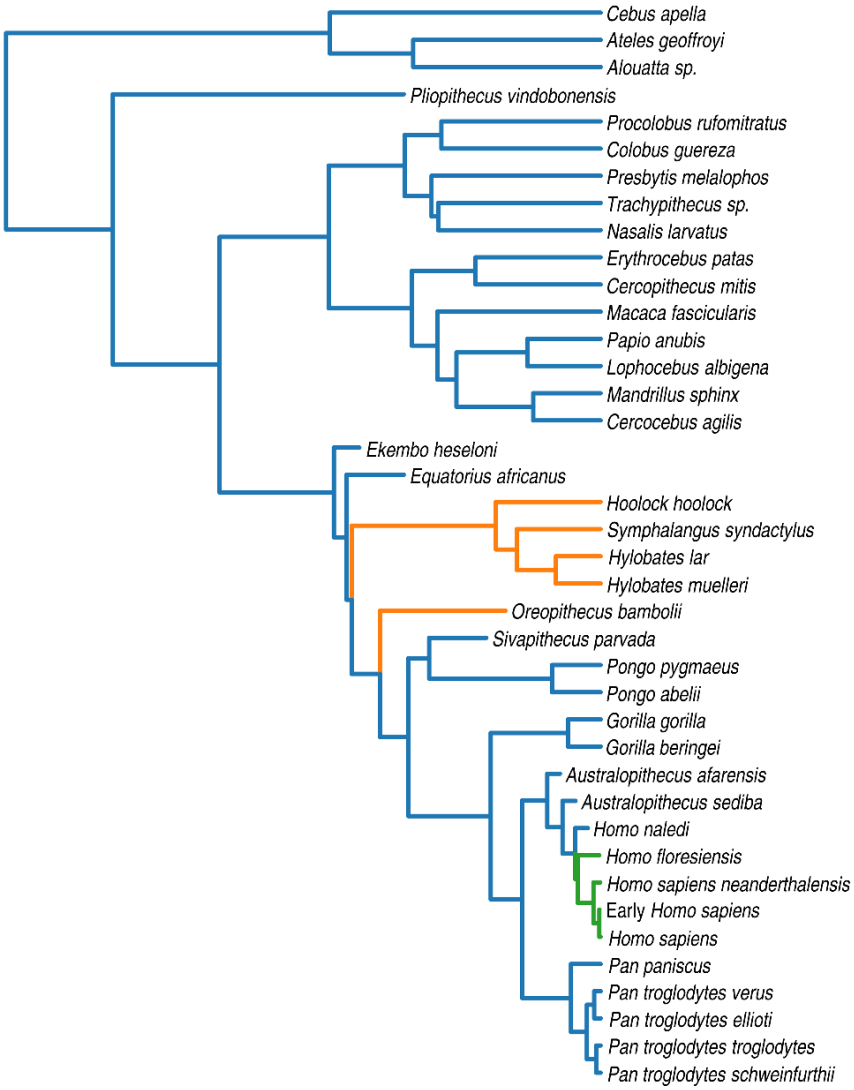

Fig. 4.6. Estimated adaptive regimes during anthropoid hamate evolution, based on the first two pPCs of all hamate shape variables, representing 66.6% of sampled variation (see Fig. 4.29 and Table 4.5b). Branches are colored according to adaptive regime; most anthropoids are estimated to have retained their ancestral adaptive regime.

As noted in Chapter 2, locomotor function is only poorly reflected in the hamate. In DFA morphospace (Fig. 4.7), most humans and fossil specimens group nearest to *Gorilla*, although a few fossil hominins are adjacent only to the outliers of extant hominid groups in the knuckle-walking region of morphospace. Consistent with the other hamate shape analyses, the *Oreopithecus* and *Pliopithecus* specimens are classified as suspensory (Table 4.12b). All other fossil specimens are assigned to the knuckle-walking class with varying levels of confidence.

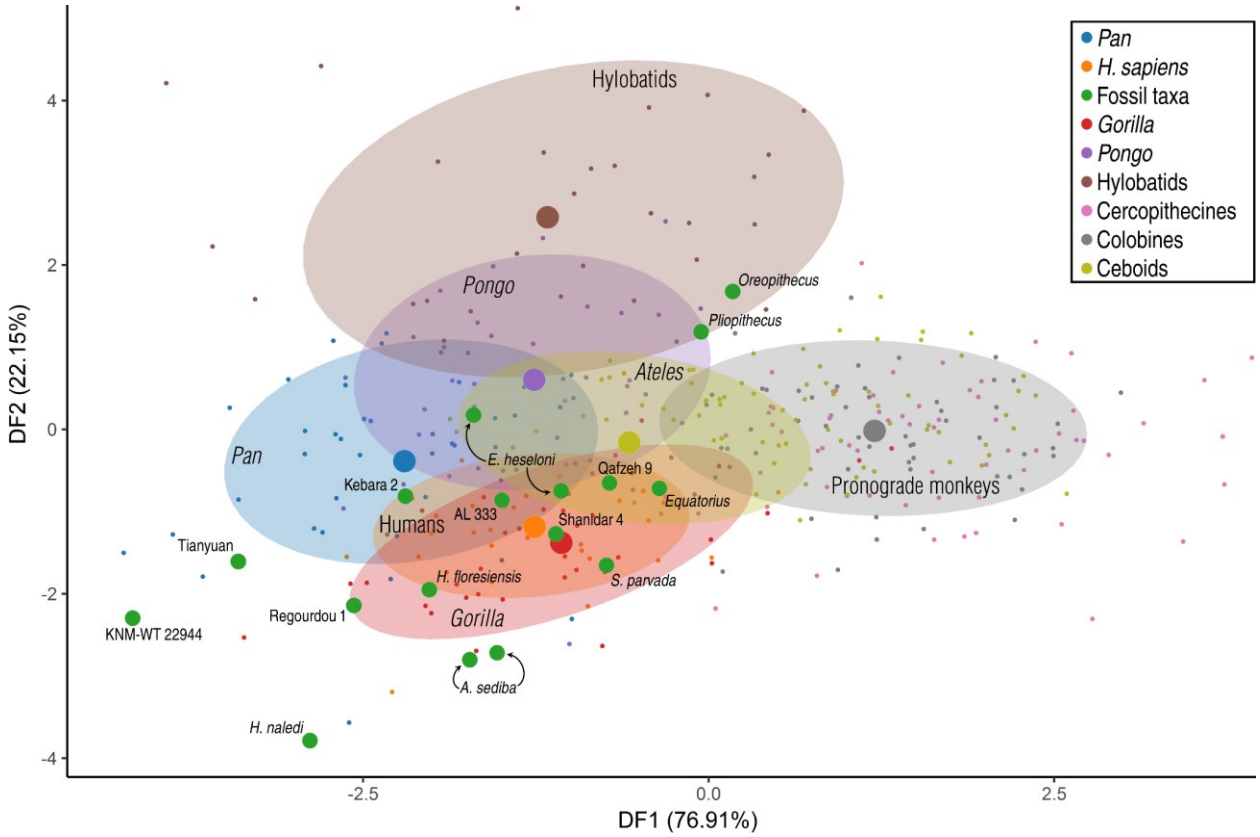

Fig. 4.7. Discriminant function analysis of five functionally diagnostic shape variables of the hamate. See Chapter 2 for selection criteria, Table 4.6b for variables and scaling, Table 4.9 for accuracy metrics, and Table 4.12b for predictions and posterior probabilities of humans and fossil specimens. Small and medium points represent extant and fossil observations, respectively. Large points represent group means; shaded ellipses are 80% confidence intervals.

While the relative lack of functionally-related hamate covariance outside of the specialized suspensors renders other functional observations of dubious value, there is again a notable discrepancy between the overall morphology of *Sivapithecus* and its DFA classification. In this case, *S. parvada* is estimated to most resemble pronograde monkeys in overall morphology, which belies its classification as a knuckle-walker. This is the expected result for a taxon that has undergone homoplastic adaptation for knuckle-walking within a primitive, monkey-like morphological template, which, unlike the capitate results, would be consistent with the hypothesized knuckle-walking habit of this genus (Begun and Kivell, 2011). However, also unlike the *S. indicus* capitate, which was estimated to closely resemble the hominid LCA, the larger and better-preserved *S. parvada* hamate is estimated to have sharply diverged from both the hominid LCA and the extant great ape lineages in overall morphology (Fig. 4.5, Fig. 4.29) at the same as it would have been adapting to knuckle-walking. Given the broad conservation of hamate morphology and the random nature of much of its variation across most of the sample, along with the contradictory functional signal of the *Sivapithecus* capitate, this knuckle-walking affinity in *S. parvada* may not merit further consideration absent additional corroboration

Unlike the other analyzed carpal elements, knuckle-walkers and suspensors are best distinguished from each other by the second discriminant function, accounting for only 22% of the variation, and then only poorly. When mapped onto the phylogeny (Fig. 4.8, Table 4.6b [DF2]), there is again very little differentiation outside of the hylobatids and convergent fossil specimens. The *Pan-Homo* and hominine LCAs fall outside the range of extant suspensors but within the ranges of all other positional categories, while

the estimated hominid LCA falls within the range of every extant group other than hylobatids.

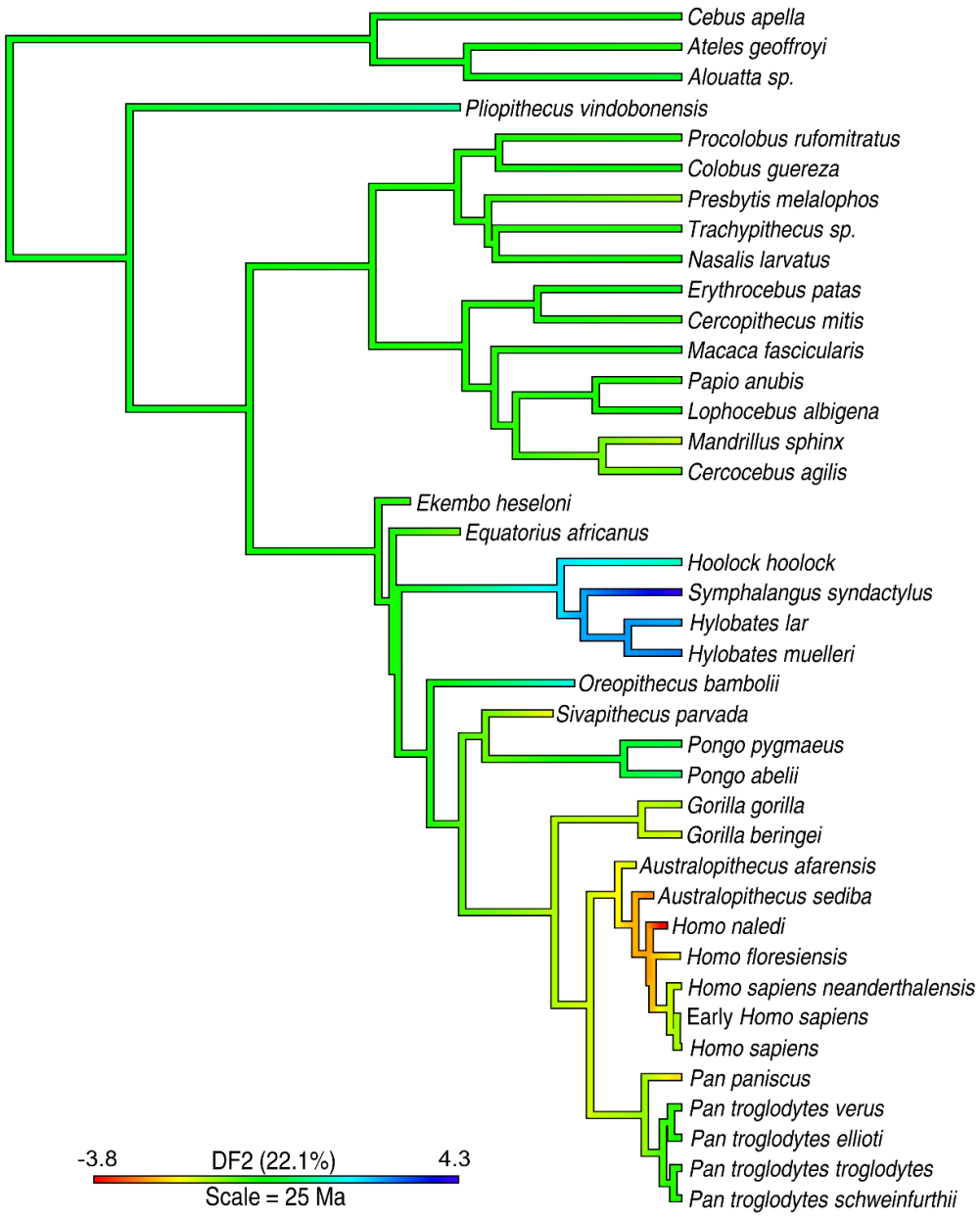

Fig. 4.8. Estimated locomotor evolution based on five hamate shape variables related to locomotor behavior. Bluer hues represent increasing suspensory specialization. Ancestral states estimated via maximum likelihood. See Table 4.6b (DF2) for variables and scaling.

Lunate

The overall morphology of the lunate covaries most closely with phylogeny of the elements analyzed here (Fig. 4.9). Humans and other hominins plot nearest other hominines, while *Ekembo* specimens, as seen in the capitate but unlike the hamate, most closely resemble sampled platyrrhines. As with the capitate and hamate, *H. naledi* is found to be more similar to *A. afarensis* than to the *H. sapiens* mean (*contra* Kivell *et al.*, 2015).

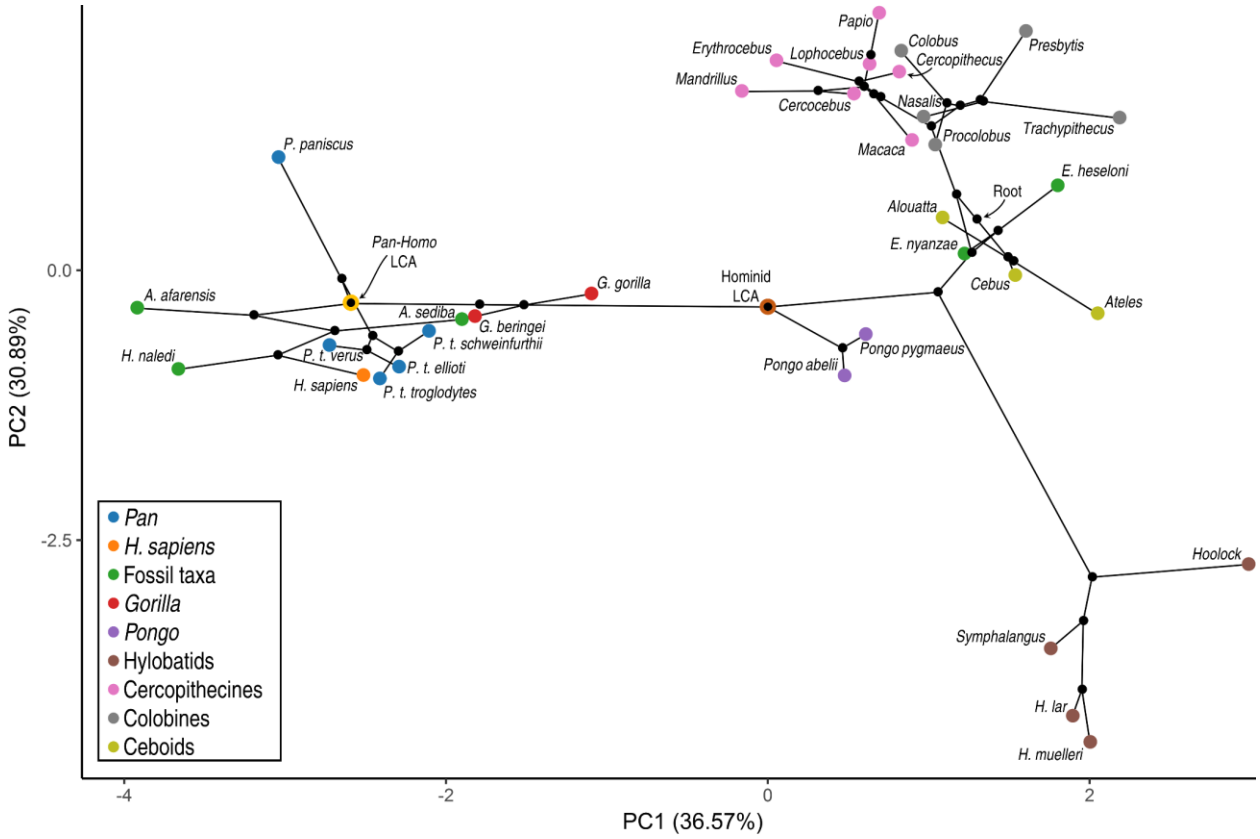

Fig. 4.9. Phylomorphospace representing the evolutionary history of anthropoid lunate morphology. The phylogeny is projected onto the first two principal components of all extant and fossil lunate shape variables, with ancestral states estimated via maximum likelihood. *Pan-Homo* and great ape LCAs are highlighted. See Table 4.4c for eigenvalues.

A functional signal is also evident in lunate morphology, as hylobatids, *Pongo*, and *Ateles* follow similar trajectories in phylomorphospace after divergence, although the magnitude of change in the latter two groups is not sufficient for the OU model (Fig. 4.10) to identify convergence of adaptive optima. The OU model instead estimates *Pongo* and *Gorilla* to have maintained the primitive regime of colobines and ceboids, and transitions toward other adaptive optima to have occurred in hylobatids, *Ekembo*, cercopithecines, and the *Pan-Homo* clade.

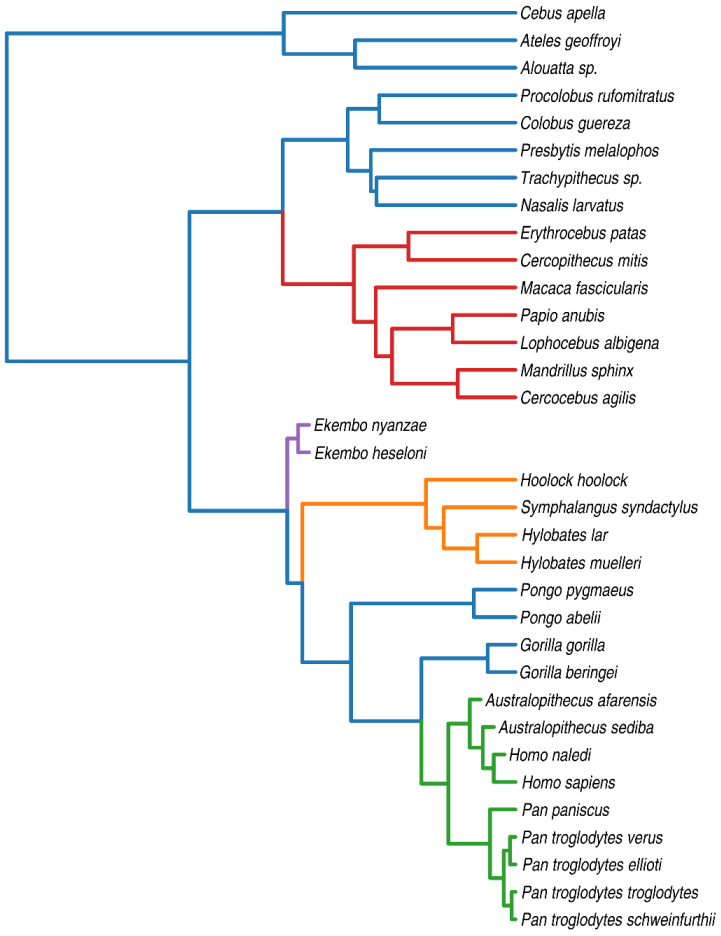

Fig. 4.10. Estimated adaptive regimes during anthropoid lunate evolution, based on the first two pPCs of all lunate shape variables, representing 51.4% of sampled variation (see Fig. 4.30 and Table 4.5c). Branches are colored according to adaptive regime; *Pongo* and *Gorilla* are estimated to have retained the ancestral adaptive regime along with ceboids and colobines.

In DFA morphospace (Fig. 4.11), the *Ekembo* specimens group among extant suspensors, while most extant humans and fossil hominins again plot among the African apes. *A. sediba* plots just outside the 80% CI of *Gorilla*, but its position in morphospace is very near the decision boundaries between knuckle-walking, suspension, and digitigrady, and, due to its score along the third discriminant function accounting for 5.9% of the variation, it is classified among the digitigrade monkeys (Table 4.12c).

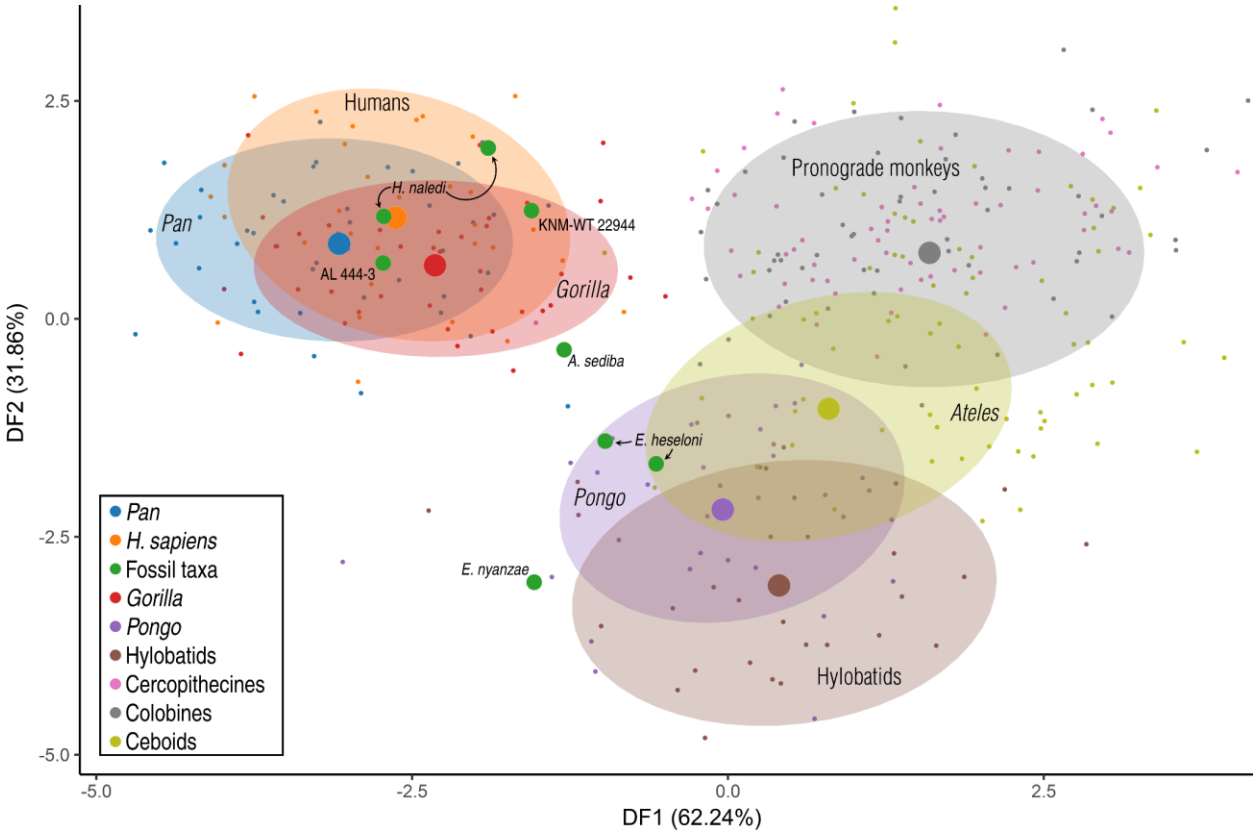

Fig. 4.11. Discriminant function analysis of six functionally diagnostic shape variables of the lunate. See Chapter 2 for selection criteria, Table 4.6c for variables and scaling, Table 4.9 for accuracy metrics, and Table 4.12c for predictions and posterior probabilities of humans and fossil specimens. Small and medium points represent extant and fossil observations, respectively. Large points represent group means; shaded ellipses are 80% confidence intervals.

The phylogenetic trait map (Fig. 4.12, Table 4.7b) estimates the most terrestrial *Pan-Homo* and *Gorilla-Homo* LCAs of the four elements, and the most suspensory hominid LCA, as measured by their ordinal positions between the minimum (greater knuckle-walking affinity) and maximum (greater suspensory affinity) discriminant values. The hominid LCA is nevertheless estimated to have been somewhat more functionally similar to extant palmigrade monkeys than most suspensors, while also falling within the *Ateles* range. Knuckle-walkers and pronograde monkeys are again not well separated along this axis, but the six lowest mean values all belong to terrestrial taxa, represented by the five *Pan* taxa and *Mandrillus*. The *Pan-Homo* LCA estimate falls between the *Pan* and *Gorilla* means, consistent with a terrestrial lifestyle. This estimate reflects the greater similarity between *Pan* and hominins (other than *A. sediba*) than to *Gorilla*, as the hominine LCA is estimated to be less terrestrial, with a value exceeded only by *Papio* among extant terrestrial taxon means and higher than those of several palmigrade monkeys. As suggested by Fig. 4.10, the terrestrial estimate of the *Pan-Homo* LCA is therefore at least partially due to phylogenetic structure.

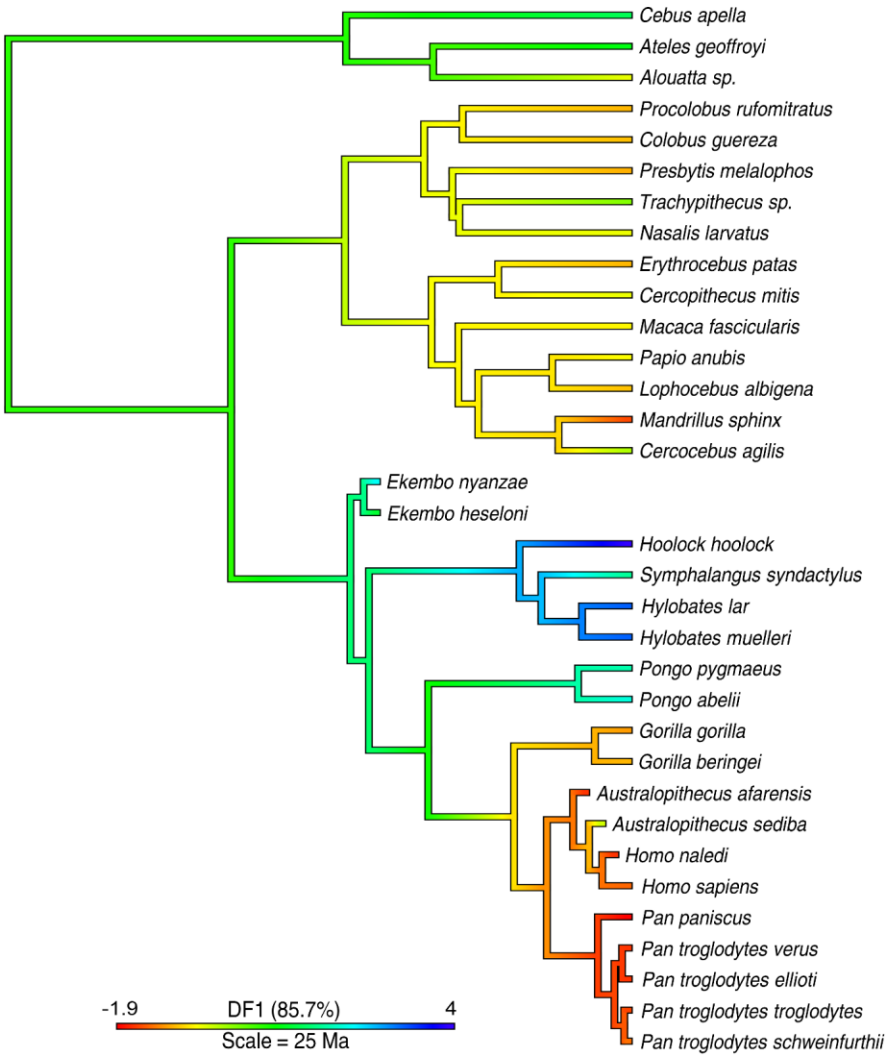

Fig. 4.12. Estimated locomotor evolution based on three lunate shape variables identified in Chapter 2 as best distinguishing knuckle-walking and suspension. Bluer hues represent increasing suspensory specialization. Ancestral states estimated via maximum likelihood. See Table 4.7b for details.

Triquetrum

The expanded range of morphological variability among hominoids relative to other anthropoids is especially evident in triquetrum morphology. The range of diversity among cercopithecoids is particularly limited, as evinced by its being circumscribed by that of the far less speciose ceboid sample in phylomorphospace (Fig. 4.13) In turn, the centroids of all sampled monkey taxa vary within a narrower range along the first PC than that separating the two *Pongo* species.

Table 4.6. Shape variable scaling of DFA biplots for each element

a	Capitate	
	DF1	DF2
CpDn	-0.43	-0.06
Cp3	0.01	-0.31
Cp2	-0.71	0.68
CpPxA	-0.58	-0.86
CpScA	-0.75	0.40
CpHmC	-0.59	-0.31
CpHP	-0.33	0.56

b	Hamate	
	DF1	DF2
Hm5	1.15	-0.06
Hm45A	0.48	-0.30
Hm5CpA	-0.05	1.36
Hm4CpA	1.40	-0.33
HmPxA	0.76	-0.24

c	Lunate	
	DF1	DF2
LuDs	-0.27	0.32
LuTq	0.05	0.23
LuSc	0.76	0.27
LuDsTqA	0.35	-1.22
LuCpRaA	1.33	0.49
LuCpC	-0.17	-0.48

d	Triquetrum	
	DF1	DF2
TqHm	-0.17	-0.99
TqPi	-0.76	0.06
TqHmPiA	-0.06	-0.94
TqHmLuA	-0.05	-0.29
TqLuPiA	0.20	-0.03
Tq1LuA	1.51	0.04

In overall morphology, modern human triquetra are found to most closely resemble the estimated condition of the *Pan-Homo* LCA among sampled taxa. Early hominins are meanwhile estimated to have evolved convergently with Asian apes. Humans' LCAs with *Pan*, *Gorilla*, and *Pongo* are estimated to be very similar, each morphologically intermediate relative to humans and *E. heseloni*, which, despite maintaining a styloid articulation, has diverged sharply from extant monkeys. *H. naledi* is again found to more closely resemble at least one species of *Australopithecus* (*A. sediba* in this case) than *H. sapiens*.

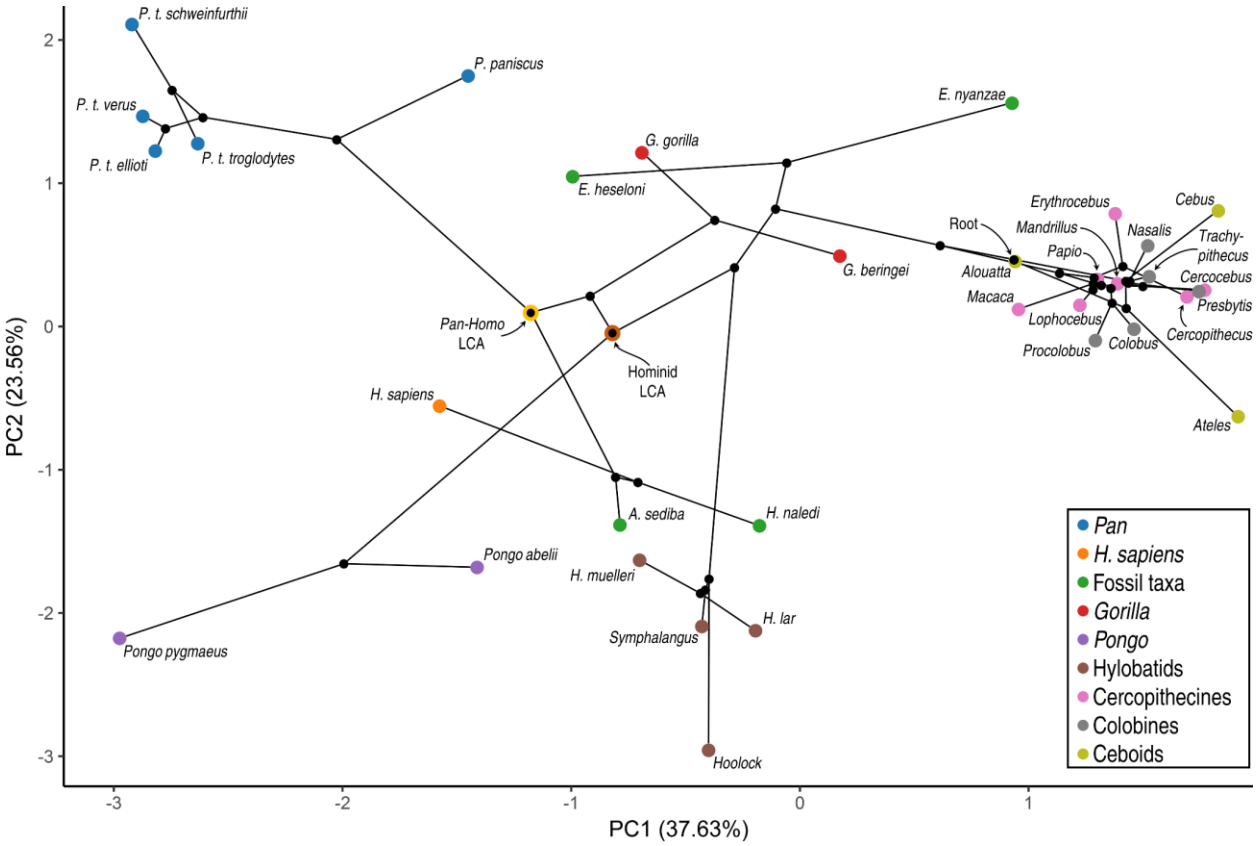

Fig. 4.13. Phylomorphospace representing the evolutionary history of anthropoid triquetrum morphology. The phylogeny is projected onto the first two principal components of all extant and fossil triquetrum shape variables, with ancestral states estimated via maximum likelihood. *Pan-Homo* and great ape LCAs are highlighted. See Table 4.4d for eigenvalues.

The multi-regime OU model estimates hominins and Asian apes to share a homologous adaptive regime, from which the African ape genera independently transitioned (Fig. 4.14). *Ekembo* is also estimated to have transitioned from the ancestral anthropoid regime. As is evidence in pPCA phylomorphospace (Fig. 4.31) the *Ekembo* triquetra depart drastically from expectation given their phylogenetic position.

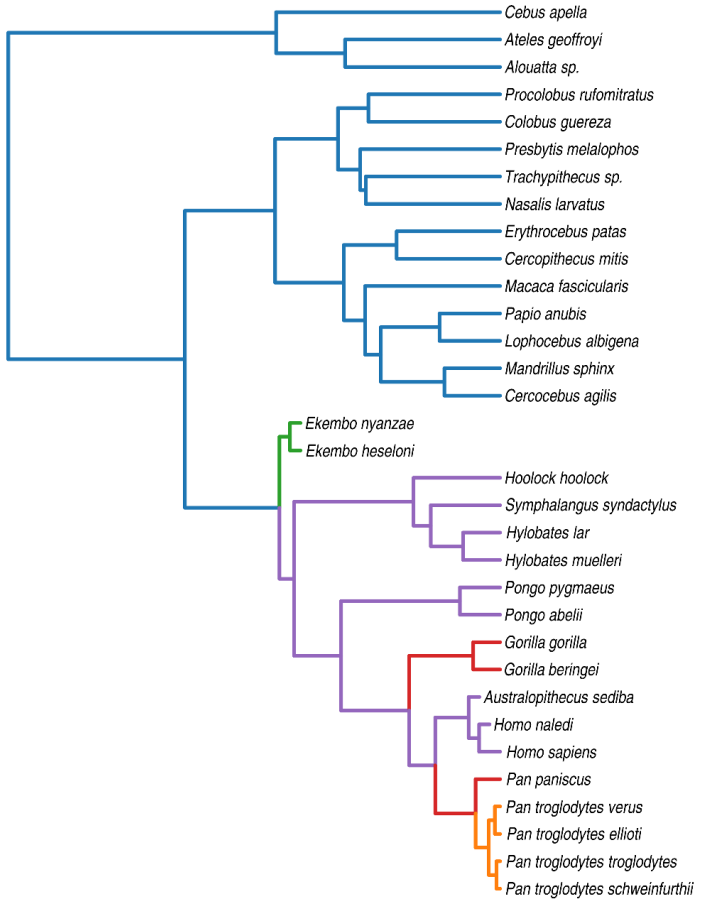

Fig. 4.14. Estimated adaptive regimes during anthropoid triquetrum evolution. Based on two pPCs representing 56.9% of sampled variation (see Fig. 4.31 and Table 4.5d). Branches are colored according to adaptive regime.

Some of the discrepancy between phylogenetic position and triquetrum morphology in *Ekembo* is influenced by its relatively basal position combined with its dissimilarity from the extant monkey sample. The greater influence results from the interaction between the morphology of the ape and great ape LCAs, which are estimated to have been generalized, and the morphology of *Ekembo*, which is found to be highly derived. This is not entirely evident in either phylomorphospace plot, but becomes more so in DFA morphospace (Fig. 4.15), in which all three *Ekembo* specimens are classified as knuckle-walking with posterior probabilities of 1 (Table 4.12d).

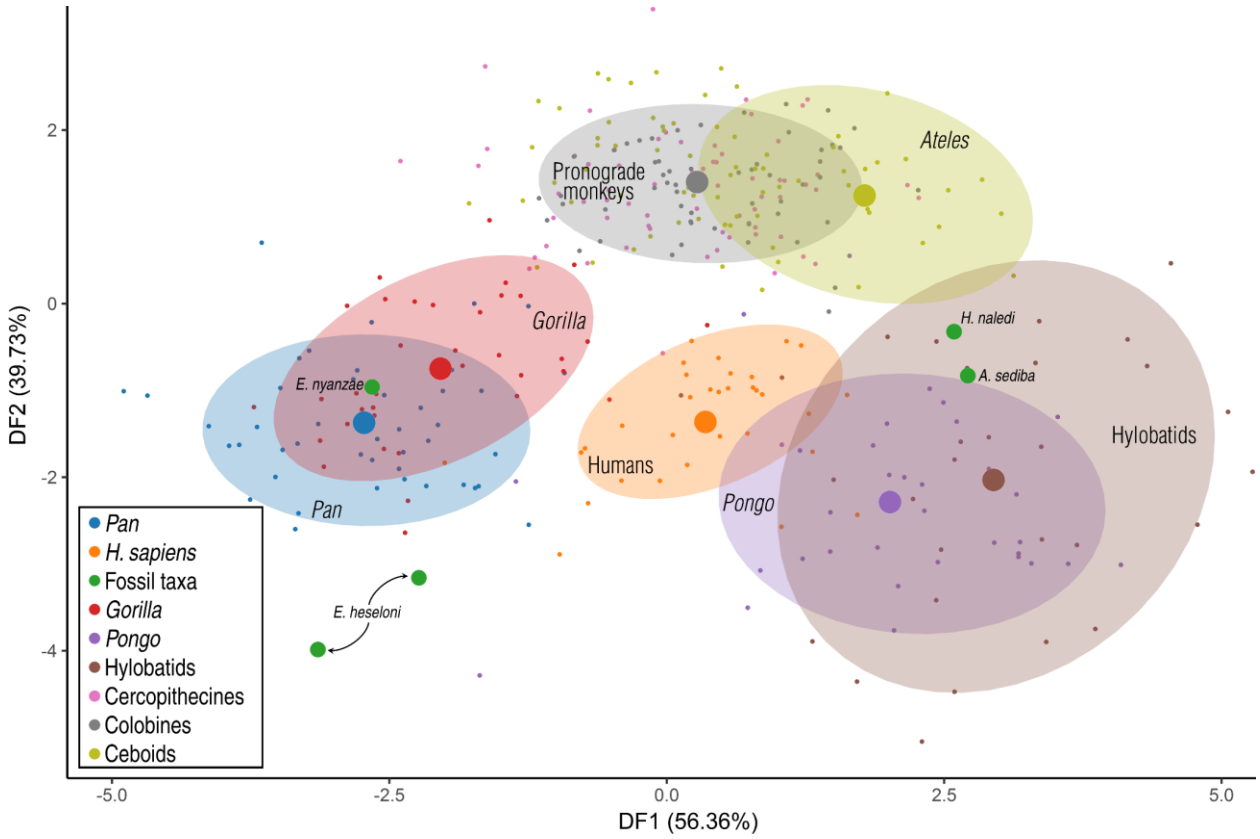

Fig. 4.15. Discriminant function analysis of six functionally diagnostic shape variables of the triquetrum. See Chapter 2 for selection criteria, Table 4.6d for variables and scaling, Table 4.9 for accuracy metrics, and Table 4.12d for predictions and posterior probabilities of humans and fossil specimens. Small and medium points represent extant and fossil observations, respectively. Large points represent group means; shaded ellipses are 80% confidence intervals.

The triquetra of both *H. naledi* and *A. sediba* are classified as suspensory with high confidence, and the mean suspensory posterior probability of the human sample also exceeds 50%. This is reflected by their position in DFA morphospace, separated from other extant hominines but overlapping only somewhat with extant Asian apes.

The phylogenetic trait map (Fig. 4.16), which distinguishes both knuckle-walkers and suspensors from pronograde monkeys, estimates the *Pan-Homo*, hominine, and hominid LCAs to have resembled extant pronograde monkeys in locomotor behavior. The former two estimates also fall just within the range of *Ateles*, but all three are well

separated from knuckle-walkers. These results are most consistent with knuckle-walking adaptations in African ape genera having evolved in parallel.

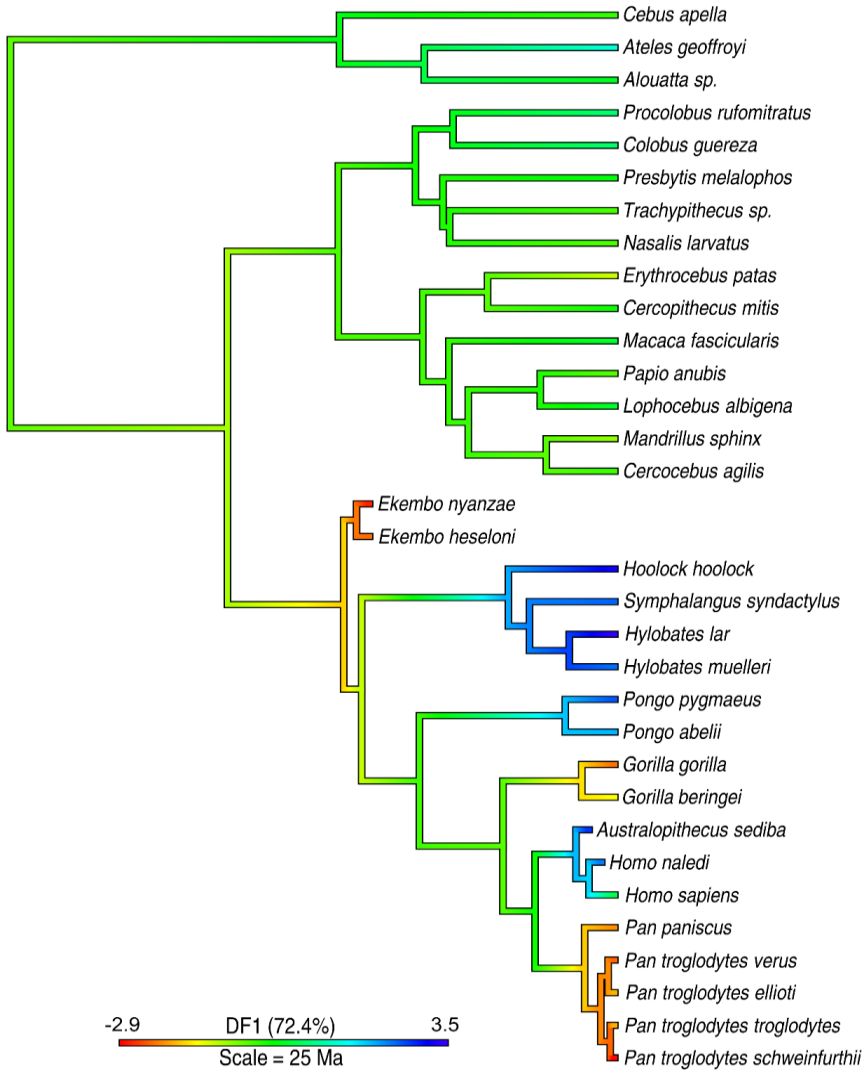

Fig. 4.16. Estimated locomotor evolution based on three triquetrum shape variables identified in Chapter 2 as best distinguishing knuckle-walking and suspension. Bluer hues represent increasing suspensory specialization, and redder hues increasing adaptation for knuckle-walking. Ancestral states estimated via maximum likelihood. See Table 4.7c for details.

Table 4.7. Shape variable scaling of discriminant functions used for each element's phylogenetic trait maps. See Table 4.6b DF2 for hamate values.

a Capitate		**b** Lunate		**c** Triquetrum	
CpHmC	-0.61	LuTq	-0.14	Tq1LuA	1.43
CpPxA	-0.99	LuDsTqA	1.40	TqPi	-0.81
CpScA	-0.43	LuCpC	0.30	TqHmPiA	0.05

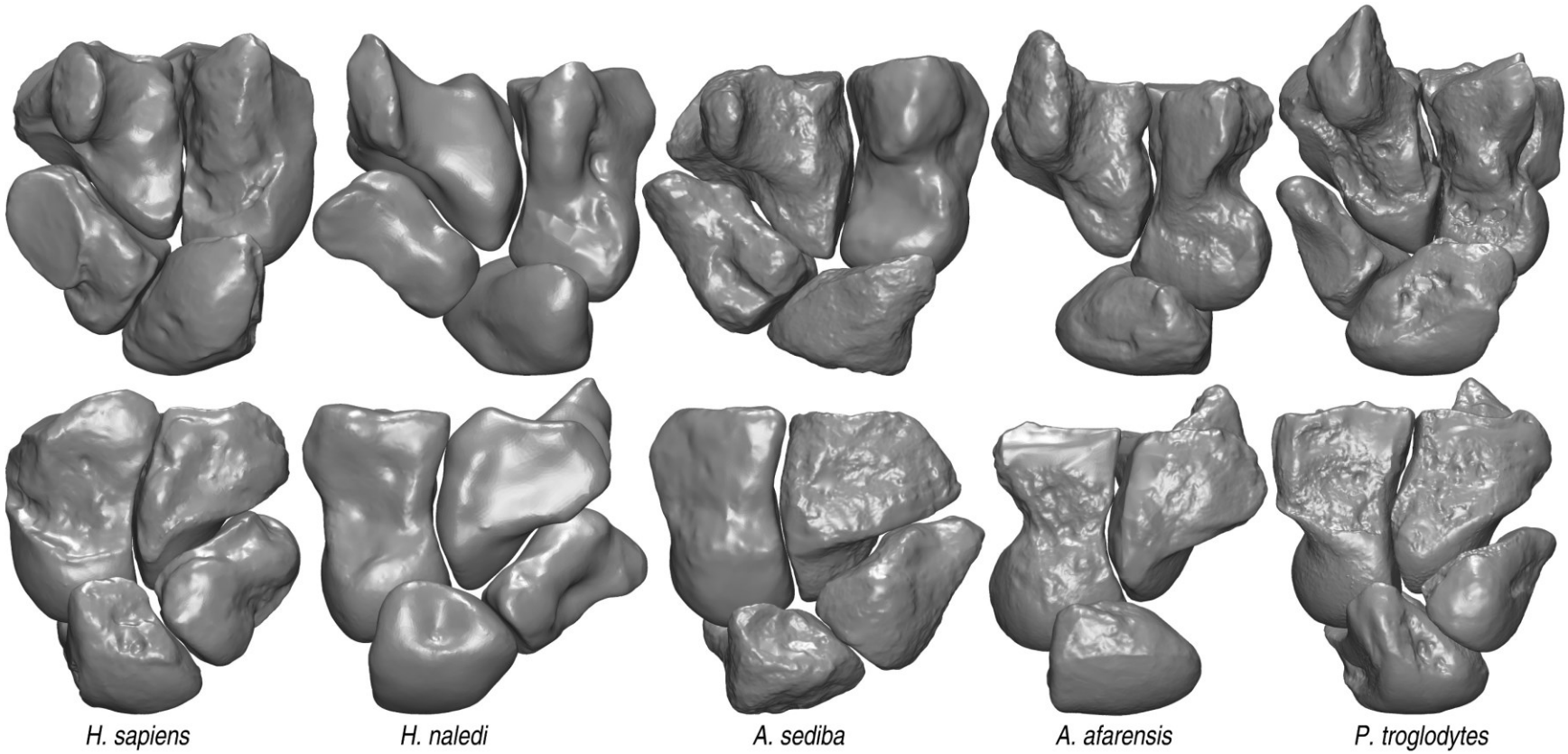

Fig. 4.17. Comparison of selected fossil hominin individuals with a modern human and a chimpanzee. Analyzed elements are shown in palmar (top) and dorsal (bottom) view.

Discussion

Diversity of variance patterns among carpal elements

Patterns of variation within Hominoidea are inconsistent among the analyzed carpal elements, with each seeming to have traversed a different evolutionary track in arriving at its condition in extant lineages. *Pan* and *Pongo* are estimated to have shared adaptive optima during capitate evolution, and, along with *Gorilla*, during hamate evolution as well. The adaptive optima of the lunate, meanwhile, are estimated to have been more similar in *Pongo* and *Gorilla*, which shared a plesiomorphic adaptive regime with ceboids and colobines, whereas the *Pan-Homo* clade transitioned toward a synapomorphic optimum. The triquetra of the hominin clade are estimated to have evolved according to the symplesiomorphic regime maintained by the Asian ape lineages, with *Gorilla* and *Pan* independently transitioning away from it and each other toward substantially divergent adaptive optima.

Patterns of variation among the most functionally diagnostic metrics also differ between carpal elements. The triquetra of humans share affinities with extant suspensors in each of the variables most diagnostic of this behavior: The long axis is oriented relatively orthogonally to its lunate facet (Fig. 4.18a), the lunate facet is relatively small (Fig. 4.18c), and the pisiform facet is both somewhat smaller (Fig. 4.18b) due to being limited to the distal aspect of the bone, and angled more palmarly relative to the bone's hamate facet (Fig. 4.18d; see Chapter 2 for biomechanical interpretation of these features). This resemblance to extant suspensors seems to be greatest in earlier hominins, judging by the high suspensory posterior probabilities of the fossil specimens analyzed here (Fig. 4.15; Table 4.12d) as well as observations by Kivell

(2011) of SKX 3498, an early Pleistocene hominin triquetrum of unknown taxonomic identity.

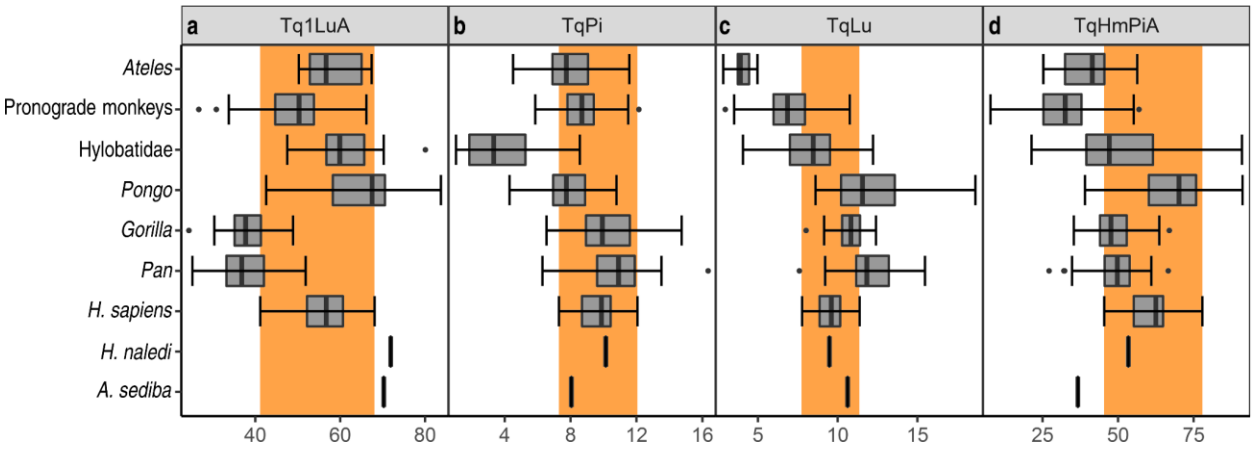

Fig. 4.18. Comparisons between extant taxa and fossil hominins of triquetrum variables discussed in the text. Boxes represent 25th and 75th percentiles, centerlines the medians, and whiskers the non-outlier ranges. The modern human range is highlighted.

Ekembo, meanwhile, more closely resembles African apes in these metrics, which is estimated to have resulted from a substantial and rapid morphological divergence from the hominoid LCA. This presents an enticing problem, as the mechanism by which this could have occurred in *Ekembo*, the positional repertoire of which is akin to the null hypothesis in the study of early catarrhine function (see Chapter 3), is opaque. This problem could potentially be explained by additional, unsampled instances of morphological convergence among either Asian apes, hominins, or both, which would serve to reverse the apparent polarity between the more terrestrial morphology of African apes and *Ekembo* and the more suspensory morphology of Asian apes and hominins. The triquetrum belonging to the IPS-21350 partial skeleton of *Pierolapithecus* (Moya-Sola *et al.*, 2004) will add clarification when it is made available

for research; the limited photos and description currently available provide little guidance.

This functional signal is largely reversed in the lunate, as *Ekembo* demonstrates functional affinity with extant suspensors, while humans and fossil hominins tend to most closely resemble *Pan* (Fig. 4.11, Table 4.12c). This is particularly evident in the angle between the lunate's distal surface and its articulation with the triquetrum (Fig. 4.19c), the metric best distinguishing between the lunates of extant knuckle-walkers and suspensors. This angle is especially acute in humans and *Pan*, as well as *H. naledi* and *A. afarensis*; it is somewhat less acute in *A. sediba*, but falls near the maximum range of the extant hominine sample, below the most acute value of sampled Asian apes. The size of the triquetrum facet in sampled extant and extinct hominins (Fig. 4.19b) also resembles that of African apes, significantly larger than the suspensory taxa but not distinct from various cercopithecoids. The lunate's distal surface (Fig. 4.19a), which is significantly larger in knuckle-walkers than other positional classes, tends to be further enlarged in humans, a condition shared by *H. naledi*, in which this facet is similar in size to the human median. The sampled australopiths are not consistent in this, however; *A. sediba* and *A. afarensis* have values near the median of sampled *Pongo* and hylobatids, respectively, although values of the latter hominin taxon remain within the range of most hominine taxa.

While variance in lunate morphology has the strongest phylogenetic structure of the analyzed carpals (discussed below), features of the lunate are well represented among those found to be most effective in extant positional classification (see Table 4.8, Table 4.10), and the lunate DFA model exceeds those of the other elements in total and

balanced classification accuracy (Table 4.9). As has been expounded elsewhere (e.g., Polly *et al.*, 2013), these influences are not dichotomous, given the high phylogenetic signal of locomotor function and the likelihood that much of the phylogenetic autocorrelation of morphological traits is attributable to similarly strong phylogenetic autocorrelation of behavioral ones. Interpreting multivariate lunate model results is therefore difficult.

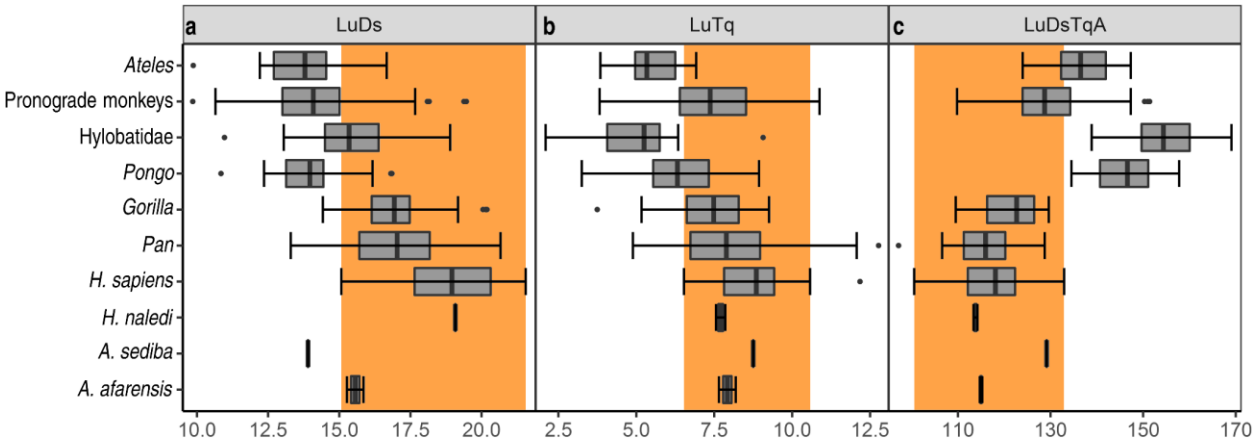

Fig. 4.19. Comparisons between extant taxa and fossil hominins of lunate variables discussed in the text. Boxes represent 25th and 75th percentiles, centerlines the medians, and whiskers the non-outlier ranges. The modern human range is highlighted.

Variation in functionally diagnostic features of the capitate is at odds with those of the lunate and triquetrum. Humans and most hominins share stronger functional affinity with pronograde monkeys than African apes (Fig. 4.3, Table 4.12a), and while human capitates are among the most derived of the sampled taxa in overall morphology, functionally-related aspects of the ancestral morphotype seem to have been either retained or secondarily reacquired in the hominin lineage. While Lovejoy and colleagues (2009a, b) favor the former hypothesis, palmigrade-like features could have evolved in

hominins to facilitate the greater palmar compliance beneficial for enhanced manipulative capabilities.

Capitate features aligning the hominin clade with pronograde monkeys over apes include the size of the Mc2 articulation (Fig. 4.20a), which, while smaller in humans than in most monkeys, tends to be larger than in other hominoids. This is true of most fossil hominins as well, particularly in *H. naledi* and the AL 333 individual of *A. afarensis*. The Mc3 facet (Fig. 4.20b) of humans and most hominins is more similar in size to those of Asian apes and various cercopithecoids, whereas it is generally larger in African ape specimens. Hamate facet concavity (Fig. 4.20d) is usually somewhat reduced in humans relative to African apes, most resembling the condition in colobines, and a relatively palmar position of the capitate head (Fig. 4.20e) distinguishes humans from African apes, in which it tends to be positioned more dorsally.

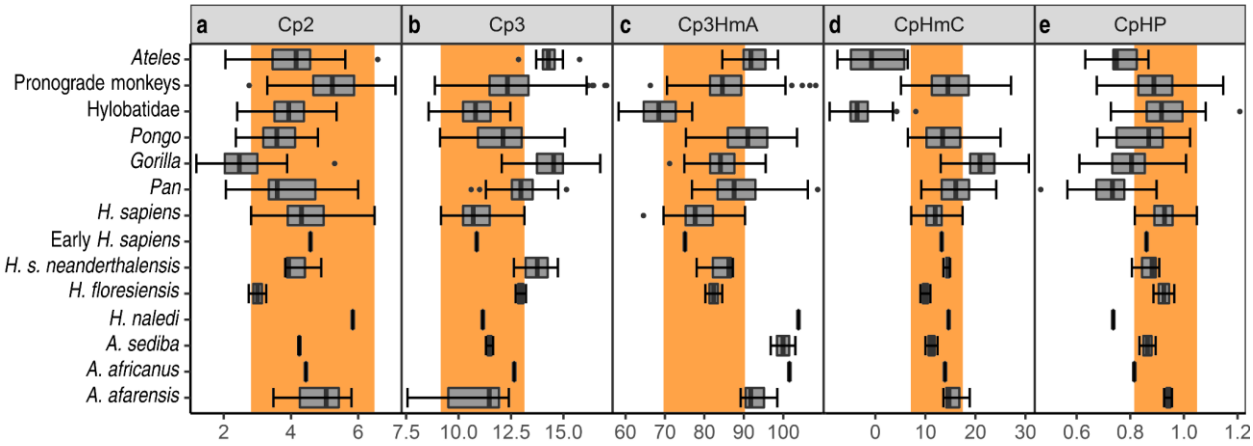

Fig. 4.20. Comparisons between extant taxa and fossil hominins of capitate variables discussed in the text. Boxes represent 25th and 75th percentiles, centerlines the medians, and whiskers the non-outlier ranges. The modern human range is highlighted.

Meanwhile, hamate articular geometry is very conservative, with relatively little variance attributable to positional behavior. The hamate is also marginally less covariant

with phylogeny than the other elements (discussed below), leaving much of its variation unattributable to either of these influences. This is reflected in the large majority of lineages estimated to share a symplesiomorphic adaptive regime (Fig. 4.6).

Analyses of these four carpal elements produce results potentially supporting three competing hypotheses regarding hominin locomotor ancestry. These discordant patterns of variation reinforce the necessity of caution in analyzing isolated fossil specimens; in assessing the locomotor affinities of a fossil hominin known only from an isolated carpal, results of a comparative functional analysis will be highly dependent on which carpal of the extinct individual was found – a hominin capitate will tend to suggest pronogrady (Fig. 4.3), a lunate knuckle-walking (Fig. 4.9), and a triquetrum suspension (Fig. 4.13, Fig. 4.15); a hamate will also likely suggest knuckle-walking while being relatively uninformative (Fig. 4.7).

Table 4.8. Results of functional analyses incorporating shape variables derived from all analyzed elements

a PCA eigenvalues			**b** pPCA eigenvalues			**c** DFA scaling		
	PC1	PC2		PC1	PC2		DF1	DF2
CpPxA	-0.37	-0.10	CpPxA	-0.24	-0.34	CpPxA	-0.29	0.44
CpScA	-0.29	0.18	CpScA	-0.27	0.15	CpScA	-0.08	0.13
CpHmC	-0.36	-0.04	CpHmC	-0.33	-0.05	CpHmC	-0.60	0.10
CpHP	0.11	0.31	CpHP	0.06	0.47	CpHP	0.19	0.29
Hm5	-0.29	0.30	Hm5	-0.19	0.11	Hm5	0.10	0.47
LuDs	0.01	-0.43	LuDs	-0.01	-0.57	LuDs	-0.40	-0.07
LuSc	0.13	0.42	LuSc	0.14	0.22	LuSc	-0.01	0.57
LuTq	-0.34	-0.09	LuTq	-0.43	0.18	LuTq	-0.21	0.09
LuCpRaA	-0.10	0.39	LuCpRaA	0.05	-0.11	LuCpRaA	0.37	0.97
LuDsTqA	0.35	0.20	LuDsTqA	0.27	0.32	LuDsTqA	0.61	-0.21
LuCpC	0.29	-0.23	LuCpC	0.26	-0.22	LuCpC	0.01	-0.18
Tq1LuA	0.20	0.10	Tq1LuA	0.34	-0.07	Tq1LuA	1.09	0.01
TqPi	-0.34	-0.17	TqPi	-0.46	-0.05	TqPi	-0.30	-0.28
TqHmPiA	0.21	-0.32	TqHmPiA	0.21	-0.24	TqHmPiA	0.36	-0.65

Hominin locomotor ancestry

Despite these discrepant results, a composite narrative begins to emerge from similarities among locomotor estimates assigned to ancestral nodes within Hominoidea, as well as results of the combined functional analyses. The phylogenetic trait maps built from each element are consistent in estimating the *Pan-Homo* LCA to have lacked morphological adaptations comparable to those of extant suspensors (Fig. 4.4, Fig. 4.8, Fig. 4.12, Fig. 4.16; Table 4.6b, Table 4.7). They also generally find this ancestor to have been functionally indistinguishable from pronograde monkeys, although the lunate trait map estimate for the *Pan-Homo* LCA, but not the hominine LCA, is somewhat more consistent with knuckle-walking, and the capitate and hamate trait maps do not distinguish between pronogrady and knuckle-walking.

Table 4.9. Extant classification accuracy of DFA models calculated after 100 repetitions of 10-fold cross validation. Tot, total accuracy. *DG*, digitigrady. *KW*, knuckle-walking. *PG*, palmigrady. *S*, suspension. Bal, balanced accuracy, which accounts for inequality of class sizes (see Chapter 2). See Table 4.6, Table 4.8c, and Table 4.11b for model details.

	Tot	*DG*	*KW*	*PG*	*S*	Bal
Capitate	0.839	0.918	0.929	0.771	0.848	0.872
Hamate	0.669	0.620	0.817	0.579	0.712	0.763
Lunate	0.875	0.959	0.948	0.797	0.925	0.892
Triquetrum	0.834	0.840	0.903	0.820	0.787	0.876
Combined function	0.952	0.995	0.987	0.917	0.968	0.947
CHL function	0.931	0.964	0.974	0.910	0.916	0.932

In analyses incorporating the shape variables from all analyzed elements best distinguishing knuckle-walking and suspension (Table 4.8), the hominid LCA is estimated to have been generalized, intermediate between *Pongo* and pronograde monkeys in combined functional phylomorphospace (Fig. 4.21, Table 4.8a). The human

LCAs with both *Gorilla* and *Pan* are meanwhile estimated to have approached *Gorilla* in locomotor function while still being positioned between them and other non-African ape anthropoids.

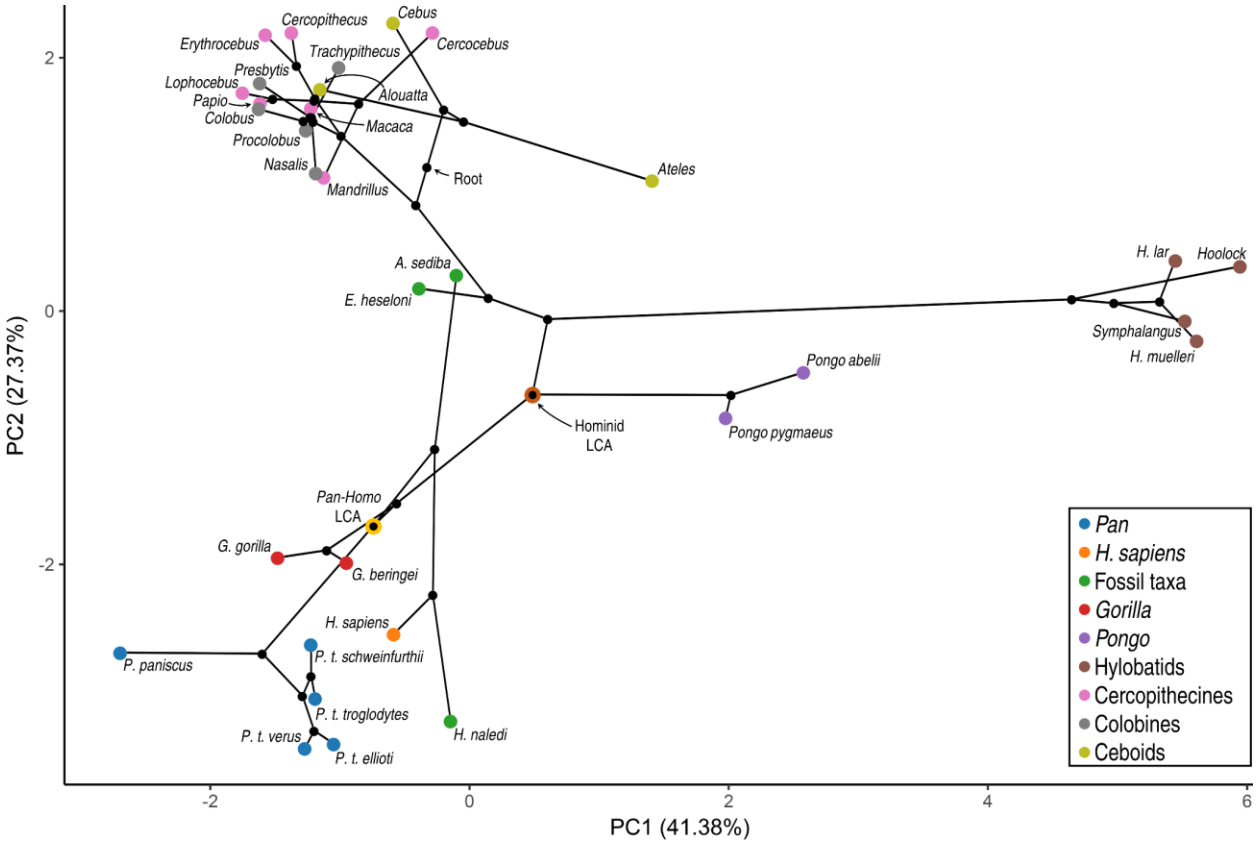

Fig. 4.21. Phylomorphospace representing anthropoid locomotor evolution based on 14 diagnostic shape variables from the four analyzed carpals. The phylogeny is projected onto the first two principal components of extant and fossil shape variables, with ancestral states estimated via maximum likelihood. *Pan-Homo* and great ape LCAs are highlighted. See Table 4.8a for eigenvalues.

However, despite comprising the shape variables most related to locomotor function, the multivariate phylogenetic signal of the combined functional subset (K_{mult} = 0.73; Adams, 2014) is greater than that of the complete variable sets of any individual element (discussed below). This enhances the potential utility of the pPCA phylomorphospace (Fig. 4.22, Table 4.8b) relative to that built on a standard PCA.

While the *Pan-Homo* and *Gorilla-Homo* LCAs are similarly adjacent to extant *Gorilla* in pPCA phylomorphospace, changes in the surrounding structure find African apes and pronograde monkeys in greater proximity, with the *Pan-Homo* and hominine LCAs positioned roughly equidistant from several palmigrade monkeys on the one hand, and the human and chimpanzee centroids on the other.

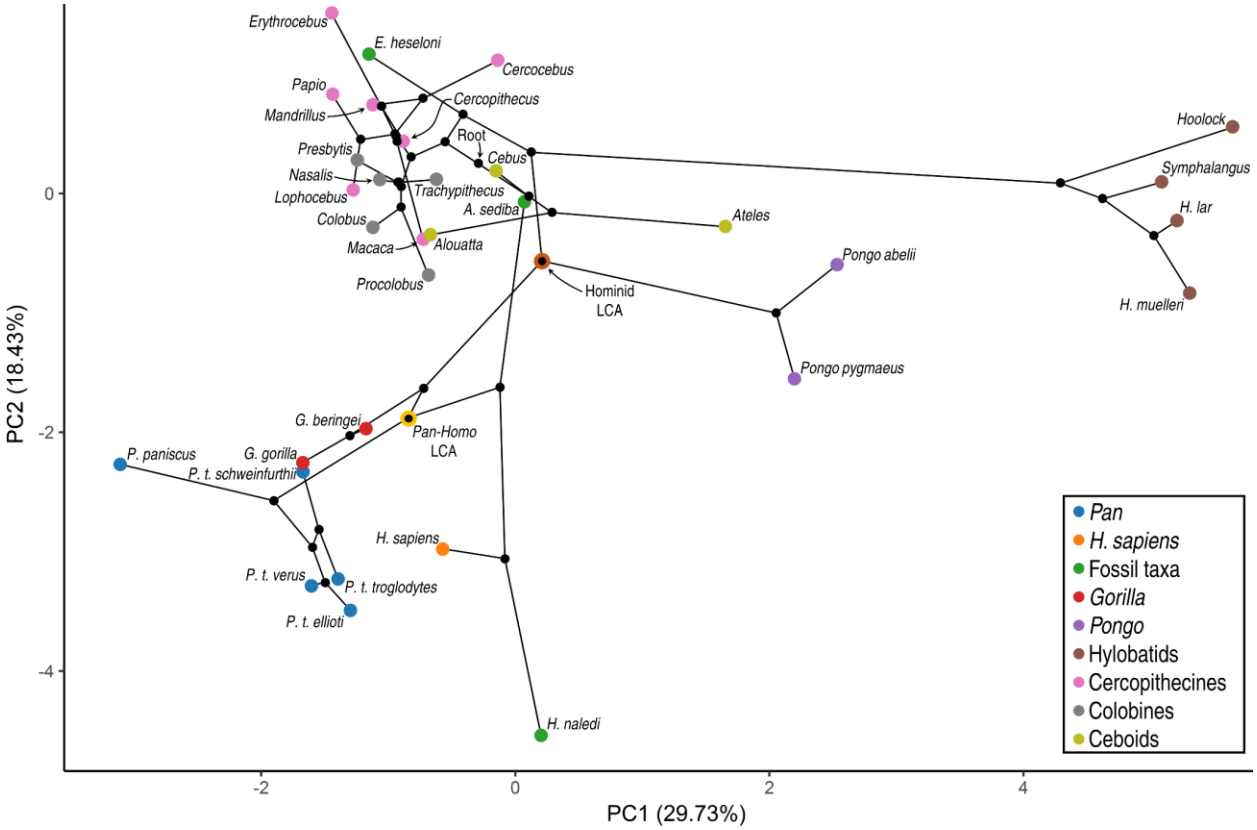

Fig. 4.22. Phylomorphospace representing anthropoid locomotor evolution based on phylogenetic PCA of 14 diagnostic shape variables from the four analyzed carpals. The phylogeny is projected onto the first two phylogenetic principal components of extant and fossil shape variables, with ancestral states estimated via maximum likelihood. *Pan-Homo* and great ape LCAs are highlighted. See Table 4.8b for eigenvalues

In contrast to the knuckle-walkers, the combined pPCA shows extant suspensors to be similarly divergent from other anthropoids with or without accounting for phylogeny. The pPCA does group African ape more closely together, however, and

further separates them from the *Homo* species, perhaps reflecting the features shared among the former in association with knuckle-walking. *H. sapiens*, meanwhile, owing to the functionally disparate *A. sediba*, is estimated to have descended from an ancestor even less similar to extant African apes after their split with *Australopithecus*.

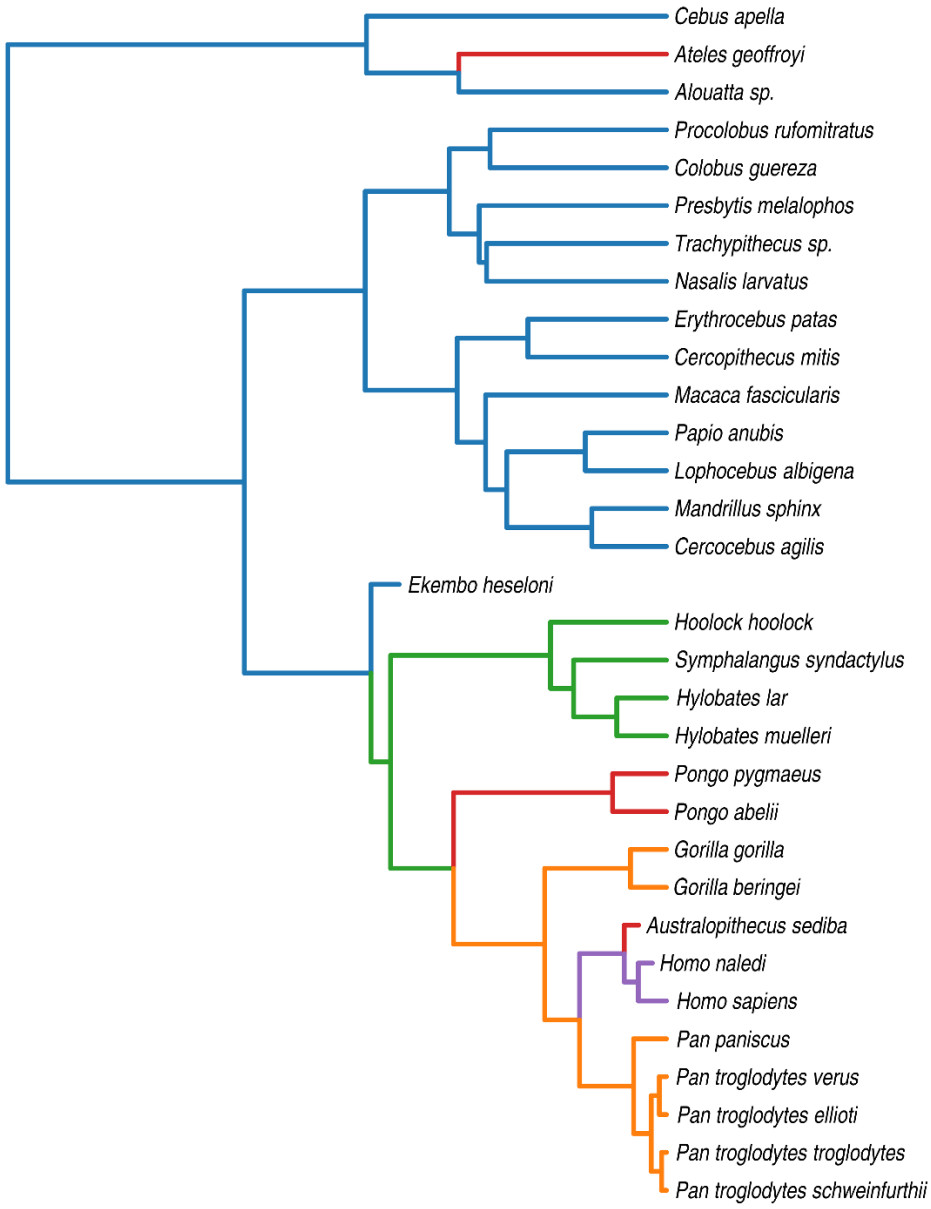

Fig. 4.23. Estimated adaptive regimes during anthropoid locomotor evolution, based on the first three pPCs of 14 diagnostic shape variables, representing 62.2% of sampled variation (see Fig. 4.22 and Table 4.8b). Branches are colored according to adaptive regime; *Australopithecus sediba* is estimated to have shared an adaptive regime with *Pongo* and *Ateles*.

The combined multi-regime OU model (Fig. 4.23) estimates *A. sediba*, *Pongo*, and *Ateles* to have converged on similarly suspensory adaptive optima, with the hylobatid clade having transitioned toward an even more specialized optimum. *Pan* and *Gorilla* are estimated to share the ancestral hominine adaptive regime, with hominins having shifted away from it after branching from *Pan*. This scenario is consistent with the hominine LCA having been a knuckle-walker, but its estimated intermediate morphology (Fig. 4.22) is also consistent with non-knuckle-walking terrestriality, or with adaptation for some other shared function such as vertical climbing.

The combined phylogenetic trait maps provide some clarity. The suspensory trait map (Fig. 4.24a, Table 4.10a) comports with the analyses of each element's overall morphology in finding a lack of suspensory adaptation at the origin of any of the major anthropoid clades, with hylobatids, *Pongo*, and *Ateles* having adapted to their suspensory habits independently. The knuckle-walking trait map (Fig. 4.24b, Table 4.10b) also estimates the morphology associated with knuckle-walking in the African ape genera to have evolved at least largely in parallel. The *Pan-Homo* and *Gorilla-Homo* LCA estimates most resemble the mean values of *H. sapiens*, *E. heseloni*, and *Mandrillus*, between the African ape and palmigrade monkey samples. Although these estimates both fall outside the range of extant African apes, the proximity of the *Pan-Homo* LCA to *Mandrillus* may be consistent with the hypothesis that even if knuckle-walking is not homologous in the African ape genera, a more generalized form of terrestriality may be (e.g., Sarmiento, 1988; Gebo, 1992, 1996).

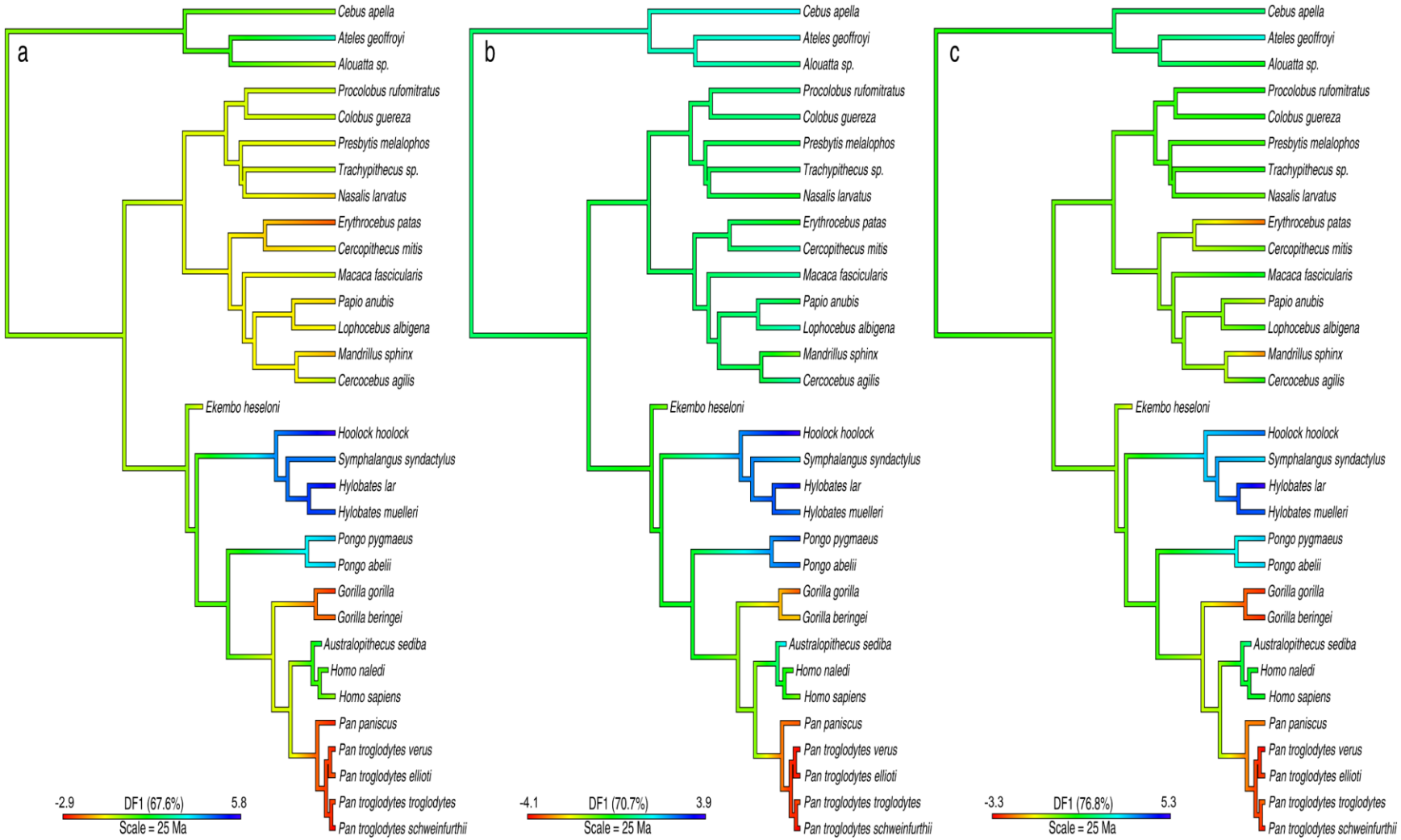

Fig. 4.24. Estimated locomotor evolution based on shape variables from all four analyzed elements identified in Chapter 2 as best distinguishing suspension (a), knuckle-walking (b), and terrestrial behavior (c) from other anthropoid positional groups. Bluer hues represent increasing suspensory specialization, and redder hues increasing adaptation for knuckle-walking or terrestrialitiy. Ancestral states estimated via maximum likelihood. See Table 4.10 for details.

Table 4.10. Shape variable scaling of discriminant functions used for phylogenetic trait maps in Fig. 4.24

a Combined Susp		**b** Combined KW		**c** Combined Terr	
CpPxA	-0.41	CpHP	0.26	Cp23A	0.39
CpHmC	-0.51	LuDs	-0.29	CpHmC	-0.56
LuTq	-0.15	LuDsTqA	0.82	LuTq	-0.16
LuDsTqA	0.77	LuCpRaA	0.64	LuDsTqA	0.88
LuCpC	0.01	TqPi	-0.52	LuCpRaA	0.63
TqHm	-0.08	Tq1LuA	1.07	Tq1LuA	1.09
TqPi	-0.21				
Tq1LuA	1.09				
TqHmPiA	0.54				

The third combined trait map (Fig. 4.24c, Table 4.10c) tests this hypothesis by estimating the evolution of terrestrialism without regard to hand posture. Tip data are distributed similarly to the knuckle-walking trait map, save for most digitigrade cercopithecines joining knuckle-walkers toward the red end of the continuum, and *H. sapiens* and *H. naledi* being positioned among arboreal monkeys, well separated from African apes. The *Pan-Homo* and *Gorilla-Homo* LCAs are both estimated as less terrestrial than any sampled individual of *Pan*, *Gorilla*, *Mandrillus*, or *Erythrocebus*. As discussed in Chapter 2, however, *Papio* frequently lacks the terrestrial features linking the other terrestrial cercopithecines. Here, the *Papio* mean is intermediate between the other digitigrade taxa and arboreal monkeys, with individual observations overlapping with both. The *Gorilla-Homo* LCA is estimated very near the *Papio* mean, while the *Pan-Homo* LCA is estimated to be marginally less terrestrial. These analyses estimate the *Pan-Homo* LCA to have lacked knuckle-walking adaptations comparable to those of extant African apes.

As previously noted, it has been speculated that adaptations associated with the ancestral hominin locomotor repertoire may have been retained in the lineage, perhaps persisting to the present. While this may yet be true of some features, for instance

scaphoid-centrale fusion (e.g., Kivell and Begun 2007), the functional signal disparities among hominin carpal elements demonstrated here could have arisen in part due to a relative lack of such pleisiomorphic retention. If the *Pan-Homo* LCA lived more than 7 million years ago (Langergraber *et al.*, 2012; Steiper and Seiffert, 2012), none of the taxa included in this analysis can be properly characterized as early hominins, and the evolution of wrist morphology may have proceeded quickly in the first few million years after the split with *Pan* upon alleviation of constraints associated with locomotor responsibilities. Increasing reliance on manipulative behaviors, which was arguably already substantial even in the earliest of the hominins sampled here (e.g., McPherron *et al.*, 2010), would serve to magnify this effect, rendering most hominin specimens uninformative at best and potentially misleading for the purpose of inferring ancestral locomotion.

Locomotor behavior of fossil hominins

Results of this study find *A. sediba* to have stronger functional affinity with extant suspensors and pronograde monkeys than with African apes, with its relative affinity to each group varying between analyses. Its position in combined DFA morphospace (Fig. 4.25, Table 4.8c), is consistent with these results, with *A. sediba* grouping just within the 80% CI of *Ateles*, better separated from other hominines than from pronograde monkeys or Asian apes.

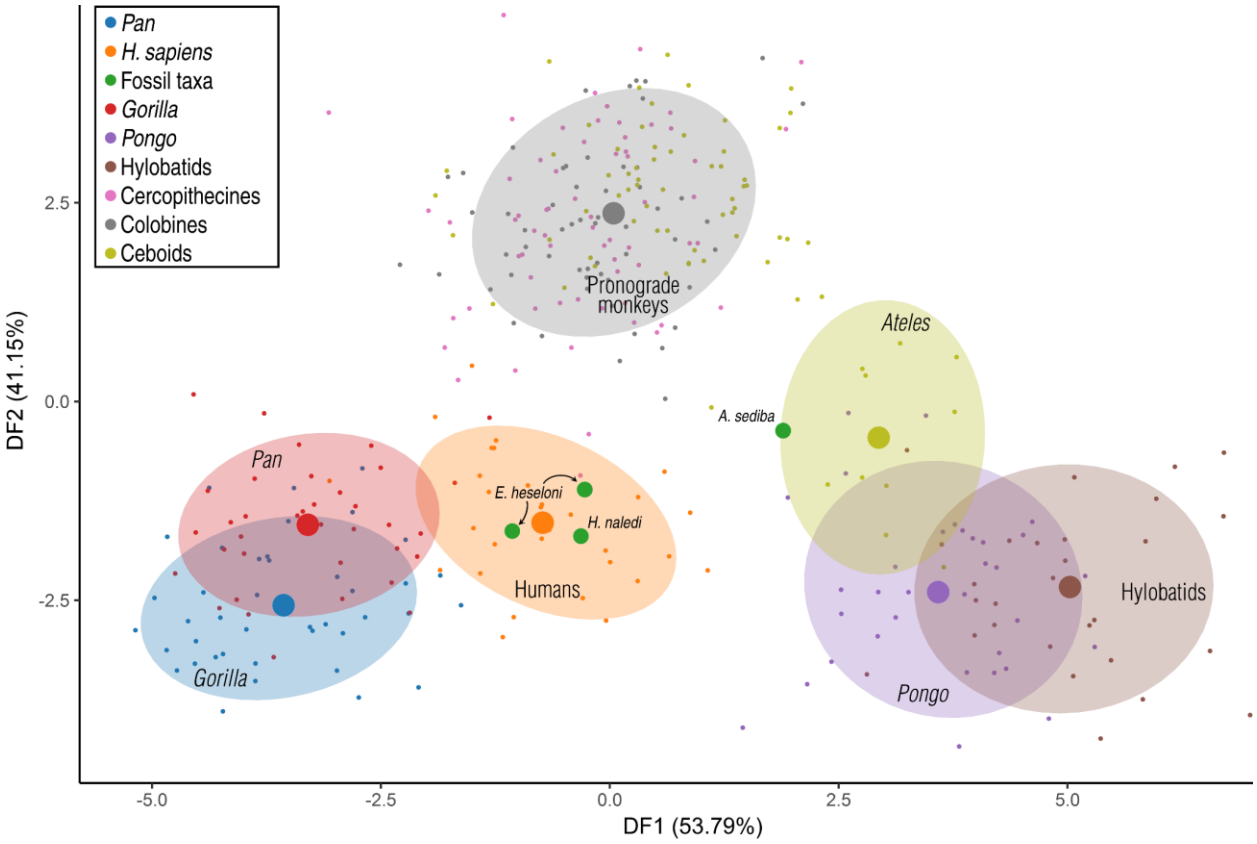

Fig. 4.25. Discriminant function analysis of 14 diagnostic shape variables across the four analyzed elements. See Chapter 2 for selection criteria, Table 4.8c for discriminant functions, Table 4.9 for accuracy metrics, and Table 4.12e for predictions and posterior probabilities of humans and fossil specimens. Small and medium points represent extant and fossil observations, respectively. Large points represent group means; shaded ellipses are 80% confidence intervals.

As shown in the previous section, the functional distinction of *A. sediba* from extant hominines is estimated to have resulted largely from convergence rather than a lack of negative selection on adaptations associated with the ancestral locomotor repertoire. This is consistent with previous functionally significant distinctions observed in *A. sediba* relative to other hominins. However, the suspensory habit inferred from more proximal morphology of the arm (Churchill *et al.*, 2013; Rein *et al.*, 2017) is only equivocally supported; in capitate morphology, the most effective of the four analyzed elements in diagnosing suspensory behavior (see Chapter 2), no suspensory signal is found in either antimere of the MH2 individual (Table 4.12a). In contrast, the capitate of

A. africanus, while classified as a knuckle-walker, is assigned a non-trivial suspensory posterior probability. This finding, while potentially consistent with previous observations of a suspensory signal in *A. africanus* (McHenry and Berger, 1998; Green *et al.*, 2007), does not support a unique degree of suspensory adaptation in *A. sediba* relative to its congeners.

Due to the problems discussed above associated with incongruent variance patterns among carpal elements, the right-hand set of four carpals from the MH2 individual of *A. sediba* is directly comparable only to *H. naledi* and extant humans of sampled hominins. Much of the suspensory signal of *A. sediba* is found in the triquetrum, however, the morphology of which, as detailed above, is similar in all sampled hominins to that of extant suspensors. The triquetrum of *H. naledi*, for example, possesses a suspensory signal approaching that of *A. sediba* in strength (see Table 4.12d), despite its other elements having suspensory probabilities of 0 (Table 4.12a-c).

To evaluate the functional distinctiveness of *A. sediba* relative to other hominins based on non-triquetrum morphology, the pPCA phylomorphospace and DFA morphospace were recreated with triquetrum-derived variables removed. This has the further benefit of allowing comparison between *A. sediba* and the articulated capitate, hamate, and lunate of the KNM-WT-22944 individual attributed to *A. afarensis.* In phylomorphospace (Fig. 4.26, Table 4.11a), *A. sediba* is again best separated from African apes of the sampled hominins, positioned very similarly to that derived from all four elements (Fig. 4.22, Table 4.8b). In this case, however, it is joined amongst the

palmigrade monkeys by *A. afarensis*, potentially contradicting the hypothesized functional distinction of *A. sediba* relative to other hominins.

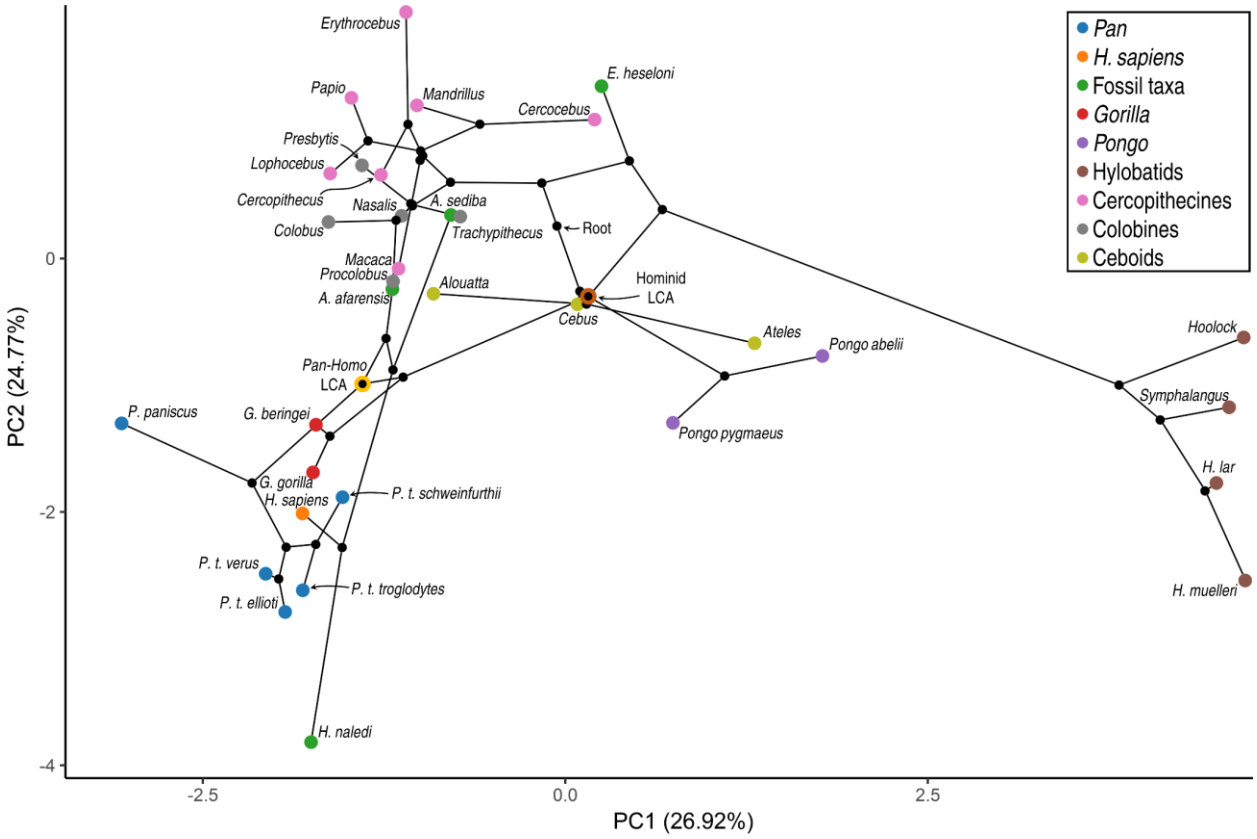

Fig. 4.26. Phylomorphospace representing anthropoid locomotor evolution based on phylogenetic PCA of 11 diagnostic shape variables from the capitate, hamate, and lunate. The phylogeny is projected onto the first two phylogenetic principal components of extant and fossil shape variables, with ancestral states estimated via maximum likelihood. *Pan-Homo* and great ape LCAs are highlighted. See Table 4.11a for eigenvalues.

The DFA analysis using the same shape variables (Fig. 4.27, Table 4.11b) clarifies this somewhat. The MH2 individual is again separated from other hominines, in this case positioned intermediately among the extant positional groups, with the greatest affinity to digitigrade cercopithecines (Table 4.12f). Meanwhile, the position of KNM-WT-22944 is shared by both humans and gorillas, and both *A. afarensis* and *H. naledi* are classified among the knuckle-walkers. As described above, withholding

triquetrum data from the analysis will tend to reduce the suspensory affinities, and increase the knuckle-walking affinities, of hominins. Nevertheless, the relative positions of the hominin taxa do seem consistent with some degree of functional divergence in *A. sediba* relative to other hominins.

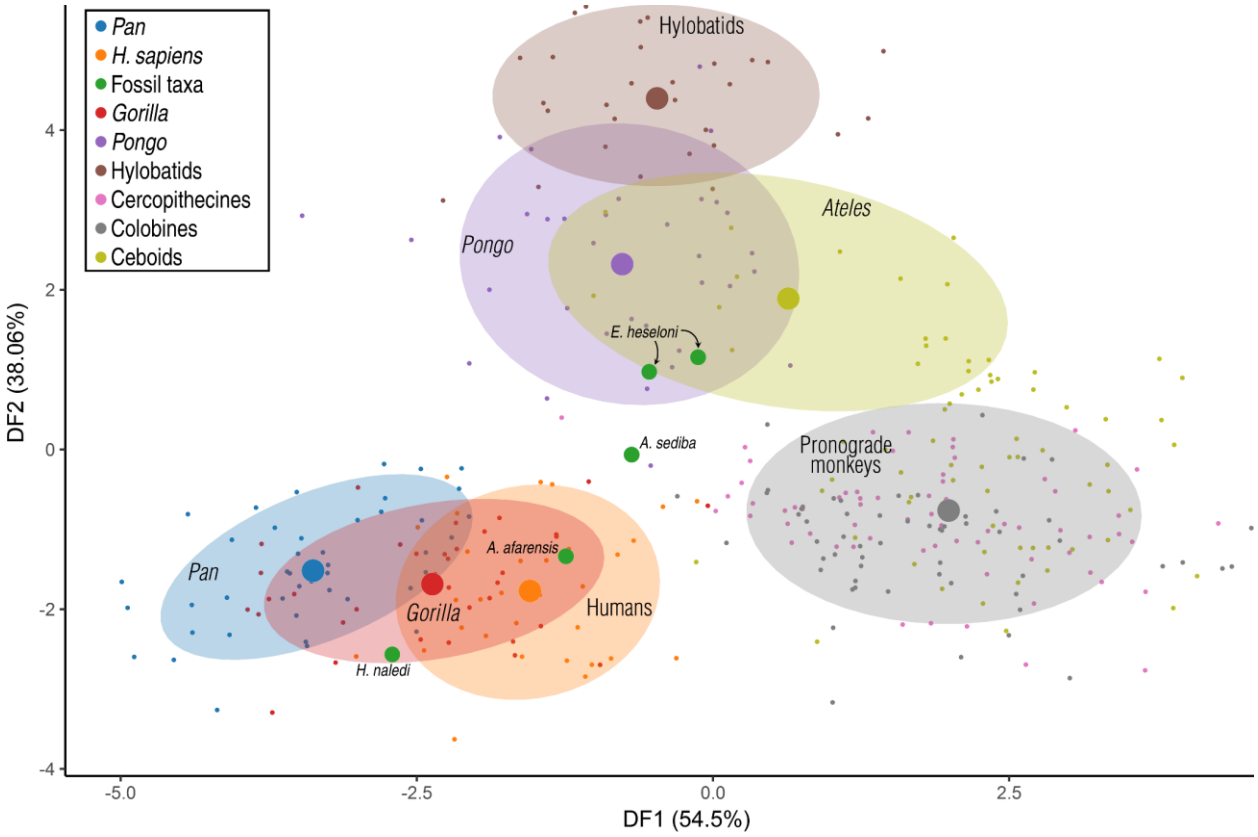

Fig. 4.27. Discriminant function analysis of 11 diagnostic shape variables from the capitate, hamate, and lunate. See Chapter 2 for selection criteria, Table 4.11b for discriminant functions, Table 4.9 for accuracy metrics, and Table 4.12f for predictions and posterior probabilities of humans and fossil specimens. Small and medium points represent extant and fossil observations, respectively. Large points represent group means; shaded ellipses are 80% confidence intervals.

While not representing a separate data point, the capitate and hamate available from the left wrist of MH2 are consistent with this assessment; the latter element is classified as a knuckle-walker in the hamate DFA with a posterior probability identical to its antimere (Table 4.12b), while the left capitate shares a digitigrade classification with

its antimere, its superior preservation notwithstanding (Table 4.12a). Other *A. afarensis* specimens are also consistent with the inferred functional distinction; only the AL 288-1 capitate substantially differs from KNM-WT 22944 in estimated function, and its knuckle-walking classification relative to the pronograde affinities of the other *A. afarensis* capitates and those of *A. sediba* would only widen the apparent functional gap between them. Whether this could be related to an arboreal habit in *A. sediba* remains unclear.

Table 4.11. Results of functional analyses combining diagnostic shape variables from the capitate, hamate, and lunate

a pPCA eigenvalues

	PC1	PC2
CpPxA	-0.40	-0.19
CpScA	-0.25	0.31
CpHmC	-0.41	0.09
CpHP	0.23	0.48
Hm5	-0.23	0.10
LuDs	-0.16	-0.57
LuSc	0.22	0.16
LuTq	-0.45	0.34
LuCpRaA	-0.03	-0.11
LuDsTqA	0.40	0.15
LuCpC	0.26	-0.34

b DFA scaling

	DF1	DF2
CpPxA	0.18	-0.69
CpScA	0.19	-0.22
CpHmC	-0.29	-0.40
CpHP	0.43	0.07
Hm5	0.46	-0.28
LuDs	-0.22	-0.40
LuSc	0.63	-0.26
LuTq	0.03	-0.12
LuCpRaA	1.16	0.03
LuDsTqA	0.16	0.78
LuCpC	-0.18	0.11

An aside on Mc3-capitate joint obliquity

Although not associated with positional behavior across the sample, the angle between the Mc3 and hamate facets of the capitate may help to inform hominin locomotor ancestry. Lovejoy and colleagues (2009a) provide two alternate metrics for quantifying obliquity in the Mc3-capitate joint (figures S23-S25 in Lovejoy *et al.*, 2009a; see also Selby *et al.*, 2016). They argue that the obliquity of this joint in African apes is associated with a "partial screw mechanism" (not to be confused with the "screw-clamp mechanism" of MacConaill, 1941) in the central joint complex (comprising the capitate,

hamate, and second and third metacarpal bases) to facilitate knuckle-walking, whereas its obliquity was independently acquired in humans, in which the embryonic transfer of a chondral anlage results in a region of ossification normally contributing to the capitate in adult humans instead forming the Mc3 styloid process. Humans would otherwise have a more neutrally- or oppositely-angled Mc3-capitate joint (depending on the measurement used) as seen in *Pongo*, *Papio*, and *Ardipithecus ramidus*. This trait as characterized here is not necessarily comparable, as the Mc3 is not analyzed. However, it is noteworthy that their metrics compare the axis of the Mc3 to that of either the proximal portion of the hamate facet or the dorsal margin of the Mc3 facet, rather than to either facet's average orientation. The former metric may therefore be problematic due to the enhanced proximodistal concavity of the hamate facet (Fig. 4.20d) in African apes compared to other hominoids, while the utility of characterizing the orientation of their Mc3 facet via a line along its dorsal margin would seem to be undermined by the authors' emphasis on the partial screw mechanism created by its opposite dorsal and palmar orientations (Selby *et al.*, 2016).

Nevertheless, when accounting for the topographical variance of these facets, the interior angle between them (Cp3HmA) is indeed less than 90° in nearly all sampled humans, most gorillas, and in a small majority of *Pan* specimens, with the *Pongo* mean being marginally closer to neutral (Fig. 4.20c). These results are in rough accord with the characterization of Lovejoy and colleagues (2009a), although the mean values of several other taxa deviate more strongly from neutral than do those of the African apes, with this angle being most acute among the hylobatids.

A pattern of variation in this trait does seem to be evident among the sampled hominins. Dorsolateral beveling of the distal capitate in association with Mc3 styloid process acquisition is only evident in sampled Neandertals and early and modern *H. sapiens*. The right capitate of the MH2 individual also has the appearance of this derived condition, but this seems to be due to diagenetic factors, as this region of the bone is abraded, and the Mc3 with which it articulates lacks a styloid process. The better-preserved left capitate of this individual also clearly lacks this trait. In likely association with this condition, the orientation of the Mc3 facet relative to the hamate facet ranges between 89° and 104° in the earlier hominin specimens, values comparable to those measured for *A. ramidus* (Lovejoy *et al.*, 2009a; Selby *et al.*, 2016), while the upper Pleistocene specimens vary between 75° and 87°, within the modern human range. The more acute angle of *H. floresiensis* despite its lack of morphology associated with an Mc3 styloid process is the exception to this trend, yet another way in which this taxon more closely resembles African apes than humans. The obtuse angle found in earlier hominin capitates potentially provides further support for the hominine LCA lacking the “screw mechanism” of African apes, joining most other results presented here in suggesting a relatively generalized arboreal locomotor ancestry.

Caveats

Similarly incongruent evolutionary scenarios derived from the analysis of different carpal elements led Kivell and colleagues (2013) to conclude that the bones of the

carpus each have a degree of independence in following distinct evolutionary pathways (but see Griffin and Yapuncich, 2015). This would seem to comport with many other recent studies in supporting the characterization of hominoid postcranial evolution as a mosaic process, with features like those of extant taxa emerging independently in separate fossil lineages (Rae, 1999; Almecija *et al.*, 2009; Kivell *et al.*, 2011; Alba *et al.*, 2012; Schmid *et al.*, 2013; Tallman *et al.*, 2013; Morgan *et al.*, 2015), their shared presence in extant taxa presumably having resulted from either later interbreeding among these lineages, or else due to many of these traits having been acquired yet again within ancestral lineages. However, while some degree of mosaicism is to be expected owing to the known vagaries of adaptive and non-adaptive evolution (e.g., Abrams, 2001), and there is a large body of evidence rejecting the parsimonious evolution of hominoid locomotor behaviors that might be suggested by a survey of the clade's surviving lineages, a combination of confounds likely contributes to enhancing the appearance of this phenomenon, particularly as it relates to the appearance of adjacent, functionally integrated bones evolving independently of each other.

The multivariate phylogenetic signal (K_{mult}) of the capitate, hamate, lunate, and triquetrum among sampled extant taxa are 0.59, 0.57, 0.69, and 0.59, respectively. When the fossil samples are considered, however, these values drop to 0.15, 0.26, 0.41, and 0.37, respectively. The attenuation of each element's phylogenetic signal (0.44, 0.31, 0.28, and 0.22, respectively), roughly corresponds with the number of each element comprising this study's fossil sample (25, 18, 8, and 5, respectively) and the number of operational taxonomic units to which they belong (14, 11, 5, and 4, respectively). This result is congruent with the consistent role fossil discoveries have

played in disrupting conclusions derived from variance patterns among extant taxa, and suggests that inconsistencies between ancestral reconstructions based on different elements are partially explained by the differential influence of respective fossil samples. However, results of this study's triquetrum analyses hint at the possibility of even greater levels of morphological convergence, as discussed above. This suggests that at least among hominoids, the low phylogenetic signal calculated in the combined capitate and hamate samples may partially reflect the high degree of mosaicism inferred in fossil hominoids, which in turn may related to the increased evolvability of the hominoid forelimb (Rolian *et al.*, 2010; Rolian, 2016), perhaps in concert with, in the case of middle and late Miocene Eurasian hominoids, increased diversity of available ecological niches after migration out of Africa (e.g., Begun, 2013).

However, because most phylogenetic comparative methods handle an individual fossil observation the same as a taxon centroid calculated from a large sample, much of the influence of a larger fossil sample on phylogenetic signal is a statistical phenomenon rather than a biological one, as it is impossible to know where the condition of each shape variable extracted from a fossil specimen would be positioned relative to the range of variation within the species it represents in the analysis. This problem may be further exacerbated among hominoids by what seems to be a real biological phenomenon, supported in this and the previous two chapters – morphological variability of the hominoid carpus drastically exceeds that of non-hominoid anthropoids, not only between taxa but within them as well. Any given hominoid fossil specimen should therefore be expected to less accurately represent the central tendencies of its species' morphology. Relatedly, the reader is cautioned

regarding the low sample sizes available for certain taxa of this study's extant hominoid sample, particularly the bonobos, in which this problem is likely culpable for much of the morphological gulf between the *Pan* species seen in several analyses.

Despite these limitations, as more fossil specimens are discovered (or made available for research), their phylogenetic affinities better characterized, and the range of morphological diversity at earlier stages of hominoid evolution more fully understood, techniques such as those used here are equipped to estimate which fossil taxa are more likely to represent the morphotypes ancestral to the various nested clades, particularly as they are improved upon to better account for intra-taxon variation and the number of individual observations contributing to the data associated with each tip of the phylogeny.

Conclusions

Results of this study provide further support for the frequency of parallelism in hominoid evolution, with specialized suspensory adaptation estimated to have been limited in the LCAs of the major hominoid clades. The LCAs of crown apes and great apes are instead reconstructed as more generalized arborealists; the prevalence of orthograde climbing in these ancestral apes is not specifically addressed, however, due to the complex and inconsistent correspondence of this behavior with carpal morphology. Therefore, while results are consistent with the positional repertoires of crown hominoids and hominids having resembled those of extant palmigrade monkeys or similarly reconstructed stem hominoids, as has been suggested (Lovejoy *et al.*, 2009a, b), it does not provide strong support for this hypothesis, as results are also

generally consistent with the supplementation of above-branch quadrupedalism with forelimb-dominated or antipronograde vertical climbing and clambering, as variously inferred for *Nacholapithecus* (Rose *et al.*, 1996; Nakatsukasa *et al.*, 1998; Ishida *et al.*, 1999, 2004; Dean and Begun, 2008; Nakatsukasa and Kunimatsu, 2009), *Pierolapithecus* (Almecija *et al.*, 2009; Alba *et al.*, 2010, but see Dean and Begun, 2008, 2010) and *Morotopithecus* (Sanders and Bodenbender, 1994; Gebo *et al.*, 1997; MacLatchy *et al.*, 2000; MacLatchy, 2004), and which may characterize *Rangwapithecus* as well (see Chapter 3).

The hominine and *Pan-Homo* LCAs are also estimated here to have been fairly generalized. Results of most analyses are consistent with a degree of terrestrialism, but only the lunate demonstrates patterns of variance most consistent with knuckle-walking having contributed to the ancestral repertoire, and the high phylogenetic structure of lunate variation among great apes attenuates its reliability in interpreting hominin functional affinities. Results of analyses of the other carpal elements and combinations thereof are most consistent with hominins having descended from a more generalized morphotype adapted for neither suspension nor terrestrial locomotion to a substantial degree. This study therefore joins other observations (e.g., Dainton and Macho, 1999; Thorpe and Crompton, 2006; Kivell and Schmitt, 2009; Lovejoy *et al.*, 2009b; Sayers *et al.*, 2012; Almecija *et al.*, 2015; White *et al.*, 2015) in questioning the utility of any extant ape species in modeling the morphology or locomotor repertoire of the *Pan-Homo* LCA, and finds parallelism, rather than homology, to better explain many of the behavioral similarities between extant African ape genera.

A. sediba is found to have diverged functionally from other hominins to some extent. While potentially comporting with previous detection of a suspensory signal in its more proximal brachial anatomy (Churchill *et al.*, 2013; Rein *et al.*, 2017), results of this study are equivocal regarding the behavioral implications of this morphology.

Finally, the inconsistent functional signals among hominin carpal elements when compared to those of extant non-human anthropoids may be explained by a lack of phylogenetic lag in hominin carpal morphology, rendering known hominin specimens relatively uninformative in reconstructing the ancestral behavioral repertoire.

Chapter 4 references

Abrams, P., 2001. Adaptationism, optimality models, and tests of adaptive scenarios, in: Orzack, S.H., Sober, E. (Eds.), Adaptationism and Optimality. Cambridge University Press, pp. 273-302.

Adams, D.C., 2014. A generalized K statistic for estimating phylogenetic signal from shape and other high-dimensional multivariate data. Systematic Biology 63, 685-697.

Alba, D.M., Almecija, S., Moya-Sola, S., 2010. Locomotor inferences in *Pierolapithecus* and *Hispanopithecus*: Reply to Deane and Begun (2008). Journal of Human Evolution 59, 143-149; discussion 150-154.

Alba, D.M., Almecija, S., Casanovas-Vilar, I., Mendez, J.M., Moya-Sola, S., 2012. A partial skeleton of the fossil great ape *Hispanopithecus laietanus* from Can Feu and the mosaic evolution of crown-hominoid positional behaviors. PLoS One 7, e39617.

Akaike, H., 1974. New look at statistical-model identification. IEEE Transactions on Automatic Control AC19, 716-723.

Almecija, S., 2016. Pitfalls reconstructing the last common ancestor of chimpanzees and humans. Proceedings of the National Academy of Sciences 113, E943-944.

Almecija, S., Alba, D.M., Moya-Sola, S., Kohler, M., 2007. Orang-like manual adaptations in the fossil hominoid *Hispanopithecus laietanus*: first steps towards great ape suspensory behaviours. Proceedings of the Royal Society B 274, 2375-2384.

Almecija, S., Alba, D.M., Moya-Sola, S., 2009. *Pierolapithecus* and the functional morphology of Miocene ape hand phalanges: paleobiological and evolutionary implications. Journal of Human Evolution 57, 284-297.

Almecija, S., Smaers, J.B., Jungers, W.L., 2015. The evolution of human and ape hand proportions. Nature Communications 6, 7717.

Arnold, C., Matthews, L.J., Nunn, C.L., 2010. The 10kTrees website: A new online resource for primate phylogeny. Evolutionary Anthropology 19, 114-118.

Bar-Yosef, O., 1998. The chronology of the Middle Paleolithic of the Levant, in: Akazawa, T., Aoki, K., Bar-Yosef, O. (Eds.), Neandertals and Modern Humans in Western Asia. Kluwer Academic Publishers, New York, pp. 39-56.

Begun, D.R., 1992. Miocene fossil hominids and the chimp-human clade. Science 257, 1929-1933.

Begun, D.R., 1993. New catarrhine phalanges from Rudabanya (Northeastern Hungary) and the problem of parallelism and convergence in hominoid postcranial morphology. Journal of Human Evolution 24, 373-402.

Begun, D.R., 2004. Knuckle-walking and the origin of human bipedalism, in: Meldrum, D.J., Hilton, C.E. (Eds.), From Biped to Strider: The Emergence of Modern Human Walking, Running and Resource Transport. Kluwer Academic/Plenum Publishers, New York, pp. 9-33.

Begun, D.R., 2007. How to identify (as opposed to define) a homoplasy: examples from fossil and living great apes. Journal of Human Evolution 52, 559-572.

Begun, D.R., 2013. The Miocene hominoid radiations, in: Begun, D.R. (Ed.), A Companion to Paleoanthropology. Wiley-Blackwell, pp. 398-416.

Begun, D.R., 2015. Fossil record of Miocene hominoids, in: Henke, W., Tattersall, I. (Eds.), Handbook of Paleoanthropology. Springer-Verlag, Berlin, pp. 1261-1332.
Begun, D.R., Kivell, T.L., 2011. Knuckle-walking in *Sivapithecus*? The combined effects of homology and homoplasy with possible implications for pongine dispersals. Journal of Human Evolution 60, 158-170.
Bishop, W.W., Miller, J.A., Fitch, F.J., 1969. New potassium-argon age determinations relevant to the Miocene fossil mammal sequence in East Africa. American Journal of Science 267, 669-699.
Bookstein, F., 2014. Measuring and Reasoning: Numerical Inference in the Sciences. Cambridge University Press, New York.
Boyer, D.M., Kaufman, S., Gunnell, G.F., Rosenberger, A.L., Delson, E., 2014. Managing 3D digital data sets of morphology: MorphoSource is a new project-based data archiving and distribution tool. American Journal of Physical Anthropology 153, 84-84.
Burnham, K.P., Anderson, D.R., 2002. Model Selection and Inference: A Practical Information-Theoretical Approach, 2nd Ed. Springer-Verlag, New York.
Butler, M.A., King, A.A., 2004. Phylogenetic comparative analysis: a modeling approach for adaptive evolution. American Naturalist 164, 683-695.
Byron, C.D., Covert, H.H., 2004. Unexpected locomotor behaviour: brachiation by an Old World monkey (*Pygathrix nemaeus*) from Vietnam. Journal of Zoology 263, 101-106.
Casanovas-Vilar, I., Alba, D.M., Garces, M., Robles, J.M., Moya-Sola, S., 2011. Updated chronology for the Miocene hominoid radiation in Western Eurasia. Proceedings of the National Academy of Sciences 108, 5554-5559.
Churchill, S.E., Holliday, T.W., Carlson, K.J., Jashashvili, T., Macias, M.E., Mathews, S., Sparling, T.L., Schmid, P., de Ruiter, D.J., Berger, L.R., 2013. The upper limb of *Australopithecus sediba*. Science 340, 1233477-1233477.
Cote, S., McNulty, K.P., Stevens, N.J., Nengo, I.O., 2016. A detailed assessment of the maxillary morphology of *Limnopithecus evansi* with implications for the taxonomy of the genus. Journal of Human Evolution 94, 83-91.
Crompton, R.H., Sellers, W.I., Thorpe, S.K., 2010. Arboreality, terrestriality and bipedalism. Philosophical transactions of the Royal Society of London. Series B, Biological sciences 365, 3301-3314.
Dainton, M., Macho, G.A., 1999. Did knuckle walking evolve twice? Journal of Human Evolution 36, 171-194.
Deane, A.S., Begun, D.R., 2008. Broken fingers: retesting locomotor hypotheses for fossil hominoids using fragmentary proximal phalanges and high-resolution polynomial curve fitting (HR-PCF). Journal of Human Evolution 55, 691-701.
Deane, A.S., Begun, D.R., 2010. Pierolapithecus locomotor adaptations: a reply to Alba *et al.*'s comment on Deane and Begun (2008). Journal of Human Evolution 59, 150-154.
Dembo, M., Radovčić, D., Garvin, H.M., Laird, M.F., Schroeder, L., Scott, J.E., Brophy, J., Ackermann, R.R., Musiba, C.M., de Ruiter, D.J., Mooers, A.Ø., Collard, M., 2016. The evolutionary relationships and age of *Homo* naledi: An assessment using dated Bayesian phylogenetic methods. Journal of Human Evolution 97, 17-26.

Dirks, P.H.G.M., Roberts, E.M., Hilbert-Wolf, H., Kramers, J.D., Hawks, J., Dosseto, A., Duval, M., Elliott, M., Evans, M., Grün, R., Hellstrom, J., Herries, A.I.R., Joannes-Boyau, R., Makhubela, T.V., Placzek, C.J., Robbins, J., Spandler, C., Wiersma, J., Woodhead, J., Berger, L.R., 2017. The age of *Homo naledi* and associated sediments in the Rising Star Cave, South Africa. eLife 6, e24231.

Einstein, A., 1905. On the movement of small particles suspended in a stationary liquid demanded by the molecular-kinetic theory of heat. Annalen der Physik 322, 549-560.

Felsenstein, J., 1985. Phylogenies and the comparative method. American Naturalist 125, 1-15.

Felsenstein, J., 1988. Phylogenies and quantitative characters. Annual Review of Ecology and Systematics 19, 445-471.

Gebo, D.L., 1992. Plantigrady and foot adaptation in African apes: implications for hominid origins. American Journal of Physical Anthropology 89, 29-58.

Gebo, D.L., 1996. Climbing, brachiation, and terrestrial quadrupedalism: historical precursors of hominid bipedalism. American Journal of Physical Anthropology 101, 55-92.

Gebo, D.L., MacLatchy, L., Kityo, R., Deino, A., Kingston, J., Pilbeam, D., 1997. A hominoid genus from the early Miocene of Uganda. Science 276, 401-404.

Granatosky, M.C., 2015. Kinetic and kinematic patterns of arm-swinging in the red-shanked douc langur (*Pygathrix nemaeus*). Vietnamese Journal of Primatology 2, 33-40.

Green, D.J., Gordon, A.D., Richmond, B.G., 2007. Limb-size proportions in *Australopithecus afarensis* and *Australopithecus africanus*. Journal of Human Evolution 52, 187-200.

Gregory, W.K., 1927. Two views of the origin of man. Science 65, 601-605.

Griffin, R.H., Yapuncich, G.S., 2015. The independent evolution method is not a viable phylogenetic comparative method. PLoS One 10, e0144147.

Hammond, A.S., Alba, D.M., Almecija, S., Moya-Sola, S., 2013. Middle Miocene Pierolapithecus provides a first glimpse into early hominid pelvic morphology. Journal of Human Evolution.

Hamrick, M.W., 1999. Pattern and process in the evolution of primate nails and claws. J. Hum. Evol. 37, 293-297.

Hansen, T.F., 1997. Stabilizing selection and the comparative analysis of adaptation. Evolution 51, 1341-1351.

Harcourt-Smith, W.E.H., 2015. The origins of bipedal locomotion, in: Henke, W., Tattersall, I. (Eds.), Handbook of Paleoanthropology. Springer, Heidelberg, pp. 1919-1957.

Harrison, T., 1991. The implications of *Oreopithecus bambolii* for the origins of bipedalism, in: Coppens, Y., Senut, B. (Eds.), Origine(s) de la Bipedie Chez Les Hominides. Editions du CNRS, Paris, pp. 235-244.

Harrison, T., 2010. Dendropithecoidea, Proconsuloidea, and Hominoidea, in: Werdelin, L., Sanders, W.J. (Eds.), Cenozoic Mammals of Africa. University of California Press, Berkeley, pp. 429-469.

Harrison, T., Rook, L., 1997. Enigmatic anthropoid or misunderstood ape?: the phylogenetic status of *Oreopithecus bambolii* reconsidered, in: Begun, D.R.,

Ward, C.V., Rose, M.D. (Eds.), Function, Phylogeny, and Fossils: Miocene Hominoid Evolution and Adaptations. Plenum Press, New York, pp. 327-362.
Harrison, T., Rein, T.R., 2016. The hands of fossil non-hominoid anthropoids, in: Kivell, T.L., Lemelin, P., Richmond, B.G., Schmitt, D. (Eds.), The Evolution of the Primate Hand. Springer, New York, pp. 455-483.
Hunt, K.D., 1996. The postural feeding hypothesis: An ecological model for the evolution of bipedalism. South African Journal of Science 92, 77.
Ingram, T., Mahler, D.L., 2013. Surface: detecting convergent evolution from comparative data by fitting Ornstein-Uhlenbeck models with stepwise Akaike Information Criterion. Methods in Ecology and Evolution 4, 416-425.
Inouye, S.E., 1992. Ontogeny and allometry of African ape manual rays. Journal of Human Evolution 23, 107-138.
Inouye, S.E., 1994. Ontogeny of knuckle-walking hand postures in African apes. Journal of Human Evolution 26, 459-485.
Inouye, S.E., Shea, B.T., 2004. The implications of variation in knuckle-walking features for models of African hominoid locomotor evolution. Journal of Anthropological Sciences 82, 67-88.
Ishida, H., Kunimatsu, Y., Nakatsukasa, M., Nakano, Y., 1999. New hominoid genus from the Middle Miocene of Nachola, Kenya. Anthropological Science 107, 189-191.
Ishida, H., Kunimatsu, Y., Takano, T., Nakano, Y., Nakatsukasa, M., 2004. *Nacholapithecus* skeleton from the Middle Miocene of Kenya. Journal of Human Evolution 46, 69-103.
Johanson, D.C., Masao, F.T., Eck, G.G., White, T.D., Walter, R.C., Kimbel, W.H., Asfaw, B., Manega, P., Ndessokia, P., Suwa, G., 1987. New partial skeleton of *Homo habilis* from Olduvai Gorge, Tanzania. Nature 327, 205-209.
Jones, A.L., 2008. The evolution of brachiation in ateline primates, ancestral character states and history. American Journal of Physical Anthropology 137, 123-144.
Jungers, W.L., 1987. Body size and morphometric affinities of the appendicular skeleton in *Oreopithecus bambolii* (IGF-11778). Journal of Human Evolution 16, 445-456.
Keith, A., 1902. The extent to which the posterior segments of the body have been transmuted and suppressed in the evolution of man and the allied primates. Journal of Anatomy and Physiology 37, 18-40.
Keith, A., 1923. Man's posture: its evolution and disorders. The British Medical Journal 1, 451-454, 499-502, 545-548, 587-590, 624-626, 669-672.
King, A.A., Butler, M.A. 2009. ouch: Ornstein-Uhlenbeck models for phylogenetic comparative hypotheses (R package).
Kivell, T.L., 2011. A comparative analysis of the hominin triquetrum (SKX 3498) from Swartkrans, South Africa. South African Journal of Science 107, #515, 510 pages.
Kivell, T.L., Begun, D.R., 2007. Frequency and timing of scaphoid-centrale fusion in hominoids. Journal of Human Evolution 52, 321-340.
Kivell, T.L., Begun, D.R., 2009. New primate carpal bones from Rudabanya (late Miocene, Hungary): taxonomic and functional implications. Journal of Human Evolution 57, 697-709.

Kivell, T.L., Schmitt, D., 2009. Independent evolution of knuckle-walking in African apes shows that humans did not evolve from a knuckle-walking ancestor. Proceedings of the National Academy of Sciences 106, 14241-14246.
Kivell, T.L., Kibii, J.M., Churchill, S.E., Schmid, P., Berger, L.R., 2011. *Australopithecus sediba* hand demonstrates mosaic evolution of locomotor and manipulative abilities. Science 333, 1411-1417.
Kivell, T.L., Barros, A.P., Smaers, J.B., 2013. Different evolutionary pathways underlie the morphology of wrist bones in hominoids. BMC Evolutionary Biology 13, 229.
Kivell, T.L., Deane, A.S., Tocheri, M.W., Orr, C.M., Schmid, P., Hawks, J., Berger, L.R., Churchill, S.E., 2015. The hand of *Homo naledi*. Nature communications 6, 8431.
Kohler, M., Moya-Sola, S., 1997. Ape-like or hominid-like? The positional behavior of *Oreopithecus*. Proceedings of the National Academy of Sciences 94, 11747-11750.
Langergraber, K.E., Prufer, K., Rowey, C., Boesch, C., Crockford, C., Fawcett, K., Inoue, E., Vigilant, L., 2012. Generation times in wild chimpanzees and gorillas suggest earlier divergence times in great ape and human evolution. Proceedings of the National Academy of Sciences 109, 15716-15721.
Larson, S.G., 1998. Parallel evolution in the hominoid trunk and forelimb. Evolutionary Anthropology 6, 87-99.
Lovejoy, C.O., Meindl, R.S., Pryzbeck, T.R., Barton, T.S., Heiple, K.G., Kotting, D., 1977. Paleodemography of the Libben site, Ottawa county, Ohio. Science 198, 291-293.
Lovejoy, C.O., Cohn, M.J., White, T.D., 1999. Morphological analysis of the mammalian postcranium: A developmental perspective. Proceedings of the National Academy of Sciences 96, 13247-13252.
Lovejoy, C.O., Simpson, S.W., White, T.D., Asfaw, B., Suwa, G., 2009a. Careful climbing in the Miocene: The forelimbs of *Ardipithecus ramidus* and humans are primitive. Science 326, 70e1-8.
Lovejoy, C.O., Suwa, G., Simpson, S.W., Matternes, J.H., White, T.D., 2009b. The great divides: *Ardipithecus ramidus* reveals the postcrania of our last common ancestors with African apes. Science 326, 100-106.
MacConaill, M.A., 1941. The mechanical anatomy of the carpus and its bearings on some surgical problems. Journal of Anatomy 75, 166-175.
MacLatchy, L., Gebo, D., Kityo, R., Pilbeam, D., 2000. Postcranial functional morphology of *Morotopithecus bishopi*, with implications for the evolution of modern ape locomotion. Journal of Human Evolution 39, 159-183.
Maclatchy, L., 2004. The oldest ape. Evolutionary Anthropology 13, 90-103.
Madar, S.I., Rose, M.D., Kelley, J., MacLatchy, L., Pilbeam, D., 2002. New *Sivapithecus* postcranial specimens from the Siwaliks of Pakistan. Journal of Human Evolution 42, 705-752.
Matarazzo, S., 2008. Knuckle walking signal in the manual digits of *Pan* and *Gorilla*. American Journal of Physical Anthropology 135, 27-33.
Matarazzo, S., 2013. Manual pressure distribution patterns of knuckle-walking apes. American Journal of Physical Anthropology 152, 44-50.

McHenry, H.M., Berger, L.R., 1998. Body proportions in *Australopithecus afarensis* and *A. africanus* and the origin of the genus *Homo*. Journal of Human Evolution 35, 1-22.
McPherron, S.P., Alemseged, Z., Marean, C.W., Wynn, J.G., Reed, D., Geraads, D., Bobe, R., Bearat, H.A., 2010. Evidence for stone-tool-assisted consumption of animal tissues before 3.39 million years ago at Dikika, Ethiopia. Nature 466, 857-860.
Meindl, R.S., Mensforth, R.P., Lovejoy, C.O., 2008. The Libben site: A hunting, fishing, and gathering village from the eastern late woodlands of North America. Analysis and implications for palaeodemography and human origins., in: Bocquet-Appel, J.-P. (Ed.), Recent Advances in Palaeodemography. Springer Science+Business Media, pp. 259-275.
Morgan, M.E., Lewton, K.L., Kelley, J., Otárola-Castillo, E., Barry, J.C., Flynn, L.J., Pilbeam, D., 2015. A partial hominoid innominate from the Miocene of Pakistan: Description and preliminary analyses. Proceedings of the National Academy of Sciences 112, 82-87.
Moya-Sola, S., Kohler, M., Rook, L., 1999. Evidence of hominid-like precision grip capability in the hand of the Miocene ape *Oreopithecus*. Proceedings of the National Academy of Sciences 96, 313-317.
Moya-Sola, S., Kohler, M., Alba, D.M., Casanovas-Vilar, I., Galindo, J., 2004. *Pierolapithecus catalaunicus*, a new Middle Miocene great ape from Spain. Science 306, 1339-1344.
Moya-Sola, S., Kohler, M., Rook, L., 2005. The *Oreopithecus* thumb: a strange case in hominoid evolution. Journal of Human Evolution 49, 395-404.
Nakatsukasa, M., Yamanaka, A., Kunimatsu, Y., Shimizu, D., Ishida, H., 1998. A newly discovered *Kenyapithecus* skeleton and its implications for the evolution of positional behavior in Miocene East African hominoids. Journal of Human Evolution 34, 657-664.
Nakatsukasa, M., Kunimatsu, Y., 2009. *Nacholapithecus* and its importance for understanding hominoid evolution. Evolutionary Anthropology 18, 103-119.
Napier, J.R., 1964. The evolution of bipedal walking in the hominids. Archives de biologie 75, 673-708.
Orr, C.M., 2005. Knuckle-walking anteater: A convergence test of adaptation for purported knuckle-walking features of African Hominidae. American Journal of Physical Anthropology 128, 639-658.
Orr, C.M., Tocheri, M.W., Burnett, S.E., Awe, R.D., Saptomo, E.W., Sutikna, T., Jatmiko, Wasisto, S., Morwood, M.J., Jungers, W.L., 2013. New wrist bones of *Homo floresiensis* from Liang Bua (Flores, Indonesia). Journal of Human Evolution 64, 109-129.
Pagel, M., 1999. Inferring the historical patterns of biological evolution. Nature 401, 877-884.
Patel, B.A., Susman, R.L., Rossie, J.B., Hill, A., 2009. Terrestrial adaptations in the hands of *Equatorius africanus* revisited. Journal of Human Evolution 57, 763-772.
Peppe, D.J., Deino, A.L., McNulty, K.P., Lehmann, T., Harcourt-Smith, W.E.H., Dunsworth, H.M., Fox, D.L., 2011. New age constraints on the early Miocene

faunas from Rusinga and Mfangano Islands (Lake Victoria, Kenya). American Journal of Physical Anthropology 144, 237-237.
Pina, M., Alba, D.M., Almecija, S., Fortuny, J., Moya-Sola, S., 2012. Paleobiological inferences on the locomotor repertoire of extinct hominoids based on femoral neck cortical thickness: The fossil great ape *Hispanopithecus laietanus* as a test-case study. American Journal of Physical Anthropology 149, 142-148.
Pina, M., Almecija, S., Alba, D.M., O'Neill, M.C., Moya-Sola, S., 2014. The middle Miocene ape *Pierolapithecus catalaunicus* exhibits extant great ape-like morphometric affinities on its patella: Inferences on knee function and evolution. PLoS One 9, e91944.
Polly, P.D., Lawing, A.M., Fabre, A.-C., Goswami, A., 2013. Phylogenetic principal components analysis and geometric morphometrics. Hystrix 24, 33-41.
Rae, T.C., 1999. Mosaic evolution in the origin of the Hominoidea. Folia Primatologica 70, 125-135.
Rein, T.R., Harrison, T., Carlson, K.J., Harvati, K., 2017. Adaptation to suspensory locomotion in *Australopithecus sediba*. Journal of Human Evolution 104, 1-12.
Revell, L.J., 2009. Size-correction and principal components for interspecific comparative studies. Evolution 63, 3258-3268.
Revell, L.J., 2012. phytools: An R package for phylogenetic comparative biology (and other things). Methods in Ecology and Evolution 3, 217-223.
Revell, L.J., 2013. Two new graphical methods for mapping trait evolution on phylogenies. Methods in Ecology and Evolution 4, 754-759.
Revell, L.J., 2014. Graphical methods for visualizing comparative data on phylogenies, in: Garamszegi, L.Z. (Ed.), Modern Phylogenetic Comparative Methods and Their Application in Evolutionary Biology. Springer, pp. 77-103.
Richmond, B.G., Strait, D.S., 2000. Evidence that humans evolved from a knuckle-walking ancestor. Nature 404, 382-385.
Richmond, B.G., Begun, D.R., Strait, D.S., 2001. Origin of human bipedalism: The knuckle-walking hypothesis revisited. American Journal of Physical Anthropology Suppl 33, 70-105.
Richmond, B.G., 2006. Functional morphology of the midcarpal joint in knuckle-walkers and terrestrial quadrupeds, in: Ishida, H., Tuttle, R., Pickford, M., Ogihara, N., Nakatsukasa, M. (Eds.), Human Origins and Environmental Backgrounds. Springer, New York, pp. 105-122.
Rohlf, F.J., 2002. Geometric morphometrics and phylogeny, in: MacLeod, N., Forey, P.L. (Eds.), Morphology, Shape and Phylogeny. Taylor & Francis, London, pp. 175-193.
Rolian, C., 2016. The role of genes and development in the evolution of the primate hand, in: Kivell, T.L., Lemelin, P., Richmond, B.G., Schmitt, D. (Eds.), The Evolution of the Primate Hand. Springer, New York, pp. 101-130.
Rolian, C., Lieberman, D.E., Hallgrimsson, B., 2010. The coevolution of human hands and feet. Evolution 64, 1558-1568.
Rook, L., Bondioli, L., Kohler, M., Moya-Sola, S., Macchiarelli, R., 1999. *Oreopithecus* was a bipedal ape after all: Evidence from the iliac. Proceedings of the National Academy of Sciences 96, 8795-8799.

Rose, M.D., 1986. Further hominoid postcranial specimens from the late Miocene Nagri formation of Pakistan. Journal of Human Evolution 15, 333-367.
Rose, M.D., 1997. Functional and phylogenetic features of the forelimb in Miocene hominoids, in: Begun, D.R., Ward, C.V., Rose, M.D. (Eds.), Function, Phylogeny, and Fossils: Miocene Hominoid Evolution and Adaptations. Plenum Press, New York, pp. 79-100.
Roth, V.L., 1984. On homology. Biological Journal of the Linnean Society 22, 13-29.
Russo, G.A., Shapiro, L.J., 2013. Reevaluation of the lumbosacral region of *Oreopithecus bambolii*. Journal of Human Evolution 65, 253-265.
Ruvolo, M., Disotell, T.R., Allard, M.W., Brown, W.M., Honeycutt, R.L., 1991. Resolution of the African hominid trichotomy by use of a mitochondrial gene sequence. Proceedings of the National Academy of Sciences 88, 1570-1574.
Ruvolo, M., 1997. Molecular phylogeny of the hominoids: inferences from multiple independent DNA sequence data sets. Molecular Biology and Evolution 14, 248-265.
Sanchez, P.M., 1974. The unequal group size problem in discriminant analysis. Journal of the Academy of Marketing Science 2, 629-633.
Sanders, W.J., Bodenbender, B.E., 1994. Morphometric analysis of lumbar vertebra UMP 67-28: implications for spinal function and phylogeny of the Miocene Moroto hominoid. Journal of Human Evolution 26, 203-237.
Sarmiento, E.E., 1988. Anatomy of the hominoid wrist joint: its evolutionary and functional implications. International Journal of Primatology 9, 281-345.
Sayers, K., Raghanti, M.A., Lovejoy, C.O., 2012. Human evolution and the chimpanzee referential doctrine. Annual Review of Anthropology 41, 119-138.
Scally, A., Dutheil, J.Y., Hillier, L.W., Jordan, G.E., Goodhead, I., Herrero, J., Hobolth, A., Lappalainen, T., Mailund, T., Marques-Bonet, T., McCarthy, S., Montgomery, S.H., Schwalie, P.C., Tang, Y.A., Ward, M.C., Xue, Y., Yngvadottir, B., Alkan, C., Andersen, L.N., Ayub, Q., Ball, E.V., Beal, K., Bradley, B.J., Chen, Y., Clee, C.M., Fitzgerald, S., Graves, T.A., Gu, Y., Heath, P., Heger, A., Karakoc, E., Kolb-Kokocinski, A., Laird, G.K., Lunter, G., Meader, S., Mort, M., Mullikin, J.C., Munch, K., O'Connor, T.D., Phillips, A.D., Prado-Martinez, J., Rogers, A.S., Sajjadian, S., Schmidt, D., Shaw, K., Simpson, J.T., Stenson, P.D., Turner, D.J., Vigilant, L., Vilella, A.J., Whitener, W., Zhu, B., Cooper, D.N., de Jong, P., Dermitzakis, E.T., Eichler, E.E., Flicek, P., Goldman, N., Mundy, N.I., Ning, Z., Odom, D.T., Ponting, C.P., Quail, M.A., Ryder, O.A., Searle, S.M., Warren, W.C., Wilson, R.K., Schierup, M.H., Rogers, J., Tyler-Smith, C., Durbin, R., 2012. Insights into hominid evolution from the gorilla genome sequence. Nature 483, 169-175.
Schluter, D., Price, T., Mooers, A., xd, Ludwig, D., 1997. Likelihood of ancestor states in adaptive radiation. Evolution 51, 1699-1711.
Schmid, P., Churchill, S.E., Nalla, S., Weissen, E., Carlson, K.J., de Ruiter, D.J., Berger, L.R., 2013. Mosaic morphology in the thorax of *Australopithecus sediba*. Science 340, 1234598-1234598.
Schroeder, L., Scott, J.E., Garvin, H.M., Laird, M.F., Dembo, M., Radovčić, D., Berger, L.R., de Ruiter, D.J., Ackermann, R.R., 2017. Skull diversity in the *Homo* lineage

and the relative position of *Homo naledi*. Journal of Human Evolution 104, 124-135.
Selby, M.S., Simpson, S.W., Lovejoy, C.O., 2016. The functional anatomy of the carpometacarpal complex in anthropoids and its implications for the evolution of the hominoid hand. Anatomical Record 299, 583-600.
Selby, M.S., Lovejoy, C.O., 2017. Evolution of the hominoid scapula and its implications for earliest hominid locomotion. American Journal of Physical Anthropology 162, 682-700.
Shang, H., Tong, H., Zhang, S., Chen, F., Trinkaus, E., 2007. An early modern human from Tianyuan Cave, Zhoukoudian, China. Proceedings of the National Academy of Sciences 104, 6573-6578.
Shea, B.T., Inouye, S.E., 1993. Knuckle-walking ancestors. Science 259, 293-294.
Stanford, C.B., 2006. Arboreal bipedalism in wild chimpanzees: implications for the evolution of hominid posture and locomotion. American Journal of Physical Anthropology 129, 225-231.
Steiper, M.E., Young, N.M., 2006. Primate molecular divergence dates. Molecular Phylogenetics and Evolution 41, 384-394.
Steiper, M.E., Seiffert, E.R., 2012. Evidence for a convergent slowdown in primate molecular rates and its implications for the timing of early primate evolution. Proceedings of the National Academy of Sciences 109, 6006-6011.
Straus, J., William L., 1949. The riddle of man's ancestry. The Quarterly Review of Biology 24, 200-223.
Susanna, I., Alba, D.M., Almecija, S., Moya-Sola, S., 2014. The vertebral remains of the late Miocene great ape *Hispanopithecus laietanus* from Can Llobateres 2 (Valles-Penedes Basin, NE Iberian Peninsula). Journal of Human Evolution 73, 15-34.
Sutikna, T., Tocheri, M.W., Morwood, M.J., Saptomo, E.W., Jatmiko, Awe, R.D., Wasisto, S., Westaway, K.E., Aubert, M., Li, B., Zhao, J.X., Storey, M., Alloway, B.V., Morley, M.W., Meijer, H.J., van den Bergh, G.D., Grun, R., Dosseto, A., Brumm, A., Jungers, W.L., Roberts, R.G., 2016. Revised stratigraphy and chronology for *Homo floresiensis* at Liang Bua in Indonesia. Nature 532, 366-369.
Tallman, M., Almecija, S., Reber, S.L., Alba, D.M., Moya-Sola, S., 2013. The distal tibia of *Hispanopithecus laietanus*: More evidence for mosaic evolution in Miocene apes. Journal of Human Evolution 64, 319-327.
Thackeray, J.F., 2015. Estimating the age and affinities of *Homo naledi*. South African Journal of Science 111, 1-2.
Thorpe, S.K., Crompton, R.H., 2006. Orangutan positional behavior and the nature of arboreal locomotion in Hominoidea. American Journal of Physical Anthropology 131, 384-401.
Thorpe, S.K.S., McClymont, J.M., Crompton, R.H., 2015. The arboreal origins of human bipedalism. Antiquity 88, 906-914.
Tocheri, M.W., Orr, C.M., Larson, S.G., Sutikna, T., Jatmiko, Saptomo, E.W., Due, R.A., Djubiantono, T., Morwood, M.J., Jungers, W.L., 2007. The primitive wrist of *Homo floresiensis* and its implications for hominin evolution. Science 317, 1743-1745.

Tuttle, R.H., 1967. Knuckle-walking and the evolution of hominoid hands. American Journal of Physical Anthropology 26, 171-206.
Tuttle, R.H., 1969. Knuckle-walking and the problem of human origins. Science 166, 953-961.
Tuttle, R., 1974. Darwin's apes, dental apes, and the descent of man: normal science in evolutionary anthropology. Current Anthropology 15, 389-398.
Tuttle, R.H., 1981. Evolution of hominid bipedalism and prehensile capabilities. Philosophical Transactions of the Royal Society of London B 292, 89-94.
Ward, C.V., 2015. Postcranial and locomotor adaptations of hominoids, in: Henke, W., Tattersall, I. (Eds.), Handbook of Paleoanthropology. Springer-Verlag, Berlin, pp. 1363-1386.
Ward, C.V., Leakey, M.G., Brown, B., Brown, F., Harris, J., Walker, A., 1999. South Turkwel: a new Pliocene hominid site in Kenya. Journal of Human Evolution 36, 69-95.
Ward, C.V., Kimbel, W.H., Harmon, E.H., Johanson, D.C., 2012. New postcranial fossils of *Australopithecus afarensis* from Hadar, Ethiopia (1990-2007). Journal of Human Evolution 63, 1-51.
Washburn, S.L., 1967. Behaviour and the origin of man. Proceedings of the Royal Anthropological Institute of Great Britain and Ireland 1967, 21-27.
White, T.D., Lovejoy, C.O., Asfaw, B., Carlson, J.P., Suwa, G., 2015. Neither chimpanzee nor human, *Ardipithecus* reveals the surprising ancestry of both. Proceedings of the National Academy of Sciences 112, 4877-4884.
Williams, S.A., 2010. Morphological integration and the evolution of knuckle-walking. Journal of Human Evolution 58, 432-440.
Wolpoff, M.H., 1997. *Australopithecus*: a new look at an old ancestor. General Anthropology 3, 1-5.
Wright, K.A., Stevens, N.J., Covert, H.H., Nadler, T., 2008. Comparisons of Suspensory Behaviors Among *Pygathrix cinerea*, *P. nemaeus*, and *Nomascus leucogenys* in Cuc Phuong National Park, Vietnam. International Journal of Primatology 29, 1467-1480.
Wunderlich, R.E., Walker, A., Jungers, W.L., 1999. Rethinking the positional repertoire of *Oreopithecus*. American Journal of Physical Anthropology 108, 528.
Youlatos, D., 1996. Atelines, apes and wrist joints. Folia Primatologica 67, 193-198.
Young, N.M., Capellini, T.D., Roach, N.T., Alemseged, Z., 2015. Fossil hominin shoulders support an African ape-like last common ancestor of humans and chimpanzees. Proceedings of the National Academy of Sciences 112, 11829-11834.

Supplementary material

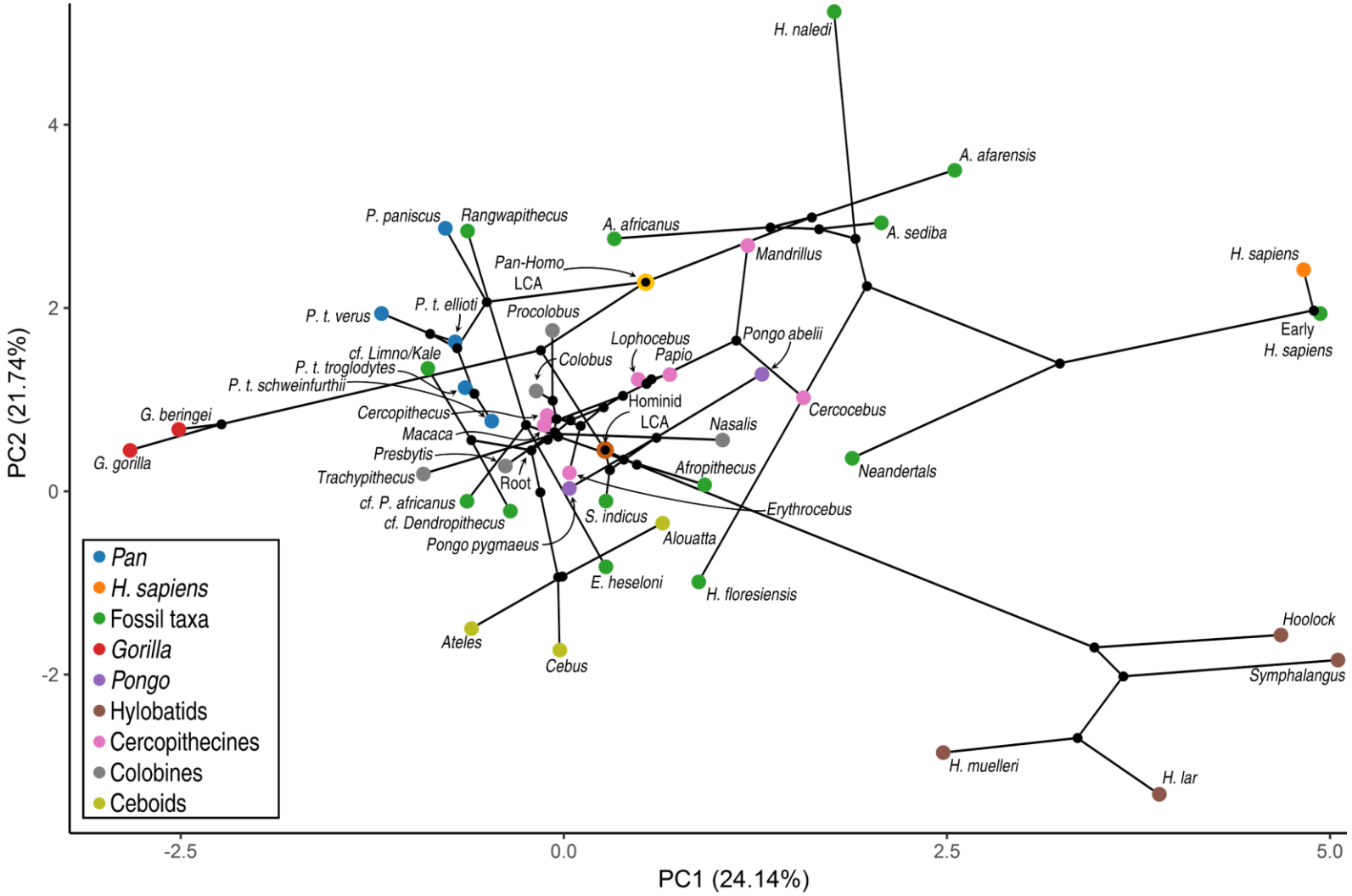

Fig. 4.28. Phylomorphospace representing the evolutionary history of anthropoid capitate morphology, based on phylogenetic PCA. The phylogeny is projected onto the first two phylogenetic principal components of all extant and fossil capitate shape variables, with ancestral states estimated via maximum likelihood. *Pan-Homo* and great ape LCAs are highlighted. See Table 4.5a for eigenvalues

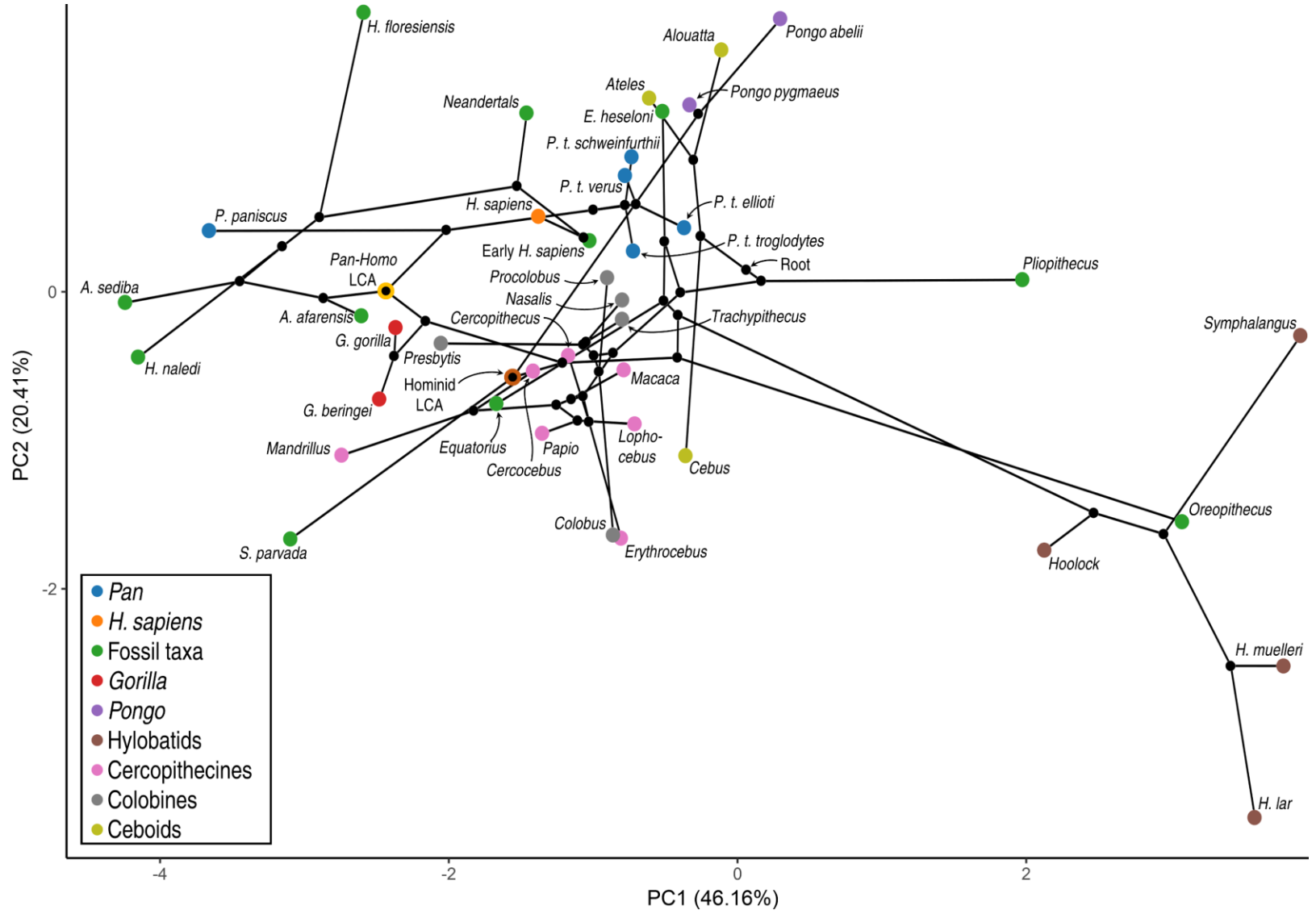

Fig. 4.29. Phylomorphospace representing the evolutionary history of anthropoid hamate morphology, based on phylogenetic PCA. The phylogeny is projected onto the first two phylogenetic principal components of all extant and fossil hamate shape variables, with ancestral states estimated via maximum likelihood. *Pan-Homo* and great ape LCAs are highlighted. See Table 4.5b for eigenvalues

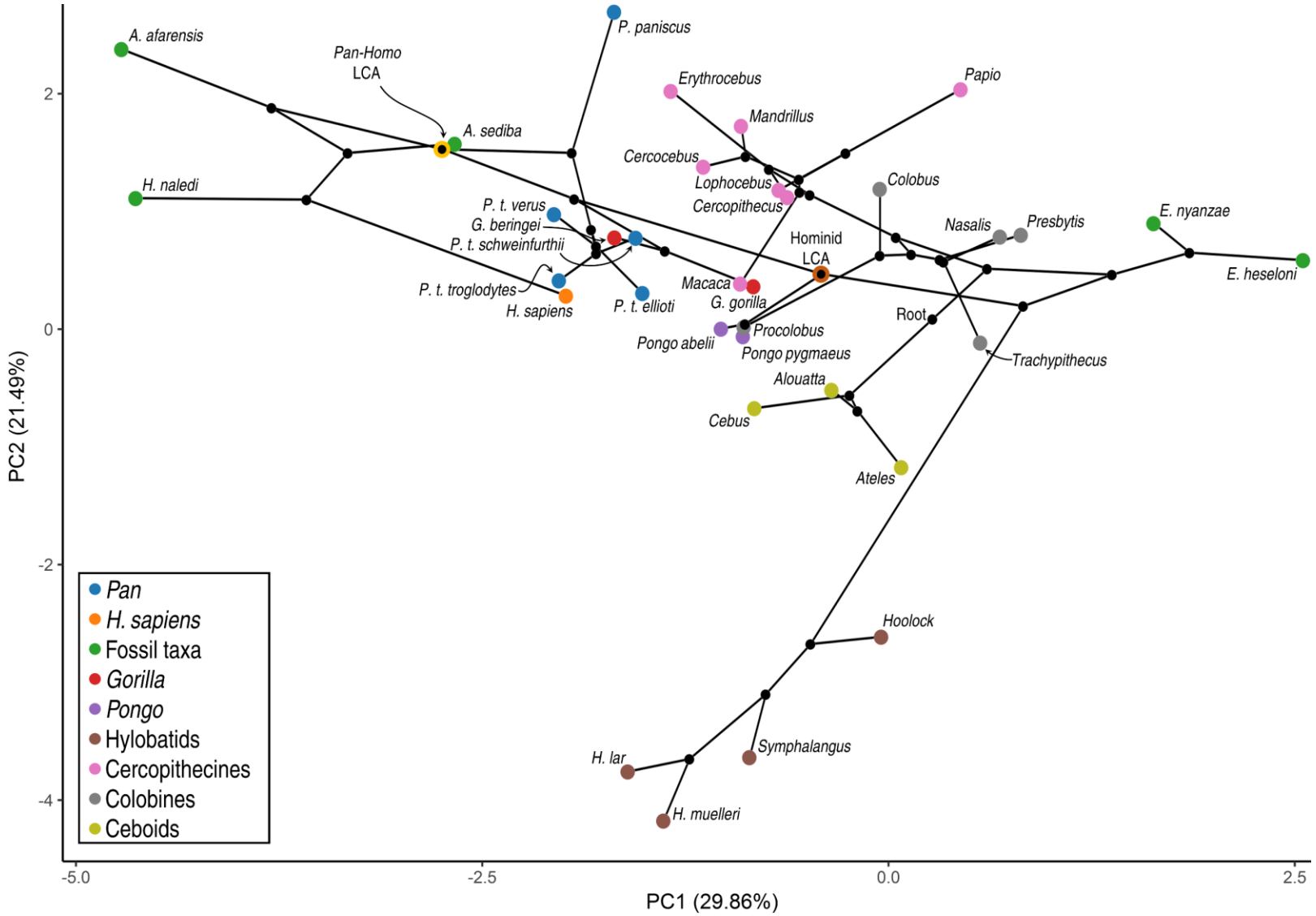

Fig. 4.30. Phylomorphospace representing the evolutionary history of anthropoid lunate morphology, based on phylogenetic PCA. The phylogeny is projected onto the first two phylogenetic principal components of all extant and fossil lunate shape variables, with ancestral states estimated via maximum likelihood. *Pan-Homo* and great ape LCAs are highlighted. See Table 4.5c for eigenvalues

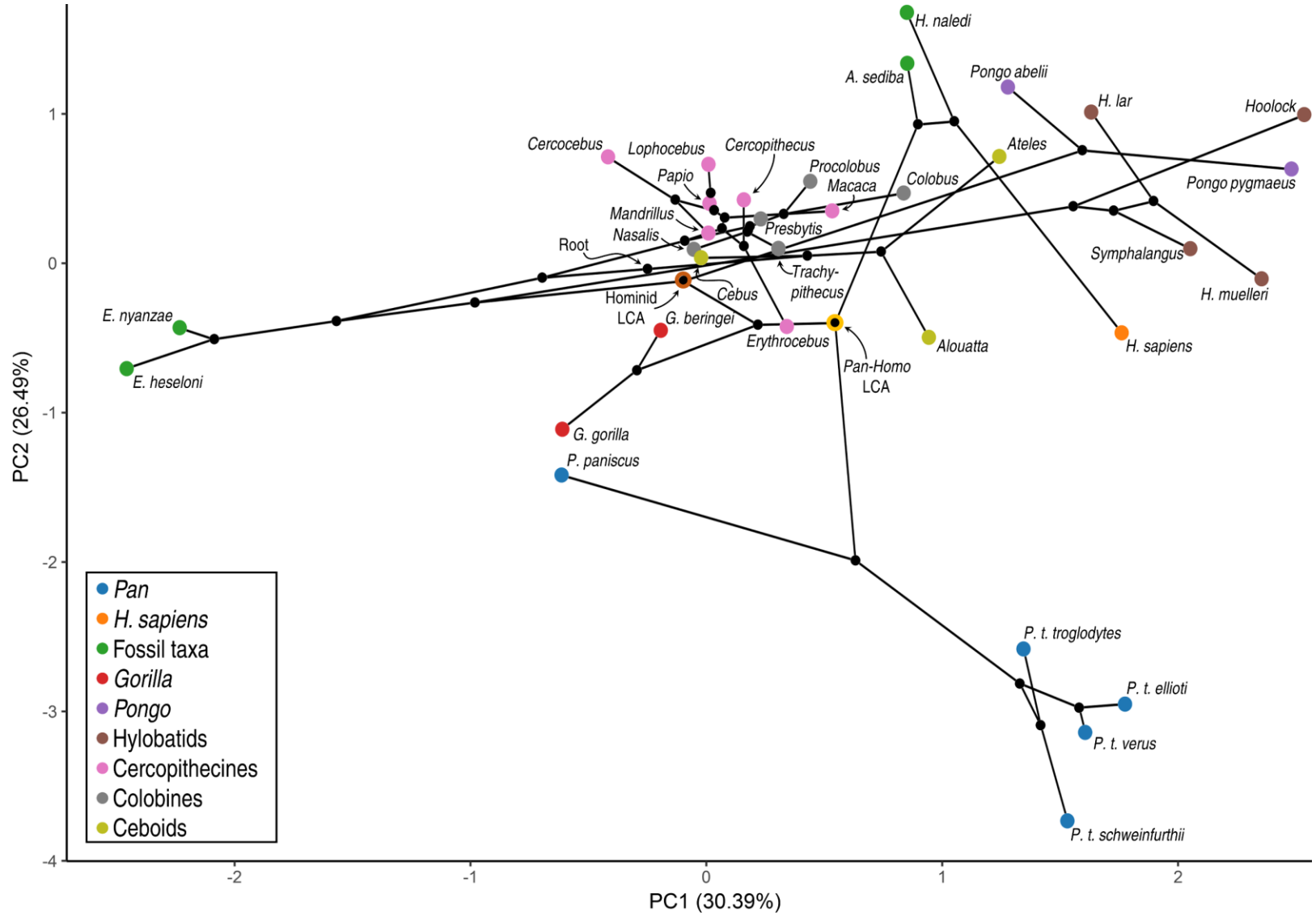

Fig. 4.31. Phylomorphospace representing the evolutionary history of anthropoid triquetrum morphology, based on phylogenetic PCA. The phylogeny is projected onto the first two phylogenetic principal components of all extant and fossil lunate shape variables, with ancestral states estimated via maximum likelihood. *Pan-Homo* and great ape LCAs are highlighted. See Table 4.5d for eigenvalues

Table 4.12. DFA positional classification and posterior probabilities of fossil and human samples. See also Table 4.6, Table 4.8c, and Table 4.11b for model details.

a Capitate	*DG*	*KW*	*PG*	*S*	Max	Class
KNM-MV 4	0.06	0.25	0.68	0.01	0.68	*PG*
KNM-CA 409	0.36	0.01	0.63	0.00	0.63	*PG*
KNM-SO 31245	0.02	0.01	0.97	0.00	0.97	*PG*
KNM-SO 31246	0.07	0.00	0.92	0.00	0.92	*PG*
KNM-SO 1000	0.01	0.44	0.09	0.46	0.46	*S*
KNM-SO 1001	0.00	0.09	0.12	0.79	0.79	*S*
KNM-SO 1002	0.01	0.67	0.33	0.00	0.67	*KW*
KPS III C26	0.58	0.00	0.42	0.00	0.58	*DG*
KPS VIII C27	0.20	0.00	0.80	0.00	0.80	*PG*
KNM-RU 2036M	0.37	0.00	0.61	0.02	0.61	*PG*
GSP 17119	0.02	0.05	0.30	0.63	0.63	*S*
KNM-WK 18365	0.25	0.00	0.75	0.00	0.75	*PG*
Qafzeh 9	0.77	0.03	0.19	0.02	0.77	*DG*
Kebara 2	0.67	0.02	0.31	0.00	0.67	*DG*
Shanidar 4	0.00	1.00	0.00	0.00	1.00	*KW*
Tabun 1	0.04	0.89	0.06	0.00	0.89	*KW*
LB1-45	0.00	0.88	0.04	0.08	0.88	*KW*
LB20	0.00	0.88	0.01	0.11	0.88	*KW*
UW 101-1730	0.38	0.37	0.25	0.00	0.38	*DG*
MH2 UW 88-105	0.38	0.26	0.35	0.01	0.38	*DG*
MH2 UW 88-156	0.39	0.02	0.59	0.00	0.59	*PG*
TM1526	0.04	0.56	0.18	0.22	0.56	*KW*
AL 288-1w	0.14	0.78	0.08	0.00	0.78	*KW*
AL 333-40	0.87	0.00	0.12	0.00	0.87	*DG*
KNM-WT 22944H	0.10	0.00	0.90	0.00	0.90	*PG*
Human mean	0.39	0.14	0.46	0.01	0.46	*PG*
b Hamate	*DG*	*KW*	*PG*	*S*	Max	Class
KPS III C12	0.02	0.77	0.07	0.14	0.77	*KW*
KNM-RU 2036L	0.00	0.56	0.02	0.42	0.56	*KW*
NG 940	0.07	0.82	0.07	0.03	0.82	*KW*
YPM30452	0.05	0.04	0.31	0.60	0.60	*S*
BH 36	0.07	0.01	0.26	0.65	0.65	*S*
KNM-TH 28860N	0.13	0.46	0.27	0.14	0.46	*KW*
Tianyuan	0.00	0.99	0.00	0.01	0.99	*KW*
Qafzeh 9	0.03	0.64	0.17	0.16	0.64	*KW*
Kebara 2	0.00	0.92	0.00	0.07	0.92	*KW*
Shanidar 4	0.01	0.89	0.05	0.05	0.89	*KW*
Regourdou 1	0.00	0.99	0.00	0.01	0.99	*KW*
LB21+22	0.00	0.99	0.00	0.01	0.99	KW
UW 101-1729	0.00	1.00	0.00	0.00	1.00	KW
MH2 UW 88-106	0.00	0.99	0.00	0.00	0.99	*KW*
MH2 UW 88-95	0.00	0.99	0.00	0.00	0.99	*KW*
AL 333-50	0.00	0.88	0.02	0.09	0.88	*KW*
KNM-WT 22944I	0.00	1.00	0.00	0.00	1.00	*KW*
Human mean	0.04	0.79	0.09	0.09	0.79	*KW*

c Lunate	*DG*	*KW*	*PG*	*S*	Max	Class
KPS III C22	0.21	0.04	0.00	0.74	0.74	*S*
KNM-RU 2036P	0.34	0.00	0.00	0.65	0.65	*S*
KNM-RU 15100B	0.00	0.00	0.00	0.99	0.99	*S*
UW 101-1732	0.00	1.00	0.00	0.00	1.00	*KW*
UW 101-418B	0.00	1.00	0.00	0.00	1.00	*KW*
MH2 UW 88-159	0.58	0.32	0.01	0.10	0.58	*DG*
KNM-WT 22944J	0.15	0.85	0.01	0.00	0.85	*KW*
AL 444-3	0.00	1.00	0.00	0.00	1.00	*KW*
Human mean	0.02	0.97	0.00	0.01	0.97	*KW*
d Triquetrum	*DG*	*KW*	*PG*	*S*	Max	Class
KPS III C38	0.00	1.00	0.00	0.00	1.00	*KW*
KNM-RU 2036DI	0.00	1.00	0.00	0.00	1.00	*KW*
KNM-RU 15100C	0.00	1.00	0.00	0.00	1.00	*KW*
UW 101-1727	0.00	0.00	0.06	0.94	0.94	*S*
MH2 UW 88-163	0.00	0.00	0.01	0.99	0.99	*S*
Human mean	0.06	0.25	0.16	0.53	0.53	*S*
e Combined function	*DG*	*KW*	*PG*	*S*	Max	Class
KPS III	0.97	0.02	0.00	0.00	0.97	*DG*
KNM-RU 2036	0.46	0.54	0.00	0.00	0.54	*KW*
UW 101	0.00	0.96	0.03	0.01	0.96	*KW*
MH2 UW 88	0.03	0.00	0.12	0.85	0.85	*S*
Human mean	0.01	0.78	0.09	0.12	0.78	*KW*
f CHL function	*DG*	*KW*	*PG*	*S*	Max	Class
KPS III	0.73	0.00	0.01	0.26	0.73	*DG*
KNM-RU 2036	0.75	0.00	0.01	0.24	0.75	*DG*
UW 101	0.00	1.00	0.00	0.00	1.00	*KW*
MH2 UW 88	0.68	0.18	0.07	0.07	0.68	*DG*
KNM-WT 22944	0.01	0.98	0.01	0.00	0.98	*KW*
Human mean	0.01	0.92	0.07	0.00	0.92	*KW*

Chapter 5

Conclusions

Summary of findings

Results of Chapter 2 demonstrate that aspects of carpal morphology strongly and consistently covary with positional behavior across the anthropoid clade, and several potential cases of convergent adaptation are identified in association with each of several behavioral modes. Many of the potential adaptations identified in association with suspension, which is found to be the behavioral mode most strongly reflected in wrist morphology, function to increase mobility at the midcarpal and antebrachiocarpal joints while stabilizing them against a broader range of force vectors. The capitohamate joint of suspensors is also found to be reinforced against the non-stereotypical force vectors thought to characterize suspensory loading regimes. Additional suspensory features enhance flexor carpi ulnaris leverage and aid in the transmission of forces generated thereby.

Digitigrady was less distinguishable than suspension from palmigrady, but several plausible adaptations were nevertheless identified. These traits aid stability of the midcarpal joint during loading at maximum extension, contribute to a distal mortise stabilizing the ulnar carpometacarpal joints, and facilitate load transmission across the ulnocarpal joint. The central column of the wrist is also found to be narrower in digitigrade taxa, perhaps related to the dominance of parasagittal movements in their

behavioral repertoires. Several features associated with knuckle-walking are also identified, most related to enhancing the transmission of axial compressive loading.

Multivariate shape is also found to strongly covary with positional behavior, allowing extant anthropoids to be classified according to positional behavior with high accuracy, and for the relative contributions of different locomotor modes to their behavioral repertoires to be accurately estimated.

Arboreal-only locomotor repertoires are found to have greater correspondence to wrist morphology than more complete characterizations of positional behavior, suggesting an outsized importance of arboreal behaviors on survivorship relative to the frequency of arboreal locomotion among terrestrial anthropoids. Climbing is found to be reflected differently in the wrists of apes and monkeys, consistent with the biomechanical dissimilarity of the behaviors between the groups, while leaping is found to have very little influence on wrist morphology. Variation of both locomotion and morphology are found to be far greater among hominoids than among other anthropoids.

Chapter 3 documents a relatively high degree of morphological variance in association with locomotion among the analyzed sample of Tinderet early Miocene catarrhine capitates, indicative of a degree of functional diversity beyond what is generally recognized among early Miocene catarrhines. The sample is found to be taxonomically diverse as well, with as many as six species represented, although the taxonomic identity of most specimens cannot be determined with confidence due to the lack of postcrania associated with many of the species known from these sites.

Two of the seven specimens are inferred to have been significantly reliant on suspensory behaviors. The largest specimen of the Tinderet sample, KNM-SO 1002, is found to be uniquely great ape-like among capitates known from the early Miocene, adding to a growing body of evidence indicating the presence of a functionally-derived, mid-sized catarrhine at Songhor. The identity of this derived ape may be *Rangwapithecus gordoni*, to which this specimen is allocated, along with the suggestion that the presence of derived postcranial features is a better criterion for distinguishing this species from *Proconsul africanus* than is body size.

Results presented in Chapter 4 provide further support for the frequency of parallelism in hominoid evolution, with specialized suspensory adaptation estimated to have been limited in the LCAs of the major hominoid clades. The LCAs of crown apes and great apes are instead reconstructed as above-branch quadrupeds, perhaps supplemented by vertical climbing and clambering. The hominine and *Pan-Homo* LCAs are also estimated to have been relatively generalized, adapted for neither suspension nor terrestrial locomotion to a substantial degree (but see below). These results suggest that extant apes are of dubious utility in modeling the morphology or locomotor repertoire of the *Pan-Homo* LCA. *A. sediba* is estimated to have diverged functionally from other hominins to some extent, but results are equivocal regarding the behavioral implications of this distinction. Finally, results of this study suggest that phylogenetic lag resulting in retention of morphology associated with the ancestral hominin positional repertoire in the analyzed hominin specimens is minimal.

Caveats and future directions

As with the construction of any scientific model, compromises must be made, and subjective choices potentially affecting analytical results are myriad. Among those choices was which morphometrics to extract from each bone. In Chapter 2 I utilize a subset of those hypothesized to be related to function, but additional morphometrics were also extracted, as shown in the subsequent chapters. Additional traits also could have been measured. For example, I did not characterize the robusticity or orientation of the hamulus, concavity of the distal portion of the hamate's triquetrum facet, or waisting of the capitate neck. These would have required bespoke quantification methods, as several other metrics did, but ultimately it was a matter of weighing the advantages of adding further to the already extremely time-consuming methods employed, and a line was drawn. Despite the partially arbitrary nature of choosing these variables, in Chapter 4 I nevertheless draw distinctions between the morphology of an element's most diagnostic features versus its "overall shape", with the latter referring to the complete set of variables I happened to extract from it. This is not uncommon, but demonstrates the point.

In Chapter 2, I describe the interactions among body size, phylogeny, and locomotor behavior. To summarize, because these factors are not independent, but rather are in some cases highly correlated, accounting for phylogeny and body size has the effect in some cases of eliminating much of the very information being sought. It is hoped that any residual signal will be more robust as a result, less likely an illusory artifact of these common confounds, but other confounding factors remain to risk false positives, while the risk of false negatives has meanwhile increased. Also discussed in

Chapter 2 is the sometimes overly parsimonious outlook of phylogenetic regression methods. Applied to extant taxa, both the PGLS and PGLMM methods will, for example, tend to see similarity between *Pongo* and hylobatids as homologous, even when there is ample evidence that much of it is homoplastic.

An additional caveat applies to the results of Chapters 3 and 4. While care was taken to limit the shape variables used to diagnose different locomotor behaviors to not only those most useful in distinguishing extant positional classes while accounting for the effects of phylogenetic and allometric autocorrelation, but also to those with plausible biomechanical roles in their facilitation, it has not been experimentally confirmed whether the condition of these shape variables in relevant taxa arose in adaptation to the locomotor behaviors with which they are here associated. As also discussed in Chapter 2, it is furthermore theoretically likely both that relatively subtle variations in the performance of a given positional behavior can modify its loading regime sufficiently to induce a divergence of adaptive optima between lineages, and that the independent emergence of a locomotor mode in separate lineages may, whether due to discrepancies of ancestral anatomy, developmental or genetic predisposition, unrelated aspects of the selective milieu, or other factors, yield wholly dissimilar morphological adaptations. The likelihood of the latter eventuality may be further increased in anatomical complexes such as the wrist in which wholly dissimilar architectures could produce similarly sufficient responses to selection associated with the behavior. And indeed, a selective pressure being overcome in separate lineages via modification of alternative bones participating in the same functional complex could manifest as incongruence of evolutionary pathway between carpal elements. The

phylogenetic toolkit as presently constituted has limited utility in identifying such cases, or in properly considering them for the purpose of estimating ancestral function.

While experimental methods of modeling skeletal biomechanics have progressed (see Orr, 2016; Vereecke and Wunderlich, 2016), the biomechanics of neither anthropoid locomotor behaviors nor anthropoid wrists are sufficiently understood to allow controlled experiments to test the effects of subtle variations in carpal morphology. The features identified as plausible locomotor adaptations in Chapter 2 may therefore be more usefully tested in the near term by sampling from a wider range of taxa. Colobine suspensors like *Pygathrix* may be especially helpful in providing an additional opportunity to investigate morphological evolution in association with autapomorphic acquisition of suspensory behavior. Early steps toward an expedition to study this genus have been taken.

Even if the variables identified as diagnostic of extant positional behavior are all supported by such future studies, it is possible that hominin carpals evolved quickly in the early stages of the lineage as constraints associated with locomotion were lifted and new pressures associated with manipulative abilities intensified. Such a scenario would tend to obscure any ancestral functional signal, making resemblance between the unique morphology Pleistocene or later hominins and extant positional groups to be of dubious functional import.

Various other caveats are discussed in Chapter 4, relating to the effect of fossil samples of different size or composition on a data set's phylogenetic signal, the estimated "polarity" of continuous traits, and decreased congruence among analyzed elements in the pathways by which they are estimated to have evolved. Additional work

is planned to evaluate this confound, as well as the robusticity of reported results, by equalizing fossil samples among the analyzed elements, removing fossils thought to be less relevant to the human lineage, or removing extant taxa that may be less representative of normal variation patterns (e.g., hylobatids), and comparing results. As ever, additional fossil specimens would also be very helpful in improving the reliability of these results. Estimation of an ancestral state is particularly benefited from being closely bracketed by known morphology; among known specimens currently unavailable for study, *Ardipithecus* and *Pierolapithecus* should be especially informative in estimating the likely morphology of the *Pan-Homo* and hominine LCAs.

Finally, as noted at the outset, the *a priori* positional classes assigned to the sampled extant taxa are crude characterizations, with significant overlap among them. This is particularly true in the context of Chapter 4; despite its relative infrequency among adult individuals, all knuckle-walkers are also capable suspensors. Various efforts were made in the preparation of Chapter 2 to detect similarities between the knuckle-walking and suspensory classes that might be attributable to shared suspensory adaptations. These attempts were unsuccessful. Such adaptations likely exist, but phylogenetic regression is not meant to be able to distinguish adaptive from non-adaptive evolution within a single clade, and the inclusion of *Ateles* was not sufficient to overcome the overwhelming phylogenetic signal. The traits used in Chapter 4 to detect suspension may therefore be inappropriate in addressing the evolution of this behavior in the hominine clade. If, on the other hand, the traits found to be morphologically convergent in Asian apes and *Ateles* adequately represent consistent ways in which suspension tends to be reflected in carpal morphology, the lack of these

features in extant African apes may relate to adaptive compromises associated with knuckle-walking. If so, the estimated lack of substantial adaptation to either behavior in the *Pan-Homo* and hominine LCAs may reasonably suggest a more generalized locomotor ancestry for hominins. Nevertheless, the estimated lack of suspension in these ancestors should perhaps have a smaller effect on the reader's Bayesian priors than the similarly generalized estimates of more ancestral nodes.

In addition to the projects mentioned above, I plan to apply the data set collected for this project and resulting insights in addressing various other questions related to the evolution of catarrhine locomotion. For example, I have plans to analyze various other undescribed fossil carpals, including the large sample known from Maboko, to evaluate the evolution of terrestriality in cercopithecoids, and to revisit the kinematic and morphological distinctions between the African ape genera.

Chapter 5 references

Orr, C.M., 2016. Functional morphology of the primate hand: Recent approaches using biomedical imaging, computer modeling, and engineering methods, in: Kivell, T.L., Lemelin, P., Richmond, B.G., Schmitt, D. (Eds.), The Evolution of the Primate Hand. Springer, New York, pp. 227-257.

Vereecke, E.E., Wunderlich, R.E., 2016. Experimental research on hand use and function in primates, in: Kivell, T.L., Lemelin, P., Richmond, B.G., Schmitt, D. (Eds.), The Evolution of the Primate Hand. Springer, New York, pp. 259-284.